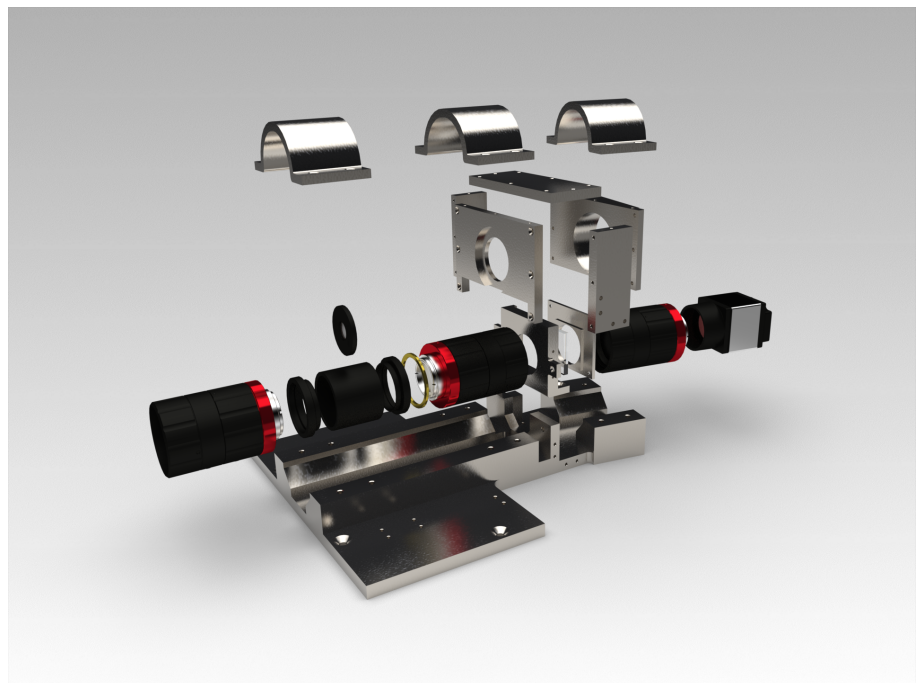Tord Hansen Kaasa

Mechanical Design Analysis and Integration of a Hyperspectral Imaging Payload for a 6U CubeSat

Master's thesis in Mechanical Engineering
Supervisor: Cecilia Haskins
June 2019

Master's thesis

NTNU
Norwegian University of Science and Technology
Faculty of Engineering
Department of Mechanical and Industrial Engineering

NTNU
Norwegian University of
Science and Technology

Tord Hansen Kaasa

Mechanical Design Analysis and Integration of a Hyperspectral Imaging Payload for a 6U CubeSat

Master's thesis in Mechanical Engineering
Supervisor: Cecilia Haskins
June 2019

Norwegian University of Science and Technology
Faculty of Engineering
Department of Mechanical and Industrial Engineering

NTNU
Norwegian University of
Science and Technology

Abstract

This thesis presents the development of a hyperspectral imager and the associated payloads onboard a 6U CubeSat owned by the HYPSO project. The thesis serves as a cover for a package of technical reports written during the research period. The reports provide a detailed description of the design process, tests, analyses and simulations done to develop the payloads. The design of the hyperspectral imager was built upon a prototype designed by Fred Sigernes, Professor in Optics and Atmospheric Research at The University Centre In Svalbard, in addition to iterative design work done by the mechanics team for their specialization project.

Preliminary mechanical and thermal simulations using NX11 were preformed. The results indicated that the total stiffness of the hyperspectral imager payload was above the requirements, while the operational temperatures present during orbit would necessitate thermal control systems for the payload.

A functional prototype of the hyperspectral imager payload was produced in aluminium 6082-T6 and tested. The results showed that the payload could operate in earth conditions, producing distinct spectral lines that shifted in a predicted manner when imaging different targets. An integration analysis was conducted on the optical COTS components present in the payload. Throughout testing it became obvious that the largest challenge related to such components were the potentially mission critical outgassing materials present inside. Mitigation strategies were developed to reduce the risk.

An architectural layout analysis was conducted to determine the different layout options inside the CubeSat. A layout that has room for every component was chosen. However, the layout necessitated a custom mechanical interface for the SDR payload. The interface was designed and simulated, and the results indicates that the mechanical integrity of the design would be appropriate.

A layout design for a dampening solution for the hyperspectral imager was created in association with the french company SMAC. While the solution is a work-in-progress, it can function as a basis for future dampening solutions.

The technical reports presents proposed design changes and tests needed in order to make the developed payloads ready for space operations onboard the HYPSO CubeSat.

I

Abstract (Norwegian)

Denne oppgaven presenterer utviklingen av et hyperspektralt kamera og tilhørende nyttelast ombord på en 6U CubeSat eid av HYPSO prosjektet. Avhandlingen tjener som omslag for en pakke med tekniske rapporter skrevet i forskningsperioden. Rapportene gir en detaljert beskrivelse av designprosessen, tester, analyser og simuleringer som er gjort for å utvikle nyttelastene.

Det hyperspektrale kameraet ble bygget basert på en prototype designet av Fred Sigernes, professor i optikk og atmosfærisk forskning ved Universitetssenteret på Svalbard, i tillegg til iterativt designarbeid utført av mekanikk teamet i forbindelse med sitt spesialiseringsprosjekt.

Foreløpige mekaniske og termiske simuleringer ved bruk av NX11 ble gjennomført. Resultatene indikerte at totalstivheten til det hyperspektrale kameraet var i henhold til kravene, samtidig som operasjonstemperaturene tilstede i omløp ville nødvendiggjøre termiske styringssystemer for nyttelasten.

En funksjonell prototype av det hyperspektrale kameraet ble produsert i aluminium 6082-T6 og testet. Resultatene viste at nyttelastet kunne operere under atmosfæriske forhold, og produserte distinkte linjer som skiftet som forventet når det avbildet ulike mål. En integrasjonsanalyse ble utført på de optiske COTS-komponentene som finnes i nyttelasten. Gjennom testing ble det åpenbart at den største utfordringen knyttet til slike komponenter var utgassende materialer tilstede. Reduksjonsstrategier ble utviklet for å redusere risikoen.

En arkitektonisk analyse ble brukt til å bestemme de forskjellige layoutalternativene i CubeSat'en. Et alternativ, med plass til hver komponent ble valgt. Dette alternativet krevde et tilpasset mekanisk grensesnitt for SDR nyttelasten. Grensesnittet ble designet og simulert. Resultatene indikerte at designens mekaniske integritet var tilstrekkelig.

En demperløsning for det hyperspektrale kameraet ble laget i samarbeid med det franske selskapet SMAC. Løsningen ble ikke utviklet ferdig, men kan fungere som et grunnlag for fremtidige demperløsninger.

De tekniske rapportene presenterer foreslåtte designendringer og tester som må gjennomføres for å gjøre de utviklede nyttelastene klare til romoperasjoner på HYPSO prosjektets CubeSat.

Preface

The work presented in this thesis has been carried out at the Department of Mechanical and Industrial Engineering in collaboration with the Faculty of Information Technology and Electrical Engineering at NTNU, as a part of the NTNU SmallSat program, HYPSO. The work presented in this thesis was done in close collaboration with Henrik Galtung and Tuan Tran, together with the HYPSO project. The focus of the thesis is the integration process of payloads consisting of readily available commercial optical parts, the design process of the mechanical interfacing of the spacecraft payloads, and the feasibility of using commercial optical parts in a camera designed for space. The HYPSO project delivers a 6U CubeSat with a hyperspectral imaging camera as its primary payload.

The work done is a continuation of the work done in the spesialization project *Mechanical and Thermal Integration of an HSI Payload in a 6U CubeSat*, coauthored by Kaasa, Galtung and Tran. The tools used for this thesis were provided by the Faculty of Information Technology and Electrical Engineering, the Department of Mechanical, Industrial Engineering and the NTNU NanoLab. The identification and ordering of usable test facilities and tools were part of the thesis work.

During the project period I have gotten help from more people than I could have imagined. Firstly, I will thank my supervisor Cecilia Haskins for providing me with this opportunity. I would like to thank my main collaborators in the mechanical team Tuan Tran and Henrik Galtung for being the best work partners anyone could ask for. I would also like to thank everyone in the HYPSO project, especially project leader Evelyn Honoré-Livermore, for creating a wonderful work environment for everyone involved with the project. Finally, I would like to thank my family for believing in me during my entire study and thesis work.

Due to the large amount of technical reports produced by the mechanics team during the research period, this thesis is structured differently than most master theses. The reports are attached in the appendix and the purpose of this document is to provide context for them and discuss their impact on the mission. Table i shows the authors for each of the reports and their location within the appendix. Even though some reports are listed with a main author, they still contain significant contributions from the other members of the mechanics team.

Table i: Technical Reports

Report Title	Author	Co-author	Appendix
Excerpt from Spesialization Report	Galtung, Kaasa, Tran	-	Appendix A
HYPSO-DR-003	Galtung, Kaasa, Tran	-	Appendix B
HYPSO-ANA-006	Kaasa	Galtung, Tran	Appendix C
HYPSO-ANA-004	Galtung, Kaasa, Tran	-	Appendix D
HYPSO-ANA-003	Galtung	Kaasa	Appendix E
HYPSO-ICD-001	Galtung, Kaasa	Tran	Appendix F
HYPSO-ICD-002	Galtung	-	Appendix G
HYPSO-TRP-OPT-002	Galtung, Kaasa, Tran	-	Appendix H
HYPSO-TRP-VAC-001	Galtung, Kaasa, Tran	-	Appendix I
HYPSO-TRP-VAC-002	Kaasa	Galtung, Tran	Appendix J
HYPSO-ANA-009	Kaasa, Tran	Galtung	Appendix K
HYPSO-ANA-008	Kaasa, Tran	Galtung	Appendix L
Test Plans	Galtung, Kaasa, Tran	-	Appendix M
Future Test Plans	Galtung, Kaasa, Tran	-	Appendix N

v

Contents

List of Tables

List of Figures

Acronyms and Abbreviations

1U	10x10x11.35 cm, Standard measuring unit used for CubeSats
6U	CubeSat made from six units of 1U in 2x1x3 (x,y,z) formation
ADCS	Attitude Determination and Control System
AUV	Autonomous Underwater Vehicle
CAD	Computer-Aided Design
CAE	Computer-Aided Engineering
CDR	Critical Design Review
CONOPS	Concept of Operations
COTS	Commercial Off-The-Shelf
CTE	Coefficient of Thermal Expansion
ECSS	European Cooperation for Space Standardization
ESA	European Space Agency
HSI	Hyperspectral Imager
HYPSO	Hyper Spectral SmallSat for Ocean Observation
ICD	Interface Control Document
IMU	Inertial Measurement Unit
MLI	Multi-Layered Insulation
NA	NanoAvionics
NASA	National Aeronautics and Space Administration
NIR	Near Infrared
NTNU	Norwegian University of Science and Technology
OPU	Onboard Processing Unit
PDR	Preliminary Design Review
PhD	Philosophiae Doctor
PLM	Product Lifecycle Management
PLSV	Polar Satellite Launch Vehicle
RGB	Red, Green and Blue
RID	Review Item Discrepancy
s/c	Spacecraft
SDR	Software Defined Radio
SMAD	Space Mission Analysis and Design
TU Berlin	Technical University of Berlin
UAV	Unmanned Aerial Vehicle
UNIS	The University Centre in Svalbard
USV	Unmanned Surface Vehicle
UV	Ultraviolet
VIS	Visible

Symbols

Table ii: Symbols

Property	Unit	Description
N	-	f-number
f	mm	Focal length
B	mm	Flange Focal Length
D	mm	Lens Pupil/ Effective Aperture Diameter
X	mm	Image Sensor Height

1 Introduction

1.1 HYPSO Mission Objective

The HYPSO (Hyper Spectral SmallSat for Ocean Observation) mission will be primarily a science-oriented technology demonstrator. It will enable low-cost and high-performance hyperspectral imaging and autonomous onboard processing that fulfil science requirements in ocean colour remote sensing and oceanography [1]. This is to be done by integrating the hyperspectral imager (HSI) into a small satellite space craft (s/c) called a CubeSat. In order to achieve a low-cost HSI solution, commercial off-the-shelf (COTS) components will be used as opposed to a space graded solution. Space grade components are relatively expensive compared to COTS due to the amount of documentation required to prove space grade authenticity for each delivered component.

NTNU SmallSat is intended to be the first SmallSat developed at NTNU with launch planned for Q4 2020 followed by a second mission due in 2021. Furthermore, the vision of a constellation of remote-sensing focused SmallSats will constitute a space-asset added to a multi-agent architecture of UAVs, USVs, AUVs and buoys that have similar ocean characterization objectives.

The main mission of the HYPSO project is to successfully integrate and launch a HSI payload into orbit, as well as to maintain the integrity of the components so it can operate in space for 5 years. The HSI in cooperation with autonomous equipment shall be able to monitor the ocean outside Norway and detect dangers such as algae blooms that can harm the local environment.

1.2 Project Organization

The HYPSO interdisciplinary project team consists of more than 20 master and bachelor students, 8 PhD and PostDoc participants and several supporting professors. The project team is structured in smaller branches based in the following work areas: Satellite bus, Payload software, Ground segment, Attitude Determination and Control, Operations and HSI Payload Hardware. All project branches work together to ensure the overall mission progress and proper information flow. A leader is assigned to all branches to establish proper communication. The project manager Evelyn Honoré-Livermore is responsible for the overall mission progress and scheduling, as well as being the branch leader for the mechanics team. The mechanics team belongs to the HSI Payload Hardware branch, and consists of three members: Tuan Tran head of thermal design, Henrik Galtung head of architecture and interface design, and Tord Hansen Kaasa head of mechanical and main payload design. These responsibilities were mutually agreed by the team members at the start of the research.

1.3 Problem Outline

As part of the HYPSO project, the main goal for this Master's Thesis was to conduct an integration analysis of the main payload, a hyperspecral imager, consisting of COTS components into a 6U CubeSat, with a focus on mechanical and material factors. This entailed establishing a mechanical design for the main HSI payload that conforms to the CubeSat system delivered by NanoAvionics (NA) based on a HSI design created by Fred Sigernes, Professor in Optics and Atmospheric Research at The University Centre in Svalbard (UNIS). The research also established a plan for examination and further testing of the COTS Components that comprised the optical system. The examination formed a basis for determining the optical components that can be used, derived from requirements based on standards given by the European Cooperation for Space Standardisation (ECSS) and the National Aeronautics and Space Administration (NASA) for space materials, elaborated on in section 4.4. Furthermore, mechanical integration of the secondary payloads, a Software Defined Radio (SDR) and an RGB camera were analyzed.

The launch of a s/c introduces numerous challenges and complications with regard to the mechanical design of the optical payload. Large frequency bands induced in the s/c from the rocket interface, vibrations caused by the acoustic pressure and pyroshock could shift the optical placement, impeding the HSIs ability to operate as required. In addition these loads could potentially damage and destroy the components. Furthermore, the payloads must survive in the environment of space. This introduces additional challenges such as thermal conditions, outgassing and microvibrations. Outgassing poses a challenge due to the materials present inside COTS components that are not rated for space. All materials shall be examined according to the outgassing requirements. Because the s/c is to be decommissioned after its life period, additional material requirements are also present. These include melting temperature and mass, as space debris needs to be accounted for, as described in the NASA published "CubeSat 101" [2]. The mechanical solution must also conform to the relevant ESA and NASA standards, discussed in section 4.4.

1.4 Scope of the Thesis

This Master's Thesis introduces the mechanical integration of the payload from the perspective of the CubeSat materials and environmental loads, from launch and operation. The research conducted during the Master's Thesis period was done in close collaboration with Henrik Galtung and Tuan Tran in the mechanics team, who focused on architecture and the thermal capabilities of the payload respectively. It follows that this thesis should be viewed as a part of the full mechanical integration report. The thesis covers the tests, analyses and simulations conducted by the mechanics team during the course of the allocated project time.

2 Background and Previous Work

This section introduces the thesis background regarding previous related work, the HYPSO mission and the CubeSat platform.

2.1 Specializaton Report

This thesis was written as a continuation of the the specialization project conducted in collaboration with Henrik Galtung and Tuan Tran for the HYPSO mission during fall 2018. All work presented in this thesis was built upon the foundation established during the specialization report. Important background information from the specialization report that will not be repeated in this thesis are presented in *Appendix A.*

2.2 HYPSO Mission

A background to the HYPSO Engineering Practice and Management was covered in the specialization report, *Apendix A*, section 2.1.

2.2.1 Preliminary Design Review

The standard CubeSat development schedule for CubeSats includes two large delivery milestones, the Preliminary Design Review (PDR), and the Critical Design Review (CDR). PDR is the first design review done in a development period as an assessment of the proposed system to establish that the requirements will be met with acceptable risk [3].

The first HYPSO PDR was held on the 30th of October 2018 followed by a follow-up meeting on the 29th of May 2019 to address open issues. Design documentation was delivered one week in advance, giving the reviewers time to add feedback and concerns to the PDR Review Item Discrepancy (RID). The RIDs were reviewed during the PDR process and appropriate actions were suggested by the experts in attendance. The RIDs were closed when the suggested action was implemented into the documentation. When all RIDs are closed, the PDR will be considered closed, and all presented designs frozen. At the time of writing, the HYPSO PDR was open. All reports presented in this thesis were used as main or reference documents during the PDR.

2.2.2 Concept of Operations

This section briefly presents the HYPSO satellite concept of operations (CONOPS). Figure 1 shows the HYPSO mission HSI CONOPS, which characterizes the systems capabilities, functions and life cycle in the operating environment [4].

The mechanical interface solution must be able to withstand all stages of the satellite life cycle. The HYPSO s/c lifecycle consists of *launch*, followed by *deploying* and *commissioning* stages where the CubeSat is deployed, detumbled and establishes down and uplink with the ground station. This is followed by the *Primary operations* phase, during which the CubeSat executes the primary task, hyperspectral imaging and data download. Images are captured during a *slew maneuvre* where the s/c scans the target area to produce a pushbroom HSI image [5]. HYPSO is planned to have a *decommissioning* stage after the initial mission end. [6]
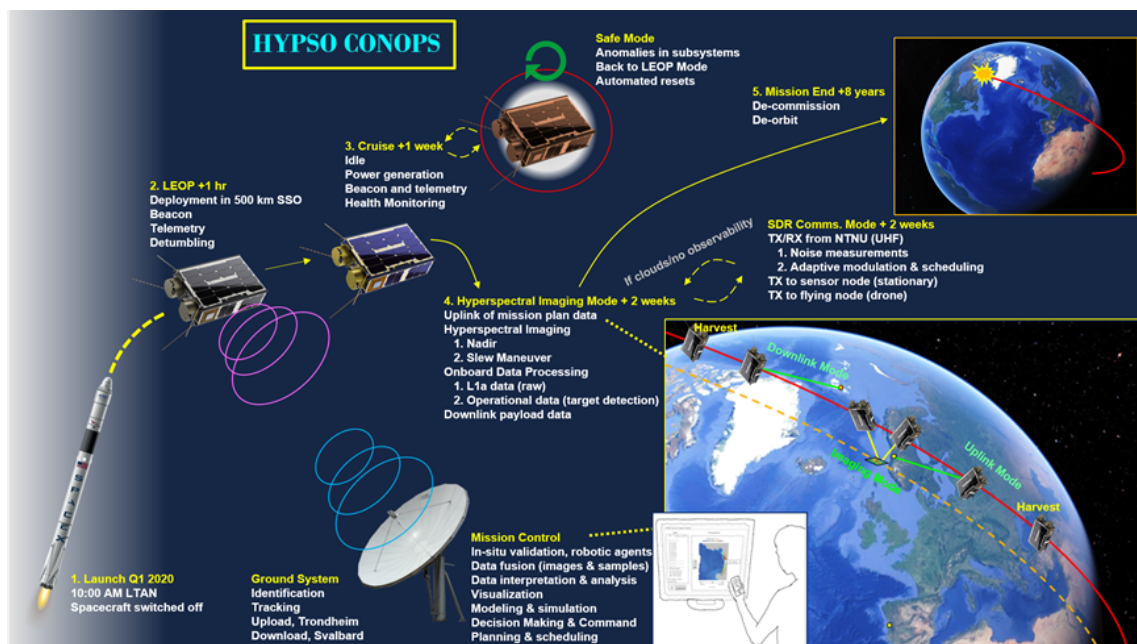
Figure 1: HYPSO Concept of Operations (Figure provided by Mariusz Grøtte)

2.3 Small Satellites

CubeSats are small satellites, *smallsats*, made from 10x10x10cm units (1U). CubeSats are commonly comprised of several units, where the HYPSO CubeSat is 6U. With the advent of smaller satellites, the threshold for developing satellite systems has been lowered significantly compared to traditional larger satellites. This can be attributed to the shorter development time and lower weight of the smallsats.

ESA recognises CubeSats as nano satellites with designs that are compliant with the CubeSat design specification developed by California Polytechnic Design Specification [7]. Smallsats are traditionally defined as weighing less than 500 kg, requiring a smaller launch and development cost [8]. This allows the smallsats to take larger risks and incorporate newer technology compared to larger satellites. The Smallsats can also *piggyback* on available room in other launchers allowing for additional cost reduction by not requiring a dedicated launcher. CubeSats are mostly classified as nano and micro satellites, a sub category of smallsats with weights of 1-10 kg and 10-100 kg, respectively, requiring even smaller investments. The advent of CubeSats, and the relatively low cost associated with development and launch, allows developers a better *trade on requirements*, meaning that more objectives can be achieved with a limited budget [8]. CubeSats are therefore a valuable tool for the space and science community and this has led to a boom in accessible space development.

2.4 Payload Description

This section gives a high level introduction to the payloads carried in the HYPSO CubeSat. The CubeSat system developed by the HYPSO project supports three main payloads in addition to the s/c system actuators and power systems delivered by NanoAvionics. The payloads include a HSI camera, an SDR and an RBG camera.

2.4.1 Primary Payload: Hyperspectral Imager

Optical Assembly The main payload of the satellite is a pushbroom HSI [9]. The imager is designed to be made from readily available COTS parts to make construction simple and reduce assembly and prototyping costs. The *HSI Pushbroom V6* was the final iteration of the prototype created by professor Fred Sigernes, designed purely as a conceptual prototype, including 3D printed parts not tailored to the launch- or space environment [10]. The V6 acted as the basis for the optical assembly that was integrated into the HYPSO s/c by the work presented in this thesis. Figure 2 shows the the initial design, while figure 3 shows a rendering of the redesigned HSI payload. A detailed design description of the newly designed HSI payload can be found in *Appendix B*.
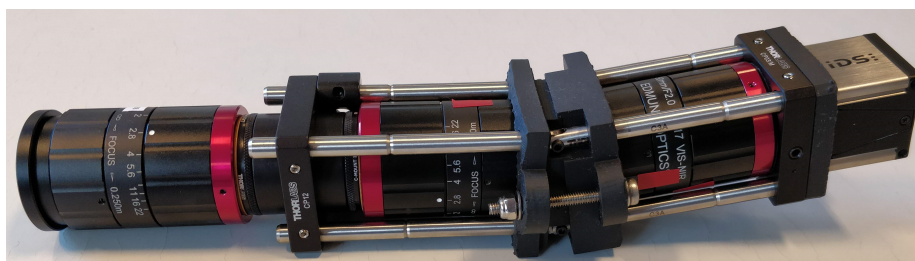
Figure 2: Conceptual HSI prototype designed by Fred Sigernes
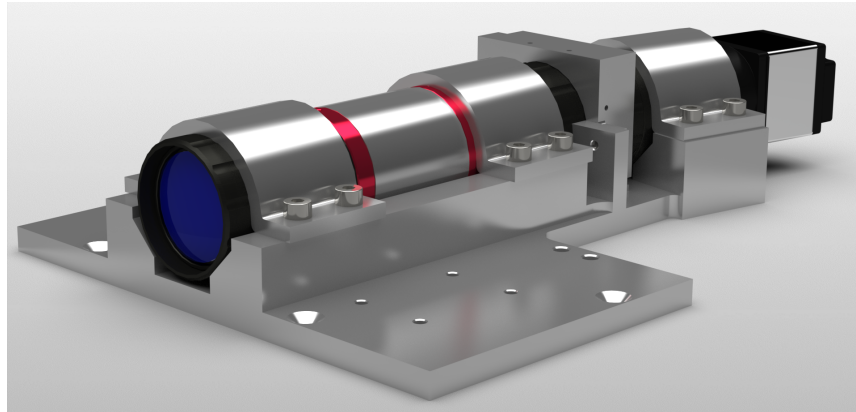
Figure 3: Re-engineered HSI payload for HYPSO

Onboard Processing Unit Payload control and data processing is managed by a PicoZed mounted on a custom carrier board, this configuration forms the s/c onboard processing unit (OPU). The HYPSO mission will require a degree of onboard processing of the hyperspectral image data. Therefore, the HSI camera must be physically linked to the OPU. The software used to operate the OPU is being developed by the HYPSO project.

2.4.2 Secondary Payload: Software Defined Radio

The secondary payload carried by the HYPSO CubeSat is proposed to be a *Software Defined Radio* (SDR). The specific SDR used for the HYPSO mission is a space proven Alén Space TOTEM SDR S-Band solution, allowing for simpler integration and less testing [11].

2.4.3 Tertiary Payload: RGB Camera

The tertiary payload in the satellite is planned to be an RGB camera. The main purpose is to provide color photography of the earth as well as georeferencing for the HSI. The RGB camera must have a rigid connection to the main payload in order to compare the pictures taken, which can be used to verify the hyperspectral images. However the RGB camera provides no additional scientific contribution to the mission. The tertiary payload will be entirely COTS components.

2.4.4 Star Tracker and Inertial Measurement Unit

The star tracker and inertial measurement unit (IMU) are managed by the attitude determination and control system (ADCS). The components are not a direct part of the onboard payloads. However, in order to provide accurate attitude control during the slew maneuvre, they must be rigidly coupled to the HSI payload.

3 Basic Theory

An extensive explanation of the underlying logic, premises and theory regarding the launch- and space environment, outgassing, architectural, mechanical and thermal CubeSat engineering was given in the specialization report. The relevant chapters can be found in *Appendix A*. The technical reports provided in the appendices provides further information and background regarding their respective subjects. Section 3. of *Appendix D* provides further information regarding outgassing in relation to CubeSats and COTS components. It follows that this section of the thesis will have a limited scope to avoid information redundancy and repetition. As such, this section will present a rudimentary overview of the optical design of the hyperspectral payload.

3.1 Hyperspectral Imaging

Hyperspectral imaging refers to a spectral imaging acquisition where all pixels within the image carries information regarding the spectrum reflected at the corresponding area of the source scene captured. The resulting hyperspectral image has two spatial dimensions and one spectral dimension. The hyperspectral imaging technique allows for a greater information sampling and additional precision compared to traditional imaging, visualized in figure 4 [12].
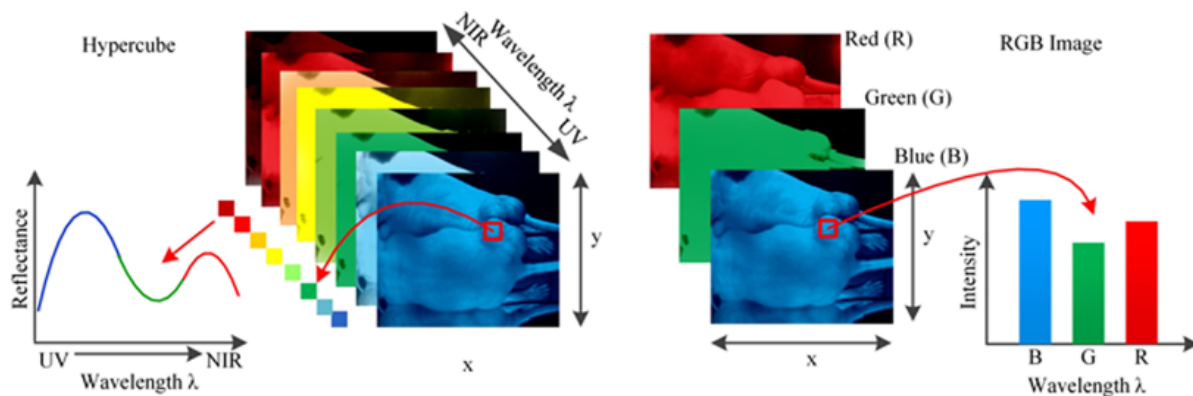
Figure 4: Hyperspecral imaging compared to RGB imaging

3.1.1 Pushbroom Method

Pushbroom is a method where several spectrograms of wavelengths are obtained by scanning narrow lines of a scene. Today, most earth observation imaging satellites carries a hyperspectral pushbroom payload. Figure 5 shows a rudimentary pushbroom HSI system operating on a satellite [5].
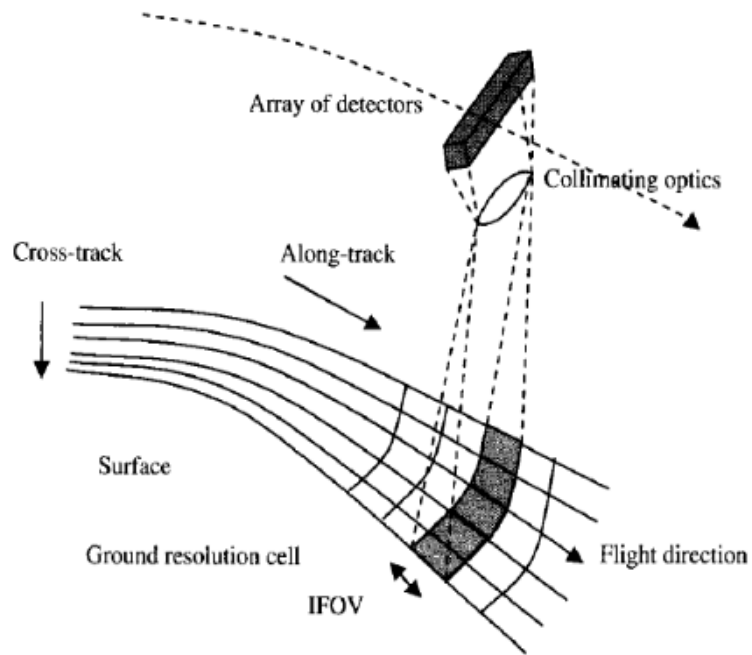
Figure 5: Pushbroom HSI operating on a satellite

Figure 6 shows the optical architecture of a basic pushbroom HSI, and the operational steps necessary to achieve the hyperspectral images [13]. The hyperspectral pushbroom technique takes the following steps: the front objective transmits the light into a slit, splitting the light into spectral bands that passes through a collimating lens. The parallel light enters the grating that disperses the light towards a detector, thus forming a spectral image. The scanned spectrograms can then be combined, to form a hyperspectral data cube, where each layer of the cube is one specific wavelength [14].
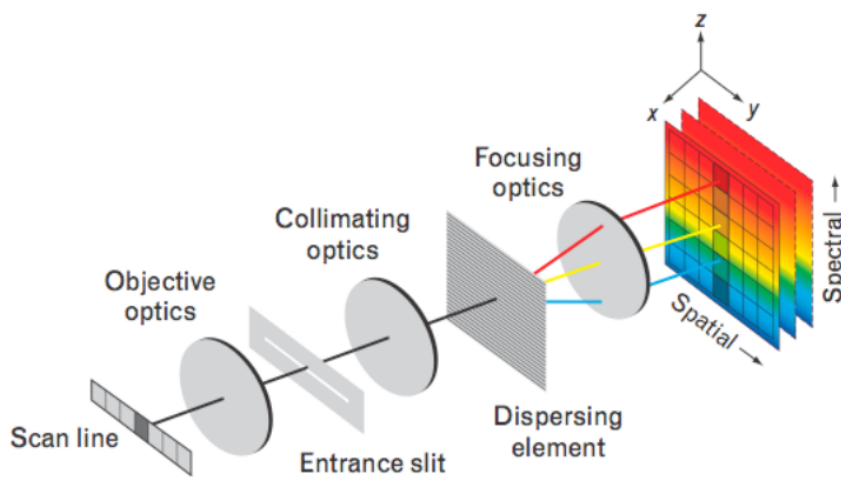
Figure 6: Optical architecture of a Pushbroom HSI

Figure 7 details a diagram of the HSI v6 optical train designed by professor Fred Sigernes [10]. In this diagram, D denotes effective aperture diameter, f focal length, L f-number, B flange focal distance, and X sensor image height.

EO Grating (G) #49-579 25mm Sq.
300 grooves/mm
Blaze angle: 17.5°

$\beta = 10.37°$

$D_1 = 18$ mm   L2 f/2.0   Range 400 - 800 nm
$f_1 = 50$mm   L1 f/2.8   X = 6.11 mm
$f_2 = 50$mm   B = 17.5 mm $f_0 = 50$ mm and up
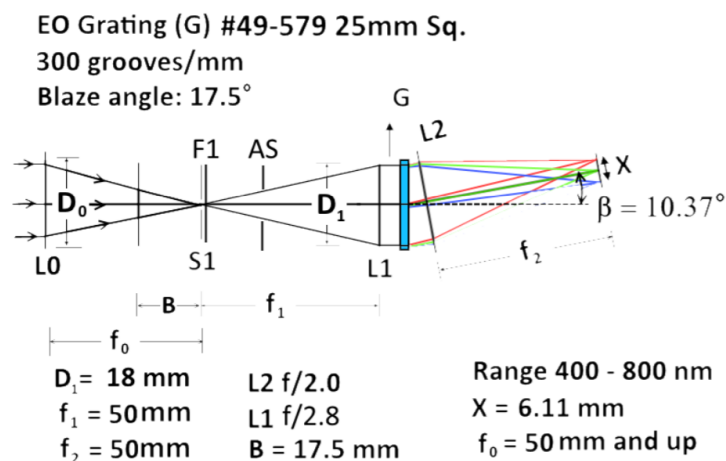
Figure 7: HSI V6 Optical Design

3.2   Hyperspectral Optical Components

This section presents the components that are used to build the pushbroom HSI presented in this report. The optical assembly consists of three lens objectives: front, collimator and detector objective. It also features an entrance slit, a transmission grating and a detector [10].

3.2.1   Lens Objectives

Objectives are classified based on their optimal transitivity of different wavelengths, ultraviolet (UV), visible (VIS) and near infra-red (NIR). This section will provide information regarding several key aspects of the objective optical properties.

Focal Length   The focal length, f, of an objective is the distance the transmitted light travels to converge, measured from the front lens centre. The focal length is therefore a measurement of how strongly the lens converge or scatters light. The image is formed at the focal point of the lens.

Flange Focal Length   The flange focal length is a measurement that describes the distance from the physical end flange of the objective to the light convergence point. Typically, an objective features a flange or metal ring at a precisely controlled distance from the focus point. This is the flange focal distance and varies depending on the manufacturer and

threading type to accurately focus the incoming light on the sensor. For the HSI, this distance is 17.526mm as it uses objectives and an imager with C-mount type threading.

Aperture and f-number   The f-number, denoted as $f/\#$ or N, is the measurement of the focal length over the entrance pupil diameter of the objective, $N = \frac{f}{D}$. The f-number can be adjusted by mechanically changing the aperture size. The aperture of modern cameras is adjusted at discrete settings using the standard *f-stop scale*, where the f-number is defined based on a geometric sequence of $\sqrt{2}$. Thus, decreasing the aperture diameter by a factor of $\sqrt{2}$ for every step, halving the light intensity and area of the pupil. The f-number is therefore a measurement of the objective light transmission, where larger f-numbers projects darker images. Figure 8 shows the changes in pupil size over varying f-numbers.

f/2   f/2.8   f/4

Figure 8: f-number of a 50mm Objective

3.2.2   Slit

An entrance slit is used in order to split the incoming light into a narrow band, effectively reducing a two dimensional image into a one dimensional slice. The height of the resulting spectrogram is dependent on the width of the slit, where a larger slit width produces a larger resulting image. The slit needs to be situated at the exact flange focal distance from the front objective and the collimator objective.

3.2.3   Transmission Grating

Transmission gratings are used to prismatically disperse incident light at a desired angle. The surface of the grating consists of a thin vacuum deposited coating or groove layer, made up of micrometer-scale prisms or grooves. The groove layer causes the light dispersion, where angular dispersion is a function of angle of incidence and groove spacing. A 17.5 blazed transmission grating was used in the HSI construction.

3.2.4   Detector

Monochrome imaging sensors are used in pushbroom HSIs in order to capture the wavelength spectrum produced by the optical train as described in section 3.1.1. The detector consists of an image sensor on a PCB board shielded by a metallic shell.

4 Method and Tools

This section is written in collaboration with Henrik Galtung and Tuan Anh Tran. It gives an overview of the work procedure and tools used by the mechanics team throughout the project. A more expansive description of the methods and tools used during this project can be found in the specialization report excerpt found in *Appendix A*.

4.1 Development

This section describes the development of the payload integration and the most important steps in this process. The first step involved mapping of various requirements and constraints. The team conducted brainstorming sessions before preliminary concepts were chosen for further development and selection. Analysis and simulation were used to explore the strengths and weaknesses of each concept. Based on the results, the design was improved and run through simulations again. When the design had matured sufficiently, manufacturing and testing of prototypes was incorporated in the development. The development pipeline shown in figure 9 is a customization and expansion of Figure 1 found in NASA-STD-5002 [15].
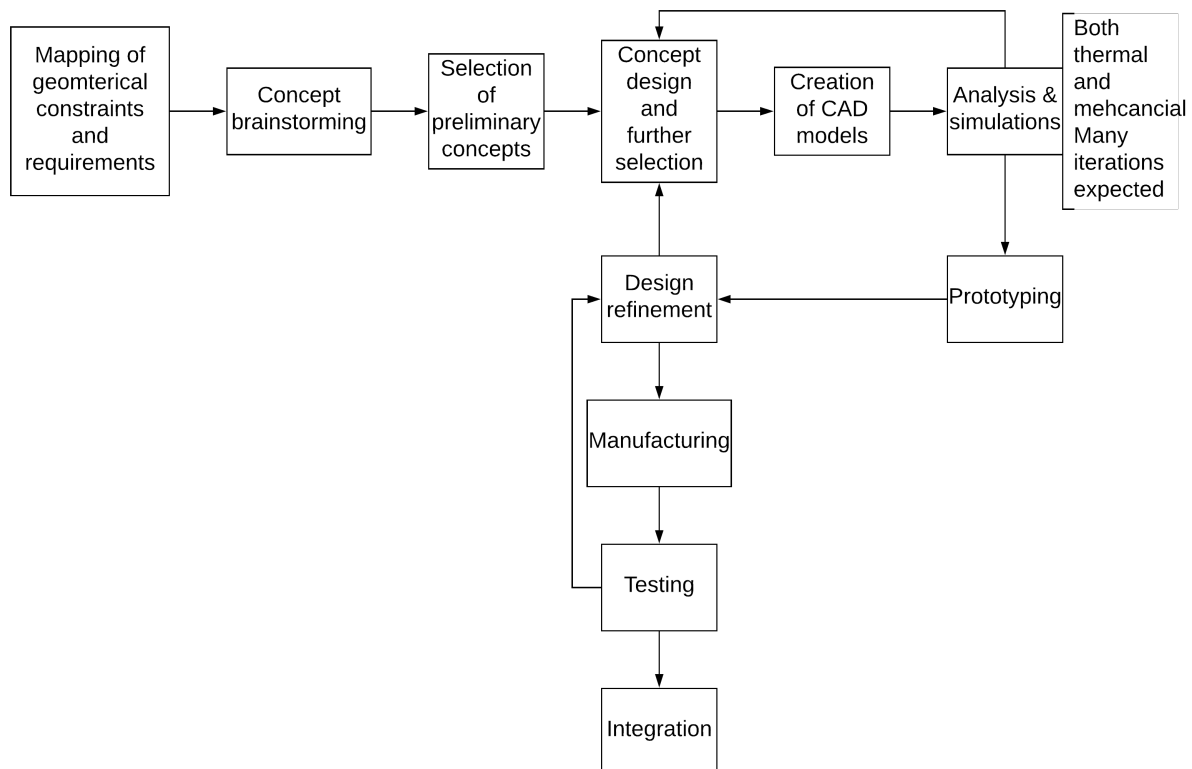
Figure 9: Development plan for HSI payload integration

Throughout the development, the design of the various components went through multiple iterations. This iterative process was fundamental to the evolution of all in-house designed components. Earlier designs focused on establishing a functionality, whereas later iterations aimed to optimize the overall complexity. Concurrently, the selection and analysis of the COTS components based mechanical and material conditions, evolved the design further. *Appendix A*, section 2.2, expands on this methodology and gives a rundown of each step and how they were intended to function.

4.2   Testing

Physical testing of a design or component is the closest engineers can get to an actual space environment without launching. While simulations provide good indicators and sometimes accurate results, the most reliable source are physical tests. Although testing allows for much higher reliability, the cost and availability of test facilities may become constraints. This mostly concerns thermal vacuum chambers and reliable vibration rigs that have limited availability. As a result, these tests were out of the scope for the thesis work. Figure 10 gives the testing approach used throughout the project. This figure is an extraction and modification of flowchart 17.1 from [16]. Testing was aimed at characterizing the performance of the design and various COTS components rather than validating against success criteria, which is referred to as *engineering development testing* by NASA [17].
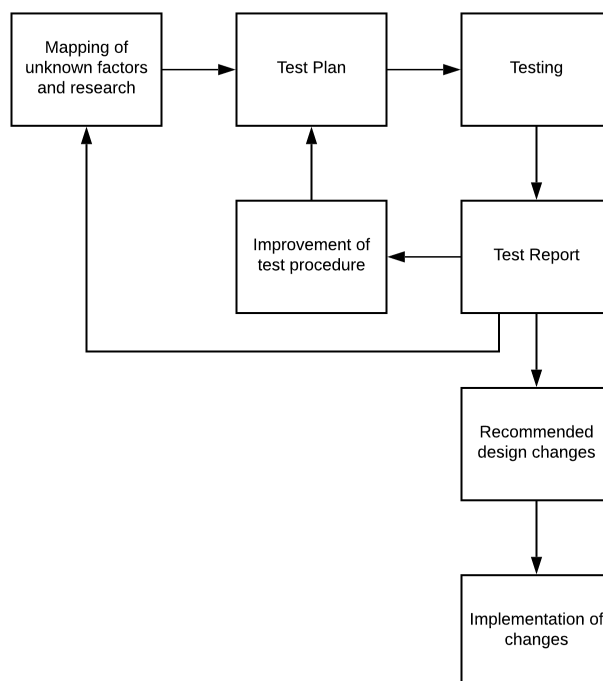
Figure 10: Testing Approach

For the first phases of design iteration, simplified tests were planned using environmental chambers and vacuum chambers. These design tests were used to gather information regarding the performance against the respective systems requirements, as well as further refining said requirements. Additionally, the results from these tests were used to further improve the reliability of the simulations.

Table 1 lists the performed tests, while table 2 lists the test planned for the future. A test plan was written for each test, listing all relevant information such that it should be repeatable in the future. Although Inspection is classified as a different verification method or a supplementary to tests [16], the disassembly inspections are listed together with the tests. After each test was performed, a technical report was created presenting the results in a concise manner to effectively disseminate the information within the project team and ensure repeatability. Later in the system development cycle, the entire system will be tested up against validation criteria with all subsystems integrated. The system must also pass a final acceptance test, subsystem level and system level, to be able to launch.

Table 1: Performed Test Overview

Test Name	Device Under Test	Test Description
HYPSO-RP-007 HYPSO-RP-008 HYPSO-RP-009 HYPSO-RP-010 HYPSO-RP-011	50 mm VIS-NIR Objective, Potential Detectors	Disassembly to uncover potentially mission harmful materials and substances *Please note that these reports are supplied at the end of Appendix J*
HYPSO-TRP-VAC-001	50 mm VIS-NIR objective, IMX 174 Detector	Items are exposed to a weak vacuum to check for potential damage
HYPSO-TRP-OPT-002	HSI Prototype	Determine the functionality of the HSI Prototype

Test Name	Device Under Test	Test Description
Material Outgassing Test	Samples of potentially volatile materials	Determine if the materials found during the Disassembly Tests are within the outgassing requirements
Cleaning Procedure Vacuum Test	50 mm VIS-NIR objective (Clean)	Vacuum Resilience Test showed damage on the objective. An objective that has been through a cleaning procedure will be vacuum tested
Component Level Vibration Test	50 mm VIS-NIR objective	Determine the COTS components resistance to vibration
Component Level Shock Test	50 mm VIS-NIR objective	Determine the COTS components behaviour under thermal loads
Component Level Thermal Test	50 mm VIS-NIR objective	Determine the COTS components resistance to shock
Component Level Thermal Test	IMX249	Determine the COTS components resistance to shock
Full Scale Vibration Test	HSI Prototype	Determine the HSI system resistance to vibration
Full Scale Shock Test	HSI Prototype	Determine the HSI system resistance to shock
Full Scale Thermal Test	HSI Prototype	Determine the thermal development of the HSI system

These tests planned for the future will have to be done to fully characterize the design and the components within. Unfortunately, there was not enough time for the mechanics team to run these tests during their project work. However, test plans for the component level shock, vibration and thermal tests were made. These can be seen in *Appendix N*.

4.3 Software Tools

This section lists all software programs used during the project. Further detail about the software, as well as other software options that fulfill similar purposes can be found in the excerpt from the specialization report in *Appendix N*, section 2.2.

4.3.1 CAD/CAE Tools

At the beginning of the project, a simple study was done to determine which CAD and CAE software would be used for the project. It was important to evaluate this properly, as it would determine much of the work-flow. Furthermore, changes in these kind of tools at a later state of the project would require rework, as all the CAD files would need conversion. This process would also cause loss in data such as underlying sketch information and material data, which would need additional work to reapply. The choice of CAD software laid the foundation for the future modeling tool used within HYPSO. Table 3 tabulates the chosen software.

Table 3: CAD/CAE Software Tools

Software	Description
NX 11	Main modelling and simulation tool
NX Nastran	FEA simulation Solver tool, structural and thermal
NX Space Systems Thermal	Thermal FEA solver specifically made for satellite development
SolidWorks 2018	Modeling tool, intuitive technical drawing module

A deciding factor when choosing the CAD software was the product lifecycle management (PLM) capabilities i.e. Team Center, PLM. NX 11 with Nastran, Space Systems Thermal and Team Center integration was chosen to minimize risk of data loss during exporting and to ensure a structured work environment for the CAD/ CAE model procedure. SolidWorks 2018 was used to create technical drawings and to convert files provided by NanoAvionics to NX 11.

4.3.2 General Software

Table 4 tabulates the general and organizational tools used during the project work. The General software was shared between the entire HYPSO team. Organizational tools such as Trello were used throughout the project, however they were phased out as the project progressed in favor of more in-depth project development software such Eclipse, which is the ESA recommended program [18].

Table 4: General Software Tools

Software	Description
CES EduPack 2018	Material library with MatML XML file support
Slic3r	Prepare 3D models for printing
Lucid Chart	Free flow chart creator
Google Drive	File storage and synchronization service, shared within the entire project
Eclipse	Project development tool
Slack	Communication and sharing platform
File Server	File storage system for larger files
Overleaf	Online LaTeX editor, for report writing

4.4 Literature

As this thesis serves as a cover for the package of included technical reports, the literature list is limited and does not represent the actual amount of literary resources read and cited throughout this project. All technical reports include a list of the respective references used, and the main bulk of material collected in conjunction with the research process. Some sources deserve a special mention; for example, during the research done for this project, open documents and reports from NASA have been very useful. Their reports and documents regarding specific space-related phenomenon like outgassing and atomic oxygen proved to be the best resources for investigating these effects in relation to a CubeSat. It is also worth mentioning the ECSS, which provides a comprehensive set of standards that are the result of a collaboration between ESA and national space agencies. It has been decided that this set of standards shall be followed by the entire HYPSO CubeSat project. The requirements outlined in the standards are therefore the basis for the design, unless otherwise stated by the launch provider.

There are some books that deserve a special mention as they have been paramount in understanding the space environment and provide a guide to solid space engineering practise.

- *Space Mission Engineering: The New SMAD [8]*

- *Dimensjonering av Maskindeler [19]*

- *Engineering Analysis with NX Advanced Simulation [20]*

The use of standards has throughout the project required evaluation of their relevance and usefulness. The complexity of CubeSat missions differs from conventional larger scale space missions. It follows that the standards used are limited or omitted. The Tailored ECSS Engineering Standards for In-Orbit Demonstration CubeSat Projects by ESA further states that the applicability of the various standards may vary according to the sensitivity of equipment as well as complexity of the particular CubeSat [7]. Following this line of reasoning, the optical main payload of the HYPSO mission can be considered highly sensitive to contamination, thus required a higher level of compliance to the standards involving contamination assessment [7]. The California Polytechnic CubeSat Design Specification was also used as a design reference [21]. The specification states the geometrical limits of the CubeSat in relation to the size of the s/c and max length of portions. In addition, NASA standards have been used as supplementary documentation. For creation of mathematical analytical models, the use of NASA standards proved to be more useful due to the stricter framework when compared to the ECSS standards.

5 Results

This section presents all relevant technical reports compiled during the master thesis time frame. The section provides an overview of the research conducted during the thesis period for the HYPSO project, in addition to providing information regarding the details of the reports. This section should be viewed as a complementary supplement to the information carried in the respective technical reports. Figure 11 displays the internal document relationship between the reports.
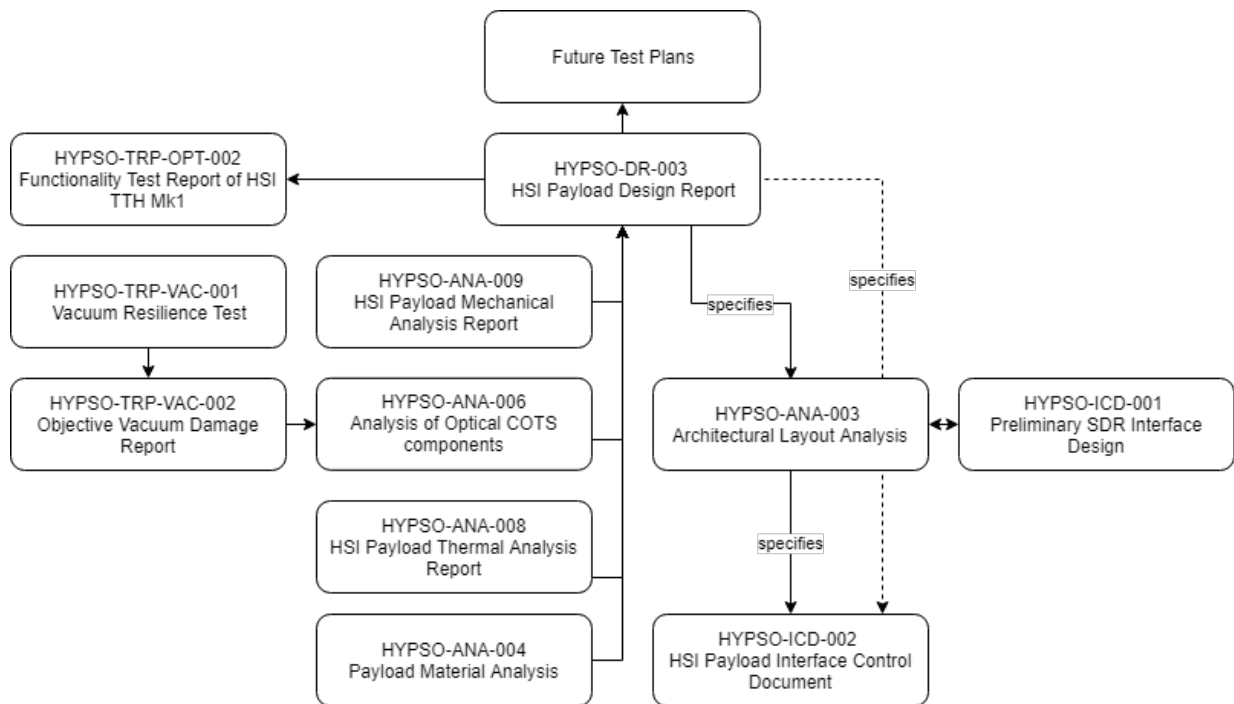
Figure 11: Report Relationship Chart

5.1 HYPSO-DR-003 HSI Payload Design Report

This report details the design process of the functional HSI prototype "TTH Mk1", providing information regarding justification of all identified design decisions, individual subsystems and components created, in addition to an analytical analysis of the design. Furthermore, the report highlights several design improvements in order to mitigate potential problems identified. The report acts as the centerpiece of this thesis, as seen in figure 11.

5.2 HYPSO-ANA-006 Analysis of Optical Components

This report outlines the analysis of the optical COTS components with respect to potential CubeSat integration. The report acts as a cover for optical component disassembly inspections and assessment reports, in addition to the venerability mitigation reports. The report outlines all potential volatile materials that can cause mission critical damage to the optical train, and possible steps needed to achieve an acceptable solution. Based on the recommendations provided in this report, the optical components and mitigation method were selected by the HYPSO management. The disassembly tests are compiled in a single document and can be found after the main report in *Appendix C*.

5.3 HYPSO-ANA-004 Payload Material Analysis

As outlined in section 5.2, several possibly volatile materials were found in the COTS components. This report details all materials present in the HYPSO payloads and provides a material analysis of the production material of the HSI payload platform. Furthermore, the report gives an insight into the outgassing phenomena that is a risk factor for all CubeSats carrying highly sensitive, optical equipment. All material inside the COTS components were analyzed and their respective outgassing characteristic identified and tabulated. The identification techniques used in order to identify the COTS materials are identified and discussed.

5.4 HYPSO-ANA-003 Architectural Layout Analysis

The CubeSat M6P delivered by NanoAvionics puts limitations on the available payload volume. As a result, an architectural layout analysis was conducted in order to place all necessary components within the given volume. Two different architectural layouts were considered, due to the large amount of systems outside the allocated payload envelope that could not be moved without instilling delays to the launch.

5.5 HYPSO-ICD-001 Preliminary SDR Interface Design

As a result of the architectural layout analysis described in section 5.4, the SDR was moved to the -Z side of the CubeSat in order to optimize the available space. The movement meant that the SDR could not be mounted using a standard stacking ring. This report outlines the design of the new mounting, in addition to a modal analysis of the SDR mounted.

5.6 HYPSO-ICD-002 Interface Control Document

The Interface Control Document provides information regarding mechanical payload interfacing, including electrical connectors.

5.7   HYPSO-TRP-OPT-002 Functionality Test Report of HSI TTH Mk1

This report outlines a functionality test designed to discover and evaluate potential flaws of the developed HSI prototype, described in section 5.1. The test indicated that the HSI payload could operate at a desired level at an atmospheric environment. Furthermore, the results indicated that the tolerances of the HSI were more forgivable than estimated in the *HYPSO-DR-003 HSI Payload Design Report.*

5.8   HYPSO-TRP-VAC-001 Vacuum Resilience Test Report

This report outlines a simple vacuum test performed on the lens objective and detector. The vacuum used was relatively low compared to the vacuum experienced in LEO, 10^{-1}Pa and 10^{-8}Pa, respectively. However, visible damage was still discovered on the objective in the form of faint scratch mark looking pattern on the front lens. It was postulated that the damage could be from outgassing or coating cracking. This led to a larger examination of the COTS components as outlined in section 5.2.

5.9   HYPSO-TRP-VAC-002 Objective Vacuum Damage Report

The damage on the vacuum tested objective described in section 5.8, was further investigated. The report outlines the examination method used in order to determine the cause of damage. The results indicated that the large amount of grease present within the objective caused the damage, however the exact dispersion method could not be identified. Possibilities includes outgassing or dispersion due to the rapid repressurization. The identification of the volatile material damage lead to the mitigation strategies discussed in the *HYPSO-ANA-006 Analysis of Optical Components* report.

5.10   HYPSO-ANA-009 HSI Payload Mechanical Analysis Report

A mechanical analysis was conducted to simulate the modal eigenfrequencies of the HSI payload, in addition to exposing the payload to expected launch loads. The eigenfrequencies of the payload were identified and checked against regulations instilled by NanoAvionics based on the launch provider, Polar Satellite Launch Vehicle (PLSV). The first recorded eigenfrequency was measured to be 695.37Hz or 1054.53Hz when using the IMU for added stiffness. This was well above the required stiffness defined at 135Hz, and suggested that the current platform was overdimensioned. Mass participation was not calculated due to time constraints.

5.11   HYPSO-ANA-008 HSI Payload Platform Thermal Analysis Report

A thermal analysis was conducted to simulate the temperature environment during operation in orbit. Two extreme cases were simulated, a hot case where all parameters yielded the largest heat, and a cold case where all parameters yielded as little heat as allowed. The results from the simulations show that the temperature range is within -39 to +50 degrees Celcius, due to the extreme cases simulated. This would lead to potentially significant future updates to the HSI payload design. However, passive thermal control techniques such as multi-layered insulation (MLI), mounting a wall at the +Z side of the CubeSat or using thermal straps to stabilize the temperature can be adapted to the current design.

5.12   Test Plans

As detailed in section 4.4.1, a test plan was created before any tests were conducted. The test plan detail general information regarding the test type, validation methods and test facilities. Furthermore, the test plans details the test purpose and expected results, as well as a detailed description of the tested item, needed equipment and test setup. A risk assessment regarding damage to the test items and general health hazards was noted. The test plans provided the HYPSO management with information regarding the planned tests, based upon this information the test was deemed go or no-go. Test plans describing tests not conducted due to the tight time frame were created, these plans will lay the foundation for future tests.

6 Discussion

This section provides a discussion on the conducted integration- and design analysis.

6.1 Mechanical Payload Design

The mechanical design of the HSI payload has gone through significant changes during the project time frame. The evolution process was based on the iterative development plan described in section 4.1. The first iteration of the design, based on the v6 prototype developed during the specialization project, was phased out in favour of a less complex design. The new design was engineered to increase the optical accuracy of the HSI camera. This was done through the use of *leading surfaces*, meaning that position of the optical components were controlled without stacking multiple tolerances.

The HSI payload was designed to provide full optical functionality, however the design was purposefully overdimensioned to provide increased support during the launch. Optimizing the payload by reducing the platforms wall dimensions and mass should be done by HYPSO in the future. The functionality of the HSI payload was tested during the project time frame, the results are provided in *Appendix H*. The results show that the produced prototype could operate on earth. The HSI produced distinct spectral lines that shifted in a predicted manner when imaging different targets. In addition, the results show the importance of the slit placement in the front optical assembly. The slit must be placed at the exact flange focal length of the front and collimating objectives. A slight deviation, less than 2mm, resulted in a defocusing effect, as shown in figure 12. In this diagram *EFL* is the focal length, $+\Delta Z$ is the displacement and *B* is the width of refracted light hitting the slit [22].
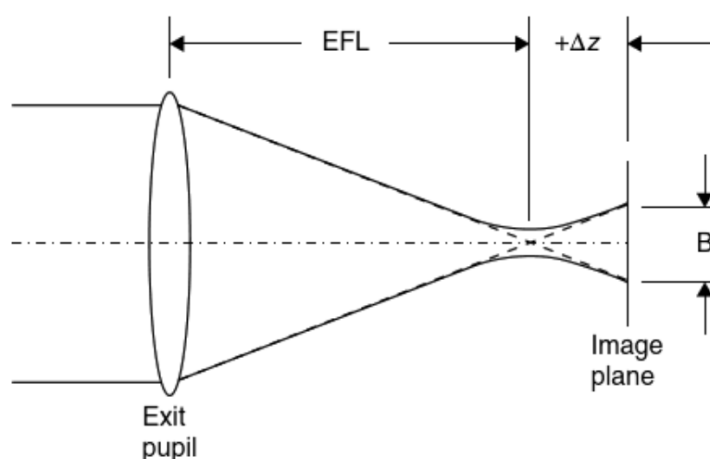

Figure 12: Diagram of Optical misalignment

The findings reinforce the importance of a design that can efficiently protect the optics during launch. A poor design is one of the many risks leading to optical misalignment due to the launch environment. Modal simulations showed that the payload had a relatively high eigenfrequency, lessening the risk of damage, as displacement is inversely proportional to the square of the frequency [23]. Additional testing must be done to conclude if the payload offers sufficient protection against expected shock and vibration loads.

6.1.1 Material Selection

Aluminium 6082-T6 was chosen as the production material for the HSI payload, as elaborated on in *HYPSO-ANA-004 Payload Material Analysis*, *Appendix D*. Aluminium is not the optimal material to encase optics operating in a thermally dynamic environment due to the relatively high *coefficient of thermal expansion* (CTE). However, 6082-T6 has a similar CTE compared to the COTS objective housing comprised of aluminium 6061-T6. This is important as materials with large CTE differences could lead to stresses between the platform and optics when exposed to large temperature variations during operation. Induced stress could lead to local yielding and optical misalignment due to the threaded connection between the optical parts allowing for no sliding when the material expands or contracts.

Exotic materials such as kovar or invar were not evaluated due the relative poor machinability, and greater cost [24]. The selected 6082-T6 material may facilitate thermal control, such as thermal straps or anodization, systems in order for the HSI payload to properly function in orbit.

6.1.2 Damping Solution

One of the largest unknowns in regards to the HSI payload design was the damping solution. The time frame did not allow for a proper investigation into the dampeners. However, a preliminary solution was proposed in collaboration with SMAC space. It is recommended that the layout and dampener stiffness should be further investigated, based upon the proposed solution.

6.1.3 Architecture

The architectural layout analysis was a challenge to resolve due to the limited space available inside the CubeSat and the often changing requirements and components being added at a late point in the development. Changes during development are normal, and proves the importance of architectural planning and developer adaptability.

6.1.4 Design Lessons Learned

Working on advanced payloads lead to several realizations amongst the mechanics team in regards to the payload design. It became apparent that the initial payload designs were not at a technical level the team felt comfortable with. The initial HSI design was too complex, assembled with a lot of individual pieces. A simplified design should almost always be preferred and pursued during development, to limit cost and assembly time, and reduce vulnerability to failure. This realization led to a change in concept and a sturdier HSI design, better adapted to the required optical accuracy and the volatile launch conditions.

The most difficult part of the design process was the creation of the technical drawings necessary to machine a functional HSI prototype and deciding the dimensional tolerances. Technical drawings had to be created for every part, inspected and approved. This was a time intensive process, as one mistake would lead to a disfunctional assembly. Involving a third person to scrutinize the technical drawings was important, as well as continued communication with the machining work shop to discuss details that were unclear in the provided drawings. To decrease the complexity, larger components were split into several sheets as recommended by the work shop. The tolerances were difficult to pin down, since no requirements with exact variable values for the spacing of the different optical equipment were established. It was decided that the prototype should be produced with a small tolerance grade. Based on results from functional testing under a controlled environment, better requirements could be established.

6.2 Commercial Off-The-Shelf Components for CubeSat Missions

6.2.1 Trade-offs associated with Commercial Off-The-Shelf Components

The use of COTS components in space is on the rise due to the low investment cost associated with CubeSat development [8]. Acquiring equivalent space graded components could cost ten to one hundred times more, depending on the specific component. As a result, the HYPSO CubeSat, was developed using primarily COTS components. The added cost of the space graded components can be explained due to extensive testing and documentation by the component provider. By developing with COTS components, the CubeSat developers become responsible for testing and documenting the components, requiring additional time and resources in a limited time frame. This in turn, introduces risk of component malfunction or reduced functionality during operation. Generally, the risk associated with COTS are tolerated, as the low development cost facilitates a higher risk tolerance [8]. The CubeSat developers must evaluate the risk associated with COTS components carefully, as complications can be revealed further down the development cycle and might not be apparent from the beginning as the investigations presented in this thesis show.

6.2.2 Optical Commercial Off-The-Shelf Components on HYPSO

One of the main goals of the HYPSO mission is to get a high degree of *return on requirements* by using optical COTS components to reduce the overall cost of the optical train. The integration analysis conducted showed that the largest problem area with the COTS components was related to particle outgassing potentially condensing on the lenses. The technical report provided in *Appendix C* elaborates further on this issue. The 50mm objectives and all considered detectors exhibited volatile materials when inspected. The objectives were assembled with a large amount of grease inside, while the detectors featured several non-removable silicone thermal pads, in addition to other problematic materials. Due to the time frame associated with the research, it was not feasible to conduct any dedicated outgassing tests of the potentially mission critical materials discovered. This lead to the mechanics team adapting the position that all potentially volatile materials should be removed or replaced in order to mitigate the risk of outgassing. The position was echoed by the HYPSO management.

HYPSO-ANA-006 Analysis of Optical COTS Components, found in *Appendix C*, presents a larger study of the possible mitigation strategies that can be instated to reduce the risk of outgassing. Due to the potentially volatile materials found within the closed detectors, it was decided that the use of a housing-less model should be pursued, circumventing the problem caused by the internal thermal pads. No problems would be introduced relating to the flange focal length of the objective, as the housing-less variant still features a threaded connection to the objective, maintaining the same distance. However, this requires the development of a new housing solution to provide radiation shielding for the components. While it is possible to remove the grease found within the 50mm objectives without causing damage, the disassembly, cleaning and subsequent reassembly introduces new risks. However, this option was deemed the most efficient solution compared to developing a new optical design. The washing procedure will be developed by the mechanics team, following the completion of the thesis. It is worth noting that the retailer of the 50mm objectives, Edmund Optics, could not provide a custom, grease free objective. It should be noted that in an ideal scenario, the people responsible for the integration of the payloads would be able to give input at an earlier stage in the development. Thus, the optical designer could be given recommendations for specific COTS components that would be easy to modify for use in space.

The findings presented in the technical reports elaborated in this section were delivered by professor Fred Sigernes to Uno Renner, Professor Emeritus, and Consultant for Space Technology at the *Technical University of Berlin* (TU Berlin). Professor Udo expressed that some satellites developed and deployed by TU Berlin carrying optical payloads exhibited unknown focus problems.

Based on the techincal reports provided, it was considered a high probability that the defocusing and blurriness were caused by contamination from outgassing of oils and grease inside the satellite. Outgassing is considered as a critical risk and TU Berlin has now started cleaning their payload optics, according to professor Fred Sigernes.

6.3 Development Testing

Testing of components and systems are integral to an efficient CubeSat development cycle. However, it is important that the amount of testing does not exceed a level where the additional information does not contribute to the development. Not all components needs to be rigorously tested, *Space Mission Engineering: The New SMAD* states that the test focus should be on functionality tests at the system level. It is further stated that testing requiring expensive equipment and test facilities should be kept to a minimum, in order to keep costs down and streamline the development. While the mechanics team shares this sentiment, it should be noted that a large amount of development testing were done at a component level during the project time frame. This was done due to the fact that no information existed on the COTS components, nor could any usable information be retrieved from the providers. Engineering development tests should be done on such components to provide information necessary for the development. Should some unknown components be ignored, fatal problems might appear at a later time in development, or even worse, after deployment, as previously mentioned in section 6.2.1.

6.4 Test Planning

During the work on the HYPSO project, the importance of thorough test planing became apparent. The objective of a well designed test plan is to be able to obtain more relevant information in less time, thus saving resources [25], [26]. A written test plan that contained the basic test setup, equipment and test steps was invaluable during the testing and reporting stages. The test plan was also an important document to convey the purpose of the test to the HYPSO project team.

During the vacuum test, it became clear that the test plan writing skills must be continuously worked on, as several factors were overlooked during the initial stage. While it is possible to deviate from the plan, it is not recommended to conduct testing *ad hoc*. Later, more thorough test plans, like the test plan for the HSI functionality test, made it possible to generate reproducible test results. Several test plans for future tests were created. Additional test plans where made in collaboration with other personnel from the HYPSO team. This was done in order to gain experience and helped further the team's understanding of test documentation. As these tests were not performed by the mechanics team, it follows that the reports will not be provided in this thesis.

6.5 The CubeSat Platform

This section discusses the CubeSat development and elaborates on the strengths and weaknesses of the platform.

6.5.1 CubeSat Development

CubeSat development differs from traditional satellite development in several areas relating to cost, typical development time frame and scope. Furthermore, CubeSat payloads are integrated and built around a standarized CubeSat frame, while traditional satellites are often designed around the payload. This puts a limitation on the CubeSat payloads, while simultaneously allowing for development of a satellite at the fraction of the cost and time.

6.5.2 CubeSat Reliability

Although the idea of the CubeSat delivering a high return on the investment and allowing for more requirements to be fulfilled for its cost is enticing, the reality is that a large number of the recorded CubeSats never completely fulfil the mission statement set out by the developers. Data taken from the Saint Louis CubeSat database [6], figure 13a, shows that only about 20 percent of all CubeSats achieve a full mission success, fulfilling all stated requirements. Furthermore, about 25 percent suffer from launch failures or are dead on arrival in orbit. University missions are even less successful, where about 37 percent fail before entering orbit, and only 13 percent fulfil the mission requirements, as shown in figure 13b. The data clearly show that CubeSats struggle with the launch, more so than in the space environment, where only 10-14 percent suffer from early loss.
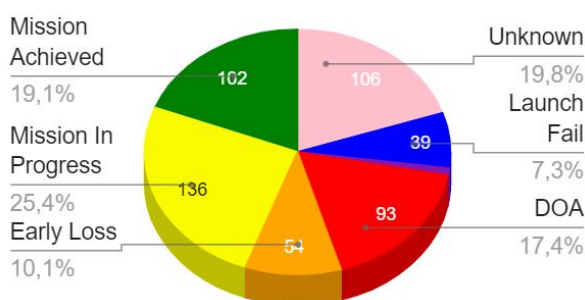
(a) All CubeSat Missions, 535 Satellites   *(b) University Missions (Hobbyists), 238 Satellites*
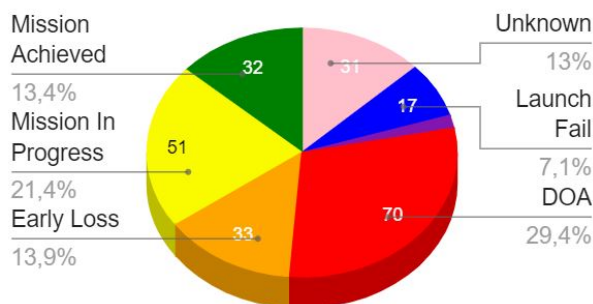
Figure 13: Mission status of all CubeSat missions, recorded from 2000- present (29.04.2019) from Saint Louis CubeSat database, (Note the amount of unknown CubeSats statuses in the data)

Figure 13b suggests that developing a successful CubeSat is a difficult task. As elaborated in section 2.3 and 6.2.1, while it is normal for CubeSat projects to accept larger risks due to the smaller scale of the project compared to traditional space design, developers are trying to fulfil the mission statement. This highlights the importance of extensive planing and testing during the development. Furthermore, as a large number of CubeSats are dead on arrival once in orbit, the data shows the importance of a solid mechanical design that can withstand the harsh launch conditions.

6.6 The HYPSO Project Environment

The team work environment within HYPSO was one of the defining aspects of the development. All dedicated project work was conducted in a designated common lab area, the NTNU Smallsat Lab, to facilitate communication and teamwork. The project also benefited from using parts of the agile development method scrum [27], having dedicated *stand up* meetings once a week. Interacting daily and working alongside colleagues with differing engineering backgrounds helped bring attention to challenges and solutions that otherwise could have gone unnoticed.

Being able work in a dedicated mechanics team, where everyone contributed toward a common goal, made the development of the payloads possible. The importance of well functioning teamwork on larger project, such as the HYPSO project, should not be overlooked.

7 Conclusion and Contributions

This thesis documents the integration analysis of commercial off-the-shelf optical components and design process of a hyperspectral imager payload into a 6U CubeSat, for the HYPSO project. During the mechanics teams one year work on the HYPSO project, the HSI payload reached a maturity level where a functional test could be conducted. The results show that the developed HSI payload could operate and produce seemingly correct spectrograms at normal atmospheric conditions. Furthermore, the results indicates that the dimensions of the produced prototype provide sufficient optical accuracy to the optical train developed by Professor Fred Sigernes.

The COTS components comprising the optical train of the HSI imager were inspected, tested and scrutenized in order to uncover volatile materials. Several potentially highly outgassing materials were uncovered, requiring adjustments to the components in order to be safely usable in space operations. It was concluded by the HYPSO management and the mechanics team that the resulting mitigation strategies should result in a successful adaptation of the current COTS components within the time frame until launch in Q4 2020.

The collaborative efforts of the Mechanics team yielded the following contributions to academia and the HYPSO project:

- Better understanding of the potential risks of using COTS optical components in space; shared with the academic community

- Initial concept for development of a housing-less HSI camera mounting for a 6U CubeSat

- Recommended layout design including preliminary damping solution and layout

- Simulation model for thermal environment and orbital parameters, and recommendation for thermal control solution

- Experiment design considerations for COTS CubeSat components

- Template for generating robust test plans for CubeSat space components

8 Further Work

This section details the high level further work needed in order to make the developed payloads ready for space operations onboard the HYPSO CubeSat.

Implement proposed design changes   The technical report provided in *Appendix B HYPSO-DR-003 HSI Payload Design Report* details design changes that would benefit the HSI payload.

Dampening solution integration   Stiffness and placement of the dampener solution must be evaluated further.

Conduct planned design tests   The planned development tests presented in table 2, section 4.1.1 must be conducted to uncover addition information regarding the mechanical integrity of the optical components and the payloads.

Improve the thermal and mechanical simulations   All simulations must be validated and compared with physical test results to increase accuracy.

Conduct Polar Satellite Launch Vehicle qualification and acceptance tests   The final payloads must undergo the appropriate tests in order to demonstrate that the delivered system can operate correctly. The qualification and acceptance parameters are provided by NanoAvionics, however, the documentation is protected under a non disclosure agreement.

9 References

[1] Hyper spectral imager for ocenaograpic applications. `https://www.ntnu.edu/ie/smallsat/mission-hyper-spectral-camera`, accessed May 2019.

[2] *CubeSat 101: Basic Concepts and Processes for First-Time CubeSat Developers.* NASA CubeSat Launch Initiative, 2017.

[3] Kevin Forsberg and H Harold Mooz. The relationship of system engineering to the project cycle. *INCOSE International Symposium*, 1:57–63, 10 1991.

[4] M. MacDonald and V. Badescu. *The International Handbook of Space Technology.* Springer, 2014.

[5] Abbas Abdollahi, Mohamad Dastranj, and Aminreza Riahi. Satellite attitude tracking for earth pushbroom imaginary with forward motion compensation. *International Journal of Control and Automation*, 7:437–446, 01 2014.

[6] Cubesat database. `https://sites.google.com/a/slu.edu/swartwout/home/cubesat-database`, accessed April 2019.

[7] TEB. Tailored ecss engineering standards for in-orbit demonstration cubesat projects, 2018. `https://www.copernicus-masters.com/wp-content/uploads/2017/03/IOD_CubeSat_ECSS_Eng_Tailoring_Iss1_Rev3.pdf`, accessed September 2018.

[8] 65 Authors from the Astronautics Community and James R. Wertz. *Space mission engineering: The new SMAD.* Microcosm Press, Hawthorne, Calif, 2011.

[9] Zhe Jiang, Zekuan yu, Yue Yu, Zhiyu Huang, Qiushi Ren, and Changhui li. Spatial resolution enhancement for pushbroom-based microscopic hyperspectral imaging. *Applied Optics*, 58:850, 02 2019.

[10] Fred Sigernes, Mariusz Eivind Grøtte, Julian Veisdal, Evelyn Honore-Livermore, Joao Fortuna, Elizabeth Frances Prentice, Mikko Syrjasuo, Kanna Rajan, and Tor Arne Johansen. *Pushbroom Hyper Spectral Imager version 6 (HSI v6) part list – Final prototype.* University Centre in Svalbard, NTNU, 2018.

[11] Nanosatellite payloads. `https://alen.space/nanosatellite-payloads/`, accessed May 2019.

[12] N Mehta, S Shaik, R Devireddy, and Mr Gartia. Single-cell analysis using hyperspectral imaging modalities. *Journal Of Biomechanical Engineering-Transactions Of The Asme*, 140(2), 2018.

[13] Francesco Dell'Endice. Improving radiometry of imaging spectrometers by using programmable spectral regions of interest. 2009. `https://www.sciencedirect.com/science/article/pii/S0924271609000677`, accessed June 2019.

[14] Photonetc. Our technology — hyperspectral imaging, 2019. `http://www.photonetc.com/hyperspectral-imaging`, accessed June 2019.

[15] Load Analyses of Spacecraft and Payloads. Standard NASA-STD-5002, National Aeronautics and Space Administration, June 1996.

[16] Peter Fortescue. *Spacecraft Systems Engineering*. Wiley, Chicester, 4th ed. edition, 2011.

[17] Nasa systems engineering handbook. `https://www.nasa.gov/sites/default/files/atoms/files/nasa_systems_engineering_handbook.pdf`, accessed May 2019.

[18] Eclipse. Providing with project and mission supports, 2019. `https://www.eclipsesuite.com/client/esa/`, accessed June 2019.

[19] G Härkegård. *Dimensjonering av maskindeler*. Tapir akademisk forl, Trondheim, 2004.

[20] T. Khalitov S. Denisikhin D. Sotnik P. Goncharov, I. Artamonov. *Engineering Analysis with NX Advanced Simulation*. Simens, 2014.

[21] Cal Poly SLO The CubeSat Program. 6u cubesat design specification rev. 1.0, 2018. `https://static1.squarespace.com/static/5418c831e4b0fa4ecac1bacd/t/5b75dfcd70a6adbee5908fd9/1534451664215/6U_CDS_2018-06-07_rev_1.0.pdf`, accessed September 2018.

[22] Keith Kasunic. *Optomechanical Systems Engineering*. Wiley, 2015.

[23] Delbert R. Wilson. *VIBRATION TESTING FOR SMALL SATELLITES*. Boeing Aerospace corporation.

[24] Scott Gibb. An introduction to invar. *College of Optical Sciences, University of Arizona, Tucson*, 2006.

[25] Systems engineering handbook: A guide for system life cycle processes and activities, 4th edition. *ProtoView*, 2(32), 2015.

[26] Charles R. Hicks. *Fundamental Concepts in the Design of Experiments*. Holt, Rinehart and Winston, 1964.

[27] H. Frank Cervone. Understanding agile project management methods using scrum. *OCLC Systems & Services: International digital library perspectives*, 27(1):18–22, 2011.

Appendices

Appendix A

Excerpt from the Specialization Report

Contents

List of Tables

List of Figures

Symbols

Property	Unit	Description
t	s	Time
m	kg	Mass
$\mathbf{M}$	-	Mass Matrix
ξ	-	Dampening Matrix
σ_y	MPa	Yield strength
σ_{UTS}	MPa	Ultimate tensile strength
E	GPa	Elastic modulus
ω	Hz	Radial Natural Eigenfrequency
f_n	Hz	Natural Eigenfrequency
k	N/m	Stiffness
$\mathbf{K}$	-	Stiffness Matrix
ρ	mg/cc	Density
F	N	Load
I_p	kgm^2	Moment of Inertia
C	J/kgK	Specific Heat
λ	W/mK	Thermal Conductivity
α	-	Absorptivity
ε	-	Emissivity
CTE	$\mu m/m$	Coefficient of Thermal Expansion
Q	Wm^2	Heat flux
s	mm	Displacement
B	-	Heat Capacity Matrix
$\dot{T}$	K/s	Temperature change with time vector
T	K	Temperature change with time vector
K_c	-	Heat Conduction Matrix
R	-	Radiation Exchange Matrix
P	-	Applied heat loads
$\mathbf{U}$	-	Grid point Temperature vector
$\mathbf{N}$	-	Non linear heat load
$\dot{H}$	J	Enthalpy

1 Background

The following section summarizes the most vital aspects of the specialization project.

1.1 Engineering Practise and Management

To be able to maintain a proper information flow within the HYPSO team, several communication methods and tools outlined in section 2.2.4 were used and the agile engineering practise scrum [1] was adapted to fit the workflow. A Systems Engineering approach to the missions requirement management was also retroactively added to filter out non mission critical, superfluous requirements. Simple Systems Engineering practise had to be learned and understood by the entire team. An intensive course held by Prof. Fernando Aguado-Agelet from the university of Vigo on the 4-7 September was attended by the mechanics team to better understand the Systems Engineering process.

1.1.1 Development Schedule

When designing and developing a CubeSat, a proper development baseline is required to be allowed to launch. The launching process is expensive, and the CubeSat must be tested and validated thoroughly to minimize the risk of failure. CubeSats are particularly susceptible to failures due to the often short and heavily pressured development schedule. It follows that proper structuring of the available time and resources is imperative. The standard CubeSat development schedule includes two large delivery milestones, the Preliminary Design Review (PDR), and the Critical Design Review (CDR). An initial Mission Design Review was done to achieve funding ahead of the outset of this project. The PDR process was a significant part of this project delivery.

1.1.2 Preliminary Design Review

Preliminary design review, PDR, is the first design review done in a development period. The PDR is an assessment of the proposed system to establish that the requirements will be met with acceptable risk [2].

The HYPSO PDR on the 30th of October 2018 was done in collaboration with Norsk Romsenter and several non affiliated Professors and phd students. Design documentation was delivered one week in advance, giving the reviewers time to add feedback and concerns to the PDR Review Item Discrepancy (RID). The RID was reviewed during the PDR process and appropriate actions were suggested. The following items and reports were delivered for the PDR by the mechanics team and are relevant for the specialization project:

- Overall payload and item placement in bus

- Preliminary design for HSI payload

- Preliminary design for HSI to bus interfacing

- Mechanical Analysis Report, ref HYPSO-ANA-001

- Thermal Analysis Report, ref HYPSO-ANA-002

- Mass budget

The PDR provided feedback on all delivered items via the RID. This feedback was used to further refine the design. As the scope of this project is focused on the pre PDR implementation phase, only a limited amount of design changes will be provided in this report.

1.2 The General Space Environment

Space is infamous for being a challenging environment to design for. There are several unique factors that must be taken into consideration when developing a design, both in regards to conditions during launch and the conditions that must be survived during the operational life. Figure 1 shows the HYPSO mission HSI Concept of Operation (CONOPS), which characterizes the systems capabilities, functions and life cycle in the operating environment [3]. Figure provided by Mariusz Grøtte. The following sections lists the most vital challenges relevant for the mechanics team during operation in the space environment.
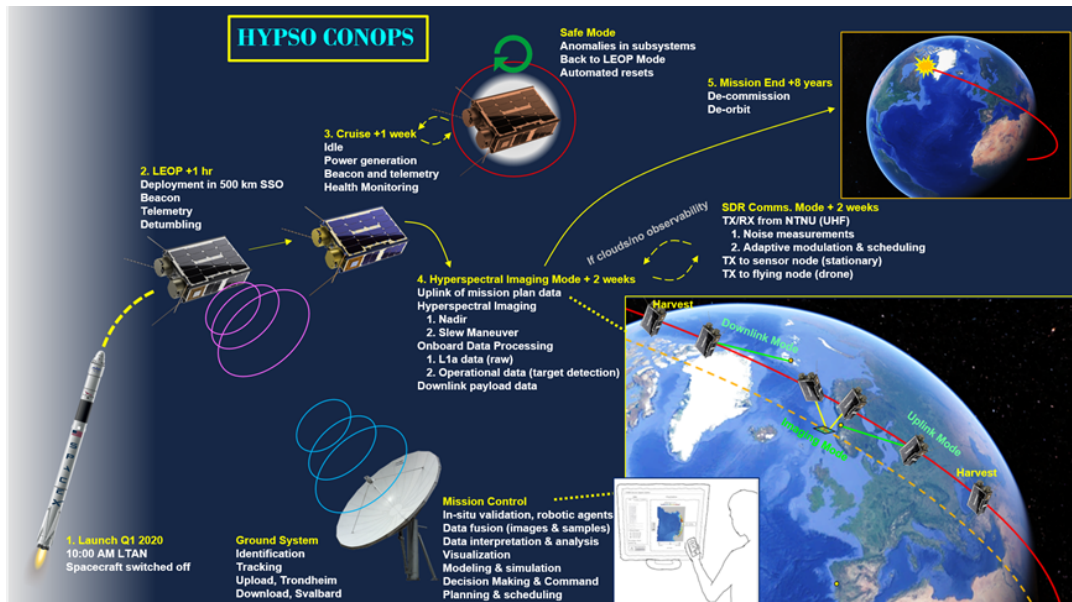

Figure 1: HYPSO Concept of Operations

1.2.1 Microvibrations

Microvibrations are vibrations induced from the mechanical parts of the s/c, such as fly wheels or reaction wheels [4]. The frequencies are relatively small compared to those present during launch, ranging from 50-200 Hz, depending on the satellite and reaction wheels. The microvibrations present during the slew maneuver, where the satellite takes pictures during its operation, are the most critical to the mission.

1.2.2 Outgassing

The lack of hydrostatic pressure in the space environment has an effect on all materials present on the s/c. Dissolved gas particles trapped in the macro structure of the material is precipitated out during space operation. The release of spurious particles is known as outgassing, and the effects are largely material specific. The particles can condensate and latch on to the s/c and surfaces such as lenses and solar cells. Since there is no effective way of cleaning the s/c, outgassing can ruin the operation. Maintaining a proper material selection is vital, as a maximum total mass loss (TML) of 1.0 percent and a maximum of 0.10 percent volatile condensable materials (CVCM) are required [5].

Outgassing limits the viable materials available, as some materials simply evaporate in the space environment [6]. Polymers are especially prone to outgassing. NASA's outgassing database [7], a suggested space material list from the CubeSat standard [5], as well as flight proven materials were used to determine potential construction materials and coating.

1.2.3 Cold Welding

In space, metal materials can fuse together from contact. This interface adhesion is caused by the lack off surface oxide layers on the materials. Oxide layers can be scraped of by impact or fretting, and the material will not be re-oxidized due to the lack of oxygen [8]. Cold welding is mostly a problem in interfaces requiring movable or deployable modules.

1.2.4 Thermal Challenges

In atmospheric conditions at sea-level heat is mainly transferred by a combination of thermal convection, conduction and radiation. For a satellite in LEO there is no air present to facilitate convection and consequently thermal management becomes significantly more complex, as radiation and conduction become the only source of heat dissipation and distribution. External sources of heat in LEO include the solar flux, infrared radiation from Earth and radiation from the earth albedo. The thermal input to the satellite from these sources will vary depending on the spacecraft orientation relative to the earth and sun.

COTS components often have a specified thermal interval that they are designed to operate within. Normally this interval is given by the ambient temperature that the part experiences. As it is not possible to control the ambient temperature in LEO vacuum, thermal gradients must be handled by other solutions than what normally would be applicable in an air environment.

Several of the components in the mission payloads produce heat:

- The HSI detector has been reported to produce a lot of heat during prototype testing. [9]

- The FPGA on the PicoZed is expected to need cooling as these types of chips are heat intensive.

- The SDR contains processing units comparable to that on the PicoZed and will most likely require cooling as well.

This report will discuss various solutions for mitigating the heat from these components. There exists both active and passive methods for dealing with heat concentrations of differing technology readiness levels, and these will be evaluated to find a suitable design.

1.2.5 Atomic Oxygen

The planned orbit for the satellite is a LEO approximately in the middle of the thermosphere. In this region of the atmosphere, there is a very low pressure nearing a hard vacuum, but some particles are still present. The most abundant matter in this region is atomic oxygen. The pressure here is too low for the oxygen to recombine in to Ozone, diatomic oxygen or other molecules. This form of oxygen is highly reactive and can cause erosion of LEO spacecrafts as they continuously collide with these particles [10].

This erosion can pose a problem for the HSI as the atomic oxygen can erode the lens surfaces and thus cause a degradation of the imaging quality. However, for the majority of the orbit (except during slew maneuvering) the front lens will have an orientation parallel to the direction of travel and therefore a minimized impact area for the atomic oxygen to affect.

1.2.6 Radiation

In space, earths atmosphere and magnetosphere are no longer there to provide protection from the present in space. For orbiting space missions, these effects can prove troublesome. There are two particularly dangerous zones known as the Van Allen Belts. Here, charged particles are concentrated in an inner and outer layer as result of solar radiation combined with the magnetic forces of the earth [6]. Because the HYPSO mission orbit is between

450 km and 550 km, it means that some parts of the orbit will be subjected to the inner radiation belt. The effect of radiation poses danger to different materials by changing or breaking them down. In mechanical structures, change in mechanical behaviour of a material can cause many unwanted problems. Materials and coatings therefore have to be chosen with these effects in mind.

Electrical components can also be greatly affected by this effect. Digitally stored information is prone to bit flips, which over time can lead to errors in the software. Effects such as these need to be accounted for by adding protective solutions around essential/prone components.

1.3 Payload Description

1.3.1 Main Payload - Hyper Spectral Imaging Camera

The main payload of the satellite will be a pushbroom HSI. This imager is designed to be made from COTS parts as to make construction simple, parts readily available and reduce costs. The final iteration of the prototype design is version number 6, shown in figure 2, and it was the template for the design that was carried over to the integration part of the process. The lens assembly features an angled center section with an integrated grating. This solution greatly reduces overall length compared to a straight version with comparable imaging quality. The prototype utilizes a cage system to ensure stiffness across the length of the lens assembly. (1) front lens, (2) CP12 gage plate, (3) collimator lens, (4) 3D printed grating holder, (5) camera lens, (6) CP03/M gage plate, (7) steel rods, (8) 3D printed camera mount insert and (9) iDS CMOS camera head. The specific part list received from Fred Sigernes given in table 1.
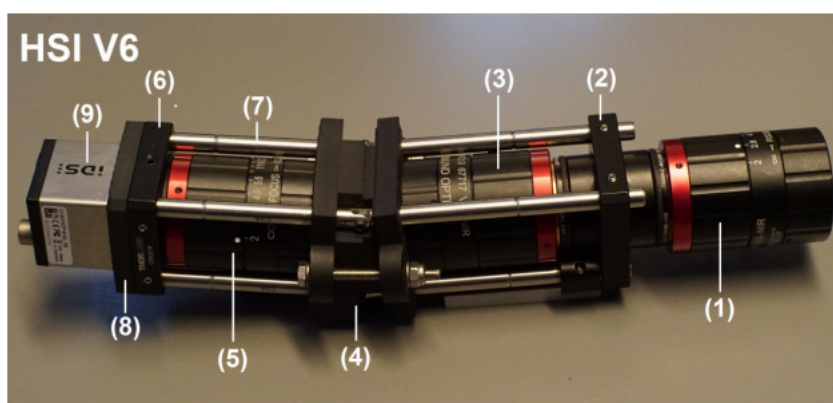

Figure 2: Assembled prototype using a standard USB 3.0 iDS camera head

5

Table 1: HSI part list from V6 document

Part/Links	Description	QTY
EO #67-717	50 mm VIS-NIR lens (Front, Collimator and Detector lenses)	3
EO #49-579	25mm Sq. 17.5deg. Blazed Trans. grating (300 lines/mm)	1
Thorlabs SM1A10	Adapter ring SM1 – C-mount internal	1
Thorlabs SM1M10	SM1 lens tube 1 inch long with internal threads.	1
Thorlabs CP12	30 mm Gage plate - SM1 tubes	1
Thorlabs S50RH	Fixed high precision mounted slit	1
Thorlabs CP13/M	C-mount 30 mm gage plate (NTNU sensor board)	1
Thorlabs CP03/M	30 mm Gage plate – 35 mm aperture (iDS-mount)	1
Thorlabs ER1.5-P4	4 x Steel rods 1.5 inch long	1
Thorlabs ER1 –P4	4 x Steel rods 1.0 inch long	1
Thorlabs C3A	4 x Rod End Swivels	1
Detector	iDS IMX174 camera head	1

1.3.2 Onboard Processing Unit

Payload control and data processing is managed by a PicoZed mounted on a custom carrier board. In-house development of software for the PicoZed is a central part of the HYPSO-groups work.

1.3.3 Secondary Payload - Software Defined Radio

When the project started, the SDR had not yet been confirmed as a secondary payload. This was mainly due to the fact that it was not expected to be ready for launch.
From the **HYPSO-DR-001-A System Design Report**

"A Software Defined Radio (SDR) is a flexible technology which enables the design of an adaptive communications system. This means that a generic hardware design can be used to address different communication needs, with varying frequencies, modulation schemes and data rates. Applying this concept to smallsats can increase data throughput, add the possibility to perform software updates over-the-air and make it possible to reuse the hardware platform for multiple missions with different requirements. Therefore, development time for future small satellite communication systems can be reduced, even though the development time of the first implementation might be longer than for a traditional radio system.

The goal of the SDR system is to enable channel characterisation in Ultra High Frequency (UHF) in the Arctic area in order to design an Arctic communication system. The main constraints for the design of the payload are cost and development time. The design proposal has to be ready for CDR in Q1 2019 and should be integrated and tested by Q3. Schedule constraints are very important in the trade-offs. The SDR will use a separate UHF monopole antenna to not influence the main communication or data link of the spacecraft."

1.3.4   Tertiary Payload - RGB Camera

The third payload in the satellite is planned to be a RGB camera. The main purposes of this is to provide color photography of the earth as well as georeferencing for the HSI. At the time of this report, the exact camera model and lens is still to be decided. The USB 2 uEye LE industrial camera with a Kowa, LM6JC, 6 mm, 2/3 lens was presented as an option at the PDR, but feedback from the review team proved that more work will have to be done on this before a decision can be made. This also means that design of a mounting solution will have to be postponed until further progress has been made.

1.3.5   Star Tracker

A star tracker is an instrument that tracks the stars in the sky to provide positional and orientational data for the satellite. The star tracker itself is not a separate payload, but a part of the bus. However, it will need to be rigidly coupled to the HSI to ensure compliance with the directional pointing of the main payload. This means that a custom mounting solution will have to be developed for this as well and it is therefore an essential consideration and part of the design process. At the time of the PDR there was still uncertainty about the exact orientation of the tracker, and consequently no design work had been done.

1.4   Architectural Design

The architectural design concerns the placement of payloads and their subsidiaries as well as the various interfaces present in the satellite. Design of these interfaces overlap greatly with the mechanical design. The various considerations and challenges for the architecture and interfacing are outlined below:

1.4.1   Center of Gravity

The CubeSat standard [5] defines a region that the center of gravity must lie within compared to an origin located in the CubeSat geometrical centre, as shown in figure 3 from the 6UCubeSat standard:

3.2.10 The CubeSat Center of Gravity (CoG) shall be located within 4.5 cm from its geometric center in the X direction, within 2 cm from its geometric center in the Y direction, and within 7 cm from its geometric center in the Z direction
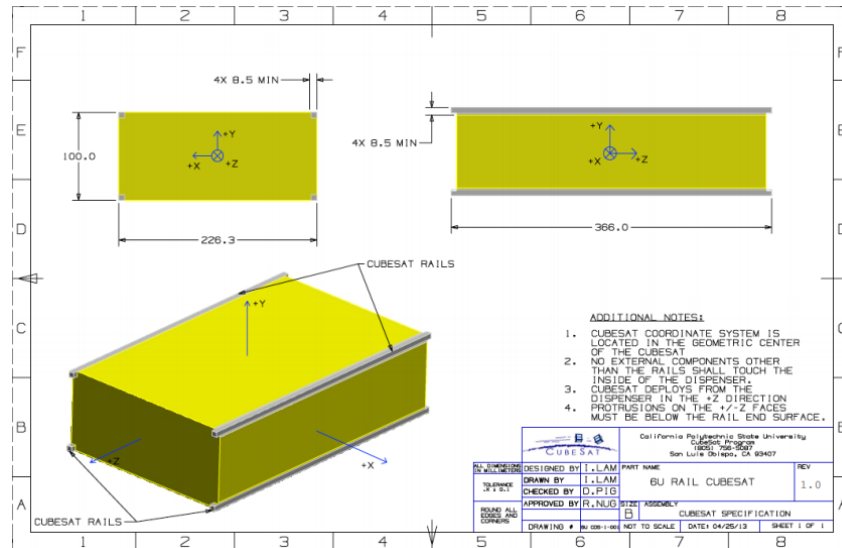

Figure 3: Definition of the geometrical center from the 6U CubeSat Design Specification

This requirement specifies the allowed displacement of the CoG compared to the geometrical center. After dialog over email with Calpoly it was discovered that this requirement can be superseded by the launch providers requirements when the satellite is manifested. However, this is an unlikely scenario and in most cases the CubeSat standard is the standard that is followed. Selection of payload placement is the main tool for moving the center of gravity. It is therefore vital that the architecture is laid out in a way that puts the CoG within the requirement. It is required by the ECSS standards that the CoG and Moment of Inertia shall be calculated using CAD tools. [11]

1.4.2 Moment of Inertia

The moment of inertia of a rigid body refers to the amount of torque needed for a specified angular acceleration about a rotational axis. This is an essential property in relation to orientation of the satellite facilitated by the reaction wheels in the bus. Similar to the CoG, the MoI is dependant on the mass distribution and therefore an important consideration for the layout. The precise placement and number of reaction wheels were not determined at the time of this report, and the MoI might need to be altered at a later stage in the design process.

1.4.3 Orientation

To ease the task of pointing the HSI in the correct direction, a centered orientation with the lenses aligned to the Z+ axis was deemed ideal. This meant that the center of the cross section of the forward pointing lenses would should have no displacement along the X- and Y axis as well as having the image-capturing end at the +Z face, as shown in figure 4.

In addition to this, the star tracker had to point at a minimum of $90°$ compared to the angle of the HSI. This meant that an orientation parallel to the X-axis or preferably further rotated towards the -Z axis was ideal.
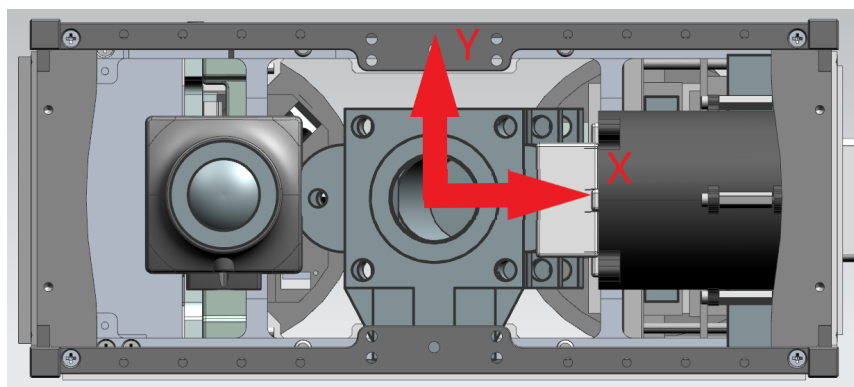
Figure 4: View of the Z face along the Z-axis

1.4.4 Fastening of Payloads

The central theme of interfacing is the fastening of the payloads. A connection needs to be created between bus and payload. This connection has two main interfaces: it needs to securely attach to the payload as well as being properly mounted onto the satellite frame. The bus comes with predrilled countersunk holes and some threaded ones as well. This is where architectural and mechanical design overlap as a mechanical solution needs to bridge the gap between the aforementioned holes and the HSI.

1.4.5 Thermal and Vibrational Decoupling

NanoAvionics gave a strong recommendation to vibrationally decouple the HSI from the bus. This would be to prevent damaging the delicate lens assembly during the violent vibrations at launch. Such a decoupling would have to be taken care of in one of the interfaces between HSI and bus. In addition to this, a thermal decoupling between the frame and HSI could also bring advantages as the frame of a spacecraft experiences a wide range of temperatures. If these gradients could be prevented from translating to the HSI this could offset potential problems with focus and mechanical distortion.

1.5   Mechanical Design

The mechanical design concerns the structural integrity of the payload and interface design, as well as several mechanical and material issues caused by the space environment discussed in section 1.2. While ensuring the structural integrity is important, considerations to the resulting mass is also of significance. Adding structural integrity will increase the mass, this again affect the costs, which is not an unlimited resource for the project. The two therefore need to be balanced according to the requirements all while keeping complexity down. The mechanical design is heavily interdependent on the interface design. Various design considerations are outlined in the following sections.

1.5.1   Deformations

To ensure that the HSI camera can operate as outlined, it is critical to the mission that the payload structure does not experience yielding or buckling in any way during launch. The chosen materials must therefore be of sufficient strength as to not experience elastic deformation nor permanent plastic deformation. This is most critical when the system experiences heavy shock loads. Any large deformation in the lens assembly can cause misalignment and impair the ability to gather image data which could prove fatal to mission success.

1.5.2   Vibrations and Shock

The launch of a rocket is a violent process. Rocket engines produce a tremendous amount of vibrations that will transfer to the satellite via the rocket fuselage. At the present day all operational orbital rockets are also staged. The separation of stages during the ascent phase are either done by pyrotechnical charges or pneumatic actuators. The shock of this separation needs to be taken into account as this would be the peak load that the satellite and its various interface solutions undergo.

1.5.3   Resonance and Eigenfrequencies

While the shock can induce a quasi static load acting on the satellite that can lead to deformations, vibrations pose another threat. The large variety of vibrations during launch can excite the entire s/c system or the individual payloads, causing them to resonate at the induced frequencies. This can happen if the system's eigenfrequencies match or are close to the induced vibrational frequencies. A system's eigenfrequency or fundamental frequency describes the frequencies where the system has a tendency to resonate violently when exposed. Normally, only frequencies exciting significant mass (large mass participation factor) in a direction are taken into consideration when designing. The eigenfrequency is entirely dependent on the system's design, stiffness and mass. Higher stiffness leads to

larger frequencies, while higher mass lowers the frequencies. The band of frequencies occurring during launch is abnormally large, from 5 to over 2000 Hz and poses a major design challenge. It is impossible to avoid any eigenfrequencies occurring in this belt. Damping solutions must therefore be explored.

Microvibrations occurring during operations must also be taken into consideration when designing the solution. The microvibrations are induced in the structure by the operation and other systems like the reaction wheels. The microvibrations do not pose any structural risk, however they can cause some shaking, disturbing the sophisticated optical equipment during the slew maneuver, blurring out the pictures taken [4].

1.5.4 Materials

Consideration of base materials and material interaction is essential when designing. The material properties like stiffness, density, yield strength, specific strength and thermal expansion are important to take into account. However the interfacing between different materials are equally important. Materials can experience corrosion induced by electrolytes in batteries or cooling systems can cause galvanic corrosion, general corrosion and stress corrosion, equivalent to on ground behaviour. Atomic oxygen can also cause corrosion due to the low orbit. The interfacing between different materials are therefore important in space. Effects such as creep and relaxations are also important to the mechanical design. When considering the case of the dampers, the material used is a polymer that tends to deform and structurally weaken with time. For sensitive equipment such as the HSI-camera, examination of these behaviours and how they occur is therefore crucial. When it comes to different materials, their susceptibility to manufacturing may also vary heavily. Some materials are difficult to machine, and can require additional annealing processes. CubeSat missions are limited in the way that they need to adhere to different environmental standards. Because of their low orbit, and short lifetime, their death need to be controlled to a sufficient degree. As a result, components using materials with high melting temperatures need to keep their mass limited.

1.6 Thermal Design

The thermal design concerns the thermal control of the satellite system. Mechanical and electronic systems each have their own thermal tolerances that need to be considered. Thermal problems often kill CubeSats and are many times underestimated or outright ignored. To ensure their survivability in space, different precautions can be made in the form of passive or active control. When considering thermal control systems, it is important to recognize the importance of their different technology readiness levels. Furthermore, because the project revolves around a CubeSat, not all control methods are equally relevant based on their TRL as cost and complexity become larger limitations.

1.6.1 Passive Control

Passive control methods involves the use of the different thermal or optical properties of materials to impose a desired thermal behaviour. Because passive control require no sophisticated systems nor control software, it is often cheaper and easier to integrate than an active control solution. For CubeSat missions, their simplicity and often low weight usually provide sufficient thermal control.

1.6.2 Active Control

Active control methods are more difficult to integrate than the passive systems. These solutions require often larger systems controlled with software, varying in complexity. With the increased complexity, additional risks are introduced to the mission. Systems such as these also require their own power, which further complicate the power budget and limits the overall mission scope.

1.6.3 Integration of Thermal Systems

The integration of the thermal control systems is dependant on several factors ranging from the observed problematic components and areas to the mechanical and interface design. The thermal solutions are a part of the mechanical and interface solutions and are therefore highly interdependent on each other. The materials chosen plays a large role in the thermal behaviour of the payload. To properly evaluate the thermal conditions in the s/c, it is important to asses and predict the effect of the operating environment and the effect of the internal s/c systems. Such predictions are heavily influenced by a multitude of factors that come with uncertainties. Because of this, it is normal to attribute a generous safety factor. For CubeSats, a commonly used number is an additional upper and lower limit of $\pm 10^{\circ}C$.

2 Method and Tools

2.1 Development

This section describes the development of the payload integration and the most important steps in this process. From the inception of the mechanics team there was a shared sentiment about the preferred design methodology. The approach started with a mapping of the various requirements and constraints. One or more brainstorming sessions were held before preliminary concepts were chosen for further development and selection. Analysis and simulation were used to explore the strengths and weaknesses of the concepts, based on the results, the design could be improved. When the design has matured sufficiently, testing of prototypes will be incorporated in the development. The planned development baseline shown in figure 5 is a customization and expansion of Figure 1 found in NASA-STD-5002.
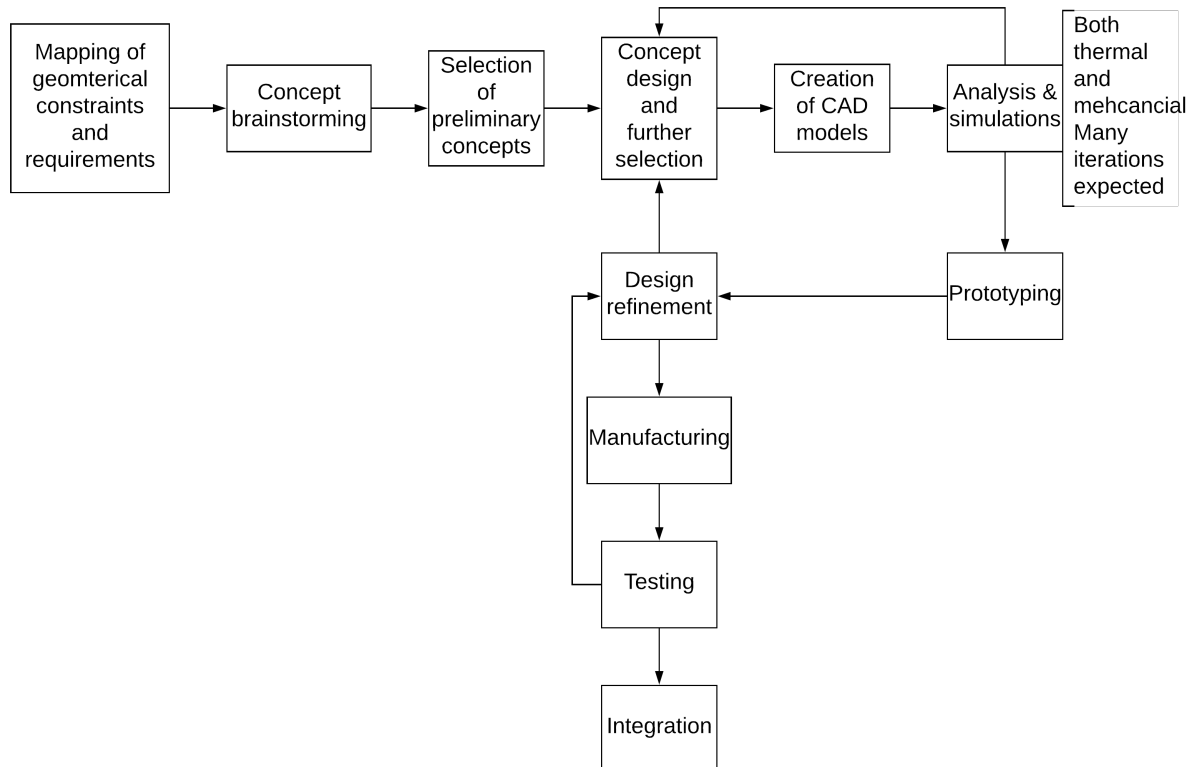
Figure 5: Development plan for HSI payload integration

The design itself was done with NanoAvionics (NA) and SMAC-SPACE as important advisors for the integration and damping respectively. It is also worth noting that this methodology will be used for the development of star tracker interfacing and thermal management solutions as well.

13

2.1.1 Requirements

Prior to concept creation, it was important to understand the framework and requirements of the part or component in question. Thus, not spend time thinking or pursuing ideas that do not actually fit the actually desired functionality. Equally, the constraints and requirement serve as a fundamental framework that concepts can be based on. The requirements are also vital to the verification and validation process of the system.

Most of the requirements were mapped out using ECSS standards, which is further elaborated in section 2.3.2. Other requirements were mapped from datasheets, industrial reports and the NASA standards. Many of the requirements for the HSI camera were defined as a result from consultation with the developer, Fred Sigernes, NA, and SMAC-SPACE. Other general requirements were defined by the team as a result of the occurring constraints and basic functionality. Note that requirements provided from the eventual launch provider will overrule requirements given by the standards.

2.1.2 Concept Design

The development of the concepts themselves started with a brainstorming session. The location chosen for productive brainstorming was en empty room with a black- or whiteboard. The most important requirements and constraints were written clearly on the board such that they could easily be pointed out and discussed. The members of the mechanics team then proceeded to present various ideas and express their opinions about the concepts that were being drawn. The usage of big drawings on a board allowed for rapid adjustments of ideas as the discussion ran. At this stage the dialogue proved essential, and the exchange of point of views and concerns evolved the original ideas. When all members were satisfied with the representation of the drawn idea it was labeled and photographed. Figure 6 shows examples of early brainstormed concept drawings.

After the brainstorming was completed the concepts were assembled in a document and then further discussion commenced. A simple selecting procedure was used to determine three concepts that would be developed further. The selection was made purely on the teams subjective beliefs, gut feeling and general concept feasibility. While it was realised that this selection type had severe limits, non scientific, and might exclude some usable concepts, it could be considered the best choice from an engineering standpoint, considering the limited time frame. The ideas that survived this process could then be moved into the next stage of the design baseline.

A simple Pugh matrix was then used as the final selection method, with adequate criteria and weighting [12]. The weighting was chosen based on individual subjective ratings, then a team discussion, to make the weights less subjective. The winning concept was then further adapted to fit the overall system design. This selection was used to narrow down the interfacing/ overall HSI payload design. This method will also be used to determine thermal solutions for the HSI, the HSI bracket design, startracker to HSI mechanical interfacing solution and the HSI grating holder solution.
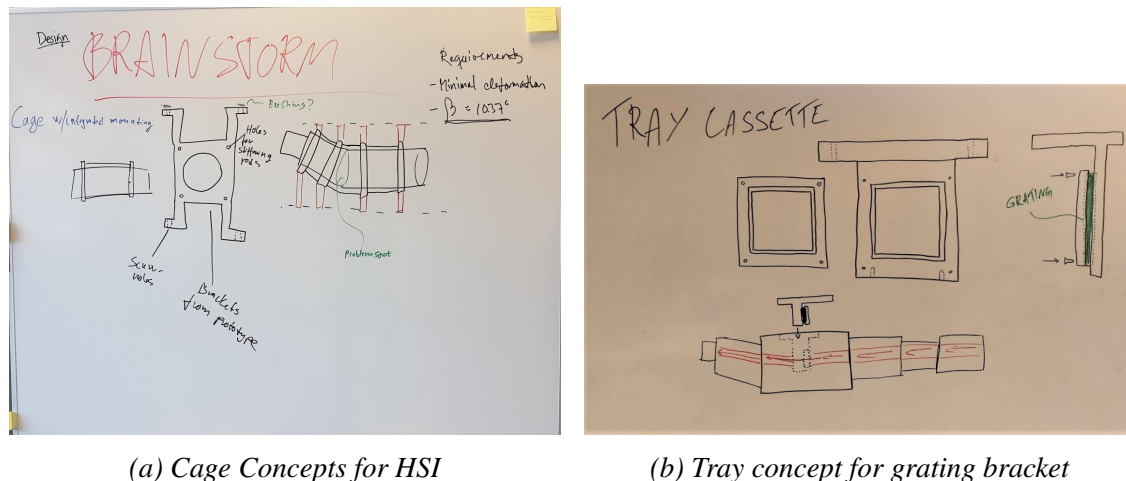
(a) Cage Concepts for HSI   *(b) Tray concept for grating bracket*

Figure 6: Examples from the concept development

2.1.3   CAD Models

The selected concepts were then moved into the next step in the baseline; modeling. The CAD models were used for the analyses and also for visual aid to further advance the understanding of the geometrical constraints and available room in the bus. One of the most important factors in this step is to draw the models in such a way that they can easily be adjusted or changed when the design matures from the analyses.

2.1.4   Analysis and Simulations

The finished 3D models were then simplified and recreated as finite element models that could be simulated using NX outlined in section 2.2.1. The complex components, mainly the COTS lenses and provided 3D bus models acquired from NA needed to be idealized and simplified. The idealization process removes unnecessary patterns and geometry that will complicate the underlying mathematical procedure used in the simulation. An idealized model should be accurate within acceptable uncertainty. An idealized body can save significant solving time due to the fact that the average mesh size can be coarser.

The idealized models were then meshed and simulation objects like loads, constrains, gluing, contact and radiation were added, depending on the active simulation solver and solution. Some simplification of the simulation objects were implemented in the simulation, this is a potential source of error. Both structural mechanical and thermal simulations were done.

Throughout the specialization project span, consultation with NTNU professor Terje Rølvåg, MSc. and a Ph.D. within finite element dynamics of elastic mechanisms, has been a vital aspect in regards to feedback for the mechanical simulations. The feedback and course curriculum provided by professor Terje Rølvåg allowed the simulations to move on with good conscious, knowing that the parameters and assumptions were correct.

The simulation was then refined several times, to achieve more realistic results. Masses were checked and changed, simulation objects adjusted and the mesh refined. However, it must be noted that the simulations must be further refined and evolved in conjunction with physical testing of the simulated subsystems to be able to provide accurate and reliable results. This will be explored further down the project baseline. The exact simulation methods are provided in the PDR analysis reports HYPSO-ANA-001 Mechanical Analysis Report sections 3.4, 3.6, 3.7 and HYPSO-ANA-002 Thermal Analysis Report sections 2.3, 2.5.

2.1.5 Prototyping

Prototyping is an important tool for understanding the behaviour of a design. At the time of this report the only prototypes produced were 3D printed plastic models of the bus frame and a mockup of the HSI payload and interfacing. The function of these prototypes has been to give a better understanding of the scale of the satellite. Designing and looking at a model on a PC screen made it hard to comprehend the actual size of components, and a model in a 1:1 scale helped tremendously with this.

Forward in time, prototyping will become more important as testing commences. Testing of prototypes made of aluminium will hopefully shed light on some of the unknowns regarding material behaviour in space conditions, both for the in-house developed components and the COTS. This will be done in addition to updating and refining the 3D printed models to use as a visual reference and for trying out solutions for attaching the star tracker and other interfaces.

2.1.6 Manufacturing

As the design is refined sufficiently it will be moved into the manufacturing stage. The production itself will most likely be done by a third party as the complex geometry requires skill and experience in machining to shape properly. Materials, dimensions and tolerances will be those that are specified in the design. The goal is to produce a high quality version of the payload that can be put trough testing and eventually be integrated.

2.1.7 Testing

Physical testing of a design is the closest engineers can get to an actual situation without actually launching. While simulations provide good indicators and sometimes accurate results, the only way to confirm the results are with actual tests. Although testing allows for much higher reliability, cost and availability of such facilities may become constraints. This mostly concerns thermal vacuum chambers and reliable vibration rigs that have a limited availability as well as a number of requirements for what is being tested. These tests should therefore not be performed until the design has reached a satisfying maturity level.

The planed tests are done on a subsystem level, requiring only the HSI payload and interfacing solution. For the first phases of design iteration, simplified tests are planed using thermal chambers, vacuum chambers and simple vibration rigs, although these also have their requirements. Additionally, the results from these tests will be used to further build the reliability of simulations. Proper tests, using special equipment and facilities will then be done. Later in the system development cycle, the entire system will be tested. The system must also pass a final acceptance test, subsystem level and system level, to be able to launch.

All acceptance tests that will be done will follow the same procedure. Tests will be linked to all relevant requirements tested, necessary equipment will be described together with a detailed test description and acceptance criteria. It is imperative that the tests can be repeatable. Simple tests used to gather data internally will be recorded and documented, but might not follow the same procedure as the acceptance tests.

2.1.8 Integration

The integration of the finished designs into the provided bus will be the final step in delivering a complete system. This step is only achievable after the system is validated and verified to fulfill the critical requirements. The mechanics team is responsible for the integration. This means that design needs to be at a complexity level that can be integrated in house.

2.2 Software Tools

This section lists all software programs used during the project. For the simulation programs, a lists of alternate tools are also given, with justification for the chosen programs provided.

2.2.1 CAD/CAE Tools

At the beginning of the project, a simple study was done in order to determine which CAD and CAE software would be used for the project. It was important to evaluate this properly, as it would determine much of how the work-flow. Furthermore, changes in these kind of tools at a later state of the project would require work, as all the CAD files would need conversion. This process would also cause loss in data like underlying sketch information and material data, which would need additional work to reapply.

A large factor to deciding was also the PLM capabilities i.e. Team Center, PLM.
NX 11 with Nastran, Space Systems Thermal and Team Center integration was chosen to minimize risk of data loss during exporting and to ensure a structured work environment for the CAD/ CAE model procedure. SolidWorks 2018 was used to convert provided files from NanoAvionics to NX 11.

NX 11 NX 11 is a simulation tool with 3D modeling capabilities. NX is comprised of multiple solvers, designed with different input and output variables. NX is industrially well known, documentation for most solvers is available. Professor Terje Rølvåg, is also available for some consultation.

NX Nastran NX Nastran is a FEM solver in NX 11, used for linear and non linear structural, and thermal analysis. Nastran has several subsolvers or solutions that provides different data. The main advantage of using Nastran is that all solvers can use the same FEM model mesh, with different simulation objects and restrictions.

NX Space Systems Thermal NX Space Systems Thermal is a special solver created to be used for thermal simulations of satellites around earth. SST has all functions built in for transient orbital simulation. SST and Nastran can't use the same FEM models. Limited knowledge exists in Europe regarding the use of SST. Limited documentation exists in previous CubeSat/ satellite project reports.

SolidWorks 2018 SolidWorks 2018 is a CAD tool with rudimentary analysis support. SolidWorks is intuitive and simple to use, but lacks features in the analysis module. However, it supports the format of CAD files received from NanoAvionics and has therefore been utilized as a file converter to open bus-parts in NX 11.

2.2.2 Other CAD/ CAE Options

The following analysis tools were considered for the project:

Ansys   Ansys is a simulation solution that incorporates interdisciplinary modules in a single work environment. Ansys incorporates thermal, structural and optical. However, the team has no experience with this software, it would require learning in designing and simulating. Ansys is a good candidate for further implementation, for a later project.

Abaqus   Abaqus an advanced simulation tool used in high end engineering. Abaqus gives the engineer a relative large control over the simulation parameters. Abaqus is also available as a solver for NX 11. Due to the complexity and lack of available time, Abaqus was not used.

Fedem   Fedem is a simulation tool used in a large range of disciplines, like robotics, space and the automotive industry. Fedem requires imported 3D models from a CAD software. Due to the limited knowledge and the fact that a single software is preferred, Fedem was not used.

ESATAN-TMS   ESATAN-TMS is a simulation tool specifically for thermal analysis. The software includes several "environments" analog to different solvers in NX. ESATAN-TMS also allows for 3D modeling. Used in several successful CubeSat launches in Europe. Acquiring a licence was the most limiting factor.

Systema-Thermica   Like ESATAN-TMS, Thermica is also a tool used for thermal analysis in space. It is also capable of advanced orbit calculations and mechanical movement simulation. Thermica has also been used in previous successful CubeSat missions. However, the use of Thermica would require the acquisition of a licence. Furthermore, Thermica would introduce more CAE programs into the workflow, as it does not provide structural analysis support.

2.2.3 General

CES EduPack 2018   CES EduPack 2018 was used as a material library. Specific material information were extracted in the form of MatML XML files and imported to NX as a custom library. System settings in NX allows the platform to read multiple XML files i a folder.

Slic3r   Slic3r was used to prepare models for 3D printing. Slic3r is an open source free software that had the necessary functionality needed for simple prototyping. Additionally, members of the mechanics team already had experience with using this software.

Lucid Chart   Lucid charts is an free flow charts creator. Lucid charts was used by the entire HYPSO team to achieve a homogeneous look and structure to all flow charts.

2.2.4   Organizational Software

Google Drive   Prior to the project, Google Drive had already been chosen as the file sharing platform by HYPSO. Drive has revision control and allows for easy sharing of work between teams. Synchronization issues and large files can provide a problem. Initially, Drive was used for storing CAD and CAE files, using an Google Spreadsheet to keep track of all the revisions and their differences.

Skype   Skype was used as a communication tool for meetings.

Trello   Trello was used to convey completed and future tasks between the group members. The tool was meant to help keep track of all tasks and be a structure for understanding other group members work agenda.

Slack   Slack was used for general communication between group members. The work space spans the entire HYPSO project.

Overleaf   Because the size of the report was expected to be fairly large, LaTeX was chosen as the type setting language of the project, providing the necessary expandability and configurability. As the document was to be written by multiple people, Overleaf the selected word processing platform. Word Online, and Google Docs were also considered as word processing platforms, but were dropped based on previous bad experiences with Word Online, mainly crashing when the document has grown too large. Google Docs, while stable, did not have the desired functionality.

File Server   At a later stage of the project, a file server was introduced to the workflow as a faster option to Google Drive. This was done because the file size of the entire satellite system kept increasing, which then increased the upload time to Google Drive, as well as requiring file compression. The server made file sharing more convenient and quick within the mechanics team. All the revision documents in Drive was still kept and followed.

2.3 Literature

2.3.1 NASA Resources

NASA has been the biggest space agency in the world for several decades. During the research done for this project, open documents and reports from NASA have been very useful. Their reports and documents regarding specific space-related phenomenon like outgassing and atomic oxygen proved to be the best resources for investigating these effects in relation to a CubeSat.

2.3.2 European Cooperation for Space Standarization

The European Cooperation for Space Standarization provides a comprehensive set of standards that is the result of a collaboration between ESA and national space agencies. It has been decided that this set of standards shall be followed by the HYPSO CubeSat project. The requirements outlined in the standards are therefore the basis for the design, unless otherwise stated by the launch provider.

2.3.3 Library Resources

The majority of references cited in this report will be online articles or reports. However, some offline sources of information were also utilized. These were gathered from the school library, the lab bookshelf and the mechanics teams private collection. Their use varies from fact-checking to information gathering, and some of them will not be directly cited as sections of them are read only to gain a general understanding of a subject. Some books deserve a special mention for this purpose:

- *Space Mission Engineering: The New SMAD [6]/*

- *Dimensjonering av Maskindeler [13]*

- *Engineering Analysis with NX Advanced Simulation [14]*

2.3.4 Previous Missions and Theses

As space is an expensive and difficult business where most missions are either run by governments or private companies, detailed information about payload and satellite design proves hard to find. However, the simplicity of the CubeSat format has made it possible for universities to delve into this subject to a much higher degree than before. A positive consequence of this is that theses regarding CubeSat and payload development are published by bachelor, master and PhD students.

The experiences of other CubeSat missions regarding mechanical and thermal challenges have provided a good foundation and awareness of potential problems for this project. The theses cited in this report have been very useful for understanding the unique demands of a CubeSat platform. It is important to acknowledge the earlier work that have made the short timeline of this mission possible, and it is the authors wish and hope that the work outlined in this report can assist others in their quest for space compatible systems.

2.4 Prototyping

2.4.1 3D Printing

When designing, having a physical model helps with giving an overview and sometimes allow the designer to easier see things that might have been overlooked. Using 3D printing, newly designed parts could quickly be manufactured. This was also helpful for other members of the project, allowing them to see the progress of design, and contribute with opinions. Furthermore, having the satellite and components in physical form would make it easier to design the wire layout when the time comes. Prototyping laboratories for 3D printing were provided by NTNU.

2.4.2 Machining

At this stage, the material used for the HSI interface is planned to be Aluminium 6061. It could be possible to 3D print in this material, but machining is a far cheaper and more predictable solution. Manufacturing is a subject that has not been prioritized at this stage in the mission, but it is still worth mentioning that machining will be a central process when functional prototypes are produced as well as for the final model. Due to the somewhat complex geometry of the grating holder, 3 or 5-axis milling will be required. The preliminary research done on the availability of such equipment on campus points to the need of outsourcing the production.

3   Mathematical Theory

This section aims to delve into the mathematical background of critical topics. For general theory regarding the topics please refer to section 2. Background.

3.1   Center of Mass and Moment of Inertia

The general equation for the center of mass is shown in equation 1. Center of mass is the balance point of an objects mass ditribution. The equation works on the assumption that all the mass of an object can be approximated as being in a single point. The distance from this point to the chosen origin is the *x, y* & *z* variables. *N* is the number of parts and *m* is their respective mass.

$$(X,Y,Z)_{Mass} = \left(\frac{\sum_{n=1}^{N} m_i x_i}{\sum_{n=1}^{N} m_i}, \frac{\sum_{n=1}^{N} m_i y_i}{\sum_{n=1}^{N} m_i}, \frac{\sum_{n=1}^{N} m_i z_i}{\sum_{n=1}^{N} m_i} \right) \tag{1}$$

The general formula for moment of inertia is:

$$I_p = \sum_{n=1}^{N} m_i s_i^2 \tag{2}$$

Where s_i^2 is the distance from the approximated point mass to the chosen origin squared. As can be seen from this equation, moving mass away from the center increases the moment of inertia. Equation 1 & 2 are the basis for the CoG and MoI calculations showcased in this report. The specific fidelity of the point assumption for each mass is however unknown. Some error estimates will be provided in the calculation, but these are also gathered from NX data. There are provided no references for these two equations as they are very common and variations are featured in every classical mechanics book.

3.2   Dynamics calculations in NX

A systems eigenfrequency can be calculated with the following formulations [15]:

$$\mathbf{M\ddot{r}} + \xi\mathbf{\dot{r}} + \mathbf{Kr} = \mathbf{F} \tag{3}$$

M is the mass matrix, ξ is the damping matrix, K is the stiffness matrix and F is the force vector. For general modal analysis the dampening is generally ignored.

$$\mathbf{M\ddot{r}} + \mathbf{Kr} = \mathbf{0} \tag{4}$$

Equation 4 forms the basis of the eigen system encountered in FEM [15]. Harmonic motion $r = rsin(\omega t)$ is then assumed.

$$(\mathbf{K} - \omega^2\mathbf{M})\mathbf{r}sin(\omega t) = \mathbf{0} \tag{5}$$

Two no frequency ($\omega = 0$) and no motion ($\mathbf{r_e} = \mathbf{0}$) solutions can be discarded, leaving the following solution:

$$\mathbf{K} - \omega^2\mathbf{M} = \mathbf{0} \tag{6}$$

M is a symmetric matrix and can therefore be factorized:

$$\mathbf{M} = \mathbf{L}\mathbf{L^T} \tag{7}$$

By introducing $\mathbf{x} = \mathbf{L^T}\mathbf{r_e}$ the following equation can be formed

$$(\mathbf{L^{-1}}\mathbf{K}(\mathbf{L^T})^{-1} - \omega^2\mathbf{I})\mathbf{x} = \mathbf{0} \tag{8}$$

A more common form of an Eigen system is expressed as the following:

$$\mathbf{A}\mathbf{x} = \lambda\mathbf{x} \tag{9}$$

And can be written as:

$$(\mathbf{A} - \lambda\mathbf{I})\mathbf{x} = \mathbf{0} \tag{10}$$

This can be solved analytically by setting the equation to $det(\mathbf{A} - \lambda\mathbf{I}) = \mathbf{0}$. For larger systems, computing methods such as Lanczos which is a power iteration method, equation 11 can be used.

$$\mathbf{A}\mathbf{x_i} = \lambda_{i+1}\mathbf{x_{i+1}} \tag{11}$$

A fundamental frequency is the lowest eigenfrequency for a system. The fundamental frequency can be calculated by the use of cantilever beam approximation [6].

$$\mathbf{f_n} = \frac{1}{2\pi}\omega \tag{12}$$

$$\mathbf{f_n} = \frac{1}{2\pi}\sqrt{\frac{3\mathbf{EI}}{\mathbf{ML^3}}} \tag{13}$$

In a single degree of freedom oscillator system:

$$\mathbf{f_n} = \frac{1}{2\pi}\sqrt{\frac{\mathbf{k}}{\mathbf{M}}} \tag{14}$$

3.3 Thermal calculations in NX

The general heat flux can be represented by the following equation [16]:

$$\dot{Q}_{net} = \dot{Q}_{in} - \dot{Q}_{out} \tag{15}$$

Where:

$$\dot{Q}_{in} = \dot{Q}_{solar} + \dot{Q}_{albedo} + \dot{Q}_{internal} + \dot{Q}_{IR.earth} \tag{16}$$

and

$$\dot{Q}_{out} = \dot{Q}_{emission} \tag{17}$$

These equations describes the balance of thermal energy that the system experiences. They can each be subdivided further, thus describing the inner thermal balances of components. This will be more important as the development proceeds, and it will be covered more substantially as part of a thesis at a later time.

For NX Siemens solves the following general equation for heat calculations to be able to predict the thermal states of the simulated models [16], [17]:

$$\mathbf{B}\ddot{\mathbf{u}} + \mathbf{K_c}\dot{\mathbf{u}} + \mathbf{R}(\mathbf{u} + T_{abs})^4 = \mathbf{P} + \mathbf{N} \tag{18}$$

Where $\mathbf{B}$ is the heat capacity matrix, $\mathbf{K_c}$ the heat conduction matrix and $\mathbf{R}$ the radiation exchange matrix. $\mathbf{P}$ is a vector of applied constant or transient heat loads and $\mathbf{N}$ is a nonlinear heat load that is a function of temperature. $\mathbf{T_{abs}}$ is the conversion adjustment for when temperatures are specified in Fahrenheit or Celsius. Finally, $\mathbf{u}$ is the grid point temperature vector. When phase change is considered, the following conversion can be made:

$$\dot{\mathbf{H}} + \mathbf{K_c}\mathbf{u} + \mathbf{R}(\mathbf{u} + \mathbf{T_{abs}})^4 = \mathbf{P} + \mathbf{N} \tag{19}$$

Where $\dot{\mathbf{H}}$ is the enthalpy vector. The equation is then solved using Newmark's method with adaptive time stepping [17].

[1] H. Frank Cervone. Understanding agile project management methods using scrum. *OCLC Systems & Services: International digital library perspectives*, 27(1):18–22, 2011.

[2] Kevin Forsberg and H Harold Mooz. The relationship of system engineering to the project cycle. *INCOSE International Symposium*, 1:57–63, 10 1991.

[3] M. MacDonald and V. Badescu. *The International Handbook of Space Technology*. Springer, 2014.

[4] W. Zhou, D. Li, Q. Luo, and K. Liu. Analysis and testing of microvibrations produced by momentum wheel assemblies. *Chinese Journal of Aeronautics*, 25(4):640–649, 2012.

[5] Cal Poly SLO The CubeSat Program. 6u cubesat design specification rev. 1.0, 2018. `https://static1.squarespace.com/static/5418c831e4b0fa4ecac1bacd/t/5b75dfcd70a6adbee5908fd9/1534451664215/6U_CDS_2018-06-07_rev_1.0.pdf`, accessed September 2018.

[6] 65 Authors from the Astronautics Community and James R. Wertz. *Space mission engineering: The new SMAD*. Microcosm Press, Hawthorne, Calif, 2011.

[7] Outgassing data for selecting spacecraft materials, 2018. `https://outgassing.nasa.gov/`, accessed November 2018.

[8] A Merstallinger, M Sales, E Semerad, and B D Dunn. Cold welding in hold down points of space mechanisms due to impact and fretting. *Proceedings of the Institution of Mechanical Engineers, Part J: Journal of Engineering Tribology*, 222(8):1005–1014, 2008.

[9] Fred Sigernes, Mariusz Eivind Grøtte, Julian Veisdal, Evelyn Honore-Livermore, Joao Fortuna, Elizabeth Frances Prentice, Mikko Syrjasuo, Kanna Rajan, and Tor Arne Johansen. Pushbroom hyper spectral imager version 6 (hsi v6) part list – final prototype, 2018.

[10] Miller Banks, de Groh. Low earth orbital atomic oxygen interactions with spacecraft materials, 2014. `https://ntrs.nasa.gov/archive/nasa/casi.ntrs.nasa.gov/20040191331.pdf`, accessed November 2018.

[11] TEB. Tailored ecss engineering standards for in-orbit demonstration cubesat projects, 2018. `https://www.copernicus-masters.com/wp-content/uploads/2017/03/IOD_CubeSat_ECSS_Eng_Tailoring_Iss1_Rev3.pdf`, accessed September 2018.

[12] H.F. Cervone. Applied digital library project management: Using pugh matrix analysis in complex decision-making situations. *OCLC Systems and Services*, 25(4):228–232, 2009.

[13] G Härkegård. Dimensjonering av maskindeler, 2004.

[14] T. Khalitov S. Denisikhin D. Sotnik P. Goncharov, I. Artamonov. *Engineering Analysis with NX Advanced Simulation*. Simens, 2014.

[15] Terje Rølvåg. *FEAinME Lecture Notes in Finite Element Dynamic Analysis*. 2018. Unpublished.

[16] Sofia de Fátima Caeiro Aboobakar. Dynamic and thermal models for ecosat-iii. 11 2016.

[17] Siemens NX. *Thermal Analysis User's Guide*. NX Nastran Documentation, 2014.

Appendix B

HYPSO-DR-003 HSI Payload Design Report

HSI Payload Design Report

HYPSO-DR-003
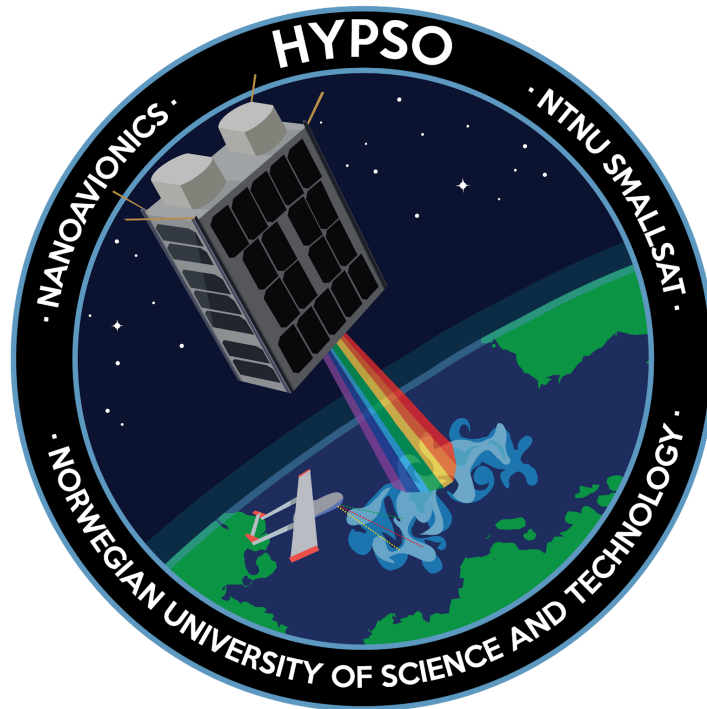
Prepared by: HYPSO Project Team
Reference: HYPSO-DR-003
Revision: 2
Date of issue: 25.05.2019
Status: Issued
Document Type: Analysis Report
Authors: Tord Hansen Kaasa, Tuan Tran, Henrik Galtung

Table Of Contents

Table 1: Table of Changes

Rev.	Summary of Changes	Author(s)	Effective Date
1	*First issue*	*Tord Hansen Kaasa, Tuan Tran, Henrik Galtung*	*23.05.2019*
2	*Formatting of text and figures*	*Tord Hansen Kaasa, Tuan Tran, Henrik Galtung*	*25.05.2019*

1. Overview

1.1 Purpose

This report documents the design process of the functional HSI prototype "TTH Mk1" shown in figure 1, and gives a background for all design decisions based on the requirements gathered for the HSI camera assembly. The prototype is planned to be used as a benchmark for functional, vibration, shock and thermal testing. Figure 1 shows an exploded view of the finished prototype.
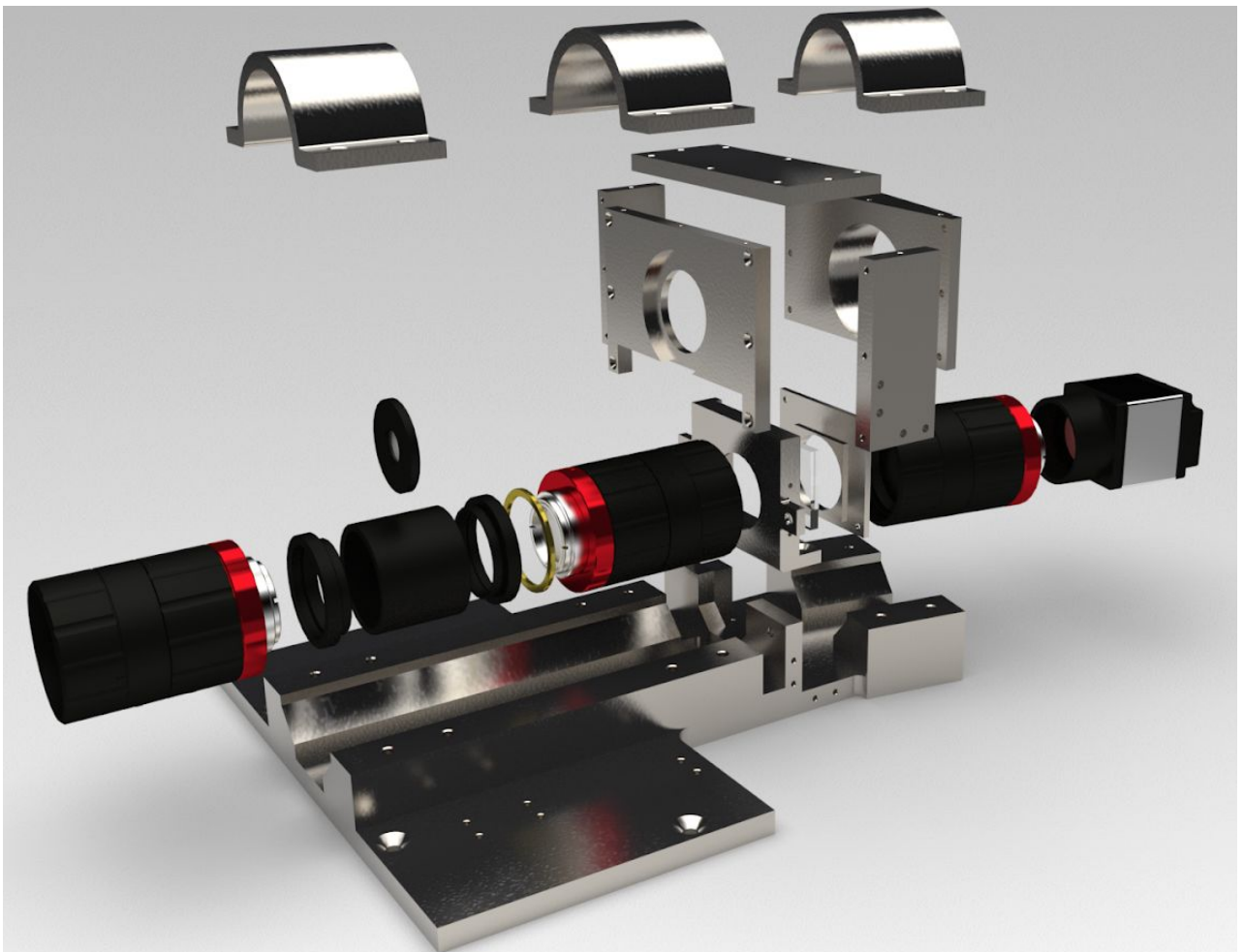
Figure 1: Exploded view render of the TTH Mk1 prototype

1.2 Scope

The optical design for the TTH Mk1 was based on the HSI Pushbroom V.6, developed by *Fred Sigernes*, professor in physics, optics and atmospheric research at UNIS. The TTH Mk1 uses the same optical layout as described in the V.6 report [RD01]. The TTH Mk1 is the redesigned version of the HSI developed for the PDR by the mechanics team, described in the specialization report [RD02]. Figure 2 shows the relationship between all the documents.

Figure 2: Document relationship

1.3 Reference Documents

The documents listed in table 2 have been used as reference in the creation of this document.

Table 2: Referenced Documents

ID	Author	Title
[RD01]	Fred Sigernes, Mariusz Eivind Grøtte, Julian Veisdal, Evelyn Honore-Livermore, Joao Fortuna, Elizabeth Frances Prentice, Mikko Syrjasuo, Kanna Rajan, and Tor Arne Johansen.	Pushbroom hyper spectral imager version 6 (hsi v6) part list – final prototype. 2018
[RD02]	Tord Hansen Kaasa, Tuan Anh Tran, Henrik Galtung.	Mechanical and Thermal Integration of an HSI Payload in A 6U CubeSat, Specialization Report. 2018
[RD03]	NanoAvionics.	Environmental Test Requirements for Polar Satellite Launch Vehicle Auxiliary Payloads. (Not published, under NDA)
[RD04]	Shyam Patidar, Pradeep Kumar Soni.	An Overview on Vibration Analysis Techniques for the Diagnosis of Rolling Element Bearing Faults. International Journal of Engineering Trends and Technology (IJETT) - Volume 4 Issue 5. May 2013
[RD05]	Tom Irvine.	An introduction to the shock response spectrum. 07 2012.
[RD06]	Wikimal.	Good CNC design practice. [Link], accessed February 2019.
[RD07]	Engineers Edge	Engineering Tolerance (IT) Grades Table Chart [Link], accessed March 2019
[RD08]	65 Authors from the Astronautics Community and James R. Wertz.	Space mission engineering: The new SMAD, Microcosm

		Press, Hawthorne, Calif, 2011.
[RD09]	H. Galtung, T.H. Kaasa, E.F. Prentice, T. Tran.	HYPSO-RP-006 HSIv6 NTNU-01 Assembly, 2019
[RD10]	T. Kaasa, T. Tran, H. Galtung.	HYPSO-RP-005 Objective Vulnerability Mitigation, 2019
[RD11]	Balaji, PS & Rahman, Muhammad & Leblouba, Moussa & Lau, Hieng Ho.	Wire rope isolators for vibration isolation of equipment and structures – A review. IOP Conference Series: Materials Science and Engineering. 78. 10.1088/1757-899X/78/1/01 2001, (2015).
[RD12]	NASA.	Multilayer Insulation Material Guideline. [Link], Accessed May 2019
[RD13]	John Williams. Cambridge University Press,	Engineering Tribology, 2005.
[RD14]	Gunnar Härkegård,,	Dimensjonering av Maskindeler, Fagbokforlaget, 3. Opplag, 2014
[RD15]	Knight Optical.	Technical / Sheet Glasses. [Link], Accessed May 2019
[RD16]	Jack A. Collins, Henry Busby, George Staab.	Mechanical Design of Machine Elements and Machines. Wiley, 2010

2. Mechanical Design

2.1 ECSS and NASA Standards

The following section contains modified excerpts from "Specialization Report section 5.3.1, Kaasa, Galtung, Tran"

The mechanical interfacing for the HSI has several requirements instated from the NASA and ECSS standards. The requirements are strict due to severe safety measures. The requirements are given by different standards in relation to tests types, simulation types and loads. The main standards followed are NASA-STD-5002 LOAD ANALYSES OF SPACECRAFT AND PAYLOADS and ECSS-E-ST-32C Structural general requirements. It should be noted that the standards are written for large scale satellites, and the requirements must be limited and scaled back to fit the development of a CubeSat system. The standards are open to reduction, section 1.3 in NASA-STD-502: "Determining the suitability of this standard and its provisions is the responsibility of program/project management and the performing organization. Individual provisions of this standard may be tailored (i.e., modified or deleted) by contract or program specifications to meet specific program/project needs and constraints". It follows that not all simulations referred to in the standards will be done. Other standards are applicable in a CubeSat development, the ESA report *Tailored ECSS Engineering Standards for In-Orbit Demonstration CubeSat Projects* gives a complete view of the ECSS standards that are relevant to CubeSat development. Some of the most important requirements for the mechanical system is outlined in section 5.3.1 in the Specialization Report [RD02], see the relevant standards for further information.

2.2 Payload Requirements

This section contains the main requirements for the HSI payload. The requirements are based on the standards presented in the last section. In addition, the requirements are made based on iterative work on the payload with a multidisciplinary team. These requirements are not final and will be changed after functional, vibration, shock and thermal testing has been completed. It follows that some of the requirements are vague and lack the proper variable values.

HSI Requirements

Table 3 shows the current list of requirements retaining to the HSI mechanical interface, optical components, thermal, material and ADCS. Furthermore the requirements for the grating bracket subsystem are included. In addition, a check mark for complete/not compete.

Table 3: HSI Requirement List

ID	C/NC	Definition
Mechanical Payload Interface		
IF-001		The mechanical and software interfaces of the HSI shall comply to the spacecraft 6U CubeSat ICD delivered by NanoAvionics
HSI-019		The total mass of the HSI payload shall be less than 1500 g, with a margin of 20%
HSI-020		The HSI platform shall be manufacturable by using a 3-axis CNC
HSI-021		The HSI payload shall withstand the pressure change during the launch
HSI-022		The HSI payload shall withstand launch loads, Provider: Polar Satellite Launch Vehicle
HSI-023		Due to geometrical limitations, the front lens shall not protrude from the spacecraft by more than 6 mm (+/-1 mm)
HSI-024		The payload surfaces exposed to outer space should survive any orientation with respect to the environmental loads
HSI-025		The HSI payload shall be decoupled thermally from the spacecraft frame
HSI-026		The HSI payload shall be decoupled mechanically from the spacecraft frame
HSI-027		The HSI payload shall encompass a rigid connection with the star tracker
HSI-028		The HSI payload shall encompass a rigid connection with the IMU
HSI-029		The HSI payload shall accommodate a rigid connection to the proposed RGB camera
HSI-030		The payload frame should be electrically coupled to the spacecraft frame to avoid static buildup
Optical Components		
PA-011		The optical components shall be comprised of non volatile materials
HSI-ASS-001		The payload shall be assembled according to an assembly procedure with an as-built list
HSI-ASS-002		The grating shall not rotate around the axis perpendicular to its plane
HSI-ASS-003		The grating shall not shift in any axis

HSI-ASS-004		The slit shall be parallel to the X and Y-axis
HSI-ASS-005		The slit, grating and detector shall be aligned, resulting in straight spectral lines
HSI-ASS-006		The sum of rotational optical misalignments of all optical components throughout orbital lifetime shall not be greater than 0.01 degrees
HSI-ASS-007		The slit shall be placed perpendicular to the XZ plane, parallel to the Y axis
HSI-ASS-008		All objectives shall share the same driving dimension from the mechanical interface to avoid stacking multiple tolerances
HSI-ASS-009		The total deformations induced by the thermal expansion should not result in the change of optical performance
HSI-ASS-010		The F/# shall be adjustable for front lens, collimator lens and detector lens during assembly
HSI-ASS-011		The F/# shall be locked for front lens, collimator lens and detector lens after assembly
HSI-ASS-012		The locked F/# shall be 2.8 for the front lens
HSI-ASS-013		The locked F/# shall be 2.8 for the collimator lens
HSI-ASS-014		The locked F/# shall be 2.0 for the detector lens
Thermal		
HSI-032-001		The heat produced by electronics for a typical slew maneuver process duration (3 min) should be within the defined operational ranges of the COTS components
HSI-032		The HSI payload shall survive the temperature fluctuations throughout its lifetime
Material		
PA-002		The HSI payload should comprise of non -ferritic and -magnetic materials as to not interfere with the magnetorquers or the magnetometers
PA-003		The HSI interface shall be made from one of the recommended light alloys listed in the 6U CubeSat Standard
PA-004		The use of heavy materials with high melting points shall be limited. The spacecraft shall not create debris after decommissioning
HSI-032-002		The HSI interface material shall have a thermal expansion rate similar to AA6061, as to not induce stress when exposed to thermal gradients
PA-005		The materials used shall have TML < 1.0%, CVCM < 0.1%
PA-006		Machined camera parts should be anodized in black (TBC)
PA-007		All aluminum components shall be designed such that anodizing can be done with uniform thickness (TBC)
ADCS		
PA-008		The spacecraft center of gravity (CoG) shall confine to the 6U cubesat standard requirements
PA-009		The moment of inertia (MoI) of the satellite shall confine to the allowable ranges defined by the ADCS team (TBD)

Grating Cassette Requirements (Subsystem)		
HSI-ASS-015		The grating cassette shall prevent the grating from translational movement in the plane with a tolerance of 0.01 mm
HSI-ASS-016		The HSI platform shall accommodate the mounting of two 50 mm VIS-NIR lenses, with a respective angle of 10.37 degree between them
HSI-ASS-017		The HSI platform shall mount the lenses such that their light points to the middle of their respective closest surface of the grating
HSI-ASS-018		The HSI platform shall mount the detector lens and collimator lens with a clearing between lens and grating of 0.5mm to 15mm
HSI-ASS-019		The HSI payload design shall not have more than one driving dimension to avoid stacking multiple tolerances

2.3 Typical Load Environment

There are several requirements in relation to the launch of the CubeSat. This section will explore the most important load requirements instated by the Polar Satellite Launch Vehicle (PSLV), the chosen launch vehicle for the HYPSO CubeSat. The specific load environment values are provided by NanoAvionics. All loads must be multiplied with a safety factor of 1.7 during testing, in accordance with the documentation.

2.3.1 PSLV Loads

The PSLV will instill a maximum load requiring the following design loads
Longitudinal ±11 g, > 135 Hz
Lateral ±6 g, > 70 Hz

The longitudinal and lateral loads acts simultaneously. Due to the uncertainties of the CubeSat placement in the launcher, the longitudinal load must be used as the design load for all axis.

The first fundamental frequency is required to be higher than 135 Hz.

Note: The first fundamental frequency is required to be higher than 70 Hz according to PSLV documentation, however due to the lack of information in regards to the CubeSat placement within the launcher, the first fundamental frequency must be the longitudinal stiffness.

The payloads shall remain fully functional after a sine vibration test with the parameters noted in table 4, based on the Environmental Testing Requirements for Polar Satellite Launch Vehicle provided by NanoAvionics [RD03]. The values are for a standard qualification test, the acceptance test requires a less severe profile as to not purposefully harm the flight model more than necessary. Where DA is the double amplitude, or one complete excitation in both directions.

Table 4: PSLV Sine parameters

Characteristic		Qualification
Profile	Frequency, Hz	Amplitude
	5- 8	34.5 (DA)
	8- 100	4.5 g
Directions		x, y, z
Sweep Rate, oct/ min		2

The payload must also be able to survive the random vibrations that are present during the flight. The vibration band present in the PSLV can be simulated and tested in the lab. Table 5 shows the recommended values for a random vibration test, the values are for all directions X, Y and Z. Where PSD is the *power spectral density*, or the distributed power of the vibrations, and RMS is the *root mean square* a measure of the overall amplitude of the random vibrational system [RD04].

Table 5: Random Vibration Test

Characteristics		Qualification
Profile	Frequency, Hz	PSD, g^2/Hz
	20	0.002
	110	0.002
	250	0.034
	1000	0.034
	2000	0.009
Acceleration, g (RMS)		6.7
Duration, sec/ axis		120

The payload must be able to survive the shock loads present under launch. Table 6 tabulates the required shock values the payload shall survive, note that the safety factor must be applied. Where the Q-factor is the quality factor related to the system damping, a Q-factor of 10 is equivalent to 5% damping, and a normal approximation of bolted transmissions [RD05].

Table 6: Half Sine Shock test

Characteristics	Qualification
Acceleration, g	70
Duration, ms	2
Q- Factor	10

3. Design for High Precision Machining

3.1 Production Methods

As can be seen in requirement HSI-020, in section 2.2, all manufactured parts shall be manufacturable in a 3-axis CNC milling machine or lathe. This requirement exists to ensure that the design can be manufactured on campus by the internal workshops to reduce cost for future machining. The use of an 5-axis CNC milling machine to provide a higher accuracy and to ease the design process was considered, as was aluminium 3D printing, but was scrapped due to the lack of campus equipment and uncertainties in regards to mechanical integrity and outgassing respectively. A limitation of the 3-axis milling machine is that the milling depth should not exceed three times the cutting tool diameter and internal radii at the corners of at least 1/3 of the depth of the cavity, all designs must be tailored to this limitation [RD06]. The sentiments were also echoed by *VerkstedPartner*, who produced the prototype.

3.2 Machining for Optical accuracy

Several different machining and design techniques were employed during the design process in order to ensure the HSI camera accuracy. Since no requirements with exact variable values for the spacing of the different optical equipment were established, it was decided that the prototype should be produced with a small tolerance grade. Based on results from functional testing under a controlled environment, better requirements could be established. T10 [RD07] was instated as the general tolerance on the machined part, while smaller tolerances was applied on the optical leading surfaces. In addition, the amount of components compromising the platform was reduced as much as possible, geometrical inaccuracies introduced from machining and assembly could be reduced considerably.

3.2.1 Leading Surfaces

Leading surfaces were used in order to limit and control the amount of surfaces that decided the position of optical COTS components. Using controlled surfaces with known position, it is possible to control the positioning of the optical equipment with a high accuracy. The leading surfaces consisted of simple geometry, designed with the limitations of the 3-axis milling process. The use of leading surfaces avoids stacking of several tolerances and the entire optical train can be secured using only one surface with the desired tolerance.

3.2.2 Countersunk Offset

To ensure the grating cassette had proper contact with the leading surfaces of the grating groove, offset countersunk holes were made in the groove. This method involved offsetting the location of the hole in the direction of the desired force vector. The concept of offsetting countersunk for high precision alignment was introduced by the CubeSat provider NanoAvionics during their workshop sections at NTNU. For the first prototype, an offset of 0.15 mm in -Y and -X direction was used at the side wings, while the bottom lip used an offset of 0.1 mm in the +Z and -X direction. Ideally, because of the lack of resources regarding this method, a smaller prototype of the cassette and grating holder would be made to test the concept. However, because of other uncertainties present in the full design, a full prototype was more desirable as more uncertainties could be tested.

4. Prototyping for testing and further design optimization

4.1 Functional HSI Prototype

The production of a functional prototype of the HSI assembly was deemed necessary in order to carry out the testing required to ensure proper alignment of the lens objectives, grating, slit and detector. Rotation or non translational displacement in the XY plane will impeach the HSI cameras ability to take pictures, the alignment of those key parts are therefore of the utmost importance. In addition the prototype would be able to serve as a benchmark for vibration, shock and thermal tests, as well as a proof of concept. The prototype was made with machinability in mind. It follows that adjustments like the total prototype mass would vary from the finished assembly. The prototype created was a deviation from the initial design outlined in the PDR documents. The changes was done with regard to the following factors: machinability, complexity, alignment, stiffness, mechanical and thermal integrity. As discussed in the material analysis report *HYPSO-ANA-004*, the chosen material for the functional prototype was Aluminium 6082 T6.

4.2 HSI Design Evolution

The HSI has gone through several iterations of design. This section gives a short overview of the evolutionary history of the HSI. Details about the various stages of iteration can be found in the specialization report and in section 4.3 of this document. The original HSI prototype, shown in figure 3, was developed by Prof. Fred Sigernes [RD01]. It used a combination of 3D printed parts and a cage system from Thorlabs to hold the optical train in the correct position. All subsequent changes to the design were developed by the authors of this document.

The first modification of the original design was the addition of a front supporting bracket and the extension of the grating holder into a "foot" that would interface with the bus frame as shown in figure 4.

This design was then modified by merging the aforementioned "foot" with the front bracket. The driving idea behind this change was to increase the stiffness of the imager while also creating a surface that could interface to the added mounting rail. The rail created a secure connection with the bus frame in addition to include an interface for damper as can be seen in figure 5.

Following this, the grating holder was redesigned. Originally it consisted of two separate parts that were pressed together. This was changed to a cassette-type solution to better control the orientation of the grating in addition to increasing the rigidity of the center of the HSI. This iteration can be seen in figure 6.

Following the gathering of new information regarding the accuracy needed for reliable hyperspectral imaging from Prof. Fred Sigernes, it was decided that the HSI interface should be redesigned in order to allow for the use of the design philosophy described in section 3.
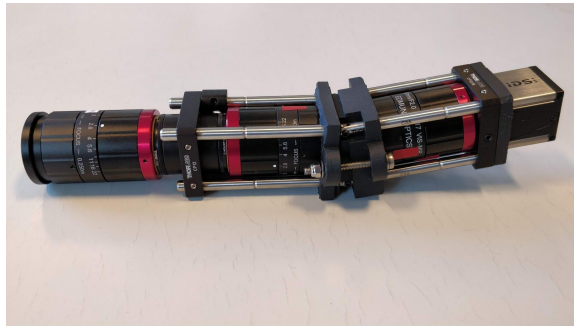
Figure 3: HSI V6 prototype from Fred
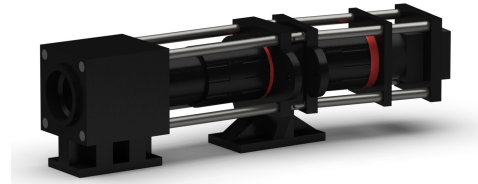
Figure 4: Aluminum version with expanded cage and front bracket
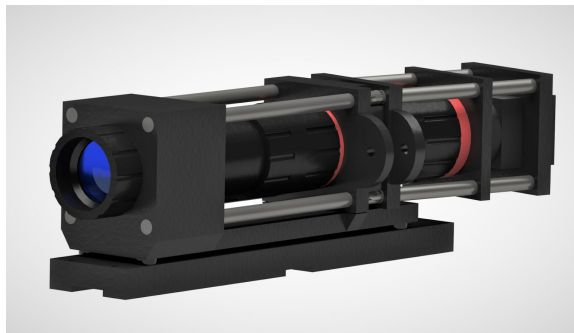
Figure 5: Merged front and center bracket with addition of mounting rail
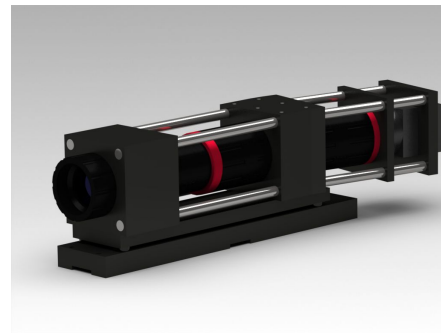
Figure 6: Redesigned grating holder
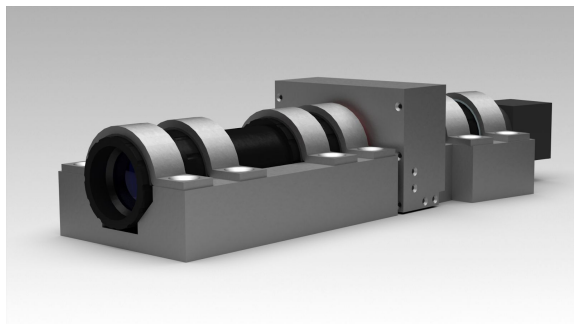
Figure 7: Complete redesign of HSI concept. Switch to rigid cradle solution
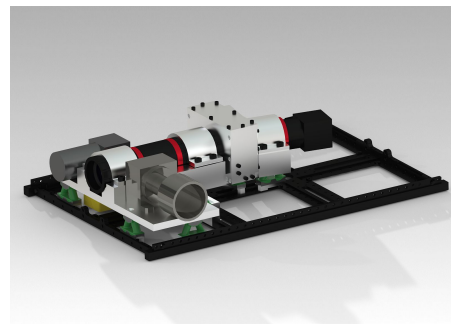
Figure 8: Sideways extension of platform front. Full platform functionality

The resulting iteration can be seen in figure 7 and fully realised and integrated in figure 8. The selection process moving to a cradle and platform solution is shown in Appendix A

4.3 Prototype Design Overview

As stated, the prototype produced was a change in design concept compared to the initial plans drafted for the PDR. This section shows all parts of the assembly that needed to be changed/ produced from the ground up in relation to the initial prototype that differs from the design outlined in the PDR documents. The HSI assembly was simplified by limiting the amount of pieces, thereby limiting the amount of critical error sources. The main assembly was simplified from three different brackets, the lens objectives would hang free between them, to one continuous machined piece.

The piece was constrained in order to be made in a 3-axis milling machine. The changes made decreased the complexity, added stiffness and bettered the alignment of the objectives to grating at the cost of increased mass.

The prototype solution and dimensions were preliminary, and made without simulations. It follows that further prototypes, and the design in general had to be tweaked and changed on the basis of the simulations and the acquired test results. Determination of bolt sizes and part thickness was decided to be somewhat overdimensioned in order to ensure proper connections and aligned leading surfaces.

The following sections will include the main assembly parts, the design process behind it and the necessary information needed to improve the parts. Note that the figures presented in the sections does not include the interfacing rail to the bus. The Front Objective Seating Groove, Back Objective Seating Groove and Platform Cassette Slot are all on the same part, the HSI Platform. The HSI platform was made this way in order to decrease the amount of parts thereby decreasing complexity and manufacturing price. The exact dimensions and technical drawing of all designed and produced parts can be found at the end of the report.

Front Objective Seating Groove

The front objective seating groove is located at the front of the HSI Platform. Acting as the main interface for the front optical assembly consisting of two lens objectives mirrored around the baffling tube containing the high precision slit. The main purpose of the part is to correctly align the optical assembly within the required tolerances, provide mechanical support against vibration, static loads and shocks during launch and thermal stability during operation. The part interfaces to the optical component through a sett of leading surfaces that provides the required stability to the assembly. Several concepts were considered for the interfacing solution, the *L-block* and *seating groove* were deemed the most stable. Different groove solutions was discussed, a 45 degree angle with an extra groove for additional padding was decided upon. The 45 degrees gives a maximum stress distribution. Back of the envelope calculations proved that such a solution would work in a static 11G, without the lens objective material experiencing yield (SF. 2). Figure 9 shows the geometry of the Front Objective Seating Groove in relation to the HSI Platform.
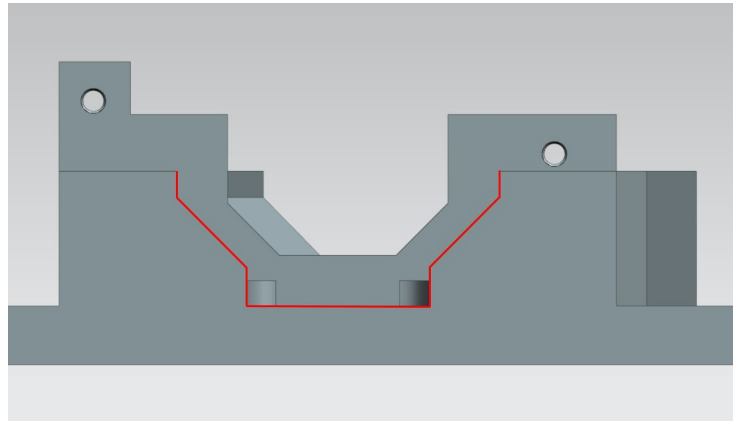
Figure 9: The Front Objective Seating Groove marked in red

The groove should in theory provide adequate and plane securing of the front optical assembly. However, the objectives are not ideal cylinders, as they have notches and patterns on the perimeter of the cylinder surface. A problem could arise should these patterns interfere with the angled leading surface. The contact point is theoretically an infinitely small line between the two surfaces. Should this contact point coincide with said patterns, misalignment could occur in the optical assembly if the contact points are not mirrored and the same for the other objective. This however, is unlikely. The best practise is to make sure that no pattern on the objectives coincides with the interfacing points. The assembly of the physical prototype will show if this approach is plausible. Professor Fred Sigernes, the creator of the HSI design, stated that movement in XY-plane only would shift the pixel register area to another location on the sensor, thus not leading to a crucial problem. However, another issue that could occur from this would be if light is lost between the different sections.

An additional factor is the elastic deformation present for cylinders on flat surfaces. As previously stated, an ideal cylinder on a different surface will theoretically have an infinitely small area of contact. In reality, this area will be a function of the force on the cylinder as well as the elastic properties of the material. This means that the position of the lens objectives will move relative to the grating, as the elastic deformation is occuring. The deformation has been calculated to result in 0.0098 mm half-width surface on both sides, section 7.2. The sf. for yield on the objectives were calculated to be 5.2, disregarding additional force induced from the mounting brackets. The tightening force produced by the bolt with regards to static G forces are allowed to be more than 40 N. This solution is more safe than the potensial cylinder to flat surface solution.

Back Objective Seating Groove

The back objective seating groove is located at the back of the assembly, as seen in figure 10. Acting as the main interface for the front optical assembly consisting of two front lens objectives mirrored around the baffling tube containing the high precision slit. The parts main purpose is to correctly align the optical assembly within the required tolerances, provide mechanical support against vibration, static loads and shocks during launch and thermal stability during operation. The part interfaces to the optical component through a set of leading surfaces that provides the required stability to the assembly. The geometry of the groove can be seen in figure 10.
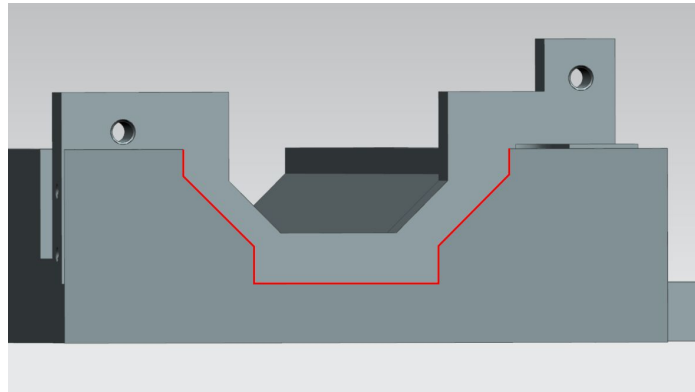
Figure 10: The back objective Seating groove marked in red

Platform Brackets

The optical assembly must be tightly secured to the leading surfaces of the groove solution. Special brackets were designed to provide the necessary force on the lens objectives. The front objectives were secured with two brackets, one on each objective. The back objective was secured with one bracket. The brackets were designed to use M4 bolts, with a 6 mm depth of threading on the grooves. Figure 11 shows the bracket design. To induce the correct uniform force on the objectives the bolts must be tightened incrementally. The exact tightening moment on the bolts were calculated to be 270 Nmm, detailed in section 7.3. The platform brackets will not provide any driving surfaces, effectively allowing for additional gaskets to be placed between it and the lens objectives. Some amount of creep is expected to occur within the gasket, this means that the tightening force must accommodate this. In addition the gasket material will be embrittled over time when exposed to vacuum and radiation. The exact gasket material and suppliers being explored.
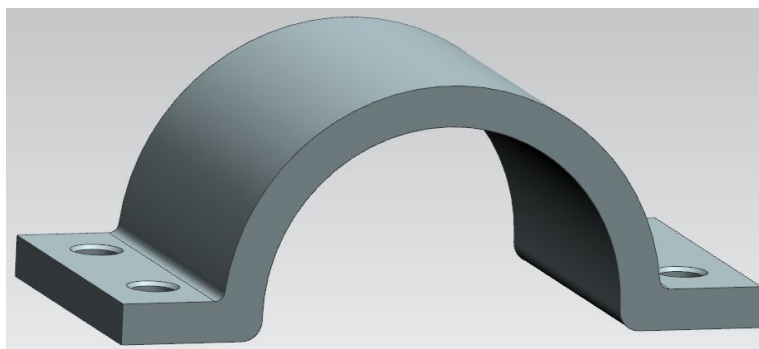
Figure 11: Platform Bracket Design

Platform Cassette Slot

The platform cassette slot was made to accommodate the grating cassette and grating shroud. The grating groove has three mounting points in the main platform. These holes are offset (M2.5), section 3.2.2, to provide force towards a set of driving surfaces for the grating cassette. The upper leading surface towards the front has two mounting points (M3) for the cassette to provide additional force toward the driving surface, these can be seen in figure 12. In addition, the mounting prevents bending in the cassette around the platform mounting. The total depth of the platform was determined by using the rule of thumb "The depth of milling must not exceed 3 times the cutting tool diameter". Some complications might occur on the side mounting due to the amount of material blocking potential milling equipment. A long drill head will be required. The grating groove has holes located in the +X and -X side for interfacing with the grating shroud. Figure 12 shows the geometry of the leading surfaces that secures the alignment of the grating cassette.
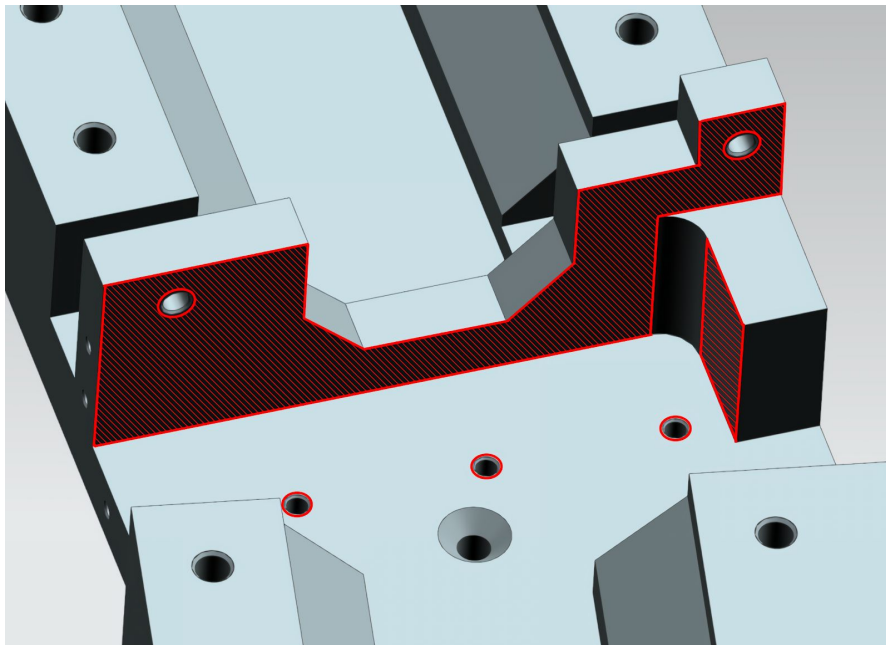
Figure 12: Driving surfaces and mounting holes for the cassette showed in red

Grating Cassette

The grating is the most sensitive component in the whole camera assembly. It is a fragile piece of glass and must therefore be securely and carefully held in place. Its alignment in regards to the incoming light is also of the utmost importance. The chosen solution for this was to utilize 3 driving surfaces, one for each plane of restricted movement. The grating itself is pressed up against these surfaces by two small brackets and the cassette back plate, this configuration is made to be able to handle gratings of a variety of sizes and can easily account for the supposed 0.5 mm tolerance present in the 25x25mm grating, tolerances provided by Edmund Optics. Figure 13a and shows the driving surfaces controlling the grating position, 11b shows the grating inserted into the cassette.
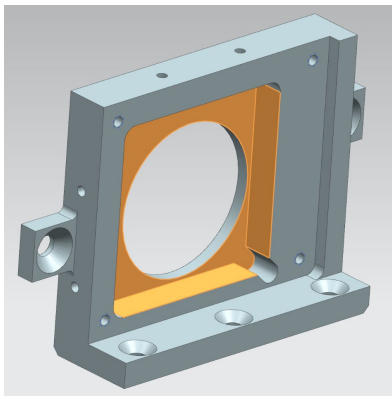
Figure 13a: Three grating driving surfaces shown in yellow
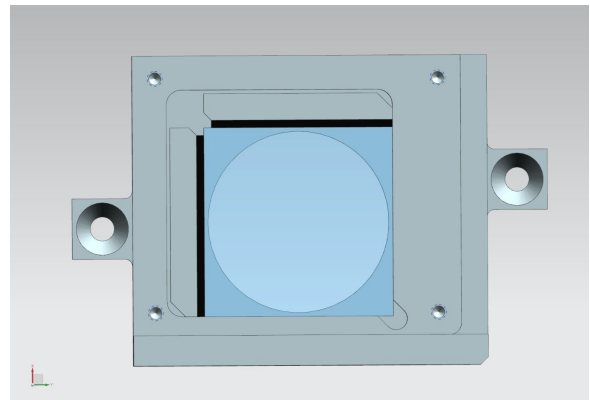
Figure 13b: Grating secured in place

The brackets themselves are pushed towards the grating by two M2 set screws each. The contact surface between the brackets and the grating will have a gasket serving as a force distributor. The back plate features an extension in the +Z direction that pushes up against the grating as shown in figure 14. The plate itself will be fastened to the cassette by four M2.5 screws. It will also have a gasket lowering the stress concentrations in the interface.
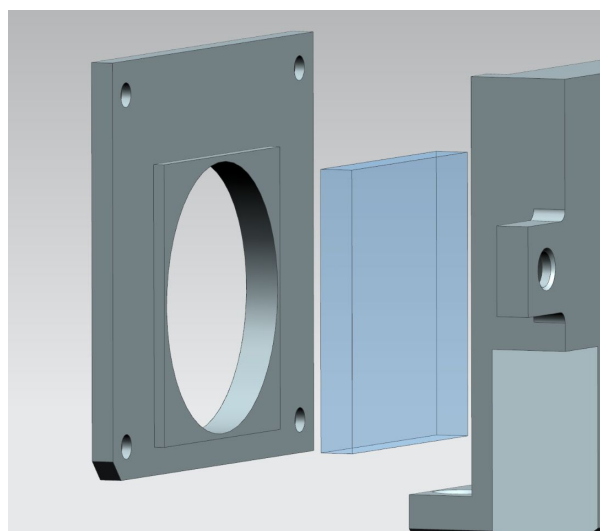
Figure 14: The cassette back plate

Furthermore the cassette features three countersunk M2.5 mounting holes at the -Y side as well as one countersunk M3 hole in each of the "ears" that protrude from the cassette -X and +X sides. The "ears" are asymmetrical to allow spacing for the cutting tool over the bend of the HSI platform and to provide additional area for the leading edge of the cassette side. Figure 15 shows an overview of the five mounting points that is used to fasten the cassette to the platform. These holes facilitate the fastening of the cassette to the platform itself. The correct positioning of the cassette is ensured by the same principle as the grating: it presses up against three driving surfaces.
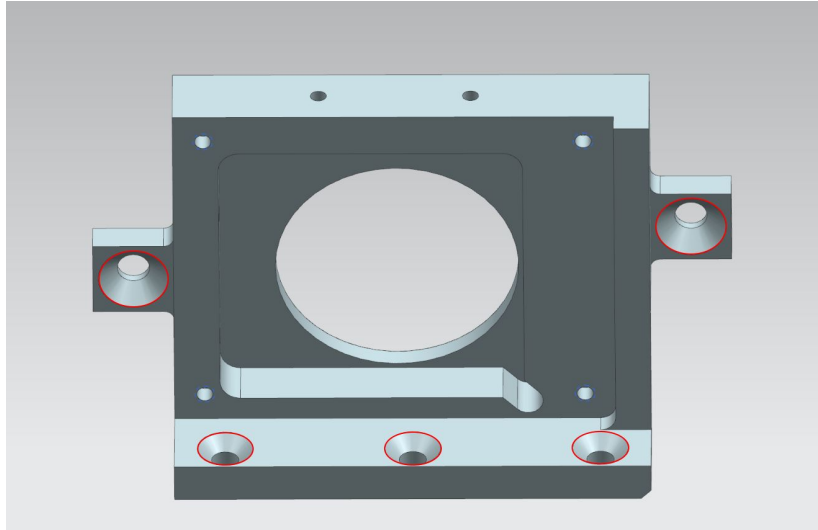
Figure 15: An overview of the cassette and its mounting holes.

The cassette also features chamfers at all the edges that run between the driving surfaces. This is done to avoid problems with imprecise machining and the need for perfect corners if chamfers are not included. These chamfers are highlighted in figure 16. A problem introduced when adding the chamfers, were that the driving surface areas on the X- and Y-axis were reduced. This meant that the position of the cassette would become more prone to follow the Z-axis driving surface. Because variation in translational positioning of the grating in the Z-plane has no effect on image quality as long as the rotational orientation is perpendicular to the slit and camera sensor, this problem was deemed acceptable.
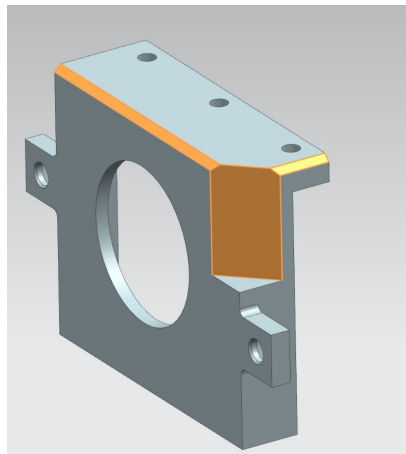
Figure 16: Chamfers on the cassette.

The front hole in the cassette has its center at the same XY coordinate as the grating itself. With a diameter of 24mm this ensures all the light from the front lens assembly reaches the grating. Figure 17 shows the designed path the light will be transmitted through the grating.
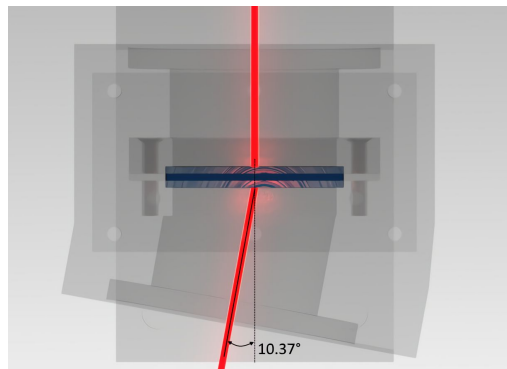
Figure 17: Illustration of diffracted light beam through the grating

This solution for keeping the grating in its correct position and orientation has gone through several redesigns. Figure 18 shows the original grating holder from the first V6 prototype, figure 19 shows the first version of a cassette-type design solution and figure 20 shows the design for keeping the grating positioned correctly.
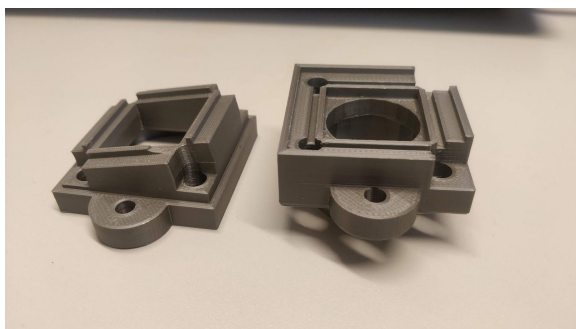
Figure 18: The original prototype grating holder
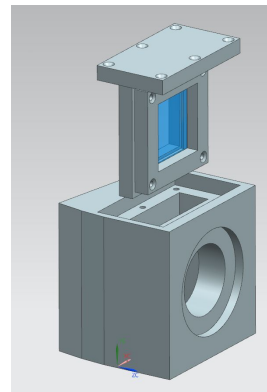
Figure 19: Early iteration of a cassette-type design
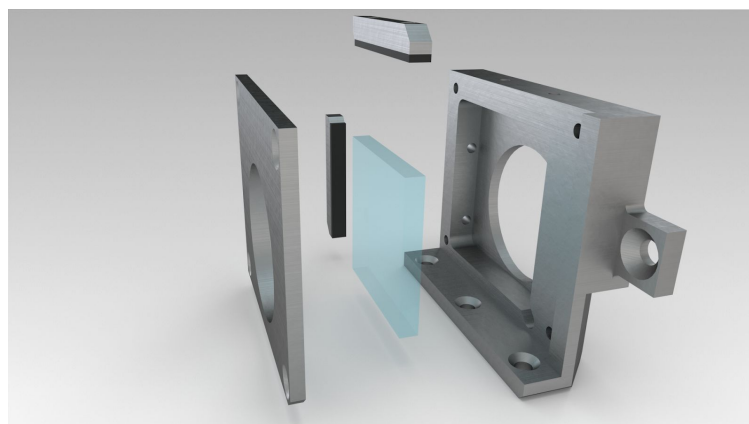
Figure 20: Current iteration of the grating cassette

Grating Shroud

The grating shroud provides light mitigation. The grating requires that the only light being led onto its surface is the light from the lens objectives. For the prototype, manufacturing time and ease of machining was deemed to be the most important factors for choosing a light-blocking concept.

The chosen concept for light mitigation was a *4-walled assembly w/o roof.* This method was deemed easy to manufacture, the walls would be tightened together well leaving no gaps for light. Gaskets and steps could be introduced to further block light if necessary in addition to the sharp internal corners giving more space to the grating holder support structure. However, the rigidity of this solution was deemed to be less than the other alternatives. It would be ill advised to include a solution with this large amount of different pieces in the flight model. The modular design was also less vibration safe. Additional modal simulations were required to decide on a further design. Furthermore a new design for the grating cassette incorporates the shroud functionality. The shroud might be omitted in the next iteration. The shroud solution can be seen in figure 21.
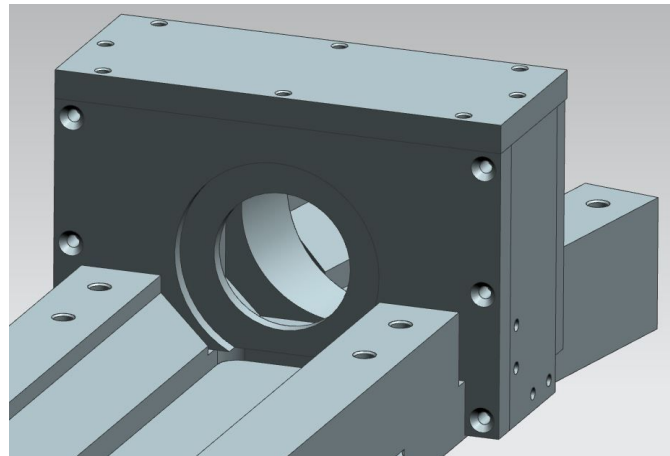
Figure 21: Shroud mounted on HSI Platform

Star Tracker Platform

The Star Tracker must be mounted rigidly to the HSI assembly. The reasoning behind this is the HSI is mechanically decoupled from the frame by the dampening solution. Consequently, the star tracker must be mounted with the same dampener solution in order to record the placement of the HSI and not the bus, since the exact relation between the two separate systems are unknown. A direct mounting solution to an extended front bracket was discussed, however this would lead to undesirable mode shapes during resonance. The rail solution has superior mounting capabilities as outlined in the star tracker design document. A 50 x 95 mm platform was added to the side of the rail. This solution was more stable than a clunky protrusion mounting. Figure 22 shows the star tracker platform, placement of holes and the driving surfaces created. Mounting holes and driving surfaces allowing for an exact placement of the star tracker at the desired 20-35 degrees were to be made further into the development due to issues relating to the Star Tracker size.
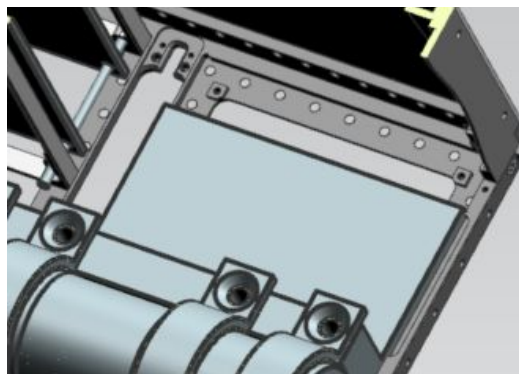
Figure 22: Star Tracker platform

The chosen star tracker has a final length of 82.6 mm, a max diagonal of about 90 mm. The large size of the star tracker facilitated a number of changes in the assembly, mainly the Front Objective Seating Groove needed to be slimmed down to accommodate the Star Tracker. The 6U CubeSat standard section 3.2.3 states that an item can protrude a maximum of 10 mm from the CubeSat sides, the +X side included. 3.2.3.1 further states that the rails act as the plane of measuring. The Star Tracker must be situated as close as possible to the outer limit of 10 mm to keep interference problems with the rest of the HSI assembly to a minimum. Further development might facilitate that the HSI assembly be offset in the -X direction, or that the Star Tracer be placed perpendicular to the HSI front objective to save space. As stated in The new SMAD, newer Star Tracker models can operate in spite of the earth albedo, thereby forgoing the placement angle [RD08]. Figure 23a shows the Star Tracker interface problem spot and figure 23b shows the available room along the Y-axis.
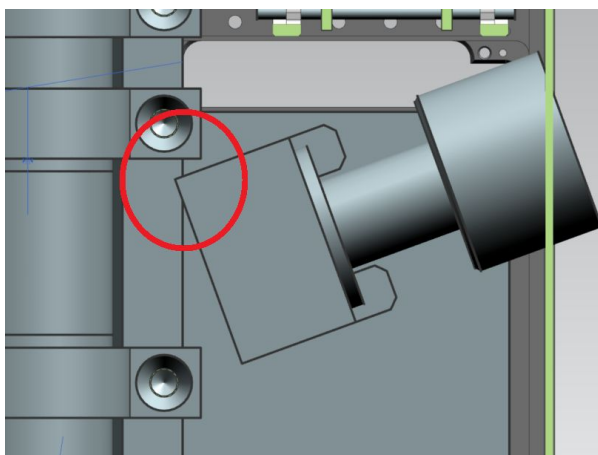
Figure 23a: Star Tracker collision
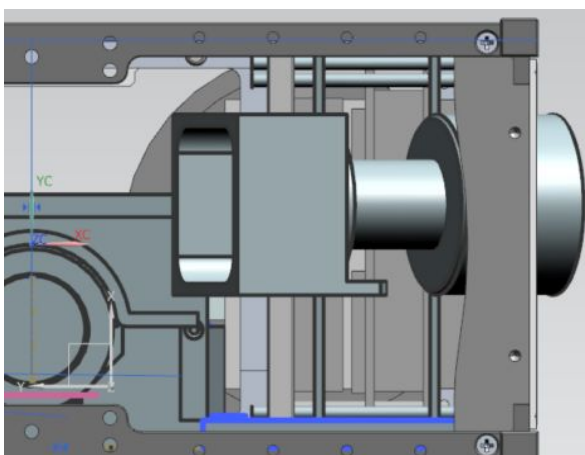
Figure 23b: Spatial room for Star Tracker

RGB Platform

The RGB camera was confirmed to be a part of the initial launch, and the specific camera chosen in early February 2019, was too close to the completion of the prototype. A mock up of the platform was created, with identical features to the Star Tracer Platform 50 x 95 mm. The RGB shell and mounting points are produced in a polymer material. This means that the entire shell had to be replaced by a new design made in a space rated material. Because of the unknown mounting factors retaining to the RGB camera, the interfacing, placement of holes and driving surfaces were decided after the initial machining of the prototype. Figure 24 sows the RGB platform and placement.
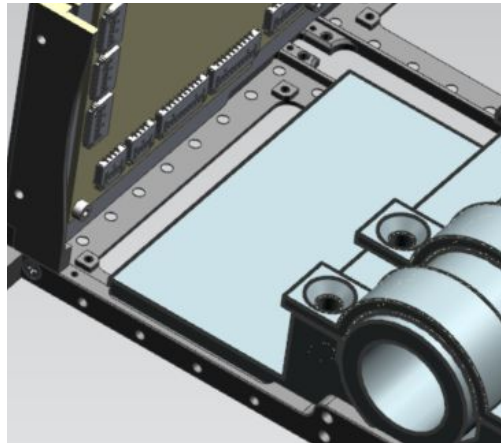
Figure 24: RGB Platform

4.4 Prototype Total Mass

Initial mass projections made during the PDR for the HSI assembly was 910g, with a 20 percent margin. The prototype was measured to be 1380g in NX, an increase of 51 percent, 70 percent if the 150g rail is included. In addition, the prototype has fastening solutions for a star tracker and an RGB camera. The additional platforms contributes 90g each, totaling in 180g additional mass not accounted for in the PDR mass projections. The prototype has a total mass of 1200g, the fastener platforms and rail excluded. However, the initial prototype was made disregarding the total mass. The main body could be slimmed down, and mass saving patterns added. The prototype was not within the 910g ± 20 percent mass projected for the PDR. The mass budget was updated, adding the 180g platform solution and 150 g rail. The new estimation was calculated at 1200g ± 20 percent.

4.5 Future Prototype Improvements

This section contains the most relevant future improvements for a potential new prototype. Results from tests, simulations and literature will be the criteria for eventral redesigns.

4.5.1 General Improvements

Mass Reduction

The initial functional prototype was designed to be simple to machine. The mass of the prototype was not a priority. Several solutions can be implemented in order to save mass in later designs. The following list contains proposed changes:

- The side walls of the prototype can be slimmed down
- The total surface area of the platforms can be lowered, however the thickness might increase
- Indentation patterns can be added to the prototype

Based on the results collected from modal simulations done in HYPSO-ANA-009, the current design would in fact benefit from mass reduction in the groove areas. The reason for this is that the first mode shape that will occur during vibration stems from bending in the groove area, which has the lowest stiffness in platform due to the low relative thickness, being almost 70% thinner than the rest of the platform. This suggests that removing weight in the groove areas as proposed would be beneficial in regards to increasing stiffness, thus elevate the frequency of the first mode shape.

Slit Tube In-House Redesign

In the current design the slit is mounted in a Thorlabs SM1M10 Housing Tube by retainer rings. This design was carried over from the HSI V6. It features one Thorlabs SM1A10 adapter in each end and utilizes spacer rings to approach the correct flange focal length. This is not an especially accurate way of getting this length precise. Thus, a better solution should be developed for the flight model to ensure the proper focus of the optical assembly. A preliminary design has been created that improves the precision of this essential part. Its main features are a slit tube with an integrated baffling plate that a slit plate can be pressed up against by a retaining ring. The slit would also be baffled in the other direction by a custom baffle ring. The proposed assembly is shown in figure 25.
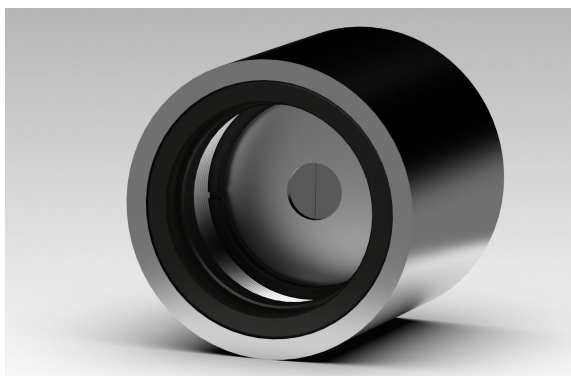
Figure 25a: Slit tube redesign   *Figure 25b: Cross section, slit tube assembly*
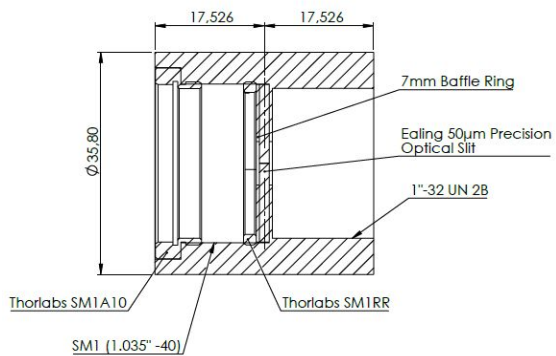
As can be seen from figure 25b, this design would eliminate the need for manually adjusting the slit to the correct flange length as is needed in the current design. A description of this manual process and its issues can be found in HYPSO-RP-006 [RD09].

Z-axis fastening of grating cassette

To lower the required drilling depth and substrate size, the positioning of the fasteners of the grating cassette towards the HSI platform was chosen to be closer towards the center for one of the sides. Moving the fastener towards the top of the grating cassette would be better for stability in ideal conditions. Whether this is necessary or not can be determined by testing. Thus, the simpler solution was chosen for now.

Light Proofing the grating area

The grating shroud solution is a simple cover to lower over the grating cassette. A more secure solution could be achieved by making "steps" to block the light. For now the idea is to screw it in place and use a gasket to seal off light.

Grating shroud rigidity

The grating shroud was made of a total of 5 parts. The front part was thin and had a large hole (D=24 mm) to accommodate for the lens objective. This part is potentially a weak part that can resonate at low frequencies. The thin walled structure comprising the shroud would also be structurally weak.

Moving the Shroud Functionality to the Grating Cassette

The main functionality of the shroud is to block light from entering the grating. However with some tweaking to the Grating cassette design, this functionality can be achieved by the cassette itself. A preliminary model of this can be seen in figure 26, where the whole shroud has been removed and the cassette modified to replace the shroud functionality. The design was 3D printed and a very basic functionality test was performed. It performed adequately for a simple 3D print and would be a very viable option as a permanent design change of the HSI geometry.
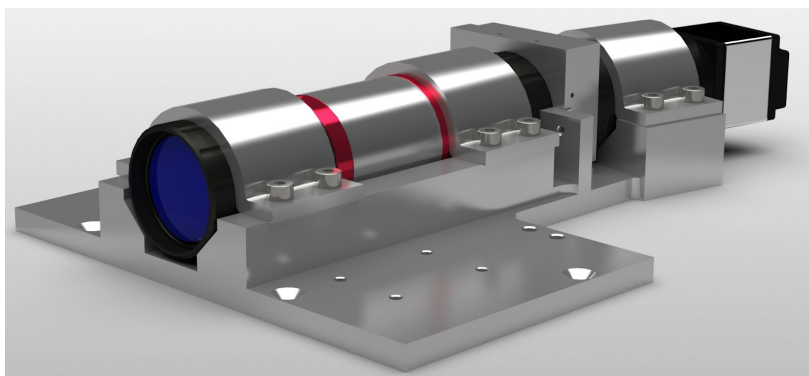
Figure 26: The shroud-less HSI redesign

Further tests would have to be performed to validate the design, but in principle it is an elegant solution that eliminates five components and lightens the payload. It also eliminates the potential problems with the shroud mentioned previously in this section regarding light proofing and the structural rigidity of the shroud.

Thin edges on cassette back plate

Due to the grating being 25x25mm and the recommended light hole diameter ~24mm, the gasket on the back-plate will have 4 edges of 0.5mm thickness. It is likely that this is too thin for practical purposes. A solution to this could be to have a gasket piece/square in each corner instead of covering the whole area.

Detector floating in air

In the current design the detector will float in space, connected only by the front threads. This is a concern, as lower frequency mode shapes induced by the vibrational loads during launch will occur at this part. For further prototyping, the detector should be secured with additional brackets. At the same time, the detector might need a thermal connector solution. Newer prototypes must accommodate the thermal solution and allow for correct wire placement.

Non-Countersunk Screw Solutions

For less complexity, non-leading screws without a countersunk profile where chosen due to simplicity. Additional tests are required to uncover if countersunk screws are necessary in those locations. These areas concern the outside of the cassette shroud and brackets.

Bolt length

The chosen length of the screw holes are somewhat flawed in this prototype. The length of these holes must be updated in the next iteration of the HSI prototype and be designed for standard screw lengths.

Objective Placement

The Front Objective Seating Groove was designed so that the front objective lens would be flush with the seating rail. For further prototyping, the objective could be pushed further out in the +Z direction. This would allow for a shorter total length of the prototype, or allow for additional support in the back for the detector. The lens can not extend beyond the body of the bus. Atomic oxygen could potentially be a risk factor with such a solution.

Objective Wall Width

As mentioned in section 1.3.1, the prototype design interfaces with the lens objectives via the seating grooves in the front and back. The objective placement in the y direction, or the distance between the contact points must be explored further.

Matt Black Anodization

To decrease the amount of reflection present on the inside of the optical assembly, anodization has been considered. However, to find out whether this is necessary or not, the first prototype was produced without anodization in mind. A risk with anodization is that outgassing and layer flaking might occur, something that is especially common for aluminium in the 7000 series. This would require additional testing as well. The anodization is a surface treatment that can alter the surface properties and tolerances. Due to the high precision tolerances required for the grating, an anodized solution will only be considered if the tolerances will not be exceeded.

Objective aperture replacement

As discussed in HYPSO-RP-005 [RD10] it would be beneficial for the objective cleaning process to disregard the aperture adjustment mechanism. A simple replacement for this would be to install a disc with a centered hole of the appropriate stop diameter instead of the current assembly. The optics follows the relationship:

$$N = \frac{f}{D}$$

Where N is the f-number (required to be f2.8 for the two front objectives and f2 for the back objective), f is the focal length (50mm for these objectives) and D is the pupil entrance diameter (effective aperture). However, it is not as simple as setting the aperture stop diameter to this pupil diameter. The front lens has a magnifying effect and this needs to be taken into consideration when designing a new aperture stop. If the aperture replacement is needed, Prof. Fred Sigernes would have to be consulted as the projects optical expert. At the present time it is not known whether enough information can be gained from Edmund Optics to accurately replicate the required aperture stop diameter in a redesign.

Back Assembly Angle

The back objective assembly is situated on a 10.37 degree angle to the grating, as this is the theoretical optimal angle [RD01]. However, a functional test was done on the prototype showing significant cut off in the image received by the detector. This could indicate that the angle should be raised. The full report can be found as *Functionality Test Report of HSI TTH Mk1.* Further testing must be done before the change of angle is solidified or scraped.

Ruggedization

In order to keep parts from vibrating loose, further steps will have to be taken to ruggedize the assembly. This will be done by adding epoxy to vulnerable parts such as screws and brackets. In addition to this, internal objective parts, as well as set screws will also be glued to prevent possible optical misalignments caused by vibrations during launch.
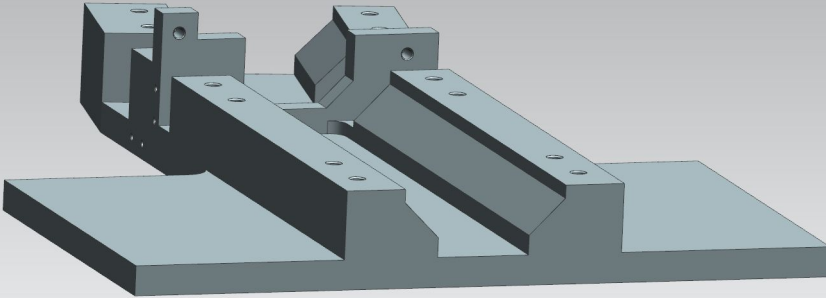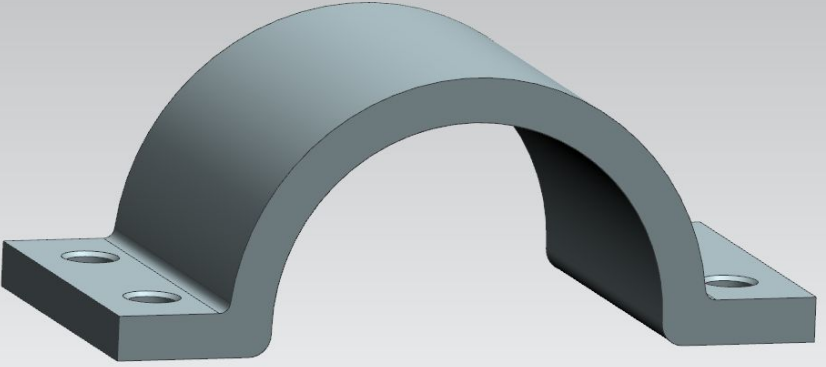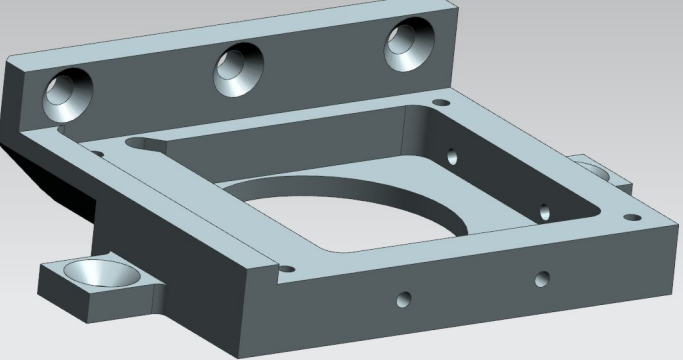
4.6 List of Prototype Parts
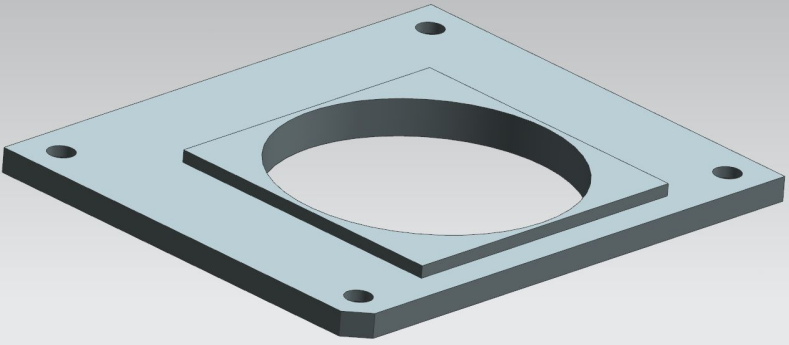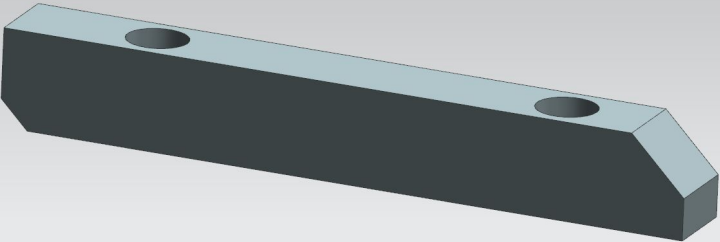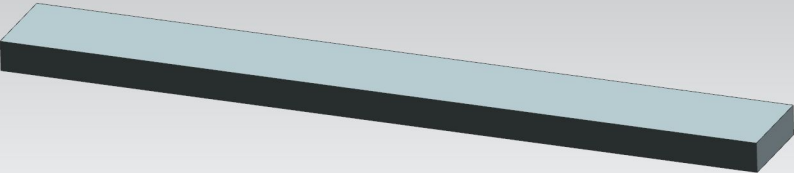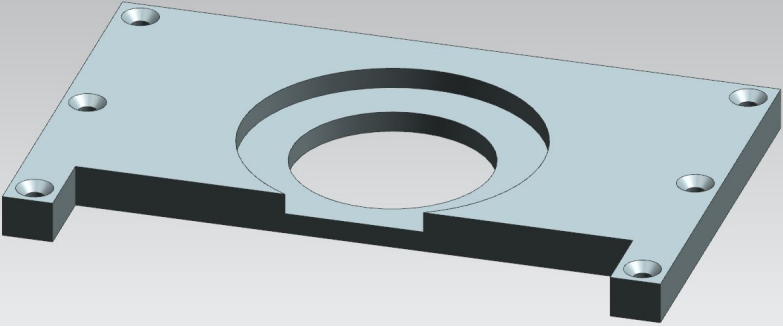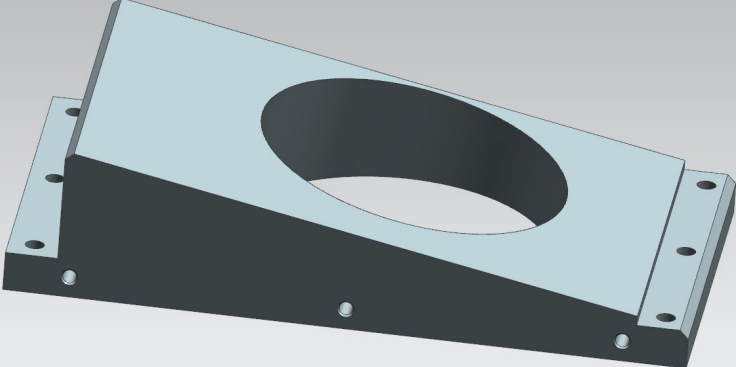
The HSI payload is made up from COTS components and specially made machined parts. The prototype consists of the following parts:

4.6.1 Machined Parts and Bolts

Table 7: Machined Parts

Part Name (Nr.)	Part Geometry	Qty
HSI Platform		1
Platform Bracket		3
Cassette Front *(Grating Assembly)*		1

Cassette Back *(Grating Assembly)*		1
Clamp Bracket *(Grating Assembly)*		2
Bracket Gasket *(Grating Assembly)*		2
Shroud Front *(Shroud Assembly)*		1
Shroud Back *(Shroud Assembly)*		1
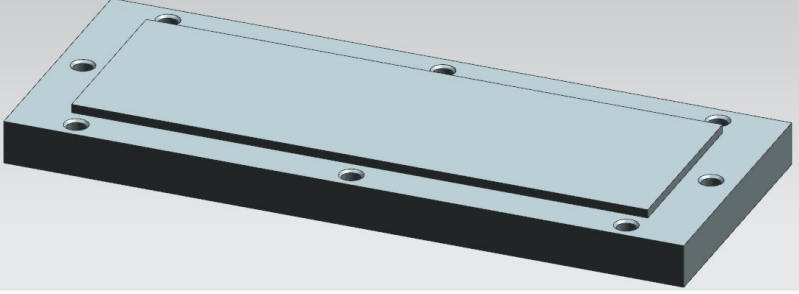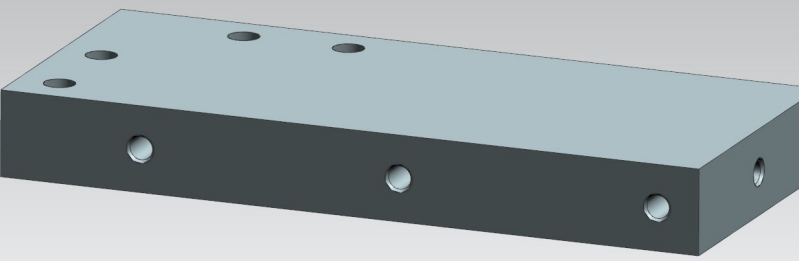
Shroud Top *(Shroud Assembly)*		1
Shroud Side *(Shroud Assembly)*		2
Shroud Gasket Front	TBD	1
Shroud Gasket Back	TBD	1

Table 8: Screws & Bolt locations

Screw & Bolt Type	Location	Qty
M2x4CSK	Cassette back	4
M2x8CSK	Shroud front	6
M2x6 Set	Grating cassette	4
M2X8CH	Shroud assembly (top,sides,back)	22
M2.5X6CSK	Cassette front-Platform (lips)	3
M3X8CSK	Cassette front-Platform (ears)	2
M4X10CH	Platform brackets	12
COTS		
M2x3 Set	Camera lens objectives	6

4.6.2 COTS Parts

All COTS components present in the prototype is tabulated in table 9.

Table 9: Optical COTS components

Description	ID	Appearance/geometry	Qty
50mm VIS-NIR Objective	EO#67-717		3
Blaze Angle Transmission Grating	EO#49-579		1
Camera Head	UI3060		1
C-Mount Spacer Ring, 0.50 mm Thick	CMSP050		2
Adapter Ring SM1 - C-mount	SM1A10		2
Slit Tube	SM1M10		1
Ø1" Mounted Slit, 50±3µm x 7mm	S50RD		1

5. Damper Integration

5.1 Purpose and preliminary work

Until specific testing of the objectives (both for the RGB and HSI) it is assumed that these payloads needs to be protected from the vibrations and shock during launch. It has therefore been decided that a damping solution for the HSI platform is necessary, should the need for the damping arise. This chapter shows the preliminary design of such a solution. The french company SMAC has provided a recommendation for a model which would be suitable for this application. The model is the 1114S shown in *figure 27a*, and can be delivered in a range of stiffnesses with an axial/radial ratio of 1.7. Thus the natural frequencies of the payload platform can be tuned to a desired frequency by choosing an appropriate stiffness along with the number of dampers.

The main purpose of the damping solution is to dampen and isolate lower frequencies that can occur during the launch of the PSLV and the micro vibrations that occur during the slew maneuver. However, according to the PSLV environmental testing requirements provided by NanoAvionics, the first fundamental eigenfrequency of the s/c is required to be above 135 Hz. The document is unfortunately under an NDA. This forces the dampener amplification over 135 Hz, it follows that the damping and isolation frequencies are also higher. Figure 27b shows a normal damping transmissibility curve. Micro vibrations are often at the 50-200 Hz frequency range, depending on the reaction wheels, which can result in a less than optimal amplification frequency. NanoAvionics has assured that the operation of the reaction wheels should not result in any harmful micro vibrations. The reaction wheels from NanoAvionics has a maximum controlled spin speed of 6500 rpm, which corresponds to roughly 110 Hz generated from each of the four reaction wheels present in the s/c. Further testing must be done in order to determine the effect of the micro vibrations on the HSI operation capabilities.
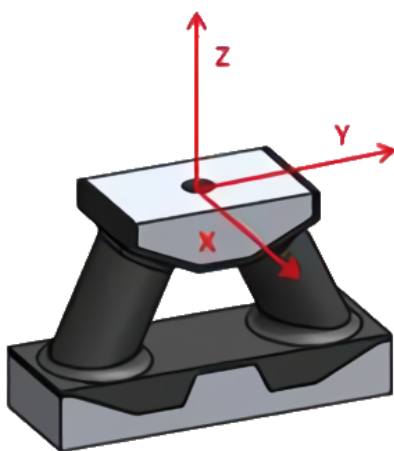
Figure 27a: The 1114S damper
from SMAC, local CS
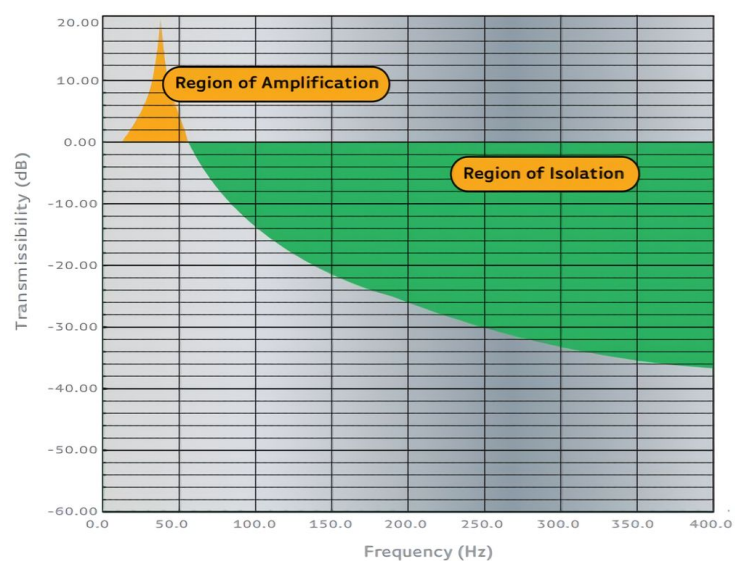
Figure 27b: General Transmissibility/ Frequency curve
for a damper. Note: not the curve for 1114S [RD11]

5.2 Mass Distribution

The eigenfrequencies of the HSI platform is dependent on its mass distribution and center of gravity. These factors are also important to determine the optimal placement of the dampers themselves. Total mass and CoG coordinates are displayed in table 10.

Table 10: Center of Gravity of Fully Assembled HSI

Total Mass [kg]	CoG (X, Y, Z) [mm]
1.73	**(-111.36**, **-56.21**, **233.86**)

The spatial location of the CoG is shown in figure 28. It is worth noting that these calculations were done with the proposed fastening solution of the dampers included as their weight directly affects the mass distribution. The cut-off point for the measured mass was set where the dampers themselves are excluded as they are the dampening element and everything above them the damped mass. This makes it possible to theoretically calculate the expected shift in the resonance frequencies when dampers are included.
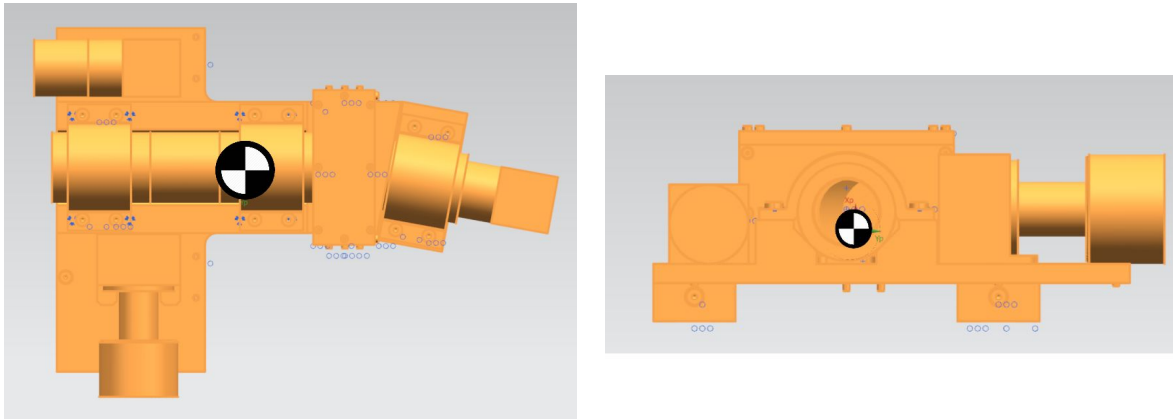
Figure 28: The location of the CoG in the HSI assembly

As can be seen from the location of the CoG it is approximately geometrically centered. It is slightly offset in the +X direction, something that was expected due to the angle of the HSI itself. However, this offset is very small and is not expected to manifest to any particular degree in the resonance frequencies. The CoG also lies somewhat offset from the main damper concentration, section 5.3, in the -Z direction. This could affect the resonance frequencies as the -Z end of the HSI has fewer dampers and could give excitement to this end in the lower end of the frequency spectrum.

5.3 Layout

The dampers shall serve a bridging function between the frame of the bus and the HSI platform. Because of this they have to be fastened securely to both components while providing a solid and strong connection. Any shifts in these connections would misalign the HSI and RGB which would heavily impact the mission. The dampeners could even be affected by creep, resulting in the same effect. However, SMAC has guaranteed that no noticeable creep will occur during the CubeSat life cycle. The orientation of the satellite in the launch vehicle is not known, and therefore it was decided that the dampers needed to be implemented with alignment along the three global axes as shown in figure 29. This was done to ensure that sufficient strength is present regardless of orientation.
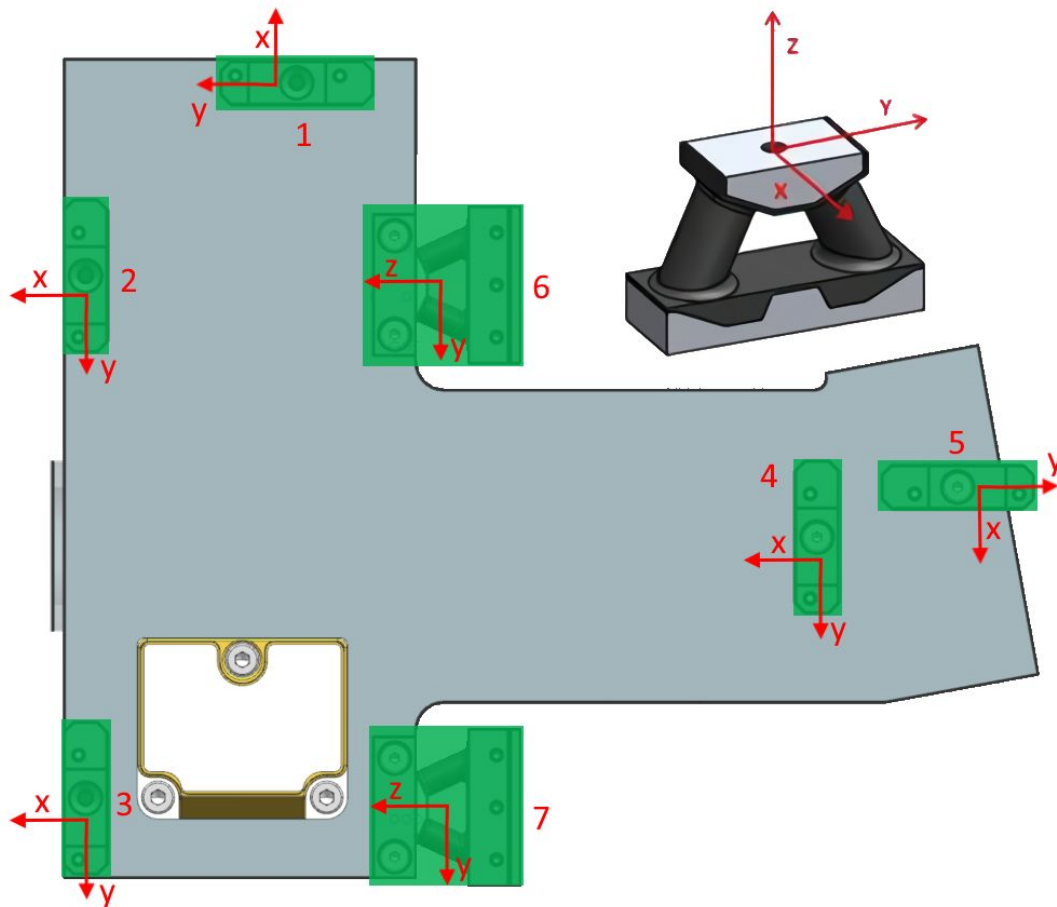
Figure 29: Layout and orientation of the dampers shown in red.

It is worth noting the asymmetrical layout of the dampers. This is a consequence of the limited space within the bus as well as the limited amount of mounting points the frame has along with the 10.37° angle of the HSI. The impact of this asymmetry is unknown until simulations are complete.

5.4 Interface Design

The 1114S comes with a M3 threaded hole on each side for mounting. The tapered end and the base end will be connected to the payload and bus frame respectively. Damper number 1, 2, 3, 4 and 5 use the same universal bracket to interface with the bus. The bracket is fastened to the bus frame by two countersunk M2.5 screws and to the damper by a countersunk M3 bolt.This bracket was designed to fit in all available positions on the frame to make it possible to move around the mounting locations in alter configurations of the layout. Using the same bracket for all vertical mounting spots also reduces cost by only needing to machine one geometry and therefore reducing the setup-time for machining operations. Its use in two of the locations are shown in figure 30.
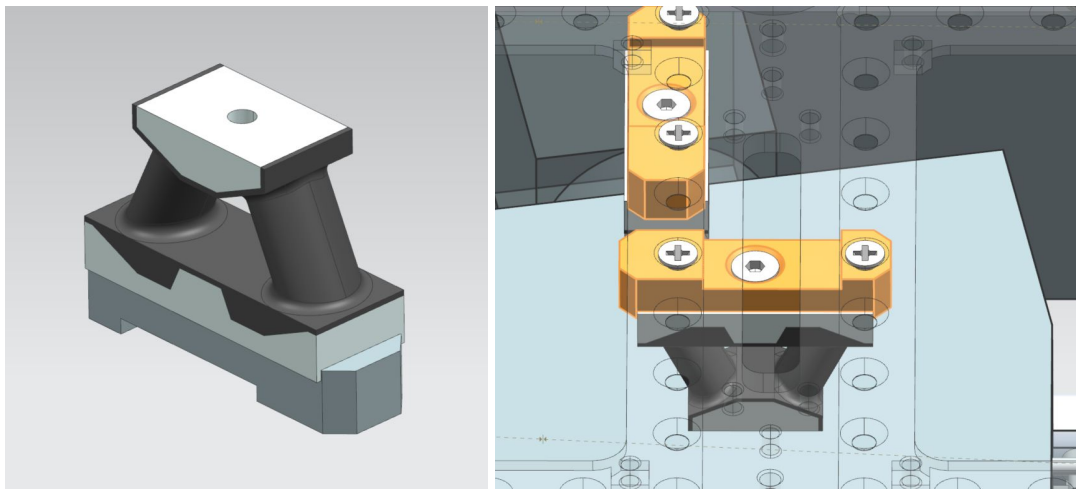
Figure 30: The universal bracket render (left), shown in position 4 and 5 (right)

The two dampers lying flat in the XZ-plane at location 6 and 7 are mounted by two custom brackets as shown in figure 31. They provide a secure mounting for the damper and are possible to move or add to other locations as well. The big bracket is fastened to the bus by three countersunk M2.5 screws and to the damper by a countersunk M3 bolt. The small bracket is fastened to the HSI platform by two Countersunk M3 screws and to the damper by one countersunk M3 screw.
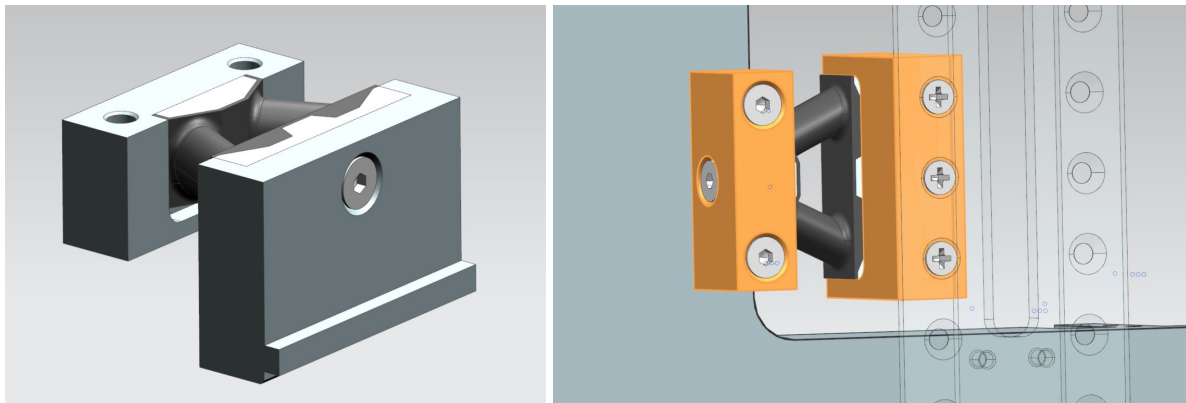
Figure 31: Horizontal damper assembly render (left), shown in position 7 (right)

5.5 Suggested Changes to the Damper Layout

The layout described in section 5.3 was presented to SMAC and then evaluated by them. The company responded with a revision to the configuration, as shown in figure 32.
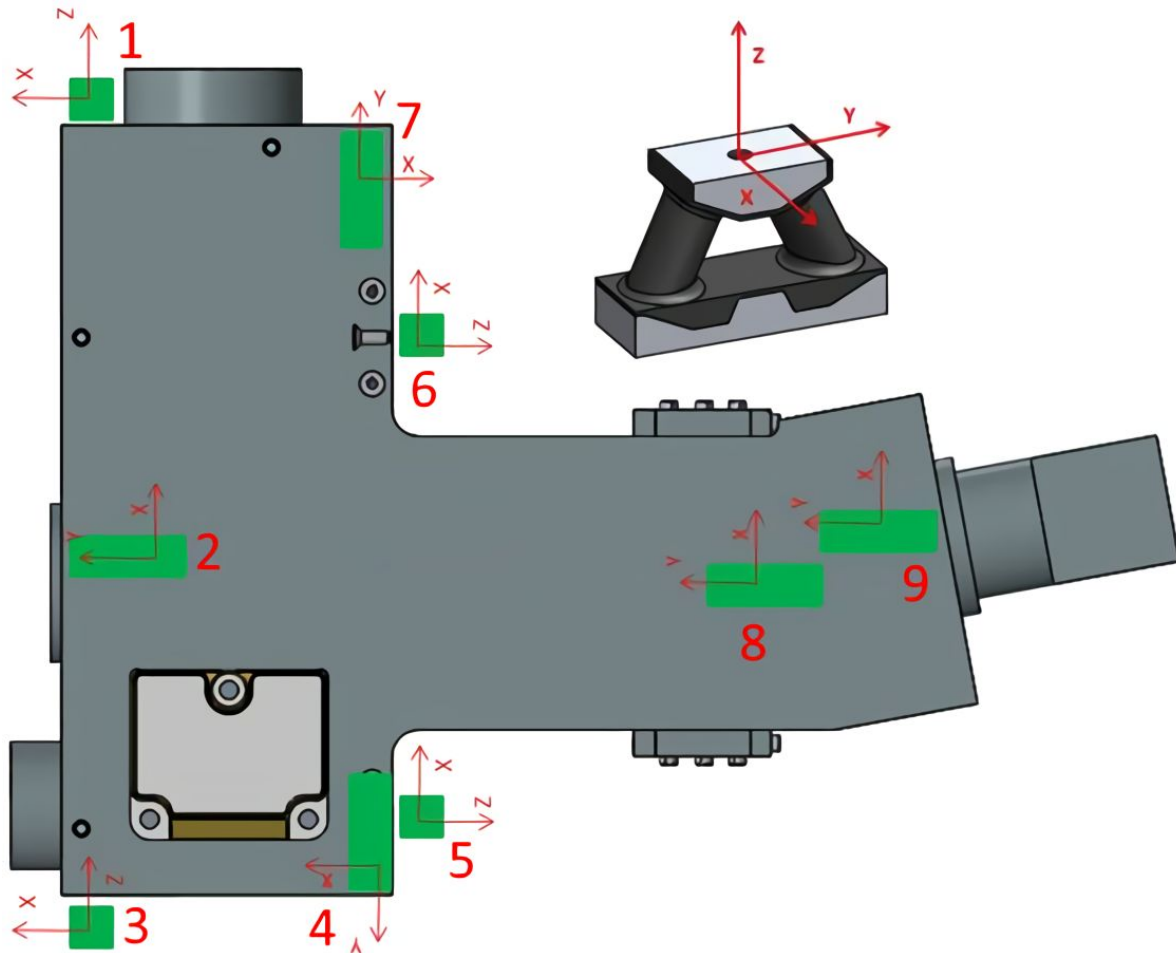
Figure 32: The suggested damper layout from SMAC

Due to limited time this configuration has not yet been implemented in the model, and therefore it is unknown how much the platform design would have to change to accommodate this new layout. The most apparent challenges are as follows:

- Limited space for damper 3 to be integrated. The inner +YZ wall of the bus is occupied by the payload controller and mounting a damper in the suggested position could therefore be very difficult.
- Damper 4 and 5 are positioned very close together and this could cause some issues with the available room on the bus frame for mounting. An alternative here could be to design a joint bracket for interfacing with said frame.
- Damper 2, 8 and 9 would have to be offset from the middle along the +/- X axis to avoid interfering with the raised middle portion of the bus frame. In the suggested configuration the universal bracket would not fit and would have to be drastically redesigned.

An approximation of the resonance frequencies under low levels of load for this layout was also calculated by SMAC, shown in table 11. The solicitation axis reference the HSI coordinate system.

Table 11: Approximation of damped resonance frequencies

Mass	1.0 kg	1.0 kg	1.0 kg
Solicitation	Axial Y	Radial Z	Radial X
Fr 0.5g	110 Hz	78 Hz	72 Hz

The approximated mass was only 1kg. This is lower than the actual platform + payloads mass, but these frequencies only serve as a preliminary estimate to base further calculations on. As can be seen the resonance frequencies are too low if compared to the PSLV launch requirements and the stiffness of the dampers would therefore have to be increased to conform to said requirements.

6. Thermal Design

This section summarizes the thermal design and considerations that has been done on the prototype and the thermal control systems that can be attached. Most of the decisions regarding the thermal control stems from the thermal analysis done in ANA-008.

According to the analysis, the unanodized platform is balanced towards the hotter side due to the thermo-optical properties of machined aluminum, measuring 29.08°C to 41.08°C in the hot case. The heat is however desired when the temperatures of the rigidly connected payloads are balanced on the colder side.

To account for the heat generation of the IMX249 processing chip, one or more PGS thermal strap connections will be added between the chip and the bottom surface of the HSI platform. To accommodate for the strap, a compression interface will be designed into the platform comprised of threaded holes and a simple aluminium plate with matching clearance holes that can be screwed on with a controlled torque.

Further steps to balance out the platform temperature is to add a plate at the front of the CubeSat. The plate will keep thermal radiation from leaking out too much at the front, something that was suggested by the analysis results. Another solution to this would be by packing the platform as well as the payload in a multi-layer insulation (MLI) packing, which would more effectively reduce the gradients along the platform [RD12]. The current iteration of the platform does however not lend itself very much to packed in MLI due to the geometric shape and time constraints. Following the analysis, the addition of a plate appears to be sufficient with respect to the thermal requirements. The satellite platform should however be tested in a TVAC environment in order to characterize the performance in this solution.

7. Analytical Analysis

7.1 Touching Surfaces

The positioning of the driving surfaces in the groove had to be calculated, so that exact positioning of the lens objectives could be determined and controlled with accuracy. This was done using basic geometry, considering the cylindrical objectives resting on the 45 degree driving surfaces of the platform groove, which would decide the position of the objectives in the XY-plane. When deciding the position of objectives, it was important to make sure that the cylinder center aligned with the center of the visible grating from the cassette. The touching area between a perfect cylinder and a flat surface is in theory a singularity or an infinitely thin line. However local deformation will occur, leading to some amount of resting area. The following equation can be used to calculate the half width of the resulting touching area [RD13].

$$b = \sqrt{\frac{4F[\frac{1-v_1^2}{E_1}+\frac{1-v_2^2}{E_2}]}{\pi L(\frac{1}{R_1}+\frac{1}{R_2})}}$$

The resulting area can be estimated with the use of two touching cylinders, one having an infinite diameter to simulate a flat surface. When both the materials are the same, the equation can be further simplified to:

$$b = \sqrt{\frac{(8FR_1)(1-\nu^2)}{\pi LE}}$$

Two cases were calculated:
Normal Case: full touching between the platform and objective
Worst Case: Limited touching, limited to the outer red rings of the objective

For the normal case the allowed clamping force will exceed 1KN due to the local deformation occurring at the touching surfaces.

The touching surfaces of one objective to the HSI platform was calculated to be roughly 0.04 mm in width, and the max allowed clamping force of 56 N for yield when experiencing a 98 G shock in the -Y direction (SF =1.4).

Despite the safety factor against yielding for the normal case, additional precautions has been planned in order to increase the structural integrity of the objectives following the reasoning behind section 4.5.1, ruggedizing. This will be done by application of epoxy to objective surfaces not in contact with the platform grooves, which will balance out the stress concentrations as well as decrease the probability of vibration induced misalignments.

7.2 Translational Lens Movement

When the lens objectives are pushed down by the platform brackets, small amounts of elastic deformation will happen. The degree of this elastic movement had to be calculated so that the position of vital optical parts are known. This made it possible to make evaluations whether preventive measures should be made or not.

7.3 Bolt Force and Frictional Forces on Objective

This section shows the calculations done for the required screw tightening moment and friction forces on the front optical assembly and the grating. Other bolted connections are deemed less sensitive and their tightening force have therefore been determined by over-dimensioning and rule of thumb principles.

Front optical assembly

The function of the brackets is to prevent the front optical assembly from sliding. The worst-case scenario for this type of sliding would be if the satellite was oriented with its Z-axis along the direction of shock detailed in section 2.3.1. Below is shown the calculation of the required bolt force and the ensuing bolt tightening moment.

$$F_S = (2 \cdot m_{objective} + m_{slit\ tube}) \cdot 98g = 313.41N$$

Where F_S is the force on the optical assembly due to shock, m is masses and $g = 9.81 \frac{m}{s_2}$

Thus the friction force imposed by the clamping pressure from the brackets needs to be higher than this value by a safety factor (SF). This SF is chosen to be 1.4 per the NASA standard and is incorporated into the shock load, as per NanoAvionics requirement.

$$F_C \cdot \mu \geq 313.41$$
$$F_C \geq 522.3N$$

Where F_C is the clamping force on the objectives from the brackets and μ is the friction coefficient between aluminium and steel, which is approximated to $\mu = 0.61$ in this calculation [RD16]. This force can then be divided among the eight screws exerting force on the brackets:

$$F_{screw} = \frac{522.3N}{8} \approx 65N$$

An approximation for the required tightening moment is given by [RD14]:

$$M_{tightening} = F_{screw} \cdot d \cdot k_s$$

Where d is the screw diameter and k_s is a dimensionless constant given by:

$$k_s = 0.0232 + 0.522\mu_{thread} + 0.67\mu_{head}$$

Where μ_{thread} and μ_{head} are the friction coefficients between aluminium and steel equal to 0.61. This gives:

$$M_{tightening} = 90N \cdot 4mm \cdot 0.75 \approx 200Nmm$$

Thus this value signifies the minimum required tightening force on each of the bracket bolts to hinder the optical assembly from sliding under shock.

The calculated tightening force per objective gives a SF of 0.92 in the worst case scenario for -Y directional shock at 98G. However as noted in SMAD, the shock will not be directly transferred into the payload, due to the bolted connections mitigating the shock propagation through the CubeSat [RD08]. The dampener solution will further mitigate the shock.

Grating clamping

The grating is a sensitive component and thus the clamping force needs to be calculated carefully to avoid damaging it due to over-compression. However, it needs to be held reliably in place as any deviation in its positioning reduces the quality of the final spectrogram. The main body of the grating is made of B270 glass which has a breaking strength of 30 MPa [RD15]. It is compressed along all three main axis, and compressive forces can be adjusted according to the tightening moment of the screws in the brackets and the back plate. To calculate the resulting stress from the compression, the Von Mises yield criterion was utilized. It was assumed even pressure distribution over all sides with:

$$\sigma_x = 20\,MPa$$
$$\sigma_y = 20\,MPa$$
$$\sigma_z = 30\,MPa$$

These values were then used to solve the reduced stress cubic equation

$$\sigma^3 - \sigma^2(\sigma_x + \sigma_y + \sigma_z) + \sigma\,(\sigma_x\sigma_y + \sigma_y\sigma_z + \sigma_x\sigma_z) - \sigma_x\,\sigma_y\,\sigma_z$$

With roots of:

$$\sigma_{11} = 20\,MPa$$
$$\sigma_{22} = 20\,MPa$$
$$\sigma_{33} = 30\,MPa$$

The principal shearing stresses can be found with the equations [RD16]:

$$\left|\sigma_{12}\right| = \left|\frac{\sigma_{22} - \sigma_{11}}{2}\right|, \quad \left|\sigma_{23}\right| = \left|\frac{\sigma_{33} - \sigma_{11}}{2}\right|, \quad \left|\sigma_{31}\right| = \left|\frac{\sigma_{11} - \sigma_{22}}{2}\right|$$

That can in turn be used to solve the Von Mises yield equation:

$$\sigma_V = \sqrt{\tfrac{1}{2}\left[(\sigma_{11} - \sigma_{22})^2 + (\sigma_{22} - \sigma_{33})^2 + (\sigma_{33} - \sigma_{11})^2\right] + 3(\sigma_{12}{}^2 + \sigma_{23}{}^2 + \sigma_{31}{}^2)}$$

$$\sigma_V = 15.81 MPa$$

Nevertheless, it is highly recommended that further testing of the grating is done as what looks like surface cracks have been observed on grating surface in the assembled NTNU-1 camera. It is postulated that the cracks observed are from the layer of diffraction material particles delaminating as a result of stress concentrations. Figure 33 shows the cracked grating surface. The test should aim to uncover a rough limit for the compressive forces allowed, or at least be a vital part to inspect for future mechanical full assembly tests. The prior is recommended, but will take additional time that should also be factored in.
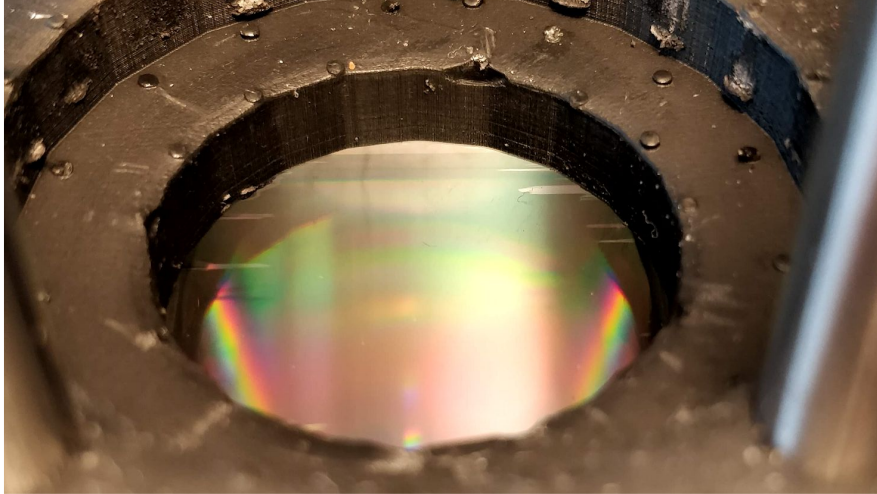
Figure 33: Flaking damage to the grating surface, HSI NTNU-2

7.4 Contact forces on objectives

Not yet available. (TBD)

7.5 Tightening Moments List

Table 12 tabulates the tightening moments that will be used for the following locations.

Table 12: Tightening moments

Location	Screw Dimensions	Number of Screws	Tightening Moment [Nmm]
Cassette Front	M3 x 8 CSK	2	250
Cassette Front	M2,5 x 6 CSK	3	250
Objective Brackets	M4 x 10 CH	8	270
Grating Bracket	M2 x 6 SET	4	-
Cassette Back Plate	M2 x 8 CSK	4	-

7.6 Thermal Absorption of Platform

Because the mass of the platform is considerable when compared to the heat energy generated by the rigidly connected payloads, the temperature should remain steady. This is however without bus environment and radiation considered, which are affecting factors. If the worst hot case scenario is considered, i.e., when all components are used at their maximum duty cycle, the maximum theoretical increase in temperature per orbit can be calculated using the simple definition of heat capacity:

$$\Delta T = \frac{E}{c * m}$$

The resulting increase of temperature was calculated using a total mass of m=997.83g for the platform only, and a total heat energy of E=1694.5J, and the specific heat of AA6082 c=899.82J/kgK, resulting in an increase of 1.89°K per orbit. This is without the mass of all the COTS components considered, which would contribute to absorption of heat energy, evening out the temperature fluctuations even more. Under the transient conditions of the orbital space environment, the heat will be dissipated through radiation, as the platform would function as a radiator. This means that the biggest influence on the temperature of the HYPSO platform will be radiation to and from the inside of the s/c environment.

8. Prototype Testing

The TTH Mk1 prototype was completed May 1st 2019. Several tests were planned for the prototype. Table 13 tabulates the planned full scale tests on the entire assembly. Note that the planned tests are limited to development tests. It follows that in addition the qualification tests must also be done on the prototype in accordance with the PSLV rules. The development tests will provide useful information regarding requirement refining and assembly functionality.

Table 13: Full HSI Assembly Test List

Test Type	Purpose	Planned Test Date
Functional Test	To uncover the functionality of the assembled optics on the prototype. In addition, the data will be used to refine the requirements and will be helpful for further prototypes and missions	10.05.2019
Vibration Test	The vibration test is done in order to uncover if the current design can survive the launch. The test will first be done without dampeners.	Summer 2019 (TBD)
Shock Test	The vibration test is done in order to uncover if the current design can survive the launch. The test will first be done without dampeners.	Summer 2019 (TBD)
Thermal Test	The thermal test will help establish numerical limits for the allowed thermal gradient in the assembly. The thermal test will also provide information on the operational temperature limits of the prototype	Summer 2019 (TBD)

Appendix A: Concept Selection

The purpose of this document is to quantify and elaborate on the concepts for the interfacing between the HSI camera and the provided bus from NanoAvionics. Several different concepts were considered, this document only presents the concepts that made it through an initial selection.

Concept Nr.1: Integrated Bracket Mounting

This concept was chosen in the specialization report, however, due to the complexity, other concepts had to be considered. The design comprised of many parts held together with threaded rods which introduced additive tolerance stacking to the optical precision. Figure 1 shows the concept sketch.
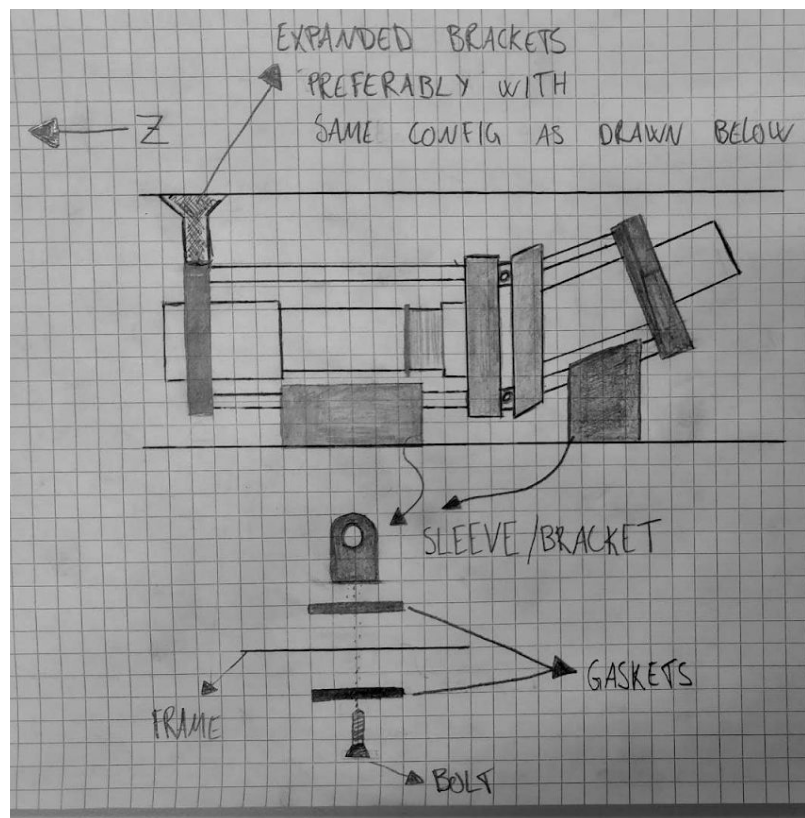
Figure 1: Integrated Bracket Mounting Concept

Concept Nr. 2: L-Shape Platform

The L-shape platform would also be possible to machine using a 3-axis CNC. It would have a low number of parts, in addition to having a controlled amount of leading surfaces. The problem of the L-shape platform was the slightly higher difficulty of applying an equal amount of force to the Y- and X-axis on the objectives. As with the bilateral platform, housing additional ADCS payloads would not be difficult. Figure 2 shows the concept sketches.
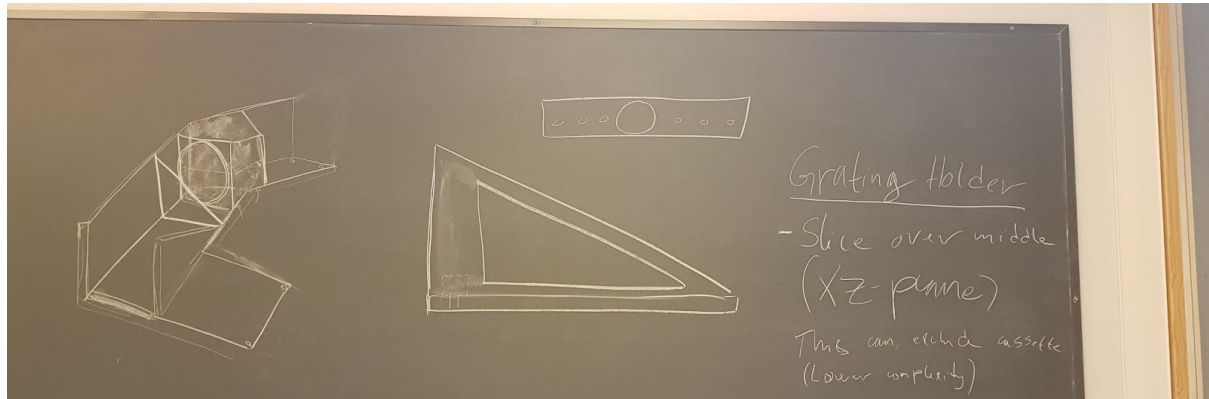
Figure 2: L-shape platform concept

Bilateral Platform

This design solves the complexity issues and also makes it easy to mount the RGB, Star Tracker and IMU with a rigid connection. It employs one platform to mount the whole optical train as well as the additional payloads and components. Another advantage is that it is possible to machine the whole platform in a 3-axis milling machine, something that makes it possible to make on campus. Figure 3 shows the concept sketch.
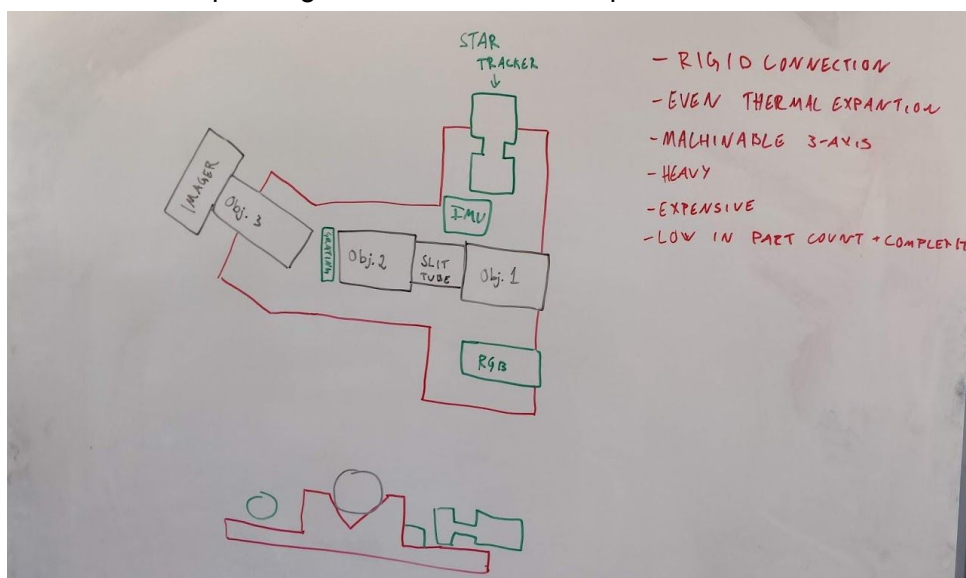
Figure 3: The bilateral platform concept

Final Concept selection

A pugh matrix was used to make the final selection. The criteria were based on interviews with NanoAvionics and the HYPSO management. The weighting for each criterion varies between 1-5, where 5 is imperative and 1 is not important. Each concept is then given a score from 1-5 where 5 is favourable properties in the given criteria and 1 is not favourable. They have all been tabulated in table 1, Selection Matrix.

Table 1: Selection Matrix

Selection matrix for HSI payload integration			
Weighted Criteria	**Concept nr: 1** Integrated Bracket Mounting	**Concept nr: 2** L Shape Platform	**Concept nr: 3** Bilateral Platform
(3) Design Complexity	1	3	2
(4) Machinability	2	2	3
(5) Optical Accuracy	1	4	5
(5) Thermal Misalignment Resistance	2	3	4
(5) Shock Resistance	1	3	4
(4) Vibration Resistance	1	3	3
(4) Stiffness to Mass ratio (Frequency)	4	4	3
(2) Total Mass	4	3	2
(2) Mechanical Integrity (Strength)	1	5	5
(3) Required Space	3	3	4
(4) ADCS Integration Compatibility	2	5	5
Total Score:	**68**	**140**	**153**

Concept 3: Bilateral Platform was chosen based on the results from the selection matrix and from consultation with NanoAvionics.
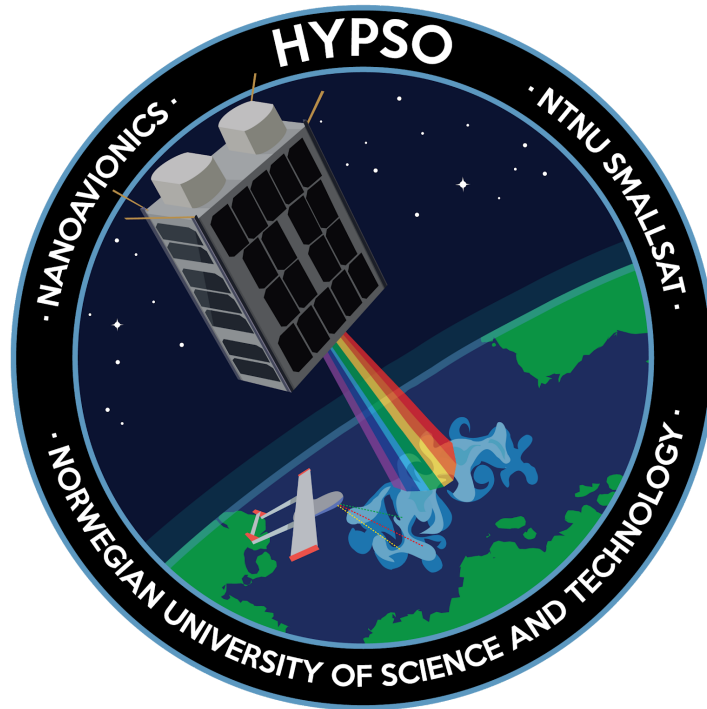
Appendix C

HYPSO-ANA-006 Analysis of Optical COTS Components

Analysis of Optical COTS components

HYPSO-ANA-006

Table Of Contents

Table 1: Table of Changes

Rev.	Summary of Changes	Author(s)	Effective Date
1	*First issue*	*Tord Hansen Kaasa,*	*02.04.2019*
2	*Formatting of text*	*Tord Hansen Kaasa, Tuan Anh Tran, Henrik Galtung*	*25.05.2019*

Executive Summary

After disassembly and assessment of all available optical COTS components (RGB lens was not assessed), several potential problems have been uncovered within all options. Based on the vulnarbilities uncovered, several mitigation strategies was created. Upon further evaluation, the following strategies and components are recommended moving forward.

HSI Objective
- Adapt the current 50mm VIS-NIR objective or order the parts if available

HSI Detector
- Create a custom housing for the UI-5261SE-M-GL PCB detector

RGB Detector
- Adapt the UI-1250SE-M-GL detector

RBG Objective
- Not evaluated

1. Overview

The HYPSO mission will enable low-cost and high-performance hyperspectral imaging and autonomous onboard processing that fulfil science requirements in ocean color remote sensing and oceanography. In order to achieve a low-cost solution, COTS components will be used as opposed to space graded solution. Space grade components are relatively expensive compared to COTS due to the amount of documentation required in order to prove space grade authenticity for each delivered component. At the same time, the use of COTS components induce several challenges regarding planning, testing and adapting to ensure that the COTS components are acceptable and fulfil the requirements set by the *6U CubeSat standard [RD01]*, and the launch provider.

1.1 Purpose of document

During the planning stages of the HYPSO project, several COTS detectors and objectives were looked into based on their optical characteristics. During disassembly of the COTS components, several potential harmful materials were found. This report contains an assessment of all potential objectives and detectors. The report also contains an evaluation of the actions that should be done in order to mitigate the risks associated with the detector and objective components. The aim is to create an overview of previous examinations and analysis of the findings as a whole. The individual assessment reports provides additional data as well as a thorough disassembly procedure for further testing and adaptations. Figure 1 shows the relation between this analysis and the design documents, while figure 2 shows the relationship with the previous assessment and mitigation reports.
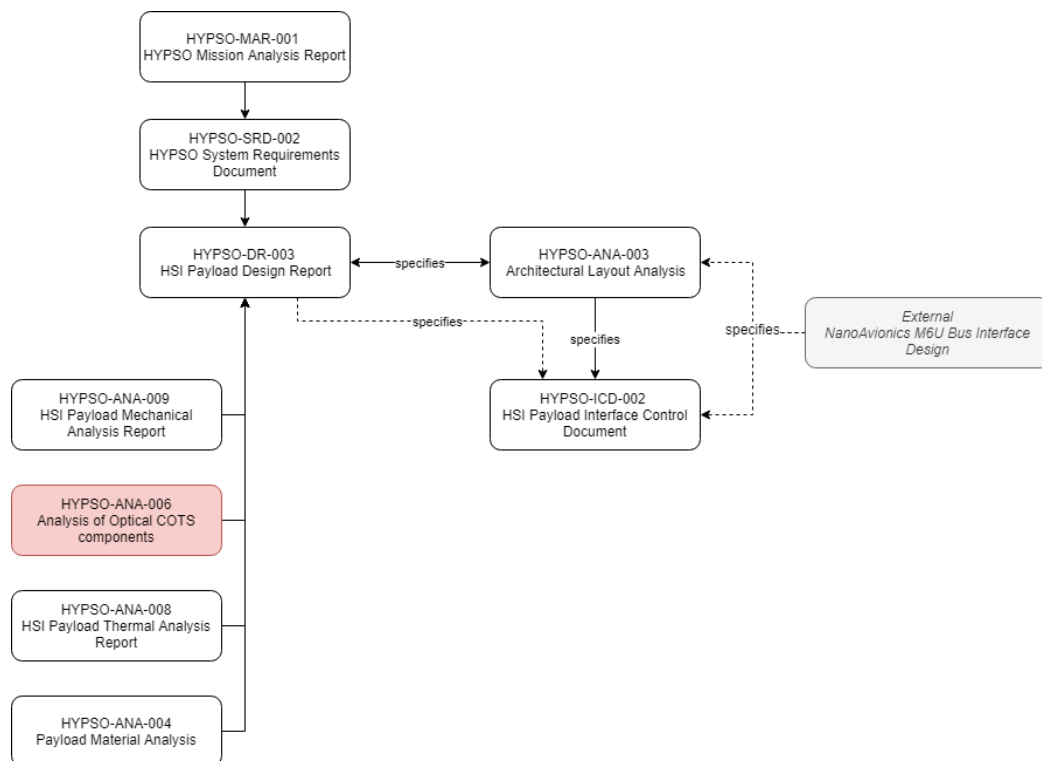
Figure 1: Document relationship to design documents
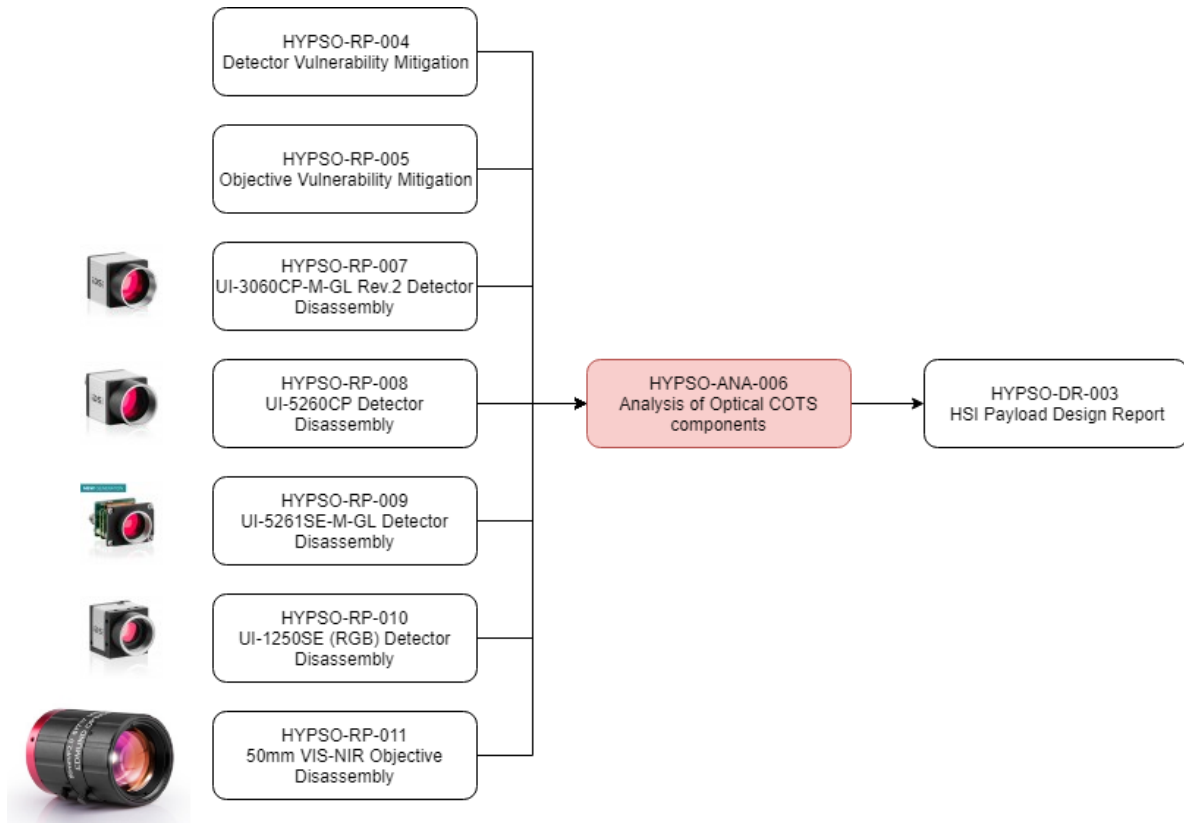
Figure 2: Document relationship with referenced documents

1.2 Requirements

The use of COTS components sets strict rules for what is acceptable to use on the mission. This is due to the fact that COTS components are not inherently space graded and must be qualified by testing and documentation. The main material requirements for components on CubeSats are listed in the *6U CubeSat standard [RD01]:*

3.1.7.1 CubeSat materials shall have a Total Mass Loss (TML) < 1.0 %
3.1.7.2 CubeSat materials shall have a Collected Volatile Condensable Material (CVCM) < 0.1%

The proposed outgassing requirements are based on typical pass/fail criteria used by NASA during qualification for most spacecraft materials [RD02]. The values are stated as *conventional wisdom,* and should not be interpreted as absolute. However, the effect of outgassing on the HSI camera by different material sources has yet to be tested, the values presented in the standard will be considered. Polymer materials will be avoided due to the high risk of outgassing [RD03]. All polymer and other potentially high outgassing materials that is necessary to bring like PCB materials, must be tested.

Ferromagnetic components can be used if no substitution can be done, however bolts should be non ferromagnetic. Ferromagnetic materials can influence the measurements from the magnetometers [RD04]. Ferromagnetic materials in the payload may potentially disrupt the magnetorquers, although tests must be done in order to characterize the disturbance.

1.3 References Documents

The documents listed in table 2 have been used as reference in the creation of this document.

Table 2: Referenced Documents

ID	Author	Title
[RD01]	Cal Poly SLO The CubeSat Program. 2018	6u cubesat design specification rev. 1.0. Accessed April 2019. [Link]
[RD02]	NASA Contractor Report 4740. 1994	Contamination Control Engineering Design Guidelines for the Aerospace Community. Accessed April 2019. [Link]
[RD03]	65 Authors from the Astronautics Community and James R. Wertz. Microcosm Press, Hawthorne, Calif, 2011	Space mission engineering: The new SMAD
[RD04]	Mohammed Chessab Mahdi. Cambridge Scholar Publishing, 2018	Attitude Stabilization for CubeSat: Concepts and Technology
[RD05]	Tord Hansen Kaasa, Tuan Anh Tran, Henrik Galtung	50mm VIS-NIR Objective Disassembly
[RD06]	Tord Hansen Kaasa, Tuan Anh Tran, Henrik Galtung	UI-3060CP-M-GL Rev.2 Detector Disassembly
[RD07]	Tord Hansen Kaasa, Tuan Anh Tran, Henrik Galtung	UI-5260CP-M-GL Detector Disassembly
[RD08]	Tord Hansen Kaasa, Tuan Anh Tran, Henrik Galtung	UI-5261SE-M-GL Detector Disassembly
[RD09]	Tord Hansen Kaasa, Tuan Anh Tran, Henrik Galtung	UI-1250SE (RGB) Detector Disassembly
[RD10]	Tord Hansen Kaasa, Joe Garrett	Objective Vulnerability Mitigation
[RD11]	Tord Hansen Kaasa	Detector Vulnerability Mitigation

2. Commercial Off-The-Shelf Components Analysis

2.1 Components

Several different COTS components have been disassembled and evaluated. Table 3 shows all assessed components. For further information regarding each component, refer to the individual assessment report. The UI-5260CP-M-GL/ UI-5261SE-M-GL are currently favoured to the UI-3060CP-M-GL due to the connection type.

Table 3: Potential COTS Components

Component Name	Description
50mm VIS-NIR Objective [RD05]	HSI objective lens, fixed focal length
UI-3060CP-M-GL [RD06]	HSI Detector, micro USB
UI-5260CP-M-GL [RD07]	HSI Detector, Ethernet
UI-5261SE-M-GL [RD08]	HSI Detector, Ethernet, PCB only
UI-1250SE-M-GL [RD09]	RGB Detector
UI-1250LE-C-HQ	RGB Detector, PCB only

2.2 Vulnerabilities

The following chapters provides a list over mission dangerous materials were found in the COTS components. Vulnerabilities marked in **bold** are challenging to remove or replace, requiring additional development time. For more information, refer to the individual disassembly reports.

2.2.1 HSI Objective Vulnerabilities

Several parts inside the 50mm VIS-NIR objective were deemed potentially unsuited for space flight [RD10]:
- **Large amount of internal grease**
- **Two *Cemented achromat type* lenses inside the objective**
- **Aperture control system must be replaced due to assembly complexity**
- Polymer cap on the aperture control screws

The most pressing matter on the objective is the grease inside. The grease might be responsible for the damage observed during the initial vacuum test, however this has yet to be proven as the damage could stem from coating cracking. The cemented lenses cannot be replaced. The aperture control will get damaged during an eventual washing and must be replaced with a fixed aperture system.

2.2.2 HSI Detector Vulnerabilities

The detectors shared several parts potentially unsuited for space flight [RD11]:

UI-3060CP-M-GL (Micro USB)
- **Polymer pads (Silicone) (3)**
- **Polymer spacer inserts (3)**
- **Non space grade thermal strap with glue**
- PCBs require epoxy coating
- Lens elastomer gasket
- Ferromagnetic bolts
- QR stickers with glue

UI-5260CP-M-GL (Ethernet)
- **Polymer pads (Silicone) (3)**
- **Polymer spacer inserts (2)**
- Lens gasket
- PCBs require epoxy coating
- Ferromagnetic bolts
- QR stickers with glue

UI-5261SE-M-GL (Ethernet, PCB only)
- **Polymer spacer inserts (2)**
- **Glue on power transformer**
- **Ferromagnetic cylindrical stack spacers**
- Polymer cylindrical washers (2)
- Lens gasket
- PCBs require epoxy coating
- Ferromagnetic bolts

The largest concern is the polymer pads present in the UI-3060CP and UI-5260CP versions. One pad must be removed destructively. This is not the case for the UI-5261SE version, however this version requires the building of customised housing. The spacers inside all detectors must be replaced by space graded spencers, as the flange focal length will be distorted if the spacers are removed. Thermal straps might be required to be added to the detectors, depending on thermal test results.

2.2.3 RGB Detector Vulnerabilities

The several parts within the detectors were found to be potentially unsuited for space flight:

UI-1250SE-M-GL
- **Polymer connector in the PCB stack**
- **Polymer Spacer Insert**
- **Elastomer Gasket**
- **Unknown coating on the front lens**
- Ferromagnetic bolts
- PCBs require epoxy coating

UI-1250LE-C-HQ (PCB only)
- **Must make a housing with correct flange focal length**
- PCBs require epoxy coating

The RGB detectors are differently built and does not contain the polymer pads found inside the HSI detectors. However there are several other challenges present inside the RGB detectors. The removal of the front elastomer gasket together with the coated lens would be preferred, if the action does not impede the detector functionality to a level outside the stated requirements. If the lens is necessary for the detector functionality, a test must be performed to characterize the external outgassing of the coating. The UI-1250LE-C-HQ is just a PCB with sensor. Unlike the HSI detector UI-5261SE-M-GL (Ethernet, PCB only), the UI-1250LE-C-HQ does not come with a lens nor a C-mount to connect with a lens. This must be made in order to use the UI-1250LE-C-HQ.

3. Mitigation Strategies

This section presents information from the *Vulnerability Mitigation* reports.

3.1 HSI 50mm VIS-NIR Objective

1) Adapt current objective. Full disassembly Required (listed in order of complexity)
    a) Remove grease - 4 weeks
        i) Remove with wiping and ultrasonic baths
    b) Replacing the aperture mechanism - 4 weeks
    c) Replace polymer parts - 4 weeks + machining
    d) Remove and replace glue
        i) Lens glue - 16 weeks
        ii) Edges and placement - 4 weeks

2) Order the parts of the current lens objectives and assemble it
    a) Order loose components
    b) Assemble in clean room
    c) No high outgassing material i.e. glue, grease and polymers
    d) Glued lenses would not be addressed (problem)

3) Find another COTS objective with fixed properties. A fixed design would remove the need for grease and aperture mechanism.
    a) Find objective with F number fixed at #F/2.8 if possible
    b) Use achromatic lens #F/4
    c) If possible, said objectives should have a fixed focus at infinite distance

4) Order space grade objectives
    a) Find supplier, ensure compatibility of camera and part

5) Make a custom objective with new lenses
    a) Design our own
        i) Hire space engineer (PhD student or from industry) or sub-contract
        ii) Require optics advisor or optics engineer
        iii) Add > 12 months to the development timeline

3.1.1 HSI 50mm VIS-NIR Recommendation

The analysis done regarding the choice of objective solution has no conclusive answers at this point in time. The recommended solution varies depending on the available time frame and the availability of manpower. It follows that a shorter time frame introduces more risk regarding the choice of solution.

- *Short time frame (additional time <3 months):*

Strategy 2 would be recommended for a short time frame, it the parts can be bought disassembled, strategy 1 would be the only option, however this would require additional time. The glued lenses would pose the largest challenge. Outgassing and characterization tests must be done to determine if the glued lenses can operate adequately in space conditions. If the single outer lenses can not be used, new lenses can be adapted with the same optical properties.

- *Long time frame (additional time >12 months):*

If the project time frame were to accommodate the full development of a custom objective, strategy 5 would be recommended. This solution is the most complicated, however it gives full control regarding material, mechanical, thermal and optical properties. The experience gained through such a project would prove more valuable than ordering a space grade objective.

3.2 HSI Detector

1) Adapt UI-5260CP-M-GL housing (listed in order of complexity)
   a) Replace polymer padding with space-grade padding.
   b) Replace thermal strap with space-grade thermal strap if outgassing test fails .
      i) Otherwise, remove glue (acetone or isopropanol) and epoxy
   c) Remove window, window gasket, and stickers
   d) Replace magnetic bolts
   e) Coat PCB boards with epoxy or Al_2O_3

2) New housing for standalone UI-5261SE-M-GL PCB detector
   a) Design our own
      i) Hire space engineer (PhD student or from industry) or sub-contract
      ii) Add > 3 months to the development timeline
   b) Order space grade (or space-plausible)
      i) Find supplier, ensure compatibility of camera and part

3) Use PCB-based detector
   a) Design our own
      i) Either hire someone internally or find a subcontractor
      ii) Add > 6 months to development timeline
   b) Order space grade (or space-plausible)
      i) Find supplier, ensure compatibility of camera and parts

4) Find space-grade camera (housing+detector+PCB to control)

3.2.1 Recommendation

A complete disassembly of the detector (UI-5260CP-M-GL) shows that the removal of the final thermal pad results in a damaged assembly. Option 1 is therefore deemed as not suitable due to the complicated removal process.

Solution 2 a) would recommended moving forward. The non enclosed version UI-5261SE Rev. 4 can be adapted and a custom housing can be made. However, his option should be further explored. The effect of the power transformer and the ferromagnetic cylindrical stack spacers on the CubeSat magnetic equipment must be tested.

If the time frame is worth the extra expenses, solution 4 would be recommended. However, a space grade solution would be expensive.

Before moving forward, it is necessary to decide what design criteria the thermal padding and strap must meet. Then quotes can be requested and the budget can be evaluated.

3.3 RGB Detector

1) Adapt UI-1250SE-M-G housing (listed in order of complexity)
    a) Replace gasket with a custom space grade design
        i)   If it can be removed, the gasket can be removed to
    b) Replace polymer spacer inserts with space grade equivalent
    c) Replace magnetic bolts
    d) Coat PCB boards with epoxy or Al_2O_3

2) New housing for standalone UI-1250LE-C-HQ PCB detector
    a) Design a new space grade housing
        i)   Must be able to connect with a c- mount lens
        ii)   Must have the correct flange focal length

3.3.1 Recommendation

Adapting the current UI-1250SE-M-GL poses several challenges. The parts must be tested, and the coated lens must be examined further. Creating a new housing for the UI-1250LE-C-HQ within the given requirements will be challenging and take up a lot of development time. Since the RGB camera is a tertiary payload, strategy 2 is not recommended. Since adapting the RBG seems simpler than creating a custom shell, *Strategy 1) is recommended.*

4. Conclusion

After disassembly and assessment of all available optical COTS components (RGB lens was not assessed), several potential problems have been uncovered within all options. Based on the vulnarbilities uncovered, several mitigation strategies was created. Upon further evaluation, the following strategies and components are recommended moving forward.

HSI Objective
- Adapt the current 50mm VIS-NIR objective or order the parts if available

HSI Detector
- Create a custom housing for the UI-5261SE-M-GL PCB detector

RGB Detector
- Adapt the UI-1250SE-M-GL detector

RGB Objective
- Not evaluated

5. Further Work

All the solutions must be further explored. All potential dangerous materials must be tested and evaluated. For now, the strategies recommended are based on safety, future tests might prove that some components deemed as potentially dangerous in fact are safe. The RGB objective must also be disassembled and evaluated as some of the challenges encountered in the 50 mm VIS-NIR objective are expected to be encountered there as well.

6. List of Abbreviations

Table 4: Abbreviations

Abbreviation	Description
COTS	Commercial Off-The-Shelf
CVCM	Collected Volatile Condensable Materials
ESA	European Space Agency
HSI	Hyper Spectral Imager
LEO	Low Earth Orbit
NASA	National Aeronautics and Space Administration
PCB	Printed Circuit Board
RGB	Red Green Blue
TML	Total Mass Loss

50mm VIS-NIR
Objective Disassembly

Table Of Contents

Table 1: Table of Changes

Rev.	Summary of Changes	Author(s)	Effective Date
1	*First issue*	*Tuan Tran* *Tord Hansen Kaasa*	*05.03.2019*
2	*New formatting, fixed spelling*	*Tuan Tran* *Tord Hansen Kaasa* *Henrik Galtung*	*25.05.2019*

1. Purpose

The main purpose of the disassembly analysis of the 50mm lens objective is to uncover if the assembly is safe to be carried on a CubeSat. Parts that are potentially prone to outgassing of condensable material will be documented. Grease, glue and polymers are unsafe, potentially lens coating as well. The disassembly will be done on a vacuum tested lens objective. During the *Vacuum Resilience Test* (HYPSO-TRP-VAC-001), unknown damage was observed occurring beneath the front lens. The damage will be further elaborated in *Objective Vacuum Damage Report* (HYPSO-TRP-VAC-001). To uncover further information regarding the damage, the tested objective must be disassembled and inspected. The lens will be separated from the shell and examined properly with a microscope, and possibly SEM machine and 3D optical profiler.

2. Procedure

Disassembling of the objective requires a structured plan both for disassembly and documentation. The objective planned for disassembly is the vacuum tested objective, with the unknown damage. For the disassembly process it is important to document every single step, as well as the reasoning and result so that future experiments may retrace the process. It is also beneficial for identifying sources of error, if something unexpected were to happen. The thought process should be shared, and before every step the intended action should be vocalized so that everyone present can hear it. In addition to this, every step should be documented in text and picture. It is recommended to have at least one person responsible in each of the three following roles: transcriber/ note taker, photo documenter, and disassembler. The current leading approach is to use a specific tool designed to screw parts of the objects. Because the assembly is suspected to be lightly ruggedized with some amount of glue, a process is needed to remove it and simultaneously document the precise location of the glue. This process shall not contaminate the damaged area, which might be a coating. Thus, methods such as heat treating and ultrasonic baths in glue solvents should be considered carefully. Furthermore, all screws available from the outside should be unscrewed to see if any parts starts loosening. Table 1 shows all equipment and equipment quantity used during the procedure.

Table 2: Equipment list

Equipment	#
50 mm VIS NIR lens (Vacuum exposed)	1
Screwdrivers	1
Tweezers	2
Isopropanol	-
Non latex gloves	-
Digital Camera	1
Ziplock bags	-
Objective disassembly tool (Specialized)	3

3. Disassembly Procedure

Wear gloves. Loosen the objective front notch key ring using the objective disassembly tool. If front remains rigid, glue removal processes should be considered. Carefully separate parts if able. It is important that movements are slow during separation attempts, so that loose parts on the inside may not fall out and become damaged. Because the insides of the objective are unknown, further steps will need improvisation. As the objective is a compact part, it follows that some force may be required in order to open the assembly. Damage can occur on the outer shell and non vital areas of the objective. The objective will not be reassembled and will be considered unusable after the entire process. The disassembled parts will be preserved in ziplock bags and marked for further investigation.

It is worth noting that the actual disassembly procedure might diverge as these are assumptions. This is an exploratory experiment and such the procedure will be adapted to the actual construction of the objective.

It is postulated by the mechanics team that the objective is made with the following parts:
- Objective housings
- Multiple lenses
- Coating film
- Spacing and calibration mechanisms
- Misc. glue, grease

4. Results

The following section provides the results found during the disassembly process. Table 2 shows the steps taken, table 3 tabulates noteworthy findings. Figures of the disassembly process can be found in *Appendix A: Objective Disassembly Figures.*

Table 3: Objective Disassembly Chart

Step nr.	Step explanation	What happened
1	Screw out set screws (5)	Unscrewed with some resistance because of glue
2	Screw out bolt screws (2)	Bolt screws were unscrewed easily as they were loose to begin with
3	*Front ring* removal in +Z direction	Front ring is successfully detached
4	Screw out *backend lens tube* using a screwdriver on the notch (normal counterclockwise)	Backend lens tube was unscrewed with use of force due to glue. Future disassemblies should use a specialized tool
5	Unscrew *back ring* (-Z)	Back ring was successfully unscrewed
5b	Remove -Z lens tube	Successfully removed
6	Unscrew *aperture adjustment ring*	Aperture ring was successfully unscrewed. The threads were extensively greased. Removal of aperture adjustment ring releases a ball inside used for generation of clicking sounds per step. This ball was dropped
7	Removal of *aperture control screws* (2)	Aperture screws were successfully removed. Substantial amount of grease observed on the inside. The caps of the screws are polymer.
8	Unscrewing of *central measurement ring*	Central measurement ring can now be rotated. However, remains connected mechanically to the central measure unit
9	Unscrew *F stop pin*	F stop pin successfully unscrewed and detached from remaining assembly
10	Pull out *aperture groove ring* in the -Z direction	Aperture groove ring successfully pulled out without any resistance
11	Loosen *aperture focus ring assembly* (8 parts) using a screwdriver	Aperture focus ring assembly was slightly scrambled, losing mechanical integrity. The parts are highly flexible, meaning they probably are polymeric
12	Turn lens upside down (-Z side down)	Assembly falls out of the lenses

13	Unscrew *control unit* from *central unit*	Parts successfully unscrew
14	Pull apart control unit from central unit	Control unit and central units are seperated. A lot of grease can be observed
15	Special step: Removal of front lens *inner key bracket*	See notes
16	Unscrew the container ring blocking the front lens and remove it	The ring was full of glue in the threads
17	Removal of front lens	Front lens successfully detached. Damage is observed to be only on the back side of the front lens
18	Removal of front spacer ring	Front spacer ring successfully removed
19	Removal of middle lens	The lens appears to be two lenses put together, due to the seam on the side
20	Special step: Disassemble the -Z lens tube	See notes. This was the final step

Table 4: Noteworthy Findings

Notes
The entire interior of the objective is covered in a thick layer of grease. This must be removed in order to avoid extensive outgassing at lower pressures. -Z lens in the -Z lens tube looks like two lenses merged as one. The entire assembly is comprised of 5-6 lenses, several fine mechanical parts and subassemblies. The part is complex and therefore structurally weak. Some parts such as some of the lenses were stored by being screwed back into the assembly. This was done to decrease risk factors of storing coated and scratch-sensitive parts in a plastic bag environment. The averaged aluminum thickness of the housing was measured to be close to 3mm.

Several parts inside the objective were deemed potentially unsuited for space flight:
- Polymer cap on the aperture control screws
- All adjustable parts contain large amount grease
- Aperture focus assembly is possibly made of polymer. However the spring response is akin to a metal material
- -Z lens in -Z lens tube appears to be two separate lenses merged together
- The middle lenses appears to be comprised of two separate lenses merged together (cemented achromatic lenses)

4.1 Removal of front lens inner key bracket

For the removal of this part, a custom cut 1 mm steel plate as shown in figure 1 was used. A round notch was machined between they key notches to account for the curvature of the lens. A 3D printed SLA tool was also made, but it was not strong enough, figure 2. The objective was fastened in place using a lathe at the available workshop. From this position the plate was pushed on to the notches of the key bracket. An adjustable wrench was clamped onto the sheet for an increased moment of inertia. Some force had to be used in the counterclockwise direction before the glue gave in. The steel part was comprised during disassembly, as yielding occurred around the round notch. After the part had been loosened, the assembly was brought back to the lab for more careful work. For future disassembly, a more customized tool is recommended as this method could damage the lens and objective.

Figure 1: Custom 1 mm steel key plate

Figure 2: Custom SLA printed notch key

4.2 Disassembly of the -Z lens tube assembly

Two special tools were made to disable the unit. Unscrew first lens key container ring. Take out the back lens. Remove second container ring. Then take out the lens tube middle lens. Glue and grease was found on the outer and inner threads.

5. Conclusion

The lenses are potentially unfit for space. Extensive actions must be done in order to prepare the part for the space environment. This includes changing all polymer parts, removing the grease, make a new fine mechanical aperture system free of polymer, remove other contaminants from the assembly, epoxy down movable surfaces. This would require a full disassembly and reassembly. The part is ruggedized and all threads are glued, making a clean disassembly complicated due to the required force to pry the container rings open. The reassembly could potentially lead to a myriad of problems, some parts can be damaged, or shifted around.

An analysis weighing the different options regarding the potential lenses should be conducted in order to uncover an appropriate solution.

Appendix A: Objective Disassembly Figures

1. Set screws

2. Unscrewing bolt screws
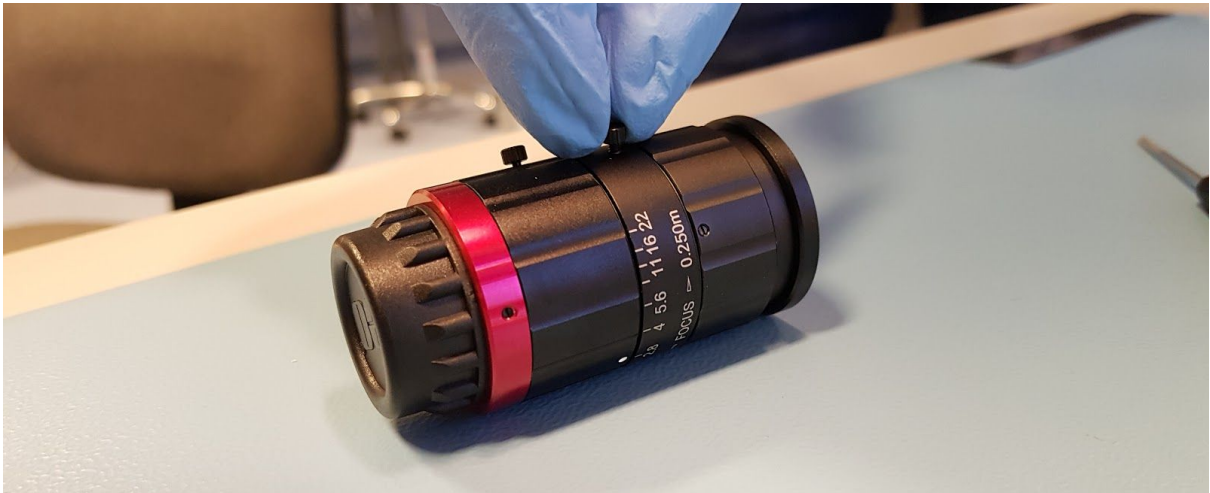
3. Unscrewing the front ring

4.Unscrewing backend lens tube using a screwdriver

5. Back ring unscrewing
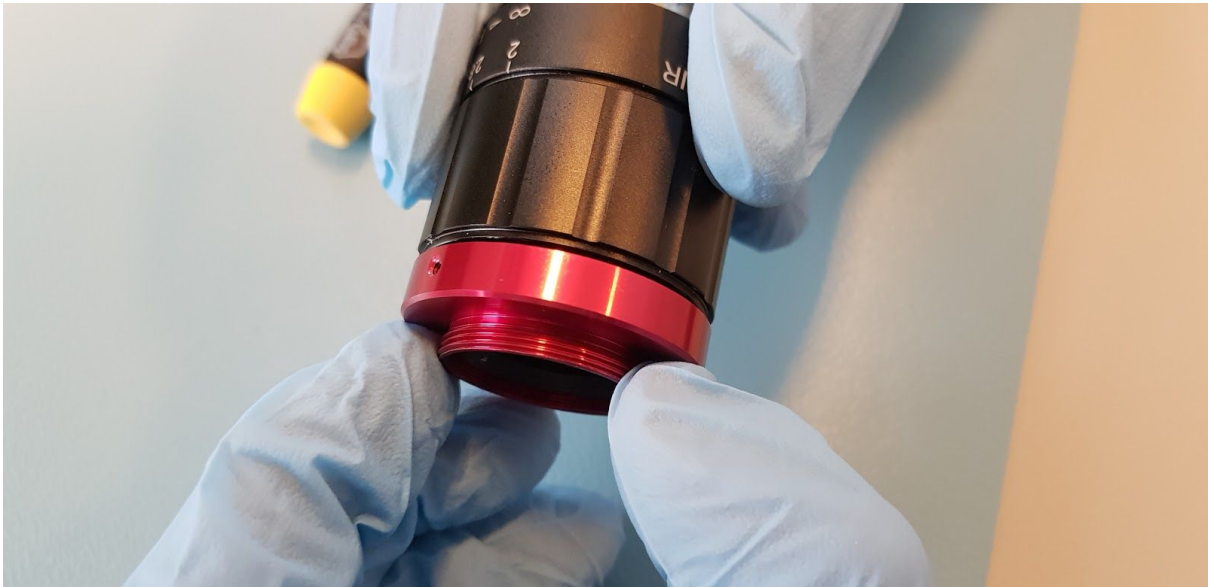
5b. -Z Lens tube

6. Removal of *aperture adjustment ring*
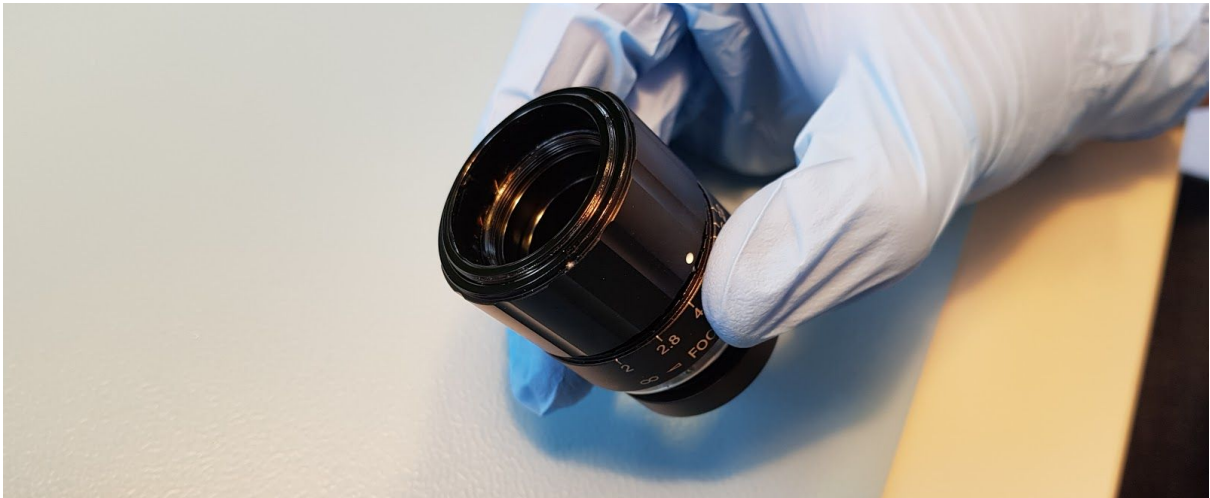
7. *Aperture control screws*

8. Grease on the inside

9. Aperture Ring

10. F stop pin

11. Additional grease on the tube

12. Aperture mechanism assembly

13. Aperture mechanism assembly

14. Polymer capped screw

15. Screws and polymer caps (2)

16. Central measurement ring remains connected to assembly

17. Removal of aperture groove ring
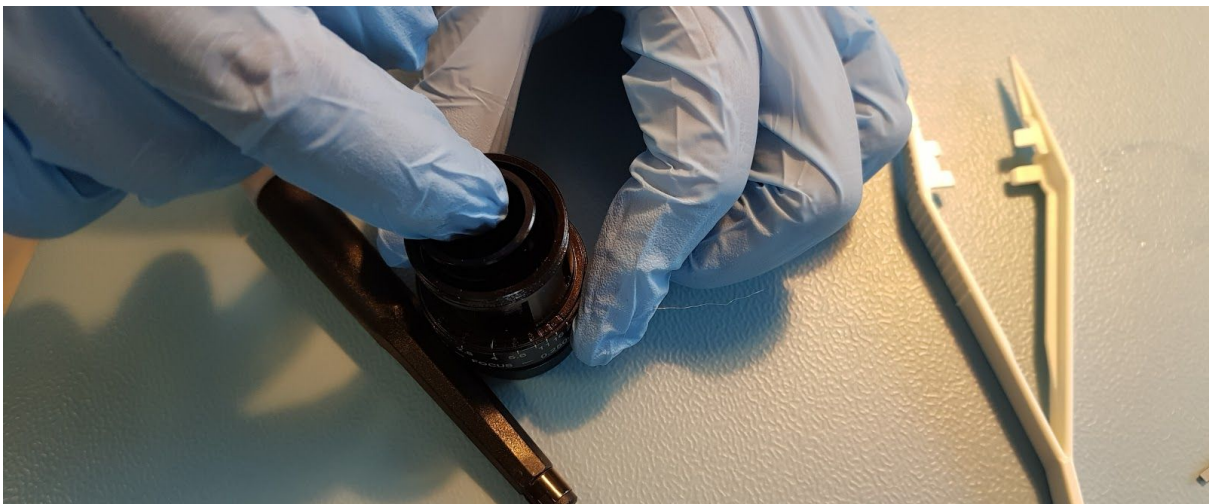
18. Aperture mechanism ring assembly dislodged

19. Aperture groove

20. Separation of control unit from central lens assembly

21. Central unit and control unit side by side

22a. Control unit

22b. Control unit

23. Central unit assembly

24. 0.8 mm key notch steel plate
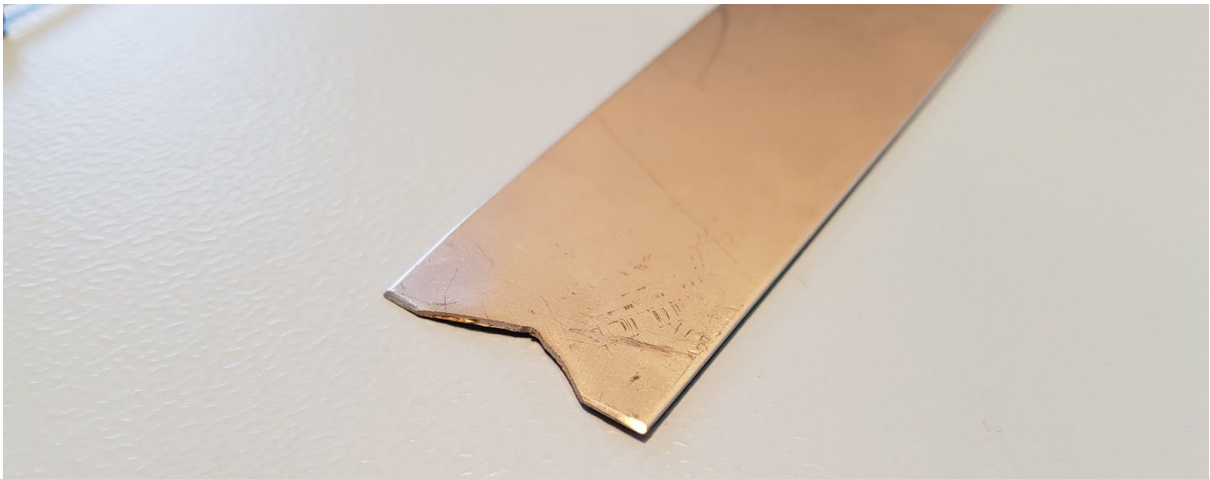
25. Removal of the outer lens ring
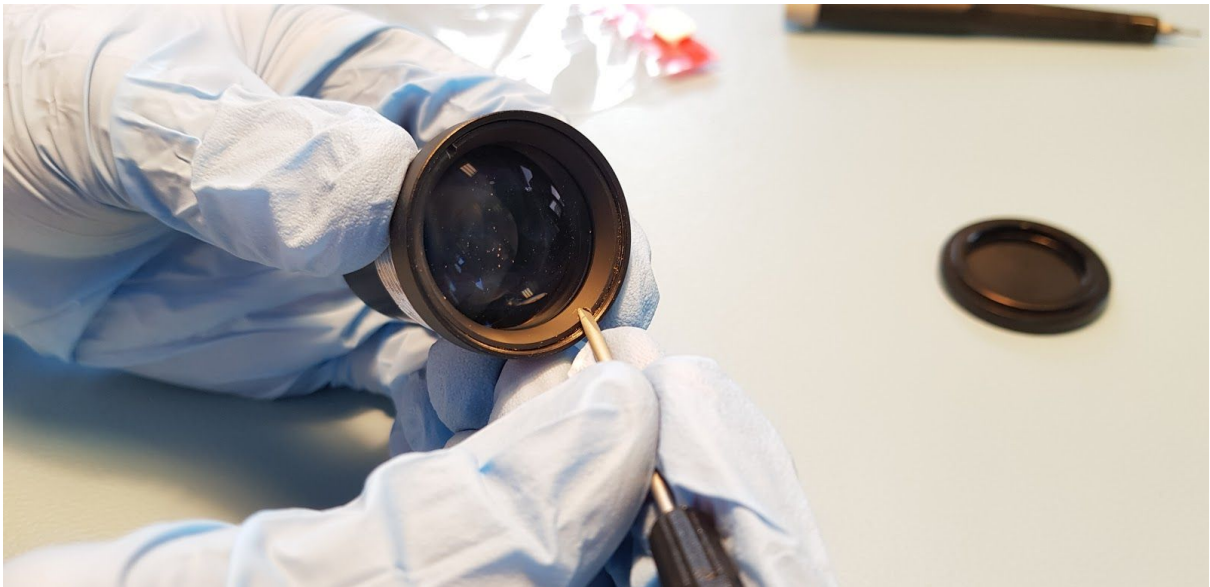
26. Outer lens ring
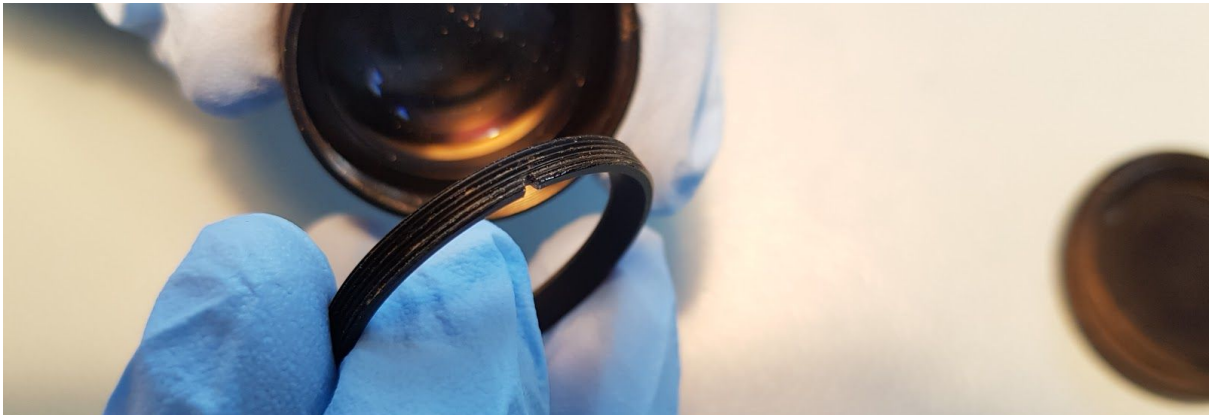
27. Removal of front lens

28. Middle lens in assembly

29. Spacer ring removed

30. Middle lens removed
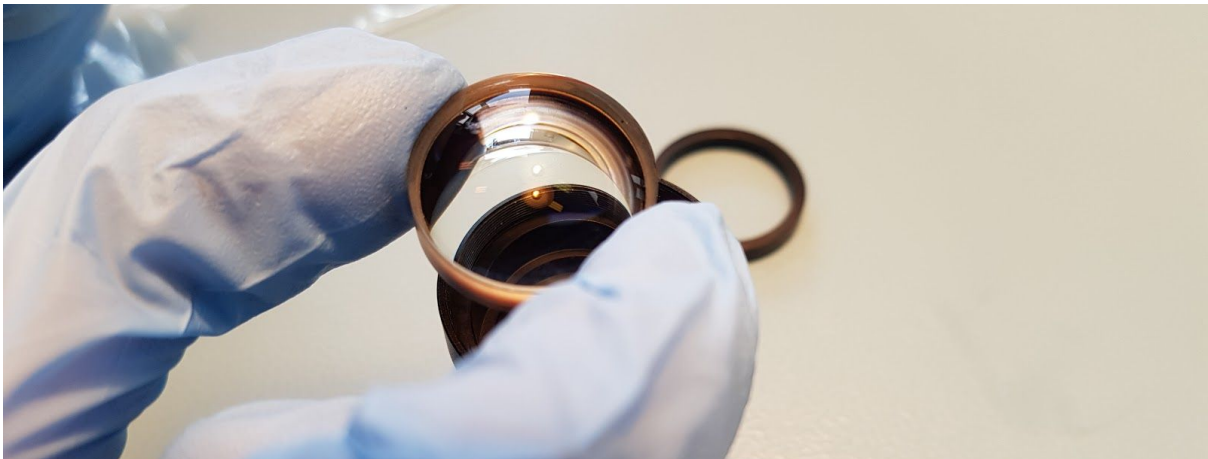
31. Middle lens with an apparent seam, appears to be glued
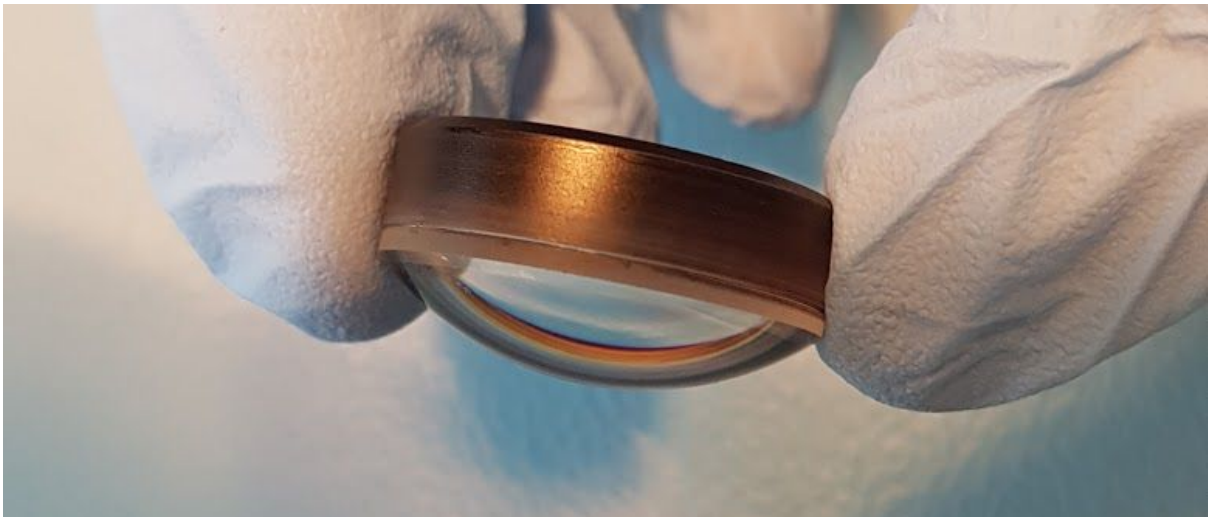
32. Bottom (-Z) of the middle lens
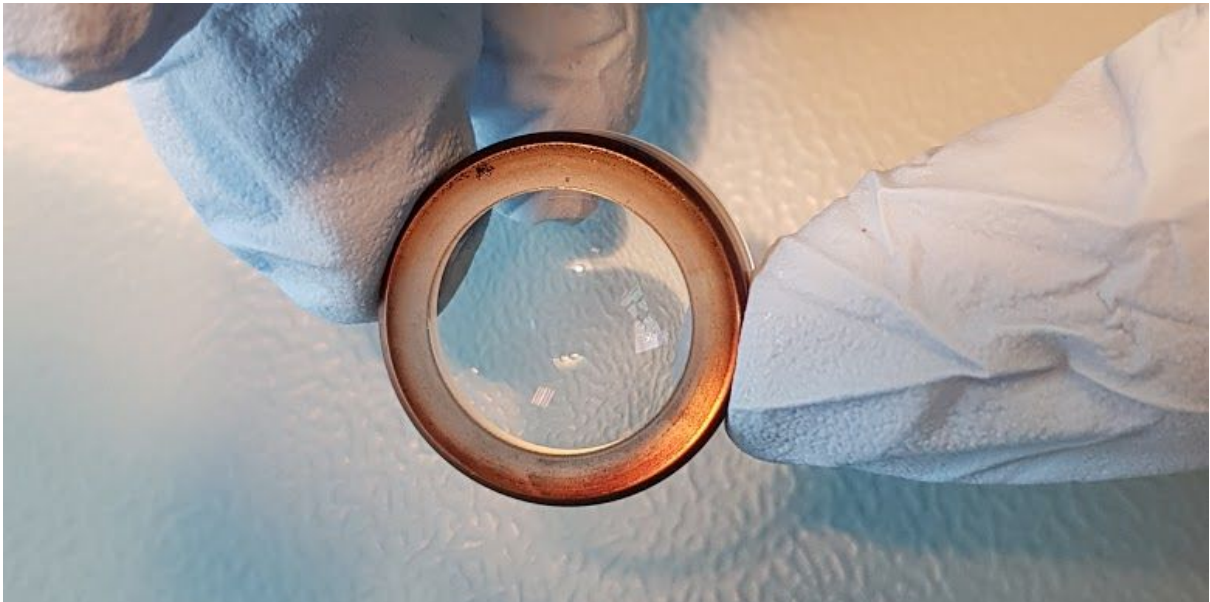
33. Middle lens front

34. Special tool used to remove the keyring on the -Z lens tube
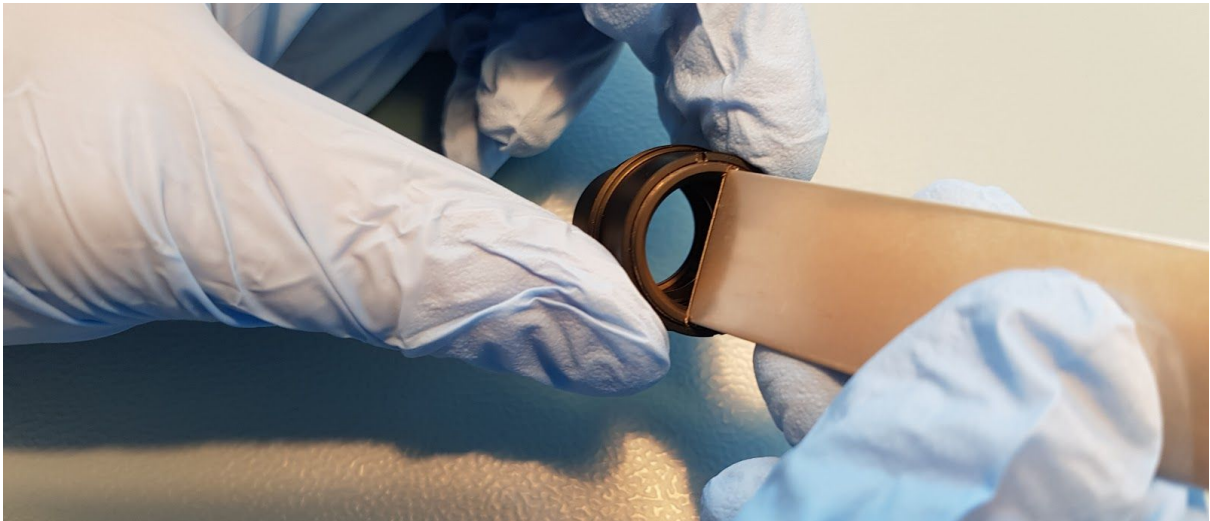
35. Removal of key ring on the -Z lens tube

36. Removal of back end lens form the -Z lens tube
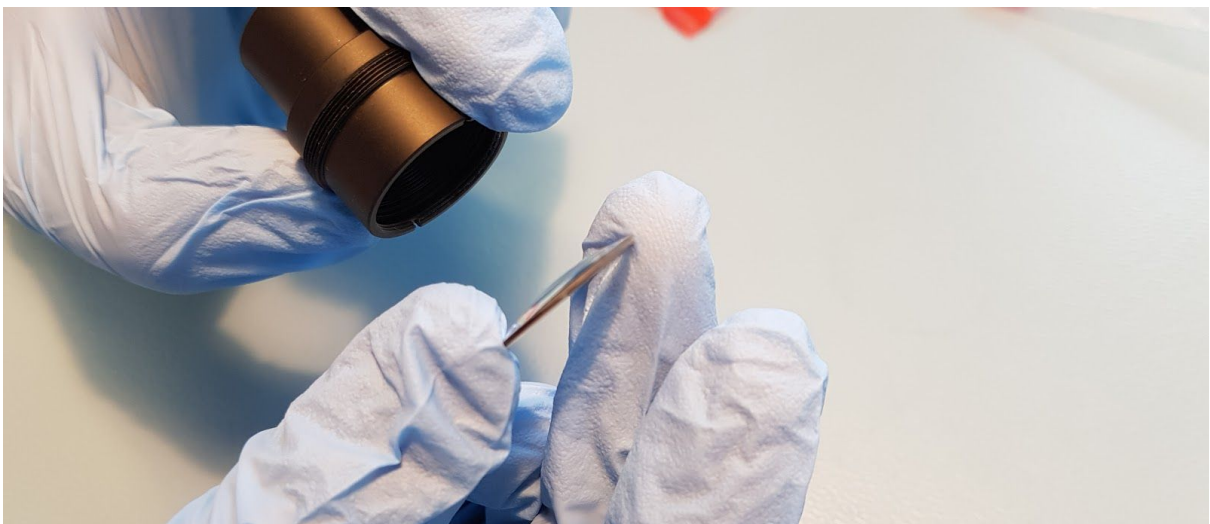
37. Using the special tool to remove the inner key ring
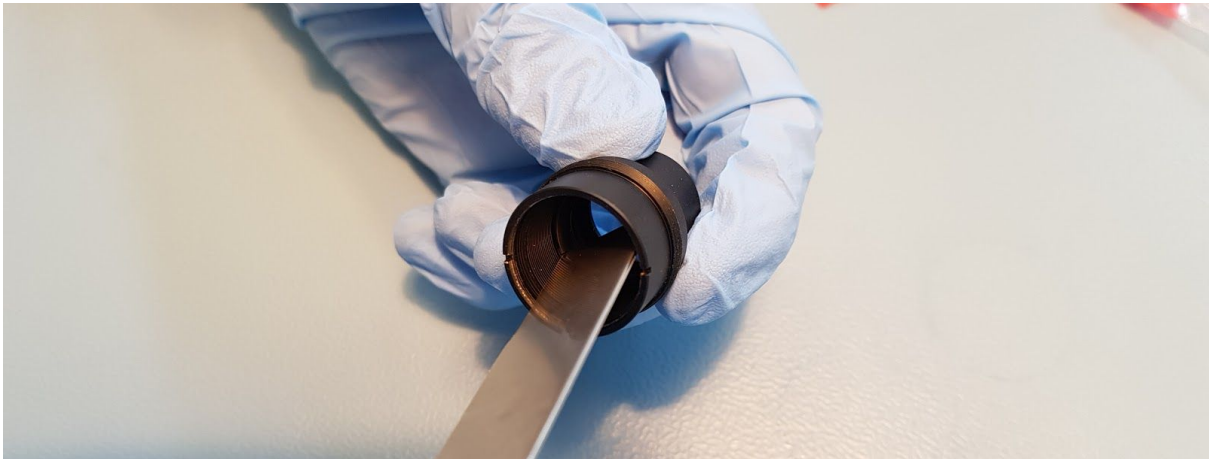
38. Removal of lens. The lens appears to be comprised of two glued lenses
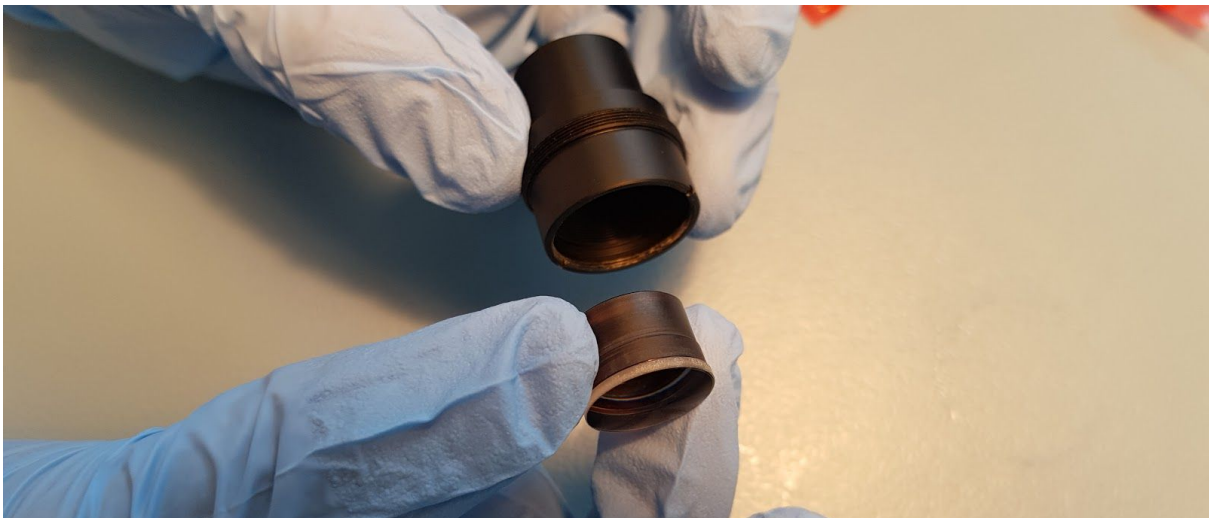
39. -Z lens tube assembly

40. Cross section of the complete objective assembly

Objective Vulnerability Mitigation

HYPSO-RP-005

Table Of Contents

Table 1: Table of Changes

Rev.	Summary of Changes	Author(s)	Effective Date
1	First issue	Tord Hansen Kaasa	05.03.2019
2	New formatting, fixed spelling	Tord Hansen Kaasa	25.05.2019

Executive Summary

Most of the vulnerabilities that were found are potentially serious. The three objectives are an integral part of the HSI assembly. It follows that changing the objectives to a fully space-compliant model would result in severe time delays as the entirety of the setup and mechanical design would change. As a result it would be beneficial to modify the current objective such that it becomes fit for space rather than replacing it fully. The following analysis explores the various paths forward that would ensure the discovered problems are mitigated.

1. Purpose

The report *HYPSO-RP-011 50mm Lens Objective Disassembly* found several aspects of the objective which are likely to cause issues in low earth orbit [RD01]. This memo outlines possible strategies to mitigate the discovered vulnerabilities.

1.1 Summary of uncovered problematic conditions

Glue on structural bolts
The structural set screws and bolts holding the objective assembly together from the outside of the chassis features glued threads. The glue is of unknown origin and can be assumed to have unacceptable outgassing levels until further testing can be done.

Polymer cap on the aperture control screws
The polymer caps on the control screws are a minor problem. It is suspected that the polymer caps are there to avoid causing wear on the mechanism, as this component slides up and down the slit. Because this part is required to stay fixed during the entire mission lifetime after calibration, it can be replaced by a glued bolt of similar size. The only complication would be the fact that the bolt would need to compensate for calibration.

Adjustable parts contains large amounts of grease
Because the amount of grease present inside the objective is alarmingly large, a complete degreasing of all involved parts might pose a big challenge. As the purpose of the grease is to spread out and smoothen the movement between moving joints, it may be present throughout the entire objective assembly. To mitigate this, a full disassembly of the objective would be needed to reach all affected surfaces. A full disassembly also increases the chance of issues arising in the reassembly process, as this is a precision component. The grease removal process would also need consideration with respect to lens coating, as damage to this should be avoided.

Aperture mechanism is made of an unknown material
The 8 small parts forming the aperture mechanism is comprised of an unknown material, possibly of polymeric nature. However the spring response of the material is akin to metallic behaviour. If the mechanism is made of polymer, it can be assumed that it would not meet the outgassing regulations outlined in the 6U CubeSat standard. It is possible that the part is a coated metal, in that case the coating must be examined for outgassing. Changing the material of the aperture mechanism would be a very complex process, however it is possible that the whole mechanism could be swapped out for a plate with a non-adjustable aperture.

Cemented lenses
The middle lens and one of the back lenses are comprised of two individual glass pieces. Initial visual inspection points to these being joined into one lens by glue. This glue is of unknown origin and can be assumed to have unacceptable outgassing levels until further testing can be done. If the glue used here is actually of non-acceptable quality, this would be close to impossible to modify internally in the project.

1.2 Reference Documents

The documents listed in table 2 have been used as reference in the creation of this document.

Table 2: Referenced Documents

ID	Author	Title
[RD01]	Tord Kaasa, Tuan Tran	*50mm Lens Objective Disassembly HYPSO-RP-011*

2. Mitigation strategies

1) Adapt current objective. (listed in order of complexity)
   a) Replacing the aperture mechanism (Highly challenging if this mechanism is polymer, if metall no change would be made) - 4 weeks
   b) Remove grease - 3 weeks (Joe can work on this in May. Not super-helpful)
   c) Replace polymer parts - 4 weeks + machining
   d) Remove and replace glue
      i) Lens glue - 16 weeks
      ii) Edges and placement - 4 weeks

2) Order the parts of the current lens objectives and assemble it
   a) Order loose components
   b) Assemble in clean room
   c) No high outgassing material i.e. glue, grease and polymers
   d) Glued lenses would not be addressed (problem)

3) Find another COTS objective with fixed properties. A fixed design would remove the need for grease and aperture mechanism.
   a) Find objective with F number fixed at #F/2.8 if possible
   b) Use achromatic lens #F/4
   c) If possible, said objectives should have a fixed focus at infinite distance

4) Order space grade objectives
   a) Find supplier, ensure compatibility of camera and part

5) Make a custom objective with new lenses
   a) Design our own
      i) Hire space engineer (PhD student or from industry) or sub-contract
      ii) Require optics advisor or optics engineer
      iii) Add > 12 months to the development timeline

3. Evaluation

With the problems of the COTS 50mm VIS-NIR objectives, adapting the current objective for space would require extensive work. Removing the grease and glue will be challenging, as it can not simply be wiped of. Potentially, ultrasonic baths could be used to clean the parts, however the result might not be satisfactory. The entire objective must be disassembled in order to properly clean it, including removing the aperture mechanism which can not realistically be reassembled. Every single HSI assembly would require complete adaptation of three objectives. Strategy 1 would introduce more risk to the system as each objective will have to be disassembled and reassembled. The risks involved in this process was deemed to be high.

Strategy 2 would bypass the disassembly and cleaning challenges, but the risk of errors involved when assembling the system is still high. The process of swapping out the glue for a space-compliant one while maintaining the integrity of the lens would require extensive knowledge of optics assembly and manufacturing skills that are currently far beyond what the project is equipped to deal with.

With a fixed aperture and focus objectives, as outlined in strategy 3, there should be no need for grease or adjustable parts. An objective with fixed optical properties should also be more rigid in nature. However, finding another COTS objective with the correct fixed properties is unlikely. Additional testing and disassembly would also be needed. Even so, there would be no guarantee that the lenses are suitable for space. Other COTS components can potentially use high outgassing coating or polymer parts. This solution requires a high amount of research and the ordering and examining of several potential objectives, adding additional time compared to solution 2.

Several space grade HSI solutions for cubesats exist in the world, some even in Europe. However, the price range of these products are beyond the scope of the HYPSO mission. Furthermore, doing so would deviate from the goal of using COTS components.

Making a custom objective lens housing at the university would require a lot of work as well as knowledge in optical and mechanical engineering. A custom objective lens housing would however provide far more control over build material and design, thus allow for greater suitability for space. If a longer timescale had been defined for the HYPSO, this strategy would be beneficial. This strategy would redefine the HYPSO mission goal of using COTS components for the mission.

4. Recommendation

The analysis done regarding the choice of objective solution has no conclusive answers at this point in time. The recommended solution varies depending on the available time frame and the availability of manpower. It follows that a shorter time frame introduces more risk regarding the choice of solution.

- *Short time frame (additional time <3 months):*

Strategy 2 would be recommended for a short time frame. If the parts can't be bought disassembled, strategy 1 would be the only option. However, this would require additional time. The glued lenses would pose the largest challenge. Outgassing and characterization tests must be done to determine if the glued lenses can operate adequately in space conditions.

- *Long time frame (additional time >12 months):*

If the project time frame were to accommodate the full development of a custom objective, strategy 5 would be recommended. This solution is the most complicated, however it gives full control regarding material, mechanical, thermal and optical properties. The experience gained through such a project would prove more valuable than ordering a space grade objective.

UI-1250SE RGB
Detector Disassembly

HYPSO-RP-010
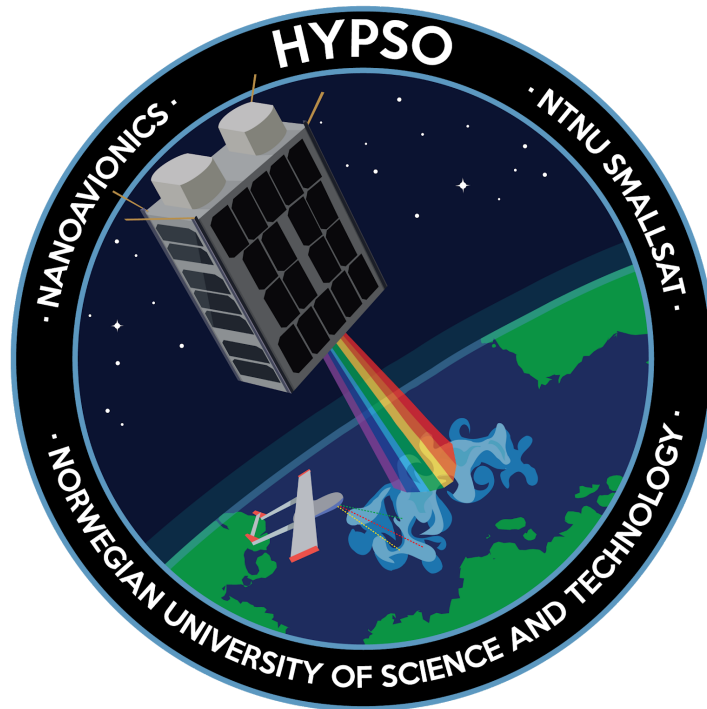
Prepared by:	HYPSO Project Team
Reference:	HYPSO-RP-010
Revision:	2
Date of issue:	25.05.2019
Document Type:	Report
Author(s):	Tord Hansen Kaasa, Tuan Tran, Henrik Galtung

Table Of Contents

Table 1: Table of Changes

Rev.	Summary of Changes	Author(s)	Effective Date
1	First issue	Tuan Tran Tord Hansen Kaasa Henrik Galtung	20.05.2019
2	Formatting of text	Tuan Tran Tord Hansen Kaasa Henrik Galtung	25.05.2019

1. Purpose

This report serves as an assessment of the UI-1250SE RGB detector that is a potensial detector in the RGB camera payload. The RGB camera payload is a low priority payload, thus an internal fatal error due to the space environment is not a concern. However, due to the close approximate placement to the main HSI payload, potential external outgassing of several components inside the RGB detector must be examined. The main purpose of this report is to uncover any components comprised of potentially high outgassing materials that could damage the primary payload. The detector will be assessed to uncover if any adaptation can be done or if another solution, like the PCB only variant, presents a better overall solution with regard to the time frame and safety requirements.

2. Procedure

Disassembly of the detector requires a structured plan both for disassembly and documentation. The disassembly process will be non-destructive. However caution must be used when disassembling the unit. For the flight model, the disassembly must be done in a clean environment.

Table 1 shows all equipment and equipment quantity used during the procedure.

Table 2: Equipment list

Equipment	#
Sony UI-1250SE (RGB Detector)	1
Screwdrivers	1
Tweezers	1
Non latex gloves	-
Ziplock bags	1 pack

3. Results

The following section provides the results found during the disassembly process. Table 2 shows the steps taken, table 3 tabulates noteworthy findings. Relevant pictures can be found in appendix A: *Detector Disassembly Figures*.

Table 3: Detector Disassembly Chart

Step nr.	Step Description	Additional Information
1	Remove +Y screw (1)	Ferromagnetic, dark. The steel prongs now fully loose.
2	Remove the -Y screws (2)	Ferromagnetic, dark. Assembly is now loose.
3	Separate assembly by pulling the +Z side from the -Z side	The assembly was separated into three different parts: PCB assembly with +Z lens front, -Z casing, and -Y plate
4	Remove QR code using tweezers	QR code was removed with some trouble. Metal tweezers had to be used instead of polymer. First attempt resulted in damage of QR code
5	Remove the -Z stacking screws on the assembly (4)	Ferromagnetic, clear.
6	Separate -Z PCB from PCB assembly	The PCB stack can be categorized in +Z PCB in front and -Z PCB in the back. Polymer connectors spotted between both PCBs
7	Remove QR code from +Z PCB	QR code successfully removed form +Z PCB
8	Remove the four stacking rods from +Z PCB	Stacking rods successfully removed from the +Z PCB
9	Separate +Z PCB from front lens	Successfully separated. Thick polymer (0.025 inches) spacer spotted between +Z PCB and front lens in addition to the rubber gasket inside.
10	Removed polymer spacer	No glue used on the spacer.
11	Removed polymer lens gasket	Polymer gasket successfully removed. Front window remains seated in the gasket.
12	Front window pushed out of the gasket in the +Z direction	Front window successfully pushed out. Only a small amount of force needed. This was the final step

Table 4: Noteworthy Findings

Notes
The overall structure of the RBG detector appears to be more flimsy and weaker than the more expensive IMX174 and IMX249 based on the disassembly procedure. The steel prong side towards the -Y is loose. The prong is only supported in +Y with one bolt. Further disassembly shows that the prong has several millimeters of space to move inside the detector when assembled, locked between the backside and -Y plate. The connector between the +Z and - Z PCBs is comprised of polymer. The outside bolts appears to be magnetic The -Z stacking screws appears to be magnetic The detector has no internal heat straps, thermal pads or shock pads. Fitting in a thermal solution might be necessary when adapting such a solution for the space environment. The front lens is seated in an elastomer gasket. Removing the gasket alone would necessitate the design of a new seating solution. Removing the gasket together with the lens would be the simplest solution, however the lens might be important for the camera characteristics. The front lens/ window has a red hue due to the coating used. This coating might be some sort of infrared inhibitor. Thus removing the lens could change the detector spectral response. Tests should be done to characterize the detector with and without the front lens to determine if making a new seating solution is necessary. The +Z PCB (with the detector) is seated on a 0.025 inch spacer to achieve the correct focal length. A new spacer that is space grade must be made. It is also worth noting that the detector can be disassembled and reassembled while maintaining full functionality.

4. Vulnerability Assessment

Several parts inside the detector were deemed potentially unsuited for space flight:
- Polymer connector on the +Z PCB
- Polymer Spacer Insert
- Elastomer Gasket
- Unknown coating on the front lens
- Ferromagnetic bolts

Some changes must be done in order to make this detector flight ready. The polymer components being the most challenging to adapt to a space grade solution.

Changing the *polymer connector* is not possible. Testing to uncover the material outgassing properties will be necessary. Space grade coating might be used to encapsulate the connector. The coating layer must be thick, as conformal coating does not mitigate a coated components outgassing characteristics. An epoxy coating might be a viable alternative.

The *polymer spacer insert* can be made of another material, however the spacer might have a secondary function, isolating the front bcb from the outer shell. The new insert must be made of a space grade material that has similar isolation effects.

The removal of the front *elastomer gasket* together with the *coated lens* would be preferred, if the action does not impede the detector functionality to a level outside the stated requirements. If the lens is necessary for the detector functionality, a test must be performed to characterize the external outgassing of the coating. Internal problems that might damage the RGB camera in the space environment such as gradual darkening due to radiation exposure or atomic oxygen wear will not be prioritized due to the nature of the RGB camera payload priority. However any damaging effects the RGB camera can have on the main HSI payload must be explored.

The ferromagnetic bolts can be replaced with non magnetic bolts of the same size.

Adapting the UI-1250SE (RGB) Detector would add an approximated 1-2 months of development time due to the uncertainties. However, accurate statistics can not be made before the assessment of the PCB only RGB detector.

5. Conclusion

The detector is easy to disassemble, removing all unwanted parts (except the polymer connectors), and reassemble non destructively. However, there unanswered questions persist with regards to the potential unsafe parts. The range of damage the parts could cause are not mapped. Due to the uncertainties surrounding the adaptation of the UI-1250SE RGB Detector, no conclusions can be reached at this time before the assessment of the PCB only UI-5261SE-M-GL variant. The inclusion of the RGB payload could potentially damage the main HSI payload. Bake out tests must be performed on the potentially unsafe components.

Appendix A: Detector Disassembly Figures
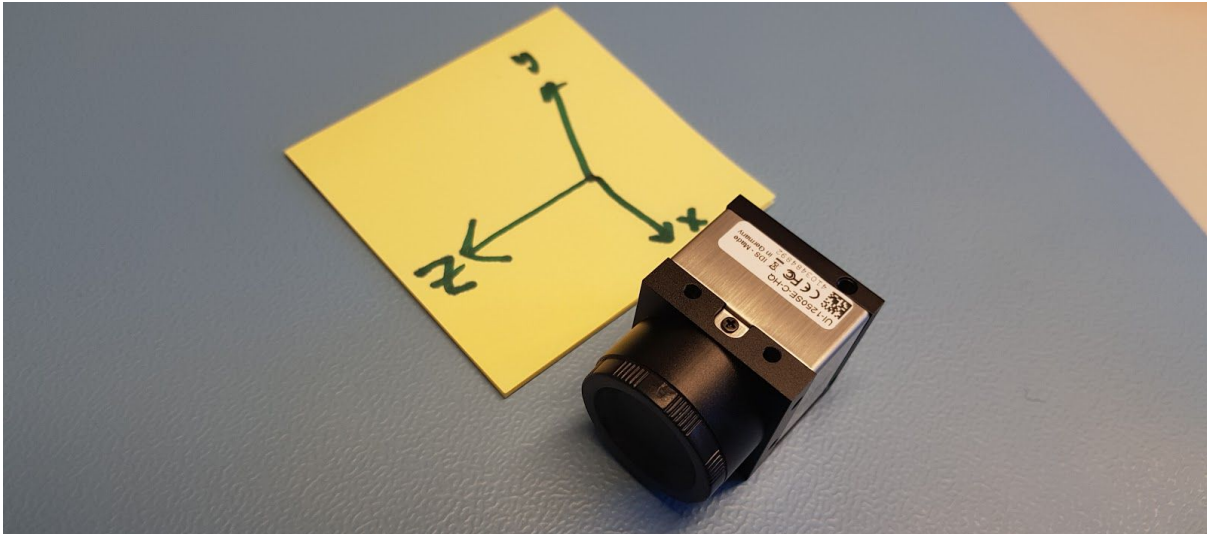
Figure 1. Detector coordinate system
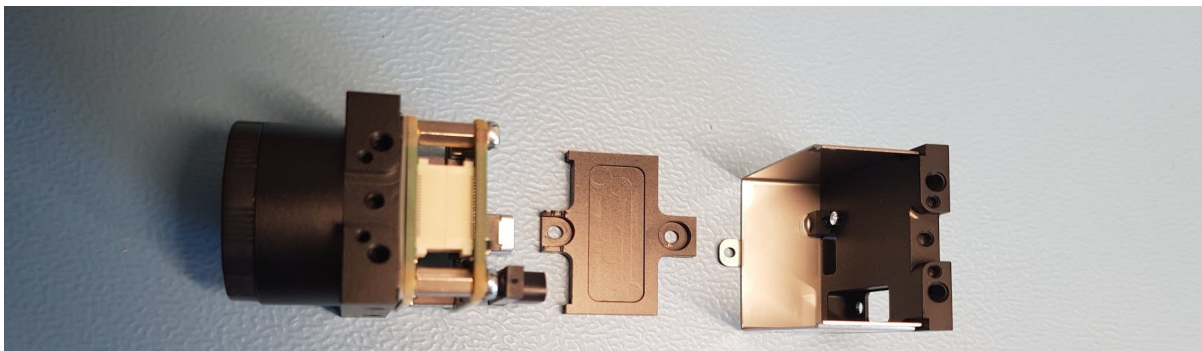
Figure 2. Main detector parts
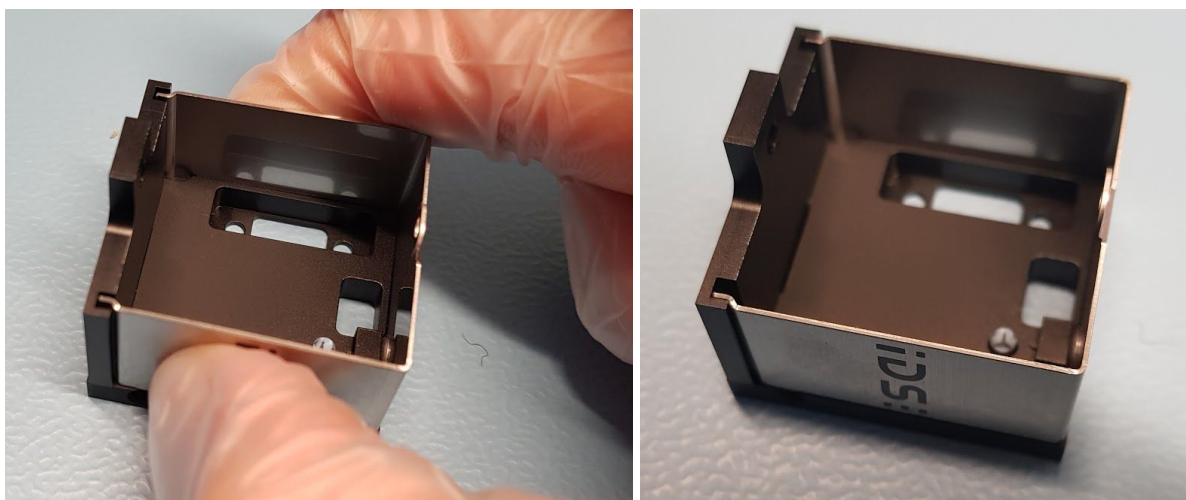
Figure 3. Loose steel prong
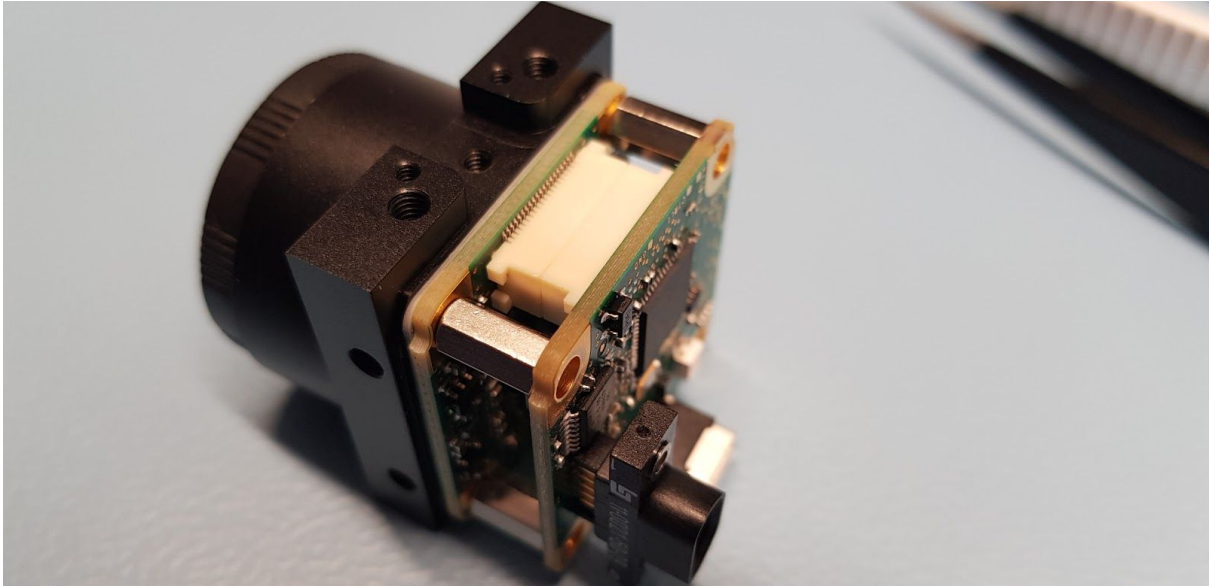
Figure 4. Polymer connector on the +Z PCB
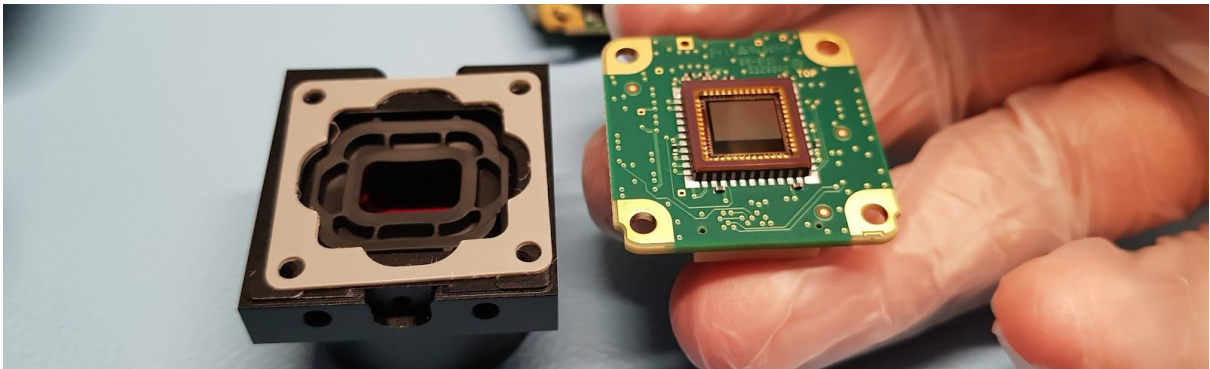
Figure 5. Polymer Spacer Insert to achieve correct flange focal length
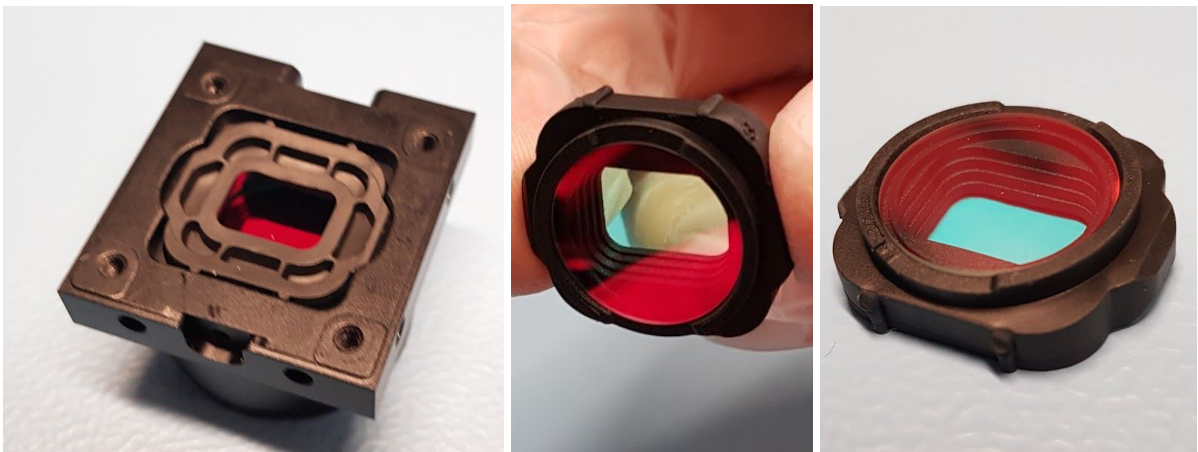
Figure 6. Elastomer Gasket with Seating for Coated lens

UI-3060CP-M-GL Rev.2 Detector Disassembly

HYPSO-RP-007

Prepared by:	HYPSO Project Team
Reference:	HYPSO-RP-007
Revision:	2
Date of issue:	25.05.2019
Document Type:	Report
Author(s):	Tord Kaasa, Tuan Tran, Henrik Galtung

Table Of Contents

Table 1: Table of Changes

Rev.	Summary of Changes	Author(s)	Effective Date
1	*First issue*	*Tuan Tran* *Tord Hansen Kaasa* *Henrik Galtung*	*12.03.2019*
2	*Formatting of text,* *Removed references to polymer front window*	*Tuan Tran* *Tord Hansen Kaasa* *Henrik Galtung*	*25.05.2019*

1. Purpose

The detector is a vital part of the HSI assembly. In spite of its importance, several key factors regarding the detector structure remain unknown. This extends to the build materials, both surface material and the inner materials. Materials inside the detector could cause damage to the CubeSat if outgassing occurs. The material comprising the detector must be identified to uncover if they impede the CubeSat mission.

It is known that the camera will heat up significantly during usage. This heat needs to be redirected and radiated through thermal coupling. Currently, the idea is to use three of the metallic surfaces of the camera to transfer the heat to the thermal control. It is however unknown if these surfaces will be equally efficient to use in vacuum conditions. This all depends on the internal electronic design of the camera. If the internal parts does not conduct the heat efficiently to the detector surface, the thermal couplings will not be an effective solution as the heat will get trapped inside the detector. The purpose of disassembling the camera is to identify how the heat is transferred on the inside, so that the thermal control can be better planned. This mitigates potential risks associated with the use of the detector in operation. Simultaneously, the inside of the detector can be well documented so that the team will have a better understanding of the COTS component being sent up in space.

2. Procedure

Disassembling of the detector requires a structured plan both for disassembly and documentation. The detector planned for disassembling is the IMX174 using micro usb. The disassembly process will destroy the detector. Currently the IMX249 using bolted down ethernet port will be used for the mission. Even though a different version will be used for the mission, it is believed that the two versions should be sufficiently close to each other in internal mechanical design.

Table 2 shows all equipment and equipment quantity used during the procedure.

Table 2: Equipment list

Equipment	#
Sony IMX174 sensor (Detector)	1
Screwdrivers	1
Tweezers	1
Isopropanol	1
Non latex gloves	-
Digital Camera	1
Ziplock bags	1 pack

3. Disassembly Procedure test

Wear gloves. Loosen the screw on the bottom of the detector. Take notice if anything loosens up. Slide any parts if able. Lift up the clamped metal surfaces on the side of the detector. Check if these can be lifted with a jack. If not, apply isopropanol (assuming it's glued together). The detector is a compact parts, it follows that some force may be required in order to open the assembly. Damage can occur on the outer shell and non vital areas of the detector. The detector will not be reassembled and will be considered unusable after the entire process. The disassembled parts will be preserved in ziplock bags and marked for further investigation. The parts will then be examined in order to determine if the parts are unsuited in a CubeSat.

It is worth noting that the actual disassembly procedure might diverge as these are assumptions. This is an exploratory experiment and such the procedure will be adapted to the actual construction of the detector.

It is postulated by the mechanics team that the detector is made with the following parts:
- Lens
- PCB stack with a camera piece
- Connectors
- Metal prong
- Clamp backside
- Clamp front

4. Documentation

The disassembly process will be documented with the following actions. All steps shall be documented with pictures. All steps shall be written down in the "Disassembly Steps " table located in section results. The large unown material pieces will be examined using an xrf scanner and microscope at the material science lab. The scanner will be able to detect non metallic material. In addition, the scanner can uncover the exact material, if the part is comprised of metal.

5. Results

The following section provides the results found during the disassembly process. Table 3 shows the steps taken, table 4 tabulates noteworthy findings. Pictures taken for every step can be found in the Appendix A : Detector Disassembly Figures.

Table 3: Detector Disassembly Chart

Step nr.	What was done	Why was it done	What happened
1	Loosen the outer phillips head screw	As a first step in opening the camera. This was the only screw present	Triangle piece loosened
2	Pull camera Z faces apart to expose the inner electronics.	To open up the assembly and make further disassembly possible	Parts were successfully pulled apart
3	Loosen the metal prong/bend it such that it can be removed.	Further loosening of the camera assembly. To avoid scratching the components	Metal prongs were bent. This step might not have been necessary. Next time this should be checked
4	Removal of the two accessible thermal pads	Make space for further disassembly of PCBs	Pads were successfully removed using tweezers
5	Removal of screws from the -Z PCB	To remove the -Z back PCB from the frame	Screws were removed. Ferromagnetic and darkened
6	Attempt to remove -Z back PCB from the frame	To allow access to the final third thermal pad as well as see what is between	PCB still remains rigid to the camera. See notes
7	Removal of screws in the middle +Z PCB	To remove the +Z PCB (sensor side) from the assembly	Successfully removed
8	Remove the +Z PCB from the stack	To allow room for further disassembly and separate the sensor side from the frame	The +Z PCB was successfully detached

9	Remove QR Code sticker from +Z PCB	Stickers not space rated	Sticker was successfully removed
10	Remove QR code sticker from +Z middle PCB	Stickers not space rated	Sticker was successfully removed
11	Removal of two screws in the +Z PCB	To loosen the PCB from the frame	Screws were successfully removed. They are ferromagnetic. Metallic
12	Removal of two additional screws (stack spacers) in the +Z PCB	To loosen the PCB from the frame	Screws were successfully removed. Not ferromagnetic
13	Removal of +Z PCB (camera sensor) with nylon tweezers	To inspect the PCB and the imaging sensor	Successfully removed. Underneath was a thin film (three layers, as a gasket between the sensor and PCB) and the camera sensor. Blue side of the gasket was on the top(-Z), then orange, then green
14	Push the lens out in the -Z direction from the lens holder	To inspect the lens/front windows and its gasket	The lens was pushed into the lens tube. There is a gasket present. The lens is most probably made of acrylics
15	Remove gasket from lens	To inspect the components further	Gaskets were successfully removed. This was the final step possible before destroying parts. nothing of particular interest was observed on the camera sensor

Post Disassembly PCB removal Steps			
The remaining pcb piece was given to the electronic lab at NTNU for disassembly. The following steps were taken by the electronic lab.			
16	Heat up area around 8 soldered pins holding the -Z PCB to the -Z housing	To more easily desolder the 8 pin connector	Area is heated up, however, a lot of heating is required. This is caused by the housing acting as a heat sink
17	Add heat on the 8 pin connection using a soldering iron	To melt the solder around the 8 pins simultaneously for removal	8 pin connector successfully removed, however an additional PCB component falls
18	Separate the PCB from the -Z back plate	To be able to remove the undesired polymer parts	Separation was successful, however required force as the parts were glued together
19	Remove thermal strap and thermal pad	High outgassing parts removed from assembly	The strap and pad suffered heavy damage.

Table 4: Noteworthy Findings

Notes
The bolts on the insides are ferromagnetic. The single bolt on the outside is not. The camera appears to be designed with thermal conduction in mind. the thickest wall is on the black side. There also seems to be a dark grey thermal strap connecting the onboard PCB chips and the backside of the chassis. The thermal strap is glued to the chips. The thermal strap is made out of multiple layers of unknown materials. There are white pads on the inside of unknown material. See zip lock bag. These pads might be thermal pads or mechanical pads to separate the PCBs in the stack. The -Z PCBs are still being investigated. It is believed that it's connected to the back plate by the power connector that is soldered on in the +Z side, while the -Z has a bushing. This keeps the structure connected unless the power connector is desoldered. The QR stickers needs to be removed from the flight model as well. The lens seems to made of some sort of polymer, possibly acrylic. Not glass. The Lens is secured with a polymer gasket. Probably not space rated. The +Z PCB (with the detector) is seated on three gaskets. These are probably not space rated. They have thicknesses of 0.20mm (Green), 0.10mm (orange) and 0.05mm (blue) respectively. High likelihood of these being spacers to ensure the correct flange focal distance. It is also worth noting that the detector can be mostly disassembled and reassembled while maintaining functionality.

Several parts inside the detector were deemed potentially unsuited for space flight:
- 4 Ferromagnetic bolts
- Lens elastomer gasket
- 3 Polymer sensor spacers
- 3 Polymer padding (Thermal/ Mechanical)
- Thermal strap with glue
- 2 QR stickers
- PCBs require epoxy coating
- Coating on the +Z and -Z material can potentially flake off

The detector might need several changes in order to make it flight ready. Due to the problems found, the detector was reassembled after removing most of the problem parts.

Table 5 shows the reassembly process. The assembly was done to indicate that removal of the potentially dangerous parts are possible, however time consuming.

Table 5: Detector Reassembly

Step nr.	What was done
1	Putting +Z PCB back
2	Screwing on one stack and one screw diagonally (incrementally)
3	The two remaining screws are screwed on
4	Two screws (blank) screwed back on the -Z PCB
5	Reattach connector between +Z PCB and middle +Z PCB
6	+Z middle PCB black screws (2) rescrewed
7	Metal shroud reattached and clicked on
8	Thermal pads (2) re-inserted
9	Squeeze full assembly together
10	Add final screw

After the reassembly, a simple test was done with a simple detector- lens assembly to uncover if the detector would operate properly. The pictures taken shows that the detector can be reassembled, however more tests will be required to secure that the detector integrity will not be harmed during such a process.

5.1 Post Disassembly PCB Removal

As previously mentioned in the disassembly notes, the removal of the -Z PCB from the -Z housing could not be done as an 8 pin connector held the assembly together. This connector had to be desoldered in order to further investigate the detector, as well as remove the final thermal pad. The following list will tabulates the additional complications and discoveries made in regards to the detectors suitability for space:

- Unknown material used as padding between the -Z PCB and -Z housing
- Padding is glued to the PCB and housing
- Desoldering of 8 pin connector is difficult, and can easily lead to damage to the surrounding area

The desoldering of the 8 pin connector required heavy heating of the surrounding area in order to melt the solder around the pins. As mentioned in the disassembly chart, this resulted in another PCB component separating from the PCB. The surrounding area in both the PCB and thermal strap experienced charring as a result of the heat.

6. Conclusion

The detector might need several changes in order to make it flight ready. After this test, it is highly recommended that an IMX 249 also be disassembled. Although the detectors are expected to be similar, it would prevent any surprises when it inevitably will have to be disassembled.

Appendix A: Detector Disassembly Figures

1.Removing the outer screw
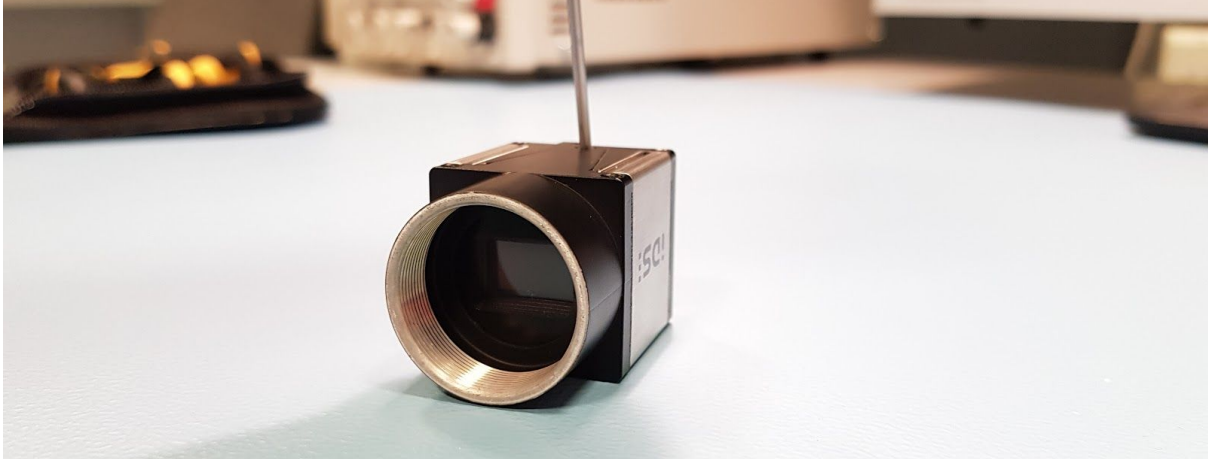
2.Pulling the detector apart
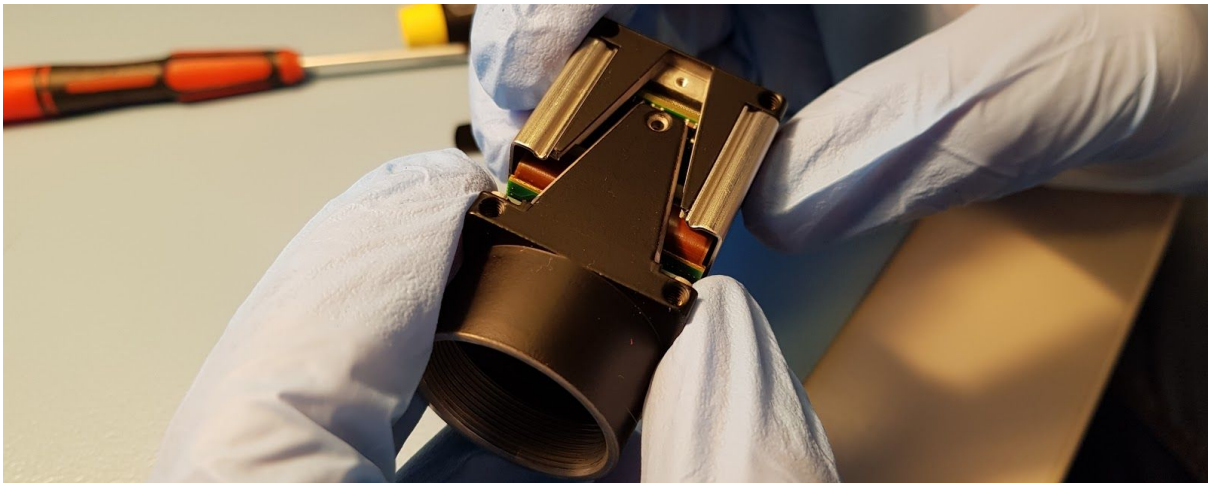
3. Metal prongs removed
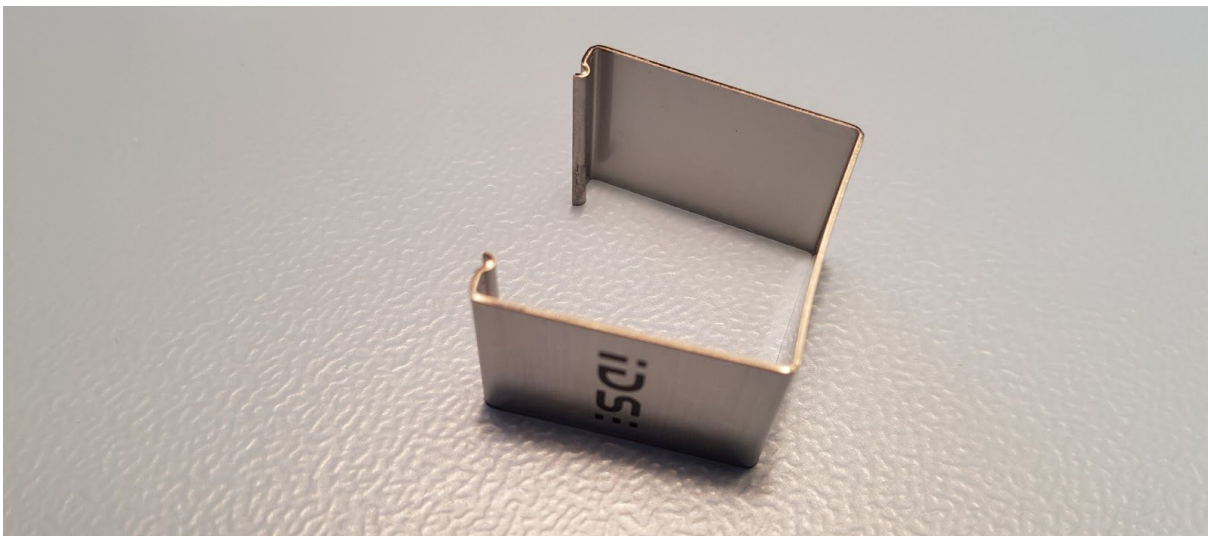
4. Removal of two polymer pads. Total of three in stack
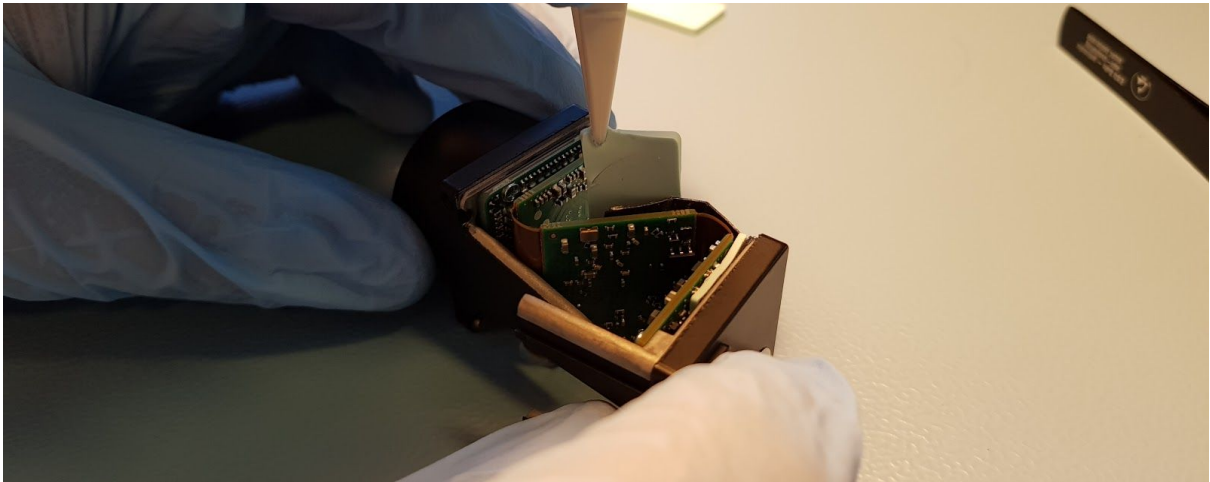
5. Removal of screws in the -Z direction
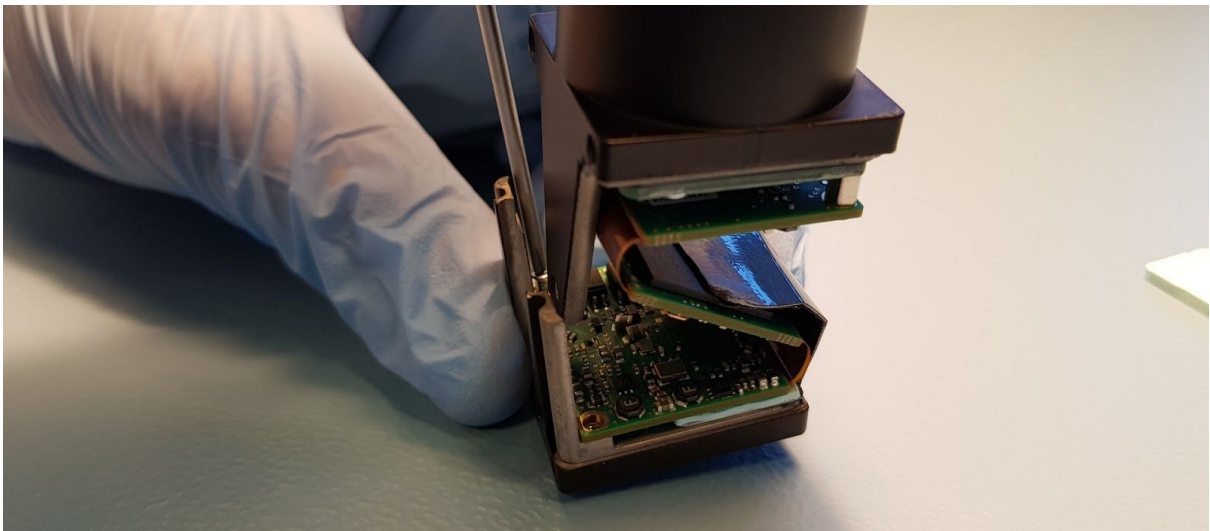
6. The PCB stack
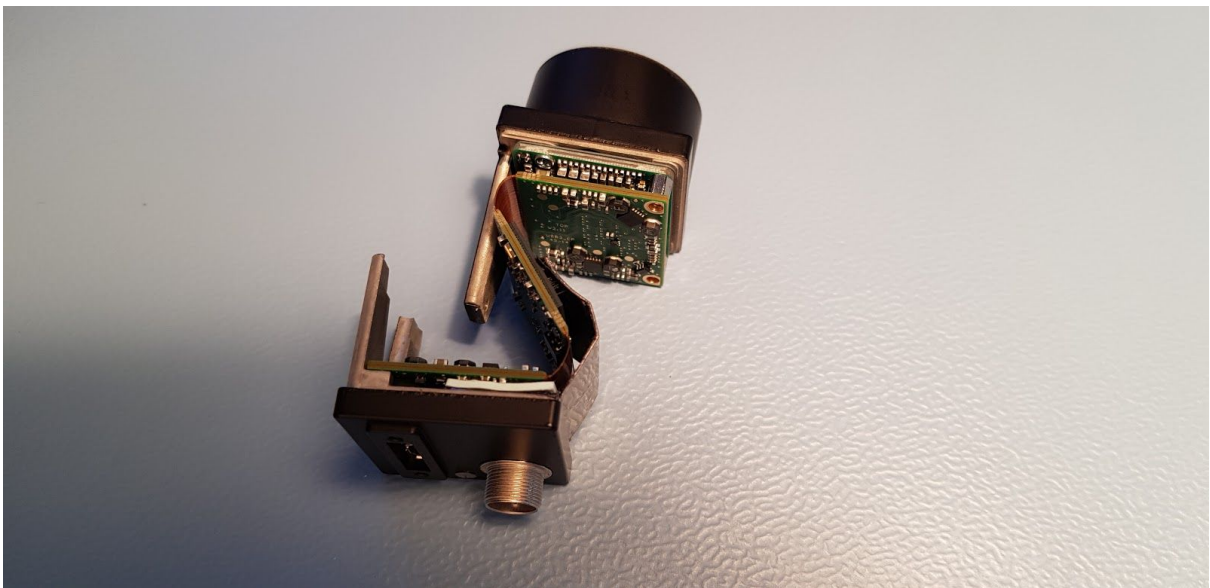
7. PCB stack and thermal coupling
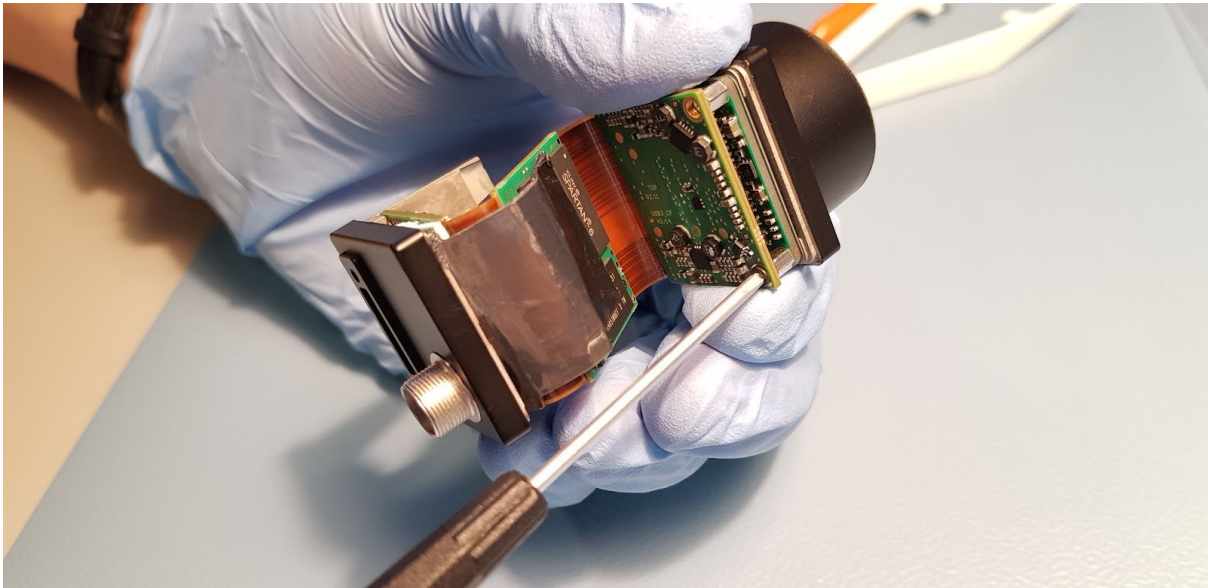
8 +Z PCB disconnected from the middle +Z PCB
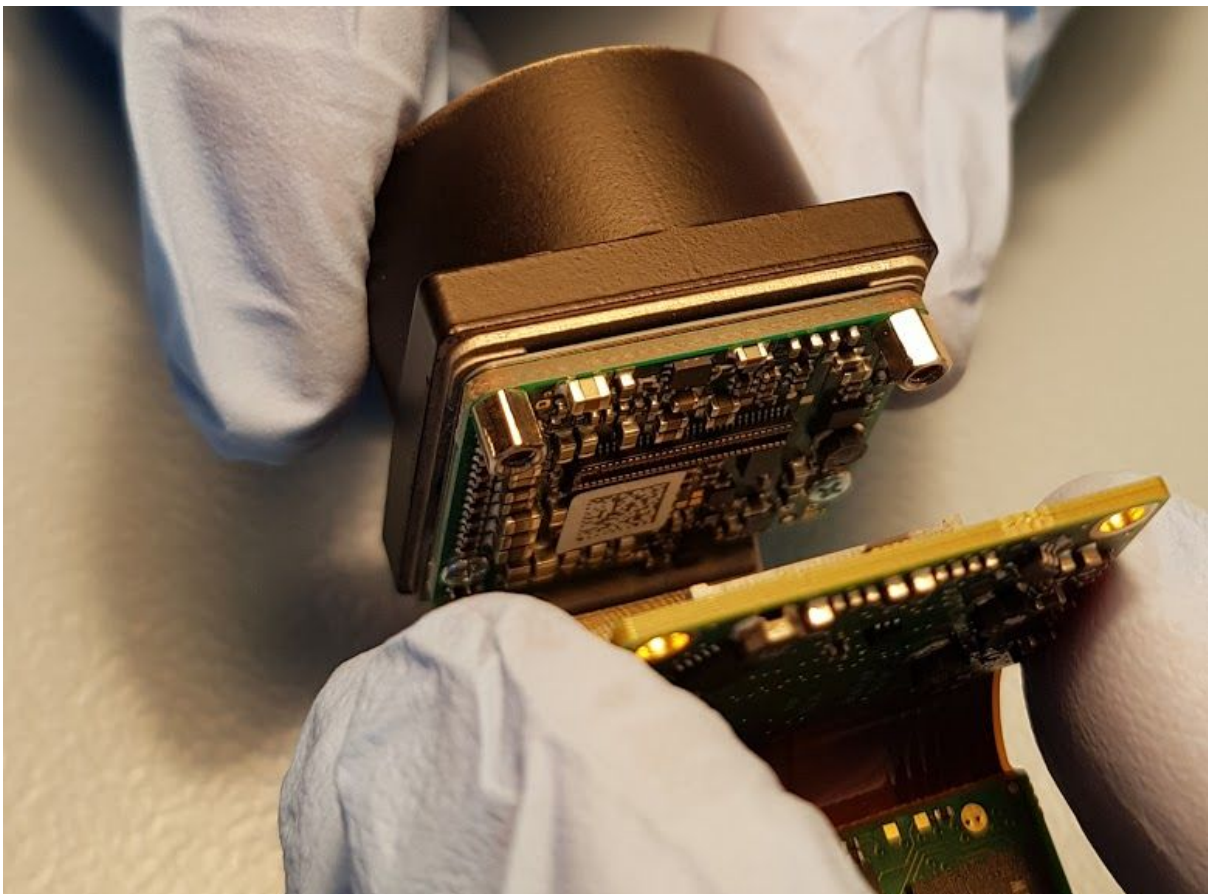
9. Removal of the +Z PCB QR sticker
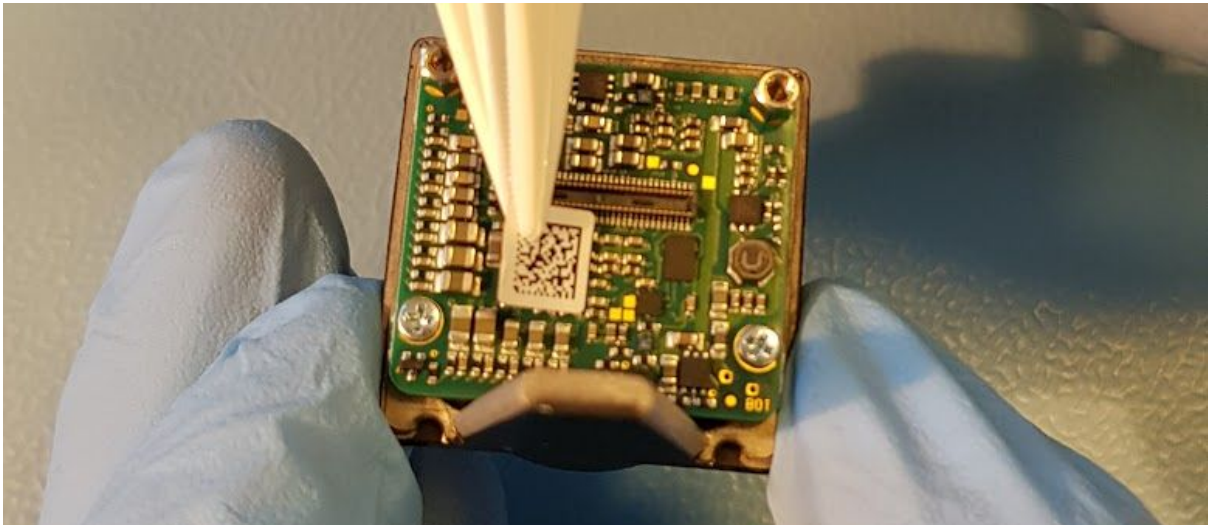
10. The QR sticker on the +Z middle PCB.
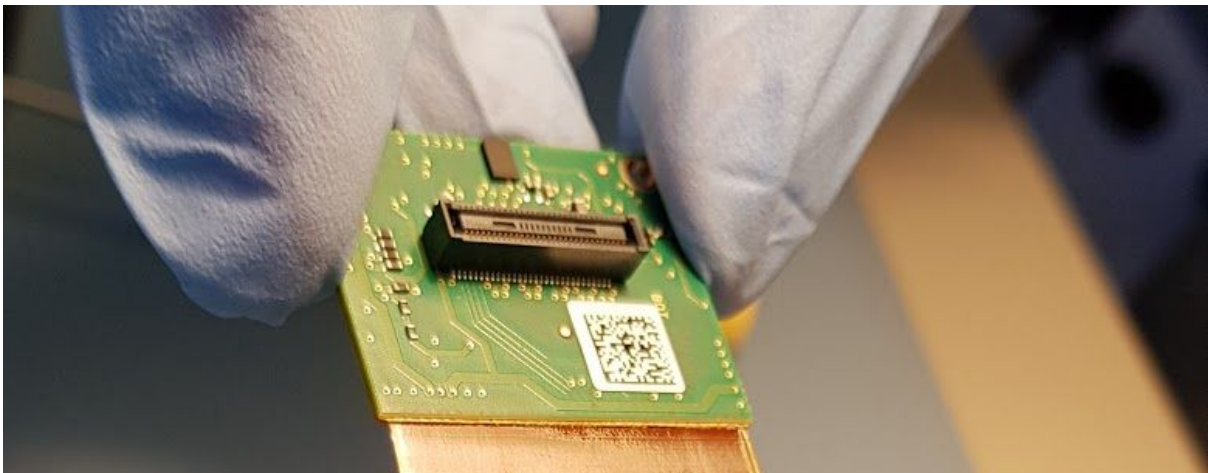
11. Removal of two normal screws from +Z sensor PCB
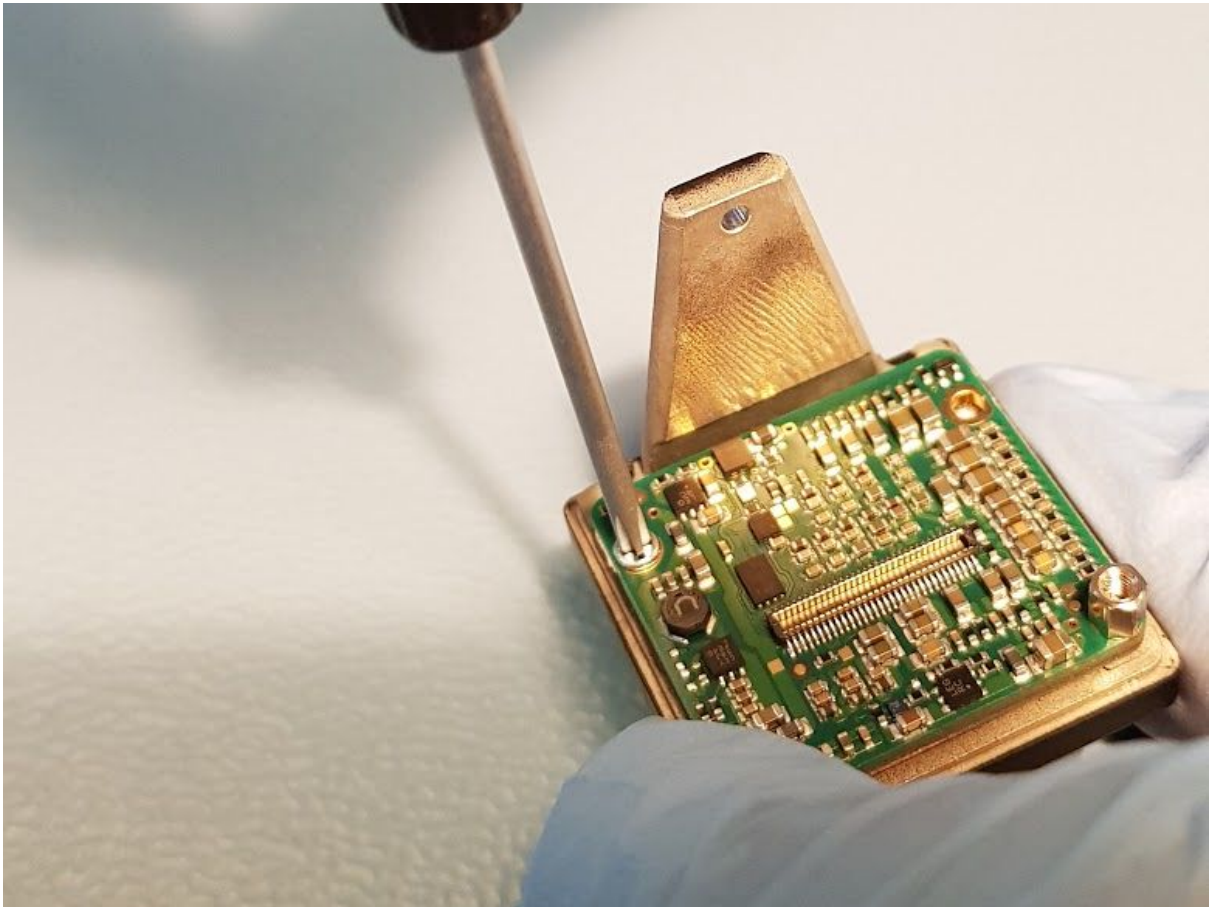
12. Removal of two stack screws from +Z sensor PCB
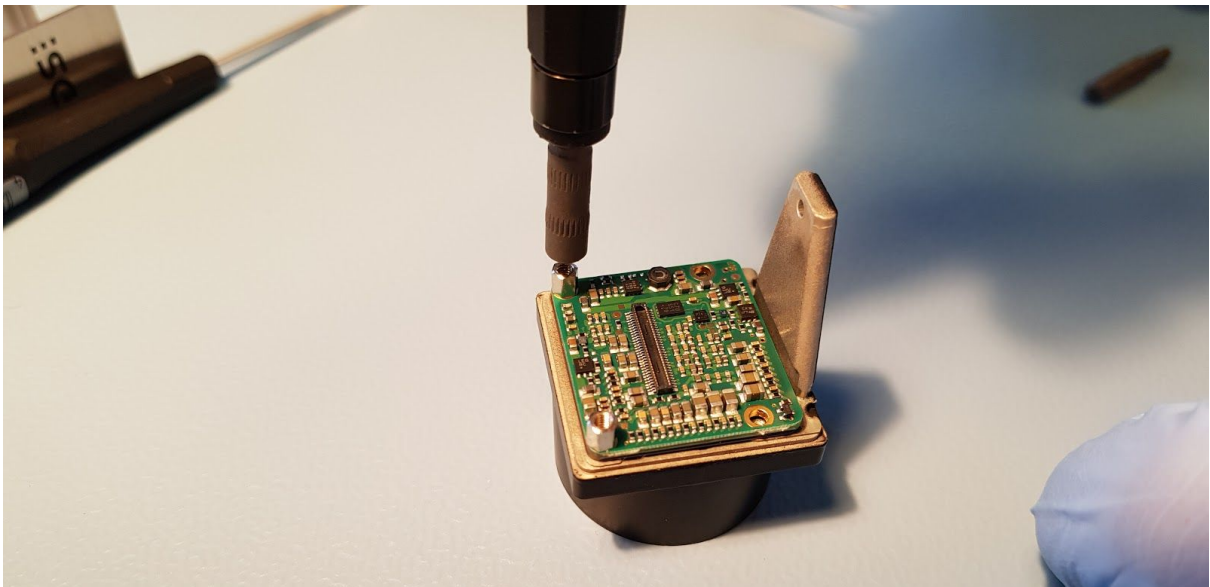
13. Removal of sensor PCB from lens housing (both sides)
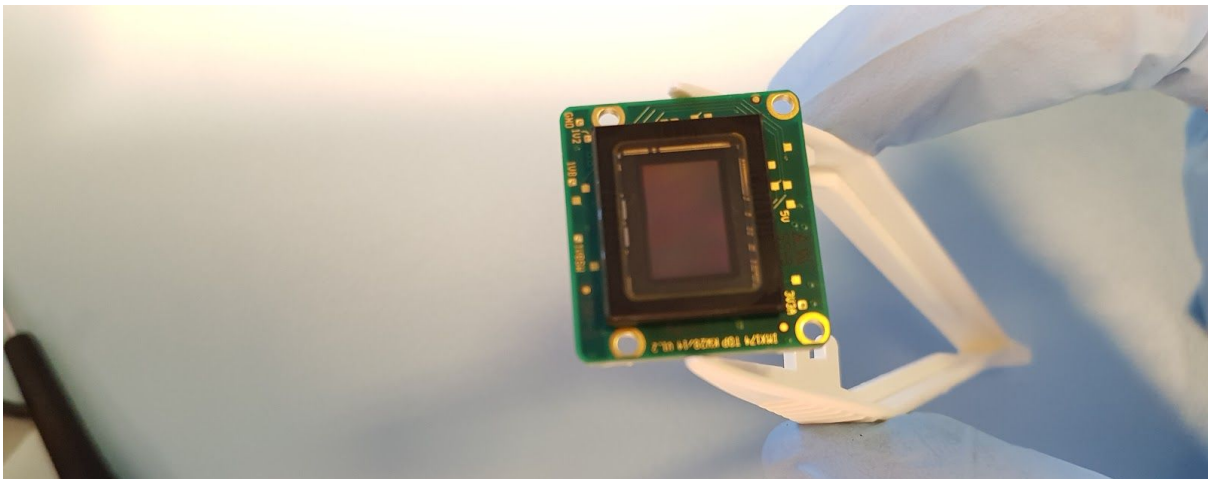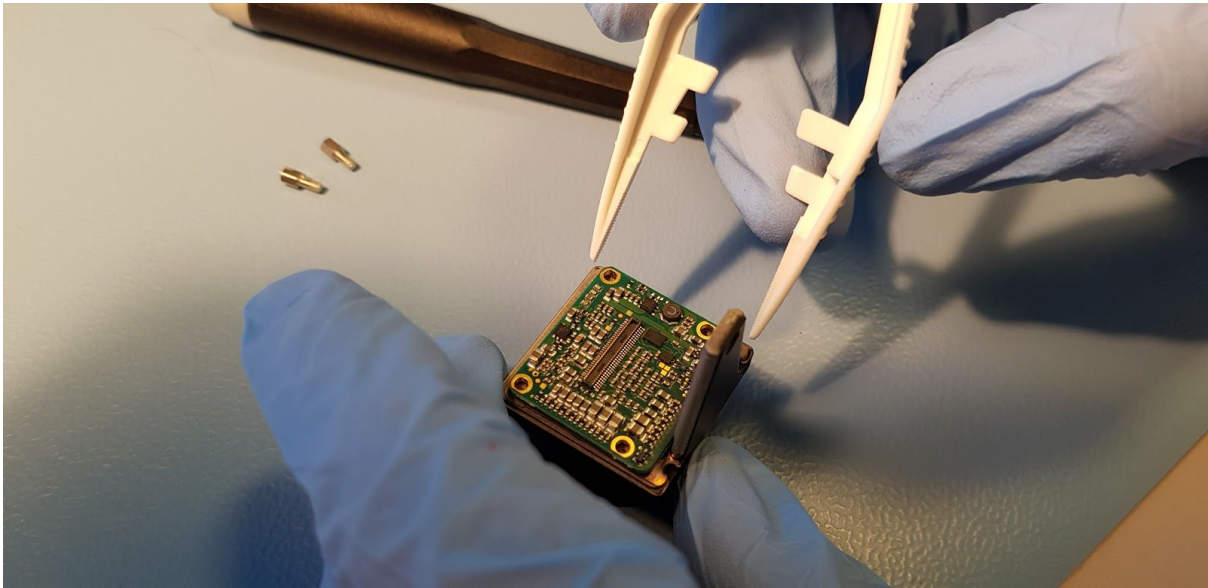
Three polymer sensor spacers
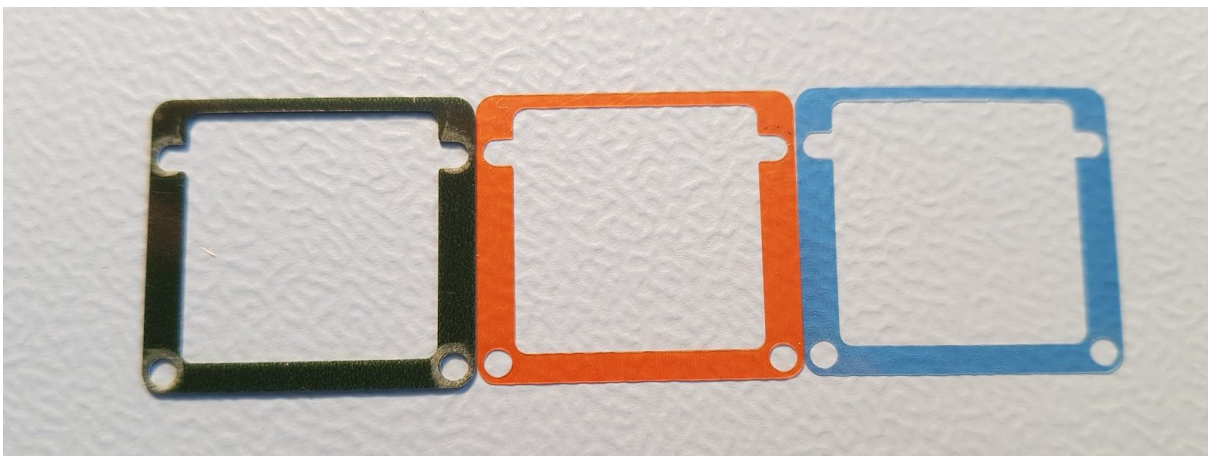
14. Pushing of gasket and lens from lens holder
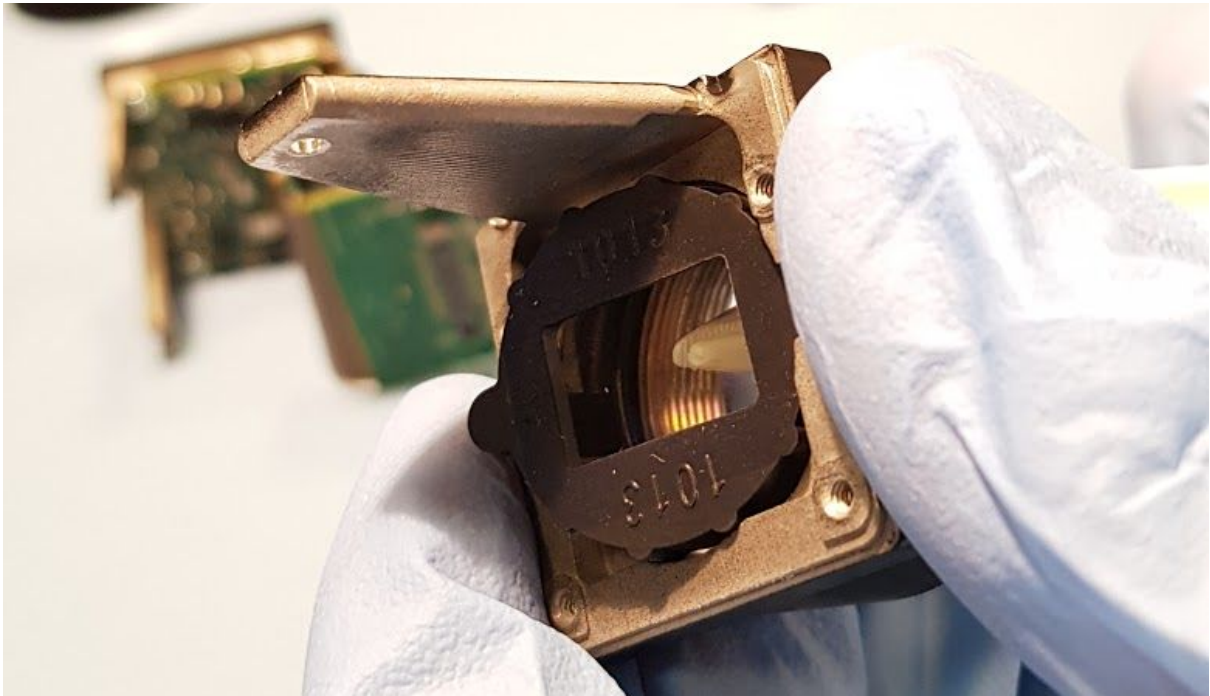
15. Gasket removed from lens
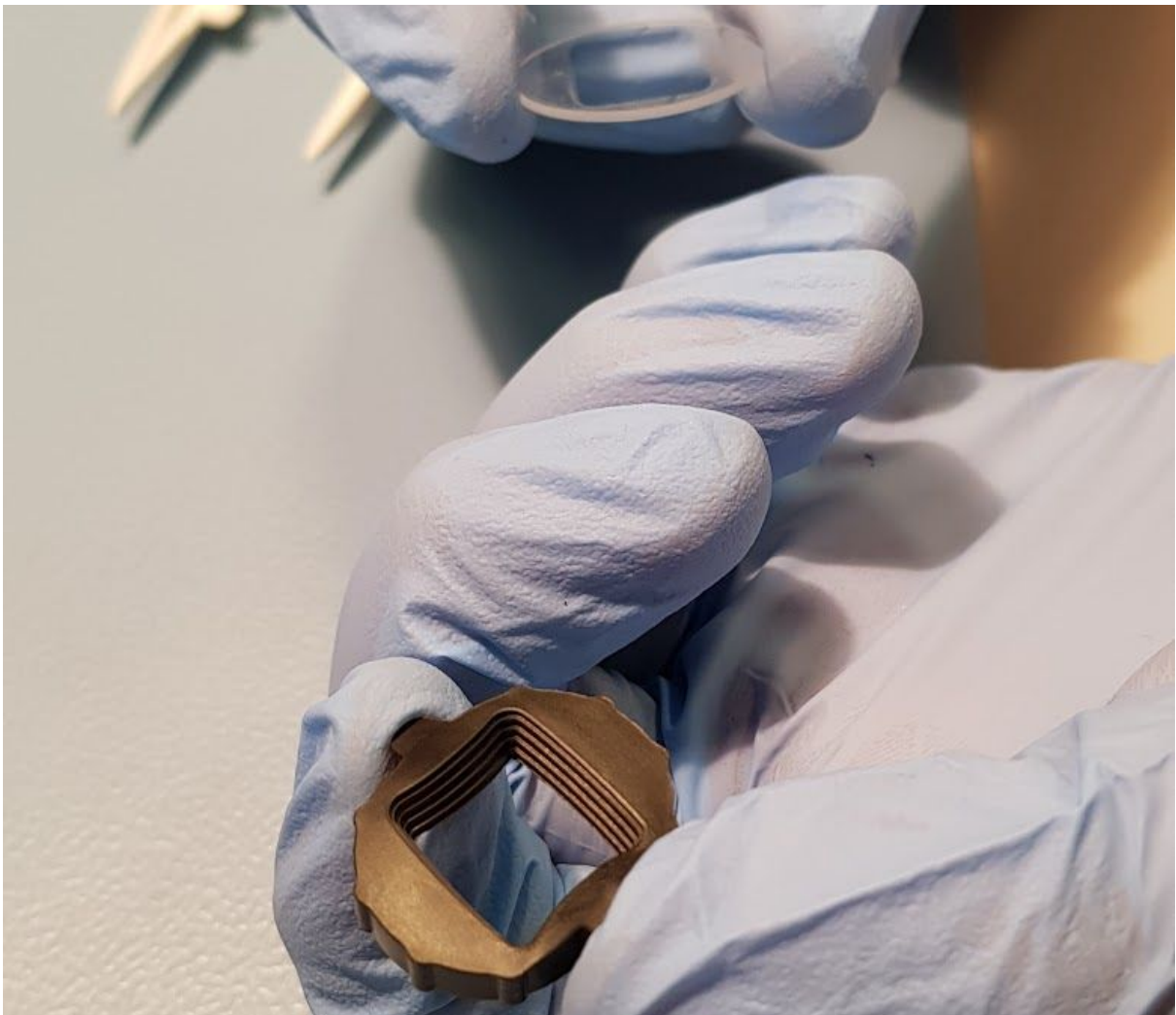
Magnetic screw
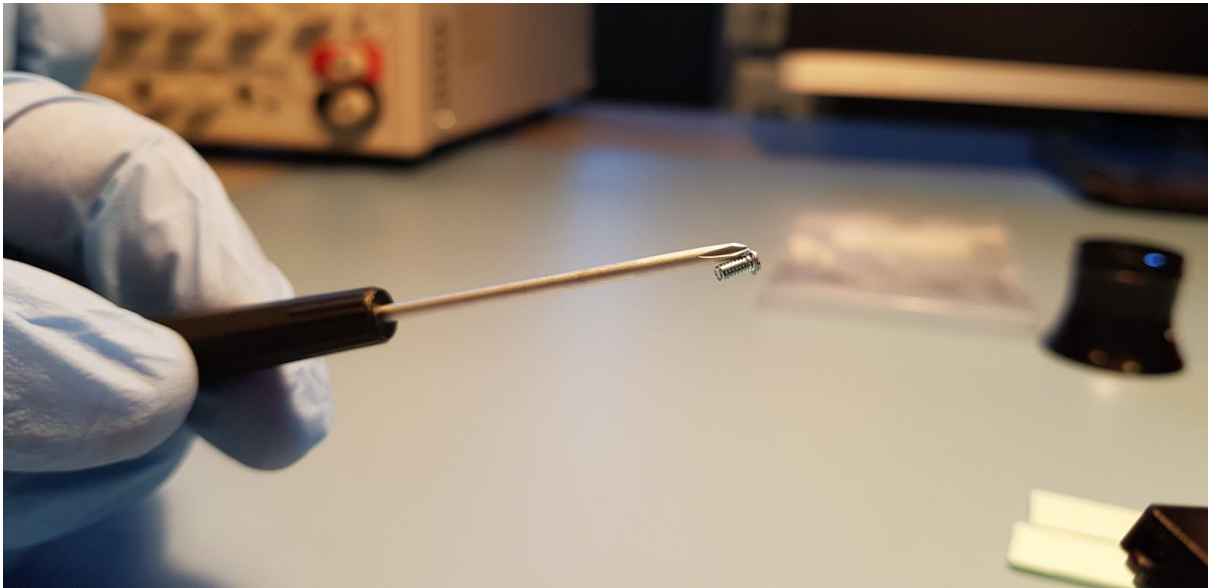
QR stickers in the stack
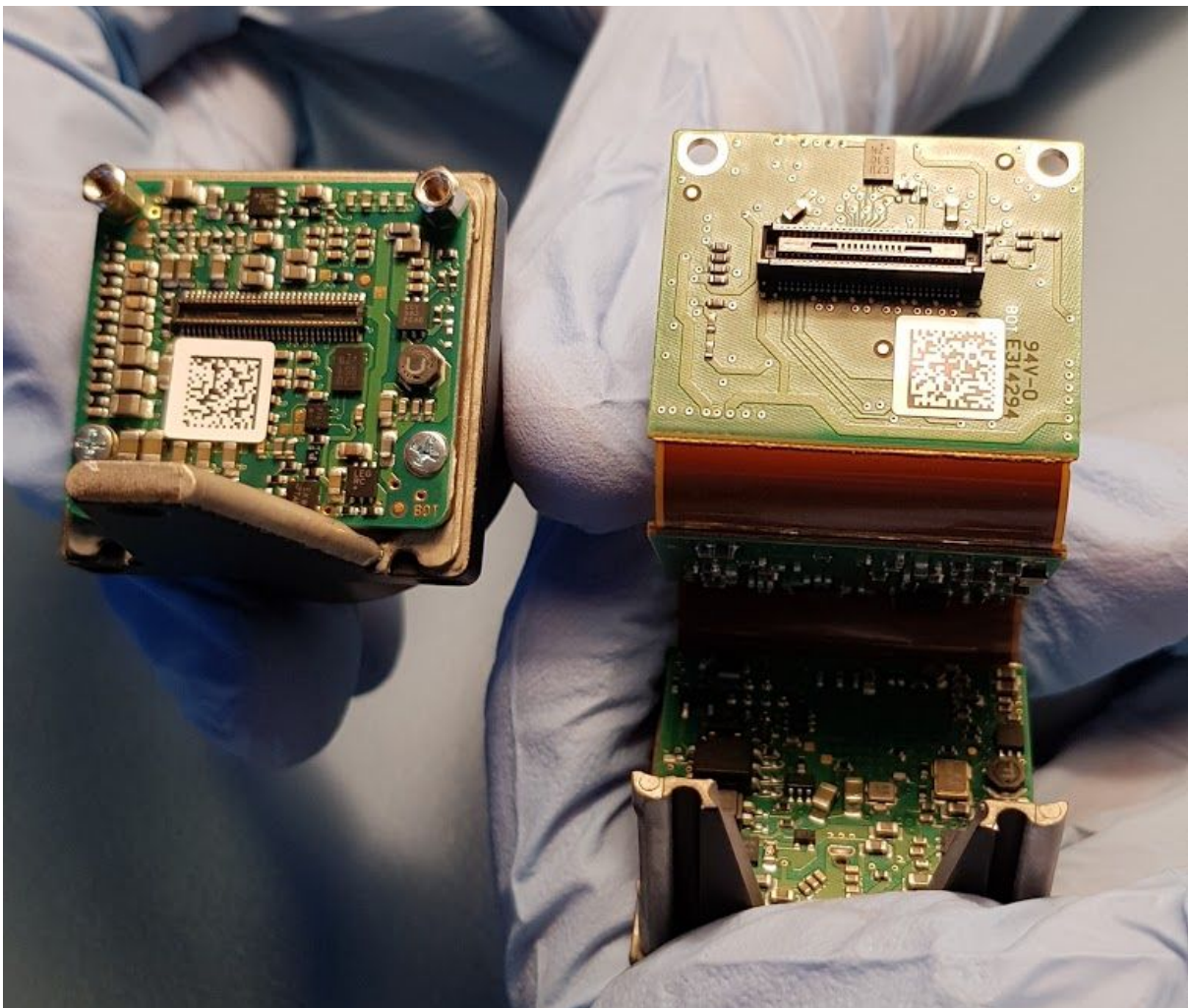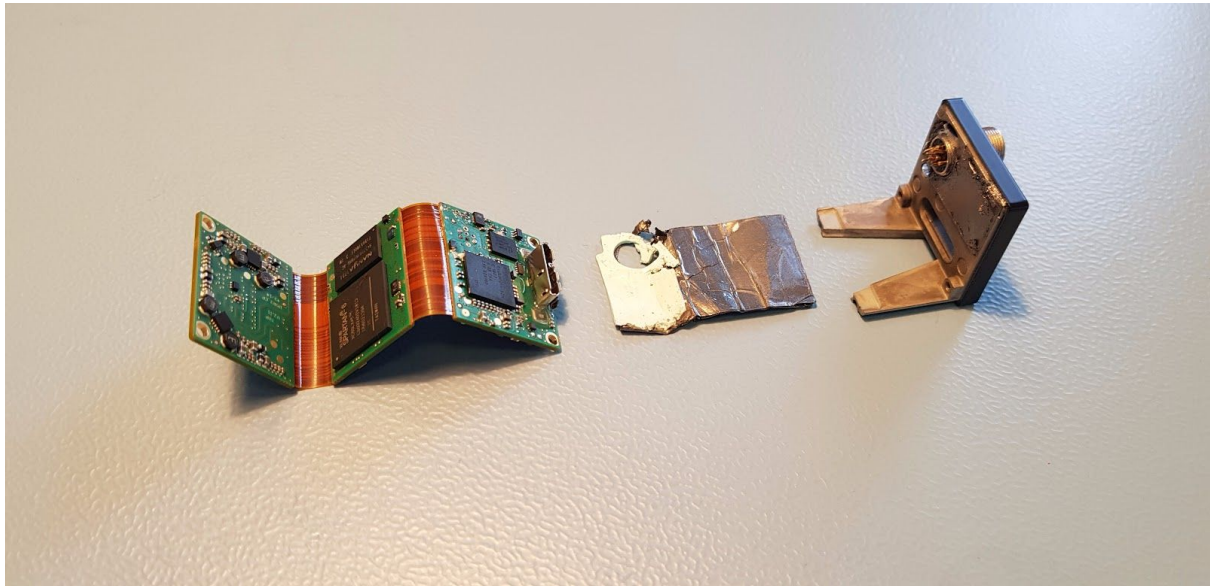
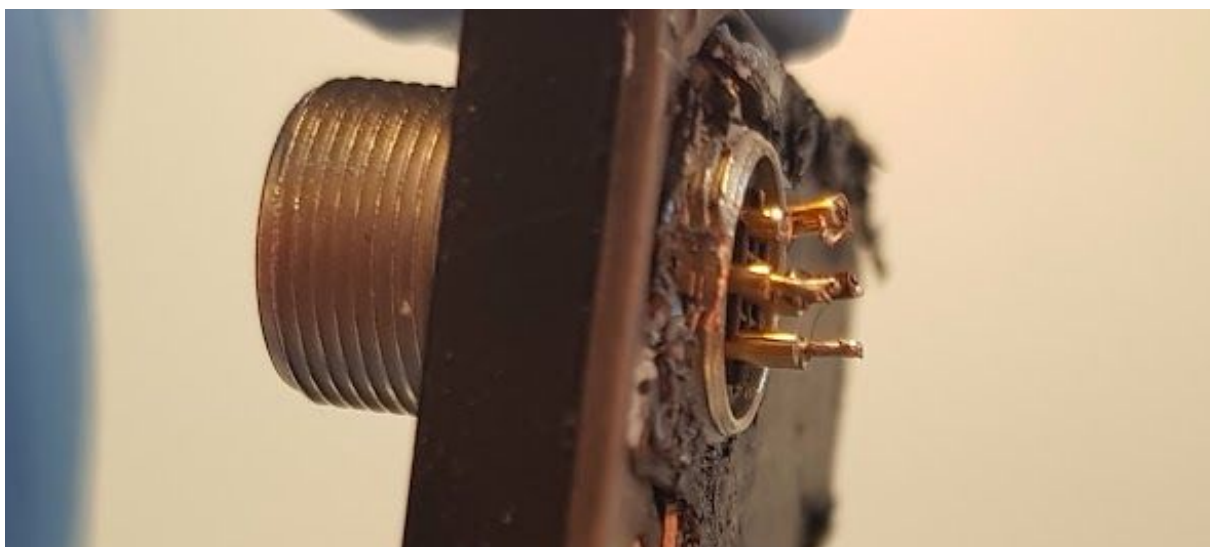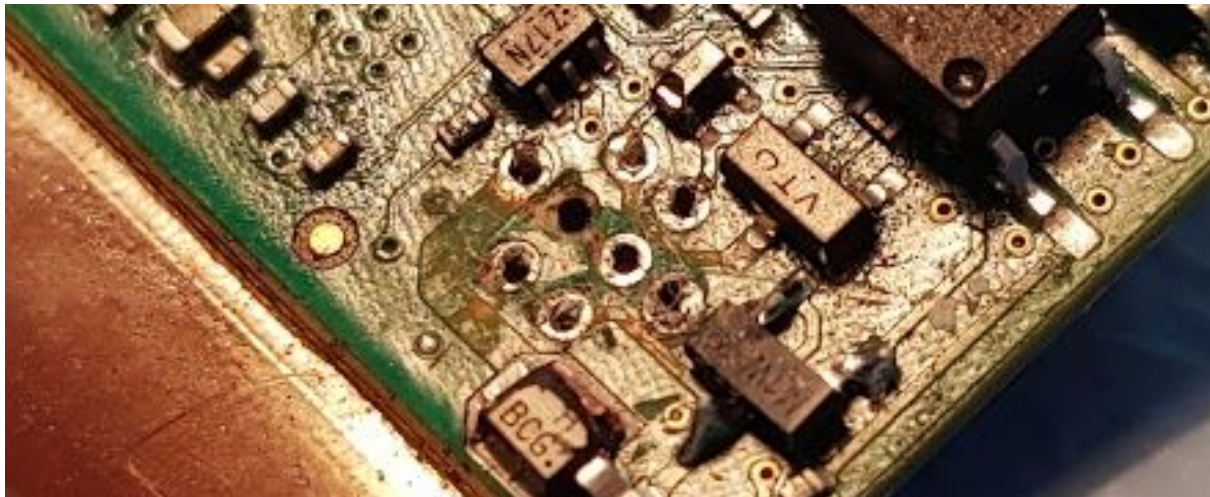## Thermal strap glue
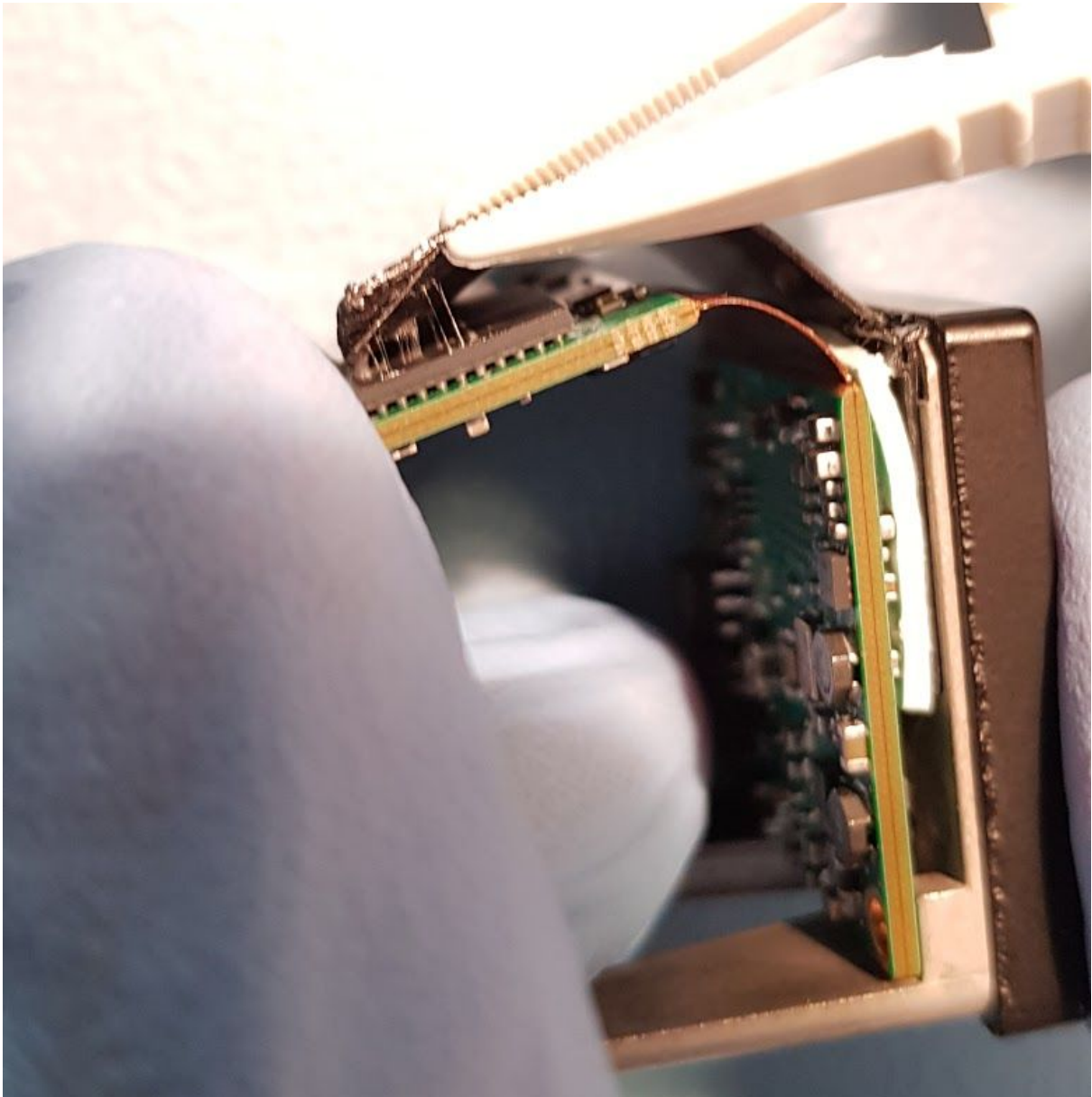
The magnetic bolts

uEye
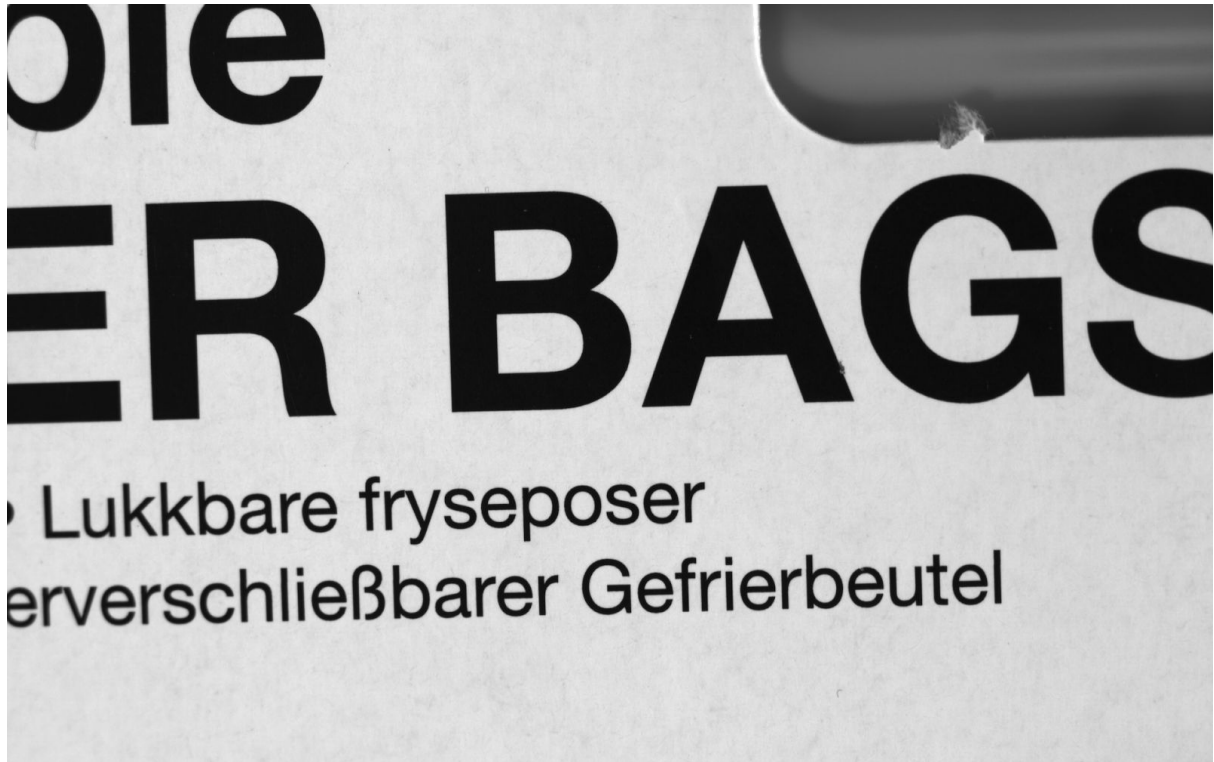
Sample pictures captured in uEye after reassembly.
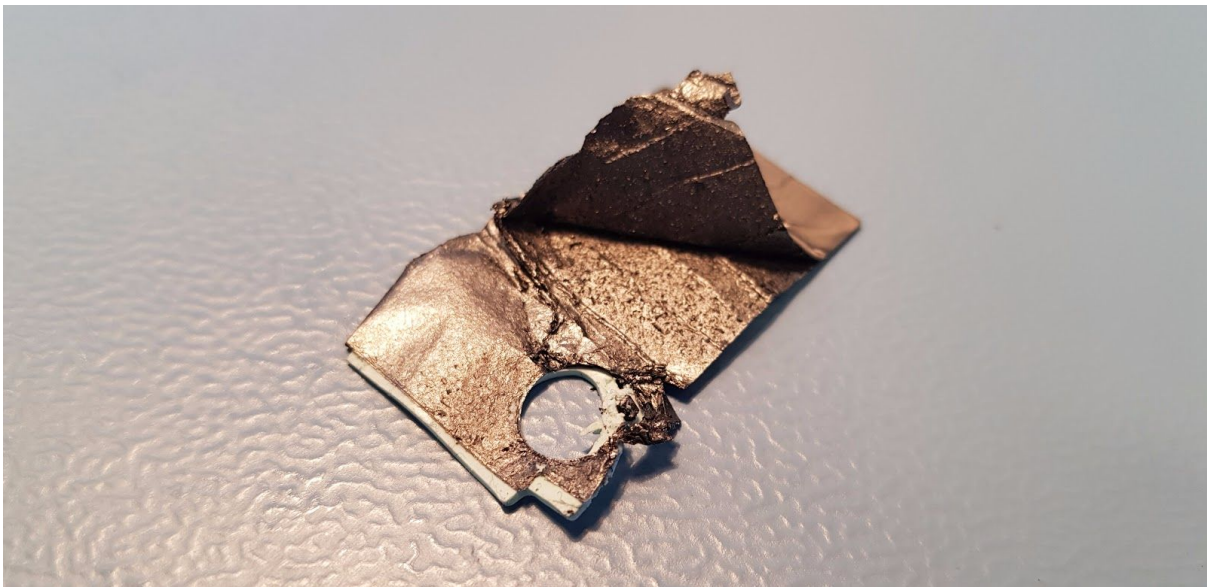
-Z PCB separated from -Z housing

Post desoldering of 8 pin connector

Leftover material from padding stuck to -Z housing

Padding of unknown material

UI-5260CP

Detector Disassembly

HYPSO-RP-008

Prepared by: HYPSO Project Team
Reference: HYPSO-RP-008
Revision: 2
Date of issue: 25.05.2019
Document Type: Report
Author(s):   Tord Kaasa, Tuan Anh Tran, Henrik Galtung

Table Of Contents

Table 1: Table of Changes

Rev.	Summary of Changes	Author(s)	Effective Date
1	*First issue*	*Tuan Tran,* *Tord Hansen Kaasa,* *Henrik Galtung*	*20.03.2019*
2	*Formatting of text*	*Tuan Tran* *Tord Hansen Kaasa,* *Henrik Galtung*	*25.05.2019*

1. Purpose

The IMX174 detector showed several problem materials during the disassembly process. Currently the IMX249 using bolted down ethernet port is the detector that is designated for the mission. Even though a different version will be used for the mission, it was believed that the two versions should be sufficiently close to each other in internal mechanical design. Based on the IMX174 disassembly, a mitigation report was created, outlining the possible solutions with regard to the feasibility of adapting the COTS components. The disassembly of a IMX249 detector with shell, a UI-5260CP Detector will be used to scrutinize the conclusions in the mitigation report. If the UI-5260CP detector can be safely disassembled while removing all unwanted parts, the adaptation of the specific detector shall be added to the list of possible options in the mitigation report.

The list of unwanted components include, polymer pads, thermal straps, glued on QR codes, polymer spacers, elastomer gaskets and ferromagnetic bolts.

2. Procedure

Disassembling of the detector requires a structured plan both for disassembly and documentation. The disassembly will be non destructive if possible. Destructive force will be used if necessary to remove a volatile component. If destructive force is applied, the adaptation of the UI-5260CP Detector will not be considered a viable option.

Table 2 shows all equipment and equipment quantity used during the procedure.

Table 2: Equipment list

Equipment	#
Sony UI-1250SE (RGB Detector)	1
Screwdrivers	1
Tweezers	1
Isopropanol	1
Non latex gloves	-
Ziplock bags	1 pack

3. Results

The following section provides the results found during the disassembly process. Table 3 shows the steps taken, table 4 tabulates noteworthy findings. Pictures taken for every step can be found in the Appendix A: *Detector Disassembly Figures*. The detector can be reassembled by repeating the non destructive steps. Characterization tests must be done on a reassembled detector to determine that no operational inhibitory damage has been sustained during the disassembly process.

Table 3: Detector Disassembly Chart

Step nr.	Step Description	Additional information
1	Remove +Y screw (1)	Screw description: Ferromagnetic, dark.
2	Remove the steel prong	Allows for accessibility of PCB stack. The stack consists of three PCBs.
3	Remove two accessible thermal pads	Large pad between the middle PCB and back PCB Small pad between the back PCB and pin connector PCB
4	Remove screws (2) connecting the front PCB to the other PCBs	The front PCB assembly is now loose. Screw description: Ferromagnetic, dark.
5	Remove the ethernet connector located between the back BCB and the shell using tweezers	This is difficult to remove. A set of tweezers must be applied to the +X and -X sides.
6	Remove QR codes from front PCB using tweezers	QR code stickers glued on, any residue must be removed.
7	Remove the two stacking rods and two screws on the front PCB	The front PCB can now be removed from the assembly.
8	Remove polymer spacer	Two spacers are inserted between the PCB and front frame.
9	Remove gasket and lens	The gasket is made of an elastomer, the lens should be removed to improve the optical capabilities of the camera.
Destructive Disassembly		
10	Removal of the I/O eight pin connector	This part must be removed by force. Necessary in order to reach the small polymer pad located between the back frame and pin connector PCB.
11	Remove the polymer pad on the back frame	Final step.

Table 4: Noteworthy Findings

Notes

The detector shares internal similarities with the IMX174 detector, however it deviates in four significant areas:
- No thermal straps are used in the UI-5260CP detector
- The thermal pads are placed differently and are of different sizes
- The back pad is not wedged around the I/O eight pin connector

Bolts appears to be ferromagnetic as with the IMX174.

The UI-5260CP contains three polymer pads (thermal and mechanical pads) in three different sizes. The pads are located between the middle and back PCBs (large size), back pin connector PCBs (medium size), and the pin connector PCB and frame (small size).

Removing the polymer pads can result in some residue on the connected PCBs. This must be removed in an eventual flight model.

Ulike the IMX174 model, the UI-5260CP detector has no internal thermal straps and appears to be less packed on the inside due to the size of the ethernet connector.

The detector sensor is located on the front PCB. To avoid damage, the PCB must be handled carefully.

The lenses are made from glass.The Lens is secured with a polymer gasket. Probably not space rated.

The +Z PCB (with the detector) is seated on two spacer gaskets.
- Probably not space rated
- Thicknesses: 0.20mm (Green), 0.10mm (orange), note color coding does not match the spacers used in the IMX174 detector
- High likelihood of these being spacers to ensure the correct flange focal distance

It is also worth noting that the detector can be mostly disassembled and reassembled while maintaining functionality, the problem spot, like the IMX174 detector is related to the I/O eight pin connector connecting the beck PCB to the back of the frame. Destructive force or desoldering is necessary in order to remove the connection. A thermal pad is located between the stated components and cannot be safely removed without a complete disassembly of the back PCB from the frame.
The I/O eight pin connector could possibly be removed and reassembled non destructively be desoldering the pins, however the results cannot be guaranteed, and would potentially not be space graded and worth the effort in comparison with adapting a PCB-only IMX249.

The ethernet connector appears to be somewhat loose. This is also likely the case with the IMX249 PCB only.

Vulnerable components

Several parts inside the detector were deemed potentially unsuited for space flight:

- Polymer pads (3)
- Lens gasket
- Polymer spacer inserts (2)
- Ferromagnetic bolts

The UI-5260CP detector need several changes in order to make it flight ready, however the vulnerable parts are easier to remove than in the IMX174 detector. The removal of the thermal polymer pad between the back frame and PCBs has been shown to be the largest problem, and can seemingly not be removed without destructive force due to the pads lack of structural integrity. If the pad could be removed non intrusively, the residue would still have to be removed. The excess polymer can be removed by using an ultrasonic bath.

4. Conclusion

The detector might need several changes in order to make it flight ready. After the disassembly of the unit and the destructive process necessary to remove problematic components, the conclusion reached in the Detector Vulnerability Report is substantiated. The adaptation of the COTS components with a shell, including the UI-5260CP detector, is deemed as a poor solution due to the complication of the removal of certain polymer parts. A review of the PCB only IMX249 detector is recommended.

Appendix A: Detector Disassembly Figures
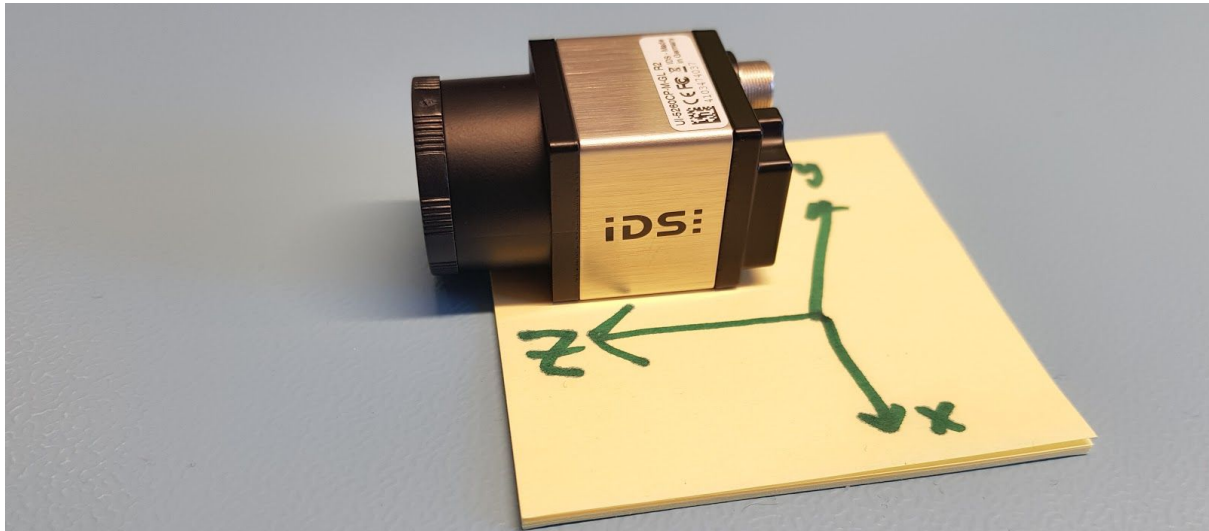
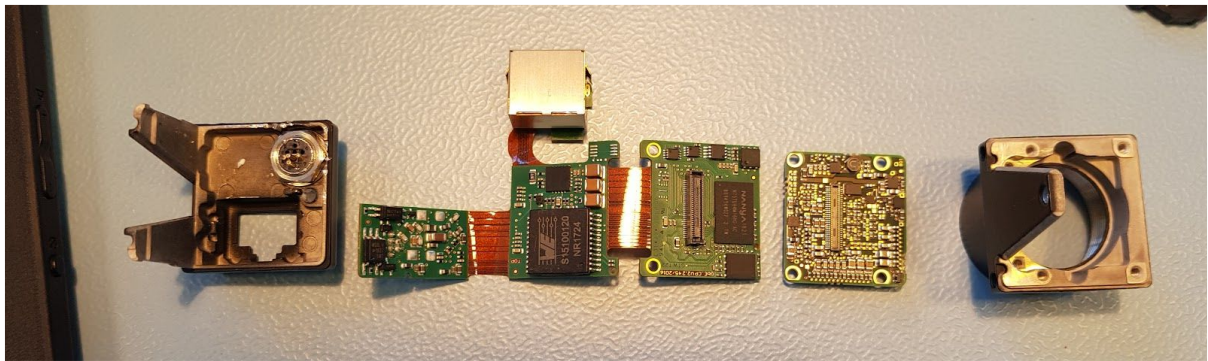*Figure 1. Detector coordinate system*
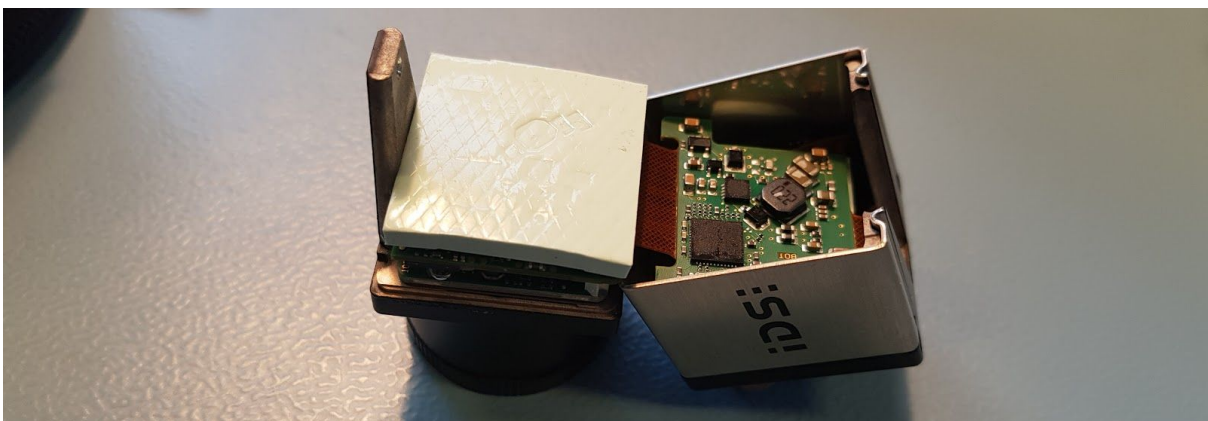

Figure 2. Detector PCB stack
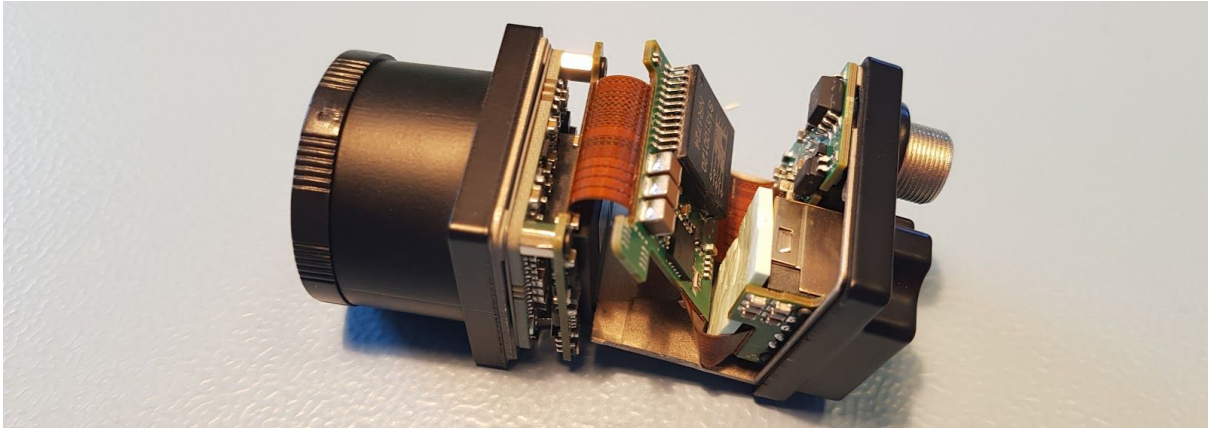

Figure 2. Thermal Pad (Large)
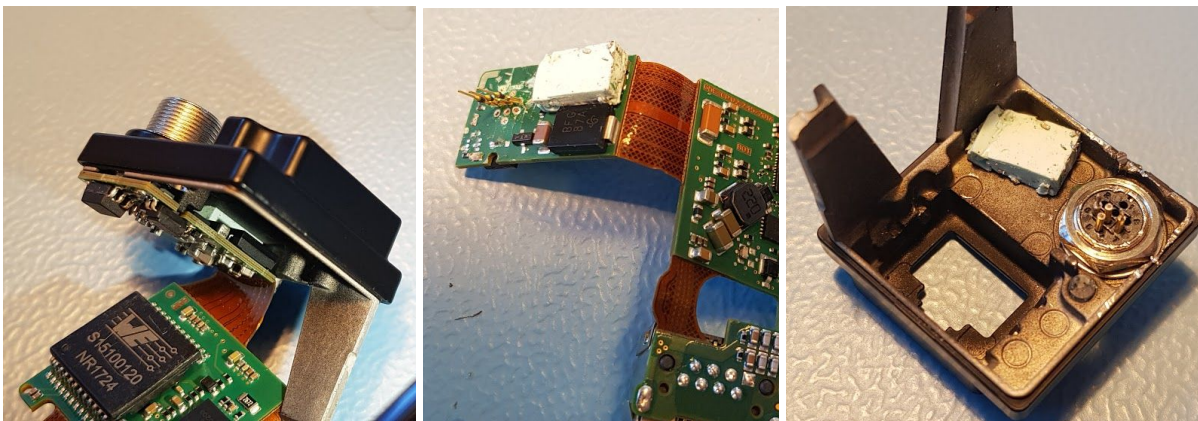
Figure 3. Thermal Pad (Medium)

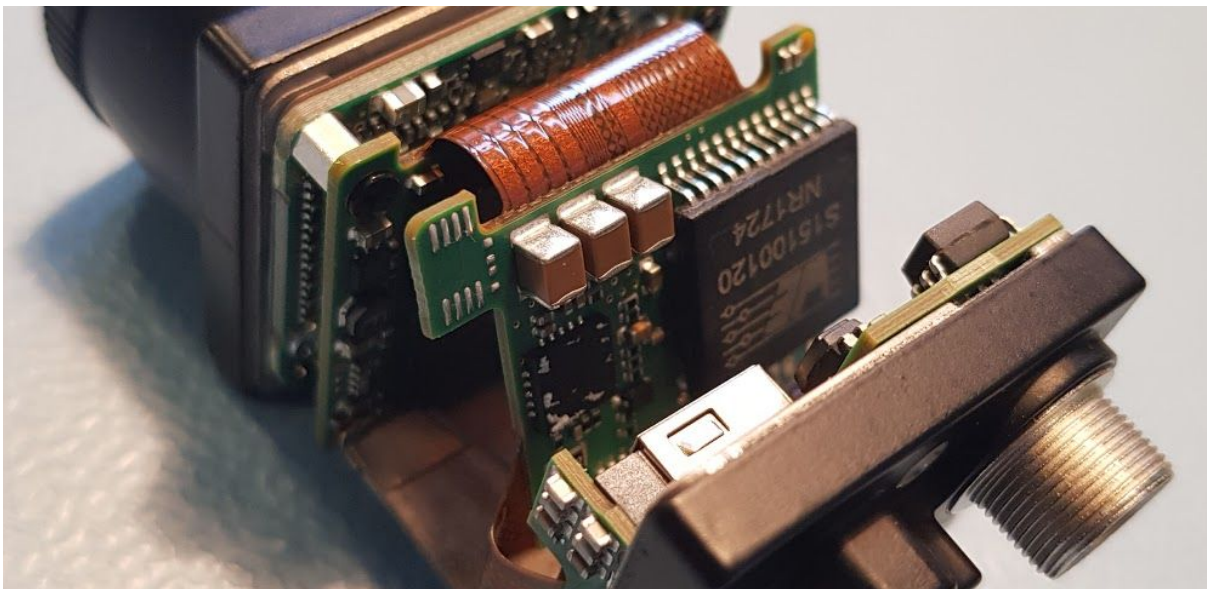*Figure 4. Hard to reach Thermal Pad (small)*
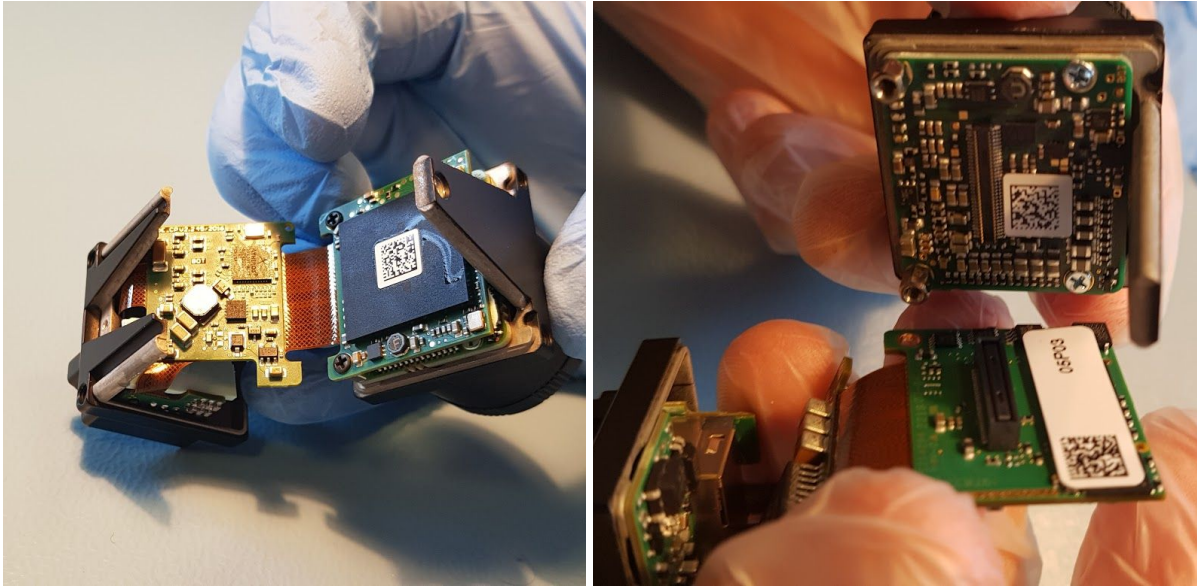

Figure 5. Polymer Residue from Polymer Pad removal
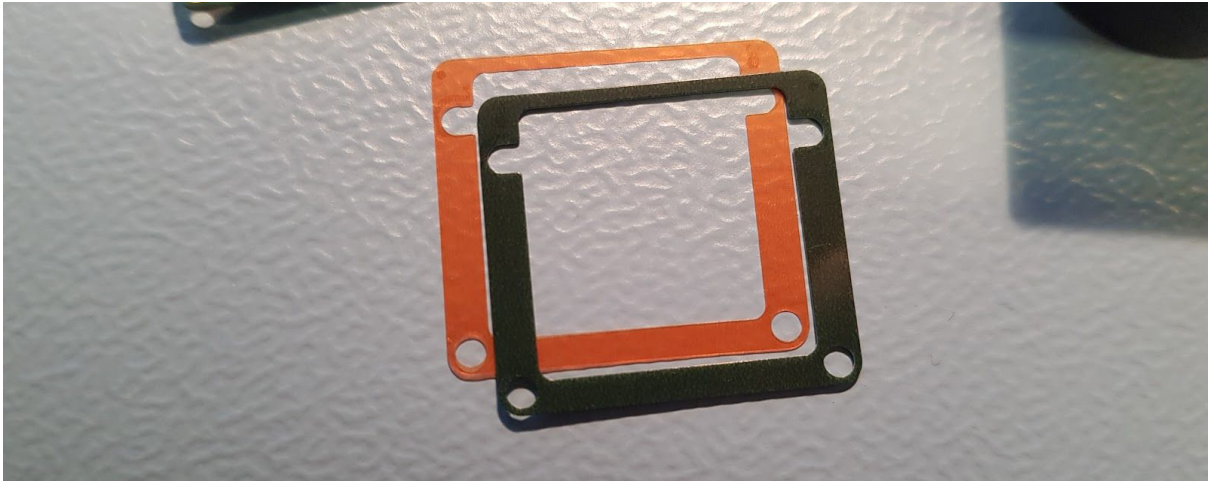
Figure 6. QR codes
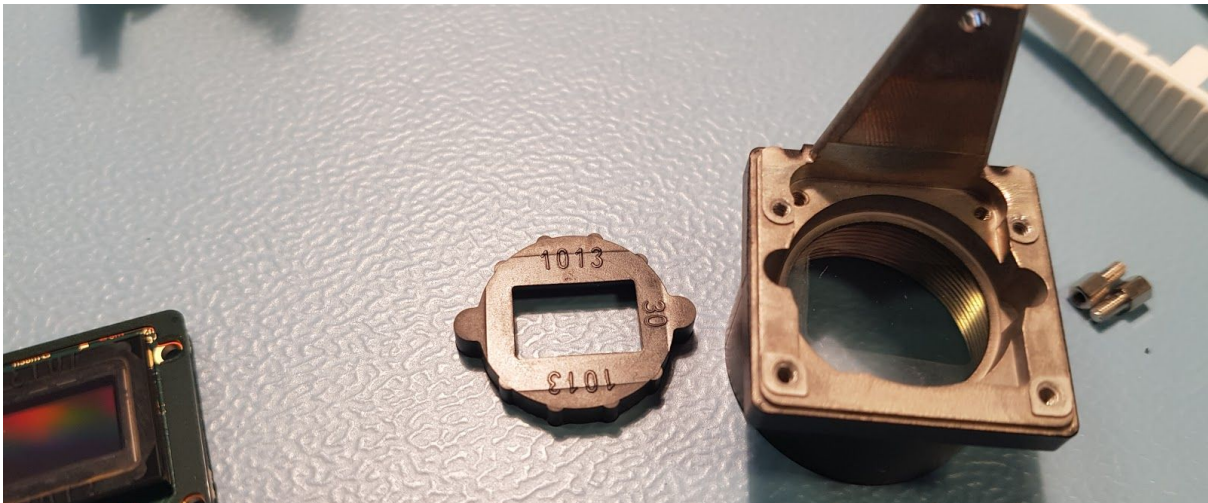

Figure 7. Polymer spacer inserts (0.40mm)

Figure 8. Elastomer Lens Gasket
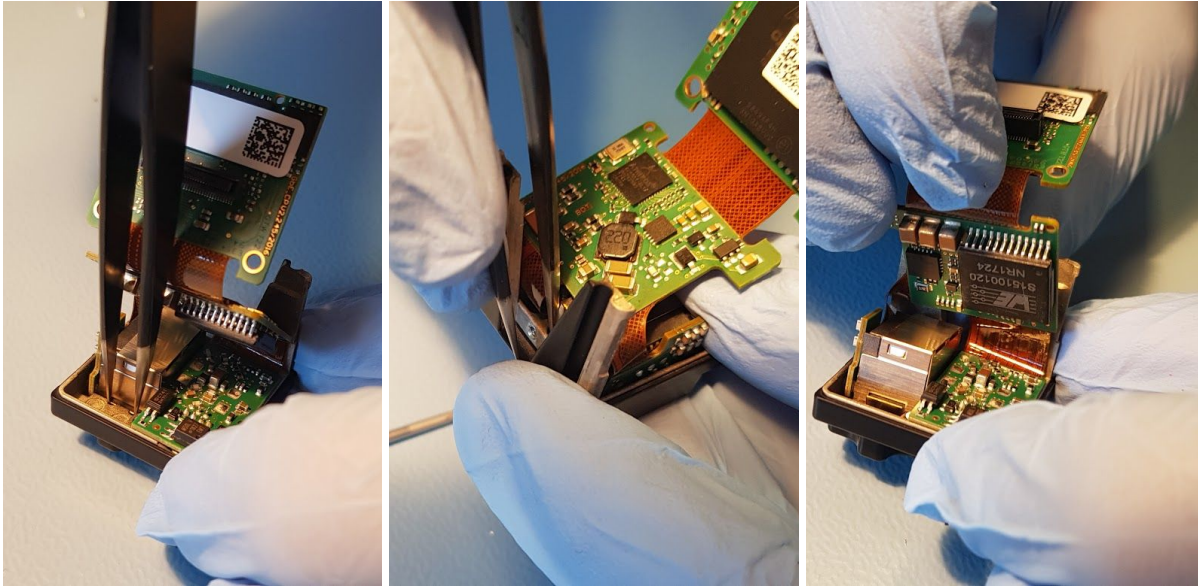
Figure 9. Removal Process of Ethernet Connector

Figure 10. Destructive removal of the I/O eight pin connector

UI-5261SE-M-GL

Detector Disassembly

Table Of Contents

Table 1: Table of Changes

Rev.	Summary of Changes	Author(s)	Effective Date
1	*First issue*	*Tord Hansen Kaasa* *Tuan Tran* *Henrik Galtung*	*20.03.2019*
2	*Formatting of text*	*Tord Hansen Kaasa* *Tuan Tran* *Henrik Galtung*	*25.05.2019*

1. Purpose

The IMX174 and IMX249 detectors showed several problem materials during the disassembly process. Currently the IMX249 using bolted down ethernet port will be used for the mission. After the assessment done on the IMX249 detector with housing, the UI-5260CP, it was concluded that the PCB only detector, UI-5261SE-M-GL, had to be assessed. The housed detectors had several vulnerabilities that could not be removed without compromising the detector structure. Most damaging was unreachable polymer thermal pads expected to outgas severely in the vacuum present in LEO. This assessment will further scrutinize the conclusions in the mitigation report.

2. Procedure

Disassembling of the detector requires a structured plan both for disassembly and documentation. The disassembly will be non destructive if possible. Destructive force will be used in necessary to remove a volatile component.

Table 2 shows all equipment and equipment quantity used during the procedure.

Table 2: Equipment list

Equipment	#
IDS UI-5261SE-M-GL	1
Screwdrivers	1
Tweezers	1
Isopropanol	1
Non latex gloves	-
Ziplock bags	1 pack

3. Results

The following section provides the results found during the disassembly process. Table 3 shows the steps taken, table 4 tabulates noteworthy findings. Pictures taken for every step can be found in the Appendix A*: Detector Disassembly Figures*. The detector can be reassembled by repeating the non destructive steps. Characterization tests must be done on a reassembled detector to determine that no operational inhibitory damage has been sustained during the disassembly process.

Table 3: Detector Disassembly Chart

Step nr.	Step Description	Additional information
1	Remove -Z QR code sticker	Located on the back PCB
2	Remove +Z QR code sticker	Located on the front lens housing
3	Unscrew T8 torx screws at -Z (2)	Screw dimensions: Length: 32.0 mm Diameter: 2.4mm Ferromagnetic Polymer cylindrical washers included
4	Remove QR code +Z middle PCB	
5	Pull the -Z PCB of the PCB stack	-Z middle PCB has a glued component. Most likely a power transformer.
6	Remove QR codes from front PCBs	QR code stickers glued on, any residue must be removed.
7	Remove screws phillips head (4) from +Z PCB stack	Ferromagnetic
8	Remove polymer spacer	Two spacers are inserted between the PCB and front frame.
9	Remove gasket and lens	The gasket is made of an elastomer, the lens should be removed to improve the optical capabilities of the camera.

Table 4: Noteworthy Findings

Notes
The UI-5261SE-M-GL detector is overall similar to the UI-5260CP detector. However, it deviates in some aspects: ● Different overall PCB stack structure ● Lack of outer housing structure ● No thermal pads ● Addition of a power transformer (HALO TGSP- P049EP7*1725LF) ● Overall more mass. Stemming from the change from a magnesium frame to Aluminum Bolts appears to be ferromagnetic. The UI-5261SE-M-GL has the addition of a power transformer in the stack. The transformer is glued on with an excessive amount of glue. The extra glue must be removed. The rods separating each PCB in the stack appears to be ferromagnetic and glued. Therese rods can not be removed from the stack. The effect of the magnetic field of the rods must be explored. The UI-5261SE-M-GL uses ribbon polymer connectors like the IMX147 and UI-5260CP. The window is glass. The Lens is secured with a polymer gasket. Not space rated. The +Z PCB (with the detector) is seated on two spacer gaskets. ● Probably not space rated ● Thicknesses: 0.30mm (Green), 0.10mm (orange) ● High likelihood of these being spacers to ensure the correct flange focal distance It is also worth noting that the detector can be fully disassembled and reassembled while maintaining functionality. The lack of polymer thermal pads makes the process more simple. The ethernet adapter appeared to be structurally stable and not loose.

3.1 Vulnerable components

Several parts inside the detector were deemed potentially unsuited for space flight:
- Polymer cylindrical washers (2)
- Glue on power transformer
- Lens gasket
- Polymer spacer inserts (2)
- Ferromagnetic bolts
- Ferromagnetic cylindrical stack spacers

Overall, as expected, the vulnerable parts in the UI-5261SE-M-GL appears to be simpler to remove and replace than on the UI-5260CP and IMX147 detectors.

Polymer cylindrical washers
Can be removed or replaced with a metal version.

Glue on power transformer
Can be removed with ethanol and acetone. Must also be cleaned in an ultrasonic bath.

Lens gasket
Can be removed together with the front window.

Polymer spacer inserts
Can be replaced with non outgassing material with the same overall thickness (0.40 mm)

Ferromagnetic bolts
The ferromagnetic bolts can be replaced with non magnetic versions.

Ferromagnetic cylindrical stack spacers
The ferromagnetic cylindrical stack spacers can not be removed and replaced easily. The easiest solution would be to include the parts and monitor the effect of the ferromagnetic material through tests and characterization.

4. Conclusion

After assessing the different available detectors, the IMX147 variant, the two IMX249 variants, the UI-5260CP with housing and the UI-5261SE-M-GL PCB only detector, the conclusion reached in the *Detector Vulnerability Mitigation* report remains supported.

It seems simpler to design a custom housing and shielding for the UI-5261SE-M-GL detector than removing the polymer pads present in the UI-5260CP version.

However, none of the options presented remains optimal due to the additional time required to develop the custom housing solution. It must be stated that the only reason for the choice of the UI-5261SE-M-GL detector remains the unremovable polymer pads inside the UI-5260CP. Should these pads be tested and shown not to outgas, the UI-5260CP would be the superior choice.

Appendix A: Detector Disassembly Figures
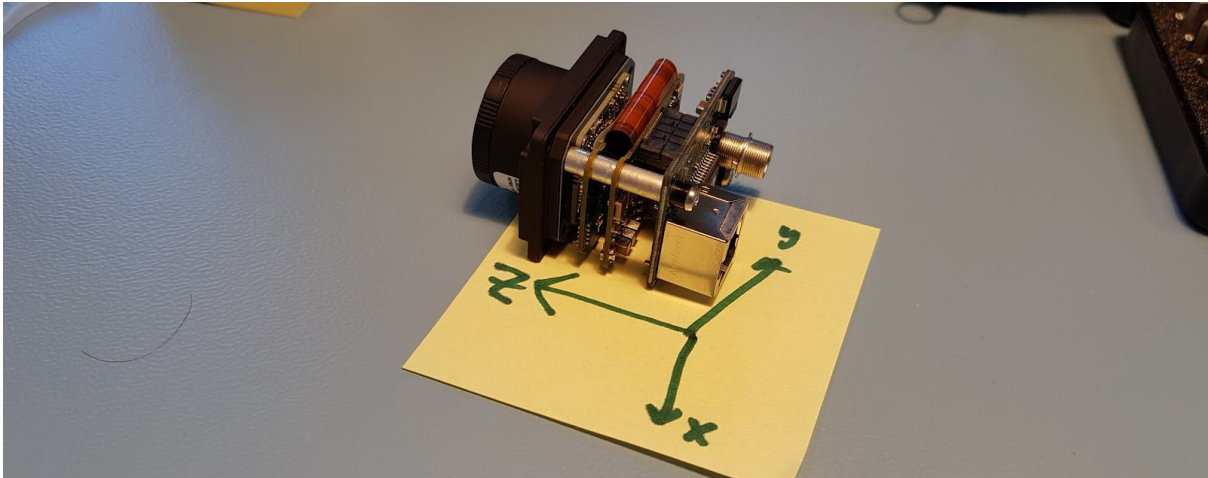
Figure 1. Detector coordinate system

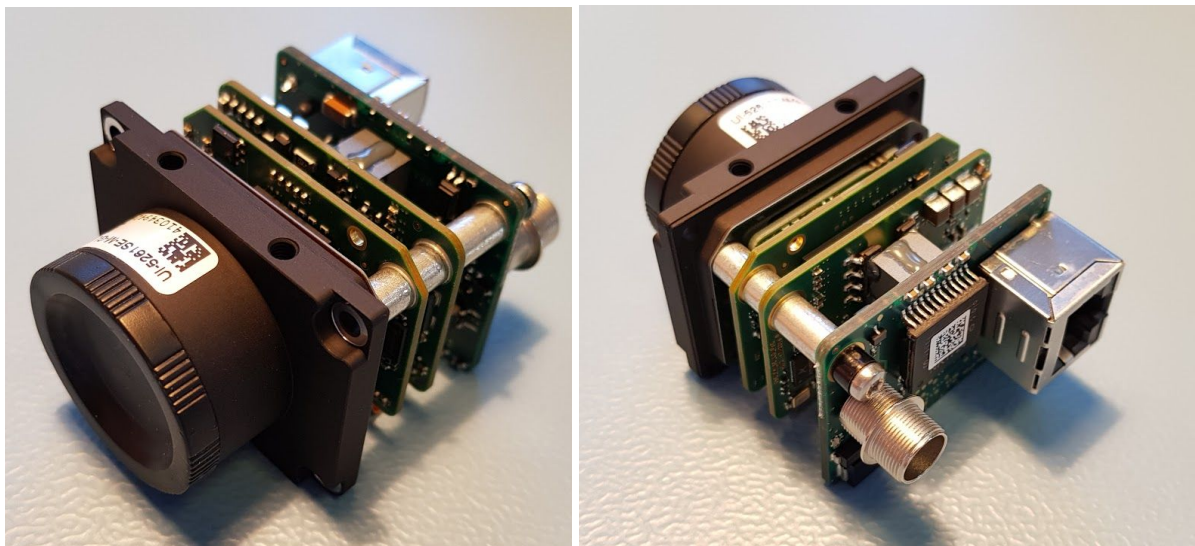*Figure 2. Detector PCB stack*

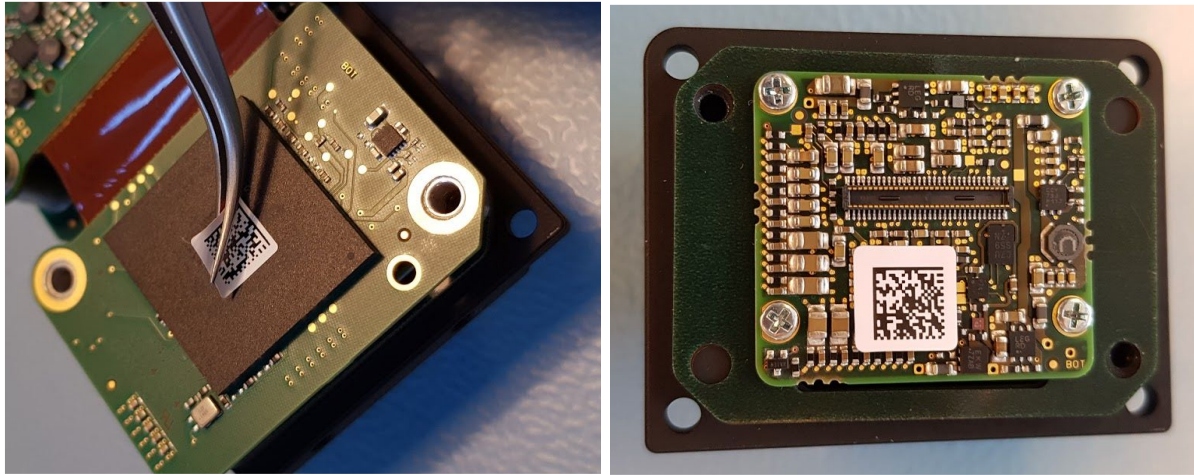*Figure 3: Ferromagnetic bolts and polymer washers*
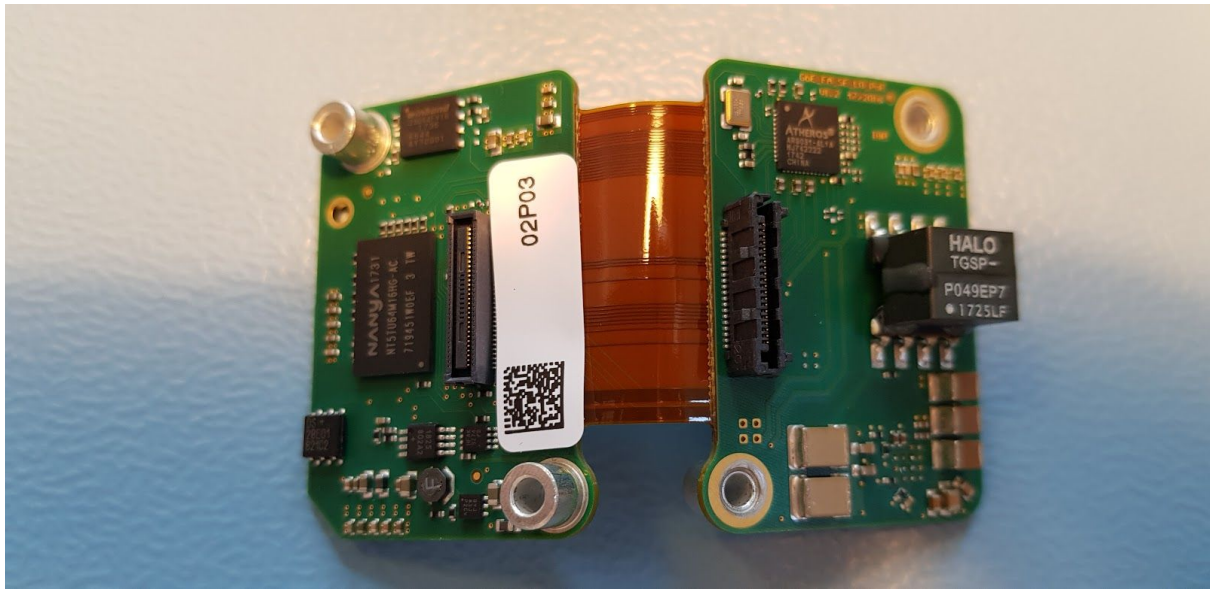
Figure 4: QR codes

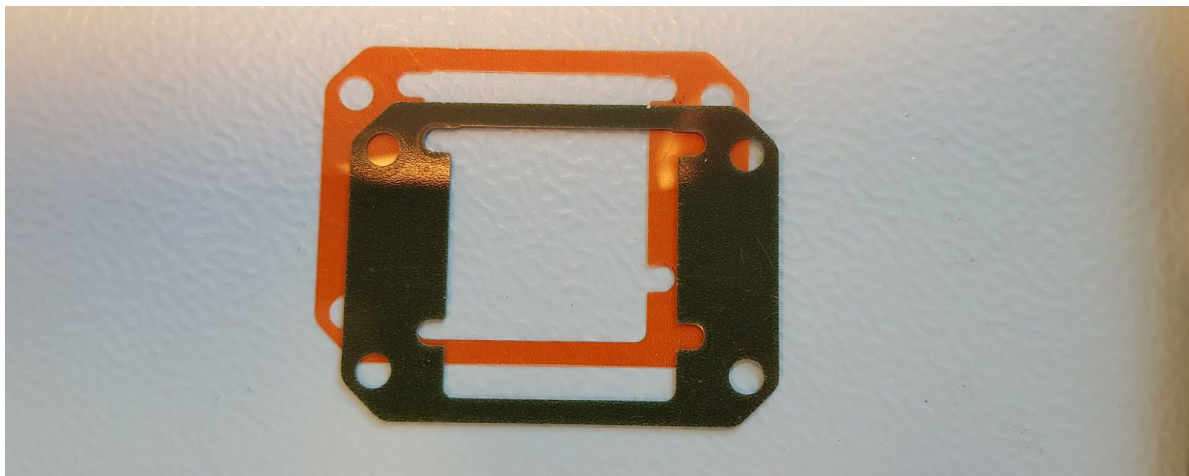Figure 5. Ribbon connector and QR code sticker

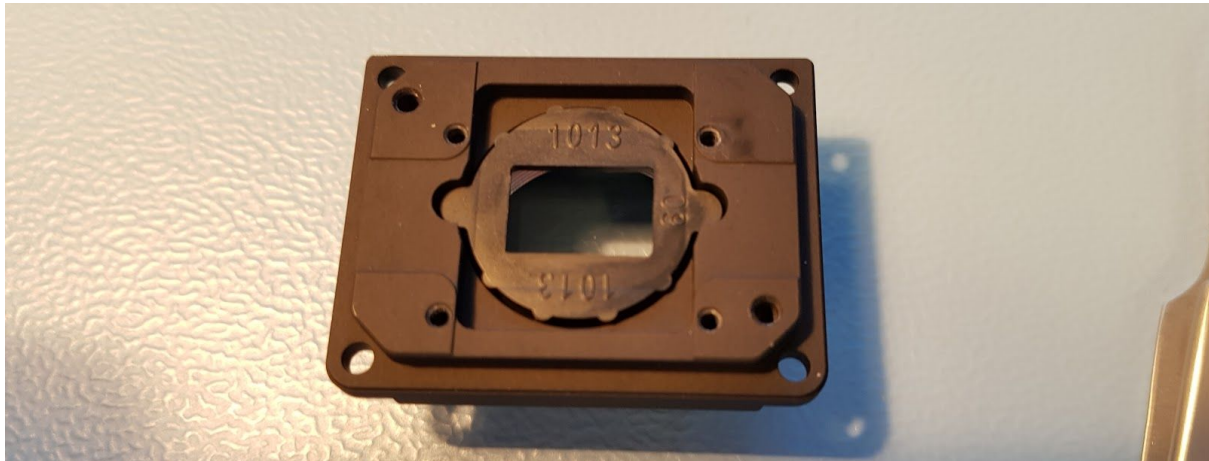

Figure 6. Polymer spacer inserts (0.40mm)

Figure 7. Elastomer Lens Gasket
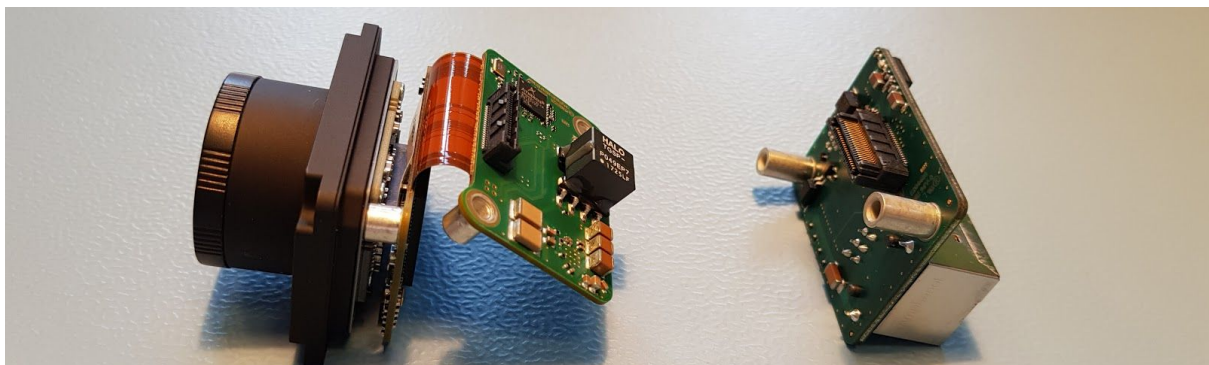
Figure 8. Ferromagnetic cylindrical PCB spacers
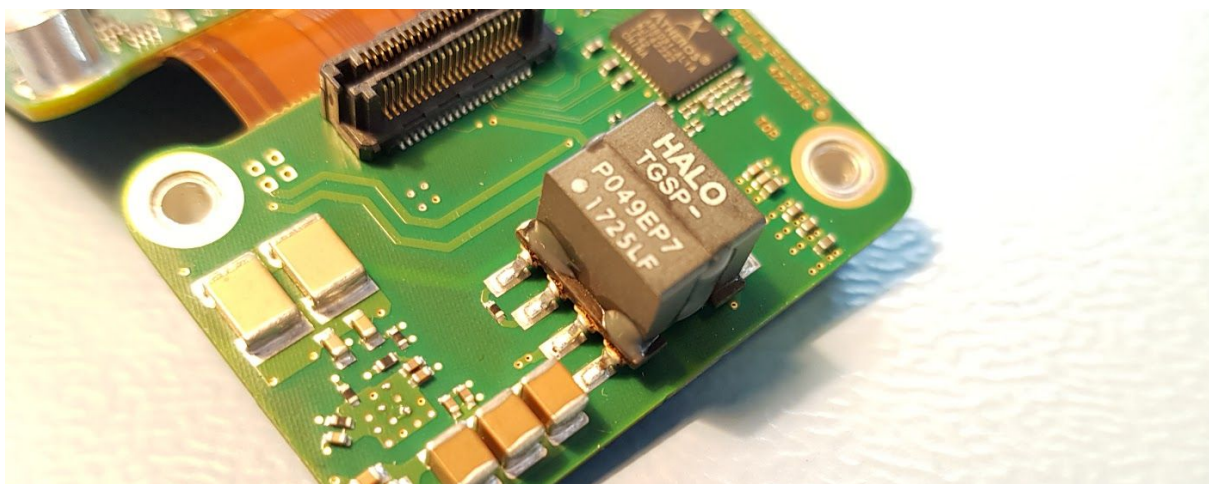
Figure 9. Power Transformer with glue

Detector Vulnerability Mitigation

HYPSO-RP-004
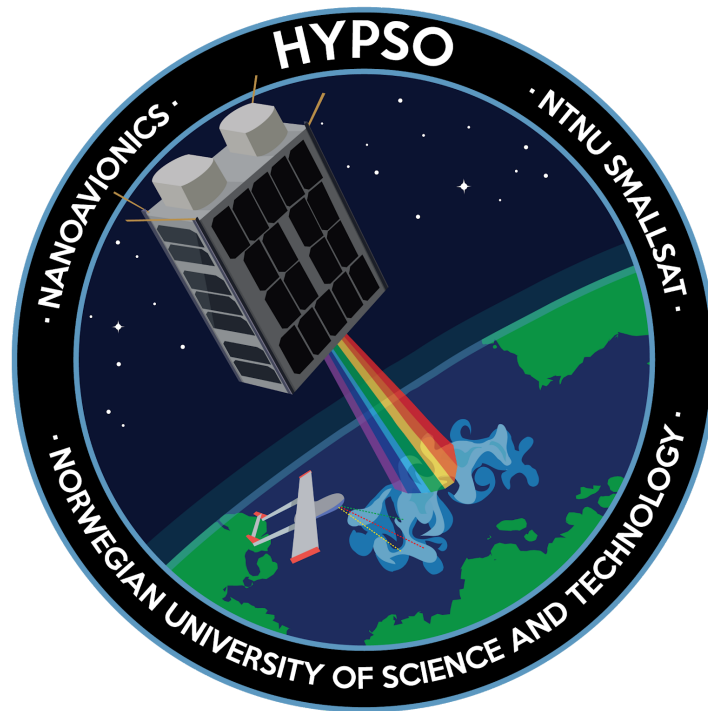
Table Of Contents

Table 1: Table of Changes

Rev.	Summary of Changes	Author(s)	Effective Date
1	*First issue*	*Joe Garrett* *Tord Hansen Kaasa*	*06.03.2019*
2	*New formatting,* *Fixed spelling,* *References to polymer window removed*	*Tord Hansen Kaasa*	*25.05.2019*

Executive Summary:

Most of the vulnerabilities that were found are potentially serious. A few are expected to not be problematic which could be verified by further testing (mainly the magnetic bolts and the ±Z coating). Because of how integral the detector is to the entire HYPSO mission, significantly changing it would result in severe time delays. Therefore, it is recommended to adapt the current detector rather than replacing it with either another detector unit or a custom PCB board designed and constructed internally in the project.

Several detector vulnerabilities can be eliminated by substituting the other non-specialized components or by removing the components entirely. Outgassing of the two remaining components could be tested, but it is expected to be severe because they seem like polymers. To remedy this, space grade alternatives to the padding and thermal strap could be found to replace the original parts in the detector. Space-grade alternatives for both the padding and thermal strap do exist, choosing them is a matter of price [RD01,RD02].

1. Purpose

The report *HYPSO-RP-007 UI-3060CP-M-GL Rev.2 Detector Disassembly* found several components of the detector which are likely to cause harm to the operation in space. This memo outlines possible strategies to mitigate the vulnerabilities.

1.1 Summary of uncovered problematic conditions

Ferromagnetic bolts
The bolts are only a minor problem. They should be simple to replace, though it is necessary to test for any differences in thermal expansion. In addition, further tests could be performed to determine whether they are actually ferromagnetic or paramagnetic.

Lens elastomer gasket
The gasket is a significant problem. It could be tested to see how much it outgasses. Other possible solutions could be to machine a similar part out of metal (which could scratch the lens) or to re-assemble without the gasket (see below).

Silicone Elastomer Thermal Pads
The padding is a major problem. Tests should be done to see how much it outgasses. If the final padding could be removed, it could presumably replace these with space-grade padding (for example, graphite fiber or copper).

Thermal strap with glue
The thermal strap is a problem. To test it and mitigate any potential effects, it must be removed. Once removed, we could test how much it outgasses. If it outgasses to much, it could be replaced with a space-grade thermal management system. If it only outgasses a little, it could be re-attached with space grade epoxy.

QR stickers
Because the QR stickers were successfully removed, they should not cause problems in space. Any adhesive residue could be removed with isopropanol.

PCBs require epoxy coating
It is feasible to coat the PCBs with epoxy or a thin film [RD03]. Outgassing testing should be performed to characterize the outgassing performance.

Coating on the +Z and -Z material
The coating could be paint or anodized metal. Should be feasible to seal it so it does not flake off. Could also test outgassing. Alternatively, the coating could be sanded off.

Polymer sensor spacers

They could be replaced with a material that conforms to the outgassing requirements. However, the replacement would need to have a very specific thickness, and this could be challenging to find. An outgassing test is advisable as the cost for a custom cut replacement of high precision thickness could be very expensive.

1.2 Reference Documents

The documents listed in table 2 have been used as references in the creation of this document.

Table 2: Referenced Documents

ID	Author	Title
[RD01]	Laird	Thermal Interface Solutions [Link]
[RD02]	Technology Applications Inc.	GRAPHITE FIBER THERMAL STRAPS (GFTS®) [Link]
[RD03]	Loughborough University	Atomic layer deposition (ALD) for tin whisker mitigation on Pb-free surfaces [Link]
[RD04]	iDS	Ui-5261se-Rev 4 [Link]

2. Mitigation strategies

1) Adapt current housing (listed in order of complexity)
   a) Remove window, window gasket, and stickers
   b) Replace magnetic bolts
   c) Coat PCB boards with epoxy or Al_2O_3
      i) (optional) ±Z should be coated as well.
   d) Replace polymer padding with space-grade padding.
   e) Replace thermal strap with space-grade thermal strap if outgassing test fails .
      i) Otherwise, remove glue (acetone or isopropanol) and epoxy
2) New housing for standalone iDS-PCB-detector
   a) Design our own
      i) Hire space engineer (PhD student or from industry) or sub-contract
      ii) Add > 3 months to the development timeline
   b) Order space grade (or space-plausible)
      i) Find supplier, ensure compatibility of camera and part
3) Use PCB-based detector
   a) Design our own
      i) Either hire someone internally or find a subcontractor
      ii) Add > 6 months to development timeline
   b) Order space grade (or space-plausible)
      i) Find supplier, ensure compatibility of camera and parts
4) Find space-grade camera (housing+detector+PCB to control)

3. Recommendation

Because of the time and personnel demands of options 2 and 3, option 1 was recommended in Detector Vulnerability Mitigation revision 1. However, complete disassembly of the detector shows that the removal of the final thermal pad results in a damaged assembly. Option 1 is therefore deemed as not suitable due to the complicated removal process.

Option 2a) would be the recommended solution, moving forward. Finding a space-plausible solution and constructing a custom shell would require extra time and effort compared to option 1. A non enclosed version of the same detector called UI-5261SE Rev. 4 is available [RD04]. This option should be explored further, to determine the feasibility of adaptation.

If the time frame is worth the extra expenses, solution 4 would be recommended. However a space grade solution would be expensive.

Before moving forward, it is necessary to decide what design criteria the thermal padding and strap must meet. Then quotes can be requested and the budget can be evaluated. Moreover, because the rgb camera has a similar layout to the HSI detector, it should also be disassembled simultaneously and inspected for similar vulnerabilities.

Appendix D

HYPSO-ANA-004 Payload Material Analysis Report

Payload Material Analysis

HYPSO-ANA-004
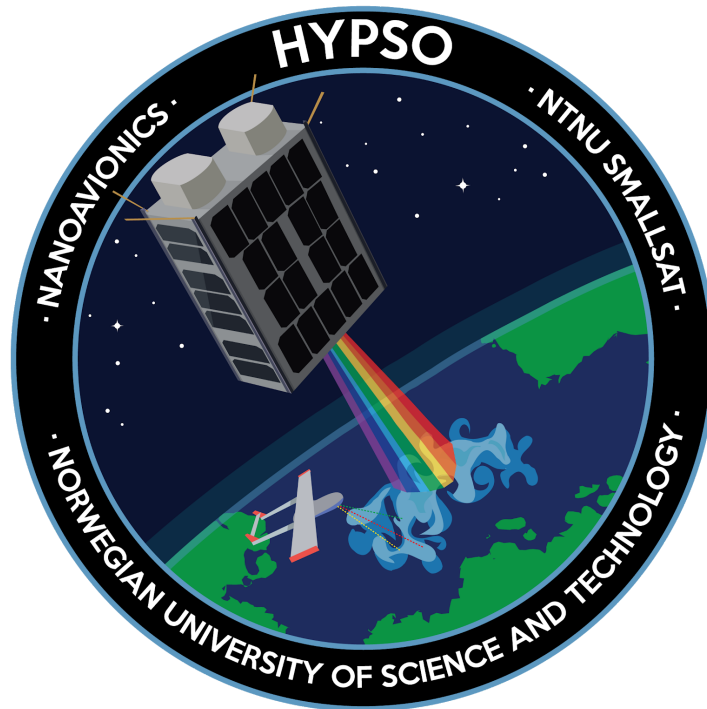
Prepared by: HYPSO Project Team
Reference: HYPSO-ANA-004
Revision: 2
Date of issue: 26.05.2019
Document Type: Internal Analysis
Author(s):   Tord Kaasa, Tuan Tran, Henrik Galtung
Related Documents: HYPSO-DR-003, HYPSO-ANA-007, HYPSO-TRP-VAC-002

Table Of Contents

Table 1: Table of Changes

Rev.	Summary of Changes	Author(s)	Effective Date
1	*First issue*	*Tord Hansen Kaasa, Tuan Tran, Henrik Galtung*	*23.05.2019*
2	*Formatting*	*Tord Hansen Kaasa, Tuan Tran, Henrik Galtung*	*26.05.2019*

Executive Summary

Table 2 presents all materials currently planned to be used in the HYPSO CubeSat, blue indicates objective, green indicates detector, yellow indicates grating and slit, while red indicates fasteners. While the HSI Platform, fastener and adhesive materials were specifically chosen based on the requirements presented in this report, the other materials were part of a larger COTS system that had to be adapted. Some of the COTS materials exhibit outgassing values higher than the NASA recommendation or exhibits an unknown outgassing characteristic and must therefore be tested. It follows that the presented materials list is subject to change.

Table 2: List of Materials Planned to be part of the Flight model

Component	Material
HSI Platform	AA6082
Sensor Thermal Strap	Pyrolytic Graphite
Objective Shell	AA6061 w. Black Anodization
Objective Lenses	SiO2 w. MgF2 AR coating
Detector Shell	Aluminum Alloy
Detector PCB Stack Spacer	Ferritic Steel
PCB Base Material	FR4 (GRP)
PCB Component	Unknown Ceram (Possibly Alumina)
PCB Component	Unknown Polymer
Grating	B270 Glass
Slit Housing	AA6061
Slit Material	302 Stainless Steel
Fastener Material (Screws)	A2 Grade Stainless Steel
Adhesive Tape (PEEK)	Acrylic
Adhesive for Connector Ruggedization	Epoxy
Cable Insulation Jacket (Uncertain)	mPPE (Modified Polyphenyl Ether)

1. Overview

This report concerns all payload materials that are part of the HYPSO mission CubeSat. The report covers the choice of material for different payloads and offers an in depth explanation of the reasoning behind the choices.

1.1 Purpose

The materials that make up the HYPSO satellite payloads are specifically chosen based on the relevant requirements and needs. Systems like the HSI payload interface requires an active choice of production materials, other parts like the COTS components require an omission of potentially volatile materials. This report aims to convey the most important aspects regarding the choice of materials for the HYPSO s/c flight model and CubeSats in general.

1.2 Scope

This report will cover the material choice selection process of the mechanical interfaces of the HSI Payload, COTS components, connectors and wires, adhesives and thermal regulators. The extent of outgassing, the largest material challenge in relation to optics in space, will also be covered as well as how to test and quantify the material outgassing. The material choices are covered first in section 1 and 2, while an overview of the outgassing will be presented in section 3. Figure 1 shows the relationship between all the documents.
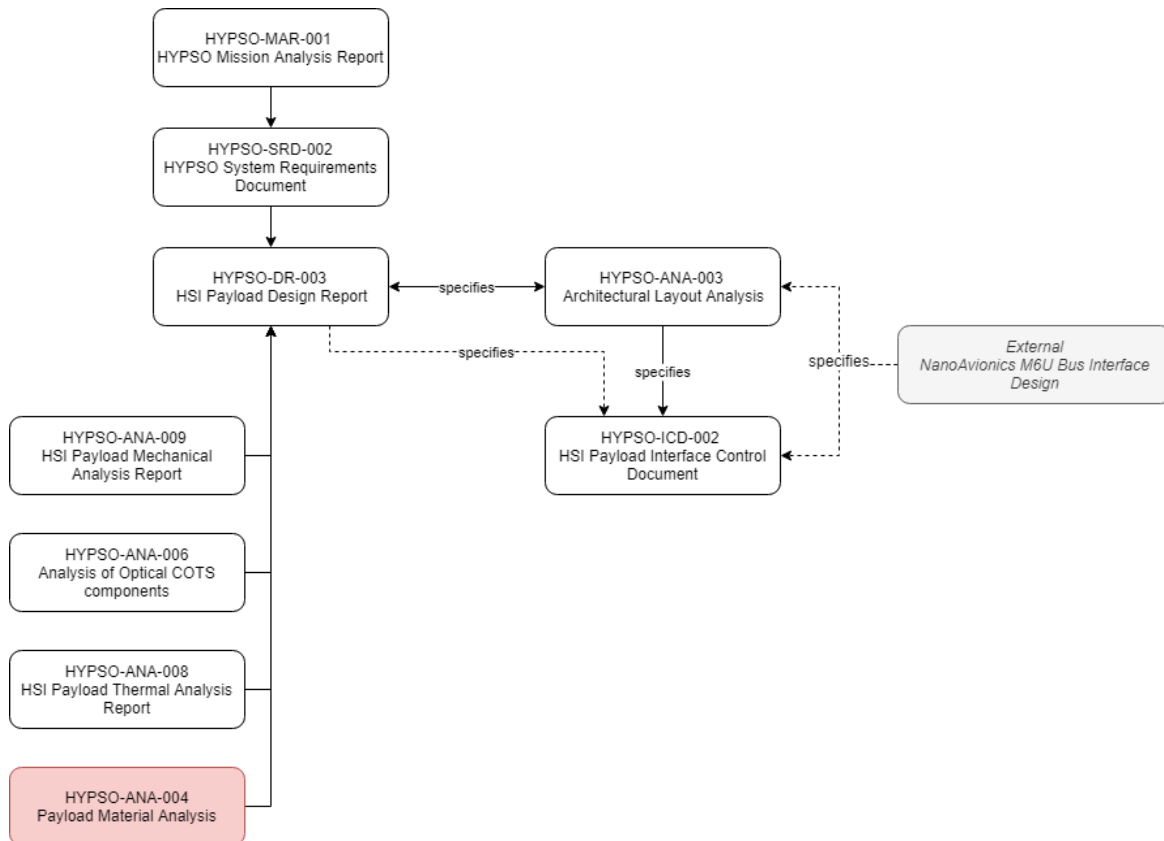
Figure 1: Document relationship

1.3 Referenced Documents

The documents listed in table 2 have been used as reference in the creation of this document.

Table 3: Referenced Documents

ID	Author	Title
[RD01]	Cal Poly SLO The CubeSat Program	6U cubesat design specification rev. 1.0, 2018. [Link], accessed April 2019.
[RD02]	NASA	State of the Art of Small Spacecraft Technology, 06. Structures, Materials and Mechanisms. [Link], accessed February 2019.
[RD03]	Tord Hansen Kaasa, Tuan Tran, Henrik Galtung	Mechanical and Thermal Integration of an HSI Payload in A 6U CubeSat Specialization Report. 2018
[RD04]	MatWeb	Aluminum Alloy Heat Treatment Temper Designations. [Link], accessed March 2019
[RD05]	SMITH	6082 Aluminium Technical Datasheet. [Link], accessed May 2019
[RD06]	ECSS	Tailored ECSS Engineering Standards for In-Orbit Demonstration CubeSat Projects. 2016.
[RD07]	Mohammed Chessab Mahdi. Cambridge Scholar Publishing	Attitude Stabilization for CubeSat: Concepts and Technology. 2018.
[RD08]	Gradeskill	Grades of stainless steel A2, A4 in relation to fasteners. [Link], accessed April 2019
[RD09]	NASA	Outgassing Database. [Link], accessed May 2019.

[RD10]	Henrik Galtung	HYPSO-ICD-001 Interface Control Document. 2019
[RD11]	3M	October 2018. Scotch-Weld Epoxy Adhesive 2216 B/A Technical Data.
[RD12]	C. Tribble, B. Boyadjian, J. Davis, J. Half-net, and E. McCullough	Contamination Control Engineering Design Guidelines for the Aerospace Community. NASA Contractor Report 4740, 1996.
[RD13]	ECSS-Q-TM-70-52A	Space product assurance. Kinetic outgassing of materials for space. 25 November 2011.
[RD14]	ASTM E 595-77/84/90	Standard Test Method for Total Mass Loss and Collected Volatile Condensable Materials from Outgassing in a Vacuum Environment
[RD15]	ECSS-Q-ST-70-02C	Space product assurance. Thermal vacuum outgassing test for the screening of space materials. 15 November 2008.
[RD16]	Tord Kaasa	HYPSO-TRP-VAC-002 Objective Vacuum Damage Report. 2019
[RD17]	Gunter's Space Page	TU-Berlin, LAPAN-Tubsat. [Link], accessed May 2019
[RD18]	H.von Münchhausen, F.J.Schittko	Investigation of the outgassing process of silicone rubber. Vacuum 13(12):549-553. 1963
[RD19]	J. Rothka, R. Studd, K. Tate and D. Timpe	Outgassing of Silicone Elastomers. 2012
[RD20]	65 Authors from the Astronautics Community and James R. Wertz. Microcosm Press, Hawthorne, Calif	Space mission engineering: The new SMAD. 2011.

[RD21]	Bruker	Handheld XRF: How it works. [Link], accessed May 2019.
[RD22]	Bergström J	Experimental Characterization Techniques. Mechanics of Solid Polymers. William Andrew Publishing 2015.
[RD23]	Norman E. Dowling	Mechanical Behaviour of Materials Engineering Methods for Deformation, Fracture, and Fatigue. Pearson 2013.
[RD24]	Engineering ToolBox	Thermal Expansion of Metals, (2005). [Link], Accessed May 2019.
[RD25]	NASA	State of the Art of Small Spacecraft Technology. [Link], accessed May 2019.
[RD26]	Hallenstvet, Merete & Mårdalen, Jostein & Bolm, Helene & Rekowski, Volker & Tanem, Steinar & Erik Lein, John	HEAT REFLECTIVE COATINGS OF ALUMINIUM. ATB Metallurgie. 45. 2006.
[RD27]	Tord Hansen Kaasa, Tuan Anh Tran, Henrik Galtung	HYPSO-TRP-OPT-002 Functionality Test Report of HSI TTH Mk1. 2019
[RD28]	Tord Hansen Kaasa, Tuan Anh Tran, Henrik Galtung	HYPSO-ANA-008 HSI Payload Platform Thermal Analysis. 2019.
[RD29]	Panasonic	"PGS" Graphite Sheets. [Link], accessed may 2019
[RD30]	Thermal-Space	Cabled Copper Thermal Straps - The Solderless Flexible Thermal Links. [Link], accessed May 2019
[RD31]	LARC	Thermal Strap Joint Relaxation and Material Creep. [Link], accessed May 2019
[RD32]	Azom	Aluminium / Aluminium 1100 Alloy (UNS J91100).

		[Link], accessed May 2019
[RD33]	MetalTek	Conductivity in Metals. [Link], accessed May 2019
[RD34]	NASA	Lessons Learned Thermal Strap Joint Relaxation and Material Creep. [Link], accessed April 2019
[RD35]	Jp Collette, P Rochus, R Peyrou-Lauga, O Pin, Nicolas Nutal, Maïwenn Larnicol, Jean Crahay. 62nd International Astronautical Congress	Phase change material device for spacecraft thermal control. 2011.
[RD36]	Pradeep Shinde, Anthony Fernandez, Ibrahim Tansel, Sabri Tosunoglu. Florida Atlantic University	Active Thermal Control System for CubeSat. 2017

2. Payload Materials

This section concerns the choice of materials in the HSI interface solution. The space environment sets a large number of challenges and restrictions in regards to the choice of materials. The environmental challenges ranges from the deep space vacuum that can cause outgassing, cold welding to atomic oxygen and radiation. The general consensus regarding spacecraft materials supports a heavy use of light metals. Aluminium 6061 and 7075, as well as the 300 series of steel are common materials used in aerospace engineering [RD01], [RD02]. Heavier materials such as Titanium are less favoured due to CubeSat decommissioning rules, requiring the satellite to burn up in the atmosphere upon a complete life cycle. However, heavier elements are allowable if the amount of material is proven to be destroyed during reentry/ decommission [RD02].

2.1 HSI Platform Materials

The mechanical design of the HSI assembly can be found in the report *HYPSO-DR-003 HSI Payload Design Document*. This section describes the process of evaluating and choosing a material for the design described there. Reports presented during the 2018 PDR concluded that Aluminium 6061 was the preferred choice of material based on the requirements presented in section 2.1.1. AA6061 was chosen over exotic metals like Covar and Invar, due to cost and potential thermal induced stresses based on the different thermal expansion of the AA6061 objective housing material and Covar/Invar. However, due to the availability of AA6061 in Europe, this study also evaluated materials more common to the European market. Due to the previous findings, only aluminum alloys were considered.

2.1.1 Material Requirements

The properties most relevant to ensure a stable HSI assembly mounting are listed below. Table 4 tabulates the relation between the properties and the overlaying requirements in the different categories. Further information regarding requirements concerning the materials can be found in the *HYPSO-DR-003 HSI Payload Design Master Document,* section 2.2.

Young's modulus: Linear ratio of stress/ strain in a material. A measure of material elasticity.

Density: Mass per volume.

Yield strength: Stress level before material suffers plastic deformation.

Specific modulus: Gives a measure over the total stiffness in the particular material. The fundamental frequencies of the parts is a function of the specific modulus and its form factor.

Thermal Conductivity: Quantity of heat transported through a material.

Coefficient of Thermal Expansion (CTE): Amount of shape changing when exposed to a temperature gradient.

Table 4: Mechanical properties required HSI mounting

Category	Properties Requirements
High Mechanical strength	High Yield Strength [MPa]
High Fundamental Frequency	High Specific Modulus [GPa/kg/m^3]
Thermal stability	High Thermal conductivity [W/mK] Low Coefficient of thermal expansion Coefficient of thermal expansion close to AA6061
Low outgassing [RD01]	TML < 1.0 % CVCM < 0.1 %
Ease of Manufacturing	High Machinability Easy Anodizing
Lightweight	Low Density

A thorough analysis of the outgassing requirements presented in the 6U CubeSat Design Specification from California Polytechnic State University, San Luis Obispo, can be found in section *3. Outgassing*.

2.1.2 Material Evaluation

The following is an excerpt of the material analysis from the specialization report:

"As mentioned the 6U CubeSat Design Specification states that the following materials AA 6061, 6082, 7075 and 5005 are commonly used in space. Comparatively, the 6000 series is simpler to handle than AA7075, and is also a cheaper option based on the price guide provided by CES EduPack 2018. Additionally, a large limitation with AA7075 is the lack of availability in regards to capable anodization facilities, thus increasing end price and production complexity further. Due to the added complexity AA7075 would add to the production, the use of this material was not explored further. In addition AA5005 has a low rated machinability and thus not a suitable mounting material." -Specialisation report, Galtung, Kaasa, Tran [RD03]. Based on the information from the 6U CubeSat Design Specification, AA6082, a common material found in the European market should be a suitable substitute for AA6061.

The material properties of aluminium are highly dependent on the tempering process. T4 and T6 are available heat treatments. T4 aluminium is heat treated, and naturally aged to a substantially stable condition. T6 is heat treated then artificially aged [RD04]. A T6 tempered material would display improved material properties, and as a result T6 is a commonly used heat treatment in aerospace engineering. Due to this It was decided that the aluminum alloy should be heat treated according to T6.

6000 series aluminium alloys were compared with each other in regards to their thermal and mechanical properties. The following figures shows the results of the property analysis: Figure 2 shows a young's modulus vs density comparison for AA 6061 and AA6082. Figure 3 shows a young's modulus vs yield strength comparison for AA 6061 and AA6082. Figure 4 shows a thermal conductivity vs Coefficient of thermal expansion comparison for AA 6061 and AA6082.

From figure 2, 3 and 4 it is evident that AA6061 and AA6082 has comparable material properties. AA6082 has superior stiffness compared to AA6061, and a higher thermal conductivity. The yield strength and density of the materials are similar. All intrinsic material properties points toward AA6082 as the superior aluminum alloy for general use in regard to the mission outline. However the COTS objective lenses are produced in AA6061. It would be preferable to avoid materials with a large deviation in their CTE. Figure 4 shows that the CTE values for AA6061 and AA6082 overlap, although small negative deviations can be seen in the AA6082 values. The relative similar CTE should not induce critical pressure on the lenses if exposed to temperature variations. From the analysis, both AA6061 and AA6082 are suitable mounting material candidates. However, AA6082 is recommended due to the additional stiffness provided. In addition, 6082 has replaced 6061 in many applications, as stated by the material distributor Smiths [RD05].

The material availability will be the driving factor for which material will be chosen. The suppliers available are Smiths and and Astrup. The available aluminium materials is limited to AA6082-T6. *Based on this analysis, AA6082-T6 was the chosen production material.*

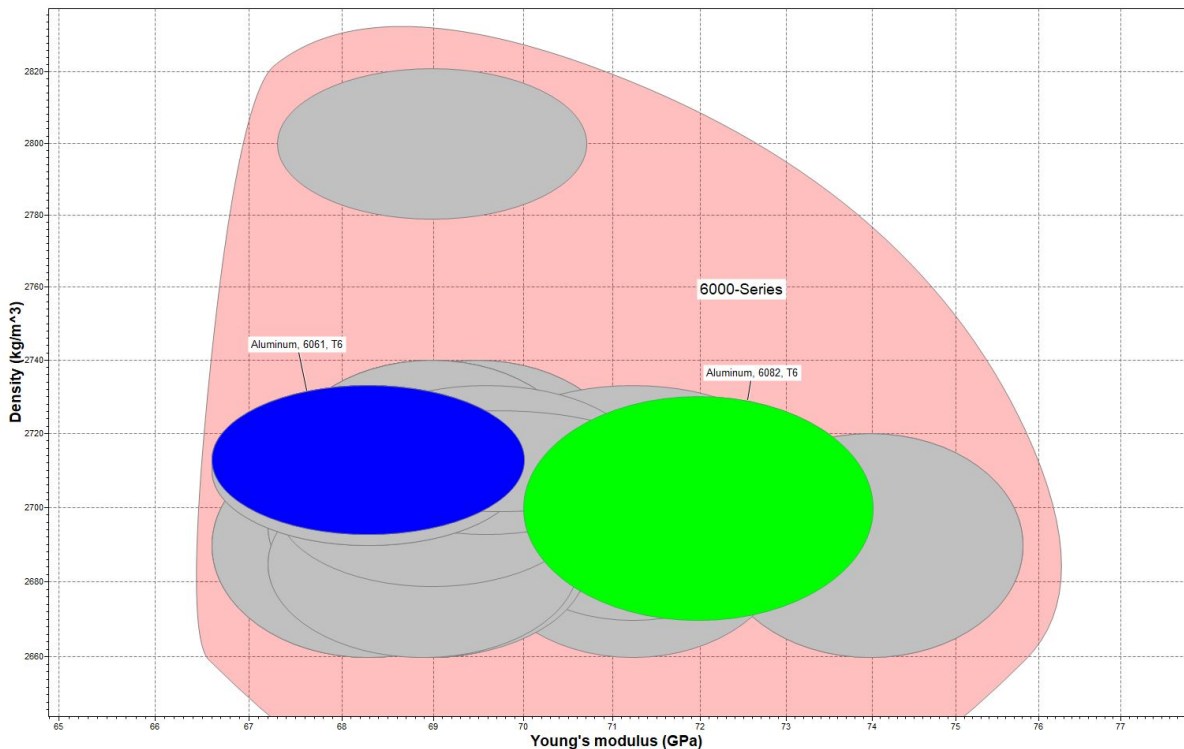**Production Material for HSI Platform: Aluminium 6082-T6.**
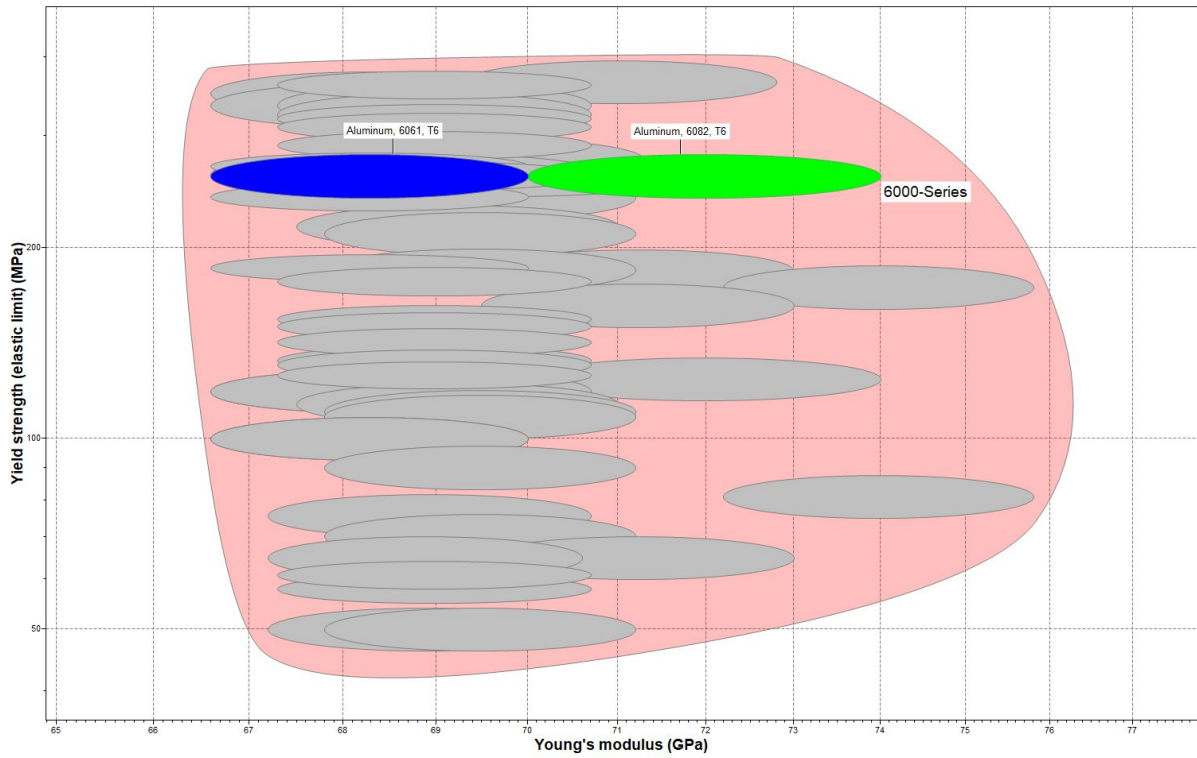

Figure 2: Young's modulus vs. Density

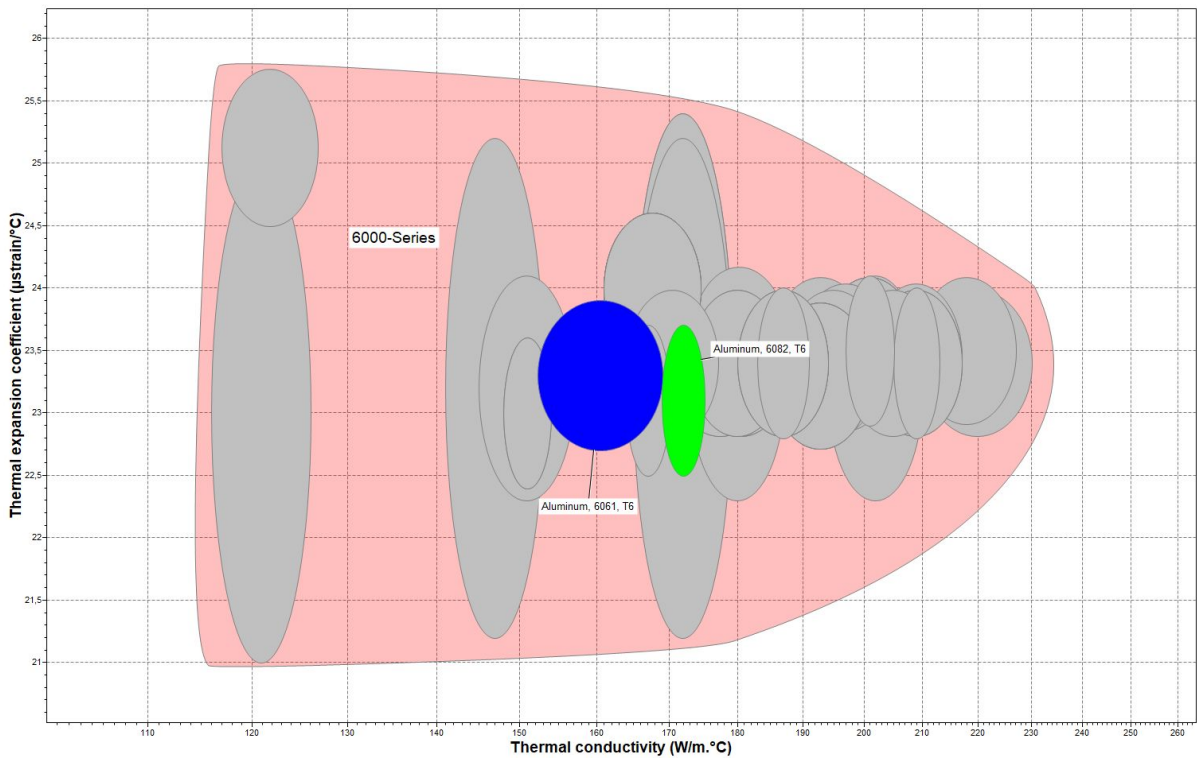Figure 3: Young's modulus vs. Yield strength

Figure 4: Thermal conductivity vs Coefficient of thermal expansion

2.2 HSI Payload COTS Materials

In order to achieve a low-cost hyperspectral design, readily available COTS components will be used as opposed to space-rated optical components in the optical train of the HYPSO HSI camera. Space grade components are very expensive compared to COTS due to the amount of documentation required in order to prove space grade authenticity. However, the use of COTS components induce several challenges in regards to planning, testing and adaptation to ensure that the components are acceptable and fulfill the requirements set by the relevant standards: *ECSS standards for Cubesats* [RD06], *Environmental Testing Requirements PSLV* [under non-disclosure agreement with NanoAvionics], and the 6*U CubeSat Design Specification* [RD01].

The materials present in the COTS components must be taken "as is" and offers little choice for customization as this would be very complex and time-consuming. However, smaller adaptations are possible. The report *HYPSO-ANA-006 Analysis of Optical COTS components* presents a larger study of the COTS components that were potential candidates for adaptation as payloads. The report also includes modifications that should be done to make them space-grade. The following subsections aims to further discuss the materials found within the flight model adapted COTS components. Some materials found within the COTS components are unknown at the time of writing. Future tests will be done in order to establish if the materials are volatile or otherwise inhibit undesirable properties in the space environment. Table 5 tabulates the optical components found within the final assembly.

Table 5: Optical COTS components

Description	ID	Appearance/geometry	Qty
50mm VIS-NIR Objective	EO#67-717		3
Camera Head	IMX249 UI-5261SE-M-GL		1
Blaze Angle Transmission Grating	EO#49-579		1
Ø1" Mounted Slit, 50±3µm x 7mm	S50RD		1

2.2.1 Objective Materials

The outer shell of the objective is manufactured in AA6061. It follows that changing the default material would require substantial rework of the lens assembly. In addition, the rework would require HYPSO to produce high quality lens housings to accommodate the sensitive optics. Therefore it was decided to use the default housings. The COTS lenses introduces several challenges to the development, partly due to the high thermal expansion of the aluminium housing material, and the large range of undesired components inside; including grease, glue and polymer materials. Section 3.2 offers an in depth exploration on the undesired COTS components in regards to outgassing.

The flight model will include an adapted solution of the lens objectives as concluded in the *HYPSO-ANA-006 Analysis of Optical COTS components* series of reports. The adapted solution will have all potentially high outgassing materials such as glue, grease and polymers removed. Replacements for these materials are outlined later in this report, where a substitute was necessary.

As the objectives will require an extensive washing procedure, the geometrically complex and fragile aperture control will be replaced with a fixed aluminium 6082 baffling ring, as described in the report *HYPSO-ANA-001 HSI Payload Design Document,* section *4.5.1 General Improvements*.

The optical build of the objectives consists of a total of four lenses, two single and two cemented achromatic lenses. The lens substrate consists of Silicon dioxide as shown in section 4. The coating of these substrates are magnesium fluoride. The materials where found using analysis described in section 4. However, these results have not been confirmed as Edmund Optics have not been willing to share such information. As a result, radiation and outgassing tests should be done prior to launch. The glue used on the cemented achromatic lenses could potentially lead to some amount of outgassing, however the effect of this has not been measured but is expected to be low due to the tiny area of the seam exposed to hard vacuum. Table 6 tabulates the materials found within the objectives. Materials marked in red can potentially harm the operation of the main payload and is therefore considered unwanted and should be examined and tested further.

Table 6: 50mm VIS-NIR materials

Material	Part	Induced Vulnerability
AA6061	Outer Shell	-
Amorphous Sio2	Lenses	Darkening, brittle, condensable surface
Crystalline MgF2	Anti Reflective Lens Coating	Darkening
Grease	Inner Objective	Outgassing
Glue	Threading, cemented lenses	Outgassing
Unknown Polymer	Inner Screws	Outgassing

2.2.2 Detector Materials

The UI-5261SE-M-GL using the IMX249 detector chip was chosen for the flight model of the HSI camera due to the unremovable silicone thermal pads found within the enclosed models. The chosen detector consists of several PCBs made of FR4 (common PCB material), fiberglass reinforced epoxy composite (FRC). The outer shell of the iDS detector models is composed of a low weight magnesium alloy and steel prongs, this is the case for all housed IMX models. The use of magnesium alloy makes the detectors lighter, while providing sufficient mechanical integrity as the part carries little load. However the UI-5261SE-M-GL is an open PCB version with a front consisting of an undisclosed aluminum alloy. The detectors from iDS generally featured unwanted and challenging to work with materials such as silicone thermal pads and polymer spacers. However, the UI-5261SE-M-GL carries no such materials and was therefore deemed more desirable for the mission as noted in the report *HYPSO-ANA-006 Analysis of Optical COTS components*.

Some components like the spacers, glue and gasket materials should be tested further in order to determine the risk of outgassing. The test procedure is described in section 3.3: *Outgassing Testing*. However, it is safer for the mission to take precautions due to the low availability of outgassing testing equipment and manpower. The glass window will be removed from the flight model to increase the total luminous transmittance of the optical train, as the only function of the window is to protect the image sensor. This function is not necessary in the flight model as interfacing with the back objective already shields it from external contamination or damage. Individual components on the imager PCBs must be investigated further to determine their material composition. These components could potentially outgas as well and this unknown will have to be solved by testing before final integration in the HSI. Table 7 shows the materials present in the UI-5261SE-M-GL detector.

Table 7: UI-5261SE-M-GL Materials

Material	Part	Induced Vulnerability
AA (Unknown)	Front	-
FR4/Cu	PCB	-
Other PCB Materials	Various	Must be investigated further
Ferritic supports	PCB Stack spacer	Ferromagnetic, effect must be investigated
Unknown polymer	Spacer insert	Outgassing
Glue	Power Transformer	Outgassing
Unknown glass substrate with AR coating	Window	Loss in total luminous transmittance
Unknown elastomer	Gasket	Outgassing

2.2.3 Grating and Slit Materials

The 300/mm Grooves, 25mm Sq, 17.5° Blaze Angle Grating substrate consist of uncoated B270 glass. According to Edmund Optics, an uncoated grating provide higher transmission efficiencies over a wider range of wavelengths while an anti-reflective (AR) coated surface will increase efficiency over an uncoated surface in the relevant range of wavelengths . The grooves are made of a vacuum deposition-coated layer, a vacuum coating technique that uses vaporised plasma of particles deposited on a substrate. Due to the small groove size, the deposited material is extremely fragile and falls off easily.. The optical behavior of grooves on B270 substrate in this configuration when exposed to changes in temperature is unknown, and should therefore be tested.

The slit housing is made from black anodized AA 6061 while the slit itself consists of a thin layer of 302 Stainless Steel with an Black Oxide Finish. The grating and slit doesn't consist of a material that poses a risk of outgassing. Table 8 tabulates the material found within the grating and slit components.

Table 8: Grating and Slit Materials

Material	Part	Induced Vulnerability
B270	Grating	Brittle
B270 (Vacuum deposited)	Grooves	Can easily break of
302 Stainless Steel	Slit	-
AA6061	Slit Housing	-

2.2.5 Onboard Processing Unit (OPU) Materials

The OPU is an assembly of two PCBs in a stacked configuration; a COTS picozed and a custom made breakout board (BoB). It follows that the OPU is comprised of FR-4/Copper composite as well as various PCB component materials. The OPU PCBs must be tested for outgassing as there are some polymers present on these boards. Table 9 tabulates the currently mapped materials and potential vulnerability.

Table 9: OPU Materials

Material	Part	Induced Vulnerability
FR4	Base material	-
Copper	Base material	-
(Alumina Ceramic TBC)	Component	-
Unknown Polymer	Component	Potential Outgassing

2.3 SDR Secondary Payload Materials

The SDR is a component bough from Alén Space; a provider of hardware and software specifically made for nanosatellites. The exact material composition of the payload is therefore unknown. However, because the component is flight proven and designed for space, further resources has not been spent on the material analysis of this component.

2.4 Fastener Materials

Ferromagnetic materials may cause disturbances in the magnetic fields inside a satellite, and therefore it was recommended by NanoAvionics that non-ferrous screws should be utilized across all payloads. The most sensitive component to this type of disturbance is the magnetometers [RD07] as their readings would be influenced by changes in the magnetic field. There is also a possibility that the magnetorquers could be affected by ferrous components. They create a magnetic field that pushes off the earth's field, and thus a disturbance to the magnetorquers field could cause issues with precise control of this effect. Tests would have to be performed to fully map this, but due to the substantial time constraints on the project, the use of non-ferrous screws should prevent any of these problems.

The most common materials used in metric machine screws are A2 and A4 grade stainless steel [RD08]. These are both austenitic steels which are non-magnetic and highly corrosion-resistant. The two grades are very similar, but A4 has an added component of molybdenum that makes it more suitable for marine applications due to increased corrosion-resistance. However, the availability of the desired screw dimensions in A4 was limited compared to A2 and it was therefore decided that A2 would be the preferred option. Their performance in vacuum should be identical as corrosion is not a factor in orbit where corroding chemicals are not present due to the vacuum.

The chosen series of screws is manufactured by the german manufacturer *Bossard* and conform to the *ISO14581* standard. The strength class of the screws was not specified, and could either have a yield strength of 500- or 700 MPa according to the standard. It was therefore assumed to be 500 MPa as a precaution.

2.5 Cable and Connector Materials

Most common electrical wire jackets are made of some type of polymer. PVC is a common type of plastic used for this application, however it is not a suitable material for Low Earth Orbit (LEO) as it has a high outgassing value compared to the NASA recommended limit, see table 10. More suitable materials for vacuum use could be PTFE (teflon) or PPE and the manufacturer *Alphawire* produces a range of cables called *ecoGen* with mPPe as the jacket material of mPPE, a modified PPE compound. The mPPe wires as listed in table 10, exhibits outgassing characteristics slightly above the limit. NanoAvionics recommends the *Alphawire* PTFE cables and wire insulation. However, the provider does not state the specific outgassing values for the PTFE wires. PTFE or teflon has historically exhibited low outgassing values.

The NASA outgassing database [RD09] was used to find other examples of PTFE wires. Table 10 shows that the PTFE wires exhibits outgassing characteristics that are lower than the NASA limits.

Table 10: Alpha Wire Outgassing Values, values given by Alphawire and NASA outgassing database

Product	TML (%)	CVCM (%)
EcoCable Insulation & Jacket	3.05	1.26
EcoWire & EcoFlex Insulation	1.95	0.84
EcoFlex Jacket	1.82	0.34
Typical PVC material	13.98 - 30.67	7.23 - 12.72
Wire Insulation Hscr PTFE Blue (Teflon alpha wire stand in)	0.10	0.03
Hft Green Wire Insulation PTFE/Kapton (Teflon wire insulation)	0.32	0.01

In addition to this the standard procedure of NanoAvionics is to bake out the wires, which removes surface contaminants and gives improved outgassing characteristics. PTFE wires should be safe to use for CubeSats carrying optical equipment.

There are several different connectors present on the various payloads as of 14.05.2019. A full list of these can be found in *HYPSO-ICD-001 Interface Control Document* [RD10]. As can be seen there, most of the connectors are planned to be swapped for picolocks/picoblades. This is due to it being close to impossible to find good material data about standard commercial connectors as they are not designed for use in space. A switch to the picolocks already present in the hardware from NanoAvionics circumvents the issue of several unknown materials. Nevertheless, the only material information available for these are that they are made of a high temperature thermoplastic resin. This is also very limited information, but as they are already space-proven in earlier NanoAvionics missions they are trusted to perform adequately for this missions use as well. If any of the standard connectors are to be used they have to pass outgassing testing to ensure they would not contaminate the optical surfaces.

2.6 Adhesives and Tape Substrate Materials

To further ruggedize components vulnerable to vibration, multiple types of adhesives have been considered. This applies to camera objectives, all threaded connections including screws as well as coupled connections such as wires and thermal straps. Adhesives have also been considered as the interface material between thermally conducting surfaces in order to transfer heat away from important heat sensitive areas. The adhesives are subjected to the same material requirements as all other materials considered for the optical assembly of the HSI.

As a primary fastener adhesive, 3M Scotch Weld DP2216 Gray Epoxy was recommended by NanoAvionics [RD11]. The epoxy can be applied to bolts in order to lock them, reducing the probability of screws unscrewing as a result of rocket launch induced vibrations. The Epoxy can also serve as a thermal interface material, even though the thermal conduction is lower when compared to other more dedicated thermal interface materials.

The 3M Scotch Weld DP2216 Gray Epoxy is space proven and should work well for general use on the payloads. No further resources were used to identify other adhesives. In order to thermally interface with COTS components, thermal straps with tape layers were considered. By using thermal straps with adhesive surfaces, PCB components can be more easily interfaced with without requiring a custom solution. For the following reasons, tape substrate materials were also investigated with respect to outgassing. Section 3 further elaborates on how the evaluation was done following outgassing requirements. Table 11 tabulates the outgassing values for evaluated adhesives and tape substrate materials using the NASA outgassing database [RD09]. It's important to note that some of the values taken from other manufacturers than what have been considered for the payloads. This means that actual properties may deviate, and should therefore be tested. In addition to fulfilling outgassing requirements, adhesives also need sufficient mechanical and thermal properties.

Precautions should be made when using adhesive materials in designs. Application of adhesives should never be a direct interface with leading surfaces or structural supports for position sensitive components. This is because of their viscous properties when subjected to temperature and pressure, which causes deformation over time.

Table 11: Tape and Adhesives Outgassing Characteristics, from NASA outgassing database

Product	TML (%)	CVCM (%)
Tapes		
PEEK Tape 37-2A with acrylic adhesive	0.40	0.01
FRALOCK 7500 Polyester tape - no adhesive	0.20	0.03
Saint Gobain Type K-102 Polyimide Tape/adhesive	1.86	0.03
3M 8901 Polyester tape with silicone adhesive	1.18	0.51
Glues		
Scotch-Weld 2216 B/A AS 5/7 Gray [RD11]	0.77	0.04

3. Outgassing

Even though outgassing is a definite concern when dealing with optics in space, it has unfortunately been the case that some engineers fail to take it into consideration in the design phase. This section provides some insight into the phenomena and presents the information necessary to test the extent of the outgassing.

Outgassing is the release of spurious particles from a material. The particles can be ejected from the material in several ways, through *desorption, diffusion* and *decomposition.* Desorption is the ejection of absorbed contaminants from the material surface. Diffusion is the homogenization that occurs from random thermal motions of contaminants. The random motion of the particles can lead them to the surface layers, should the particles have sufficient thermal energy they can escape the material and evaporate into the environment. Decomposition is a type of chemical reaction where a compound divides into two or more simpler substances which may then outgas through desorption or diffusion [RD12]. The forms of outgassing are all thermally activated and the reaction rates can be mathematically approximated with the use of the Arrhenius law [RD13].

$$k = A\,e^{\frac{-Ea}{RT}}$$

Where
k: Outgassing time constant of material/ Reaction rate
A: Arrhenius pre-exponential factor [s]
E: activation energy of this material [kJ/mol]
R: Gas constant [0,00831 kJ/mol·K]

The activation energy of desorption is low, diffusion has midrange activation energy and decomposition has the comparatively highest activation energy [RD12].

The extent of the outgassing is mainly measured in two ways, Total Mass Loss (TML) and Collected Volatile Condensable Material (CVCM). TML is the measured mass loss percent in a material while CVCM is the fraction of the TML that could condense on a 25 degree celsius surface [RD12]. Outgassing is more severe in space due to the lack of hydrostatic pressure that keep contaminants inside the material. Furthermore, outgassing can be damaging to the operation of satellites. Satellites carrying optical payloads, are especially prone to outgassing related problems as the ejected material can damage the operational capabilities of the optical payloads. The outgassed particles have a tendency to condense on surfaces and can latch on to camera lenses, PCBs, glass and solar panels. Because there is no effective way of cleaning the surfaces, the condensed material will accumulate over time and cover the surface. The distance between the outgassing material and the critical component decides the risk level. For a satellite carrying a camera as the main payload, outgassing is a real concern that must be taken into account when designing and integrating the various payloads. The extent of the outgassing is material specific. In general, polymers are more prone to outgassing related contamination than metals due to the lower activation energy. However, space graded polymers still exist such as nylon. A list of the outgassing characteristic of various components can be found in the NASA database [RD09].

3.1 Outgassing Requirements for CubeSats

The most commonly referred reference regarding outgassing is the NASA rules for spacecraft materials: TML < 1.0 %, CVCM < 0.1 %. These values are the current standard for acceptance of space materials. However the requirements are seen as controversial and the limits somewhat arbitrary [RD12]. The requirements do not take into consideration the opacity of the outgassed particles or the color of the outgassing. Furthermore, a material with a large TML and a near zero CVCM would not be accepted even if the TML does not matter.

As a baseline, the 6U CubeSat Design Specification from California Polytechnic State University, San Luis Obispo recommends that the NASA standard for space material shall be followed to avoid outgassing related contamination of payloads and other s/cs during integration, testing and launch [RD01]. However in some cases the material requirements are not considered or outright ignored, during CubeSat development. The ECSS tailored standard for CubeSats states that the standard *Requirements for contamination assessment* are partially applicable for CubeSat development, it is stated that "Assessment to be performed only if the spacecraft has equipment (e.g. optics) with a high contamination sensitivity. Additionally, since the spacecraft is enclosed in its deployment system during launch, only materials outgassing products shall be considered." [RD06].

CubeSats are required to be tested for outgassing before launch, however the individual materials are not. It follows that some CubeSats can pass the acceptance tests while still carrying potentially volatile materials on board. Some materials has a high activation energy but can outgas over an extended period of time and would not display abnormal outgassing values during a CubeSat acceptance test [RD12]. Materials with a comparatively higher diffusion or decomposition compared to desorption would also result in skewed data due to the activation energy required for outgassing would be higher [RD12]. Thus, the time sensitive outgassing might not initiate, even at the elevated temperature present during the test (normally higher than 125°C [RD13], [RD14], [RD15]). Similarly, internal outgassing in a non ventilated part would not be detected as the total mass wouldn't change.

Several smallsats and CubeSats have had an early loss of optical functionality that is theorised to be the result of outgassing related contamination. The satellite LAPAN-Tubsat/LAPAN A1 exhibited focusing problems some time after deployment. After sharing the findings presented in *HYPSO-TRP-VAC-002 Objective Vacuum Damage Report* [RD16] Prof. Fred Sigernes proposed that the damage could be attributed to outgassing. When contacted, Professor Uno Renner, Professor Emeritus, Consultant for Space Technology at TU Berlin informed that the project had not completed testing of the optical equipment in vacuum and that the engineers had not considered the outgassing contamination that grease and oil could inflict on the telescope. This serves as a real-life example of the dangers of outgassing.

When dealing with outgassing in CubeSat development, the requirements are rather difficult to relate to due to the somewhat arbitrary limits. However, the material outgassing must be inspected and tested due to the severe ramifications the contamination could have on the equipment and other CubeSats. Even when not carrying highly sensitive optical equipment, outgassing is a valid concern that should be estimated and controlled to a certain degree.

3.2 Outgassing in COTS Components

This section discusses the outgassing characteristics of the potential and chosen optical COTS components present in the HYPSO CubeSat. COTS components are a huge issue when integrating optical equipment into a CubeSat as the components were not made with the space environment in mind and could potentially carry high outgassing or volatile material. The fact that acquiring the material information from the suppliers is such a difficult ordeal as most companies are protective of their design and production methods, makes the testing and potential adaptation of the components a tedious process. It is recommended to use space proven equipment. However, most COTS objectives and detectors are simply not usable in space in their default configuration.

Objectives are difficult to adapt due to the large amount of grease normally present inside the unit. The grease used in the COTS parts are not rated for space as vacuum grease is expensive and unnecessary for atmospheric use. Some parts inside the objectives can also be made of polymers that are potential outgassing sources. The objectives planned to be carried by the HYPSO CubeSat, the 50mm VIS-NIR Objectives from Edmund Optics, showed contamination damage due to outgassing of grease. This is further elaborated on in the *HYPSO-TRP-VAC-002 Objective Vacuum Damage Report [RD16]*. It follows that the grease must be cleaned of the objectives. This should be done with an ultrasonic bath and a fat dissolver chemical like *Isopropanol.*

The various detectors considered for the mission all had the same problems: mainly the large amount of polymers and glue found within. All closed detectors were fitted with silicone elastomer thermal pads, as can be seen in section 4. The NASA database suggests that some silicone based thermal pads can exceed the NASA outgassing requirements [RD09]. Table 12 tabulates some of the silicone thermal pads found in the NASA database.

Table 12: Silicone Outgassing Characteristics

Material	TML (%)	CVCM (%)
APTEK Therm-Pad 1100 Thermally Conductive Silicone	0.11	0.02
CHO-THERM 1673 Therm Cond Sheet Green Silicone	1.18	0.10
CHO-THERM 1663 Therm Cond Sheet White Silicone	1.53	0.14

The behaviour of such silicone pads varies depending on heat treatment. It has been reported that the rate of outgassing can be lowered by two orders of magnitude [RD18]. Heat treating the silicone causes a reduction of low molecular weight silicone oils inside the compound. After curing, the silicone must be allowed to ventilate as the compound will continue to outgas, as the low molecular compounds will vaporize, for an extended period of time [RD19].

For the purpose of the HYPSO mission, it was decided to drop the detectors carrying the silicone thermal pads. The reasoning behind this decision was that without easy access to a dedicated outgassing vacuum chamber fitted with a CVCM apparatus, (see section 3.3), no assessment could be made regarding the outgassing characteristics of the silicone. To avoid any potential outgassing, a PCB only detector from iDS was chosen, which aligned with the potential in house detector PCB planned for the next HYPSO CubeSat project.

The other plastic parts present in the COTS components must be further examined for outgassing. Polymers are known for their poor outgassing characteristics in the vacuum environment, and some polymers can completely evaporate due to the lack of hydrostatic pressure [RD20]. Although it would be wrong to say that all polymers exceeds the NASA standard values, most certainly do. Therefore it is imperative to check all polymer materials that are close to critical and cold, condensable surfaces.

3.3 Testing of Outgassing

The standards ASTM E 595-77/84/90 [RD14] and ECSS-Q-ST-70-02C [RD15] describes the standard test procedure for outgassing screening tests for space materials for NASA and ESA respectively. The standard analysis includes measurements of TML and CVCM by the use of an micro-CVCM apparatus or micro VCM equipment [RD14], [RD15]. The micro-CVCM apparatus described in the ECSS-Q-ST-70-02C consists of a temperature and vacuum controlled chamber (TVAC) holding the test sample and a collector made of chromium-plated aluminium plates for material condensation situated above. Figures, exact measurements and further physical description can be found in the mentioned standards.

Should single materials within the HYPSO CubeSat be tested for outgassing, it is recommended to conform to either of these standards.

For outgassing of larger systems, the described method would not be applicable. However, other outgassing tests exists such as Kinetic outgassing analysis. A special vacuum chamber equipped with a residual gas analyser can be used to simulate the space environment and analyse the outgassed particles emitted from the test item. The company TS SPACE SYSTEMS are currently planned to perform an outgassing test on the 50mm VIS NIR objectives to validate that an eventual cleaning procedure could remove the necessary grease inside the item. The method is further elaborated on in the standard ECSS-Q-TM-70-52A [RD13].

4. Material Identification Tests

This section will cover the methods used for material identification during the CubeSat design process. This section provides an understanding of why these methods where used and how to use them moving further into the project life time.

There are several ways to identify and characterize an unknown material. Physical tests such as appearance and spark tests can be utilised, hardness tests by using brinell, vickers or the rockwell methods can help identify metal materials. However, these tests gives only a partial description of the material properties. Newer methods exist today that produce definitive evidence as to what material is being analysed; for metal identification X-ray fluorescence spectrometers (XRF), *scanning electron microscopy (SEM)* paired with *Energy dispersive X-ray spectroscopy (EDS)*, and *X-ray Powder Diffraction (XRD)* were used.

XRF gives an overview of the elements the material is comprised of. This is done by emitting an X-ray beam with sufficient energy to affect the electrons in the inner shells of the atom. The X-ray then displaces the electron from the shell due to the energy difference, creating an electron vacancy. The vacancy causes the atom to become unstable, necessitating a higher orbit electron to fill the vacancy. The electrons in higher orbits further from the nucleus carries more energy. By filling the vacancy of the lower orbiting electrons, the energy difference is emitted as a photon. The emitted energy can then be read by the XRF apparatus which uses the information to identify the element [RD21]. An XRF gun was used to identify the material that comprises the iDS detectors. Figure 5 shows the XRF gun used during the identification process.

Figure 5: XRF Gun

Scanning electron microscopy (SEM) is a method for high-resolution imaging of surfaces [RD22]. SEM works by generating a beam of electrons that is scanned over the material surface. The SEM machine can be used by applying a high vacuum (10^-3 Pa) thereby allowing electrons to to travel from the beam source to the samples and detectors. For identifying the lens substrate and coating found within the 50 mm VIS NIR lenses SEM and EDS were used. Energy dispersive X-ray spectroscopy (EDS) is a chemical microanalysis technique where secondary X-ray radiation is analyzed as a result of electron sample bombardment [RD22]. It is a requirement of the SEM and EDS techniques that the test sample is electrically conductive. Glass is therefore often coated with a carbon powder before analysis, facilitating electrical conductance. The results of the SEM and EDS analysis are EDS spectrums showing the chemical elements present in the tested sample. The test does not specify the molecular structure [RD22]. Figure 6 shows the EDS analysis done on the second lens in the 50 mm VIS NIR objective. Based on the results, it can be concluded that the lens substrate appears to be Silicium Oxide (SiO2) with a Magnesium Fluoride (MgF2) anti reflective coating. Figure 7 summarizes the EDS results.
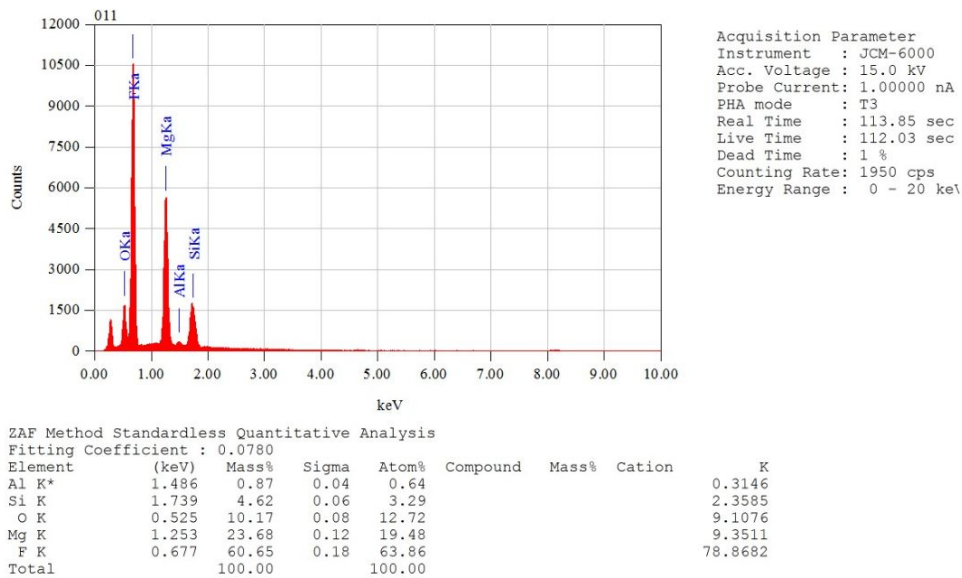
Figure 6: EDS Result for second Lens, (Provided by Vebjørn Kristvik)

	Glass 1				Glass 2			
Element	F	Mg	O	Si	F	Mg	O	Si
Mass %	54	18	5	1	60	23	10	5
Sigma	0.13	0.09	0.06	0.10	0.18	0.12	0.08	0.06
Atom %	70	18	9	1	63	20	13	3
	Glass 3				Glass 4			
Element	F	Mg	O	Si	F	Mg	O	Si
Mass%	36	7	30	11	63	18	9	6
Sigma	0.36	0.12	0.26	0.12	0.41	0.24	0.18	0.15
Atom %	34	6	35	7	67	15	12	4
	Glass 5				Glass 6			
Element	F	Mg	O	Si	F	Mg	O	Si
Mass %	56	18	17	9	52	10	12	3
Sigma	0.14	0.09	0.07	0.07	0.30	0.12	0.15	0.13
Atom %	58	14	21	6	65	10	18	3

Figure 7: Element breakdown of all glass, (Provided by Vebjørn Kristvik)

X-ray Powder Diffraction (XRD) was used in order to test the degree of crystallinity of the lenses found within the 50 mm VIS NIR objectives. The technique uses an X-ray beam directed on the sample over a variation of 180 degree angels, while measuring absorption, scattered and transmitted X-rays. XRD provides a diffractogram of intensity over angle. Sharp peaks represent a distinct crystallography and a chemical substance, no distinct sharp peaks indicate amorphous structure [RD22]. Figure 8 shows the results of the XRD analysis on the first lens. The figure indicates an amorphous substrate material, typical of glass, with a crystalline MgF_2 coating.
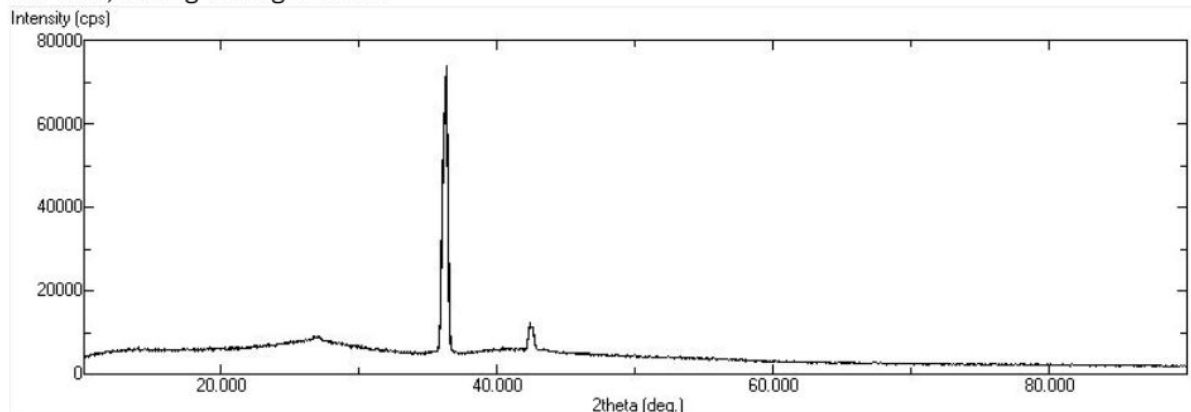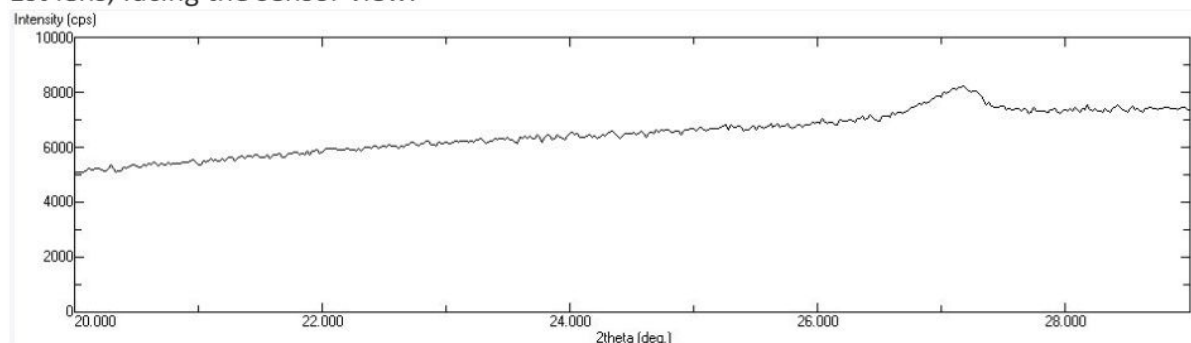
Figure 8: XRF Results on the first lens, (Provided by Vebjørn Kristvik)

For polymer identification SEM and XRF can not be used due to the vacuum and the fact that the XRF was calibrated to determine heavier metal elements. For the identification of polymers, a chemical identification method is recommended. However, for the purpose of identifying the polymer thermal pads present in the closed iDS detectors, a simple burn test was performed. The test is somewhat subjective, however, it gives a clear identification of the material when paired with other information. The test is done by pressing a heated material against a small sample of the polymer. If the polymer goes soft it is an indication that the polymer in question is a thermoplastic. If the material does not soften it is a thermosetting polymer. The different reaction to thermal energy is due to the internal cross linking between the monomer chains in the thermoset polymer. The cross linked polymer structure keeps the chains from separating, therefore the material can not be soften or melted upon reheating, only decompose [RD23]. The resulting flame color, and flame odour can be used to identify the material further.

By cross referencing the results with a *Plastic Identification Flow Chart,* like the one offered by Partec, the polymer can be identified as seen in figure 9. This method can obviously not give an insight to the exact material composition and polymerization, but it can help identify the general polymer type. Figure 10 shows the yellow flame resulting from the burn test, indicating that the thermoset polymer is an epoxy or a silicone, by cross checking with common materials used in thermal pads, the polymer was identified as a silicone.
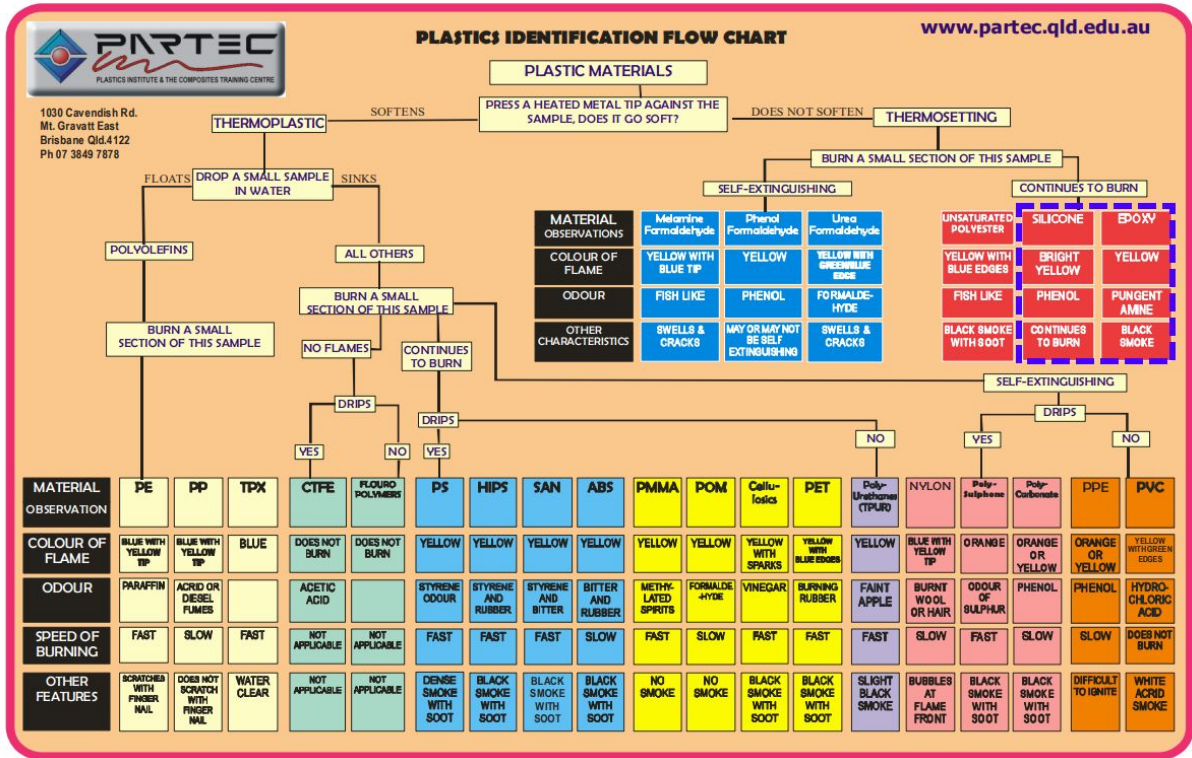
Figure 9: Plastic Identification Flow Chart
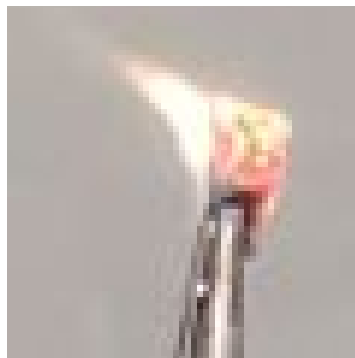
Figure 10: Yellow flame indicating silicone or epoxy

5. Thermal Control

The HYPSO mission requires thermal control of multiple heat sensitive and heat generating payload components. The HSI camera is an optical component crucial to the mission. It is comprised of COTS components assembled together with specified distances that are sensitive to movement causing misalignment. Considering the fact that the objectives are made out of aluminium, a material with one of the higher thermal expansion ratios, the thermo-optical behavior will need to be characterized and controlled [RD24]. Furthermore, the analysis *HYPSO-ANA-008 HSI Payload Platform Thermal Analysis* concludes that thermal control is necessary in order to stay within the thermal ranges of the different payloads. In CubeSat missions this is generally done using passive control methods, which is generally more associated with a lower cost, volume, weight and risk [RD25]. These methods involve changing the thermo-optical properties of a surface, material choice, and conducting heat away. The following sections will describe and evaluate the materials considered for the chosen methods with respect to their effectiveness and adaptability to the space environment.

5.1 Surface Treatments

Material surface treatments can be used to change a materials thermal properties without the need for external straps and other connectors. The mechanism behind the property adjustment is a direct change in the material emissivity and absorptivity, as a consequence the heat transfer caused by radiation is determined by the surface thermal emittance properties [RD26]. The types of surface treatments evaluated were anodization, hard-anodization, coatings, as well as untreated metal surfaces. Because the HSI camera is sensitive to light, changing the optical properties of a surface could be beneficial to avoiding stray light. It is recommended to use hard-anodization or coating materials to counteract stray light, as they are capable of providing more matt surfaces. However, based on the *Functionality Test Report of HSI TTH Mk1*[RD27] done on the TTH Mk.1 prototype using untreated manufacturing surfaces, it was uncovered that the amount of stray light present on the inside of the camera was negligible. The lenses receiving incoming light faces away from all machined parts, and the optical reflectance values were therefore not a concern when deciding on whether to utilize surface treatments. Anodizing the aluminium surfaces would also introduce uncertainties in the tolerances as the process adds a thin oxidation layer. All the aforementioned factors played into the decision of not coating or treating the machined surfaces. Furthermore, according to the thermal analysis performed in *HYPSO-ANA-008 HSI Payload Platform Thermal Analysis* [RD28], it was uncovered that surface anodization probably is not necessary. However, in order to eliminate uncertainties, it was recommended by the analysis.

5.2 Thermal Strap Materials

Thermal straps are planned to be used for passive thermal control on the HSI payload. As thermal straps rely on transferring heat effectively, the material comprising the strap must have high thermal conductivity. Due to the launch environment they also need to inhibit a certain degree of strength as well as flexibility such that they can be adapted to the cramped interior of a CubeSat. The following subsections discusses the various materials that were considered for this application.

Pyrolytic Graphite Sheets (PGS)

PGS material is a thin sheet of highly thermally conductive material. It is flexible and can be cut into desired shapes, something that makes it ideal for CubeSat applications. PGS can be delivered on a substrate of either PEEK or POLYIMIDE tape, covered in table 11, section 2.6, which would ensure a uniform connection between the thermal strap and the joined components. It can also be delivered without a substrate which could be applicable if the aforementioned substrates features undesirable outgassing properties. The PGS material has varying thermal conductivity based on its thickness. Table 13 gives an overview of the thermal conductivity for the different thicknesses [RD29].

Table 13: Thermal conductivity of various thicknesses of PGS

Thickness [*μm*]	17	25	70	100
Thermal Conductivity [*W/m*K*]	1700 - 1800	1500 - 1700	750 - 950	600 - 800

An effective conductance can be calculated in order to compare the various thicknesses by using the equation:

$C = kA/L$, where

C: Total thermal conductance [W/K]
k: Thermal conductivity [W/K·mm]
A: Cross sectional area [mm^2]
L: Substrate length [mm]

Basing the case on the IMX249 processing chip cooling, the width of the strap needs to be at least 19 mm to match the chip, yielding A=0.019m*thickness.

Copper

Copper is a conventional material used for thermal straps. Coppers thermal conductivity is typically around 380-400 W/mK [RD30], and if used in a cabled or braided configuration the copper threads can be quite flexible. One option is to design a small bracket for each interface point and run a conventional electrical copper-cored wire between them. This is a simple solution, and is already in use on the bus delivered from NanoAvionics. There are also several suppliers that could deliver customized pure copper thermal straps, which would lessen the workload of developing an in-house interfacing solution. However, these would come with a significant economic cost.

Aluminium 1100

The 1100 series is a material used in some space-applications for thermal control. It can be somewhat difficult to interface with this material without a bolted connection [RD31], something that would be necessary for mounting on the heat generating chips. Its thermal conductivity is typically around 218 W/mK [RD32], which puts it in the lower end of the materials considered. The 1100 series is a pure aluminum (99% [RD32]) and therefore has a higher conductivity compared to other aluminum alloys [RD33] and it is quite flexible [RD34], however the strength is low [RD32] and threadings should be avoided due to the softness of the material [RD34]. Based on the material properties the 1100 series were considered, but ultimately excluded as an option due to the increased complexity it would introduce in the design.

Phase Change Materials (PCM)

Phase-change cooling is a type of thermal control that resembles the method used in conventional refrigerators. PCM has not been used much in european satellites, however the demand for a low mass passive thermal control system on micro and nano satellites makes PCM lucrative for CubeSats moving forward [RD35]. It functions by absorbing thermal energy in a phase transition from liquid to gas during a pressure reduction. The gas is then passed through a radiating element before being compressed and condensed back to liquid. There exists a range of commercially available PCM, and such the cooling effect of a custom made system could be tailor-made to keep components to the optimal operating temperature. Examples of such materials are shown in table 14. There are a vast number of these products and the displayed materials are just examples to show the precision of properties that are available for a PCM based design.

Table 14: Properties of suitable commercially available organic PCM [RD36]

Material	Melting Point	Heat of Fusion [kJ/kg]
A43	43	165
A44	44	242
A15	15	130

A PCM solution was considered, however, the Technology Readiness Level (TRL) of the solution in relation to CubeSats was too low to justify the added complexity this would add to the system. This might be something that could be considered in future iterations of the HYPSO mission if appropriate resources could be assigned to develop it.

6. Conclusion

Table 15 shows all materials currently planned to be used in the HYPSO CubeSat. While the HSI Platform, fastener and adhesive materials were specifically chosen based on the requirements presented in this report, the other materials were part of a larger COTS system that had to be adapted. Some of the COTS materials exhibit outgassing values higher than the NASA recommendation or exhibits an unknown outgassing characteristic and must be further tested. It follows that the presented materials list is subject to change. The table excludes any thermal materials due to the uncertainty surrounding the solution, as testing is planned to be done at a later stage due to time constraints.

Table 15: List of Materials Planned to be part of the Flight model

Component	Material
HSI Platform	AA6082
Sensor Thermal Strap	Pyrolytic Graphite
Objective Shell	AA6061 w. Black Anodization
Objective Lenses	SiO2 w. MgF2 AR coating
Detector Shell	Aluminum Alloy
Detector PCB Stack Spacer	Ferritic Steel
PCB Base Material	FR4 (GRP)
PCB Component	Unknown Ceram (Possibly Alumina)
PCB Component	Unknown Polymer
Grating	B270 Glass
Slit Housing	AA6061
Slit Material	302 Stainless Steel
Fastener Material (Screws)	A2 Grade Stainless Steel
Adhesive Tape (PEEK)	Acrylic
Adhesive for Connector Ruggedization	Epoxy
Cable Insulation Jacket (Uncertain)	mPPE (Modified Polyphenyl Ether)

8. List of Abbreviations

Table 12: Abbreviations

Abbreviation	Description
AA	Aluminium Alloy
BoB	Breakout Board
COTS	Commercial Off-The-Shelf
CTE	Coefficient of Thermal Expansion
CVCM	Collected Volatile Condensable Materials
ECSS	European Cooperation for Space Standardization
EDS	Energy dispersive X-ray spectroscopy
ESA	European Space Agency
GRP	Glass Reinforced Plastic
HSI	Hyper Spectral Imager
LEO	Low Earth Orbit
mPPE	Modified Polyphenyl Ether
NASA	National Aeronautics and Space Administration
OPU	Onboard Processing Unit
PCB	Printed Circuit Board
PCM	Phase Change Material
PDR	Preliminary Design Review
PEEK	Polyether ether ketone
PGS	Pyrolytic Graphite Sheets
PPE	Polyphenyl Ether
PSLV	Polar Satellite Launch Vehicle
PTFE	Polytetrafluorethylene
PVC	Polyvinyl Chloride
s/c	Spacecraft
SDR	Software Defined Radio
SEM	Scanning electron microscopy
SMAD	Space Mission Analysis and Design
TML	Total Mass Loss
TRL	Technology Readiness Level
TVAC	Thermal Vacuum
XRD	X-ray Powder Diffraction
XRF	X-ray fluorescence

Appendix E

HYPSO-ANA-003 Architectural Layout Analysis

Architectural Layout Analysis

HYPSO-ANA-003

Prepared by: HYPSO Project Team
Reference: HYPSO-ANA-003
Revision: 2
Date of issue: 26.05.2019
Document Type: Internal Analysis
Author(s):   Henrik Galtung, Tord Hansen Kaasa

Table Of Contents

Table 1: Table of Changes

Rev.	Summary of Changes	Author(s)	Effective Date
1	*First issue*	*Tord Hansen Kaasa, Henrik Galtung*	*22.03.2019*
2	*Formatting of text and figures*	*Tord Hansen Kaasa, Tuan Tran, Henrik Galtung*	*26.05.2019*

Executive Summary

Two architectural layouts, *Configuration 1. "SDR at the Back"* and *Configuration 2. "RGB Camera and Star Tracker Same Side"* were proposed to mitigate the challenges introduced by the addition of a larger S-band transceiver. While the redesign done on the mechanical design of the HSI (Hyperspectral Imager) payload post PDR (Preliminary Design Review) somewhat mitigated the spacement problem introduced by the S-band transceiver, the original configuration was deemed to be undesired due to the small space for wiring coming from the HSI detector. The disadvantage of cabling space behind the HSI detector were deemed manageable by designing a custom SDR (Software Defined Radio) mounting solution around the limitations. In addition to this, the spacious nature of such a layout opens up several possibilities for mounting the IMU as well as preserving the possibility of angling the star tracker at a later time if deemed necessary.

Configuration 1. "SDR at the Back", section 4.1, was therefore chosen as the optimal architectural layout.
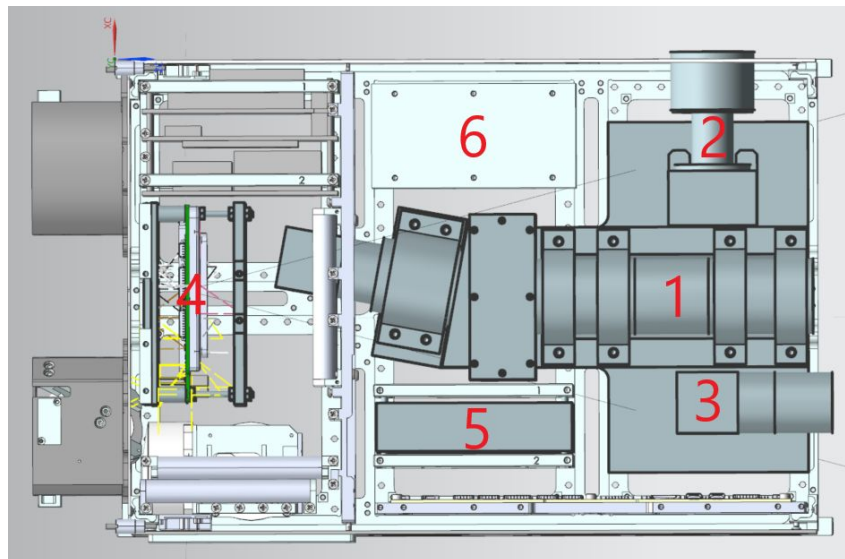
Figure 1: Configuration 1: (1) HSI, (2) Star Tracker, (3) RGB, (4) SDR, (5) OPU, (6) S-Band

1. Purpose

Due to the limited space inside the bus caused by the size of the included payloads, various components and the required space for connectors and cables, the layout needs careful consideration. During the PDR a preliminary architectural design for the payload components was decided. However, the addition of the larger S-band transceiver post-PDR necessitated compromises to the bus layout in order to fit all vital components. This document will present various configurations of the components along with pros and cons of each. This will serve as the justification for the final placement and facilitate further work on mechanical design, cable management and interface solutions. Figure 2a shows the PDR architectural design configuration, figure 2b shows the problem caused by the introduction of the larger S-band transceiver.
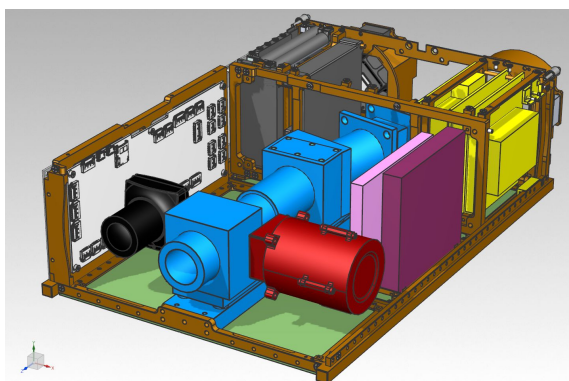
Figure 2a: Bus layout as presented in the PDR   *Figure 2b: S-band transceiver collision*
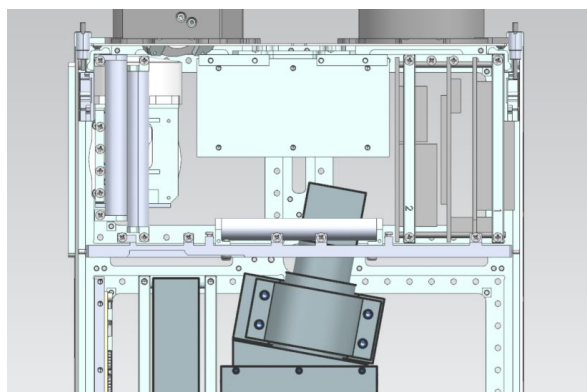
1.1 Scope

This report is limited to exploring the feasible architectural solutions in light of the current design and the changes necessitated by the inclusion of the S-band transceiver, conforming to the *6U CubeSat standard* [RD01]. In addition, the report will state if a non critical component shall be omitted due to architectural limitations. The report will not directly propose solutions for changes in mechanical and thermal design. However, the possible solutions will be considered when weighing the different options. Cable management and specific interface solutions for the chosen configuration will be further elaborated in the report *Interface solutions and Architectural Design Document.* Figure 3 shows the relationship between all the documents.
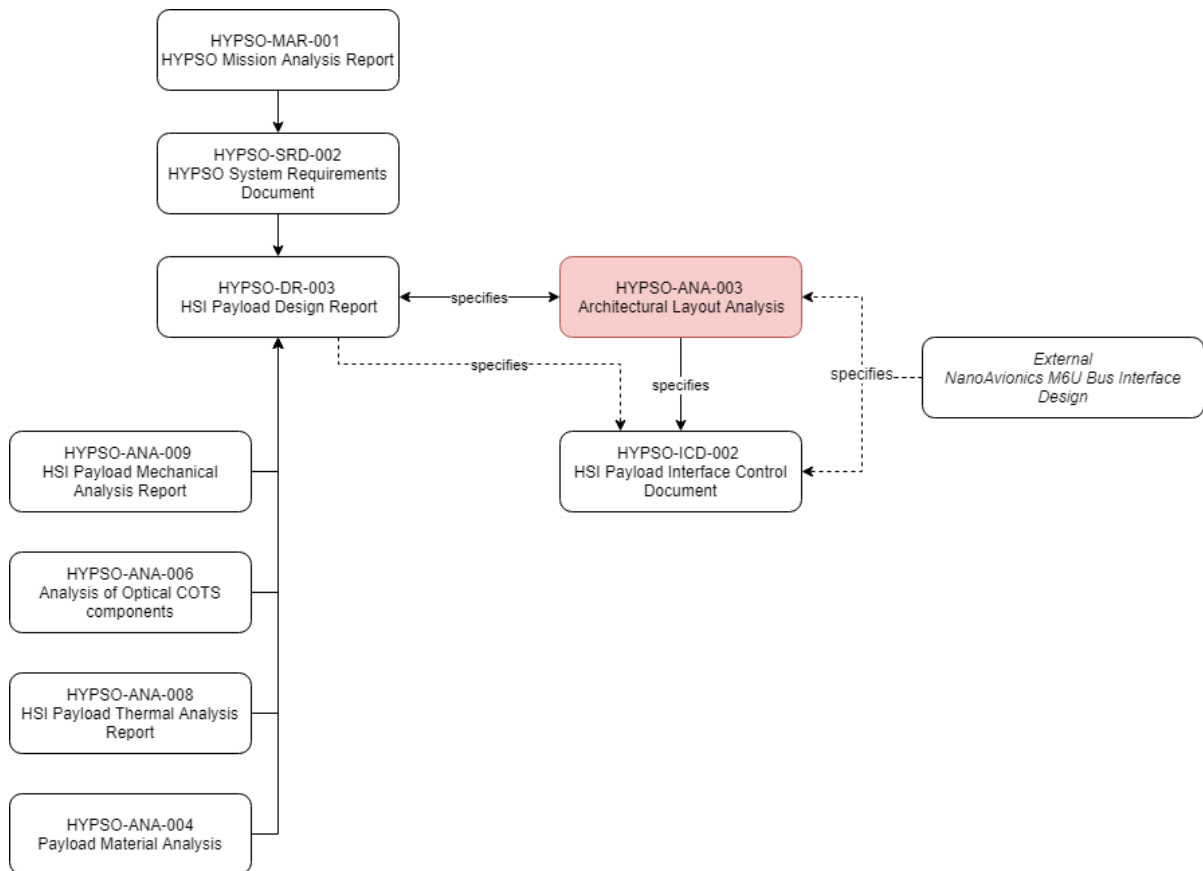
Figure 3: Document relationship

1.2 Reference Documents

The documents listed in table 2 have been used as reference in the creation of this document.

Table 2: Referenced Documents

ID	Author	Title
[RD01]	Cal Poly SLO The CubeSat Program.	6u cubesat design specification rev. 1.0, 2018 .[Link], accessed March 2019.
[RD02]	PC/104 Embedded Consortium.	PC/104 Specification Version 2.6, 13. October 2008. [Link], accessed May 2019.
[RD03]	Tord Hansen Kaasa, Tuan Anh Tran, Henrik Galtung.	HYPSO-DR-003 HSI Payload Design Report
[RD04]	James R. Wertz, David F. Everett, Jeffery J. Puschell. Microcosm Press, Hawthorne, Calif	Space mission engineering: The new SMAD. 2011.
[RD05]	Sensonor.	STIM210 Multi-Axis Gyro Module Datasheet. [Link], accessed March 2019.

2. Movable Components

This section quantifies all components which location can be changed inside the bus.
The importance level of each component can be derived in the following categories:
- *Critical:* The component is mission critical
- *Beneficial:* The inclusion of the component would be beneficial for the mission
- *Non critical:* The component would be advantageous to include, but not necessary

The components that can be moved are presented in the following sections:

2.1 Onboard Processing Unit

-Importance level: Critical

At this stage in the process the Onboard Processing Unit (OPU) still has an unknown stack height. The height discretion is caused by the expectation that a cooling solution will be needed in the form of a passive thermal control solution (heat sink). This would add significant thickness perpendicular to the main plane of the Printed Circuit Board (PCB) stack. The preliminary thickness is set to 25mm as this is the maximum design thickness of the carrier board with picozed stacked. The carrier board is designed to conform to the pc104 form factor [RD02]. The preliminary dimensions are shown in figure 4.
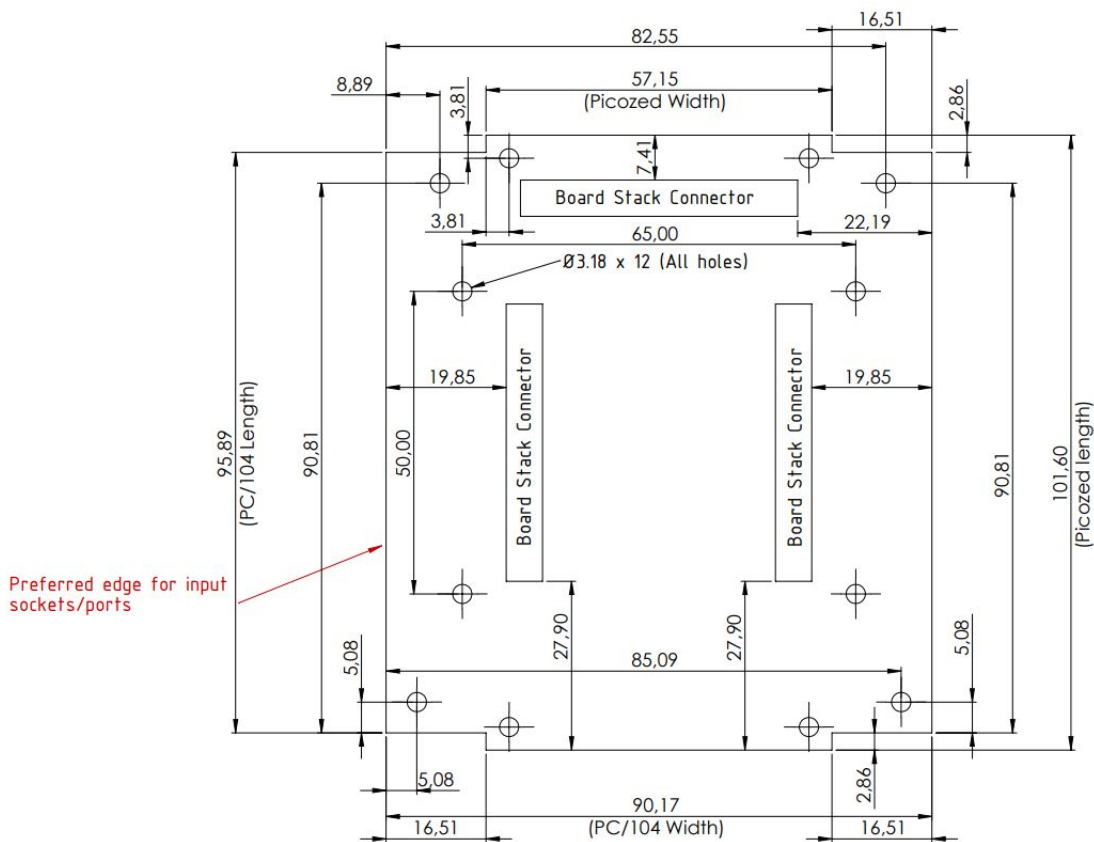
Figure 4: Preliminary dimensions of breakout board

2.2 SDR

   -Importance level: Beneficial

The SDR is a unit bought from Alén Space and thus has a set size. The thickness is shown in figure 5:
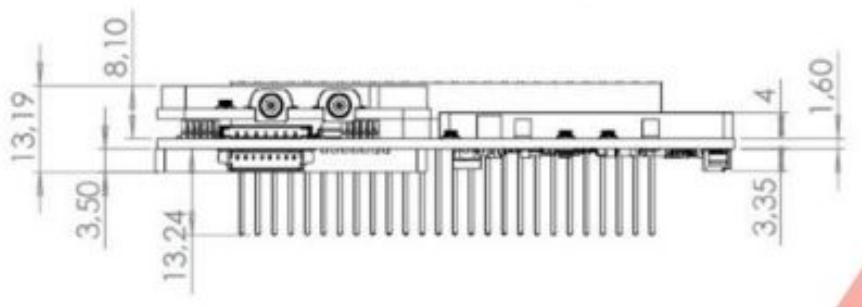
Figure 5: Dimensions along the SDR Thickness

The dimensions along the other axis are 89.3 mm x 93.3mm.
The Alén Space SDR follows the PC104 form factor for mounting.

2.3 S-band Transceiver

   -Importance level: Critical

The S-band transceiver was a post PDR payload addition by NanoAvionics, requiring significant space necessitating the restructuring of the overall architectural layout. The S-band transceiver has the shape of a box with the following dimensions:
97mm x 49.5mm x 59mm.

2.4 HSI Payload

   -Importance level: Critical

The HSI is the primary payload of the HYPSO mission. The HSI camera will be mounted on a platform with the dimensions given in figure 6. It is important for the purpose of the analysis to note that the platform dimensions are preliminary, and can be reduced by 5-10mm in the X-axis, resulting in additional space on the sides of the platform. The new platform developed also limited the length of the payload, somewhat mitigating the S-band spacing issue.

The HSI is positional required to point straight in the +Z-direction. The fact that a centralized position within the bus makes the mechanical design and interfacing with the frame easier will be taken into consideration when considering the layout. In addition, a proposed dampening solution from SMAC space will also necessitate a raising of the platform in the +Y-direction [RD03]. The HSI payload will therefore be considered as taking the entire available space i the Y axis. The HSI platform also supports the star tracker and RGB (Red Green Blue) camera, on the +X flange and -X flange respectively.
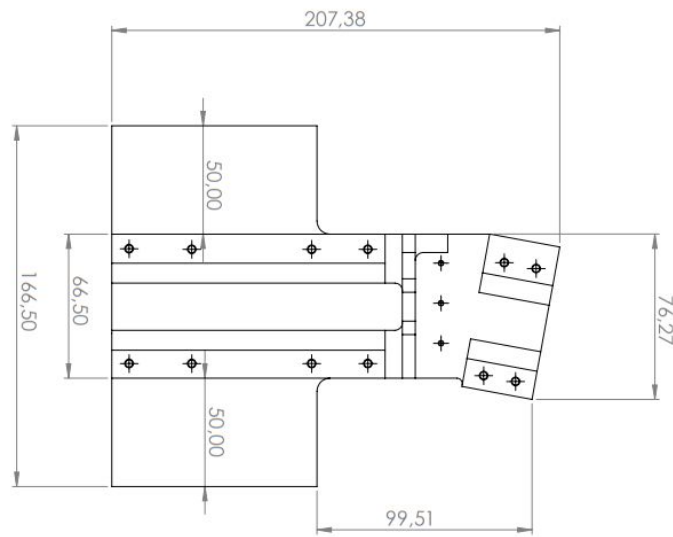
Figure 6: The external dimensions of the HSI Platform

2.5 Star Tracker

-Importance level: Critical

The star tracker is a 3rd party unit with set dimensions shown in figure 7. The star tracker is required to point in the +X-direction, preferably 20 degrees along the -Z-axis from the straight X-axis as to avoid the earth albedo light. However, the albedo does not affect new star trackers to a dangerous degree [RD04]. Since the 20 degree angle is not rooted in a requirement nor necessitated by any reports, the angeling will be considered as a bonus feature when judging the various layouts, to decrease the risk associated with the star tracker view.
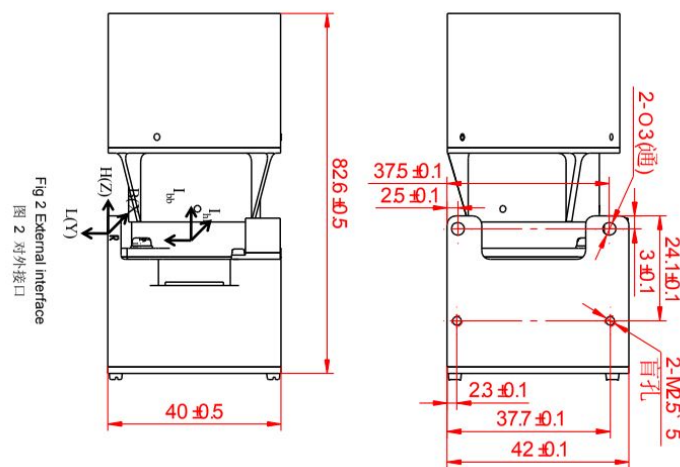
Figure 7: Star tracker external dimensions

2.6 IMU

-Importance level: Critical

The IMU (Inertial Measurement Unit) shall be mounted on the HSI payload. The main purpose of the IMU is to relay information regarding the payloads specific force and angular rate, acting as a combination of a gyro and an accelerometer [RD05]. The IMU has the following dimensions: 38.6mm x 44.8mm x 21.5mm. The mechanical dimensions and drilling pattern of the IMU are shown in figure 8a and 8b respectively. For simplicity of orientational calculations, the IMU axes need to be parallel to the bus axes, but not necessarily X with X, Y with Y, and Z with Z [RD05]. It follows that this component has several possible placements, combined with its small size and ease of mounting, will not be considered directly in this analysis. All possible layouts will have options for placing the IMU at a later time.
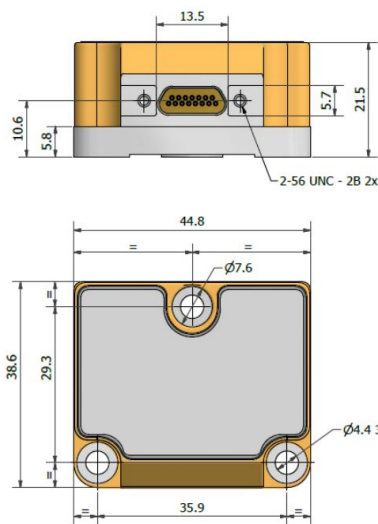
Figure 8a: Mechanical dimensions
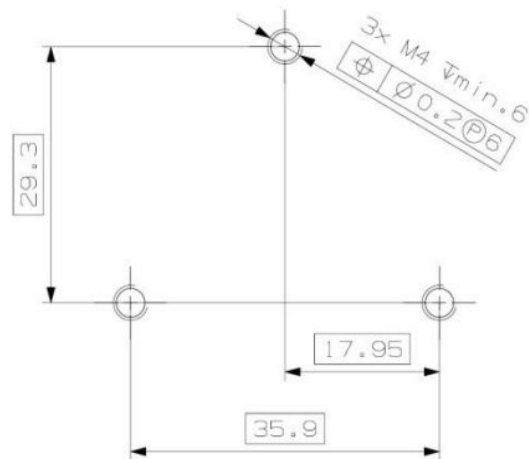
Figure 8b: Drilling pattern

2.7 RGB Camera

-Importance level: Non Critical

The RGB camera is an assembly consisting of a camera housing and a lens. These have combined dimensions as shown in figure 9. The inclusion of the RGB camera was made to complement the HSI camera in case the HSI should fail or not respond, and also be used for georeferencing. The RGB camera is required to point straight in the +Z-direction, the same direction as the main HSI payload.
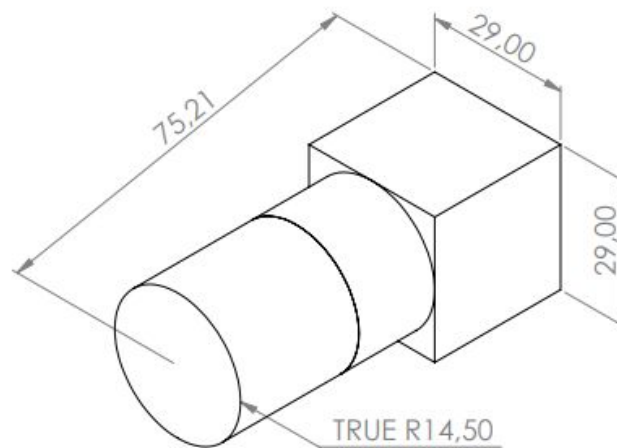
Figure 9: RGB assembly dimensions.

3. Cable Management

All components listed above requires one or more connectors and cables to supply power and exchange data. Due to this, space around the components will also be an important consideration to make when judging the layouts. At this point in the project, several of the component designs still being in the development phase. Consequently, for this analysis, the exact location of the connectors for each component is not set. Because of this it will be assumed that each component will require more free space than will be the case when all designs are finalized.

4. Configuration Overview

The following sections displays the considered layouts. Note that the IMU is not included in these illustrations as this can be mounted at several different locations for all configurations due to its relatively moderate size.

4.1 Configuration 1. "SDR at the Back"

This layout provides the most evenly divided space amongst the components. The HSI is located centrally with each of the other payload components placed in their own of the available 4U as shown in figure 10. Due to the available space, there is room for adjustments in each components precise placement. It also gives considerable options for cable management with ample room for both connectors and wires. The drawback of this configuration is the need for developing a custom interface design for the SDR as stacking rings does not fit in the desired orientation. This is however a minor challenge as there are several suitable mounting points for a custom solution at the -Z side of the frame. There is also the possibility that the custom interfacing solution for the SDR would interfere with the cabling running out of the HSI detector. This is also a minor challenge that could be mitigated in the SDR mounting design.
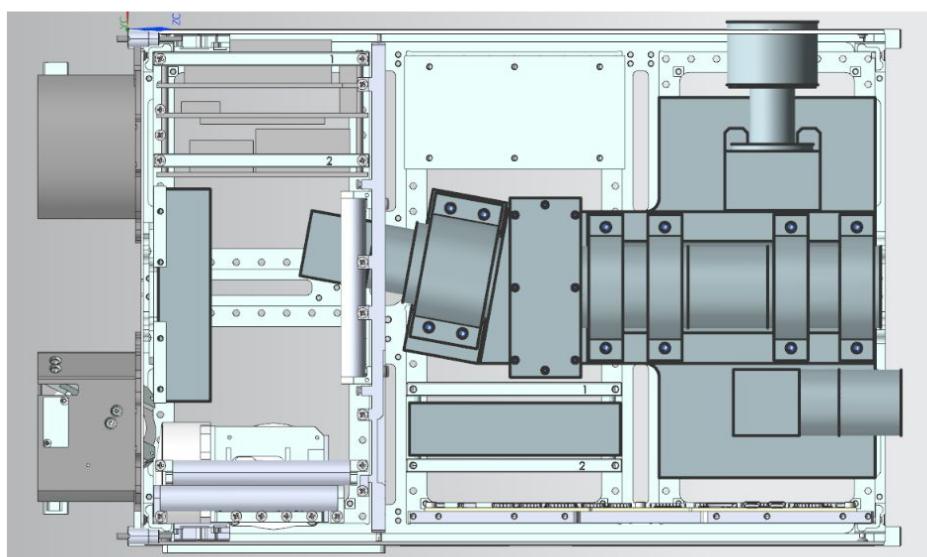
Figure 10: The "SDR at the back" configuration

The main reason the SDR is moved to the back and not the OPU is simply due to dimensional reasoning, the OPU is too large to fit in the available space. The main concern with this solution is the available space for the star tracker. The length of the star tracker might facilitate an offset of the HSI payload in order to be properly fitted in. However, the HSI platform is expected to be slimmed down allowing for more space for the star tracker. In addition, the star tracker can protrude a maximum of 10 mm from the bus frame outer datum plane in the +X-direction [RD01]. Based on this reasoning the HSI platform will remain centered in respect to the X axis.

4.2 Configuration 2. "RGB Camera and Star Tracker Same Side"

This layout moves the RGB camera over to the opposite side of the HSI compared to Configuration 1. as shown in figure 11. The star tracker is moved further in the -Z-direction, eliminating the possibility of angling, as discussed in section *2.5 Star Tracker.* The main advantage of this configuration is the ease of mounting both the OPU and the SDR. There is ample room for mounting both in their own stacking ring assemblies in addition to creating room for their respective connectors and cables. It also opens up room behind the HSI detector such that the cable running of this in the -Z-direction would not interfere with any other components.

There is also a possibility that this configuration introduces problems with the cable management for both the RGB and the star tracker. Due to their close proximity there might arise problems where the connectors and respective cables would interfere with the placement of the other component. Thermal considerations must be taken as well when considering the proximity of the two heat sources of the cameras. Another concern with this layout is the concentration of mass on the +X side of the HSI platform if both the star tracker and the RGB is situated here. There is a very serious risk of this affecting the resonance frequencies of the whole HSI assembly in an unfavourable way and potentially damaging the camera assembly during launch conditions.
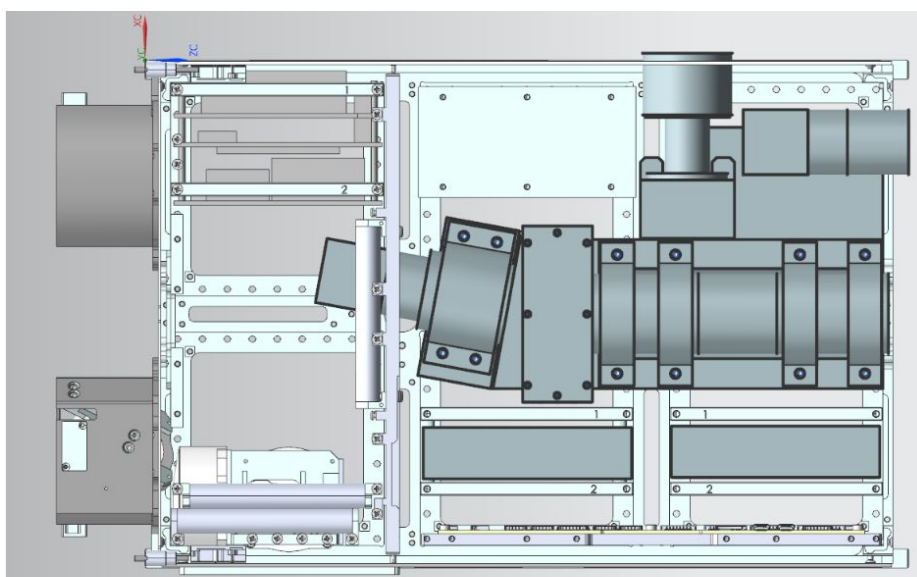
Figure 11: RGB and star tracker placed at the +X side of the HSI

5. Conclusion

While the redesign done on the mechanical design of the HSI payload post PDR somewhat mitigated the spacement problem introduced by the larger S-band transceiver, the original configuration was deemed to be undesired due to the small space for wiring from the HSI detector. Due to heavy time constraints in making a layout decision there was no time to do a modal analysis of the two considered configurations. Due to this, the uncertainties about the natural frequencies along with the limited space for cables and connectors running from the star tracker and the RGB were deemed too risky for further developing this design, as the weight on the HSI platform would get rather lopsided.

The disadvantage of cabling space behind the HSI detector were deemed manageable by designing the SDR mounting solution around them. In addition to this, the spacious nature of this layout opens up several possibilities for mounting the IMU as well as preserving the possibility for angling the star tracker at a later time if deemed necessary. Moving the SDR to the available space behind the HSI was therefore the chosen solution and the one to be developed further.

Based on the analysis, configuration 1. "SDR at the Back" was chosen as the optimal architectural layout. Figure 12 shows the finalized layout and corresponding systems colorized.
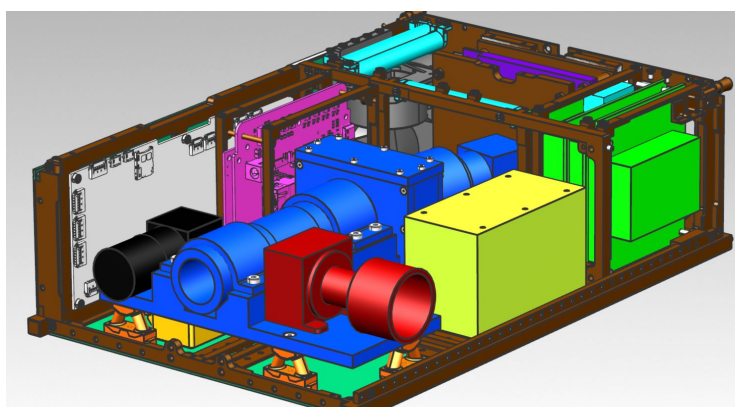
HSI	RGB Camera
SDR	OPU
Star Tracker	Reaction Wheels
Magnetorquers	Payload Interface Board
Solar Panels	Dampers
Battery Pack Unit	IMU
S-Band Radio	Frame and mounting structures

Figure 12: Cubesat architecture/layout

6. Further Work

6.1 Cable Architecture

As outlined in section 3, the connectors and cables running between the various components are important for the layout design. At the time of this report the design of the OPU is still being finalized and the specific location of its connectors are still undetermined. When all connector-locations have been set, the work of routing all the wiring can start.

6.2 X-axis space

All available architectural options shares a common challenge, the interface board present in the -X-direction of the bus. This board serves as the interface between all payloads. This board gives significantly less room in the -X-direction and must be taken into account when planning the wires and detail plan the layout.

6.3 Mechanical Interface Improvements

During the writing process of this report, the mechanical design of the HSI payload changed significantly in order to accommodate a higher required accuracy. The redesign changed the total length of the payload, compared to the PDR version and introduced platforms for the star tracker and RGB camera. However, the design is still preliminary and is expected to slim down considerably in the X-axis. The choice of layout was done considering the v1 prototype platform. It is expected that eventual changes will further support the chosen layout and provide further mounting space on the +X and -X sides. Significant changes to the platform geometry should not occur at this point, in order to freeze the chosen architectural layout.

7. List of Abbreviations

Table 3: Abbreviations

Abbreviation	Description
HSI	Hyperspectral Imaging
IMU	Inertial Measurement Unit
OPU	Onboard Processing Unit
PDR	Preliminary Design Review
PSLV	Polar Satellite Launch Vehicle
RGB	Red Green Blue
SDR	Software Defined Radio

Appendix F

HYPSO-ICD-001 Preliminary SDR Interface Design

SDR Interface Design

HYPSO-ICD-001

Table Of Contents

Table 1: Table of Changes

Rev.	Summary of Changes	Author(s)	Effective Date
1	*First issue*	*Tord Hansen Kaasa, Henrik Galtung*	*22.03.2019*
2	*Formatting of text and figures*	*Tord Hansen Kaasa, Tuan Tran, Henrik Galtung*	*26.05.2019*

1. Purpose

The SDR (Software Defined Radio) is the tertiary payload of the HYPSO mission. The layout plan presented on the PDR (Preliminary Design Review) had the component mounted in a NanoAvionics stacking ring assembly along with the onboard processing unit. However, due to the necessary inclusion of a S-band module post PDR, an alternative layout had to be developed to fit all the various components within the bus. This document presents the new layout along with the custom interface support solution developed to mount the SDR in its new location. The document also provides the simulation basis to support the new interface design and to provide a foundation for further redesign and optimization. This document should be seen in relationship as shown in Figure 1.
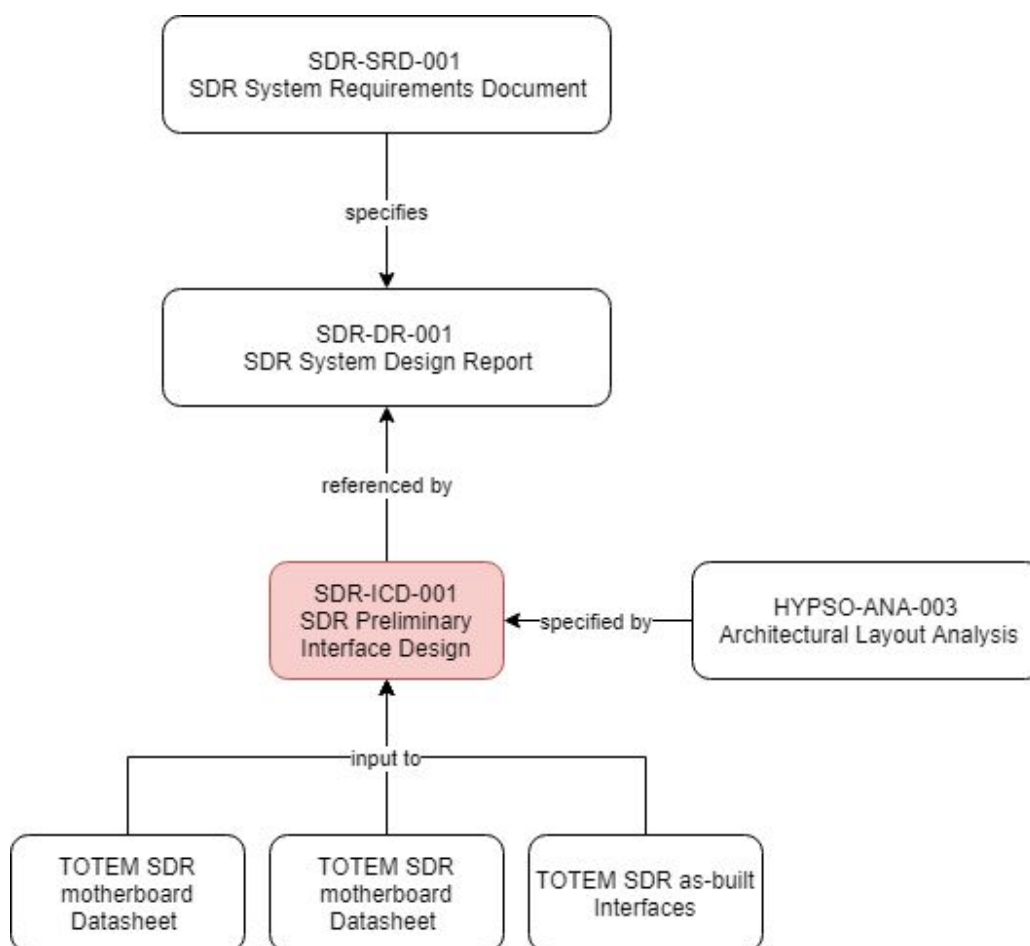
Figure 1: Document relationship

1.1 Reference Documents

The documents listed in table 2 have been used as references in the creation of this document.

Table 2: Referenced Documents

ID	Author	Title
[RD01]	Henrik Galtung, Tord Hansen Kaasa	HYPSO-ANA-003 Architectural Layout Analysis
[RD02]	PC/104 Embedded Consortium	PC/104 Specification Version 2.6, 13. October 2008. [Link], accessed May 2019.
[RD03]	André G. C. Guerraa, Diego Nodar-Lópezb, Ricardo Tubó-Pardavila	Thermal analysis of the electronics of a CubeSat mission. 2018
[RD04]	Tuan Tran, Tord Hansen Kaasa, Henrik Galtung	HYPSO-ANA-008 HSI Payload Platform Thermal Analysis. 2019
[RD05]	Tord Kaasa, Tuan Tran, Henrik Galtung	Payload Material Analysis. 2019

2. Bus Layout

The previous layout for the first PDR had the OPU (Onboard Processing Unit) and SDR placed together in a planned stacking ring assembly as seen in figure 2. The inclusion of the S-band radio made it necessary to move around various components to fit everything with extra room for cables to be run from each component as well. The solution reached after the analysis covered in *HYPSO-ANA-003 Architectural Layout Analysis* [RD01] is shown in figures 2 and 3. As a result of the additional component and the relative size of the components eligible for moving, the SDR was placed behind the HSI (Hyperspectral Imager). This placement made it possible to fit every component with some extra room to spare.
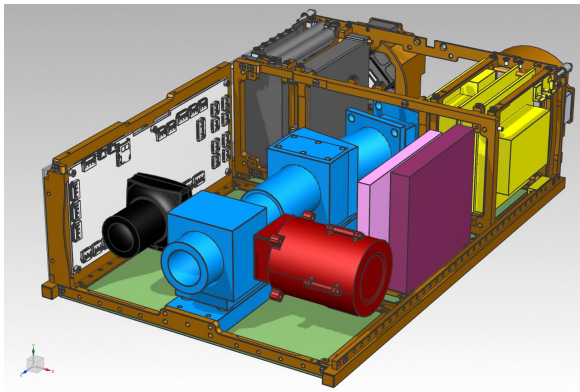
Figure 2: Bus layout as presented in the PDR, SDR(purple), OPU(pink)
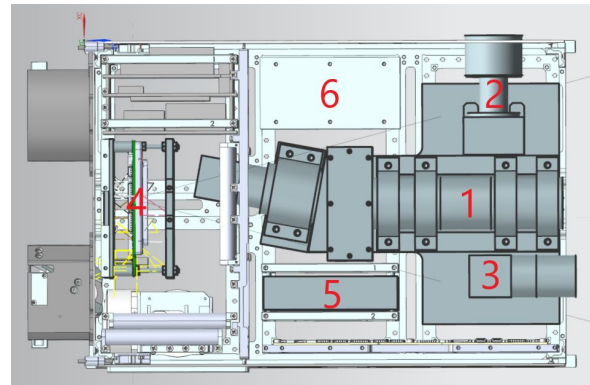
Figure 3: The improved layout of the bus. (1) HSI, (2) Star Tracker, (3) RGB, (4) SDR, (5) OPU, (6) S-Band

3. Custom Interface

The SDR comes with mounting holes conforming to the PC104 form factor [RD02]. This is the main reason that the original design was to mount it in the default stacking rings. However, the new placement prevents this solution from being used as there is no available mounting space for stacking rings at the new location (-Z direction at the back of the bus). Furthermore, the stacking rings would only work in an orientation perpendicular to the configuration necessitated by the available space. Thus a custom interface had to be developed for securely mounting the SDR, shown in figure 4.
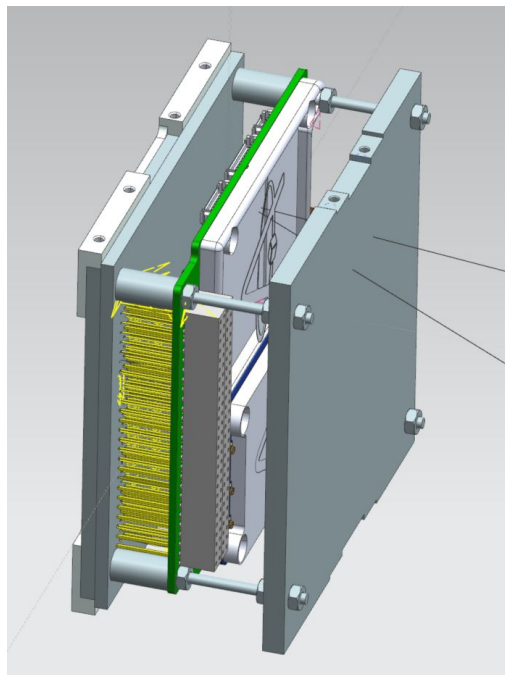
Figure 4: The Custom SDR interface solution

The solution was designed to facilitate the use of the PC104 form factor and to ensure a stable and rigid fastening of the SDR to the bus using several mounting points. The secondary reason for the design was to provide additional stiffness to the bus frame as stacking rings would provide. Key components in this assembly solution are listed in the following sections.

3.3 Mounting Plate

A mounting plate is located at the -Z wall of the bus, as shown in figure 5. The plate provides a mounting surface for an adapter to the SDR and it comes provided by NanoAvionics as part of the bus structure. It features a pattern of countersunk M2.5 holes that can be used to fasten a custom adapter to. The mounting plate is offset by 3mm in the -X direction, resulting in a uncentered interface.
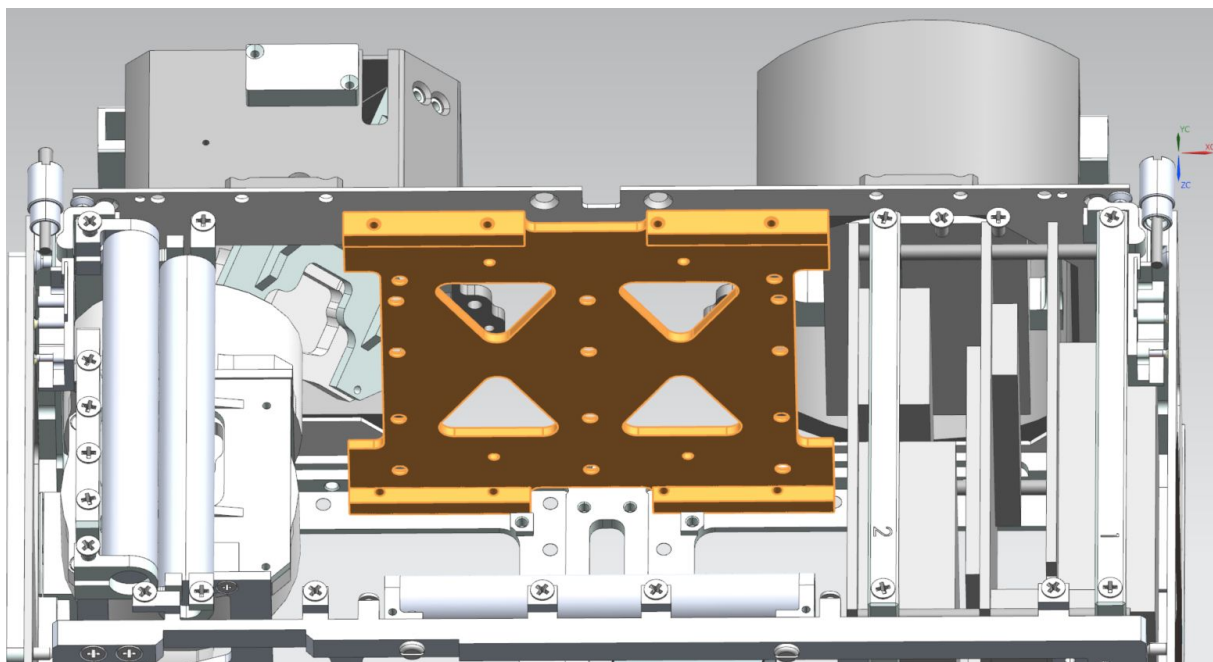
Figure 5: The mounting plate used as the base for the SDR interface solution

3.4 Base Plate

This plate serves as a platform for the mounting. It screws tightly to the mounting plate with M2.5 threaded holes at its -Z face (shown in figure 6a) and also features four M3 threaded holes that are spaced to the PC104 form factor at its +Z face (shown in figure 6b). Thus it enables the existing mounting holes in the SDR to be utilized.
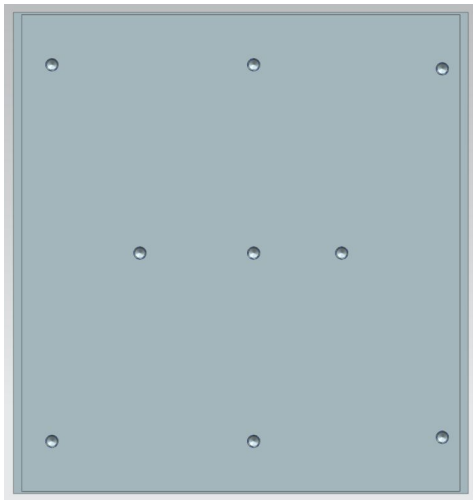
6a: -Z face of the base plate   6b: +Z face of the base plate
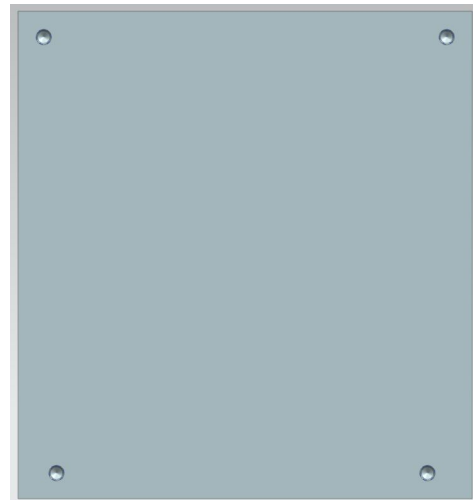
Figure 6: Z Base Plate configurations

3.5 M3 Threaded Rods

Fully threaded rods of 50 mm length (M3 rods) are screwed into the four holes on the +Z face of the base plate. These are used as an extended interface on which to attach the rest of the components. Figure 7 shows the profile of the rod and figure 8 shows their placement within the assembly.

Figure 7: Example of a M3 rod   *Figure 8: The M3 rods in the assembly highlighted in dark yellow*
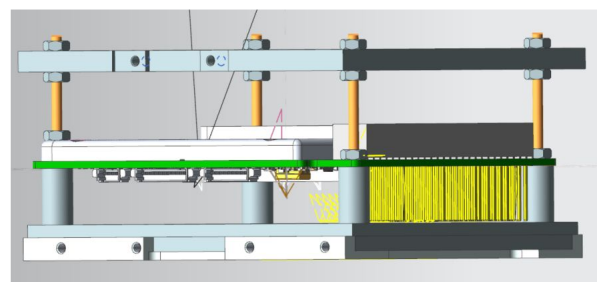
3.6 Cylinder Spacers

The design features four cylindrical supports slotted over the M3 rods resting against the base plate. Their function is to extend the support from the base plate to the SDR and provide a stable base to press the SDR up against. As the SDR has a raised area around one of the mounting holes, one of the cylinders are shorter than the other three to accommodate for this, this is shown in figure 9.
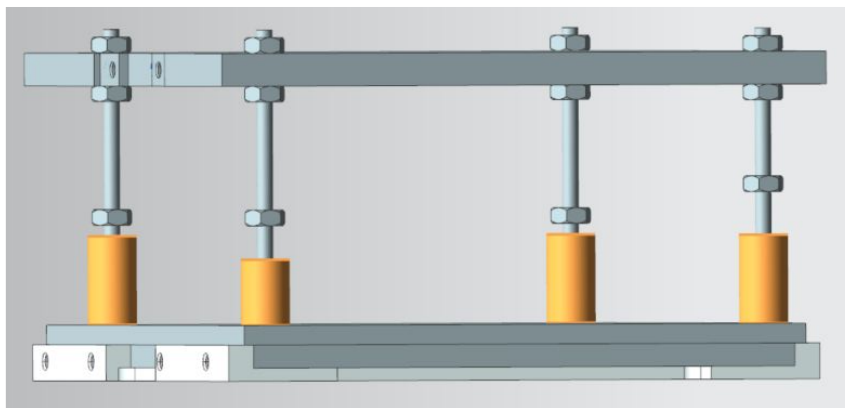
Figure 9: The Cylinder Spacers highlighted in dark yellow.

3.7 Support Plate

An additional custom plate is added at the +Z end of the assembly. Its function is to provide support for the M3 rods and eliminate much of the moment that the SDR would impart on these. It has a profile that conforms to the bus frame walls at the +/- Y faces and also two M2.5 threaded holes at these side to be used with the countersunk holes in the frame. Its placement in the assembly and its general profile are shown in figure 10 and 11, respectively.
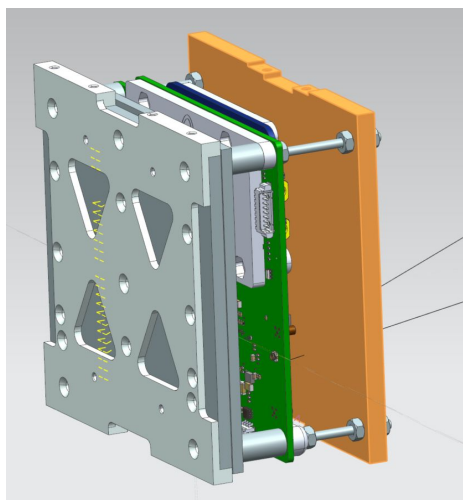
Figure 10: Support plate mounted in assembly
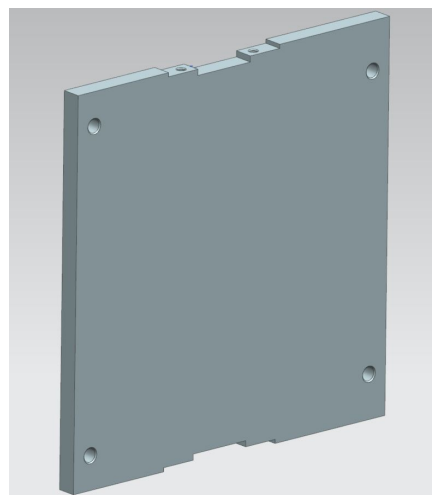
Figure 11: Mockup of the support plate.

3.8 M3 Nuts

Standard M3 threaded nuts are screwed onto the M3 rods to tighten the SDR against the cylinder spacers. They are also used to created a stiff connection between the rods and the support plate. In addition to being threaded, they will also be glued in place with epoxy to prevent any unscrewing due to vibration experienced during launch (this is standard procedure). Their location within the assembly is shown in figure 12.
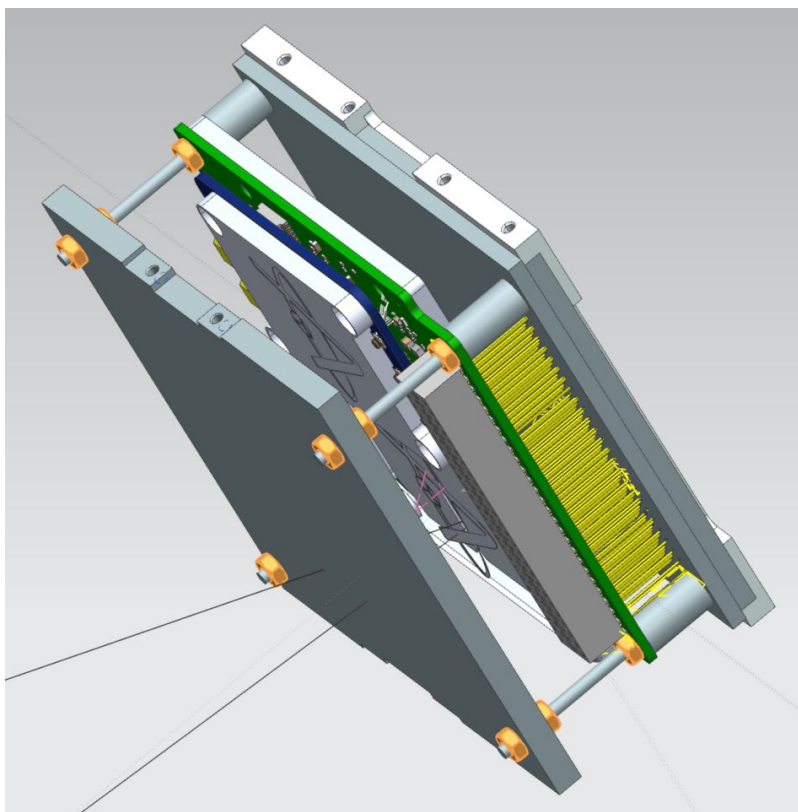

Figure 12: M3 nuts of the assembly highlighted in dark yellow

3.9 Thermal Integration

With the heat dissipation generated from the SDR, heat concentration problems may arise. Alén Space has issued a paper analysing the SDR using thermal simulation[RD03]. However, the simulations were performed using a slightly different space environment, considering a 1U CubeSat in a 400km sun-synchronous orbit. The paper states that the iteration of the SDR simulated may overheat when the amplifier is turned on, reaching a maximum temperature as much as 103°C in steady-state simulation. This surpasses the defined operation range of -40°C to +85°C. The SDR has however improved since then as a result of their analysis and testing, following the future work outlined by adding an additional aluminium shielding to the back of the board, working as a radiator and heat absorber [RD03].

Furthermore, based on temperatures measured on board their satellite, 5°C and 35°C on the motherboard, -2°C and 55°C on the frontend board, overheating appears to no longer be a problem. These are however under the same different thermal conditions as previously mentioned. Additional simulations were made of the entire bus mainly focusing on the HSI payload platform. In this simulation the SDR was for simplicity only modelled as a dummy with the estimated heat dissipation per orbit averaged out [RD04]. The temperature ranges measured at the mounting plate in the hot and cold analysis yielded 17.64ºC to 31.67ºC and -14.48ºC to -5.26ºC respectively at node 79670. These temperatures align with the operational and storage ranges defined for the unit, thus, thermally strapping the SDR to this plate should not result in any thermal problems.
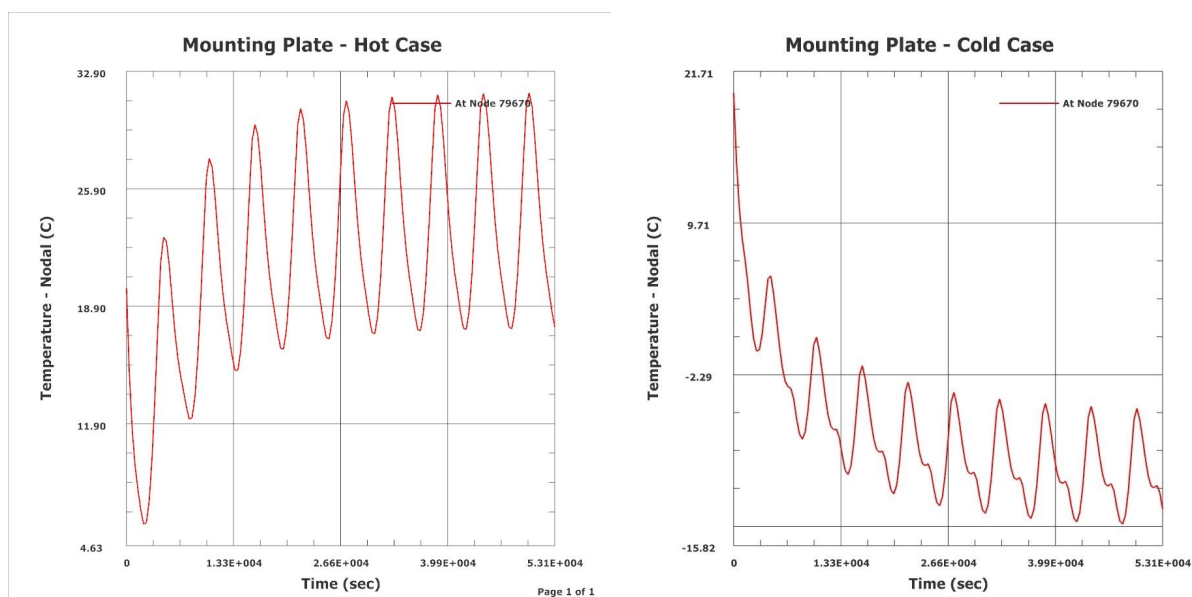
13a: Hot Case   13b: Cold Case

Figure 13: Mounting plate temperatures

Because of this, adaptation of thermal straps between the SDR and the mounting plate with the use of pyrolytic graphite sheets (PGS) has been facilitated [RD05]. Additionally, thermally coupling the adapter plate to the SDR would further increase the thermal coupling to the unit, as they are mounted on to each other. The coupling should ensure the unit always stays within the allowed ranges, as a decrease in temperature should not be a problem with the unit. However, further testing is recommended before any permanent decision is made.

4. Modal Simulation of SDR Interface

All subsystems in a CubeSat are required to have a stiffness (first natural frequency) over 135Hz longitudinal and 70Hz lateral in order to be eligible for the PSLV (*Polar Satellite Launch Vehicle*) the chosen launcher for the HYPSO mission. Due to the uncertainties regarding the axial bus placement in the launcher, the worst case longitudinal condition must be assumed for all axis. Resulting in an overall stiffness of at least 135Hz. Applying a safety factor of 2, the first eigenfrequency should be over 270Hz.

4.1 Simulation Setup

This simulation is quite rough. The simulation of the SDR interface was done in two steps. The first simulation was done with the default support plate, the second simulation was done with a 50X50mm hole centered on the plate. This was done in order to prove that a hollowed out support plate would provide the necessary stiffness to the system.

The simulation was carried out using the SOL103 Real Eigenvalues solver on NX Nastran. The bodies were meshed and meshmated, providing a perfect bonding between the parts as if glued or welded. The mesh applied was TET(10) 10mm to the SDR dummy TET(10) 30mm to the plates and HEX(20) 10mm to the rods and cylinders. The system was restricted with a constraint in the bolted surfaces (DOF1, DOF2 and DOF3 fixed). Figure 13 shows the mesh and constraints added.
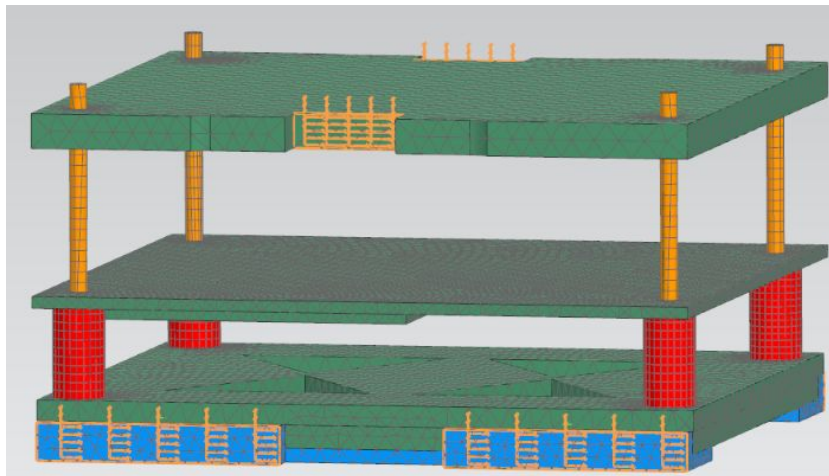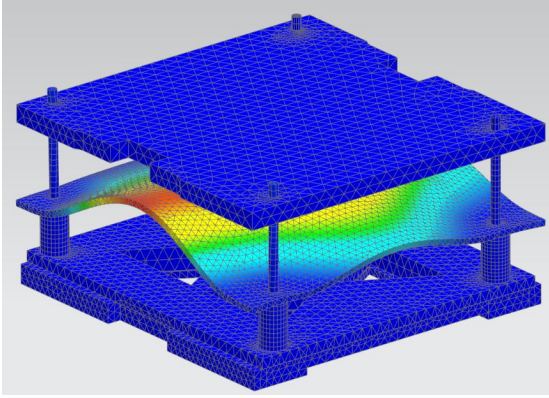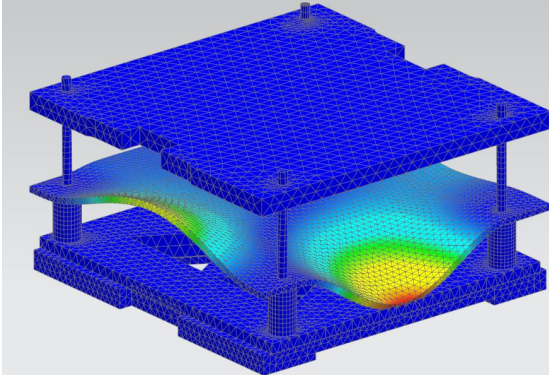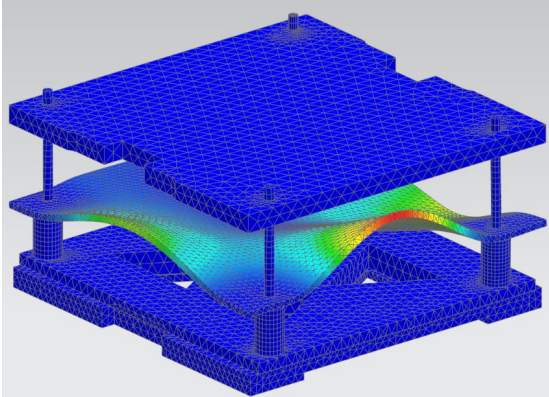

Figure 13: Mesh and constraints

4.2 Modal Results

Table 3: SDR Modal Results

Frequency (Hz)	Mode shape
379.811	
678.474	
747.923	
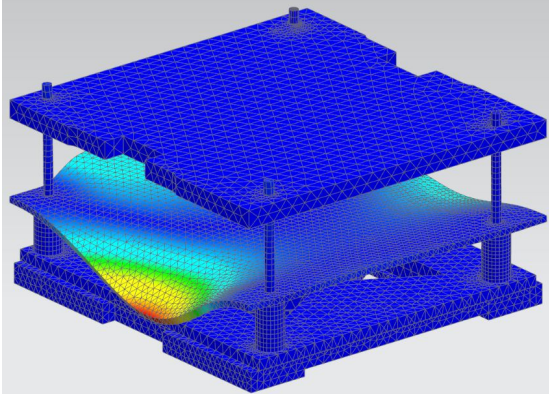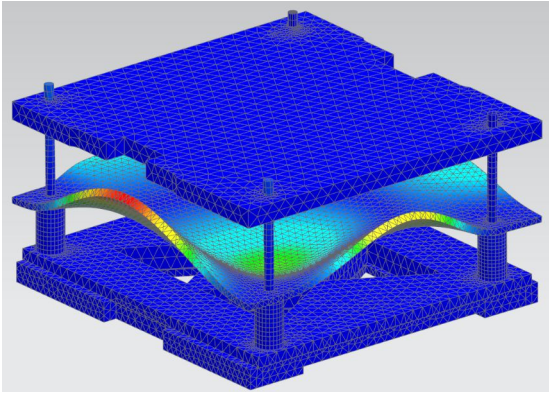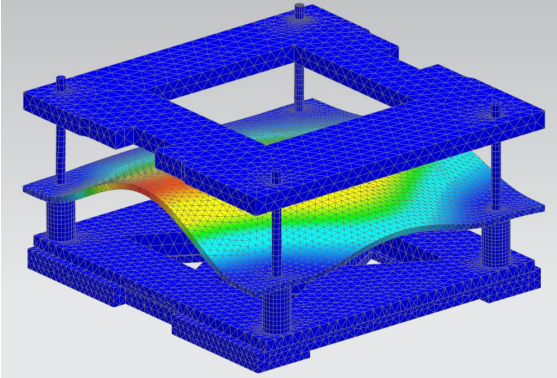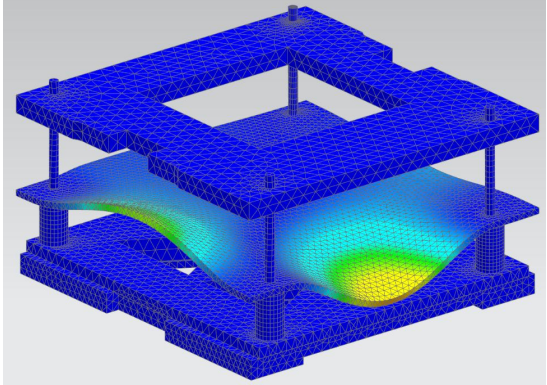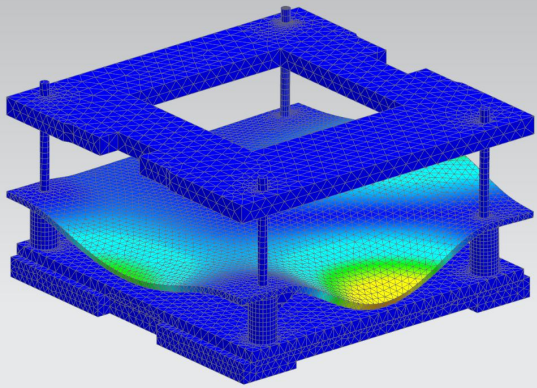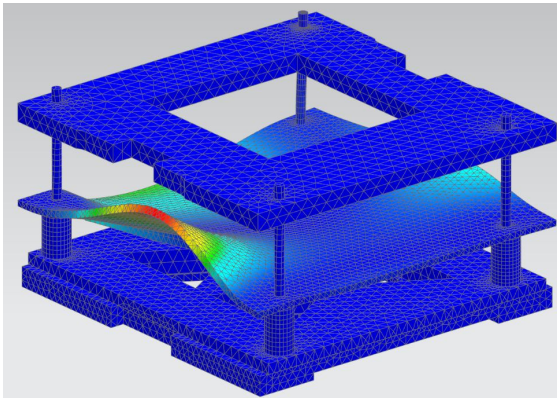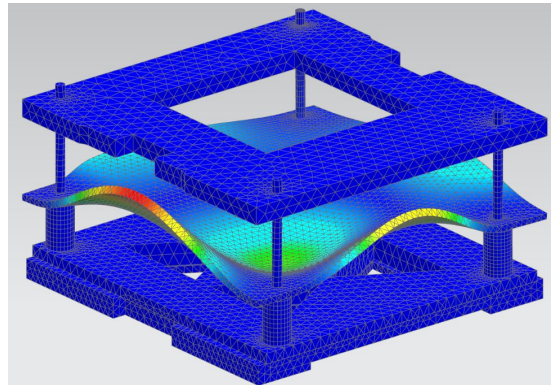
919.913	
1238.01	

Table 4: SDR Modal Results With Hole

Frequency (Hz)	Mode shape
379.175	
678.544	
747.996	

920.156	
1238.55	

4.3 Simulation Conclusion

The results of the simulation shows that the SDR has the lowest eigen frequency in the subsystem. This is also the case for the hollowed support plate case. However, the lowest frequency exceeds 270Hz. The simulated safety factor of the system is 2.8. This simulation is deemed valid for other outlined cases, like shortening the length of the system as it would not impact the system rigidity to a high degree. Without the SDR the lowest frequency for the system was about 2000Hz.

5. Further Work

As this is the first iteration of the design for a prototype, there are several improvements that can be done to the solution. The most relevant improvable factors are described in the following sections.

5.1 Weight Reduction

Both the base plate and the support plate are modeled as whole plates without any chambering or holes to reduce weight. With a mass of about 147.3g and 123.2g respectively. Removing some of the material in these could lighten the assembly considerably, by an approximated 100g +-20%, without negligible reduction to the structural rigidity. A comparable example can be seen in the mounting plate with its four triangle shaped holes.

5.2 Dimensional Reduction of the SDR

The SDR features a big row of pins that extend in the -Z direction. They are meant to serve as a power and data interface for several pcbs in a PC104 stack, but due to the SDR being a single unit, the pins are not necessary. Removing the pins would reduce the height of the assembly by close to 9.5mm which would give a considerable increase to the assembly stiffness. However, there is a high likelihood that it would be a difficult process to remove them without damaging the hardware. As a first step it is recommended to contact Alén Space and enquire whether the SDR could be delivered without these pins before planning an eventual adaptation of the SDR.

5.3 Support Plate Offset

The current iteration features a considerable distance, about 9.6mm, between the SDR and the support plate. This is done to ensure that there is room for any connectors extending in the +Z direction. There will be developed a custom connector from the pin connector that will have some extension in this direction, but at the time of this report, the design is not done and there is therefore left ample room for this. There is a high likelihood that the spacing can be reduced in the later iterations when the connector design is complete.

6. List of Abbreviations

Table 5: Abbreviations

Abbreviation	Description
HSI	Hyperspectral Imaging
OPU	Onboard Processing Unit
PDR	Preliminary Design Review
PGS	Pyrolytic Graphite Sheet
PSLV	Polar Satellite Launch Vehicle
RGB	Red Green Blue
SDR	Software Defined Radio

Appendix G

HYPSO-ICD-002 HSI Payload Interface Control Document

Interface Control Document

HYPSO-ICD-002

Prepared by:	HYPSO Project Team
Reference:	HYPSO-ICD-002
Revision:	1
Date of issue:	09.06.2019
Status:	Preliminary
Document Type:	Reference Document
Author(s):	Henrik Galtung

Table Of Contents

Table 1: Table of Changes

Rev.	Summary of Changes	Author(s)	Effective Date
1	*First issue*	*Henrik Galtung*	*18.05.2019*
2	*Formating*	*Henrik Galtung, Tord Hansen Kaasa*	*09.06.2019*

1. Overview

The HYPSO Mission will primarily be a science-oriented technology demonstrator. It will enable low-cost & high-performance hyperspectral imaging and autonomous onboard processing that fulfill science requirements in ocean color remote sensing and oceanography. NTNU SmallSat is prospected to be the first SmallSat developed at NTNU with launch planned for Q4 2020 followed by a second mission later. Furthermore, vision of a constellation of remote-sensing focused SmallSat will constitute a space-asset platform added to the multi-agent architecture of UAVs, USVs, AUVs and buoys that have similar ocean characterization objectives.

1.1 Purpose

The purpose of this ICD is to describe the various interfaces inhibited by the payloads inside the satellite. It serves as a reference document for mechanical and electronic interfaces.

1.2 Scope

This ICD covers all payloads inside the satellite that are not pre-installed by NanoAvionics. Due to the project still being in the development phase it is limited in some regards to the level of detail it can provide about the specific fastening solutions for each component, but should still serve to present the general idea of how each payload will interface with other payloads and the bus itself.

1.3 Summary

The document consists of the following:
- Section 2: A rundown of the mechanical interfaces of all HYPSO payloads and associated components.
- Section 3: Electrical interfaces of the payloads
- Section 4: Thermal Interfaces in the imager, OPU and platform
- Section 5: Data Interfaces

1.4 Referenced Documents

The documents listed in have been used as reference in the creation of this document. Documents under NDA or otherwise unavailable documents are marked in red.

Table 2: Referenced Documents

ID	Author	Title
[RD01]	Tord Hansen Kaasaa, Tuan Anh Tran, Henrik Galtung	HYPSO-DR-003
[RD02]	PC/104 Embedded Consortium	PC/104 Specification, Version 2.6. 2008. [Link], accessed 2019.
[RD03]	NanoAvionics	M6P/Payload ICD
[RD04]	Tord Hansen Kaasaa, Henrik Galtung	HYPSO-ANA-003
[RD05]	Tord Hansen Kaasaa, Henrik Galtung	SDR-ICD-001
[RD06]	BICE	NanoStarSensor ST-MA-APS1-1& ST-MA-APS1-1C Datasheet
[RD07]	IDS	IDS UI-1250SE-M-GL Datasheet
[RD08]	Sensonor	STIM210 Multi-Axis Gyro Module Datasheet
[RD09]	Tord Hansen Kaasaa, Tuan Anh Tran, Henrik Galtung	HYPSO-ANA-004 Payload Material Analysis
[RD10]	Molex	Pico-Lock Connector System. [Link]. Accessed 2019
[RD11]	Panasonic	Thermal Management Solutions. [Link] Accessed 2019.

2. Mechanical Interfaces

2.1 Overview

An overview of the various components inside the bus is given in figure 1. The mechanical interfaces of the HYPSO-developed payloads are detailed in the following sections.
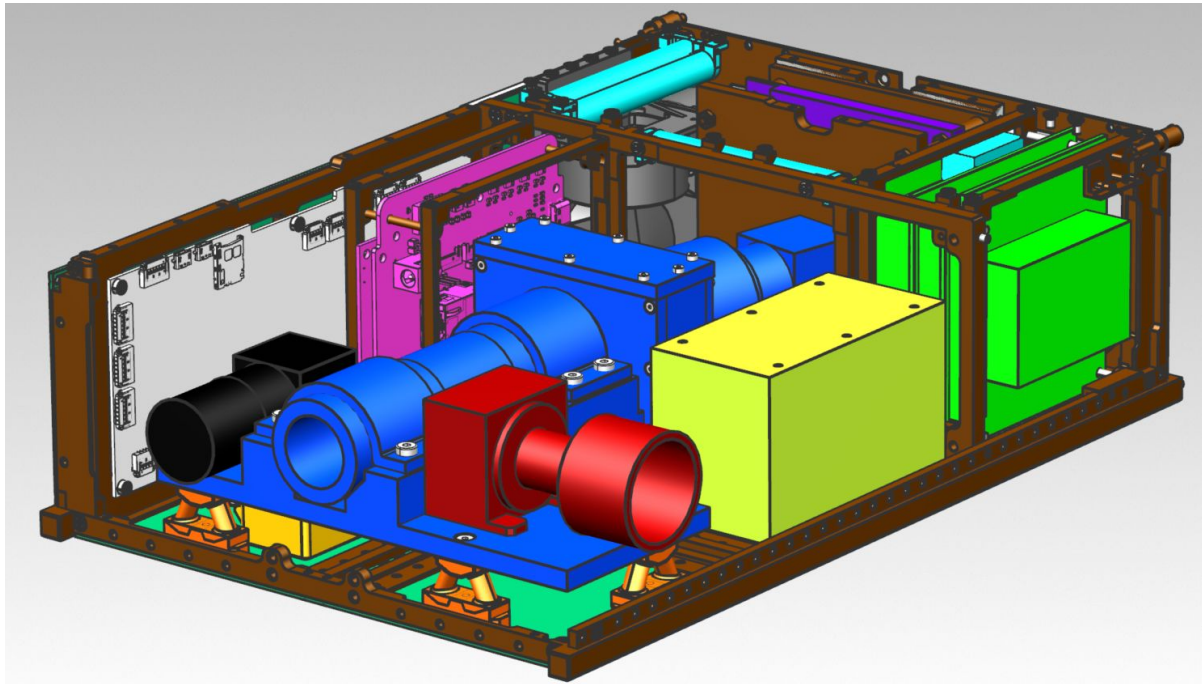
HSI	RGB Camera
SDR	OPU
Star Tracker	Reaction Wheels
Magnetorquers	Payload Interface Board
Solar Panels	Dampers
Battery Pack Unit	IMU
S-Band Radio	Frame and mounting structures

Figure 1: Architecture/layout of the 6U CubeSat

The reference coordinate system for the bus is shown in figure 2. The origin is placed in the center of the bus.
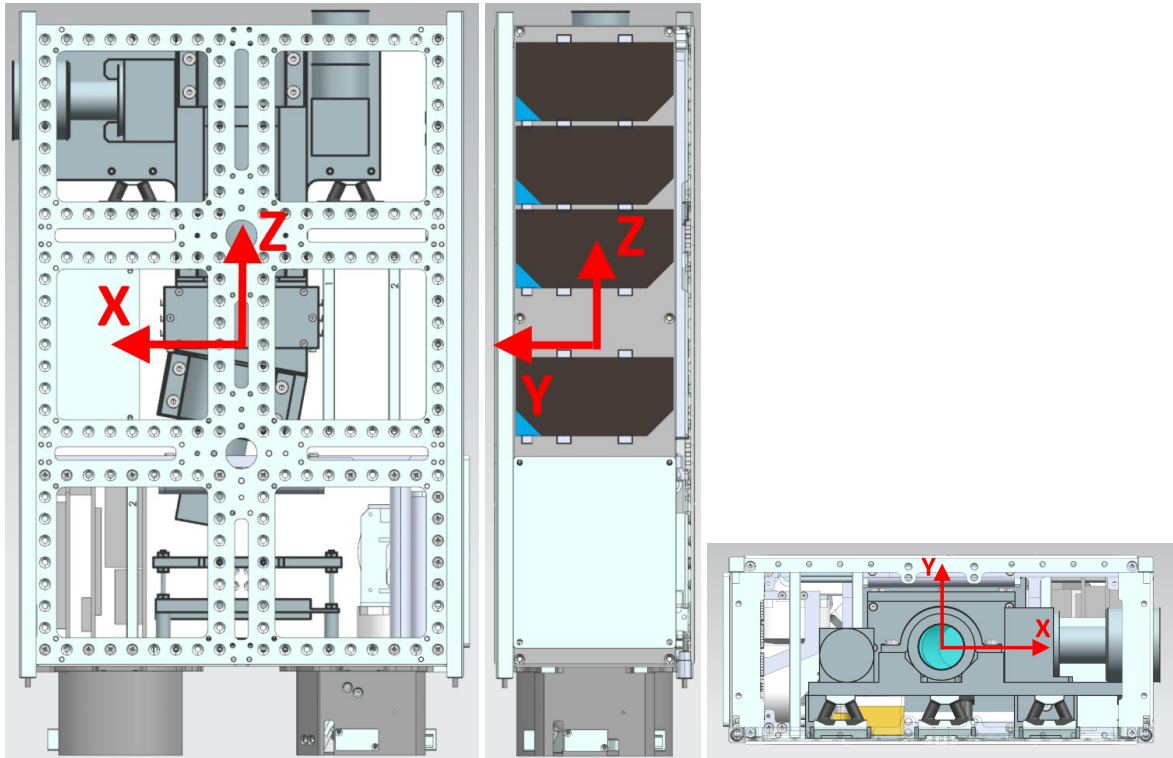

Figure 2: Native coordinate system origin of the satellite

2.2 HSI

The HSI will be mounted to the bus frame by 1114S dampers delivered by SMAC. The exact placement of these dampers are not set yet, as the specific layout have not been determined yet due to time constraints. A recommended layout by SMAC is shown in figure 1, and it is expected that this represents the final amount of dampers and orientations even though the exact locations are subject to change at a later stage due to limited space and fine-tuning of the payload resonance frequencies.
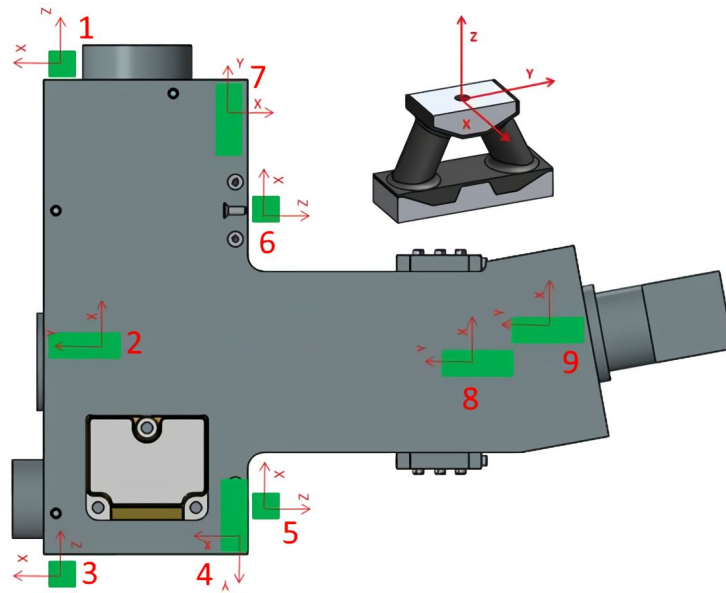
Figure 1: The damper layout inside the bus

The dampers will be connected to the bus and payload with custom brackets. These are described in detail in the *HSI Payload Design Report* [RD01] *section 5.4.* The optical axis of the HSI is aligned with the +Z direction and centerline of the satellite. The orientation and location is shown in figure 2. Technical drawings of the HSI platform can be found in appendix A. Note that the location of mounting holes are not featured there as the specific location of other payloads and dampers are still subject to change. The HSI functions as a mounting platform for the RGB, Star Tracker and IMU and as such these components needs to have their exact location confirmed before the final mounting hole pattern can be set in the HSI geometry.
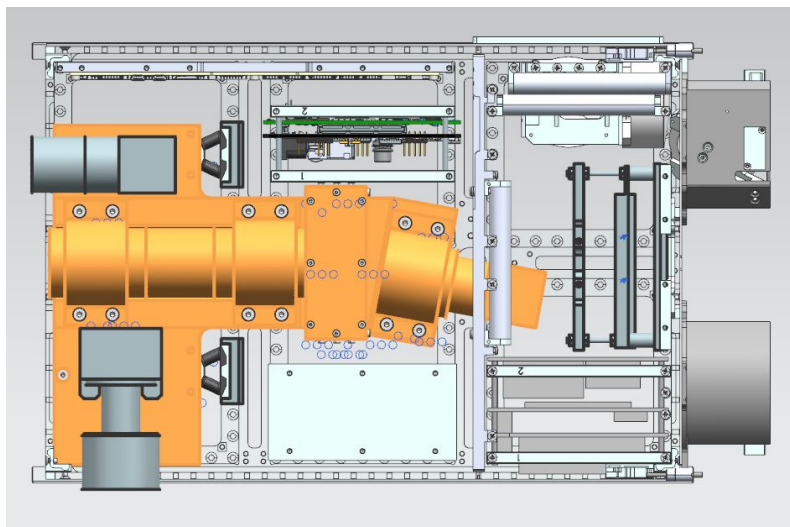

Figure 2: The HSI location and orientation inside the bus (yellow)

2.3 Breakout Board

The breakout board (BoB) conforms to the PC104 form factor [RD02]. It will be mounted to the bus via the provided stacking rings [RD03], from NA and four M3 threaded rods and M3 nuts. The locations of the mounting holes on the PCB are shown in figure 3 and the BoB location inside the bus is shown in figure 4.
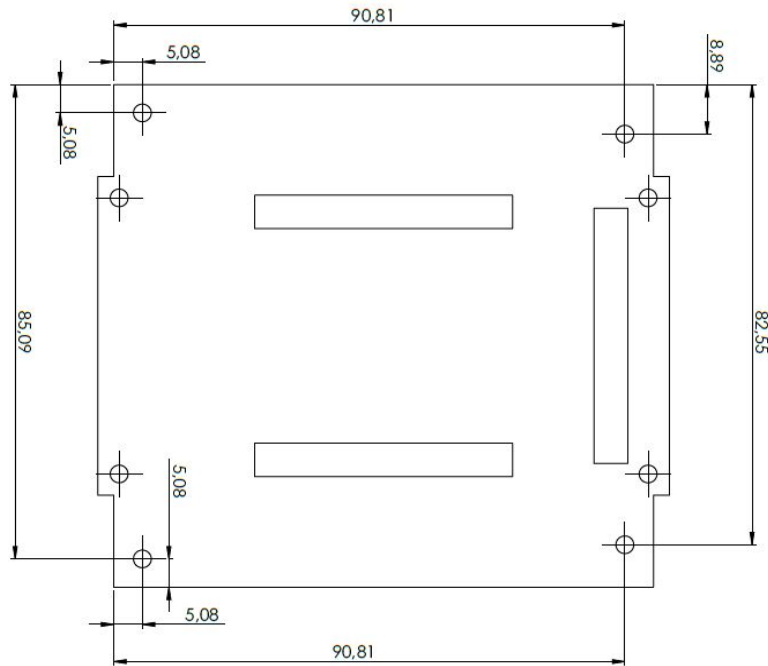

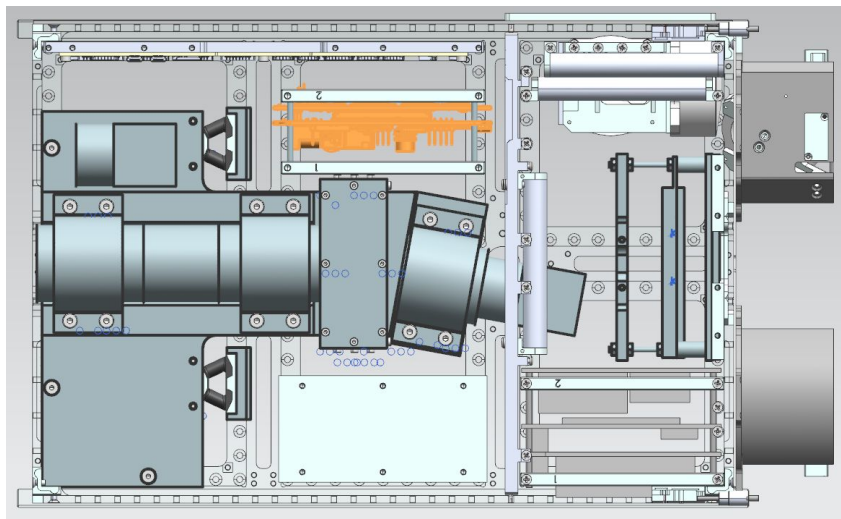*Figure 3: BoB mounting hole positions (PC104)*

Figure 4: The BoB location inside the bus (yellow)

2.4 SDR

The SDR conforms to the PC104 form factor [RD02] from the manufacturer. A custom made adapter plate and support plate was designed to make it possible to place the SDR in the -Z end of the bus. The justification for this placement is detailed in reference [RD04]. A detailed description of the geometry of the adapter solution is shown in reference [RD05], and technical drawings in appendix C. The hole layout is shown in figure 5, and the SDR location inside the bus is shown in figure 6.
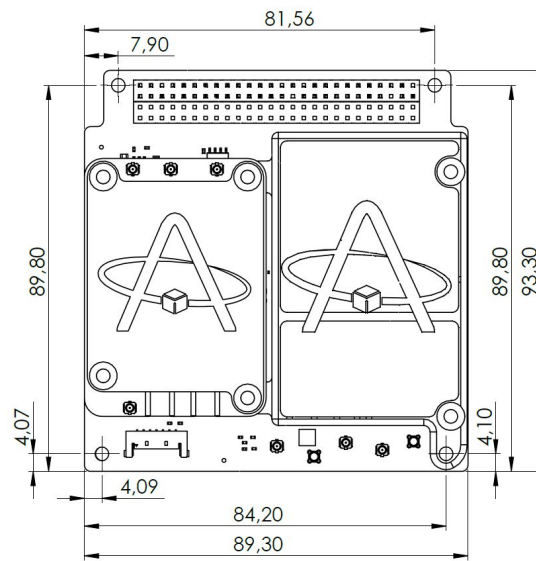
Figure 5: The SDR general dimensions and mounting hole locations
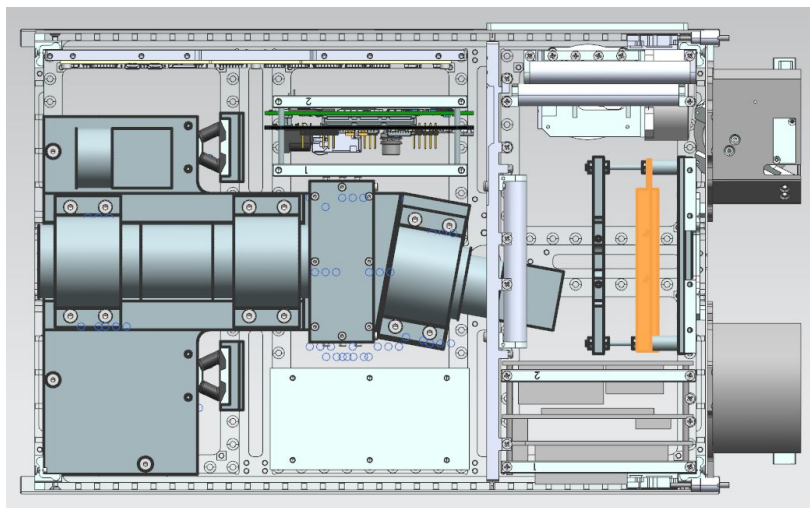
Figure 6: The SDR location shown inside the bus (yellow)

2.5 Star Tracker

The star tracker shall point in the +X direction and also be rigidly connected to the HSI [RD01]. This is facilitated by screwing it directly to the HSI platform. The external mechanical interface and geometry is shown in figure 7, and its location on the HSI platform is shown in figure 8.
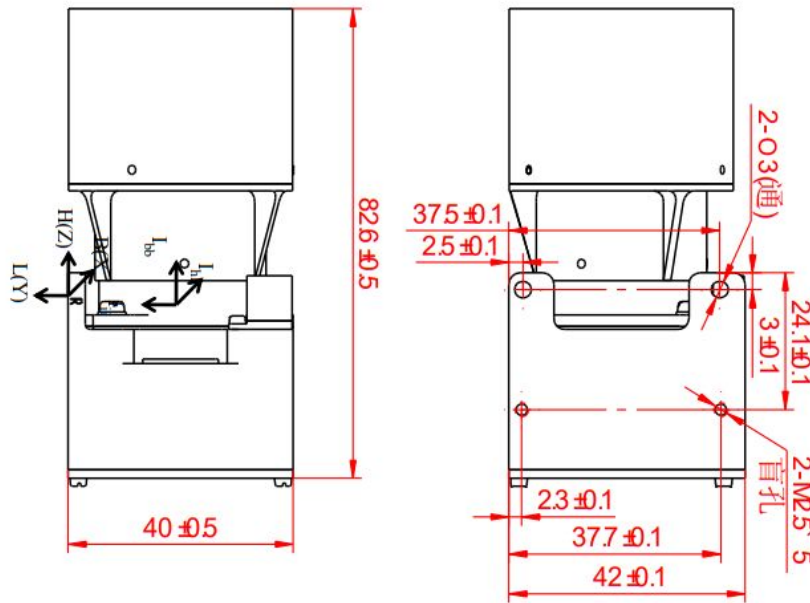
Figure 7: The external interface from the star tracker manufacturer documentation **[RD06]**
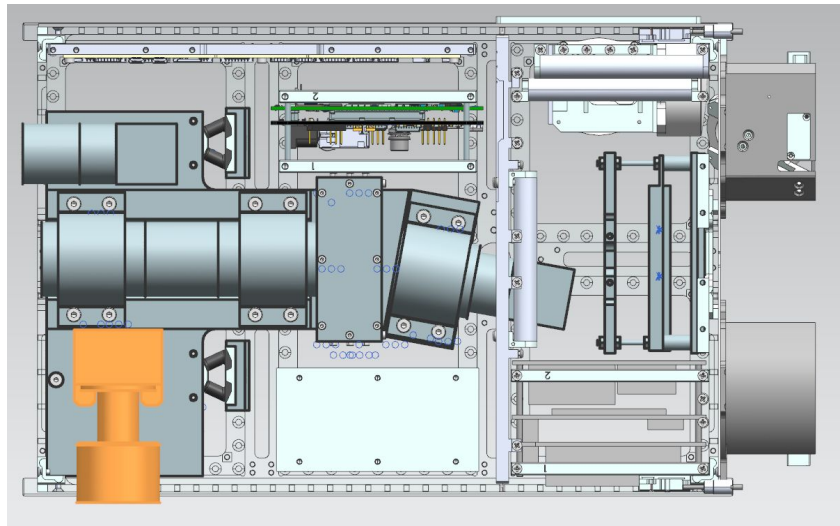
Figure 8: The Star tracker location on the HSI platform (yellow)

2.6 RGB camera

The RGB faces parallelly in the same direction as the HSI (+Z) and is rigidly connected to the platform to secure as little deviation between the HSI and RGB optical axes as possible. Its mechanical interfaces and external geometry is shown in figure 9 and its placement on the HSI platform is shown in figure 10.
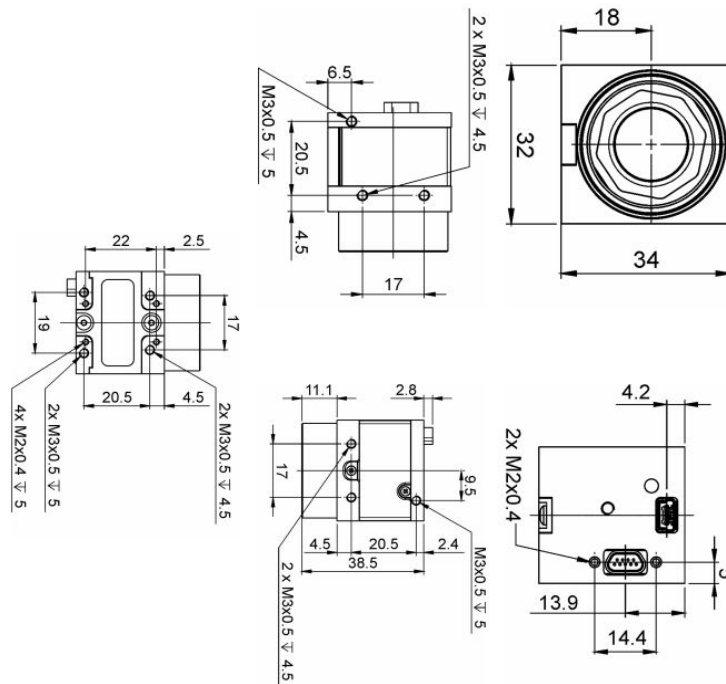
Figure 9: The mechanical interface and dimensions of the RGB **[RD07]**
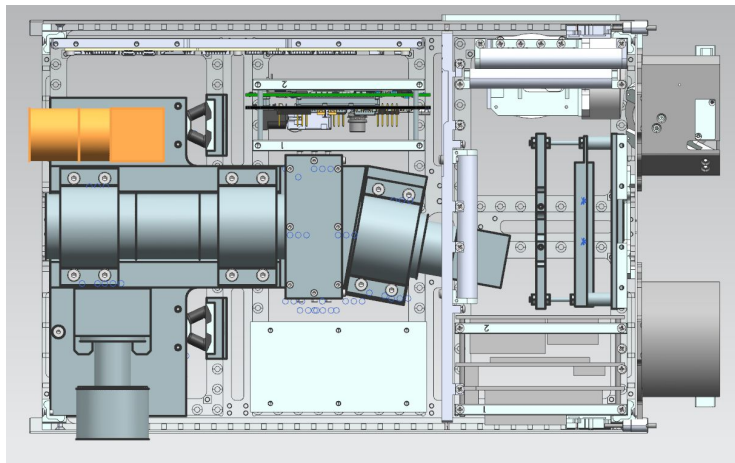
Figure 10: The RGB camera location on the HSI platform (yellow)

2.7 IMU

The IMU shall be rigidly connected to the HSI [RD01] and will be screwed to the underside of the HSI platform to make space for other components. Its geometry and mechanical interface along with the required drill pattern for proper mounting is shown in figure 11, and its location on the HSI platform underside is shown in figure 12. Its alignment to the global reference axes is arbitrary since any deviation can be calibrated for. However, its alignment compared to the global axes should not deviate over time, and it is therefore important that it has a rigid connection to the HSI to preserve the default alignment between these two. For simplicity it will be mounted with its axes parallel to the global axes if this is feasible in the final design.

Figure 11: The external geometry (left), reference axes (top right) and required drilling pattern (bottom right) for the IMU [RD08]

Figure 12: the IMU location on the underside of the HSI platform (yellow)

2.8 Masses

Table 3 displays the estimated or measured masses of the various payloads along with the estimated total mass of the bus. The rightmost column features a 20% safety margin in the mass estimations. The masses for in-house developed hardware is subject to change, and the values displayed for wires, cables and screws are very rough estimates.
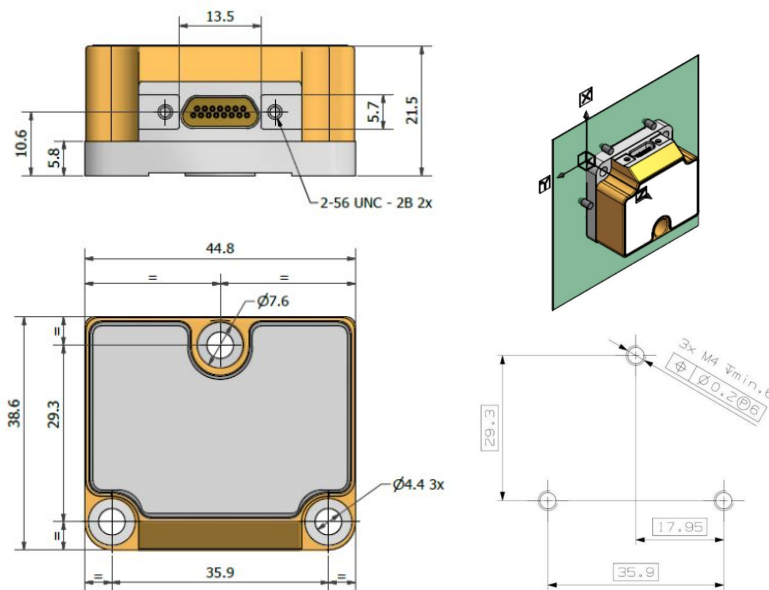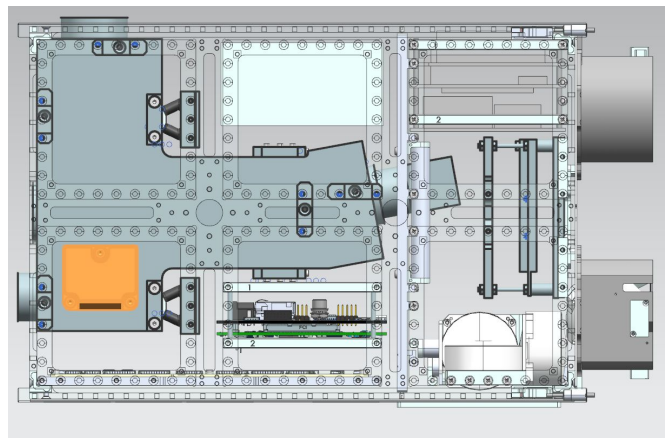
Table 3: Mass estimates

Subsystem	Nominal Mass [g]	Mass w 20% margin [g]
HSI	1444.4	1733.28
SDR front end (TOTEM)	20	24
SDR motherboard (TOTEM)	130	156
RGB Camera	169	202.8
Picozed	31.55	37.86
SDR mounting assembly	299.7	359.64
IMU	52	62.4
Breakout Board	40	48
Total (Payload)	2186.65	2153.94
Main structure assembly	1083	1299.6
Stacking rings x 2	28.8	34.56
Structure Stack Rods	123	147.6
Mechanisms/Deployment	60	72
Screws	150	180
Wires & cables	200	240
Reaction Wheels x 4	549.3	659.16
Star-tracker	108	129.6
Fine Sun Sensor	75	90
Magnetorquers	200	240
Radio S-band	191	229.2
Antenna S-band	60.9	73.08
Radio UHF/VHF	60	72
Antenna UHF turnstile	16.5	19.8
GPS	78.7	94.44
Flight Computer	135.6	162.72
EPS (incl 4 batteries)	194.3	233.16
Batteries (4)	437.9	525.48
Solar Panels	820.5	984.6
Total	6759.15	7640.94

2.9 Center of Gravity and Moment of Inertia

According to the 6U CubeSat Design Specification [RD02]:

"The CubeSat center of gravity shall be located within 4.5 cm from its geometric center in the X direction, within 2 cm from its geometric center in the Y direction, and within 7 cm from its geometric center in the Z direction"

This has been confirmed by the authors of the document to specify the allowable displacement from the center along each axis.

Calculation of the Center of Gravity (CoG) on earlier iterations of the payload design displayed results well within this requirement. As the design has been under constant change, the CoG has changed with it. There was no time to do a new calculation for the current design for this document as it is a very time consuming process, but it is expected that it would comply to the design specification as well. Added mass to the design has primarily been focused at the +Z side of the bus as well as primarily lying at , or spanning symmetrically over the ZX-plane. This would limit the magnitude of displacement of CoG compared to earlier estimates, and in theory push it closer to the origin. Table 4 displays the CoG and MoI values calculated for the early design presented at the HYPSO-projects first PDR. The displayed values were calculated in Siemens NX.

Table 4: CoG calculation of early satellite configuration

Axis	X	Y	Z
Distance from geometric center [mm]	-0.93	0.9	-42.26
Error estimates [mm]	0.08	0.08	0.07

As the moment of Inertia (MOI) is directly correlated to the CoG, table 5 displays the MoI values for the same design iteration as for table 4.

Table 5: MoI of early satellite configuration

WCS	Ix	Iy	Iz
MoI [kg*mm^2]	71199.63	92147.04	29943.58
Error estimates [kg*mm^2] (Symmetrical deviation)	94.95	98.20	98.34

As the MoI is central to the proper calibration of Attitude Determination and Control System (ADCS) these values will be crucial when the project progresses further.

2.10 Screw Fastening

The values presented in table 6 are the calculated values **[RD01]** of tightening torque for the HSI payload. TIghtening torques for the grating-related parts and other payloads will have to be determined through testing, something that has not been prioritized at the time of writing this document:

Location	Screw Dimensions	Number of Screws	Tightening Moment [Nmm]
Cassette Front	M3 x 8 CSK	2	250
Cassette Front	M2,5 x 6 CSK	3	250
Objective Brackets	M4 x 10 CH	8	270
Grating Bracket	M2 x 6 SET	4	-
Cassette Back Plate	M2 x 8 CSK	4	-

Vibrational unscrewing of screws on the payloads and on the bus generally will be avoided my gluing the connections with epoxy. 3M Scotch Weld DP2216 Gray Epoxy is the preferred option for this use [RD09].

3 Electrical Interfaces

During the development phase the default connectors of each payload was utilized on each end of their respective wire. For the flight-model all connectors on the breakout board will be swapped for picolocks [RD10] with the same number of terminals if possible. This is reflected in the connector names in table 3.

3.Connection Map

Table 7: Connectors and wire configuration for all payloads.

HSI	ID	Connector 1	Connector 2	# of conductors /cores	Purpose	Comments
BoB	1	8 pin	8 pin/Pico-Lock 8 ch.	8		The 8-pin on the BoB should be replaced with a picolock
PC	2	RJ45	RJ45 / Pico-Lock 8 ch.	8		
SDR	3	USB Mini B	USB mini B / Pico-Lock 4 ch.	4		
RGB	4	Pico-Lock 504051-0401	Pico-Lock 504051-0401	4	CAN Bus	
UHF	5	Pico-Lock 504051-0401	Pico-Lock 504051-0401	4	Power EPS HSI	
	6	Pico-Lock 504051-1001	Pico-Lock 504051-1001	10		
	7	Pico-Lock 504051-1001 / Pico-Lock 2 ch.	Pico-Lock 504051-1001	2	PPS	
	8	Custom (H1)	? / Pico-Lock	2	Power & CAN	
		Custom (H2)	? / Pico-Lock			
	9	MCX Plug, 50 Ohm	Mcx Plug, 50 Ohm	Coax (2)		

4. Thermal Interfaces

There are two main thermal interfaces that connect a heat-generating component with a passive component to even out thermal gradients. These interfaces are described in the following sections with the arrow indicating the direction of the thermal flux. Both interfaces use Pyrolytic Graphite Sheet (PGS) manufactured by Panasonic [RD11] as thermal straps between the relevant components. This material is a thin sheet of highly thermally conductive material. It is also flexible and can be cut into the desired shape, something that makes it ideal for CubeSat applications. PGS can be delivered on a substrate of POLYMID tape which would ensure a uniform connection between the thermal strap and the joined components. In addition to this, a seam of epoxy will be added along the edge where the PGS meets each component to secure it in place.

3.1 Imager chip → Platform

The IMX 249 features a processing chip inside that generates significant heat. This energy will be funneled to the HSI platform by a thermal strap. One end of the PGS will be glued straight to the chip in order to ensure optimal heat transfer away from the electronics. It is important that the PGS covers as much of the chip as possible to maximize this transfer. The other end will be glued to the platform which will act as a heatsink.

3.2 OPU → Dedicated Heat Sink/Shielding

The OPU will have a custom made plate mounted at the PicoZed side to shield it from harmful radiation. This plate will also serve as a heat sink for the internally generated heat in the FPGA chip. A PGS will be glued to the entirety of the outwards-facing PicoZed surface and extend to the heat sink where it will also be glued in place.

5. Data Interfaces

5.1 Overview

The payloads are connected to the NanoAvionics Payload Controller via a CAN-bus. The communication over this link is encapsulated in CSP packets. All CSP packets that are routed from the Payload Controller to the payloads' CAN interface. There are six available addresses provided that the two extra addresses that are reserved by NanoAvionics may be made available. Four of these are reserved for the HSI payload, and two of these are reserved for the SDR payload. In the case that the extra reserved addresses will not be available, two addresses will be reserved for each of the payloads.

5.1.1 HSI

Four CSP addresses are allocated to the HSI payload. They represent services that provide the endpoints for telecommands and telemetry. The addresses are: {12, 13, 14, 15}

CSP Address	Service name	Service function
12	*Housekeeping Service*	Monitors satellite systems and generates diagnostic reports.
13	*Onboard Operations Procedures & Scheduling Service*	Receives telecommands for operating the payload. This includes schedules for executing procedures. Responds with results whether schedules have been successfully stored and/or executed. Combines service types *On-Board Control Procedures*, *Timed-Based Scheduling*, *Position-based Scheduling*, *Parameter Management* (ECSS-E-ST-70-41C).
14	*Large File Transfer Service*	Transfers datasets from payload to groundstation. Receives new executables/data from groundstation to payload. Combines services types *Large Packet Transfer* and *On-board Storage and Retrieval* (ECSS-E-ST-70-41C).

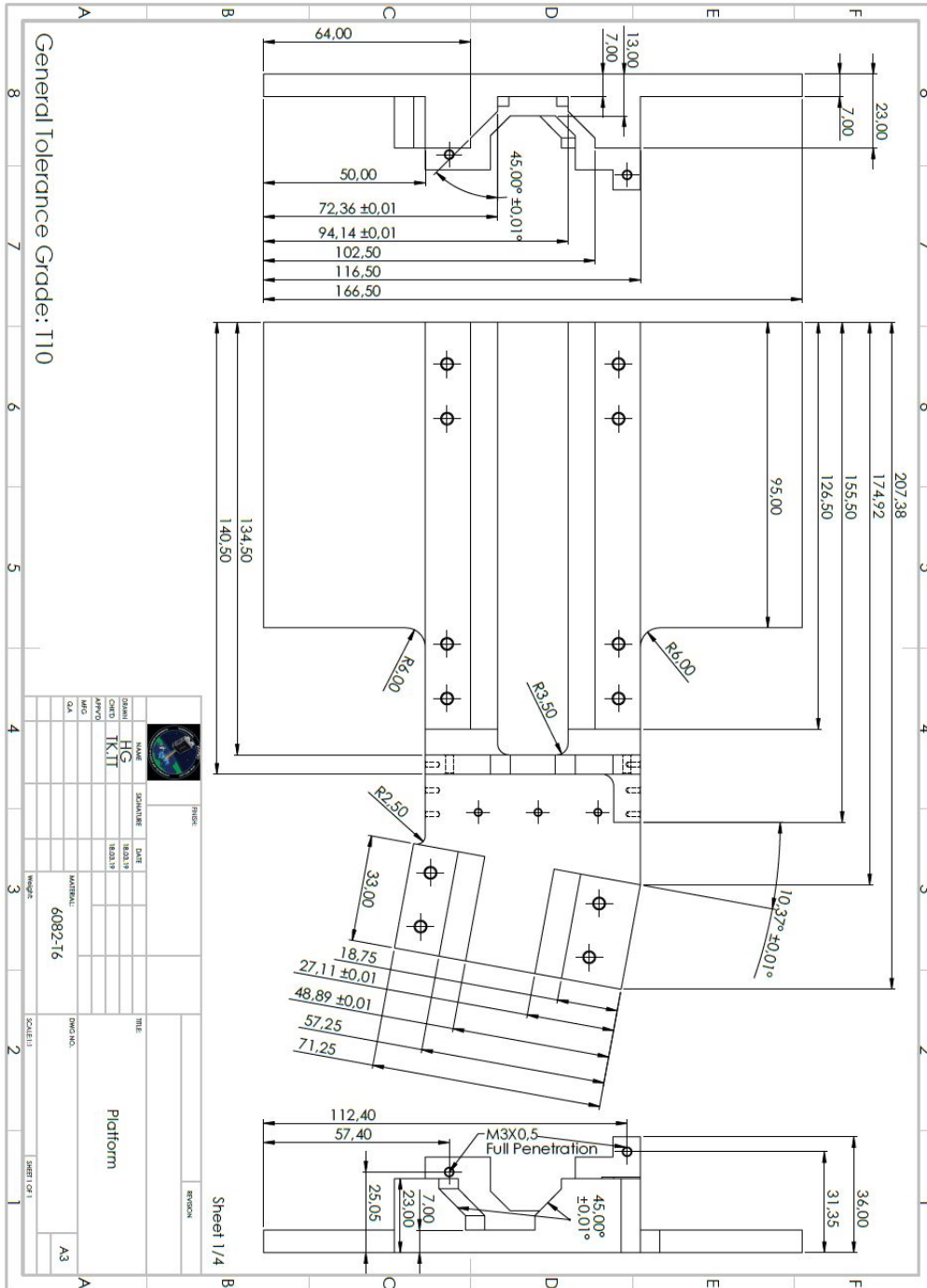| 15	*Testing Service*	Responds to telecommands by running one or more on-board self tests, returning the results of the tests as telemetry reports.

6. List of Abbreviations

Table 4: List of Abbreviations

Abbrv.	Description
ICD	Interface Control Document
NA	NanoAvionics
HSI	Hyper Spectral Imager
BoB	Breakout Board
IMU	Inertial Measurement Unit
RGB	Red Green Blue
SDR	Software-defined Radio
PC	Payload Controller
UHF	Ultra High Frequency
FPGA	Field-Programmable Gate Array

Appendix A

HSI Technical Drawings

General Tolerance Grade: T10

8X M4X0,7
Depth = 7mm

6,75   6,75

30,00
13,00
117,00
100,00

25,00
8,00
6,75
11,50
25,00
8,00

NAME
HG
TK,TT

SIGNATURE   DATE
DRAWN   18.03.19
CHKD   18.03.19
APPVD
MFG
Q.A

FINISH:

MATERIAL:
6082-T6

Weight

SCALE:1:1

DWG NO.

TITLE:
Platform

Sheet 2/4

REVISION

SHEET 1 OF 1

A3

General Tolerance Grade: T10

DETAIL B
SCALE 2 : 1

DETAIL C
SCALE 2 : 1

MATERIAL: 6082-T6

TITLE: Platform

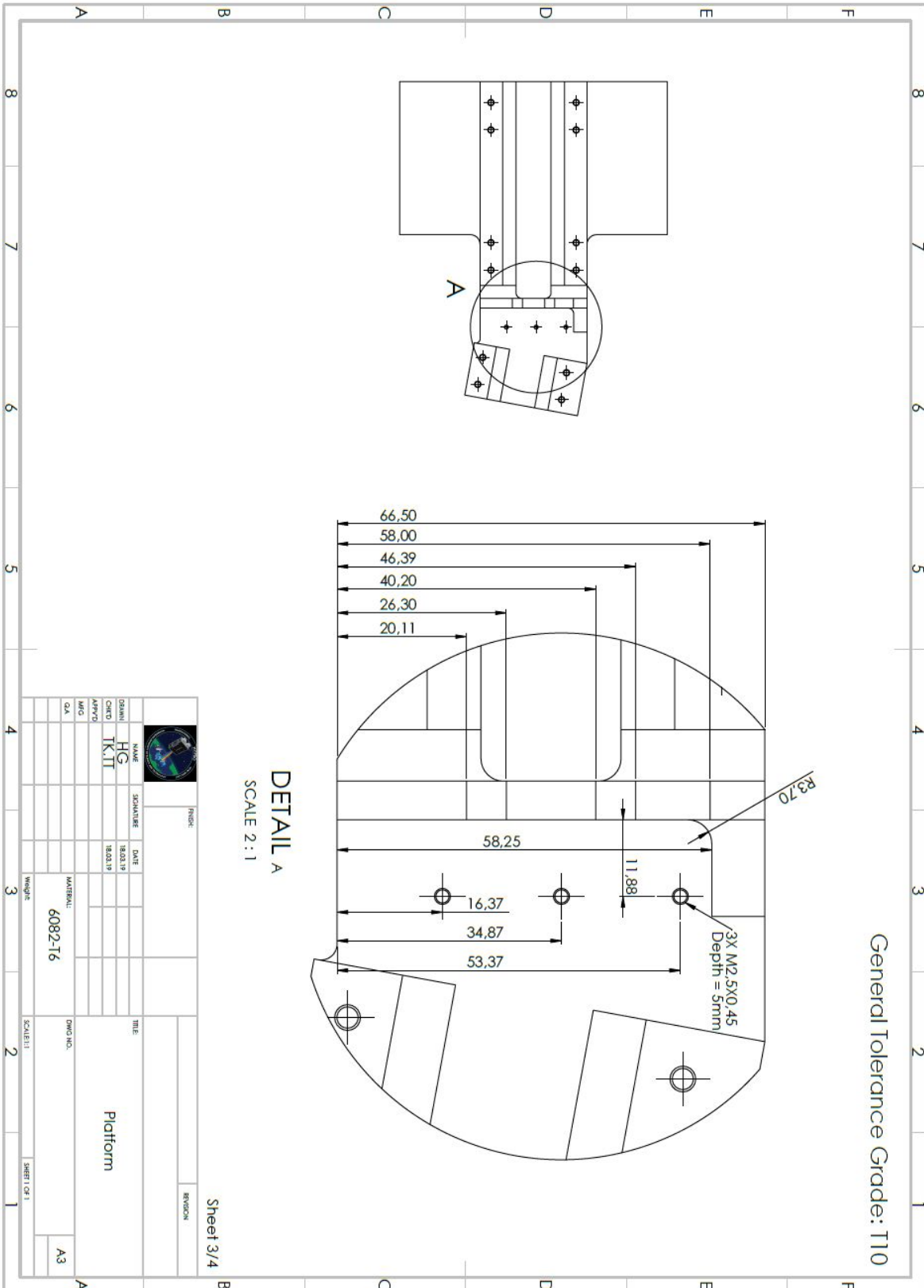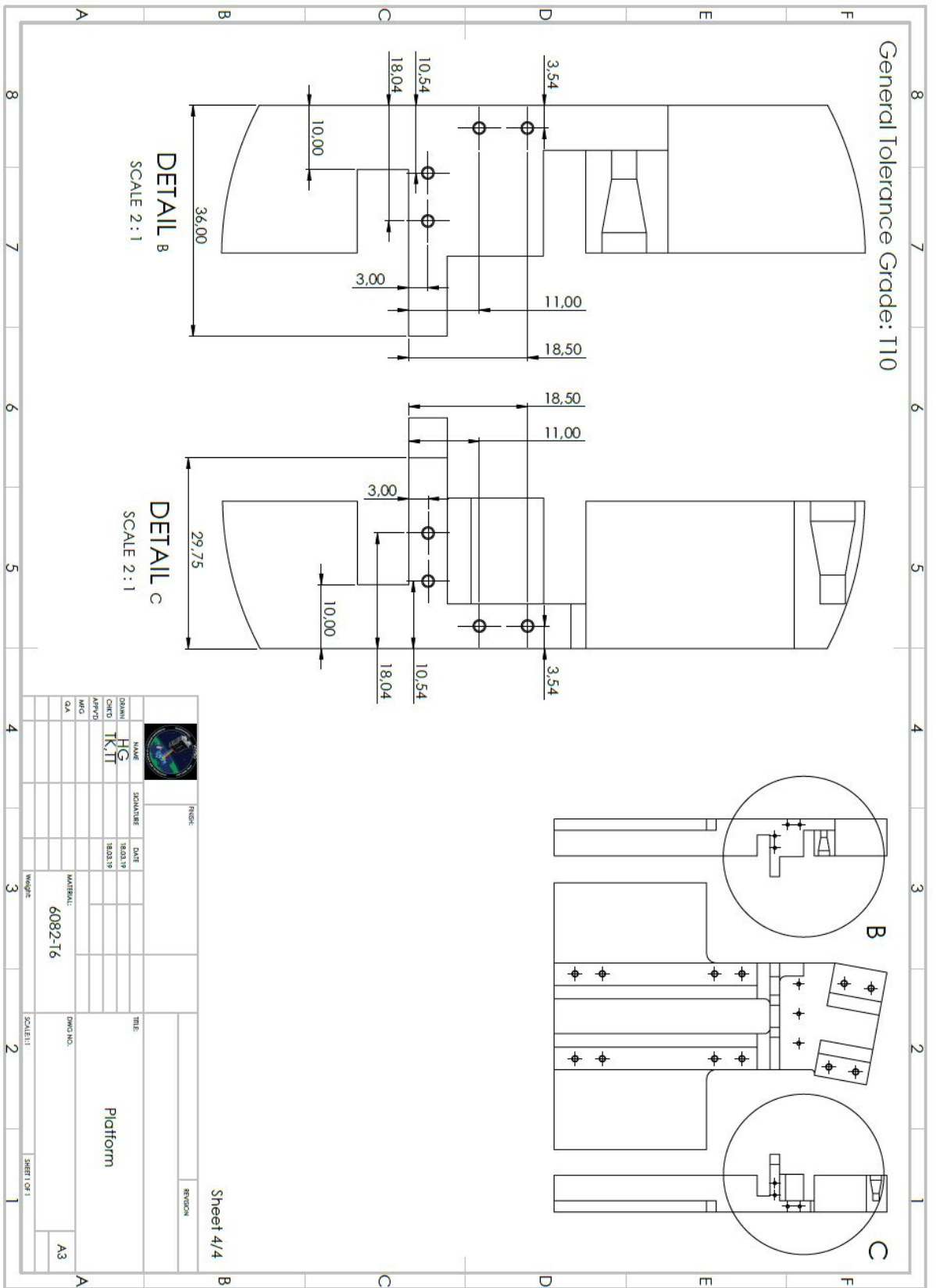Sheet 4/4
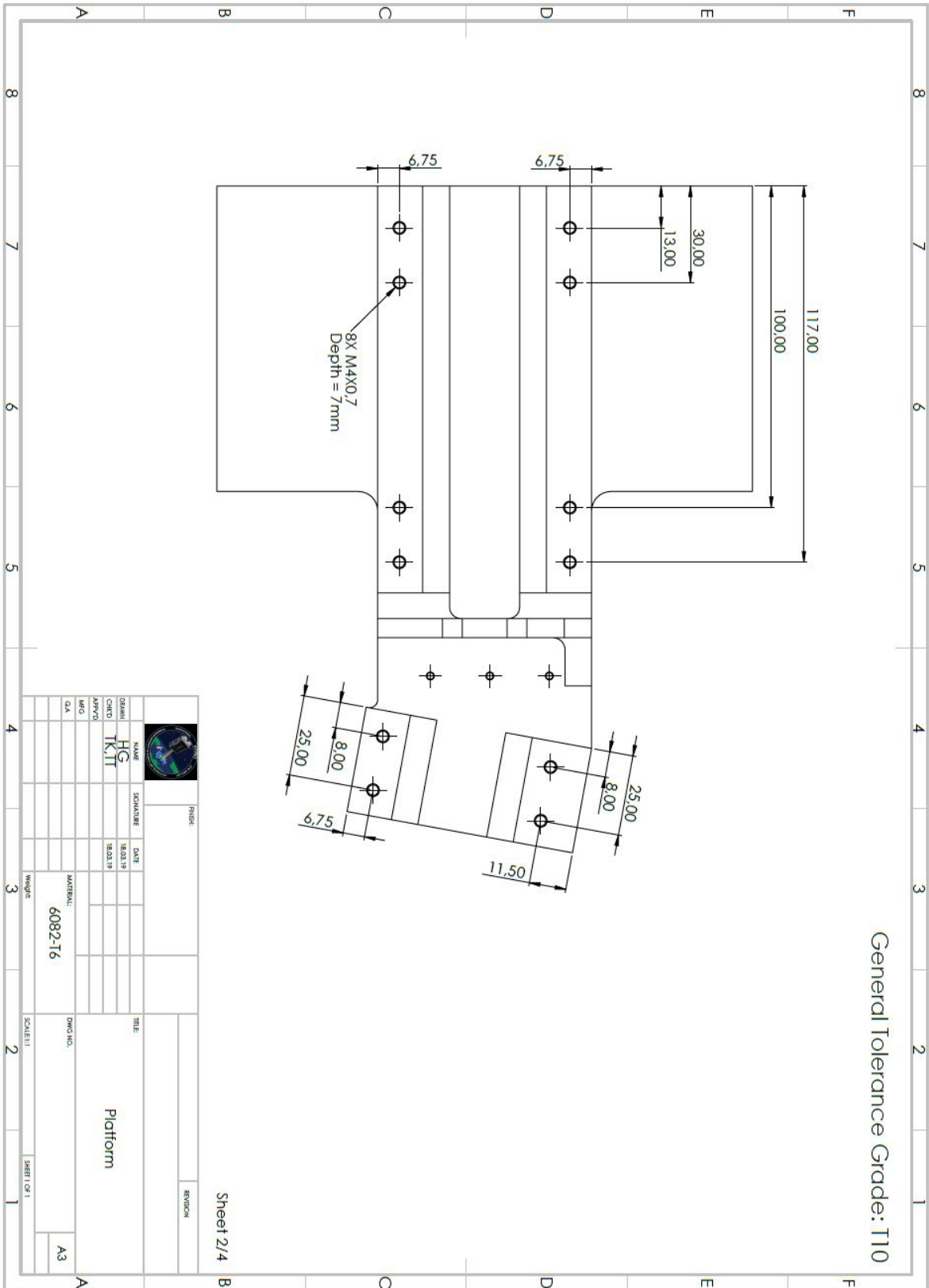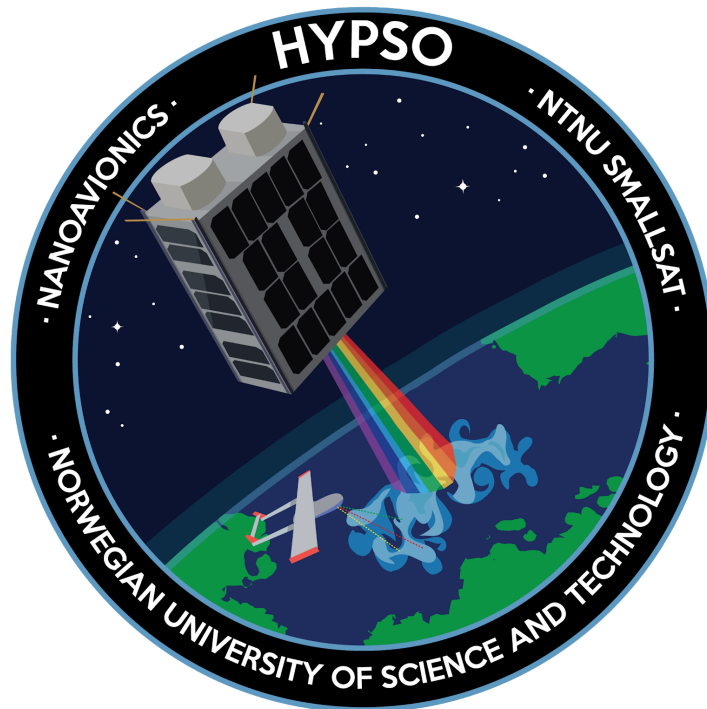
Appendix H

HYPSO-TRP-OPT-002 Functionality Test Report of HSI TTH Mk1

Functionality Test Report of HSI TTH Mk1

HYPSO-TRP-OPT-002

Prepared by:	HYPSO Project Team
Reference:	HYPSO-TRP-OPT-002
Revision:	2
Date of issue:	25.05.2019
Document Type:	Test Report
Author(s):	Tord Hansen Kaasa, Tuan Tran, Henrik Galtung

Table Of Contents

Table 1: Table of Changes

Rev.	Summary of Changes	Author(s)	Effective Date
1	*First issue*	*Tord Hansen Kaasa, Tuan Anh Tran, Henrik Galtung*	*15.02.2019*
2	*Formatting of text*	*Tord Hansen Kaasa, Tuan Anh Tran, Henrik Galtung*	*25.05.2019*

1. Introduction

1.1 Purpose

The main purpose of the test is to discover and evaluate potential flaws of the HSI prototype. Even though several aspects in regards to machinability, assembly, tolerances and functionality have been considered during the design phase, flaws may still occur, and should always be tested for. These may comprise of misalignments, miscalculation of tolerances, impossible to reach assembly locations, and collision of parts. The functionality of the assembled HSI camera will also need to be characterized and compared to other working models. Another uncertainty of the TTH Mk1, is the unknown level of stray light protection given by the shroud. Furthermore, reflective surfaces of the platform and cassette parts may cause degradation of image quality. These aspects will also be investigated.

The tests will be done in two steps and can be treated as two separate tests:

Test 1: *Assembly and general functional test*. The general assembly will be tested and scrutinized for potential flaws and irregularities. This test can potentially highlight problems that can be addressed in the next HSI design iteration.

Test 2: *General Tolerance test.* Explore the impacts of deviations in positioning and alignment on the imaging. Since the requirements does not list measurable properties here, this testing aims to better understand the impact of changes in the geometry of the optical assembly.

1.2 Background

This test report was conducted following the Functional Test Plan for HSI TTH Mk1 procedure at the smallsat lab the 15th of May 2019.

1.3 Reference Documents

Table 2: Referenced Documents

ID	Author	Title
[RD01]	Elizabeth Frances Prentice.	HYPSO-RP-006 HSIv6 Assembly, Fred's Design
[RD02]	Fred Sigernes, Mariusz Eivind Grøtte, Julian Veisdal, Evelyn Honore-Livermore, Joao Fortuna, Elizabeth Frances Prentice, Mikko Syrjasuo, Kanna Rajan, and Tor Arne Johansen.	Pushbroom hyper spectral imager version 6 (hsi v6) part list – final prototype, 2018.

2. Method

The parts involved in the assembly has been tabulated in table 3. Prior to inspection and assembly, the parts were cleaned using non-lint cleaning wipes, swabs doused in isopropanol (IPA). Considerable amounts of grease and oil was observed on the parts. An ultrasonic bath was considered for the cleaning procedure, however, due to limited access, cleaning wipes were deemed sufficient. For future assemblies, ultrasonic baths should be used to increase the procedure replicability as well as decrease surface contamination risk factors. When exposed to vacuum, grease and oil will start to outgas, and might condense onto lens surfaces.

Table 3: HSI part list

HSI Part Name	Qty
HSI Platform	1
Platform Bracket	3
Cassette Front *(Grating Assembly)*	1
Cassette Back *(Grating Assembly)*	1
Clamp Bracket *(Grating Assembly)*	2
Bracket Gasket *(Grating Assembly)*	2
Shroud Front *(Shroud Assembly)*	1
Shroud Back *(Shroud Assembly)*	1
Shroud Top *(Shroud Assembly)*	1
Shroud Side *(Shroud Assembly)*	2
Shroud Gasket Front	1
Shroud Gasket Back	1
Bolts	
M2x4CSK	4
M2x6CSK	6
M2x6set	4
M2X8CH	14

M2X10CH	8
M2.5X6CSK	3
M3X6CSK	2
M3X8CSK	5
M3X10CSK	2
M4X10CH	12
COTS Components	
50mm VIS-NIR objective (OBJ-13 to OBJ-15)	3
25mm Sq. 17.5 deg Blazed Grating (300 lines/ mm)	1
SM1 lens tube 1 inch long with internal threads, and 2 threaded rings	1
Adapter ring SM1 – C-mount internal	1
Fixed high precision mounted slit (50±3µm x 7mm)	1
iDS MX249 Detector	1

2.2 Assembly Procedure

The assembly process was done using the predicted assembly procedure from *Functional Test Plan for HSI TTH Mk1* and *HYPSO-RP-006 HSIv6 Assembly, Fred's Design* [RD01]. In addition to these reports, the Pushbroom *Hyper Spectral Imager version 6 (hsi v6) part list – final prototype* [RD02] was used. The assembly process contains steps for the shroud, which only serves as a light protection for the grating groove area. Future designs will not have these steps, as shroud functionality will be integrated with the cassette.

The parts were weighed, visually inspected and photographed before the assembly process was initiated. The mass and pictures are shown in section 3.1 *Mass measurements and* 3.2 *Visual Inspection,* respectively. Table 4 shows the complete assembly procedure. Figures of the entire assembly procedure can be found in Appendix A: *Assembly Figures*.

Table 4: HSI TTH Mk 1 Assembly Steps

Step	Description	Comments
1	Place all parts neatly on a levelled surface	Use gloves when handling the parts
2	Perform the pre assembly cleaning procedure	No contaminants shall
Grating Cassette		
1	Unpackage the grating	
2	Clean grating surfaces using pressurized air	There seemed to be dust particles already present on the grating before opening
3	Insert four M2 set screws in their respective threads from the outside of the cassette.	This is done in order to ease the mounting when the grating is inserted into the mount
4	Insert the grating along with the two clamping brackets into the cassette while ensuring that the arrows point in -Z and +X directions	The placement of the grating is important, the markings on the grating will show the correct placement in accordance with figure 1
5	Hand tighten the m2 set screws carefully	This should be done incrementally. Do not use much force when tightening as the grating substrate is brittle
6	Place gasket on back cassette	Duct tape was used instead, as gasket have not been procured yet
7	Apply the back cassette plate and insert its four countersunk M2x4 screws	The back cassette applies pressure to the grating and secures the placement to the driving surface of the cassette
8	Hand tighten M2 incrementally	This is done to ensure an even pressure over the grating surface
9	Position cassette assembly on the platform and insert three M2.5x6 screws in the vertical direction and two M3x8 screws in the horizontal direction	The vertical direction refers to Y-direction, as in the three holes at the "foot" of the cassette. The horizontal direction refers to the Z-direction, as in the "ears"
10	Incrementally hand tighten the three M2.5x6 and two three M2.5x6 to ensure a snug fit	The holes have been purposely offset in order to push the cassette into the corner of the driving surfaces. It's therefore very important that the tightening is done in small incrementations.

Shroud Assembly		
1	Attach the shroud sides to the shroud back	The shroud should only provide sheltering from light inside the grating surface. The shroud has no other purpose, and can therefore be assembled with less care than the optical equipment.
2	Screw three M2x8 bolts in loosely for each shroud side, totalling six bolts	
3	Place assembly on it's back, and fasten the shroud top	
4	Screw five M2x8 bolts in loosely in the top to the back and side shroud plates	
5	Place shroud front onto assembly	
6	Screw six M2x8 bolts to the front side and three M2x8 from the top down to front	
7	Fasten the shroud assembly to the platform using three M2x8 screws on each side of the bottom (total of six)	The shroud can be quite tight. Some force required in order to secure it to the platform
Back Objective and Sensor Assembly		
1	Screw 50mm VIS NIR lens onto IMX249 using the C-mount connections present on the parts	
2	Use set screws to fix the camera objective to **f/2**	
3	Plug in the camera into a laptop and use UEye Cockpit to adjust focus until a clear image at "infinity" is displayed	Target should be more than 50 meters away
4	Fix focus in place with the set screws.	The set screws will hinder the settings from shifting when adjusting the objective
5	Place back objective assembly on platform groove	The shroud back is extremely tight, some difficulties will occur. The Objective should optimally be placed
6	Make sure the camera sensor is properly levelled	This is best done with a level on the flat detector top. Make sure that this is done on a levelled surface

| 7	Push assembly into the back shroud	In the +Z-direction, making sure that the assembly is pressured against the backplate of the shroud
8	Place a platform bracket over the back assembly and tighten it with the four M4x10 bolts	Make sure the back assembly remains levelled while tightening incrementally
Front Objective Assembly		
1	Position locking ring in slit tube	The slit should be placed 11 mm from the front edge. When measuring using the Socket Wrench, 9 mm should be measured due to the 2 mm locking ring thickness
2	Twist adapter on to slit tube	
3	Add spacer ring to collimator objective	
4	Screw together slit tube and collimator objective	
5	Fix collimator objective setting	Adjust F numbers to **f/2.8** for both of the front assembly objectives. Plug the imager into a laptop and use UEye Cockpit to view the image from the camera. Adjust the focus while looking at infinity. (object 50m or more distant) Fix the focus with the set screw.
6	Place the Front Objective Assembly into the front HSI Platform grooves	
7	Slide the objectives into place within the shroud opening	
8	Secure the objectives with the two HSI platform brackets	The brackets are designed to have a small gap to the platform
9	Hand tighten the four M4x10 bolts incrementally on each platform bracket until the objectives are securely placed	The total amount of M4x10 bolts used in this step should be 8, try to keep the gap between bracket and platform level as you tighten. A torque wrench should be applied in further updates
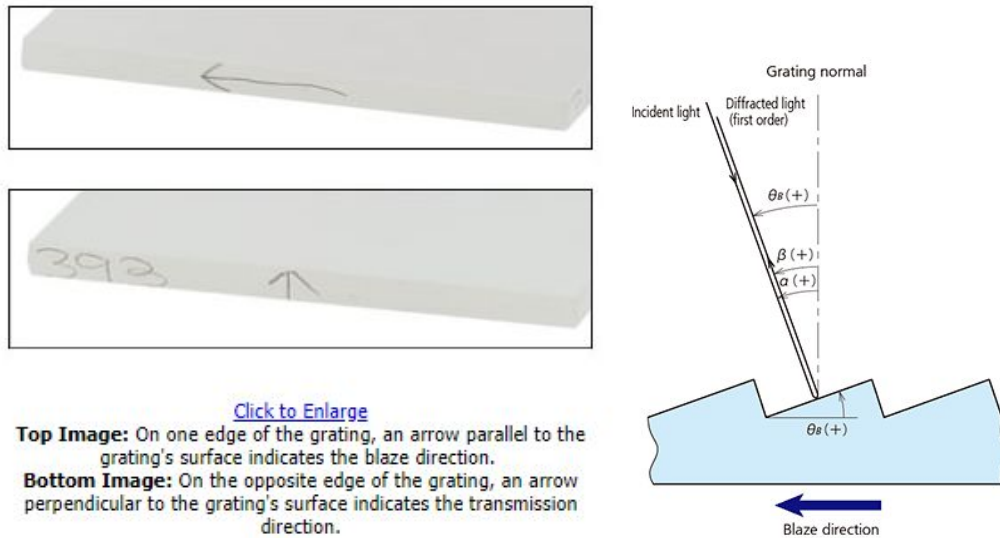
Figure 1: Grating placement indicators, image provided by Edmund Optics

2.2 Experimental Set-up

Following the assembly of the HSI prototype, several key parts were manipulated relative to the *Functional Test Plan for HSI TTH Mk1* General tolerance test. The experimental setup is noted below. Furthermore note that the steps below should be reverted to their original state before moving on to the next step. All displacements shall be measured and documented by the distance, location, and resulting spectrogram for every iteration.

The baseline captured with the TTH Mk1 were initially blurry. After consulting the v6 paper [1], it was clear that the HSI needed manual adjustments to the slit tube and spacer rings in order to get the high precision slit in a correct position. The following calculations shows the new spacer rings to better fit the flange focal length of the objectives. The old configuration used two 0.5mm, one on both sides of the slit tube. The new configuration consisted of one 1.5mm spacer ring on the back of the slit tube. Section 3.3.1 shows the configured optical measurements.

General Tolerance Test
1) The Objectives were placed on a level table facing out an open window connected to the detector and uEye pointing at a group of trees at more than 50m away.
2) The focus of the objectives were calibrated so that all pictures appeared sharp, this is a subjective step.
3) The finished assembled HSI prototype was hooked up to a pc with uEye installed. Using a micro usb cable, the HSI was connected to the software.
4) The HSI camera was then pointed at a white paper with a 0.5m distance at a room with a controlled light.

5) The software camera adjustment settings was set to manual with the following values: PixelClock=118, FPS=1.5, EXP=563.793, GAIN=0, the exact settings will vary depending on the light conditions.

6) Reference spectrograms where established using white, green and orange papers, all further spectrograms should be compared to the white baseline

7) The 1.5mm back spacer ring on the front lens assembly was removed and replaced with a 1.0mm spacer, 0.55mm, 2.0mm followed by no spacer. The impact on the spectrogram was then recorded with the use of the uEye software.

8) The front optical assembly was moved (0.5), (1.5), and (5)mm in the +Z direction and a spectrogram was captured at each displacement.

9) The back optical assembly was displaced (0.5), (1.5) and (5)mm along its axial direction and a spectrogram was captured at each displacement.

10) The shroud was removed and a spectrogram was captured in this configuration

11) An M3 washer was inserted between the cassette and the HSI platform in the location shown in figure 3, equaling +-1 degree. A spectrogram was captured and another washer was added before another capture. This process was repeated one more time.

12) The front optical assembly was rotated 45, 90 and 180 degrees.
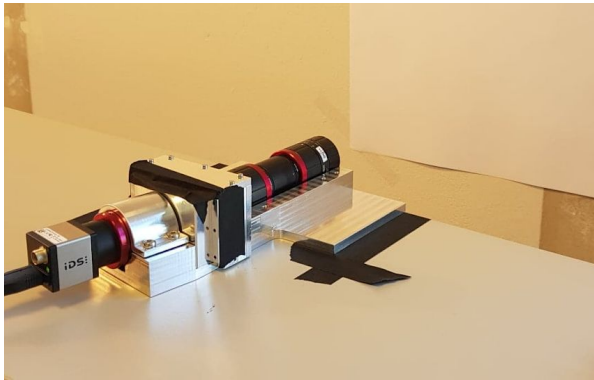
Figure 2: Test-Setup
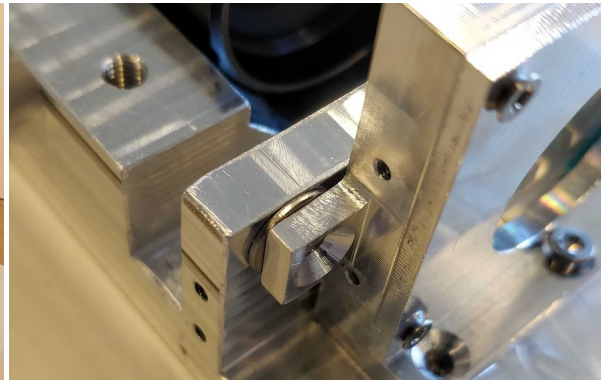
Figure 3: Washer Placement,
done on both sides of the cassette

Figure 4: White, Green and Orange Colors used for Baseline

3. Experimental data

3.1 Mass measurements

All the parts were weighed using a 0.05g precision scale and compared to the estimated massed from NX CAD models. Parts that were similar were measured separately and averaged out. In addition, the deviation between the measured and estimated masses, measured in percentage was calculated. The total mass of the TTH Mk1 assembly without bolts or camera COTS components was measured to be 1023.45g, which deviated by 21.76g from the estimated 1001.69g. Table 5 tabulates the measured mass of all parts, and the entire assembly with bolts assumed as being an additional 2% mass. No mass deviations were recorded between the parts with larger quantity. The deviation percent recorded is in relation to the original CAD calculations on NX. The gasket parts materials had not been decided on at the time of this test, and was therefore not measured or estimated.
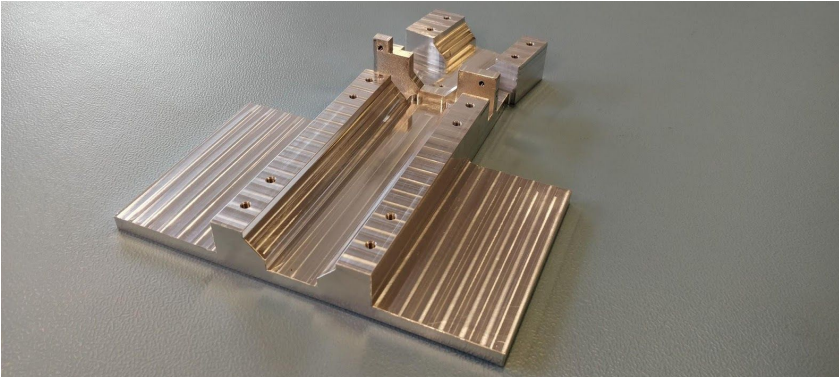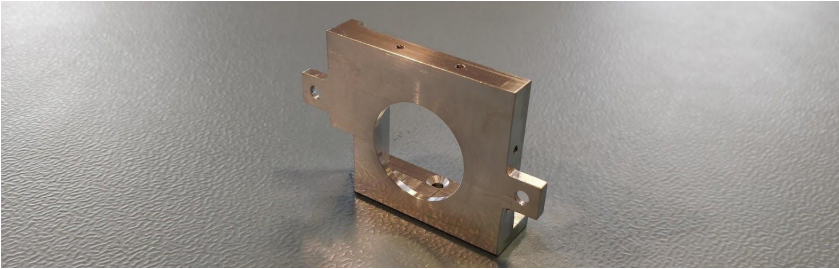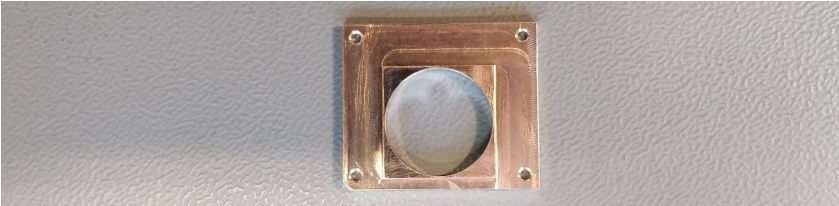
Table 5: Assembly Part Measurements

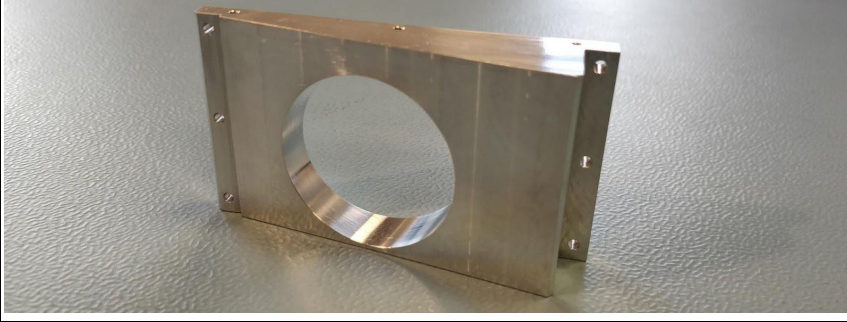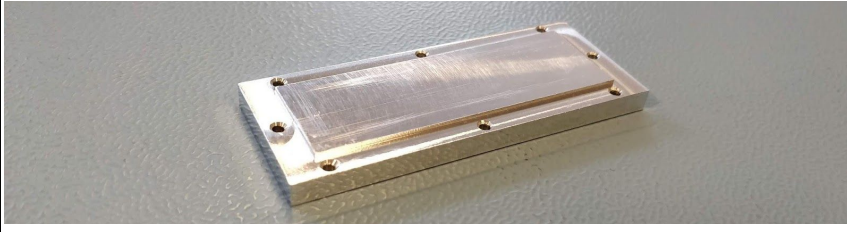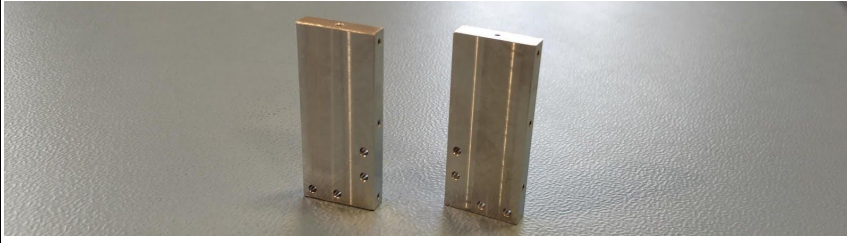| HSI Part Name	Qty	Estimated Mass (g)	Measured Mass (g)	Deviation CAD (%)
HSI Platform	1	723.18	727.15	0.55
Platform Bracket	3	29.53	30.05	1.75
Cassette Front *(Grating Assembly)*	1	25.69	25.60	0.36
Cassette Back *(Grating Assembly)*	1	6.51	6.80	4.40
Clamp Bracket *(Grating Assembly)*	2	0.645	0.60	6.67
Bracket Gasket *(Grating Assembly)*	2	-	-	-
Shroud Front *(Shroud Assembly)*	1	34.25	34.45	0.58
Shroud Back *(Shroud Assembly)*	1	68.74	67.85	1.29
Shroud Top *(Shroud Assembly)*	1	36.43	36.45	0.06
Shroud Side *(Shroud Assembly)*	2	17.01	16.90	0.63
Shroud Gasket Front	1	-	-	-
Shroud Gasket Back	1	-	-	-
Assembly w/o Bolts, COTS		1001.69	1023.45	2.17
Full Assembly		**1383.79** (1411.5 Bolts added, 2%)	**1444.40**	**1.97**

3.2 Visual Inspection

The following figures included in table 6 were taken from the visual inspection prior to assembly. Additional pictures of surface deformations and scratches have been taken. No notable deviations or damage was observed on critical surfaces and geometry. The machining has been done with precision and are functionally identical to the original CAD models.

Table 6: Visual Inspection Result

Part Name (Nr.)	Part Geometry	Qty
HSI Platform		1
Platform Bracket		3
Cassette Front *(Grating Assembly)*		1
Cassette Back *(Grating Assembly)*		1
Clamp Bracket *(Grating Assembly)*		2

|		
Shroud Front *(Shroud Assembly)*		1
Shroud Back *(Shroud Assembly)*		1
Shroud Top *(Shroud Assembly)*		1
Shroud Side *(Shroud Assembly)*		2

3.3 Functional Tests

3.3.1 Baseline Spectrogram

After assembly, a spectrogram was taken as described in the test procedure using the prototype, seen in figure 7. All spectrograms taken were compared to previous working models such as the FRED-2 and NTNU-1, seen in figures 5a-b and 6a-b respectively. The settings used in uEye Cockpit for these spectrograms were based on the ones used in the report *HYPSO-RP-006* [RD01]. The spectrograms captured by the Fred-2 and NTNU-1 were taken during clear skies and pointing to a light bulb. The exact conditions were not recorded.
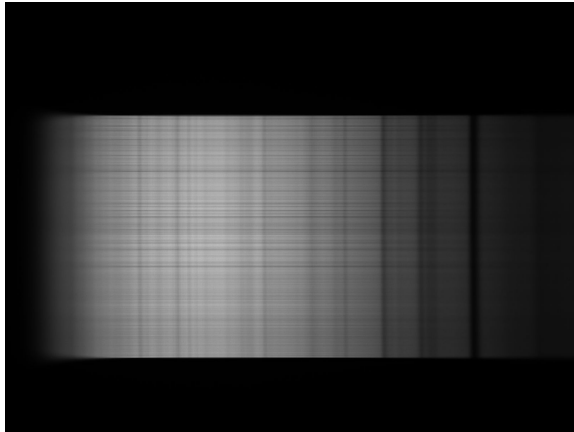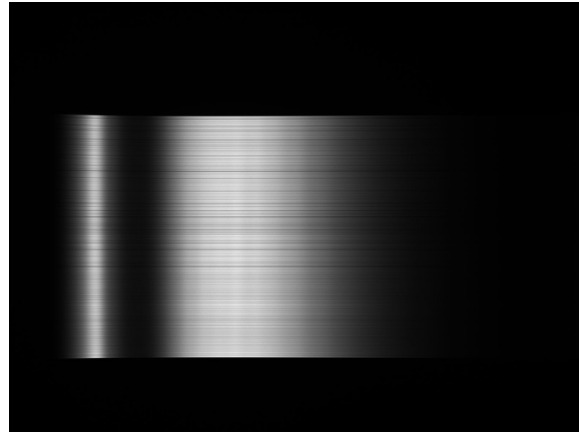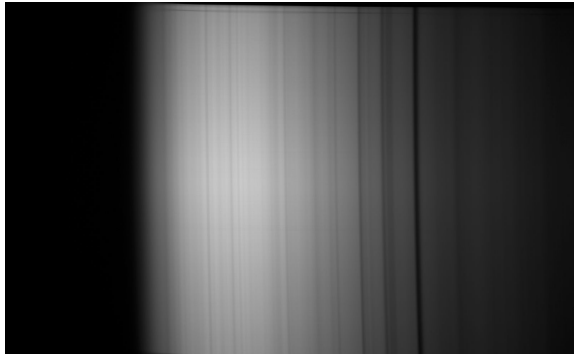
5a: Clear Skies   *5b: Light Bulb*

Figure 5: Spectrogram Fred-2

6a: Clear Skies   *6b: Light Bulb*
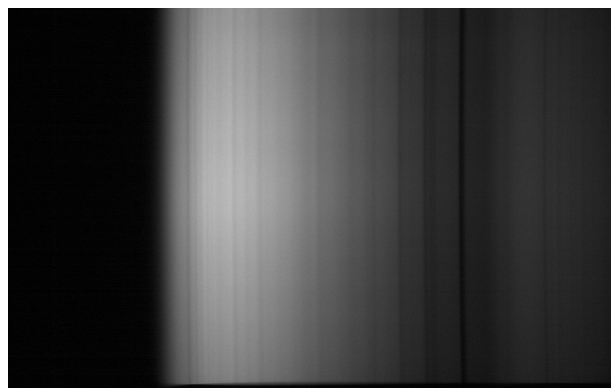
Figure 6: Spectrogram NTNU-1

Figure 7:Spectrogram TTH Mk.1 Clear Skies

The clear skies spectrogram captured with the TTH Mk1 following the v6 paper [RD02] were initially blurry. After consulting the v6 paper, it was clear that the HSI needed manual adjustments to the slit tube and spacer rings in order to get the high precision slit in a correct position. The following calculations shows the new spacer rings to better fit the flange focal length of the objectives. The old configuration used two 0.5mm, one on both sides of the slit tube. The new configuration consisted of one 1.5mm spacer ring on the back of the slit tube. Figure 8 shows the configured optical measurements and the basic calculations done to find the slit position and check the flange focal distance.
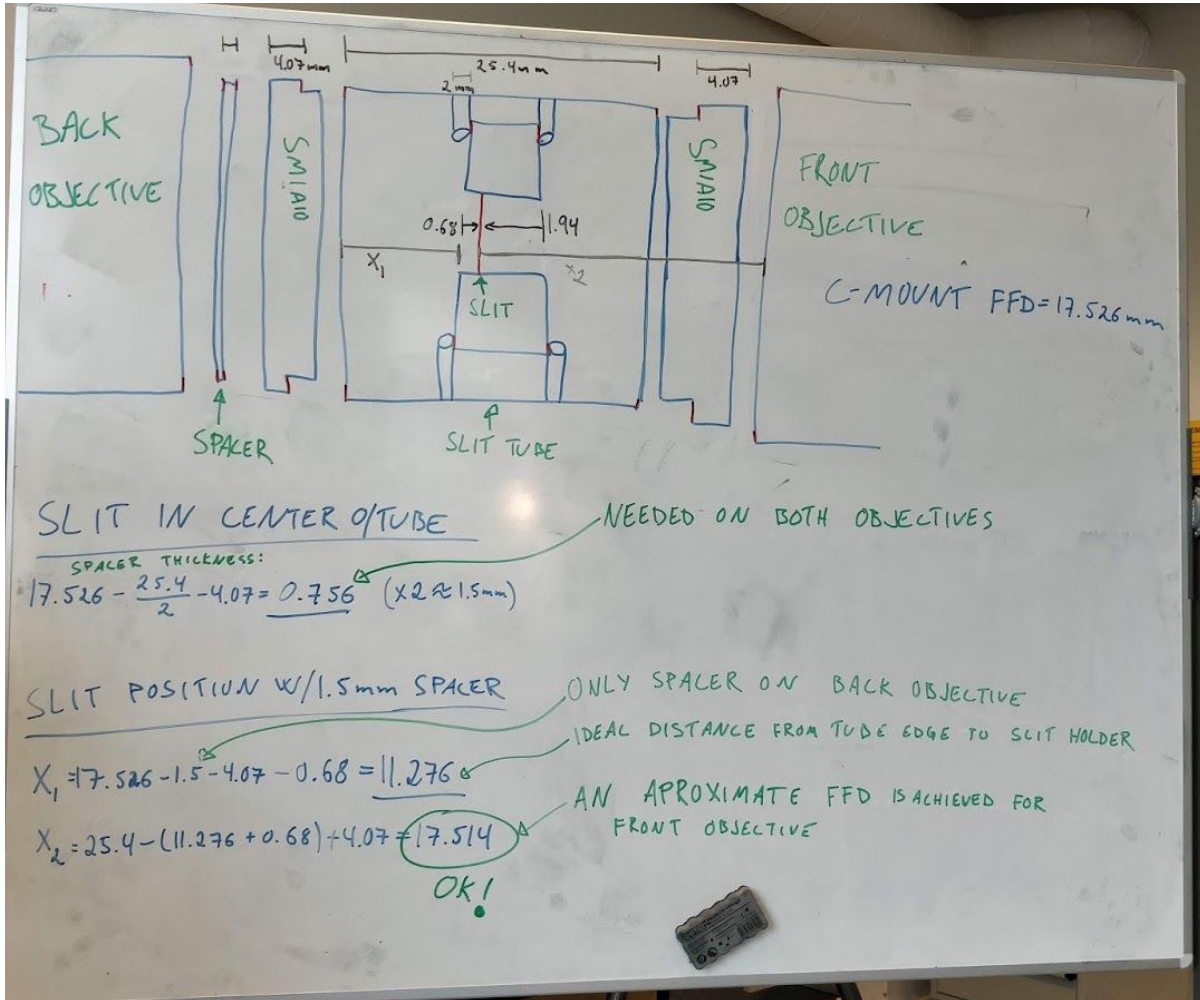

Figure 8: The basic distances and calculations for spacer thickness and slit position

Figure 9a-c show the baseline based on the new calibrations made to the slit position.
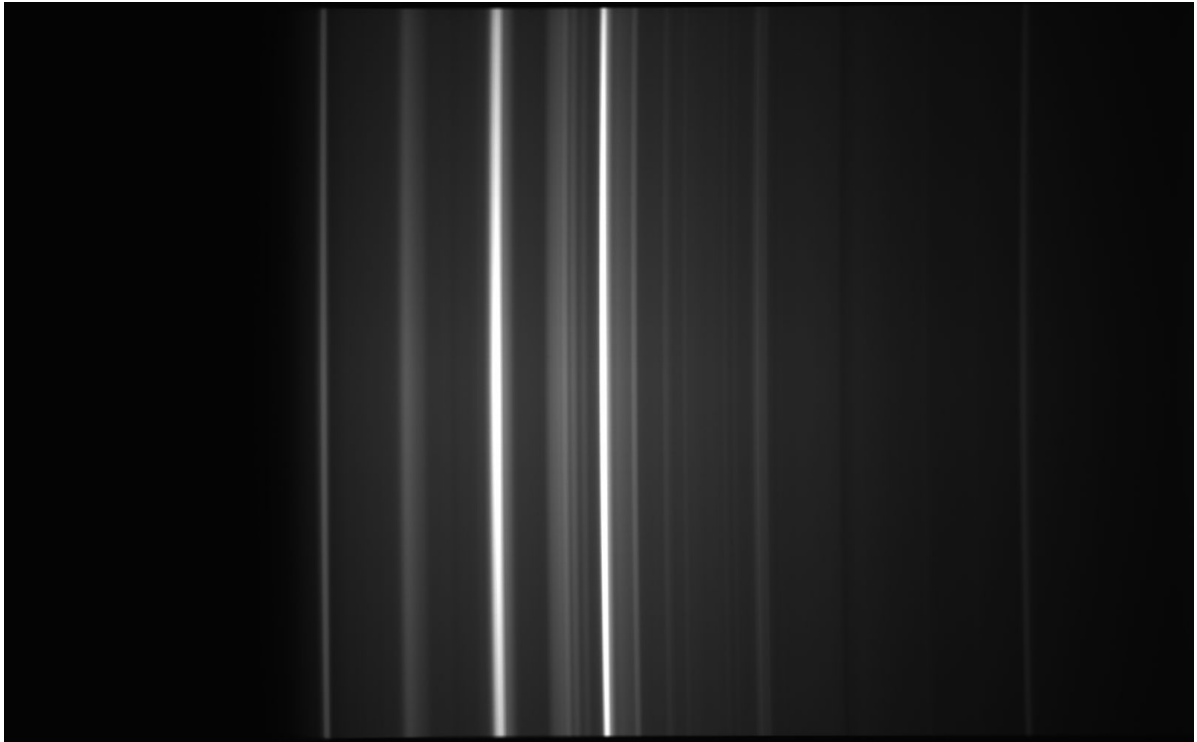
9a: Baseline - White Target
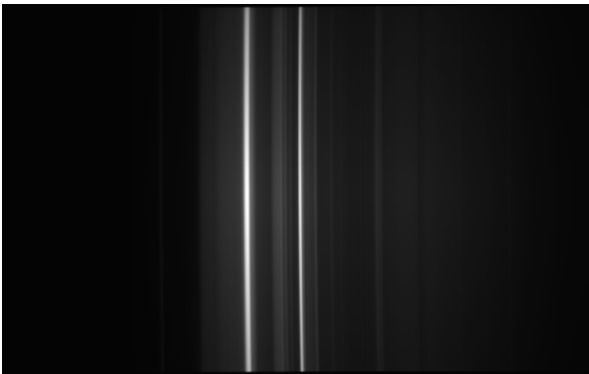
9b: Baseline - Green Target   *9c: Baseline - Orange Target*
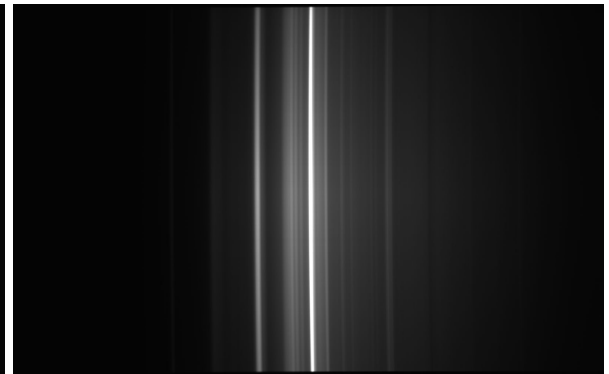
Figure 9: Calibrated Baseline

3.3.2 Spacer Ring Change Spectrogram

Figure 10 a-d shows the spectrogram captured by manipulating the spacer rings. The spectrograms captures a white paper.

10a: No Spacer Ring   *10b: 0.55 mm Spacer Ring*

10c: 1.0 mm Spacer Ring   *10d: 2.0mm Spacer Ring*
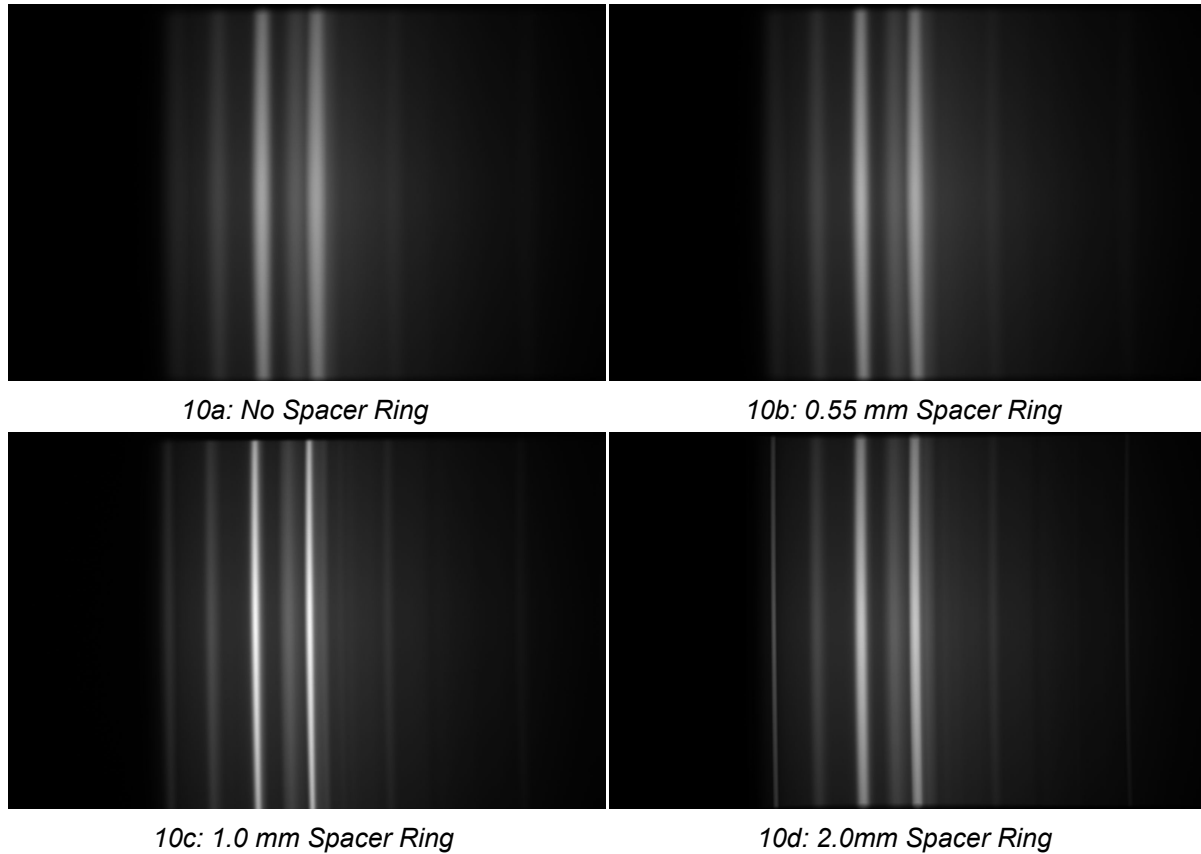
Figure 10: Change of Spacer Rings

3.3.3 Front Optical Assembly +Z Displacement Spectrogram

Figure 10 shows the resulting spectrogram after a displacement of the entire front assembly in the +Z direction (CubeSat LCS), away from the grating.

11a: 0.5 mm Displacement   *11b: 1.5 mm Displacement*   *11b: 5 mm Displacement*
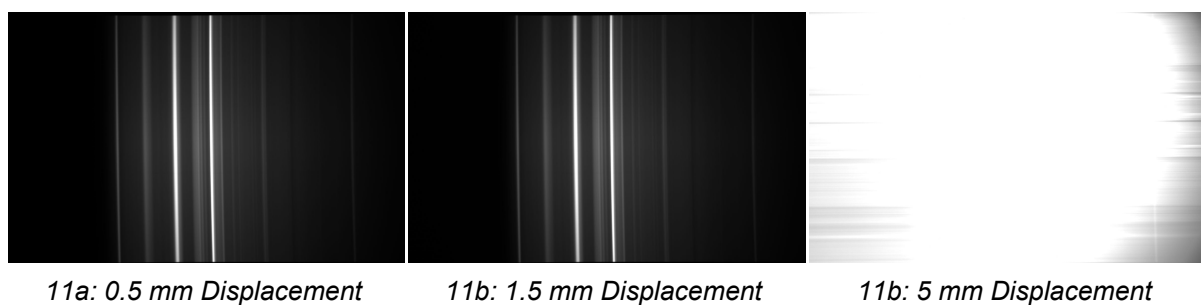
Figure 11: Front Assembly Displacement in +Z Direction

3.3.3 Back Optical Assembly -Z Displacement Spectrogram

Figure 12 a-c shows the resulting spectrogram after a displacement of the entire front assembly in the -Z direction (CubeSat LCS), away from the grating.
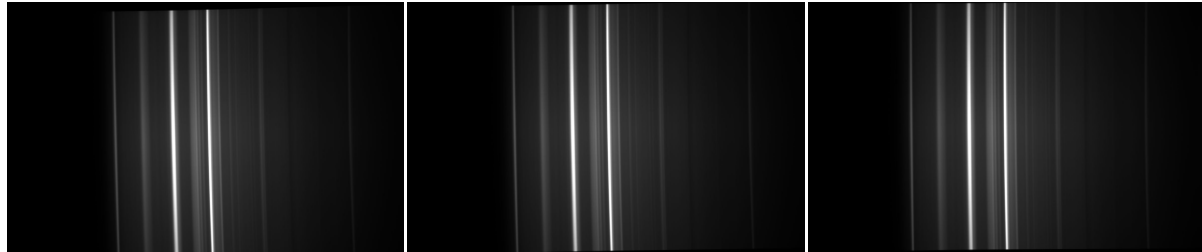
12a: 0.5 mm Displacement   *12b: 1.5 mm Displacement*   *12b: 5 mm Displacement*

Figure 12: Back Assembly Displacement in -Z Direction

3.3.4 Stray Light Entering the Grating Spectrogram

Figure 13 shows the resulting spectrogram after the shroud assembly was removed.
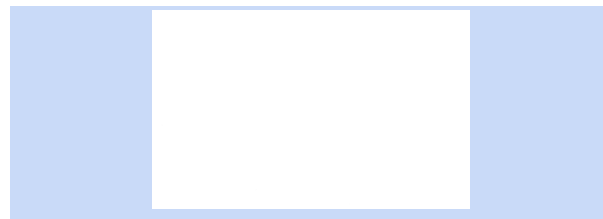
Figure 13: Without Shroud
(Overexposed)

3.3.5 Grating ± 1 Degree Offset Spectrogram

Figure 14 a-b shows the resulting spectrogram after a 0.81mm washer had been placed at the location shown in figure 3.
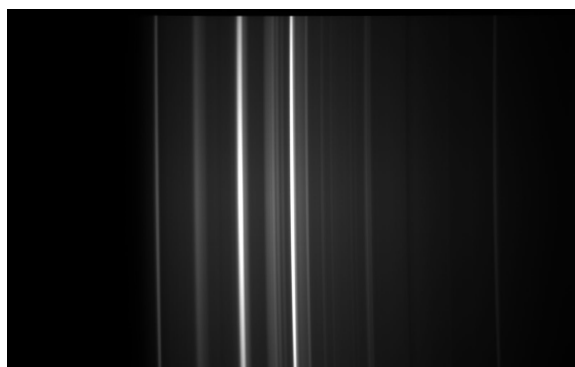
14a: One Washer on +X Side   *14b: One Washer on -X Side*
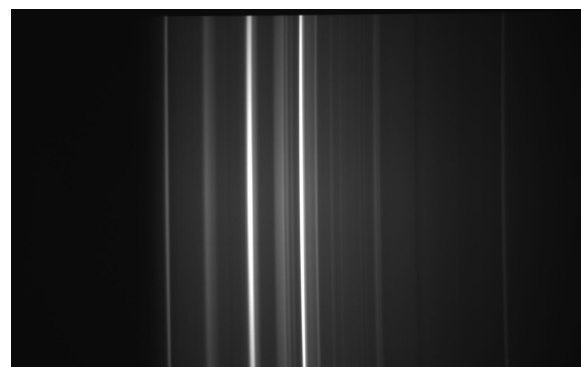
Figure 14: Rotation on Grating Cassette by Washers

3.3.6 Rotation of Front Optical Assembly Spectrogram

Figure 15 shows the spectrogram resulting from a rotation of the front optical assembly.
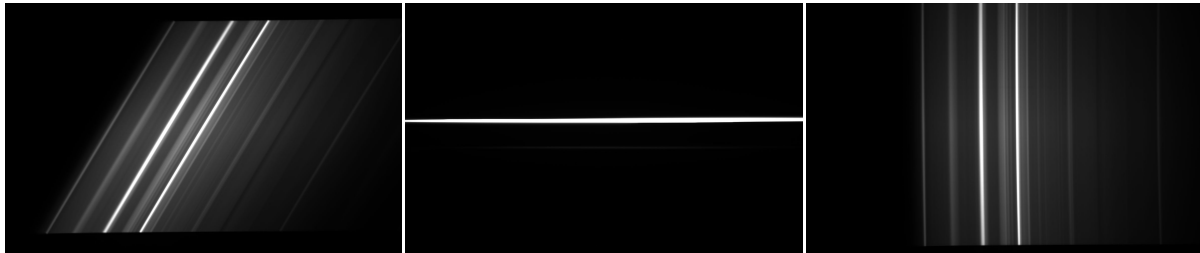
| *15a: 45 degrees* | *15b: 90 degrees* | *15c: 180 degrees* |

Figure 15: Rotation of Front Assembly

4. Discussion

4.1 Spectrogram Results

As mentioned in section 3.3.1, the pictures taken by the assembled camera, following procedures based on the v6 paper schematics [RD02], resulted in unfocused spectrograms. In addition to this, the spacer rings by Edmund Optics seemed to vary in size by up to 10% from the labelled values. This resulted in difficulties when spacing for the correct flange focal length in the front objective assembly. A new configuration was calculated that fitted the measured spacer rings. The new configuration resulted in sharp spectral lines. After assembly, the spectrogram was also observed to be shifted towards the left side. This meant that the grating to detector angle of 10.37 degrees was not sufficient and should be increased in future iterations of the prototype.

After a proper baseline was established, tolerance testing was done following the plan in section 2.2 in order to investigate the sensitivity of the HSI camera with respect to translational and rotational displacement of various parts of the assembly. The intention was to uncover the resulting behavior of the spectrogram when subjected to displacements.

As shown in figure 10 a-d, varying the distance of the spacer rings outside of the defined distances caused the spectrogram to defocus. Shifting the front and back assemblies as seen in figure 11 and 12 did not seem to cause any effect on the spectrograms, with the exception of moving it in some cases. This is however believed to be caused by calibration procedure that was necessary in between each step, which required tightening using an arbitrary amount of force and placement. The back assembly was moved up to 5 mm without causing any observable effects on the spectrogram. Too much translational movement of the front assembly in the +Z axis did however cause surrounding stray light to pass through, as gaps expanded essentially opening the assembly. Removal of the shroud produced the same result to a much higher degree, overexposing the entire view of the sensor. Overall the most dangerous shift is in the slit position as a shift in less than 1 mm caused the spectral lines to become blurry. The grating was also rotated around the Y-axis by approximately one degree using a washer to offset one side. The resulting spectrogram did not seem to change

Another displacement with potential effect to image was rotation of any of the components which led to rotation and compression of the spectrogram, potentially causing loss of data. A 180 degree rotation of the slit was also seen to have an effect on the image, meaning that the slit probably is asymmetric. Future assembly should therefore take this into consideration.

4.2 Sources of Error

- The back objective assembly had to be removed and reinstalled several times during the course of the test. This could have led to small variations in where the image hit the camera sensor due to the difficulty in installing this component in the exact same way each time. The tightening of the back objective bracket can shift the orientation of the back objective slightly if unevenly tightened across the four screws.
- Fading daylight and clouds over the course of the test could have led to small variations in the exposure of the images.
- The slit is not a press-fit in the slit tube. Due to this it is not certain that the slit is perfectly centered in the optical train. This could limit the size of the image hitting the sensor to a small degree.
- The flange focal distance from the objective flanges to the slit plane is not exactly 17.526mm. There is some deviation to this as shown in *figure 8, section 3.3.1*. This has the consequence of slightly unfocusing the image. However, the deviation is small and can be eliminated with a redesign of the slit tube.

4.3 Improvements to the HSI design

The following points were noted during the assembly process of the HSI prototype
Improvements based on Inspection

- Holes in the cassette back plate should be changed to make additional space for other screws
- A tiny amount of epoxy should be used to hold the gaskets in place inside the grating cassette
- The shroud front had to be filed down, as tolerances to the platform were not defined. However, as the shroud function is to be transferred to the grating, this has no bearing on further iterations.
- Side holes from shroud to platform were difficult to screw due to the tolerances on the shroud
- The shroud back objective hole should have a bigger diameter, i.e give more slack for the objective to fit through. The reason is that with a good fit, the position of the objective becomes determined by the shroud, instead of the groove. With the next version of the cassette with shroud incorporated, the back hole should be like the shroud front hole.
- Keeping the platform brackets level while tightening was difficult. For future assembly, the use of elastomer or metal gaskets should be considered. This way the tightening force can still remain dynamic. Another solution would be to calculate the necessary gap tolerance for desired tightening force
- The slit tube should be redesigned to eliminate the need for spacers and to ensure the proper focal flange distance is preserved. The current design makes it very difficult to properly mount the slit in the right position and requires extensive fiddling with the spanner wrench, the slit tube rings and a caliper.

Improvements based on Spectrogram Results

- The second brass spacer ring should be 1.5 mm in the front lens-slit-collimator assembly mount. The spacer is 0.5 in the current design, however this does not center the slit between the two front objectives. A change to 1.5 mm resulted in a clearer spectrogram.
- The 10.37 degree bend can be changed to 11, possibly 12, degrees based on the results. The image was skewed to the right on the detector, resulting in a cut off of some of the longer wavelengths. Increasing the angle would result in a shift back towards the left side, as there is ample space at the left side of the detector.

5. Conclusion

The assembly of the prototype mainly followed the pre-planned procedure but had to be tweaked slightly at some points. Some difficulties were encountered during the assembly and solutions to these issues were proposed and will be reviewed and implemented in the next design iteration.

The prototype provided a good quality spectrogram after proper tuning of the parts. The lines in the resulting image was in focus and shifted in an expected fashion when imaging different plain colours.

While the effect of changing the distance of the front and back assembly longitudinal in relation to the grating had little impact on the resulting spectrogram, a large rotation of the optical assembly resulted in an equally large rotation of the spectral lines, and should be avoided. However, the prototype is not as prone to potentially mission critical spectrogram shifts from translational and rotational displacement as previously expected based on interviews with Professor Fred Sigernes. This is good news for the mission and proves that the HSI tolerates small component displacements. Larger displacements would still be an issue, but that is less likely to occur. The functional tests gives a good indication of the design being resilient to mechanically harsh environments.

Appendix A: Mk1 Assembly Figures

Cassette Assembly
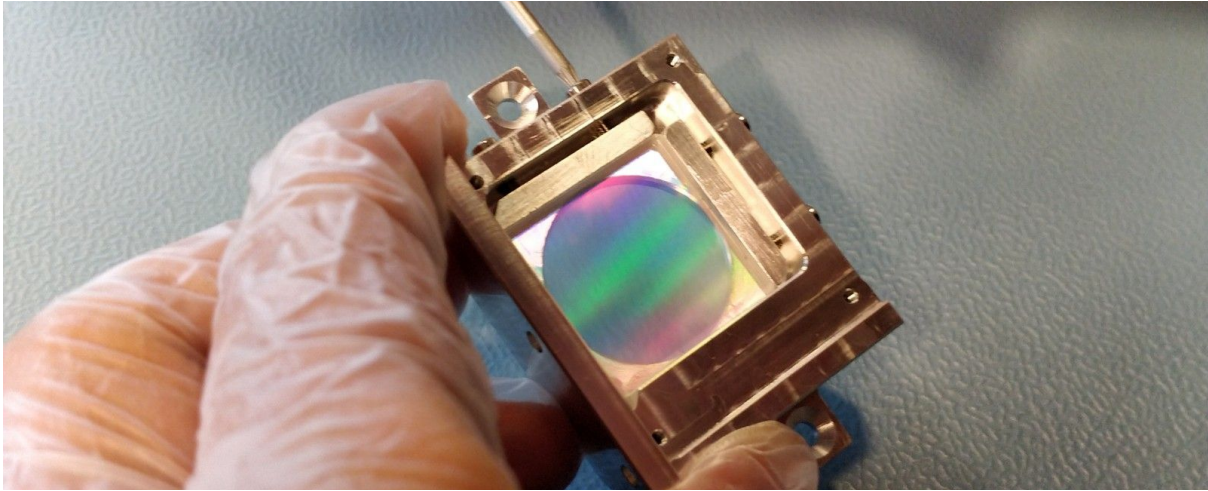
Hand tighten the m2 set screws carefully
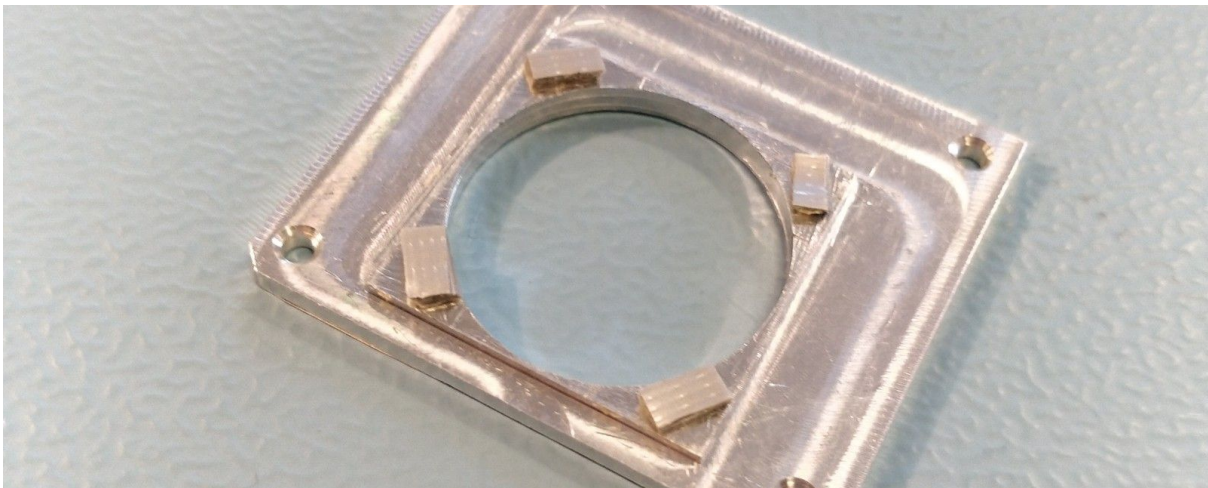
Back plate gaskets (duct tape)

Apply the back cassette plate and insert its four countersunk M2x4 screw
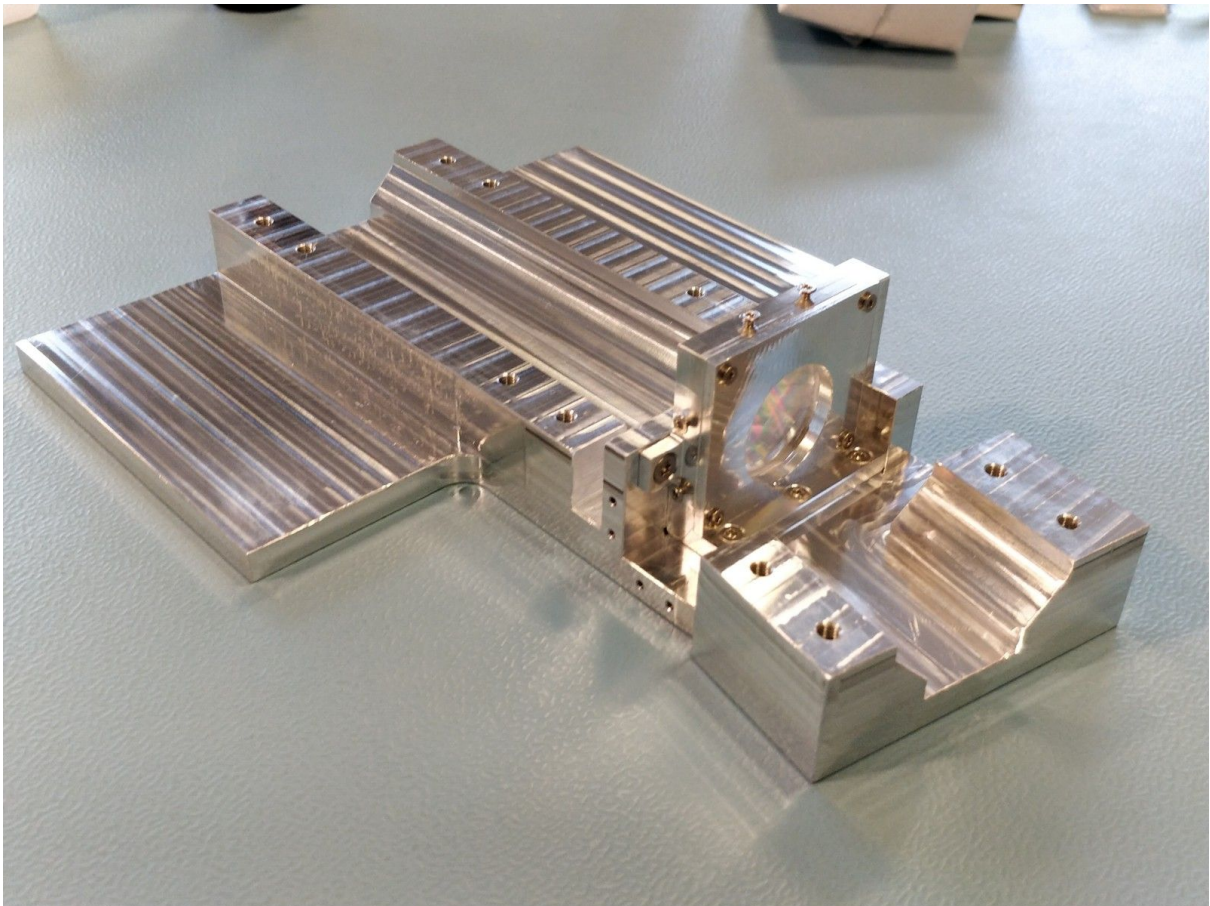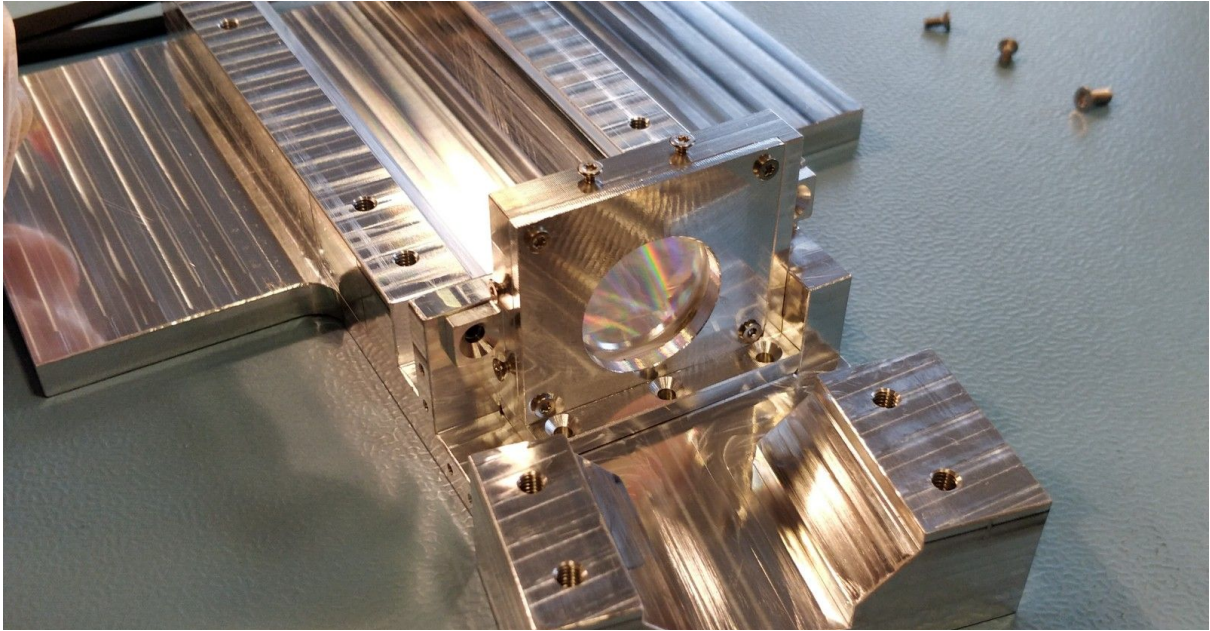
Position cassette assembly on the platform and insert screws

Shroud Assembly
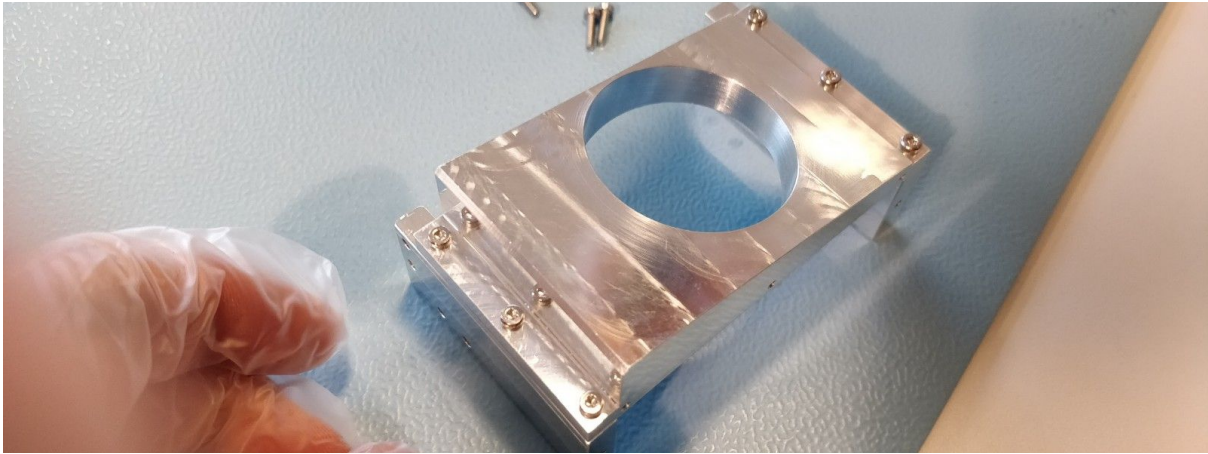
Attach the shroud sides to the shroud back
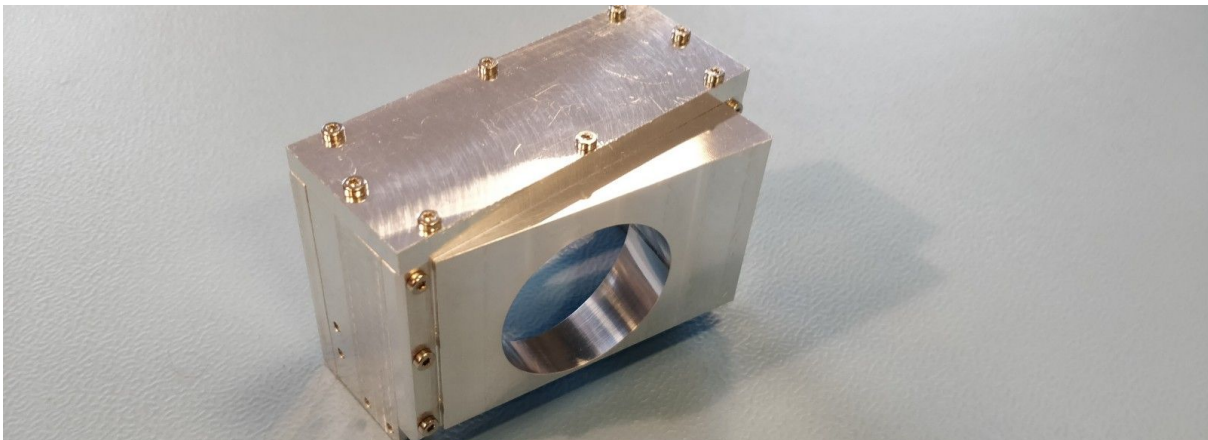
Fasten the shroud top
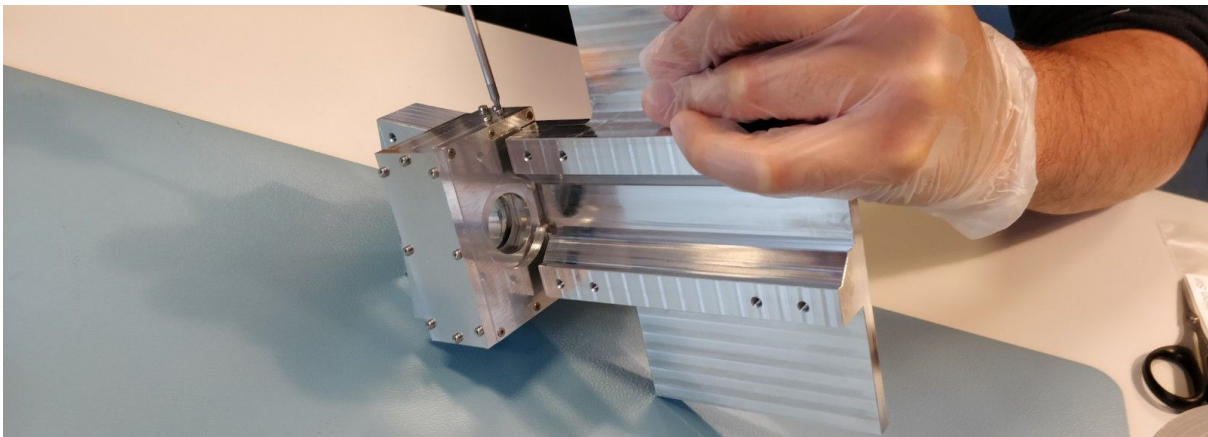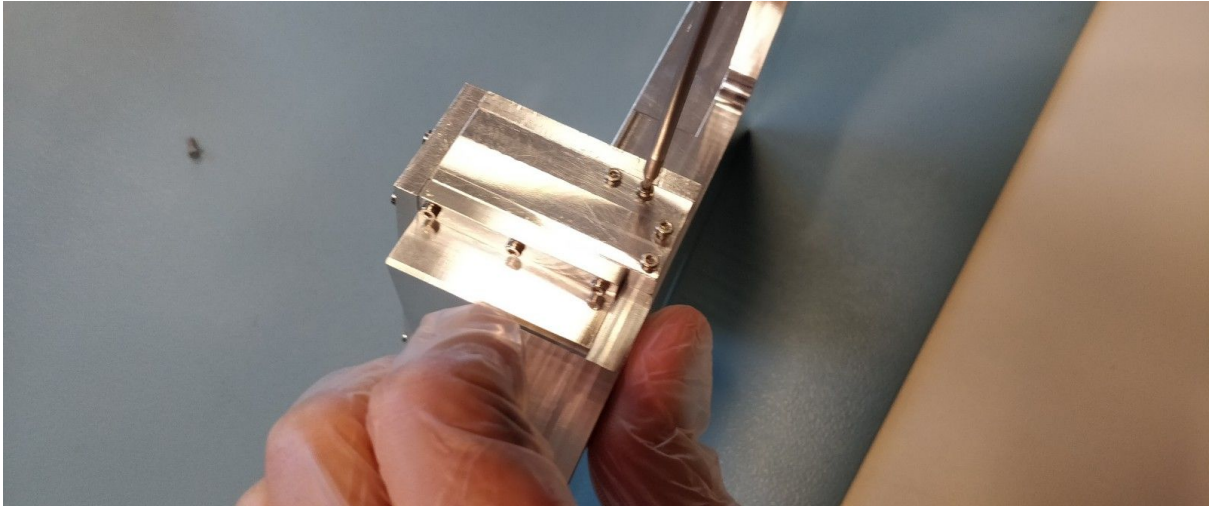
Fasten the shroud assembly to the platform

Objective Assembly

Use a level and fasten the bracket bolts incrementally on the back optics
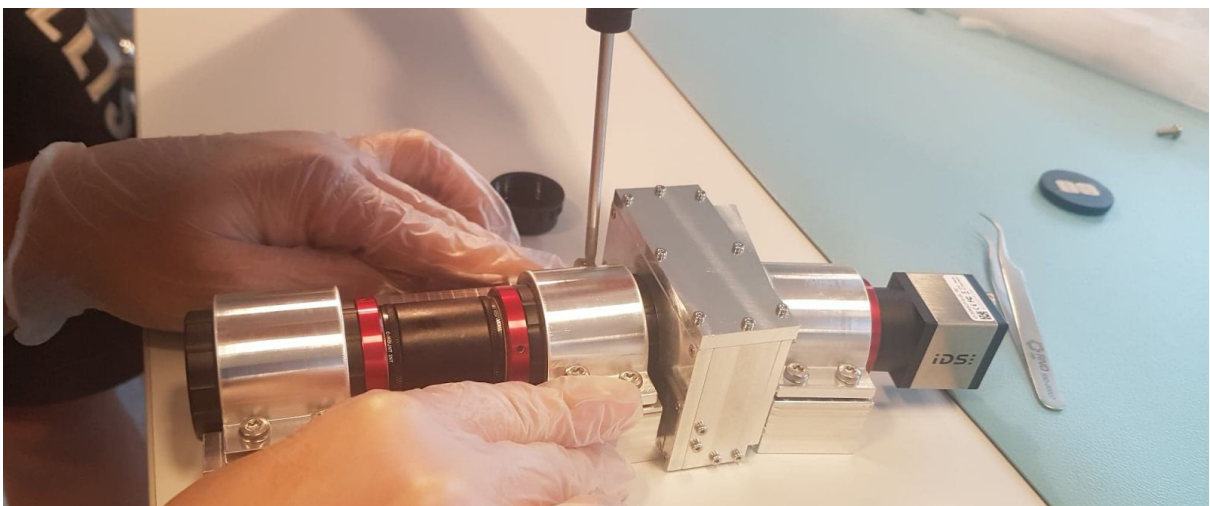
Fasten the brackets bolts incrementally on the front optical assembly

Appendix I

HYPSO-TRP-VAC-001 Vacuum Resilience Test

Vacuum Resilience Test
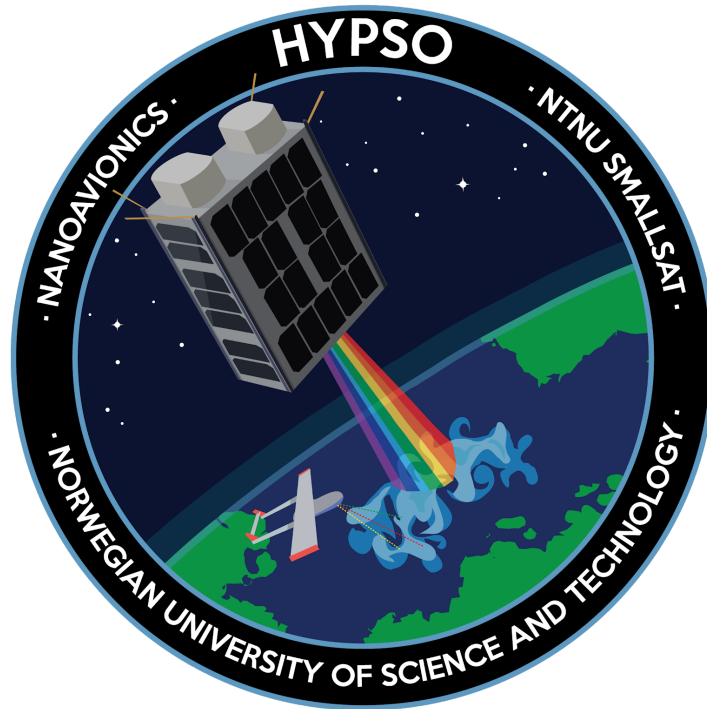
HYPSO-TRP-VAC-001

Prepared by:	HYPSO Project Team
Reference:	HYPSO-TRP-VAC-001
Revision:	3
Date of issue:	25.05.2019
Document Type:	Test Report
Author(s):	Tord Hansen Kaasa, Tuan Anh Tran & Henrik Galtung

Table Of Contents

Table 1: Table of Changes

Rev.	Summary of Changes	Author(s)	Effective Date
1	*First issue*	*Tord Hansen Kaasa, Tuan Anh Tran, Henrik Galtung*	*08.02.2019*
2	*Added info regarding the vacuum induced damage on objective*	*Tord Hansen Kaasa*	*28.02.2019*
3	*Formatting of text*	*Tord Hansen Kaasa, Tuan Anh Tran, Henrik Galtung*	*25.05.2019*

1. Introduction

This report outlines a vacuum test done on COTS optic components. Two items, 50mm lens and detector were subjected to $1.2 \cdot 10^{-1}\,Pa\,(1.2 \cdot 10^{-3}\,mbar)$ pressure over 90 minutes and $1.9 \cdot 10^{-2}\,Pa\,(1.9 \cdot 10^{-4}\,mbar)$ over 60 minutes respectively. The tested items were characterized pre and post vacuum chamber exposure using the standard *Checkerboard Pattern* test, standard *Dark Current* test and visual inspection. The main purpose was to uncover the effect of a low pressure environment on the optical COTS components and test their viability in a near space environment.

2. Method

2.1 Equipment

Table 2 shows all equipment and equipment quantity used during the test procedure.

Table 2: Equipment list

Equipment	#
Compact Arc Melter MAM-1 (Vacuum Chamber)	*1*
50 mm VIS-NIR lenses	*2*
Sony IMX174 sensor (Detector)	*1*
Mass scale	1
Computer with uEye Cockpit	1
Micro USB 3.0 cable	1
Checkerboard calibration pattern	1
Dark room	1
Controllable light source	1
Non latex gloves	-

2.2 Experimental Set-up

Prior to the vacuum test, the optical parts had to be characterized and visually inspected. The characterization process of the lens and detector was done by using the standard *Checkerboard Pattern* test and *Dark Current* test. The characterization test has strict requirements for repeatability, a consistent test set-up had to be constructed. Due to the short time frame available, the set-up had to be made of materials that made rapid prototyping possible. Additionally, the optical parts needed to point from the same distance and position with a high repeatability to ensure usable data. The set-up allowed for high light source control, giving consistent light conditions in all tests. High repeatability and consistent light conditions are imperative for quality data collecting.

The set-up consisted of:
- A cardboard box with a lid for mobility and light isolation capabilities
- A checkerboard pattern printed on an A4 paper
- A 3D printed mounting piece for the optical parts
- A clamp
- A smaller box to lift the optical parts
- A 50mm VIS-NIR lens
- A Sony IMX174 sensor
- Micro USB 3.0 cable
- PC with uEye Cockpit

The front lens was positioned approximately 32.5 cm away from the checkerboard, within the [25 cm - infinity] requirement. The checkerboard pattern consisted of 20mm 14x10 squares printed on size A4 paper. Figure 1 shows the characterization set-up.
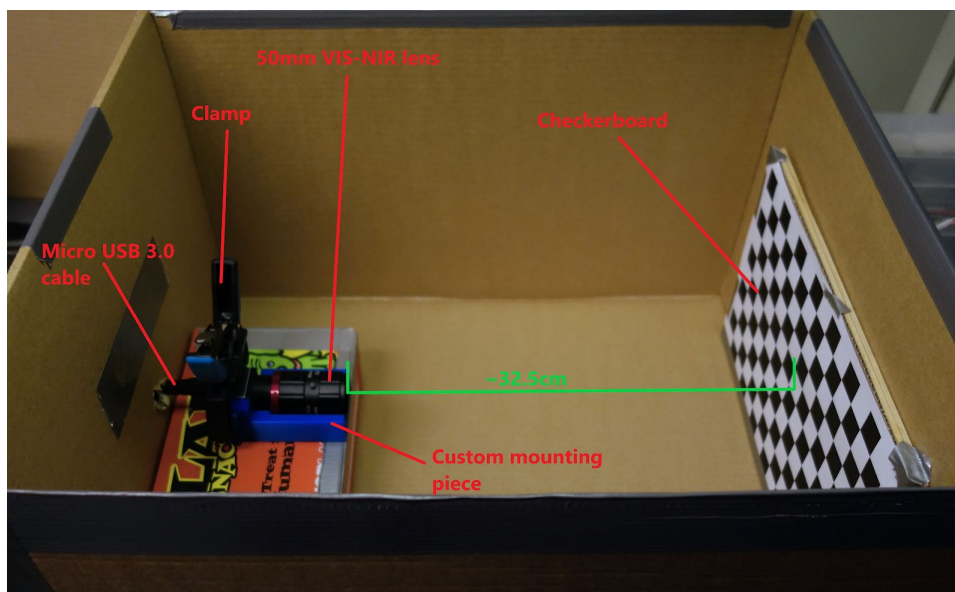
Figure 1: Characterization set-up

The mounting consisted of a 3D printed piece designed with reliable positioning in mind, using three driving surfaces to position the camera sensor, seen in figure 2. An additional clamp made sure nothing would move during testing, shown in figure 1.
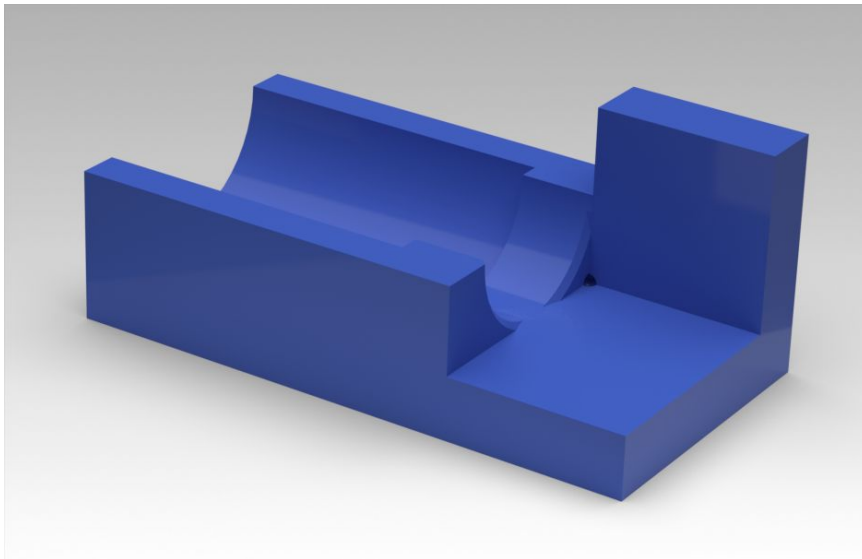
Figure 2: CAD model of the 3D printed mounting piece

The characterization tests were done pre/ post every vacuum exposure test. 5 pictures (.png) were taken per test. All the characterization tests were performed in a dark room, where light conditions could be controlled without the influence of outside light. The *dark current* tests were taken without any form of ambient light, with the exception of laptop screen (which had to be on), other laptop lights, and the green "on"-light located at the back of the sensor. For the *checkerboard pattern* tests, only ambient static ceiling lights were used. Note that the light conditions must be the same for every characterization test. A magnifier lamp desk was present in the dark room. Because of noticeable flickering of the light intensity the lamp had to be dropped.

The #F was set to 2.8 and the focus manually adjusted to get a sharp image of the grid. After the calibration, the #F and focus remained unchanged for the duration of the testing, by tightening the set screws on the lenses. When taking pictures, everyone except one person left the room lowering the chance of light condition changing movement.

A visual inspection was then performed in the same room with the use of the magnifier lamp desk for better lighting. The goal was to detect sources of error or other possible contamination that could affect the parts and their optical properties. This consisted of mainly looking for dust or other particles, scratches and cracks or other deformities.

The following are the settings used in the uEye Cockpit software. Camera image format was set to *Sensor raw 12*. *Gain* and *Black level* was set to 0. *Hotpixel correction* was unchecked. For all the other settings, auto calibration of the camera was turned off. Figure 3 shows the camera settings used. The camera settings were set to an arbitrary exposure value where the only requirement was to make sure no pixel was overexposed. I.e., low exposure was preferred over overexposure.
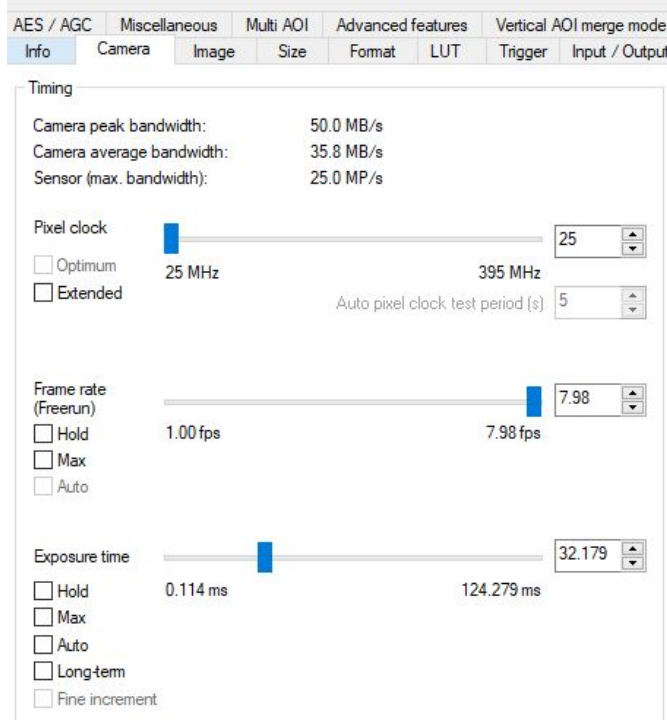
Figure 3: Camera Settings

Figure 4 shows the vacuum chamber used for the vacuum exposure. The specific chamber used was originally designed for material melting under a controlled environment, but it can serve as a normal vacuum chamber by disabling the internal furnace. The volume, leak rate, and vacuum rate of the chamber was given as 1.1 dm^3, less than 1×10^{-6} mbar l/s, and less than 5×10^{-6} mbar l/s respectively.

Figure 4: Compact Arc Melter MAM-1 Vacuum Chamber

The chamber was cleaned using ethanol before securing the 50mm lens. A small cradle of low outgassing aluminum foil was used to secure the lens inside the chamber, keeping it from moving out of place. Figure 5 shows the secured lens.
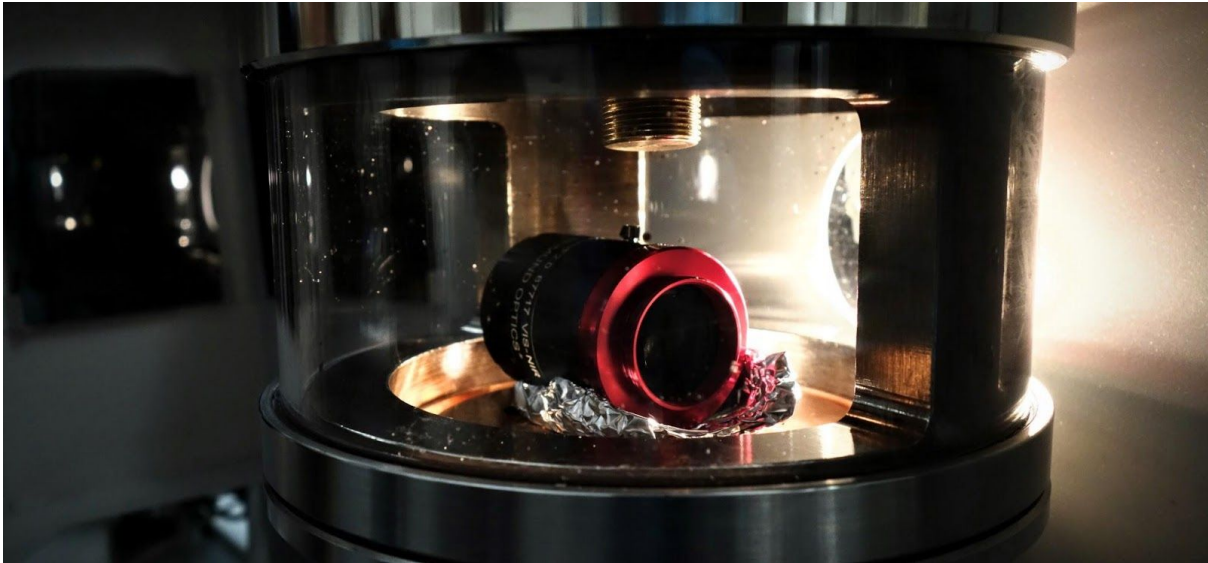
Figure 5: 50mm lens in vacuum chamber

The same cleaning procedure was followed when placing the detector, however the sticker present on the detector had to be removed as to not contaminate the chamber. The remaining glue residue were removed with isopropanol. Figure 6 shows the detector in the chamber.
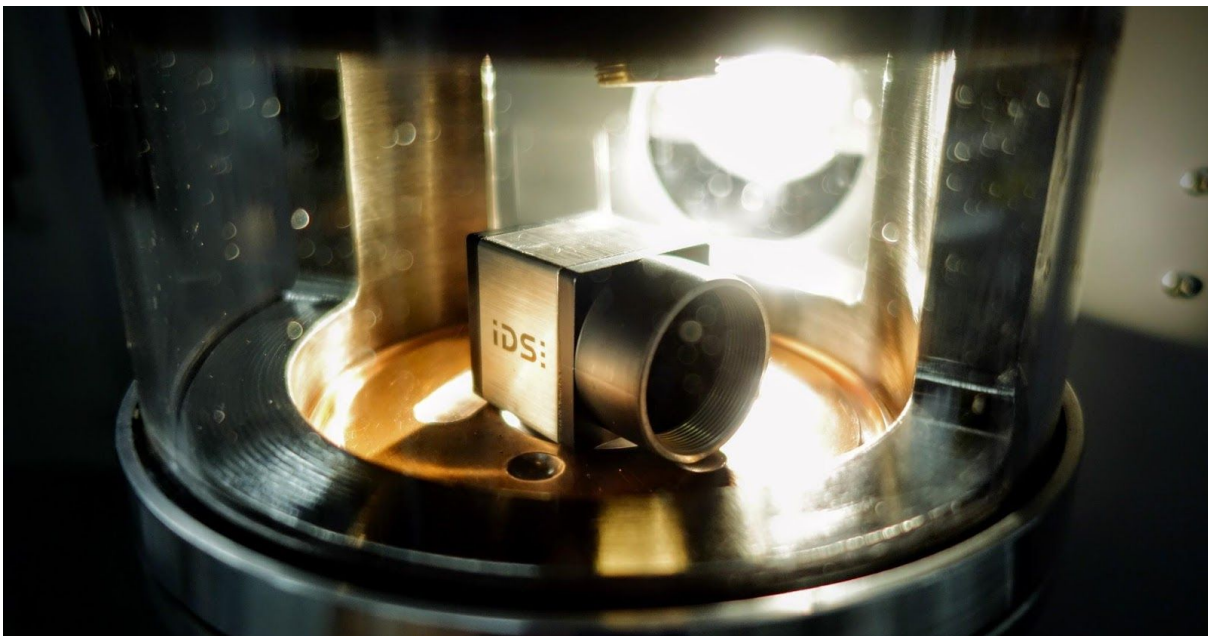
Figure 6: iDS detector in vacuum chamber

The chamber was pumped down to 23 Pa, before isolating turbopump circuit. The turbo pump was activated at the 15 minute mark for the lens test and 5 min for the detector.

To gain more data from the tests, weight measurements were taken before and after each test. This would allow pre- and post-comparison, which could allow possible detection of outgassing. The weight of the tested parts were measured using a Sartorius CP324s scale with precision up to four decimals. This meant that the atmospheric pressure of the room could influence the measurements. Figure 7 shows the weighing set-up. The weighing room was positioned in a smaller room within the vacuum testing lab.
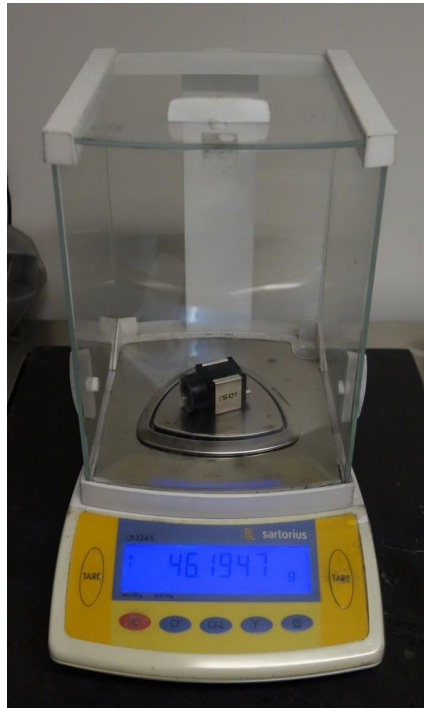
Figure 7: Sartorius CP324s scale

3. Experimental data

3.1 Pressure- Time plots

Pressure data could not be logged from the machine and had to be written down at set intervals of 1 minute for the first 20 minutes of exposure, then every 5 minutes. Figure 8 and figure 9 shows the pressure change over time for the lens and detector respectively.
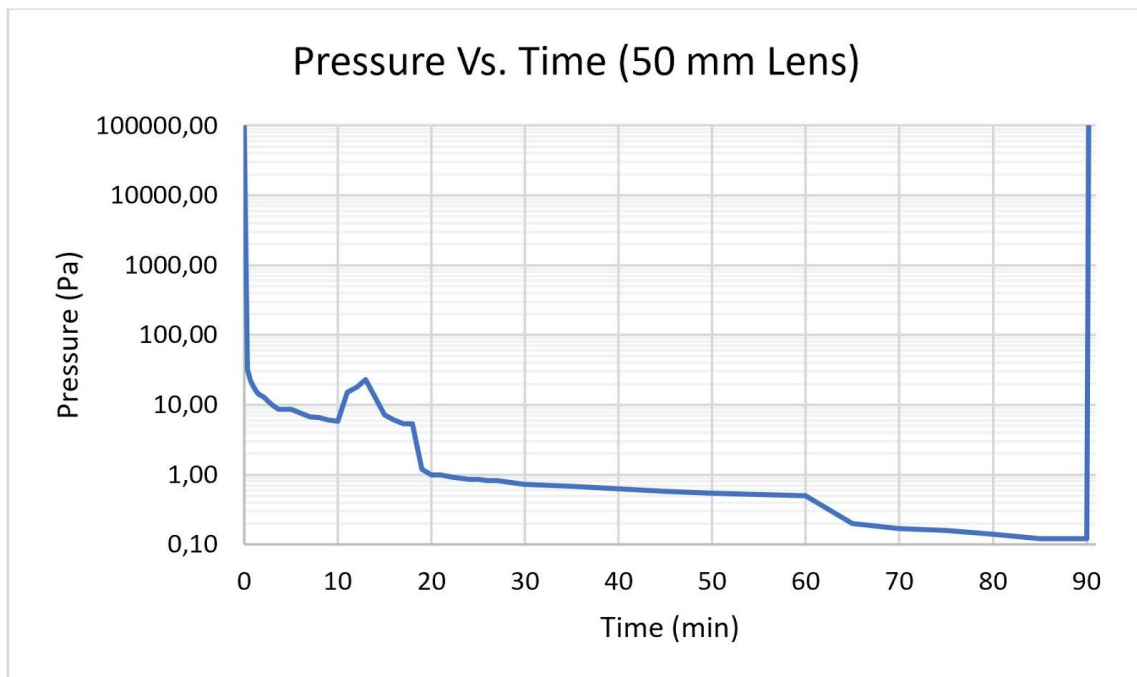
Figure 8: Pressure- time plot 50 mm lens
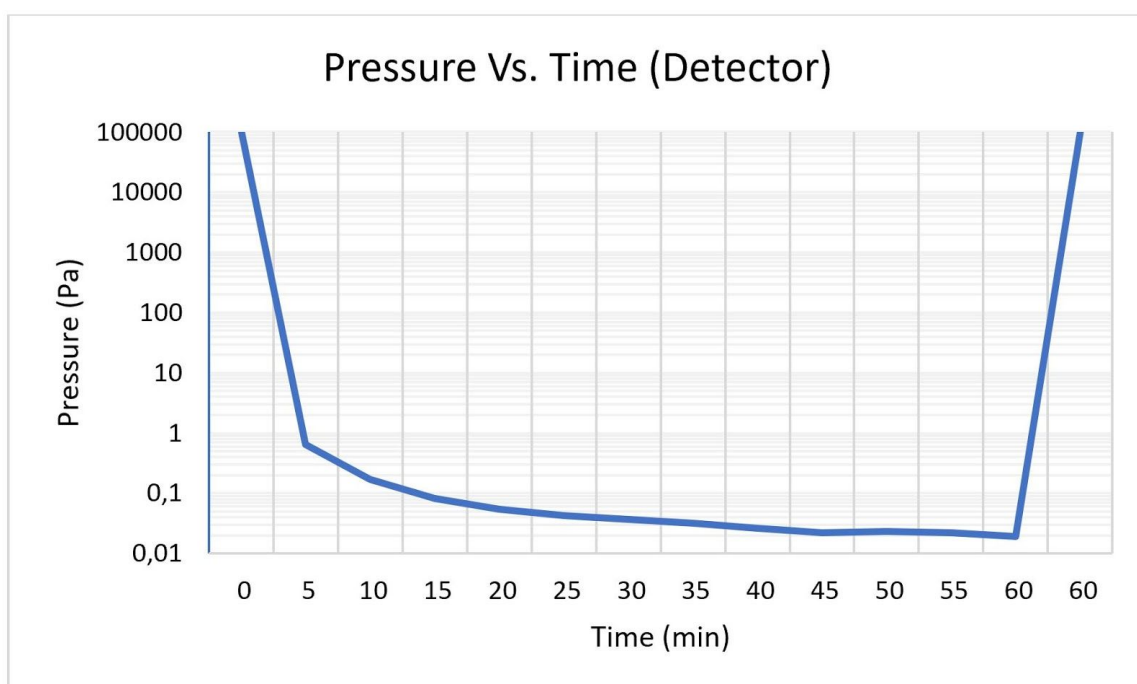
Figure 9: Pressure- time plot detector

3.2 Mass measurements

All the tested components were weighed three times pre and post vacuum chamber exposure. The following values were then averaged to decrease probability and influence of error sources. The resulting values are tabulated in tables 3 and 4 below.

Table 3: 50mm VIS NIR Lens mass measurement

#	Mass pre vacuum test (g)	Mass post vacuum test (g)	Mass loss (%)
1	104.9015	104.8776	-
2	104.9015	104.8778	-
3	104.9015	104.8780	-
Average	**104.9015**	**104.8778**	**0.0226**

Table 4: Sony IMX174 sensor (Detector) mass measurement

#	Mass pre vacuum test (g)	Mass post vacuum test (g)	Mass loss (%)
1	46.1718	46.1691	-
2	46.1720	46.1686	-
3	46.1719	46.1686	-
Average	**46.1719**	**46.1664**	**0.0119**

3.3 Visual Inspection

The following figures were taken during the visual inspection pre/post experiment. Figure shows the front of the 50mm lens pre and post vacuum exposure respectively, figure 11 shows the back side of the lens. Figure 12 shows the detector pre and post vacuum exposure respectively.
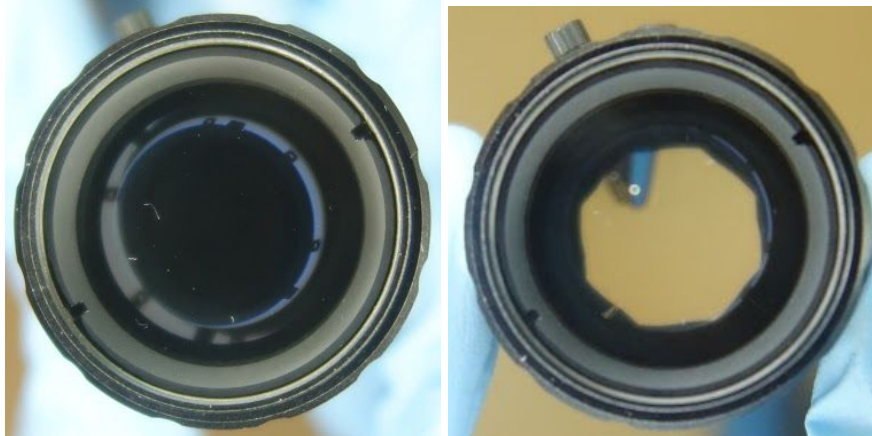
Figure 11: Lens shows no visual change in glass, the color difference was due to the c-mount cap
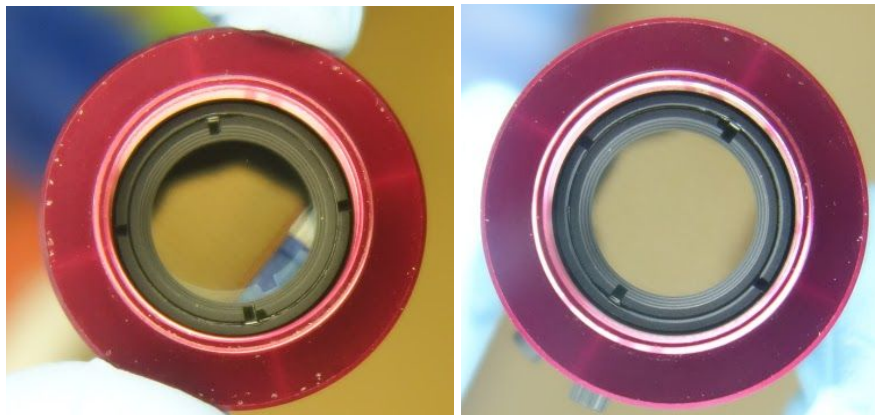
Figure 12: The visual inspection shows no lens cracking nor outgassed residue on the lens
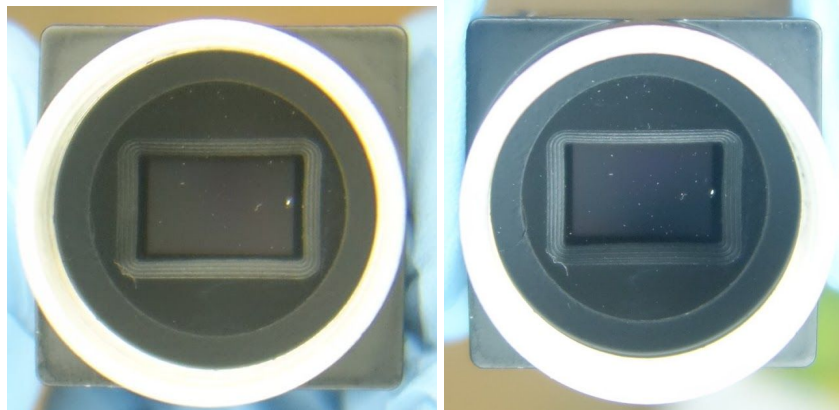
Figure 13: The detector was undamaged by the vacuum exposure

After the general inspection, the front lens of the tested 50 mm lens was inspected more thoroughly to check for eventual outgassing or other problems. Figure 14 shows clear unknown damage occurring on the front lens. The damage was localised on the front lens, no detectable damage was observed on the back lens, nor the detector lens.

Figure 14: Unknown damage on 50 mm front lens

3.4 Checkerboard Pattern Images

Figure 15 shows the resulting images of the checkerboard pattern.

15a: Pre vacuum exposure

15d: Post vacuum exposure (objective)

15d: Post vacuum exposure (detector)

15d: Post vacuum exposure (both)

Figure 15: Before and after vacuum exposure
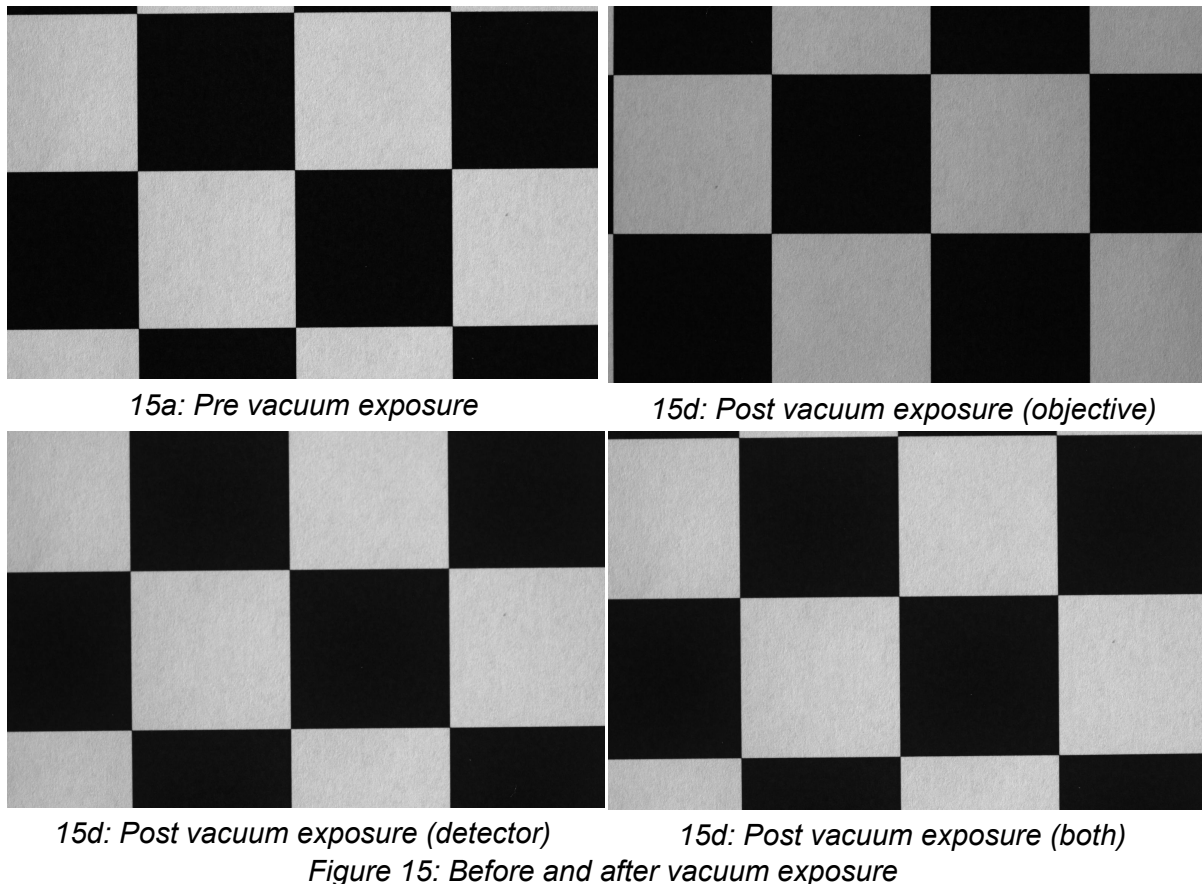
4. Discussion

4.1 Sources of Error

The following list contains the perceived sources of error encountered during the testing procedure and characterization:

- The items were not baked in a controlled owen before the vacuum testing
- Deviation between pressure rates experienced in the vacuum chamber vs a real launch, the pressure rate in lab was to small compared to launch environment
- Difference pressure behavior in the vacuum chamber compared to space
- The chamber could have been polluted by some particles post cleaning
- The test parts could have been polluted due to cleaning restrictions on the lenses
- During the initial test, a light source heated the 50mm VIS NIR lens
- Repressurization of the chamber occurred at a fast rate (15 sec)
- For the detector test, a sticker and some glue had to be removed from the sensor
- Logging of chamber pressure was done manually
- The vacuum chamber was operated manually, switching between pumps and airflow
- Pressure sensor in the chamber needed calibration
- Visual inspection was done with varying light sources and camera settings
- For the dark current test, the camera green light not covered which could have been reflected by the tape inside the box
- Movement of camera as consequence of switching parts between each test
- The repeatability of set-up is deemed as low due to the available time

4.2 Pressure Change Rate

The vacuum chamber available could not simulate the absolute pressure change expected after launch. The expected pressure in a low earth orbit is approximated to be 10^{-8}Pa, while the chamber could deliver at most 10^{-2}Pa, depending on the test item ventilation/ outgassing. Vacuum qualification testing requires the absolute pressure to be below 10^{-5}Pa. Most of this pressure change is experienced over the first moments of the launch, spanning probably over 5 to 10 minutes. Therefore, the rate of pressure change is more interesting than the absolute pressure experienced in the chamber. It was deemed that the pressure delivered by the Compact Arc Melter MAM-1 Vacuum Chamber sufficed for initial testing. Figure 8 and 9 shows the rate of pressure change for depressurization and repressurising of lens and detector. The depressurization rate was measured to be 5048,89 Pa/s and 333,33 Pa/s for the lens and detector respectively. Note that the likely real pressure drop for the detector were closer to the measured drop for the lens. The measured deviation is due to poor plotting of data. The figures shows a near instant repressurization occurring with no throttling or pressure control. The rates were calculated to be 6666,66 and 6666,67 Pa/s for the lens and detector respectively. Due to the relative lack of control in this phase the presented numbers are taken from the least threatening time scale of 15 sec. In reality, the pressure change rate is presumed to be higher, but to an unknown extent. From the tested rates, no damage was detected on the tested items. Therefore it can be presumed that the COTS components can handle the necessary pressure rate changes expected from the launch.

4.3 Item Ventilation

One of the unknowns before the vacuum test, was the capability of air ventilation of the lenses. Based on the pressure behavior of the vacuum chamber during the lens test, one could postulate that the slow air evacuation of the chamber was caused by air escaping into the chamber from within the lens. Other sources that could have caused this kind of behavior are outgassing from either lenses or contamination within the chamber. The air evacuation of the chamber was considerably slower for the lens compared to the detector, taking as much as 4 times longer to reach a pressure of 1Pa, as well as never reaching the same final pressure over a longer time span. The order of magnitude in time difference further strengthens the theory that the lens leaked air out into the chamber, making it more difficult to achieve lower pressures. The source of the air leakage is still unknown, however the lenses has shown their capacity for ventilation even without prebaking.

4.4 Unknown Damage

Figure 14 shows that the vacuum test induced damage on the front lens. Whether the damage was present prior to the vacuum test or not cannot be confirmed due to lacking pre-test inspection. However, because the tested part was new, and fresh out of the box, this is not very likely.

The source behind the damage is currently unknown. The COTS lens build is also unknown, the front lens could be two lenses glued together or one lens, so the exact damage type is also not known. The damage could be decomposition of glue inside the lenses, outgassing of coating or random contamination from the test chamber. The damage seems to be located behind the lens surface, indicating that inner outgassing accumulating on the lens or glue cracking is probable.

4.5 Characterization results

Due to the inconstancy of the checker pattern results as well as the lack of time and competence regarding optical analysis, the results were not analyzed. The pattern can be observed to move between every vacuum exposure in figure 15. This is however most likely a result of the positioning of the camera assembly changing between every test.

There was also captured dark current images, and they were to be analyzed by a separate HYPSO team member. Due to time constraints this was not done. There was a very low probability that the exposure to vacuum would lead to disturbances in the dark current, and such it was not prioritized to characterize these results. There would be no point in using visual inspection for these images as they are pure black to the naked eye. One would need to do a software analysis to figure out any variations from pre- to post-test.

4.6 General Discussion

A vacuum chamber with limited control, without data logging was used to test COTS components. For further testing it will be recommended to use a pressure chamber, going from 2 bar to 1 in a controlled manner or a more adequate vacuum chamber. The results from this experiment is flawed due to the sources of error, however the data obtained is considered of adequate quality to conclude the components pressure resilience. The data and experience gained from the tests also served as valuable information to improve future tests. Particularly the approach to the characterization tests, and the visual inspection. One of the biggest problems with the visual inspections were that there had been no procedure planned. The pictures taken before and after from the visual inspection were taken in different light conditions and with different camera settings. This makes post-analysis more difficult, as proper comparison no longer becomes possible. The inspection must be improved to easier spot changes or damage on items tested.

5. Conclusion

The main purpose of the test was to confirm the structural integrity of the COTS components when subjected to pressure conditions experienced during a launch. Experimental data obtained shows that the COTS components likely will survive the expected pressure changes. The mechanical integrity of the items are adequate for surviving the rapid change in pressure. However, the 50 mm lens experienced unknown damage during the test. This damage can potentially impair the HSI cameras ability to operate properly post launch. The lens was in low pressure (sub 1 Pa) for about 70 minutes. It is unknown if this damage will continue to accumulate at longer exposure times, or at lower experienced vacuum. Further testing must be done to uncover the damage source and damage type. This test must include better characterization tests and clareere procedures.

Appendix J

HYPSO-TRP-VAC-002 Objective Vacuum Damage Report

Objective Vacuum Damage Report

HYPSO-TRP-VAC-002
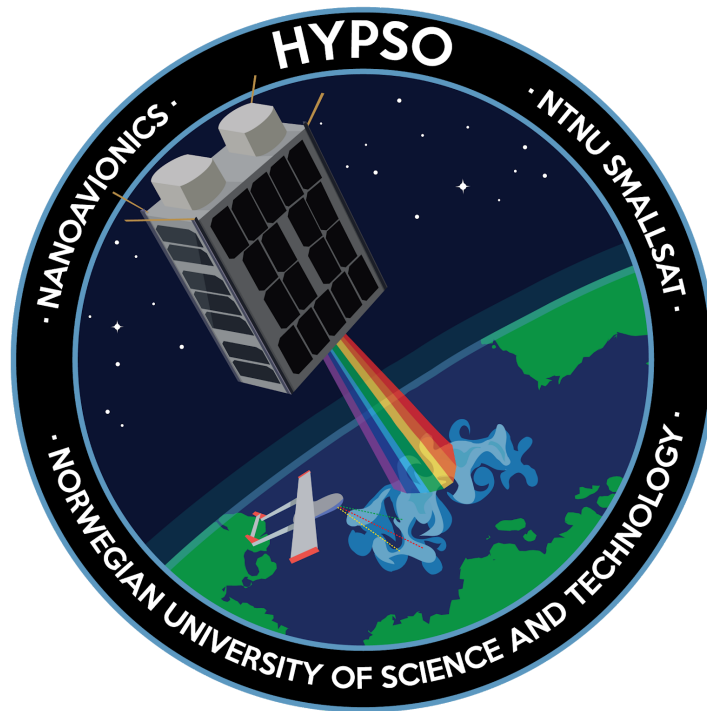
Prepared by:	HYPSO Project Team
Reference:	HYPSO-TRP-VAC-002
Revision:	2
Date of issue:	25.05.2019
Document Type:	Test Report
Author(s):	Tord Hansen Kaasa

Table Of Contents

Table 1: Table of Changes

Rev.	Summary of Changes	Author(s)	Effective Date
1	*First issue*	*Tord Hansen Kaasa*	*07.03.2019*
2	*Formatting of text*	*Tord Hansen Kaasa, Tuan Anh Tran, Henrik Galtung*	*25.05.2019*

Table 2: Referenced Documents

ID	Author	Title
[RD01]	Tord Hansen Kaasa, Tuan Anh Tran, Henrik Galtung.	HYPSO-TRP-VAC-001 Vacuum Resilience test. 2019
[RD02]	Tord Hansen Kaasa, Tuan Anh Tran, Henrik Galtung.	HYPSO-VAC-002 Post Vacuum Objective Disassembly. 2019
[RD03]	Tord Kaasa, Tuan Tran	HYPSO-RP-011 50mm VIS-NIR Objective Disassembly. 2019

1. Introduction

This report outlines the examination of the damage that occurred in a 50mm lens objective exposed to $1.2 \cdot 10^{-1} \, Pa \, (1.2 \cdot 10^{-3} mbar)$ pressure over 90 minutes as elaborated in *HYPSO-TRP-VAC-001 Vacuum Resilience test [RD01].* The unknown damage was observed beneath the front lens. The observed damage can potentially block light from entering the detector, skew the spectrum or cause other unknown effects, barring the HSI total efficiency. The effect will also stack with multiple objectives. From the evidence collected, several options are present such as cracking in film, internal lens fracture, loosening of coating, outgassing of glue or decompression (error source). It is also possible that the damage is a mixture of any of these, as well as something entirely different. *Post Vacuum Objective Disassembly HYPSO-VAC-002 [RD02]* outlines the steps taken to disassemble the unit and the layout inside. The initial microscope screening was done before disassembly, in order to get as much information as possible in case the part would break or suffer unforeseen damage under disassembly.

2. Method

2.1 Experimental Set-up

The objective was depressurised to $1.2 \cdot 10^{-1} \, Pa \, (1.2 \cdot 10^{-3} mbar)$ pressure over 90 minutes (*VAC-001).* The lens objective was observed in a x200 microscope post vacuum exposure. Pictures were taken covering the entire lens surface. Figure 1 shows the microscope set-up.

Figure 1: Microscope Set-up

The damaged lens sample was then further investigated through the use of a swab and tweezers to check the type of damage.

3. Experimental data

There are three lens objectives in series in the HSI assembly. Two are located on the front of the grating, separated by a slit. The third lens objective is located directly behind the grating at an 10.37 degree angle. Each objective is a complex part, comprised of several lenses, coatings, shell and potentially other unknown substances, that be glue, films or grease. When light travels through a lens substrate, about 4 % is lost to scatter by reflection (anti reflective coating included in this figure). During the *Vacuum Resilience Test* [RD01], unknown damage was observed occurring beneath the front lens. The damage will be further elaborated on in this report. The observed damage can potentially block more light, skew the spectrum or cause other unknown effects, barring the HSI total efficiency. The effect will also stack with multiple objectives. However, the cause of the damage is not entirely understood. From the evidence collected, several options are present such as cracking in film, internal lens fracture, loosening of coating, outgassing of glue or decompression (error source). It is also possible that the damage is mixture of any of these, as well as something entirely different.

To uncover further information regarding the damage, the tested objective must be disassembled and inspected. The lens will be separated from the shell and examined properly with a microscope, and possibly sem machine and 3D optical profiler.

3.1 Pre Disassembly Microscope

Figures taken with a 200 times magnifying microscope. Figure 2 shows the resulting composite image taken from the microscope.
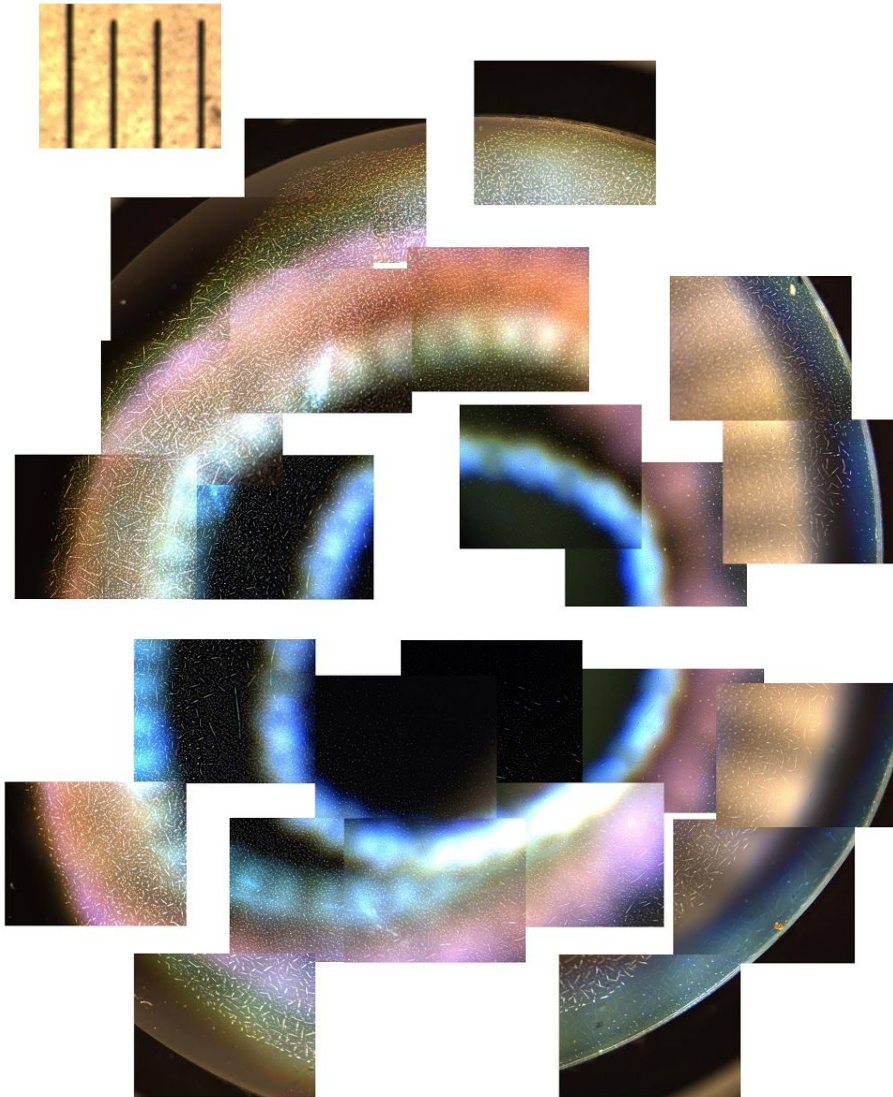
Figure 2: Vacuum induced damage on front lens

3.2 Mass measurements

All the tested components were weighed three times pre and post vacuum chamber exposure. The following values were then averaged to decrease probability and influence of error sources. The resulting values are tabulated in tables 2 and 3 below.

Table 3: 50mm VIS NIR Lens mass measurement

#	Mass pre vacuum test (g)	Mass post vacuum test (g)	Mass loss (%)
1	104.9015	104.8776	-
2	104.9015	104.8778	-
3	104.9015	104.8780	-
Average	**104.9015**	**104.8778**	**0.0226**

Table 4: Sony IMX174 sensor (Detector) mass measurement

#	Mass pre vacuum test (g)	Mass post vacuum test (g)	Mass loss (%)
1	46.1718	46.1691	-
2	46.1720	46.1686	-
3	46.1719	46.1686	-
Average	**46.1719**	**46.1664**	**0.0119**

3.3 Visual Inspection

The damage was localised on the front lens, no detectable damage was observed on any other lenses. The damage was concentrated on the backside of the front lens, as shown in figure 3. The front appeared to be damaged free.
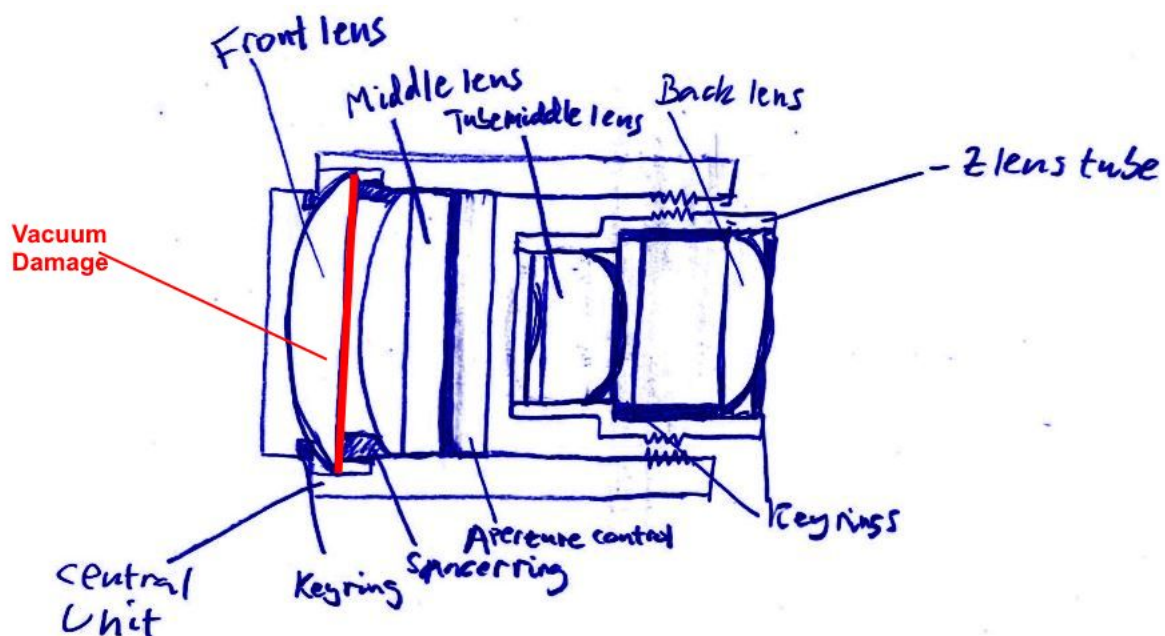
Figure 3: Vacuum damage location

Figure 4 shows the result from introducing a swab to the damaged area. The damage was smeared out. The damage had also evaporated and the damage area grown smaller over a period of 2 weeks.
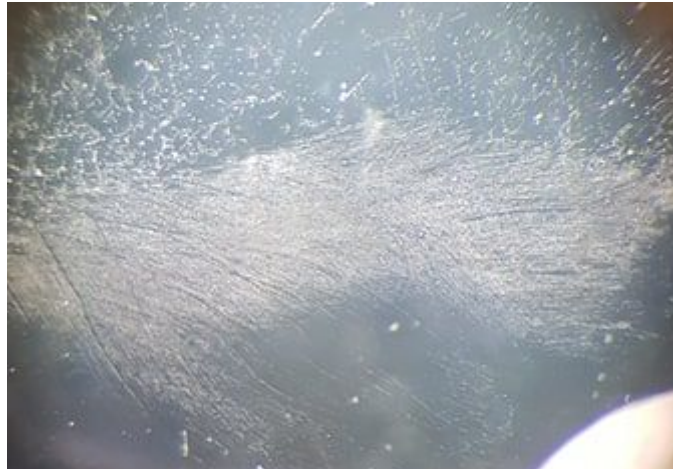
Figure 4: Damage Smear

The damage observed was similar to damage from outgassing contamination. A thorough disassembly of the objective was done and large amounts of grease was observed within the objective. Figure 5 shows on of the greased areas inside the objective.

Figure 5: Grease inside the objective

4. Discussion

4.1 Vacuum Damage

The damage observed was proposed to be either the cracking of an anti reflective coating layer or the result of outgassing from either glue or grease. Based on the pictures taken with the electron microscope, no conclusion regarding the damage origin could be reached. The *HYPSO-RP-011 50mm VIS-NIR Objective Disassembly [RD03]* report indicates that the objectives are full of non vacuum rated grease. Based on the reaction of the damaged area to the introduction of a swab, figure 4, it can be concluded that the damage was dispersed particles, most likely grease.

However it is baffling that the damage was localised on just one lens surface. The entire inside of the objective is full of grease and it would make sense for the outgassed particles to follow the ventilation paths inside the objective due to the air current created during the vacuum pumping process.

4.2 Sources of Error

The following list contains the perceived sources of error encountered during the testing procedure and characterization:
- The items were not baked in a controlled owen before the vacuum testing
- Deviation between pressure rates experienced in the vacuum chamber vs a real launch, the pressure rate in lab was to small compared to launch environment
- Difference pressure behavior in the vacuum chamber compared to space
- The chamber could have been polluted by some particles post cleaning
- The test parts could have been polluted due to cleaning restrictions on the lenses
- During the initial test, a light source heated the 50mm VIS NIR lens
- Repressurization of the chamber occurred at a fast rate (15 sec)
- For the detector test, a sticker and some glue had to be removed from the sensor
- Logging of chamber pressure was done manually
- The vacuum chamber was operated manually, switching between pumps and airflow
- Pressure sensor in the chamber needed calibration
- Visual inspection was done with varying light sources and camera settings
- Movement of camera as consequence of switching parts between each test
- The repeatability of set-up is deemed as low due to the available time

5. Conclusion

The damage experienced on the back of the front lens was due to contamination from grease or glue present inside the objective body. The damage was not surface cracking of anti reflective coating. Additional test must be conducted in order to conclude whether or not this damage is due to the poor vacuum properties of the objective or due to the sources of error present during the test. However, a method for cleaning, and subsequently test the cleaned objectives to be sure of no contamination can occur during operation in space is recommended by the mechanics team.

Appendix K

HYPSO-ANA-009 HSI Payload Mechanical Analysis Report

HSI Payload Mechanical Analysis Report
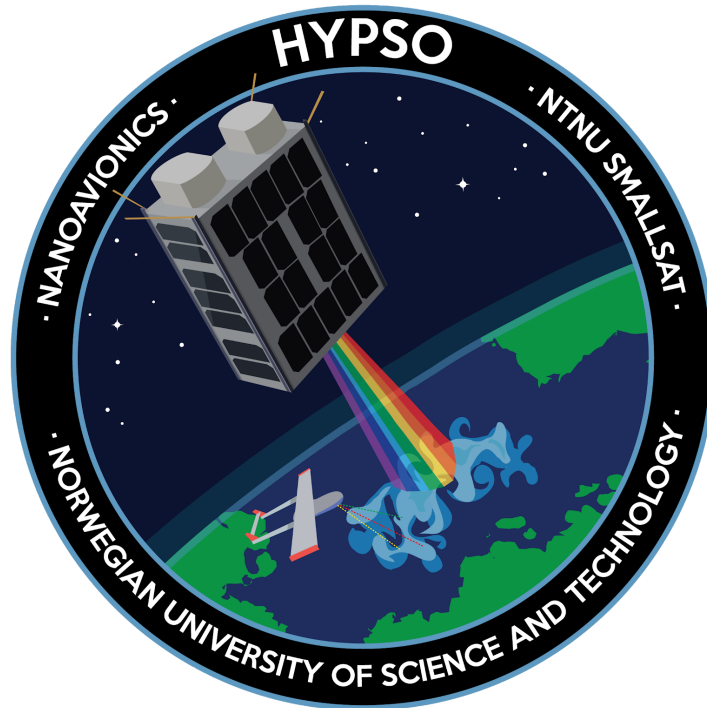
HYPSO-ANA-009

Prepared by:	HYPSO Project Team
Reference:	HYPSO-ANA-009
Revision:	2
Date of issue:	26.05.2019
Status:	Issued
Document Type:	Analysis Report
Author(s):	Tord Hansen Kaasa, Tuan Tran

Table Of Contents

Table 1: Table of Changes

Rev.	Summary of Changes	Author(s)	Effective Date
1	*First issue*	*Tord Hansen Kaasa, Tuan Anh Tran*	*14.05.2019*
2	*Formatting*	*Tord Hansen Kaasa, Tuan Anh Tran, Henrik Galtung*	*26.05.2019*

1. Overview

The HYPSO Mission will primarily be a science-oriented technology demonstrator. It will enable low-cost & high-performance hyperspectral imaging and autonomous onboard processing that fulfill science requirements in ocean color remote sensing and oceanography. NTNU SmallSat is prospected to be the first SmallSat developed at NTNU with launch planned for Q4 2020. Furthermore, vision of a constellation of remote-sensing focused SmallSat will constitute a space-asset platform added to the multi-agent architecture of UAVs, USVs, AUVs and buoys that have similar ocean characterization objectives.

1.1 Purpose

The purpose of the "Preliminary Mechanical Analysis Report" is to describe the structural analysis set-up, assumptions, and analysis results in relation to the relevant requirements, retaining to the HSI payload solution. The mechanical integrity of the simulation subject is expected to be high, based on the results gathered from the previous *Mechanical Analysis Report HYPSO-ANA-001 [*RD01*],* however since the fundamental design has been altered, new simulations have been prepared. The simulations are meant to give a rough estimate of the systems structural characteristics.

1.2 Scope

This document covers the preliminary mechanical analysis of the HyperSpectral Imager payload. The specific payload simulated is the TTH Mk1. A complete description of the prototype including all the components can be found in the *HYPSO-DR-003 HSI Payload Design Report* [RD02]. The spacecraft satellite bus is developed by NanoAvionics, as such they have the responsibility of simulating the delivered system. The simulated payload will not include any potensial dampening solutions. The IMU payload positioning is not yet decided, the simulations can give some indications on were it should be placed. Figure 1 shows the relationship between all the documents.
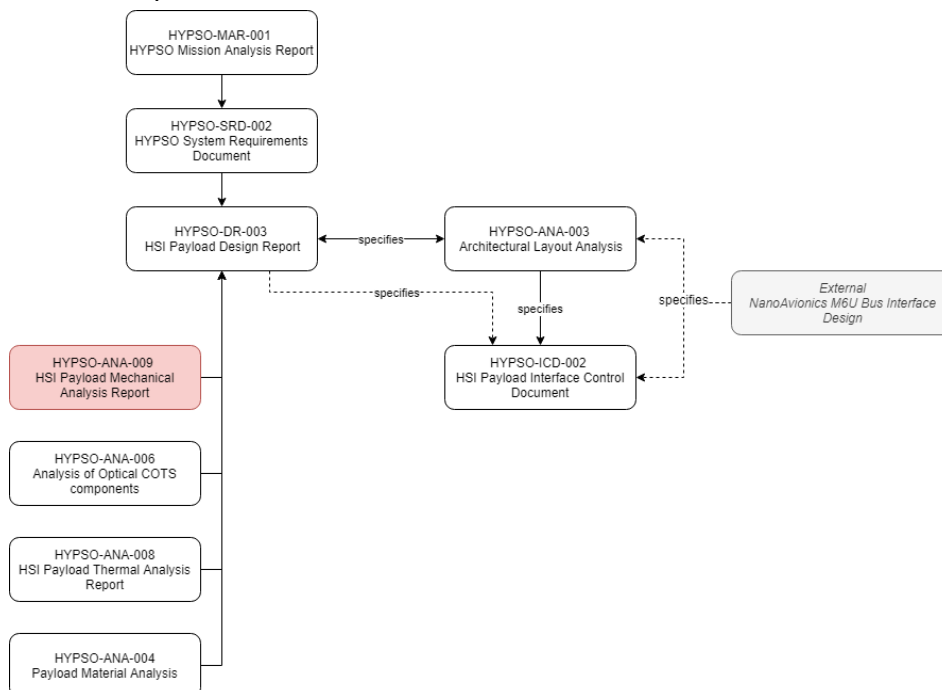
Figure 1: Document relationship

1.3 FEM Description

The finite element method (FEM) is a variation-differential method, which is based on representing an original area with a complex boundary as a collection of simple subareas (finite elements) [RD03]. This approach means that a continuous surface can be broken down into a finite amount of smaller surfaces or elements. This allows for analysis of the elements using underlying mathematical formulations built into the different solvers in the simulation program. NX NASTRAN will be used for all structural simulations.

1.4 Simulation Item

The simulated item a HyperSpectral Imager payload. The payload simulated is the TTH Mk1. Figure 2 shows the HSI payload, while figure 3 shows the payload placement in the bus.
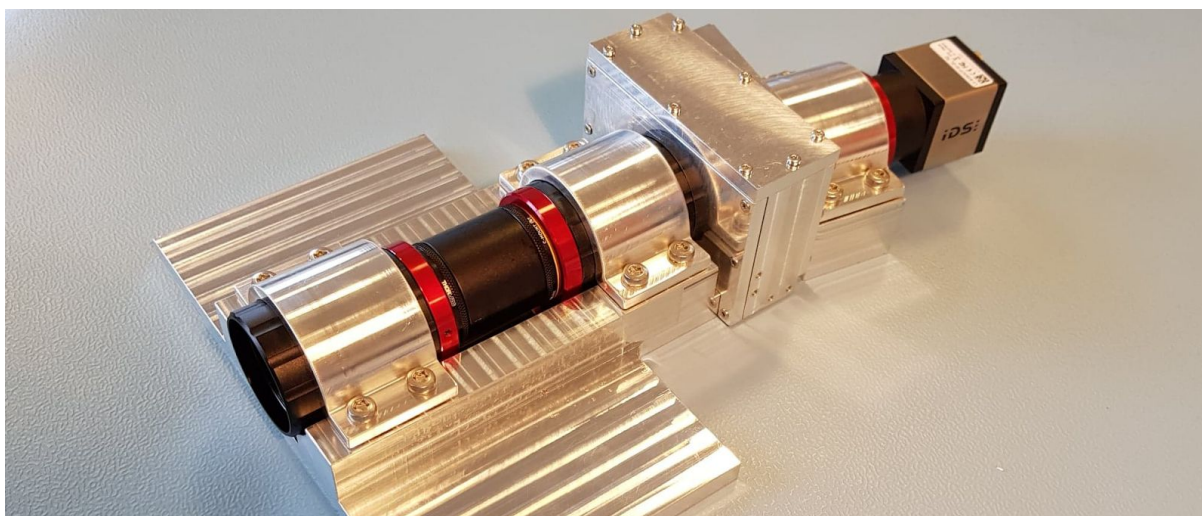
Figure 2: HSI Payload Prototype TTH Mk1, without Star tracker and RGB
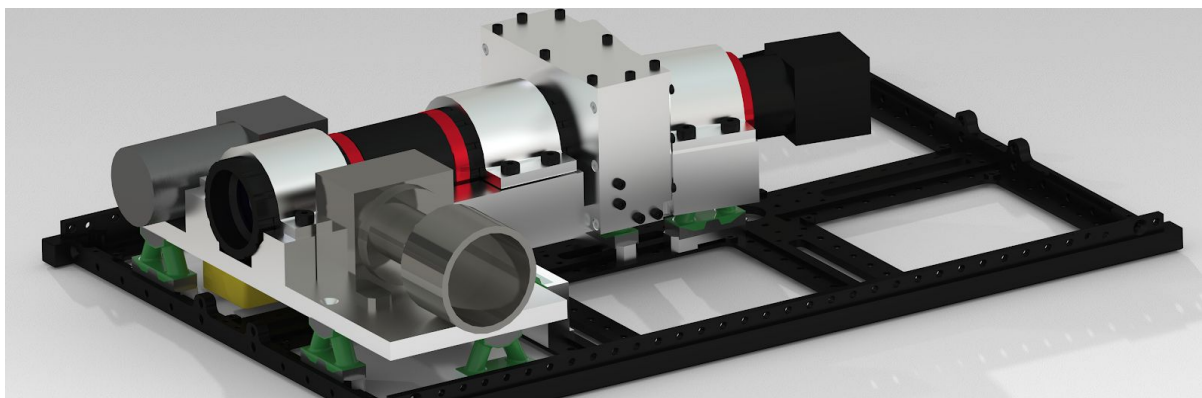
Figure 3: Payload on a 6U CubeSat frame, complying to the ICD

1.5 Referenced Documents

The documents listed in table 2 have been used as reference in the creation of this document.

Table 2: Referenced Documents

ID	Author	Title
[RD01]	Tord Hansen Kaasa, Tran Anh Tran, Henrik Galtung	*Mechanical Analysis Report HYPSO-ANA-001. 2018*
[RD02]	Tord Hansen Kaasa, Tran Anh Tran, Henrik Galtung	HYPSO-DR-001 HSI Payload Design Report. 2019
[RD03]	P. Goncharov, I. Artamonov, T. Khalitov. Lulu Publishing Services.	Engineering Analysis with NX Advanced Simulation. 2014
[RD04]	NASA	NASA-STD-5002. [Link], accessed 2019
[RD05]	Delbert R. Wilson	Vibration Testing for Small Satellites, Boeing Aerospace corporation. [Link], accessed 2019
[RD06]	ECSS	ECSS-E-ST-32-03C Space engineering Structural finite element models. 2008
[RD07]	T. Rølvåg	Finite Element Dynamic Analysis (Unpublished). 2018
[RD08]	M. Hamdi, N. Aifaoui, B. Louhichi, A. BenAmara	Idealization of CAD model for a simulation by a finite element method. [Link], accessed 2019
[RD09]	Mitch Muncy	Autodesk Nastran for Inventor: Unlocking Dynamics. [Link], accessed 2019
[RD10]	Tord Hansen Kaasa, Henrik Galtung	HYPSO-ANA-003 Architectural Layout Analysis. 2019
[RD11]	California Polytechnic State University	6U CubeSat Design Specification, Rev1.0. [Link], accessed 2019

2. Requirements

Based on the information given in [RD04] the following requirements are governing the preliminary design:

"For use in preliminary design, the spacecraft developers shall develop envelopes that bound the accelerations for components. These component load factors may be defined as a function of component weight, frequency range, structural support type, or other variables. The load factors should be based on available flight data, test data, analyses, and experience"

"There are three basic types of flight environments that generate dynamic loads on payload components:

a. The low-frequency dynamic response, typically from 0 to 50 Hertz (Hz), of the launch vehicle/payload system to transient flight events.

b. The high-frequency random vibration environment, which typically has significant energy in the frequency range from 20Hz to 2000Hz, transmitted from the launch vehicle to the payload at the launch vehicle/payload interfaces.

c. The high frequency acoustic pressure environment, typically 31Hz to 10,000Hz, inside the payload compartment. The payload compartment acoustic pressure environment generates dynamic loads on components in two ways: (1) by direct impingement on the surfaces of exposed components, and (2) by the acoustic pressure impingement upon the component mounting structures, which induces random vibrations that are mechanically transmitted to the components.

Combinations of these loads occur at different times in flight and shall be examined for each flight event."

"The resonant frequencies of a structure shall be restricted to specified bandwidths which have been chosen to prevent dynamic coupling with major excitation frequencies (e.g. launch vehicle fundamental frequencies)" Excerpt from ECSS Mechanical — Part 2: Structural.

In addition, when evaluating the results, these factors must be taken into account:

"Resonance conditions must be evaluated on a case by case basis. Generally the higher the frequency the lower the risk of damage as displacement is inversely proportional to the square of the frequency." Excerpt from Vibration Testing for Small Satellites, Boeing Aerospace corporation [RD05].

The mass participation (x, y, z) of a frequency mode, is proportional to the threat level of the mode. A low frequency mode with a large mass participation must be avoided.

Table 3 tabulates the design loads recommended by NanoAvionics for the s/c. The quasi static loads does not include shock. The smallest fundamental frequencies are based on the entire s/c, however since the HSI payload will most likely be a decoupled system, its fundamental frequencies would transfer directly to the s/c as well. Please note that since the CubeSat positioning within the launcher is not known at the time of designing, all requirements are taken as the worst case (longitudinal) for all directions (x, y, z lcs). Table 4 shows other minimum recommended frequencies for the rockets other launch providers.

Table 3: Design Loads from for PSLV, Provided by NanoAvionics

	Static load (g)	**Smallest fundamental frequencies (Hz)**
Longitudinal	11	135
Lateral	6	70

There are several requirements in relation to the launch of the CubeSat. This section will explore the most important load requirements instated by the Polar Satellite Launch Vehicle (PSLV). Load environment values provided by NanoAvionics. All loads must be multiplied with a safety factor of 1.7, in accordance with the documentation.

The longitudinal and lateral loads acts simultaneously. Due to the uncertainties of the CubeSat placement in the launcher, the longitudinal load must be used as the design load for all axis.

*The first fundamental frequency is required to be higher than **135**Hz (230Hz with SF)*
Note: The first fundamental frequency is required to be higher than 70Hz according to PSLV documentation, however due to the lack of information in regards to the CubeSat placement within the launcher, the first fundamental frequency must be the longitudinal stiffness.

Table 4: Minimum recommended spacecraft fundamental structural frequencies [RD03]

Vehicle	**Axial (Hz)**	**Lateral (Hz)**
Ariane 5	27-31	7.5-10
Atlas V	15	8
Delta II (two-stage)	35	12
Dnepr	20	10
Minotaur IV	N/A	25
Proton	25	8.5
Soyuz	35	15
Zenit	20	8

3. Assumptions

All assumptions made shall lead to a worst case scenario and a lower stiffness [RD06]. The Commercial Off-The-Shelf (COTS) components were assumed to not add significantly stiffness to the system but contributing significant mass and was therefore replaced with CONM2 0D elements with the appropriate mass connected to platform groove using rigid RBE2 elements. The RBE2 element is stiff with independent degrees of freedom defined for one node and dependent degrees of freedom defined for several nodes [RD01], while CONM2 is a simple concentrated mass at the node [RD03]. Two CONM2 elements where used per platform side (X direction), with an assigned mass equal to half of the sub system mass, this was done for the front optical assembly, front brackets, detector and detector objective assembly and back bracket. The mass distribution has been assumed homogeneous. The mass center of the CONM2 elements were set to be at the geometrical center of the COTS components in the Y and Z directions. The star tracker, IMU and RGB were also replaced with CONM2 and RBE2 elements that connected to the corresponding area of the platform, the mass center of these components were also placed at the geometrical center of the components.

To simulate the stiffness the brackets would add to the assembly, CBUSH elements where used situated between the RBE2 element master node. The CBUSH element is a generalized spring-damper structural scalar element that is used to connect two non coincident points [RD03]. The x and y directional stiffness of the brackets were calculated based on the simple finite element analysis (FEA) cantilever beam equation, one side bolted down (0DOF), while the other side can not rotate. The length of the beam was estimated to be the length of the bracket in the x and y directions respectively. The calculation should be a conservative estimate of the bracket stiffness, refer to section 5.2 for more details. The M4x10 bracket bolts were not simulated, as each bracket uses a total of 4 bolts resulting in a stiff connection, therefore the bracket-objective-platform grove was approximated as perfectly stiff RBE2 elements. This assumption had to be done in order to reduce the complexity of the simulation, a simulation using more realistic interfaces are out of the scope of this simulation and should in addition not change the report conclusion to a significant degree.

The HSI payload was simulated without a shroud assembly, designed for blocking light from entering the grating. The grating cassette designed to confirm to the HSI platform and secure the grating is slated to incorporate the shroud functionality and block stray light in further updates. On the basis of this fact, the shroud assembly was omitted from the simulation. The shroud placement is on a surface that has little excitation, the omission should not affect the result to a significant degree.

The mass of the COTS components where estimated based on measurements taken in the lab [RD02]. The connectors and adhesives used where estimated to add 10 % weight to the CONM2 elements. This should be an upper estimate of the mass, and is considered a worst case.

The dampening effects of the interface dampeners are not known, as the specific bushings are not chosen yet. It is known that the bushings will lower the eigenfrequencies of the payload. It is expected that the eigen frequency of the HSI payload will be lowered, based on the viscoelastic properties of the dampeners, the amount of dampeners, and the placement of the dampeners. Previous simulations were run using a 4 % reduction in frequencies due to the viscoelasticity, however due to the uncertainty surrounding the dampener solution, no viscoelastic reduction has been applied to the simulation system.

The bus was taken into consideration as a completely rigid body when simulating the preliminary interfaces. This, however, is not a realistic case, as the bus structure will be prone to system modal deformation. The bus structure will in reality not exhibit the characteristics of a completely rigid body, however this should have little bearing on the HSI payload.

The IMU placement is not yet decided, however it seems to make sense to place it underneath the grating area of the platform based on the preliminary simulation results as seen in section 8.1. The grating area (the middle of the platform) does not show large excitations. If the placement of the IMU changes, new simulations should be initiated to reflect the movement of mass.

4. Method

4.1 Simulation scope

Preliminary simulations will focus on the payload prototype integrity. The base payload will be simulated first to establish a frequency baseline. Then additional elements will be added as to ensure the stability of the simulation.

Modal

Simple eigenfrequency analysis of the HSI Platform with increasing complexity added to the model.

Case 1: Simulation of HSI Platform
Case 2: Simulation of HSI Platform, all optical parts and brackets added
Case 3: Simulation of HSI Platform, all optical parts, brackets, star tracker, IMU and RGB added
Case 4: Simulation omitting the IMU due to the fact that the placement is not decided

Quasi-static

Acceleration of HSI Platform based on static design loads from NanoAvionics specified in table 3 in longitudinal and lateral directions at the same time. The design loads were multiplied with a safety factor of 1.7, yielding 18.7G longitudinal and 10.2G lateral. Gravity was incorporated as 1G in the opposite direction of the longitudinal direction.

Case 5: Acceleration of HSI platform with Z-axis as longitudinal and Y-axis as lateral
Case 6: Acceleration of HSI platform with Y-axis as longitudinal and X-axis as lateral
Case 7: Acceleration of HSI platform with X-axis as longitudinal and Z-axis as lateral

The following simulations should be run:
- Modal
- Force response (frequency)
- Force response (random vibration)
- Force response (transient/shock)

Due to time constraints, it has been decided that only a modal and quasi-static analysis will be run at this time. The required setup, boundary conditions and loads will be included for all mentioned simulations. In addition, force response are encouraged on CubeSats carrying highly sensitive equipment. Physical tests done on a functional prototype will be used to test for shock in addition to validate the modal analysis.

4.2 Solver approach

NX operates on different solvers depending on the specific simulation case. Identifying the right solvers to use for the HYPSO mission is therefore necessary to be able to provide acceptable results. NX has a large assortment of solvers, some of them overlapping in terms of usability and function, but all providing differing inputs and outputs. Dynamic cases are favoured compared to static ones as a result of the vibrational forces experienced under launch are better described as a function of time [RD07]. Modal and force response simulations will be done using NX.

Preliminary simulations will be carried out strictly with linear solvers. Linear solvers will not be able to calculate plasticity and body interaction [RD07]. Dampening of the payload will needed to some extent, therefore nonlinear solvers shall be explored later in the design process. Table 5 shows potensial dynamic solvers, and the associated result type. Solvers marked in green were chosen for the preliminary simulations. Solvers in red were discarded.

Table 5: NX Solvers

DYNAMIC SOLVERS		
Modal		
Solver	**Damping (Y/N)**	**Result type**
SOL 103	No	Real eigenvalues
SOL 107	Yes	Direct complex eigenvalues
Forced Response (Frequency)		
Solver	**Linear (Y/N)**	**Result type**
SOL 111	Yes	Modal frequency response
SOL 103 RS	Yes	Modal frequency response
SOL 108	No	Direct frequency response
Forced Response (Transient/Shock)		
Solver	**Linear (Y/N)**	**Result type**
SOL 103 RS	Yes	Modal Transient Response
Quasi Static Solver (Not Dynamic)		
Solver	**Linear (Y/N)**	**Result type**
SOL 101	Yes	Static Analysis

SOL 103RS or SOL 103 Dynamic Response has been chosen as the preferred solver to run all force response analysis due to the fact that all necessary data and functions is included in the user interface. SOL 103RS is a modal solver, this means that instead of solving all coupled equation related to the response, only simplified equations related to the modes that have the highest mass participation in the simulated direction will be solved, thus shortening required simulation time [RD07]. The downside is more manual work with choosing the adequate modes and some loss in accuracy depending on the total mass participation included. A rule of thumb is to include over 85 percent mass in order to have decent accuracy, more should be included to improve the simulation results [RD07].

4.3 Material and Mass Properties

Table 6 tabulates the material data for the HSI payload. All material data exported from the CES EduPack 2018 database to NX. Table 7 tabulates the estimated mass of all components. Note that the slit tube assembly consists of the slit tube, slit, two spacer rings and 2 threaded connectors.

Table 6: HSI materials

Material Properties			
Material	**Density, ρ (g/cc)**	**Young's modulus, E (GPa)**	**Yield Strength, σ_y (MPa)**
AA 6016-T6	2.6998	69.479	210.39
AA 6082-T6	2.6998	71.92	259.23
AISI 303	7.9696	195.97	238.64
B270	2.5500	71.5	30 (Breaking)

Table 7: Payload Mass

Mass Properties		
Component	**Mass (g)**	**Adjusted Mass +10% (g)**
HSI Platform	723.18	NA
Platform Bracket	29.53	32.483
50 mm VIS-NIR Objective	106	116.6
IMX249 Detector (UI-5261SE)	50	55
Slitt Tube Assembly	25	27.5

5. Finite Element Model

For the initial simulation, the TTH Mk1 prototype is going to be analysed. For this simulation, a mockup model of the payload was used, with a precision within 1 mm. When taking other unknown factors and sources of error into consideration, this precision is acceptable. The current model analysed is not the finalized version. Some modifications that change the mechanical behavior has been made. An example of this is the grating bracket redesign and the slit tube redesign. However these redesigns should have no significant effect on the results as explained in section 3.

5.1 Idealization

The model must be simplified in order to avoid complications, and made to make the underlying mathematical model work. In addition, removal of such geometrical details save simulation time while not affecting the quality of the result [RD08]. The following actions have been taken using the idealization tool and synchronous modeling approach:

- All bolts and screws are removed, bolt and connector mass added as a 10% increase in COTS component mass
- Objectives removed, replaced with CONM2 and RBE2 elements
- Detector removed, replaced with CONM2 and RBE2 elements
- Brackets removed, replaced with CONM2 and RBE2 elements
- Star tracker, IMU and RGB removed, replaced with CONM2 and RBE2 elements
- All inner blends chamfers etc. were removed
- All small features and troublespots removed
- All holes on the platform were removed
- Faces with multiple bends etc. were made into simple flat faces

To simulate the stiffness of the lenses, RB2 elements could be used. These behave as infinitely stiff connections between faces or edges of the model [RD03]. Adding the lenses would only stiffen up the payload and since the model is already stiffer than the real camera, this was not deemed necessary.

To use idealized geometry, all faces on the platform had to be joined. This allowed for easy removal of holes and blends. Figure 4 shows the platform before and after the idealization process.
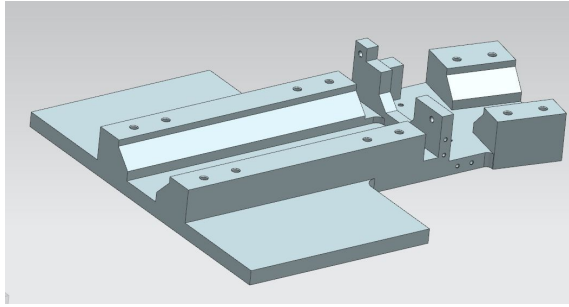
3a:
HSI Platform pre idelization
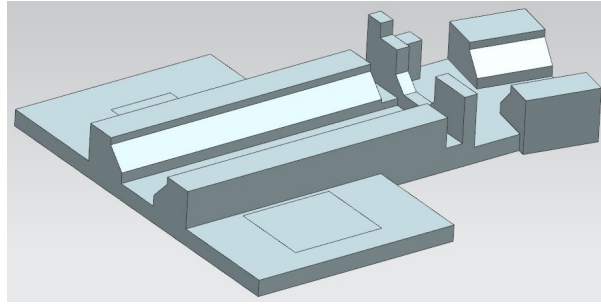
3b:
HSI Platform post idelization

The mass of the platform changed due to the idelization from 723.18G to 726.05G, a rise of 0.4%. The idelization should therefore not stiffen the platform, but decrease the stiffness by an insignificant margin.

The star tracker and RGB were replaced with CONM2 and RBE2 elements that connected to the measured geometry of the components, 29x29mm and 42x36 for the star tracker and RGB respectively. The IMU estimated to be 44.8x38.6mm, was centered in the X-axis of the platform, 115mm from the +Z front in the Z-axis at the bottom of the platform. The connected areas were placed 2mm from the platform inner edge due to machining tolerances, worst case. The platform face was partitioned with the divide face tool using a simple sketch as the dividing object. Figure 5 shows the distribution of the CONM2 elements with the RBE2 connectors and the CBUSH stiffness elements.
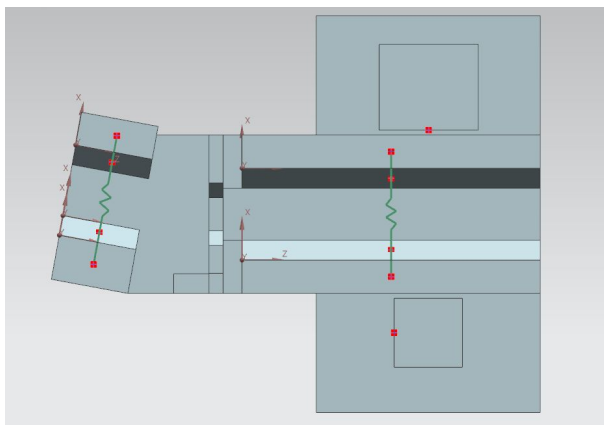
Figure 5a:
CONM2, RBE2 and CBUSH Element placement on the platform front, in addition to the measured geometry of the star tracker and RGB. Note that the LCS for the -Z CBUSH was made do coincide with the geometry of the geometry of the platform
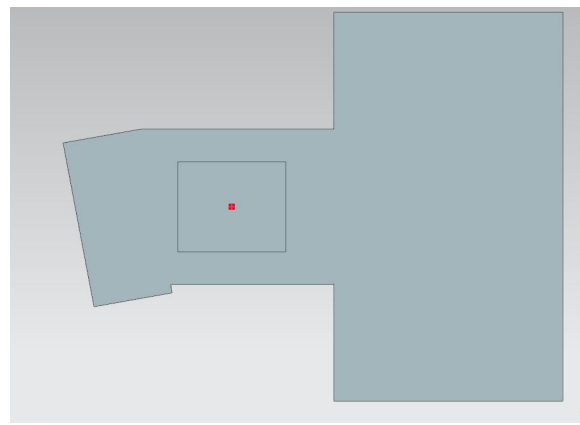
Figure 5b:
CONM2 element placement and estimated geometry of IMU. The IMU placement is preliminary, and could change in further iteration updates

The idealized mass of the components and the described offset from edges of the HSI platform face are tabulated in table 8.

Table 8: CONM2 masses and offsets

Component	Location	Offset X,Y,Z (mm)	Adjusted Mass (g)
HSI Camera			
Back optical assembly	Back groove	0, 10.24, -19.19	171.6
Back bracket	Back wall top	0, 0, 0	33.0
Front optical assembly	Front groove	0, 10.24, 0	260.7
Front bracket (2)	Front wall top	0, 0, 0	66.0
Payloads			
RGB Camera	-X wing	0, 14.5, 36.9	119.9
Star Tracker	+X wing	41, 20, 0	108.0
IMU	Under platform	0, -10.75, 0	57.2

5.2 Finite Element Model Mesh

All mesh and associated mesh data can be found in table 9. Note that the only meshed geometry is the HSI platform. To make sure that all plate thicknesses had more than two elements in between, the *Minimum Two Elements Through Thickness* setting was checked. *Element Quality* check was used to make sure that no errors or failed elements were present in the mesh. The total number of elements and nodes for the mesh was 60275 and 98982 respectively. Figure 6 shows the fully meshed platform.

Table 9: Mesh Data

Mesh HSI Dummy (PDR)				
Body	**Mesh Type**	**Element Type**	**Element Size (mm)**	**Material**
HSI Platform	3D Tetrahedral	CTETRA (10)	3	AA 6082
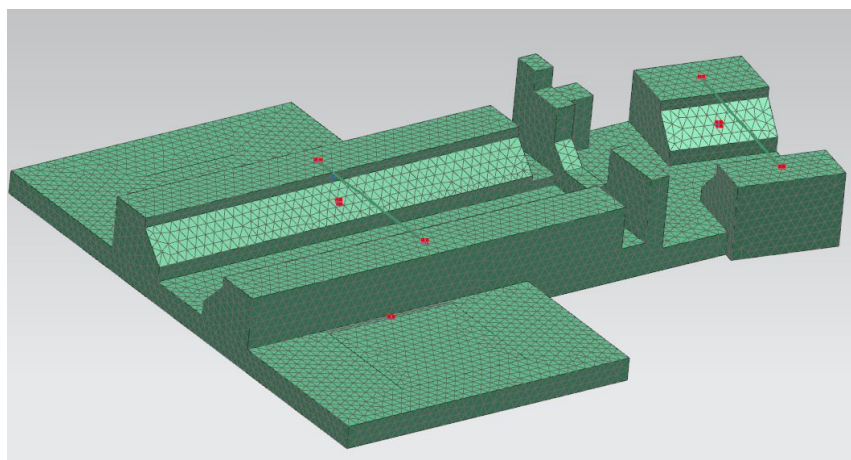
Figure 6: Platform mesh, 3mm CTETRA 10

The brackets were simulated using 1D CBUSH elements with a calculated stiffness as described in section 3. The stiffness used for the brackets in back groove was calculated using the beam equation for stiff beams as described in section 3:

$$k = \frac{12EI}{L^3}$$

Where k is the beam stiffness, E is the Young's modulus of the material, I the second moment of inertia, and L the length. I was simplified to a rectangular shape, and could thus be calculated with the following equation:

$$I = \frac{wh^3}{12}$$

Where h is the height of the beam in the bending direction along the beam axis, and the width of beam perpendicular to the height. The distance between each bolted side of a bracket, bolted side to bracket top and bracket width was measured to be 35.9mm, 23.0mm, and 32mm respectively. The cross-section thickness was measured as 4mm. For the Young's modulus, the values for AA6082 from table 6 were used. Inputting these into the equations using correct axis orientations, the stiffness was calculated to be in the 12114 N/mm X-direction and 3185.71 N/mm in the Y-direction. The same stiffness multiplied with two was used at the front brackets, assuming that they represented two springs in parallel.

5.3 Simulation Objects

Due to the omission of all other components, in addition to the simplistic nature of the HSI platform interface solution, no simulation objects were added to the simulation model.

6. Boundary conditions and load cases

6.1 Boundary conditions

The modal analysis has no boundary conditions however, should a response simulation be made, the following boundary condition was applied to the base of the fastener brackets:

Fixed in all six degrees of freedom (DOF), except the relevant axis movement. Three different simulation had to be run, one for each axis ie. the X-axis, the Y-axis and the Z- axis. To simulate a fully fixed payload to bus interface all DOF where fixed. The shall be applied in each of the corresponding axes, table 10. The fixtures should be placed on the bottom of the platform, for a more realistic approach, holes corresponding to the bus interfacing locations could be used as the anchor faces for the fixtures.

Table 10: Constraints

Degrees of Freedom	Load in X-direction	Load in Y-direction	Load in Z-direction	Fully fixed
DOF1	Free	Fixed	Fixed	Fixed
DOF2	Fixed	Free	Fixed	Fixed
DOF3	Fixed	Fixed	Free	Fixed
DOF4	Fixed	Fixed	Fixed	Fixed
DOF5	Fixed	Fixed	Fixed	Fixed
DOF6	Fixed	Fixed	Fixed	Fixed

In order to simulate a quasi-static environment for the HSI payload, fixed constraints were added to the interfacing faces for the dampener placements. The dampener interface locations were at the time of the simulation yet to be locked. The locations used for the simulation are based on the HSI Payload Design Report, following the suggestion from SMAC [RD02]. By fully constraining the dampener interfaces, the result should yield numbers that are exaggerated compared to what may be expected in realistic cases, as fixed faces will introduce larger stress concentrations to the system. Figure 7 shows the dampener interface locations used.
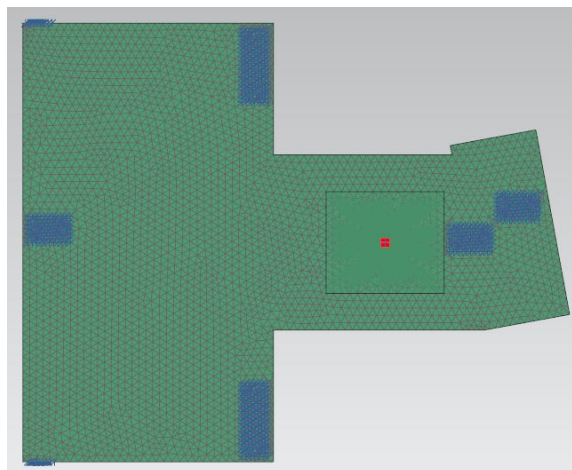

Figure 7: Dampener Fixed Constraints

6.2 Load cases

No loads were used in the modal simulations.

Forced response simulations would need an input load however. The following section is an excerpt of section 2.3.1 PSLV Loads [RD06] and describes the s/c design loads. **All load cases were provided by NanoAvionics**, and supported by the ESA and NASA standards.

The payloads shall remain fully functional after a sine vibration test with the parameters noted in table 11, based on the Environmental Testing Requirements for Polar Satellite Launch Vehicle provided by NanoAvionics. The values are for a standard qualification test, the acceptance test requires a less severe profile as to not purposefully harm the flight model more than necessary.

Table 11: PSLV Sine parameters

Characteristic		Qualification
Profile	Frequency, Hz	Amplitude
	5- 8	34.5 (DA)
	8- 100	4.5 G
Directions		x, y, z
Sweep Rate, oct/ min		2

The payload must also be able to survive the random vibrations that are present during the flight. The vibration band present in the PSLV can be simulated and tested in the lab. Table 12 shows the recommended values for a random vibration test, the values are for all directions X, Y and Z. Where PSD is the *power spectral density*, or the distributed power of the vibrations, and RMS is the *root mean square* a measure of the overall amplitude of the random vibrational system.

Table 12: Random Vibration Test

Characteristics		Qualification
Profile	Frequency, Hz	PSD, G^2/Hz
	20	0.002
	110	0.002
	250	0.034
	1000	0.034
	2000	0.009
Acceleration, G (RMS)		6.7
Duration, sec/ axis		120

The payload must be able to survive the shock loads present under launch. Table 13 tabulates the required shock values the payload shall survive, note that the safety factor must be applied. Where Q-factor is the damping equal to 5% viscous damping applied to the model.

Table 13: Half Sine Shock test

Characteristics	Qualification
Acceleration, G	70
Duration, ms	2
Q- Factor	10

In addition, a margin of safety of 1.4 should be incorporated in the described load factors to comply with the NASA standards.

The quasi-static simulation loads and load vectors are described in section 4.1. In order to simulate acceleration in NX, a field function expressing the factor of acceleration had to be defined [RD01]. This was simply defined as F(X) = 1 for the entire model, resulting in an isotropic behavior of acceleration.

7. Simulation

7.1 Modal Checks

These checks are relevant for checking the model

- Free free check
- Mass distribution check
- Constraint check
- Static load check

For the purpose of the PDR only Free free check will be done.

7.2 Free Free Check

Because the modal analysis was ran as a free free system, free free checks were done to after every iteration with added complexity to verify that the model was correctly defined. This was done by examining the frequency and mode shape of the first six modes for every iteration. For a model with no fixtures, the first 6 eigenfrequencies are expected to be zero [RD09]. All of the simulations ran in the analysis passed the free free check.

Possible errors sources that can produce additional zero frequencies are:

- Multiple free bodies due to mesh mating or gluing errors
- Corrupted elements
- Element nodes connected non coincident with no gluing
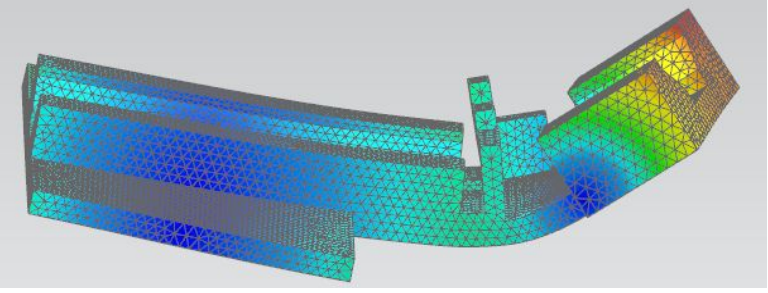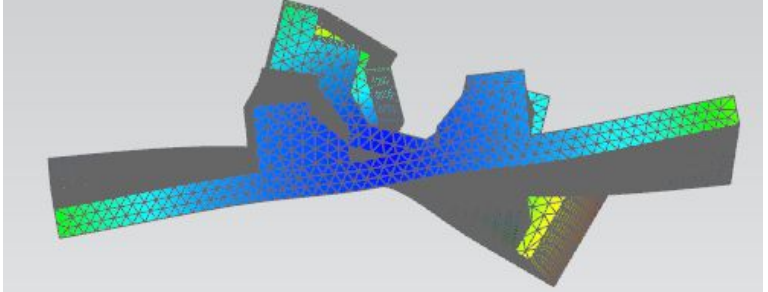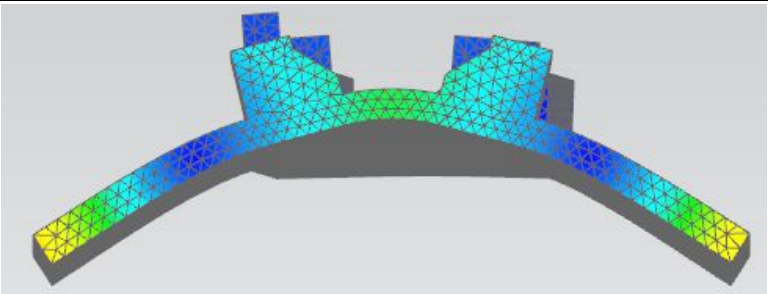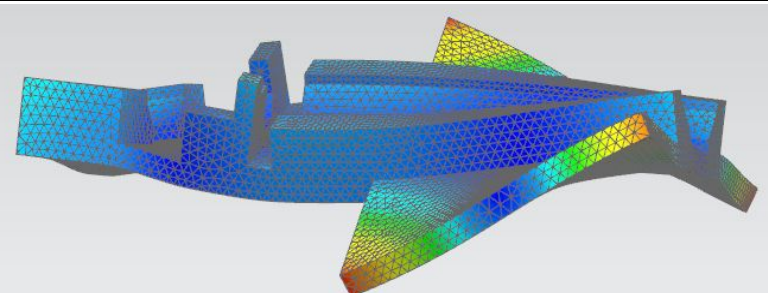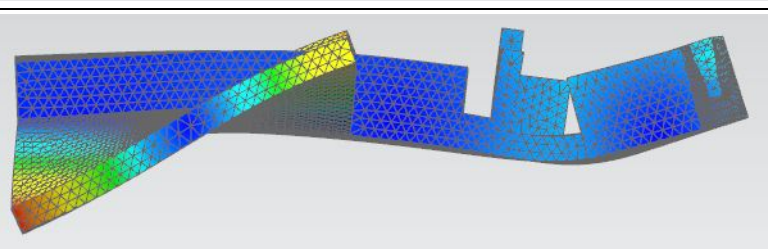
8. Results

The following results were obtained from the modal (frequency) simulations in SOL 103RS.

8.1 Preliminary HSI Platform
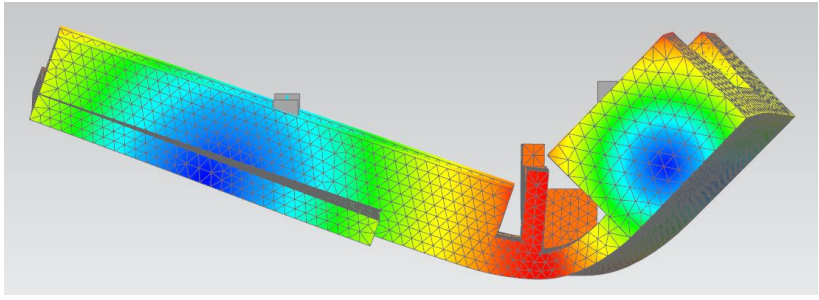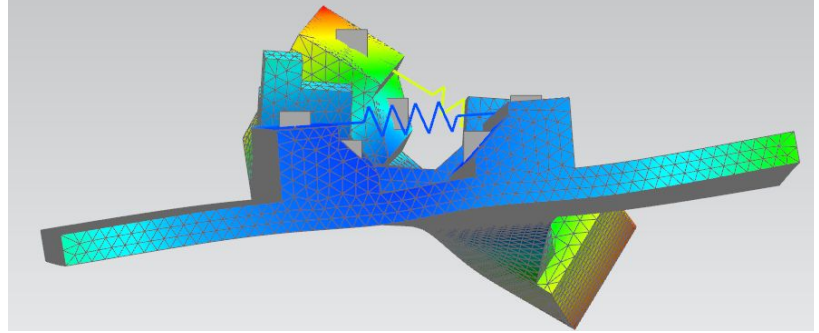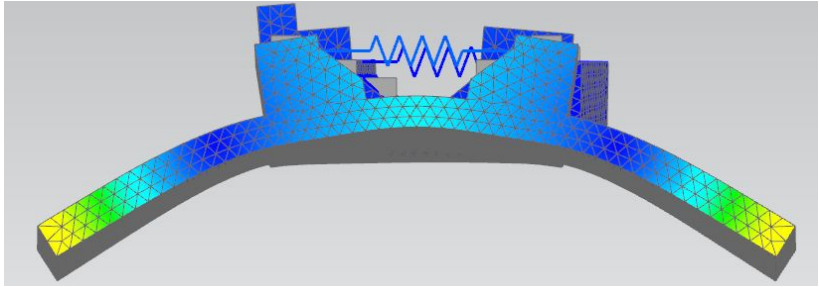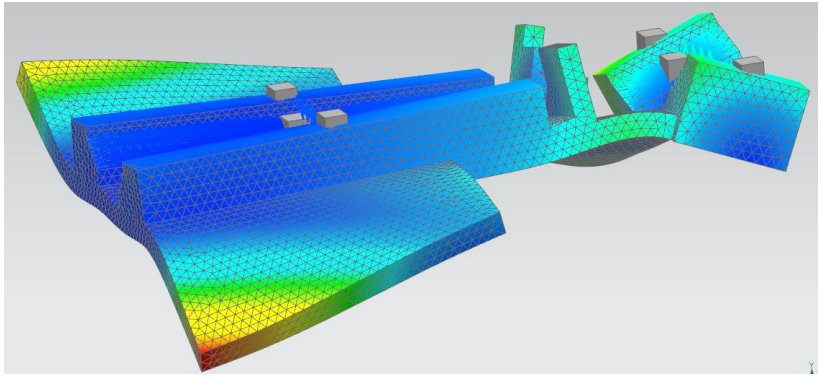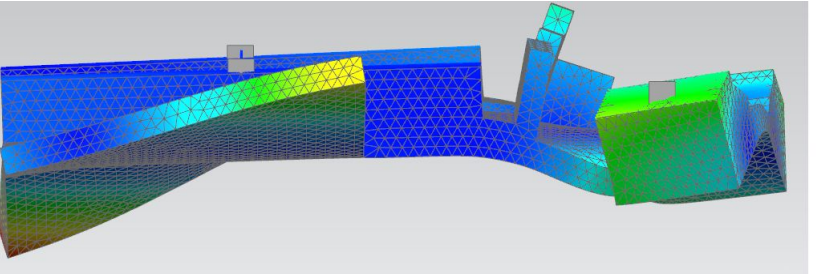
Table 14: Mode shapes Platform only

Modal Frequencies [HSI Platform]		
No.	Freq. (Hz)	Visual view
1	1200.01	
2	1438.85	
3	1640.02	
4	2500.02	
5	3005.57	

8.2 HSI Platform with Full Optical Assembly
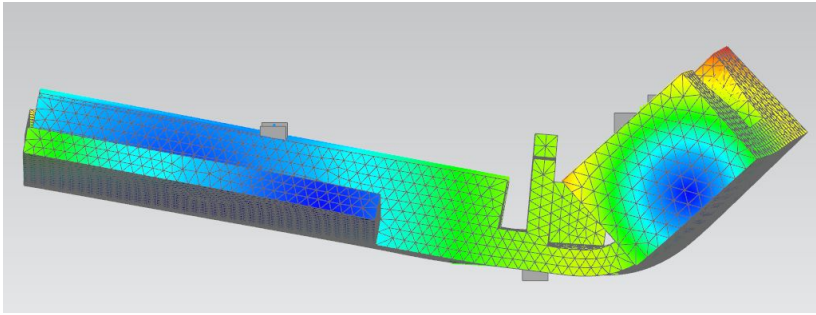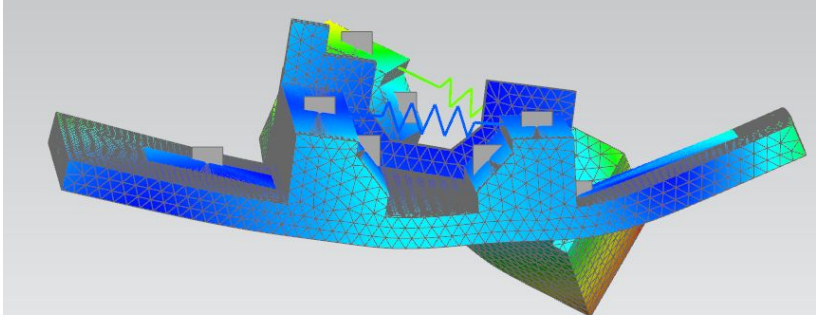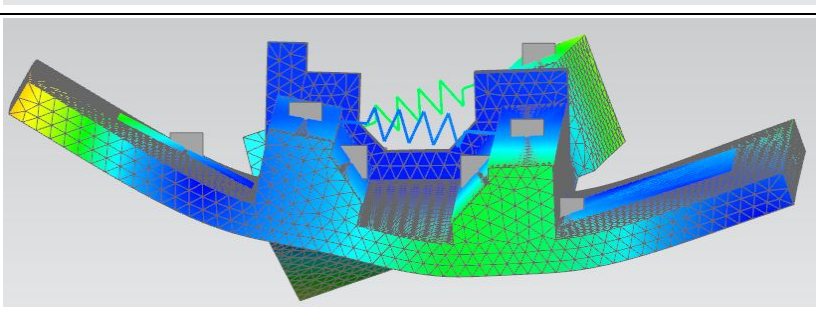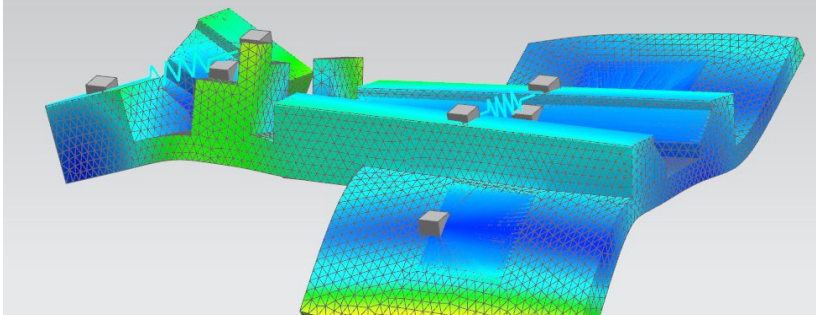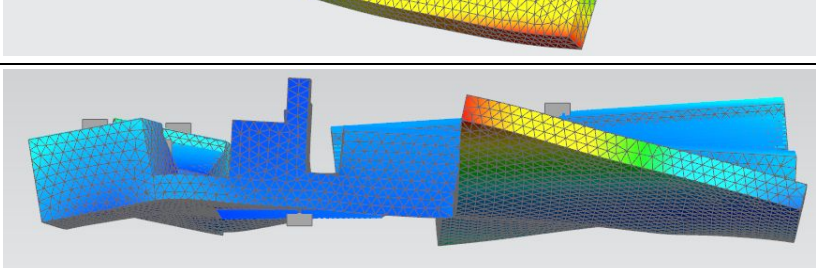
Table 15: Mode Shapes Full Optical Assembly

No.	Freq. (Hz)	Visual view
Modal Frequencies [Full Optical Assembly]		
1	728.94	
2	1051.65	
3	1716.64	
4	2505.54	
5	2968.20	

8.3 HSI Platform with Full Optical Assembly and Payloads
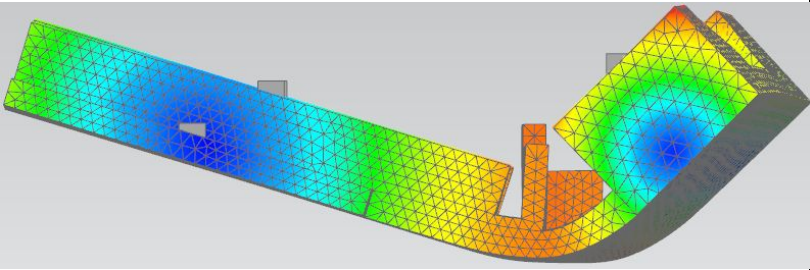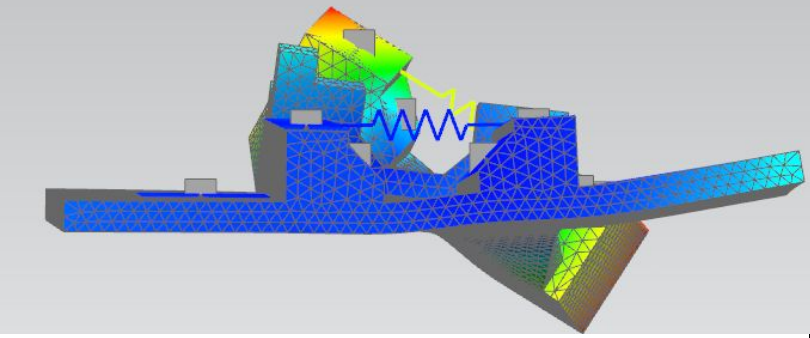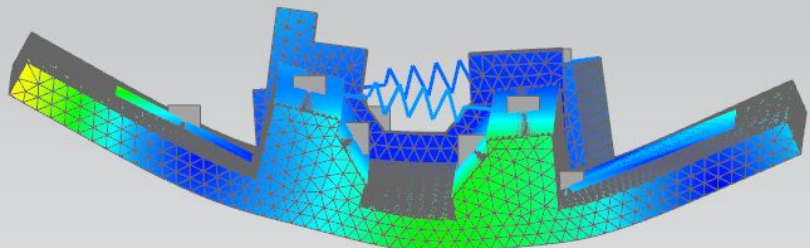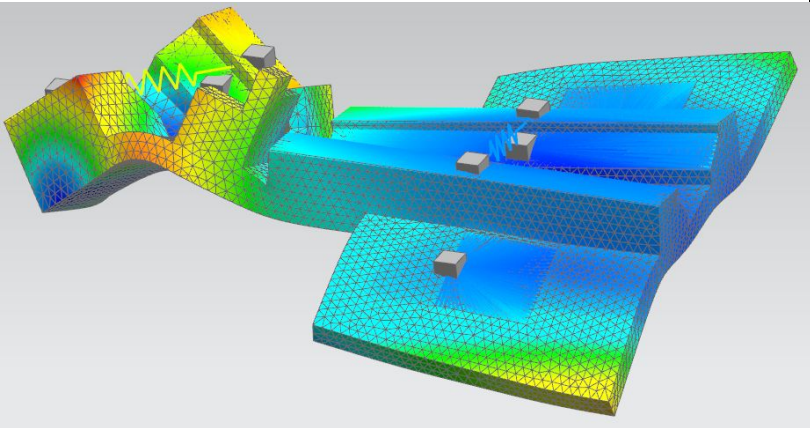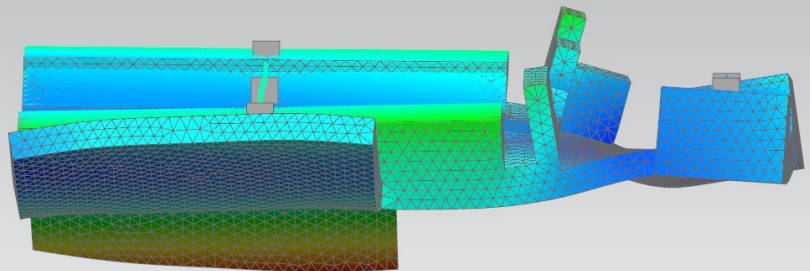
Table 16: Mode Shapes Full Optical Assembly and Payloads

Modal Frequencies [Complete Assembly]		
No.	Freq. (hz)	Visual view
1	1054.53	
2	1260.01	
3	1454.56	
4	2532.70	
5	2823.94	

8.4 HSI Platform with Full Optical Assembly and Payloads Without IMU

Table 17: Mode Shapes No IMU

No.	Freq. (hz)	Parts	Visual view
1	695.32		
2	990.73		
3	1305.26		
4	2377.59		
5	2660.95		

8.4 HSI Platform with Full Optical Assembly and Payloads Without IMU

Table 17: Mode Shapes No IMU

8.5 Quasi-static Case

Table 18 shows the results for case 5, 6 and 7.

Table 18: Von Mises Stress Concentrations

<table>
<tr><td colspan="4" align="center">Quasi-static Load with Fixed Dampeners</td></tr>
<tr><td align="center">No.</td><td colspan="2" align="center">Result Data</td><td align="center">Visual View</td></tr>
<tr><td rowspan="5">1</td><td>Longitudinal</td><td>Z</td><td rowspan="5"></td></tr>
<tr><td>Lateral</td><td>Y</td></tr>
<tr><td>$\sigma_{v,max}$</td><td>5.447 MPa</td></tr>
<tr><td>Location</td><td>Back bracket</td></tr>
<tr><td rowspan="5">2</td><td>Longitudinal</td><td>Y</td><td rowspan="5"></td></tr>
<tr><td>Lateral</td><td>X</td></tr>
<tr><td>$\sigma_{v,max}$</td><td>6.935 MPa</td></tr>
<tr><td>Location</td><td>Back bracket</td></tr>
<tr><td rowspan="5">3</td><td>Longitudinal</td><td>X</td><td rowspan="5"></td></tr>
<tr><td>Lateral</td><td>Z</td></tr>
<tr><td>$\sigma_{v,max}$</td><td>2.961 MPa</td></tr>
<tr><td>Location</td><td>Back bracket</td></tr>
</table>

9. Discussion

The lower complexity of new HSI platform allowed the finite element model for simulations to be simpler, which meant that the number of simulation objects could be reduced to zero. This in turn contributed in lowering the uncertainties following the simulations. As written in section 3, all assumptions taken in order to emulate the platform aimed to reflect worst case scenarios and lead to a lower structural stiffness. The first mode shape at 695.32Hz for the platform and payloads without the IMU should therefore in theory be a good representation of the lowest possible frequency that can occur for the HSI platform. Considering the fact that the frequency limit defined for launch conditions given by NanoAvionics is set at 130Hz, 695.32Hz should be well above. Some of the assumptions made did however contribute to an increase in stiffness. Even so, the realistic frequency is not expected to lower significantly. This becomes even more unlikely when considering that all masses added through element simplifications had a 10 percent added margin. The model should be a sufficient indicator to base design decisions upon [RD07].

Several factors affected the overall stiffness of the simulated payload. The RBE2 element connectors make the connected geometry perfectly stiff, so the faces connected can not bend [RD03]. This fact raises the overall stiffness of the HSI platform, however the implementation of the RBE2 elements on the selected faces does not contribute to a significant amount of total stiffness in the platform as the system did not experience any large bends in the particular faces stiffened by the RBE2 elements in the platform only simulation, table 14. The idealization process changed some inner and outer blends and could have lowered the stiffness of the HSI payload, however measurements indicates that the overall mass of the prototype only changed by +0.4%. The idealization process should realistically not induce any significant errors into the simulation results [RD08].

By adding complexity to the model in iterations, large and unrealistic changes could be detected early in the process, thus leading to easier troubleshooting. At the same time, the iterations could be used to make sure that the assumptions and complexity added still represented a realistic simulation. Nevertheless, the only way to properly know what frequencies will occur will be by running a frequency sweep test.

Throughout the analysis, the optimal position of the IMU in regards to frequency mode shapes was also uncovered. This position was determined to be underneath the platform and grating area, where the relative stiffness was much lower than the grooves. The relative stiffness of the grating area was further decreased due to the connected payloads on the platform wings, as weight was placed further away from the center. By comparing table 16 and 18, with and without the IMU, frequency for the first mode can be observed to increase from 695.37Hz to 1054.53Hz by adding the IMU at said location. This change could be even higher if the mass of the IMU was added somewhere close to the front wing area, which would increase the mass of the front groove. However, further analysis taking interface, and other factors into consideration should be done before making this decision.

Based on the results from the analysis, the mass of the HSI platform could be decreased at the groove walls. This could be done by making the walls thinner or grooving out patterns. Both of these methods would result in a lower weight to stiffness ratio when looking at the whole platform. This further supports the suggestion from Section 4 in [RD02] and [RD10], to slim down the platform width in order to fulfill the allowed protrusion requirements of the star tracker [RD11].

The initial mode shapes can also be used as good indicators to the position of dampeners with in order to control the frequency. By looking at the extremal displacement points of the first mode shapes in table 16, the back and front assembly grooves can be observed to twist the most relative to each other. Furthermore, the platform wings are also shown to displace. This corresponds to effective dampener positions in order to control eigenfrequencies of the platform. This leads to the fact that further analysis should be done including dampeners in the system for a more accurate prediction. In addition this, using SOL 103 RS to run a transient modal analysis, giving additional data such as mass participation for every mode is desired in order to properly evaluate the importance of each mode shape.

Based on the static-linear simulations adding acceleration loads, the stress concentration experienced by the actual current platform design are considerably below yielding values. The highest stress experienced by the platform itself was measured to be at 6.935 MPa, as tabulated in table 19, while the yield stress for aluminium 6082 is given as 259.23 MPa. This results in a safety factor of 26.1 against yielding. Furthermore, the location of the stress concentrations appear to be at the back bracket, which was modelled using RBE2 and CBUSH elements with a defined stiffness. This is the most likely outcome of the concentrated mass in the back groove in combination with the lowered stiffness of the platform floor being pushed back by the bracket stiffness when subjected to an acceleration load. Even so, due to the low level of stress experienced by the platform, no further consideration is required with respect to the structural integrity of the HSI platform when subjected to the quasi-static design loads provided by NanoAvionics. On the contrary, the structural integrity of the optical assembly is more complex and most likely more fragile. Especially when subjected to load environments involving vibration and shock. Because of the larger complexity, lens objectives and optical assemblies will not be simulated, but instead tested.

10. Conclusion

The simulated frequencies seems to be within expectation for all simulation cases, and the design has passed the fundamental frequency requirements based on the results. The lowest fundamental frequency recorded at worst case with no IMU, case 4, was 695.32Hz well over five times the required stiffness, SF notwithstanding. Based on the results, it can be assumed that the payload should not resonate at the expected low to mid level frequencies (0-200Hz) expected during the launch. High level resonans due to acoustic pressure might be a problem (20-2000Hz), however the lower frequencies are more dangerous due to the corresponding displacement is larger.

As can be seen from the modeshapes of the fundamental frequencies in table 16 and 17, the most critical point seems to be the bending motion in the back of the platform. The platform is prone to bending and movement in the Y direction. A forced response analysis must be one in order to calculate the mass participation of the mode. Additional supports might be necessary in the back, and some concepts for this have already been informally discussed amongst the members of the mechanics group. Further simulations are required to expand on the analysis outlined in this report and also when changes to the design are incorporated.

The platform itself should not experience yield to any degree as a result of the quasi-static design load environment provided by NanoAvionics. Even when subjected to acceleration loads in the worst configuration, with 18.7G in the Y-axis and 10.2G in the X-axis, stress levels appears to be well below the yielding stress. The highest measured stress values for this configuration was 6.935 MPa.

11. Further Work

Further simulations are necessary in order to uncover the payloads mechanical characteristics. Only simple modal simulations were performed. Forced response analysis must be run to identify the payloads reaction to the described frequency band (0-200Hz) and random vibrations (20-2000Hz). Shock simulations should also be done to check the integrity of the lenses. From the described simulations payload excitation response to the loads can be obtained, and Von Mises stress should be obtainable to check for yield.

Further simulations with the payload attached to the bus through the proper dampener solution should also be done. The effect of the payload on the viscoelasticity of the dampeners must be explored.

Further analysis and simulation will also be needed as the design matures. This is the case both for pure structural changes and when specific dampers are chosen. This will be an ongoing process for some time as iterations in the design are made based on analysis. The role of mechanical analysis in the design pipeline is detailed in [RD04].

The prototype will also be tested thermally. Should the prototype prove to be inadequate for the mission, new design changes will need to be iterated through using the same process.

Model cross-checks must be improved to verify that the simulations are correct. All loads must be confirmed.

Physical modal test results on the TTH Mk1 should be used to further the accuracy of the simulations.

A thorough simulation done on the grating cassette and grating should be done as this part is sensitive. This was not done due to time constraints and due to the low excitation of the interface placement as seen in table 14 section 8.1.

12. List of Abbreviations

Table 19: Abbreviations

Abbrv.	Description
AA	Aluminium Alloy
CAD	Computer Aided Design
COTS	Commercial Off-The-Shelf
FEA	Finite Element Analysis
FEM	Finite Element Method
ICD	Interface Control Document
LCS	Local Coordinate System
PDR	Preliminary Design Review
SF	Factor of Safety
PSD	Power Spectral Density
RMS	Root Mean Square

11. Symbols

Table 20: Symbols

Symbol	Unit	Description
$\sigma_{v,max}$	MPa	Max von mises stress
E	MPa	Young's Modulus
I	mm^4	Second Moment of Inertia
L	mm	Length
w	mm	Width
h	mm	Height
k	$\dfrac{N}{mm}$	Stiffness
$Q - factor$	-	Damping quality factor
PSD	$\dfrac{G^2}{Hz}$	Power Spectral Density
DA	-	Double Amplitude

Appendix L

HYPSO-ANA-008 HSI Payload Thermal Analysis Report

HSI Payload Platform Thermal Analysis Report

HYPSO-ANA-008
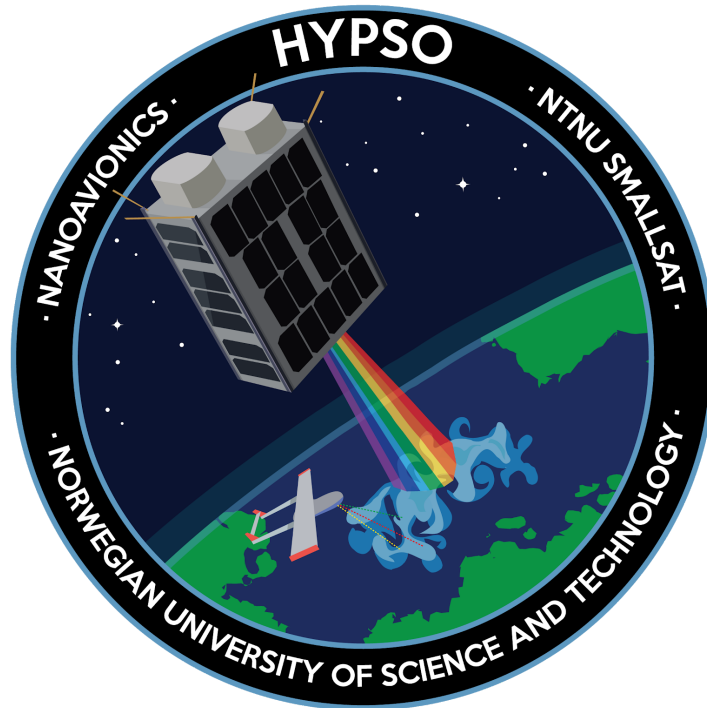
Prepared by: HYPSO Project Team
Reference: HYPSO-ANA-008
Revision: 2
Date of issue: 26.05.2019
Document Type: Analysis
Author(s):   Tuan Tran, Tord Hansen Kaasa, Henrik Galtung

Table Of Contents

Table 1: Table of Changes

Rev.	Summary of Changes	Author(s)	Effective Date
1	First issue	Tuan Anh Tran, Tord Hansen Kaasa, Henrik Galtung	23.05.2018
2	Formatting of text and figures	Tuan Anh Tran, Tord Hansen Kaasa, Henrik Galtung	26.05.2019

Executive summary

A thermal analysis was conducted to simulate the temperature environment during operation in orbit. The thermal environment inside the CubeSat is expected to be within the -20 to +40°C range based on NanoAvionics internal analysis. Two extreme cases were simulated, a hot case where all parameters gives the largest heat, and a cold case where all parameters provides as little heat as allowed. The results from the simulations shows that the temperature range is within -39 to +50, due to the extreme cases simulated. temperatures of the objectives, detector, RGB camera, IMU and star tracker payloads are under the respective temperature limits for the cold case. The hot case shows that the front objective and RGB camera reached temperatures under the limit. The results shows the need for thermal control within the payloads, if the assumptions provided are realistic. Based on the results, it can be concluded that some sort of thermal control system, passive or active.

1. Overview

The HYPSO Mission will primarily be a science-oriented technology demonstrator. It will enable low-cost & high-performance hyperspectral imaging and autonomous onboard processing that fulfill science requirements in ocean color remote sensing and oceanography. NTNU SmallSat is prospected to be the first SmallSat developed at NTNU with launch planned for Q4 2020. Furthermore, vision of a constellation of remote-sensing focused SmallSat will constitute a space-asset platform added to the multi-agent architecture of UAVs, USVs, AUVs and buoys that have similar ocean characterization objectives.

1.1 Purpose

The main purpose of this analysis is to uncover the thermal environment the HYPSO Payload Platform will be subjected to in order to successfully integrate the Hyperspectral Imager (HSI) Camera and crucial mission payloads. The main functionality of the platform is to provide a structural integrity to the HSI camera assembly, which consists of three 50 mm VIS-NIR lens objectives, a 25mm Sq, 17.5° blaze angle grating, a 50µm slit and a monochrome IMX249 sensor, which are all COTS components. In order to satisfy mission requirements in regards to orientation and pointing accuracy, the camera is required to have a rigid connection with an IMU, star tracker and a RGB camera for georeferencing. Each of these have their own thermal operating ranges, as well as contributing to heat dissipation and will therefore also need to be considered in the analysis. The thermal environment inside the CubeSat is expected to be within the -20 to +40°C range based on NanoAvionics internal analysis, (NanoAvionics could not share further information regarding the simulation).

1.2 Scope

In order to determine the thermal integrity of the main payload, the bus environment will need to be simulated used finite element method (FEM). This requires a thermal model of the 6U CubeSat Bus that will be provided by NanoAvionics. A simulation model of the HYPSO platform along with rigidly connected payloads was also created. Depending on the thermal integrity of the payloads, various modifications can be done to the platform in order to shift or lower the gradients. Passive thermal control can be done through changes in a surface thermo-optical property, or through thermal coupling with either heat sources or radiators. Because a material already have been chosen for the platform, changes in the thermal expansion properties can not be done. This is further elaborated on in *HYPSO-ANA-004 Payload Material Analysis* [RD01]. If passive control is required, anodization or application of multi-layer insulation to the platform will be investigated.

The IMX249 sensor investigated in this report will be the "housingless" version, UI-5261SE-M-GL. In contrary to the housing model, the housingless version does not rely on any internal thermal straps to transfer the heat from the microprocessor, as it has direct exposure to a high convection environment in the atmospheric environment it is designed for. A thermal strap will be added the the HSI camera sensor in order to transfer heat from the microprocessor to the platform. Figure 1 shows the relationship between all the documents.
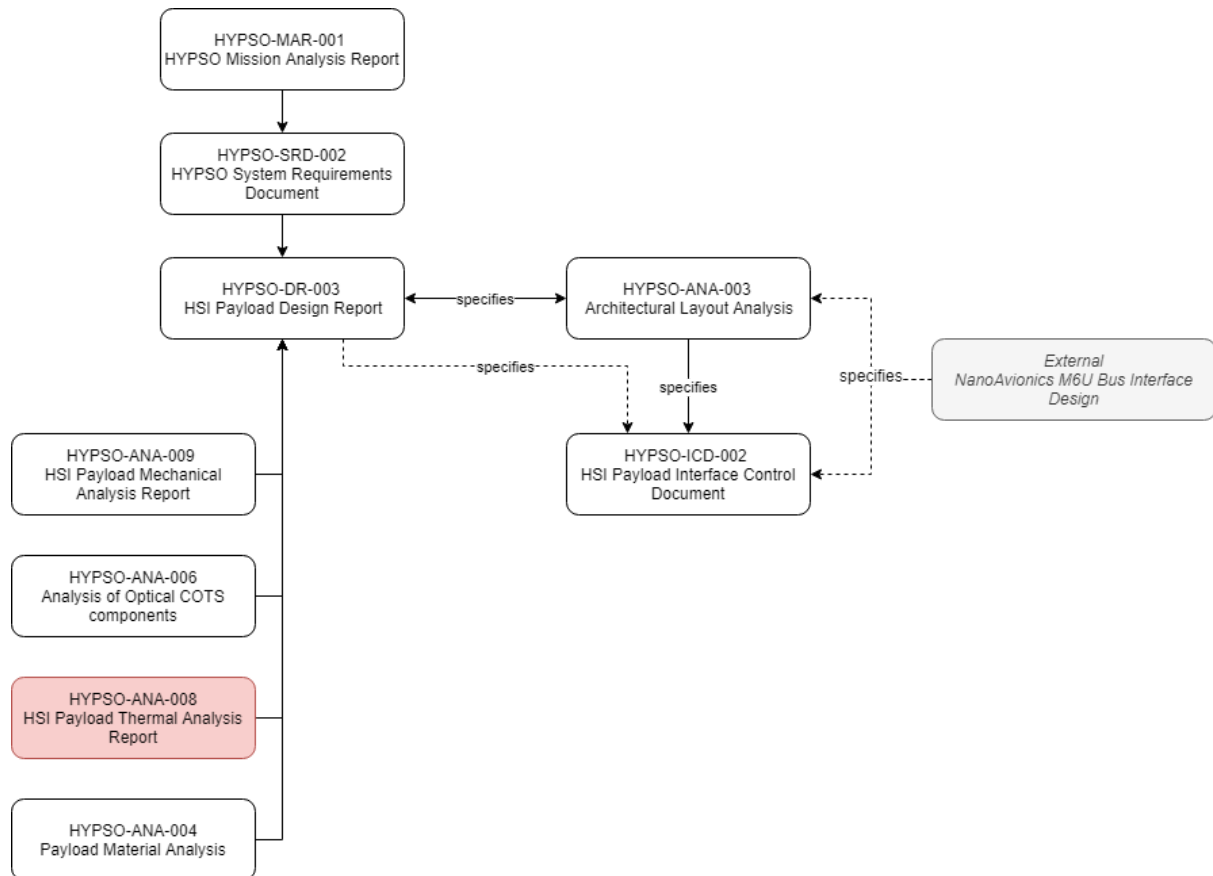
Figure 1: Document relationship

1.3 FEM Description

The finite element method (FEM) is a variation-differential method, which is based on representing an original area with a complex boundary as a collection of simple subareas (finite elements) [RD02]. This approach means that a continuous surface can be broken down into a finite amount of smaller surfaces or elements. This allows for analysis of the elements using underlying mathematical formulations built into the different solvers in the simulation program. NX Space Systems Thermal (SST) will be used for all thermal simulations.

1.4 Simulation Item

The simulated item a HyperSpectral Imager payload, SDR and the bus system delivered by NanoAvionics. The payload simulated is the TTH Mk1. Figure 2 shows the HSI payload, while figure 3 shows the payload placement in the bus . Figure 4 shows the complete bus system and high level component architecture, figure 5 shows the external thermal interfaces of the bus.
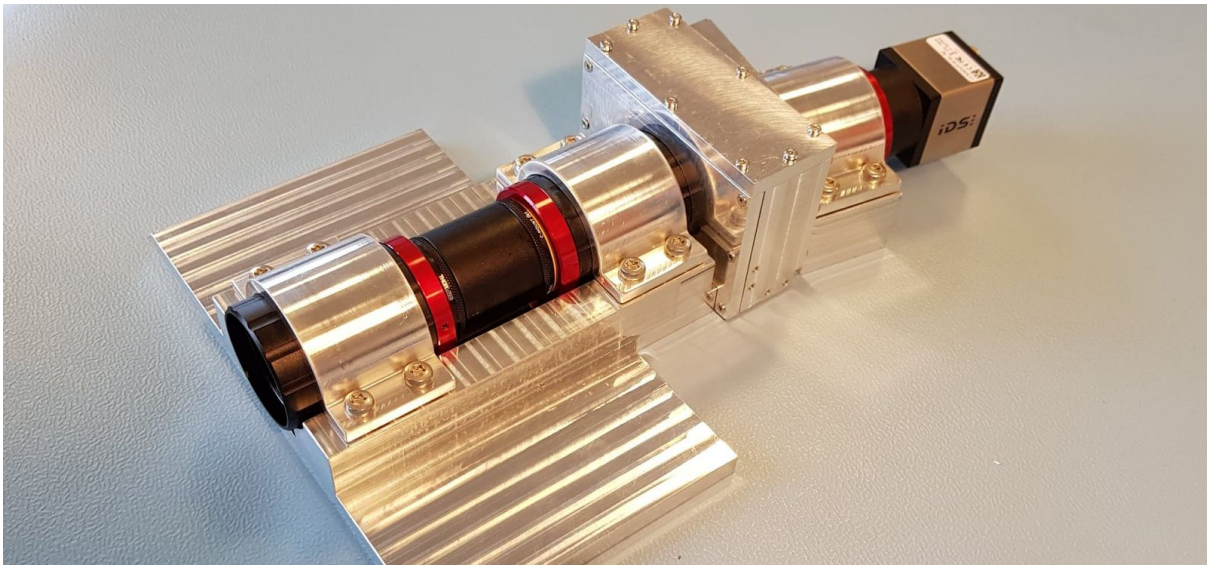
Figure 2: HSI Payload Prototype TTH Mk1, without Star tracker and RGB
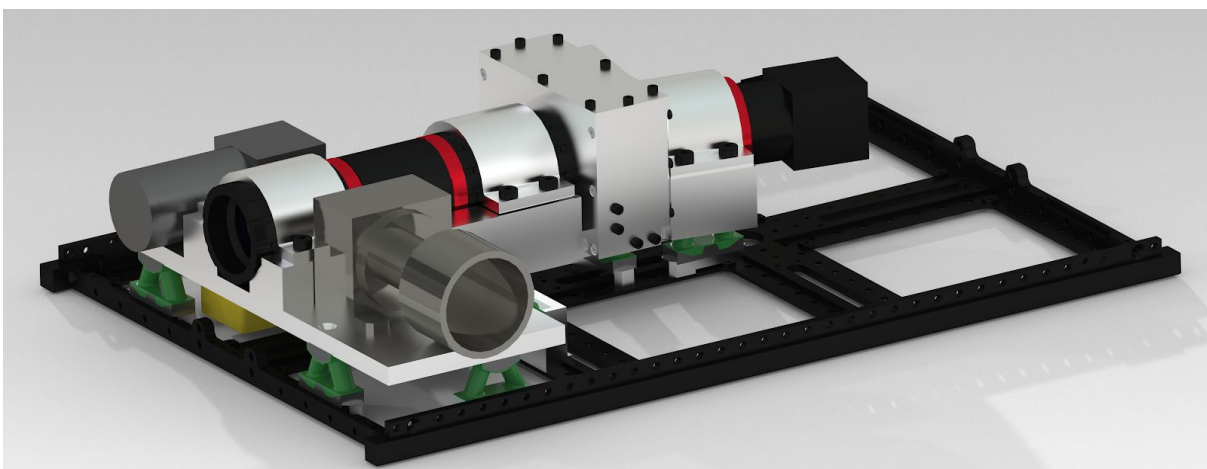
Figure 3: Payloads mounted on a 6U CubeSat frame wall
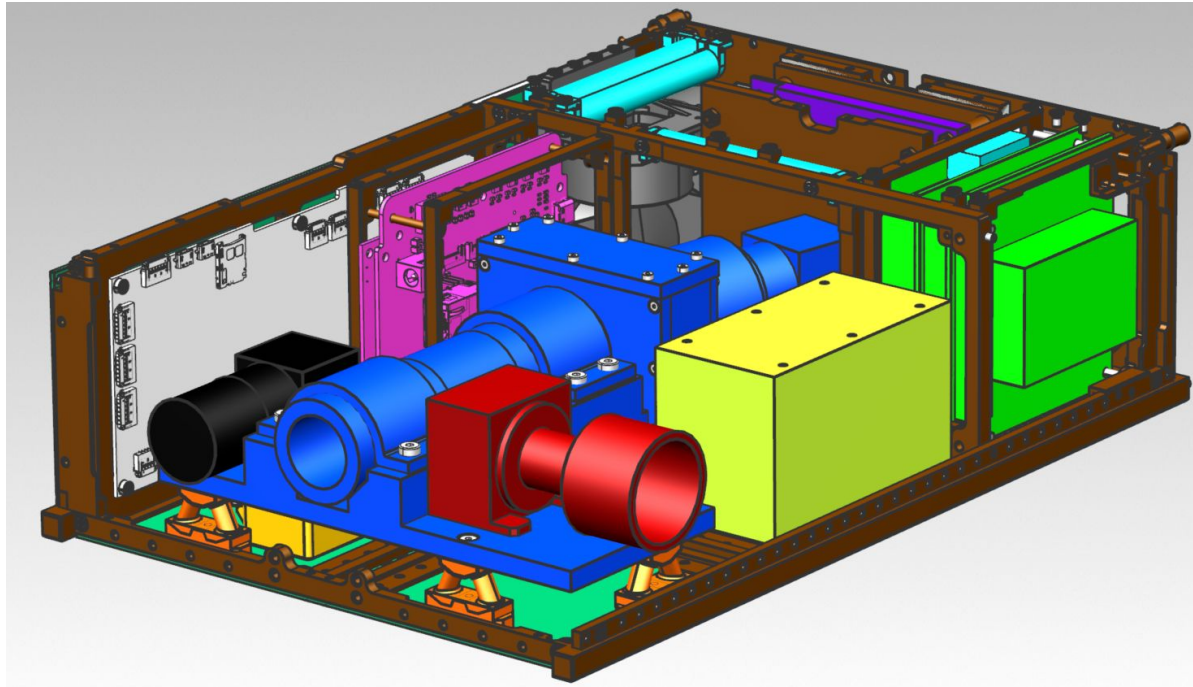
HSI	RGB Camera
SDR	OPU
Star Tracker	Reaction Wheels
Magnetorquers	Payload Interface Board
Solar Panels	Dampers
Battery Pack Unit	IMU
S-Band Radio	Frame and mounting structures

Figure 4: Cubesat architecture/layout

Figure 5: External thermal interfaces, Engineering model from NanoAvionics

1.5 Referenced Documents

The documents listed in have been used as reference in the creation of this document.

Table 2: Referenced Documents

ID	Author	Title
[RD01]	Tord Hansen Kaasa, Tuan Tran, Henrik Galtung	HYPSO-ANA-004 Payload Material Analysis
[RD02]	P. Goncharov, I. Artamonov, T. Khalitov	Engineering Analysis with NX Advanced Simulation
[RD03]	T. Walker, S.-C. Xue and G. W. Barton	Numerical Determination of Radiative View Factors Using Ray Tracing
[RD04]	Tord Hansen Kaasa, Tuan Tran, Henrik Galtung	HYPSO-DR-003 HSI Payload Design Report
[RD05]	NASA	GSFC-STD-7000A
[RD06]	HYPSO Project Team	NTNU Smallsat Budgets
[RD07]	NASA	Guidelines for the Selection of Near-Earth Thermal Environment Parameters for Spacecraft Design
[RD08]	Data Sheet, Knight Optical	Datasheet: B270 Properties Knight Optical
[RD09]	NASA	Spacecraft Thermal Control Coatings References
[RD10]	Several Authors, Editor: David G. Gilmore	Gilmore DG (2002) Spacecraft thermal control handbook Volume 1: Fundamental technologies.
[RD11]	Kenneth Wood, Barbara Whitney, Jon Bjorkman, and Michael Wolf	Introduction to Monte Carlo Radiation Transfer
[RD12]	Albin K J. Hasselström, U. Eskil Nilsson	Thermal Contact Conductance in Bolted Joints
[RD13]	Love Fältström	Graphite sheets and graphite gap pads used as thermal interface materials
[RD14]	NanoAvionics	Datasheet:GaAs Solar Arrays
[RD15]	AZUR SPACE	Datasheet: 28% Triple Junction GaAs Solar Cell

2. Requirements

Direct requirements are not given in the ESA nor NASA standards. The standards state that thermal effects must be accounted for in regards to the design process. Thermal requirements will, therefore, be defined by the payload components. The following criterias governs the HSI OPU and SDR Payload thermal design, the criteria are elaborations from the HYPSO thermal requirements HSI-032 and HSI-032-001.

> The HSI payload shall survive the temperature fluctuations throughout its lifetime. *(HSI-32)*

> The heat produced by electronics for a typical slew maneuver process duration (3min) should be within the defined operational ranges of the COTS components. *(HSI-32-001)*

> The payload shall perform satisfactorily within the vacuum and thermal mission limits.

> The thermal design and the thermal control system shall maintain the affected hardware within the established mission thermal limits during planned mission phases, including survival/safe-hold, if applicable.

> The hardware shall withstand, as necessary, the temperature and/or humidity conditions of transportation, storage, launch, flight, and manned spaces.

> The quality of workmanship and materials of the hardware shall be sufficient to pass thermal cycle test screening in vacuum, or under ambient pressure if the hardware can be shown by analyses to be insensitive to vacuum effects relative to temperature levels and temperature gradients.

Table 3 tabulates the thermal operating and non operating surviving temperature ranges for the optical components. Note that the values are based on those given in the data sheets. Section 9 shows a simple thermal tolerance test done to the HSI optical equipment, it can be seen that the optical equipment can survive well over these set limits without distorting the resulting spectrogram to a mission critical degree, however the resulting spectrogram will get blurry. Note that all temperature ranges are defined in earth conditions, the lack of a convection medium in LEO can change the limits, the extent must be tested in a thermal vacuum chamber at a later date.

Table 3: Payload Component Temperature Ranges

Component	Model	$T_{min,op}$	$T_{max,op}$	$T_{min,surv}$	$T_{max,surv}$
Main Payload					
Camera Detector	IMX 249 - Monochrome	0	55	-20	60
Optical Assembly*	50mm C Series VIS-NIR*	-20*	40*	-	-
Onboard Processing Unit					
PicoZed	PicoZed 7Z015 / 7Z030 SOM	-40	85	-20	30
Breakout Board**	Custom**	-	-	-	-
ADCS Pointing*					
Startracker	Nano Star Sensor ST-MA-APS1-1	-30	85	-40	85
Inertial Measurement Unit	STIM210 Multi-Axis Gyro Module	-40	85	-55	90
Secondary Payload					
Software Defined Radio	TOTEM SDR Motherboard	-40	85	-40	85
Software Defined Radio	UHF RF front-end	-40	85	-40	85
Tertiary Payload					
RGB Camera Detector	UI-1250SE	0	55	-20	60
RGB Objective	OPTIC C FIX 08MM MP 1/1.8 TAM	-10	60	-	-

*Values Depends on calibration, the range was found using a simple tolerance test for the HSI Payload, Section 9

**Currently no information on the custom BoB, however the PCB is mainly for interfacing the PicoZed

***Values gathered from partially classified material from Alén Space

3. Assumptions

A number of simplifications had to be done in order to build the simulation models within a reasonable time span. In addition there exist a large number of unknowns in relation to the thermal simulations, component materials and surface thermo-optical properties. This section attempts to summarize the most important assumptions taken during the thermal simulation process.

In order to numerically calculate the view factors of radiating surfaces, the Monte Carlo method was used. This method traces the radiative rays leaving every surface in random directions from random points in the surfaces [RD03].The advantage with this method is that more complex models can be more accurately modelled in comparison to deterministic and hemicube view factor calculation methods [RD02]. The disadvantage with the method is the lower efficiency compared to the other methods. This effect is elevated even more when the complexity of the model increases [RD02].

As no testing in thermal vacuum chambers have been done, and the simulations were done in a limited time frame, no measurement of components conducive values have been made. The current thermal analysis will therefore assume a worst case contact between the HSI platform and the items connected to it, by the use close parallel plates radiation (1 to 1 ratio on the view factor). This will result in a temperature difference between the platform and the items connected. The results will therefore reflect a worst case scenario. The results should in reality average out between the platform and the simulated items, resulting in a smaller temperature gradient. Further simulations should be done, once conductivity is determined.

Estimations of the lumped solar panels taking the conversion of solar radiation into electricity were made. The effective absorptivity of this surface can be estimated as $\alpha_{eff} = \alpha_c - \eta$. The averaged absorptivity was calculated to be $\alpha_{avg}=0.588$. Even when using upper values for absorptivity in the solar panel back plate material, the lumped properties still appear below the provided values. This could contribute to exaggerated absorption rates of heat flux, as elaborated in section 8.

All models have been idealized, meaning that the geometrical complexity was reduced. This was done in order to decrease the simulation time. The effect of this is a reduction of accuracy and reliability, as changes in mass and conductive interfaces may have changed. To account for the change in mass, parts with a change of mass larger than 5 percent were given a specific density to account for the change in volume. Additionally, because conductive properties between interfaces in the satellite is unknown, a pure radiative heat exchange has been assumed. The properties of this assumption is further elaborated on in section 5.3. Removing all screws and screw holes in the bus frame also means lowering the conductivity, since the cross-sectional area is effectively increased. The frame was also made thicker to remove small contours and to accommodate a coarse mesh.

The HSI payload is required to be decoupled from the frame in order to reduce the vibrational and shock load on the payload, per requirement HSI-025. It follows that the direct thermal heat flux experienced from the bus frame would be reduced due to the added interface. However the exact design of the decoupling is unknown. The decoupling solution at the time of writing is to use elastomeric dampers from SMAC Space. The number and placement is still not decided, however the HSI Payload Design Report [RD04] section 5 states that 7-9 dampeners placed at the extremal points of the HSI platform should suffice for mechanical dampening and thermal decoupling. The simulation uses 9 dampeners which was averaged out over the surface of the platform, additional details in section 5.3.

Material properties are highly uncertain. Little information regarding the complex thermal properties of the chosen materials exists online. Therefore, all material data is purely preliminary. All payloads were simulated with uniform, homogeneous material properties. This includes the HSI, PCB, SDR and RGB camera. The material properties of these modules were approximated based on the thermally dominating material. This approach induces some amount of uncertainty within the simulation. The exact material properties of the approximated materials can be found in *Appendix A: Simulation Overview*.

The index of refraction was set to one for all the materials in the analysis, as the medium is vacuum.

Orbit parameters where simplified. The first orbits are not considered. Only the equilibrium orbits are considered when discussing the results.

To simulate heat dissipation from components, their heat load had to be averaged out for the entire orbit, as NX does not have a function to activate and deactivate simulation objects as a function of time or position. This meant that the experienced temperatures resulting from the transient analysis may have lower extremities in temperature. To account for this, steady state simulations can be run in order to properly determine maximum hot cases for crucial components.

The external surfaces of the satellite were modelled to have a single lumped material property. This was due to lumped properties being the only information available regarding the external surfaces, as they were given by the CubeSat provider.

The SDR stack was approximated as a cube with the correct mass. This will affect the thermal properties. The SDR must be further investigated, however the SDR thermal operational span is high as the system is space graded.

In addition to the base assumption, further assumptions are made by using FEM, which itself carries a chain of assumptions. The FE models are mathematical representations of the original polygon geometry. The use of simulation objects, which are approximations of real life phenomena like thermal transfer and heat generation. Simulations are not exact and should not be taken as such until sufficient support can be gathered from testing and real life monitoring of the s/c system once in orbit.

4. Method

3D models for all systems and single components were produced and simplified. The polygon modeles where then converted to finite element models through meshing, converting them to mathematical models consisting of elements and nodes. The FE models where then prepared in the NX Space Systems Thermal module for simulation. The NASA standard GSFC-STD-7000A provides a description of the simulation of the orbit parameters in a thermal vacuum chamber [RD05]. The standard is aimed at physical testing by simulating the thermal input conditions. However, some notes can be taken from this standard. Section 2.6.3.3 states that all simulations should be done as worst case scenarios. All thermal simulation done on the CubeSat will present the worst case scenarios. An additional 10°C will be added to the resulting thermal range for all individual components.

4.1 Hot and Cold Cases Worst Case Scenarios

The worst thermal scenarios have been considered in order to uncover the extremals of the systems. By designing against these extremes, the payloads should in theory also work within the range. To determine the cases the worst satellite orientations, solar radiation conditions, earth albedo conditions and the IR flux from the earth were examined and used as environmental inputs. The worst case orientations were found to be a sun synchronous orbit with the -Y side of the s/c locked towards the sun for max heat exposure and heat transfer to the internal HSI payload interfaced to the -Y frame of the bus. The -X side locked towards the sun provided the least thermal energy to the payloads, the -Z side was not used due to the lack of solar panels on this side.

Two cases will be considered during this analysis, a hot and cold case. The hot case will be achieved when all heat sources produce the maximum amount of heat with a -Y sun orientation, the cold case is similarly achieved when all heat sources produce the minimum amount of thermal energy with a -X sun orientation. The hot and cold cases represents the extreme temperature range of the s/c. To simulate the heat dissipation of each component, an average power consumption based on the duty cycles for every orbit was calculated. An additional heat dissipation margin of 5 percent was added to each component before averaging out the duty cycle, this margin exist due to the power consumption estimation margin present in the calculations in the Power Budget [RD06]. The duty cycles for all components and payloads can be found in the Power budget [RD06].

The hot case is based on a scenario where all components are powered on for the designated time in the case for taking hyperspectral images using a slew maneuver, the duty cycle is designated as critical in the power budget. The cold case is defined after the safe mode duty cycle, where only the essential systems are powered on. The cold and hot cases were defined based on the SmallSat power budgets. The calculations can be found in Appendix A: *Simulation Overview* spreadsheet. Table 4 tabulates the conditions for both of the cases. The duty cycles for the payloads and relevant ADCS components are tabulated in table 5. The estimated online time for the RGB camera was based on the boot time of 15s and picture taking time of 15s with an additional safety factor of two.

Table 4: Worse Case Scenarios, thermal loads per orbit

Heat Source	Hot Case	Cold Case
Environment Heat (W/m^2) [SMAD]		
Solar Irradiance [RD07]	1419	1317
Albedo vs. Latitude	0.306	0.306
IR Flux	69.8	58
Satellite Orientation	-Y locked at sun	-X locked at sun
Component Heat Dissipation (mW) [Power Budget]		
HYPSO		
HSI Camera	32.233	0.0
OPU	550.18	0.0
Star Tracker	75.600	0.0
IMU	183.33	0.0
SDR	2419.933	1560
RGB Camera	7.780	0.0
NanoAvionics (mW) [Power Budget]		
EPS	168.0	168.0
BUS CAN Interface	31.50	31.50
Flight Computer	332.640	332.640
UHF	665.280	328.482
Gyroscope	51.975	0.0
Payload Controller	367.290	0.0
Payload CAN Interface	31.50	0.0
Sun Sensors (6)	207.90	207.90
GPS	183.645	183.645
Reaction Wheels (4)	1688.610	0.0
Magnetorquers (6)	1315.125	1315.125
S-Band RX	83.664	0.0
S-Band TX + RX	1464.120000	0.0

4.2 Orbit Parameters

The orbital parameters determines the time the s/c is in the eclipse (the umbra and penumbra). It follows that the orbit has a direct impact on the thermal environment of the s/c. Table 5 shows the HYPSO orbital parameters. A visual representation of the orbit is provided in figure 6.

Figure 6: HYPSO s/c Orbit

Table 5: HYPSO Orbital Parameters

Parameter	Value
Orbit Type	Sun-synchronous
Orbit Period	5668.22 s
Minimum Altitude	450 km
Maximum Altitude	550 km
Orbit Inclination	97.374°
Argument of Periapsis	0°
Local time at Ascending Node	00:00:00

For the simulations a maximum of 20 orbits around the earth was chosen. Table 6 tabulates the orbital setup in NX SST.

Table 6: Orbital Transient Parameters

Transient Setup	
Maximum Number of Orbits	20
Number of Time Steps	100
Calculations per Orbit	16

The numbers presented in table 6 were chosen based on a test with coarse mesh. However the selected number of orbits provides accurate results as equilibrium is achieved on all components.

4.3 Material Properties

In order to properly simulate the thermal behavior of the satellite, material and thermo-optical properties had to be mapped out. Table 7 the material properties of the components considered in the analysis. The material properties for more common materials were taken from the material database in CES EduPack 2018.

Table 7: Material Properties

Material	Density [g/m^3]	Conductivity [W/m K]	Specific Heat [J/kg K]
AA6061	2712.9	160.43	895.82
AA6082	2699.6	171.97	899.82
AA7075	2799.8	133.97	945.42
B270 [RD08]	2550	0.92	860
Copper C10100	8920	387	386
FR-4	1250	0.35	1300
Alumina Ceramic	3890	35.4	880

Table 8 tabulates the thermo-optical properties of the surfaces considered in the analysis. The thermo-optical properties of external surface properties were provided as lumped properties by NanoAvionics. For other surface properties, NASA studies were consulted [RD09].

Table 8: Thermo-optical Properties

Surface	Emissivity, ε	Absorptivity, α
Aluminium		
Black Anodized	0.87	0.83
Clear Anodized	0.76	0.27
Clear Polished [RD10]	0.05	0.25
Clear Rough [RD10]	0.07	0.525
External Surfaces		
Solar Panel +Y Lumped	0.852	0.635
Solar Panel -Y Lumped	0.852	0.635
Solar Panel +X Lumped	0.866	0.556
Solar Panel -X Lumped	0.876	0.294
Splitter -Z Lumped	0.924	0.248
Misc		
Copper Oxidized	0.8	0.9
Black Body	1	1

5. Finite Element Model

To simulate the environmental temperature effects on the payloads, the bus has to be taken into consideration. The mockup sent from NanoAvionics was used for this.

5.1 Idealization

The model must be simplified in order to avoid complications, and to make the underlying mathematical model work. Additionally, depending on the complexity of a model, thermal simulations can take a lot of time. For the preliminary analysis, it was decided to simplify the geometric complexity of the model to save computing time. The following actions have been taken using the idealization tool and synchronous modeling approach:

NanoAvionics Bus
- All screws and screw holes have been removed
- All surface details have been removed.
- PCBs have been made into 2D plates with 3D PCB components
- Heat generating elements such as processors have been replaced with simulation objects
- Solar panels merged with solar cells made into simple 2D shapes

HSI Camera Payload
- Edge blends removed
- Screws and holes removed
- Grating cassette subsystem removed, the mass transferred to the grating
- AA 6082-T6, polished surface assumed for the entire platform
- Objectives replaced with simple cylinder geometry, inner diameter of 25 mm, outer diameter of 35.8 mm, with the correct mass of 106 g assigned
- The glass lenses and internal geometry of the objectives are removed
- Collamiter tube simplified to a cylinder with inner diameter of 42.1 mm, and outer diameter of 30.7 mm
- Slit and restraining rings removed from collamiter tube
- Platform Brackets Removed, mass added to the base platform

SDR and Onboard Processing
- PCBs simplified into a simple 2D shapes
- All parts of the SDR stack were made into a single 3D cube with the total dimensions and mass of the stack.
- All payloads are simulated via PCB components. Heat generation can be traced.

RGB Camera
- Simplified massive dummy
- AA 6061-T6, white anodized assumed for the entire model

5.2 FE Model Mesh

The mesh was coarse to decrease computing time. For nastran, the mesh might be too rough. However for thermal simulations the amount of elements seems to matter less to achieve accurate results. For the final simulations a finer mesh should be used. Tetrahedral 3D mesh were used in order to mesh geometrically complex parts with high thickness, at least 2 elements per thickness was used. 3D swept mesh was used on simpler swepable geometry, swept mesh was used if possible. A simple 2D thin shell mesh were used on thinner parts, that could be substituted with a plate for computational time. Mesh mating was done on parts that had direct contact. Every part and components were meshed individually in order to assign the correct material, corrected weight if the part was simplified and surface Thermo-optical Properties. Table 9 tabulates the mesh method, element type, element size and material assigned to the different components. The total amount of mesh nodes in the simulation was measured to be 81013.

Table 9: Mesh Data

HYPSO Systems				
Bus				
Body	**Mesh Type**	**Element Type**	**Element Size (mm)**	**Material**
Walls (2)	3D Tetrahedral	TET (10)	16	AA 7075-T6
Brackets (4)	3D Tetrahedral	TET (10)	10	AA 7075-T6
Solar Panels PCB/ Cell (±Y)	3D Swept	HEXA (20)	30	FR4,Glass Copper Composite
Solar Panels PCB/ Cell (±X)	3D Swept	HEXA (20)	30	FR4,Glass Copper Composite
Splitter (-Z)	3D Swept	HEXA (20)	15	AA 7075-T6
Tuna Can (2)	3D Tetrahedral	TET (10)	14	AA 7075-T6
Battery Stack, (Inside Tuna Can)	3D Swept	HEXA (20)	15	AA 7075-T6
Battery Bracket (2)	3D Tetrahedral	TET (10)	6	AA 7075-T6
Reaction Wheel (4)	3D Tetrahedral	TET (10)	16	AA 7075-T6
Reaction Wheel Bracket (4)	3D Tetrahedral	TET (10)	9	AA 7075-T6
Magnetorquer Solenoid (4)	3D Swept	HEXA (10)	14	C10100 Copper
Magnetorquer Brackets (8)	3D Tetrahedral	TET (10)	3	AA 7075-T6
Star Tracker	3D Tetrahedral	TET (10)	15	AA 7075-T6

IMU	3D Swept	TET (20)	15	AA 7075-T6
Payload Controller Frame	3D Tetrahedral	TET (10)	10	AA 7075-T6
Payload Controller Ring	3D Tetrahedral	TET (10)	11	AA 7075-T6
Payload Controller Interface Plate	2D Thin Shell	QUAD (8)	6	FR4,Glass Copper Composite
Stacking Ring PC104 (4)	3D Swept	HEXA (20)	10	AA 7075
Stacking Ring Rod (8)	3D Swept	HEXA (20)	7	304 Stainless Steel
Stack Magnetorquers Combined	3D Swept	HEXA (20)	15.5	C10100 Copper
Battery Pack, (Inside stack)	3D Swept	HEXA (20)	16.4	AA 7075
Flight Controller	3D Swept	HEXA (20)	10	AA 7075
Flight Controller PCB	2D Thin Shell	QUAD (8)	13	AA 7075
Electrical Power System, Battery (2)	3D Swept	HEXA (20)	16.5	AA 7075
EPS PCB board	2D Thin Shell	QUAD (8)	13	FR4,Glass Copper Composite
S-Band Transceiver TX+RX	3D Swept	HEXA (20)	30	AA 7075
S-Band Antenna	3D Swept	HEXA (20)	30	AA 7075
GPS	3D Swept	HEXA (20)	10	AA 7075
OPU	3D Tetrahedral	TET (10)	15	Custom FR4/Alumina
HYPSO Payloads				
Primary HSI Payload				
HSI Platform	3D Tetrahedral	TET (10)	16	AA 6082-T6
HSI Platform Shroud	3D Tetrahedral	TET (10)	16	AA 6082-T6
IMX249 Detector	3D Swept	HEXA (20)	15	Custom Detector Material
50 mm VIS NIR	3D Swept	HEXA (20)	15	AA6061

Objective (3)				
Collimator Tube	3D Swept	HEXA (20)	15	AA6016
Grating	3D Swept	HEXA (20)	15	B270
OPU (Picozed Breakout Board)	3D	TET (10)	15	Custom FR4/Alumina
Secondary SDR Payload				
SDR (Motherboard + UHF)	3D Tetrahedral	TET (10)	10	Custom FR4/ Aluminium
Mounting Plate	3D Tetrahedral	TET (10)	10	AA 7075-T6
Adapter Plate	3D Tetrahedral	TET (10)	10	AA 6082-T6
Support Plate	3D Tetrahedral	TET (10)	10	AA 6082-T6
M3 Rod (4)	3D Swept	HEXA (20)	7	304 Stainless Steel
Tertiary RGB Camera Payload				
RBG Camera	3D Tetrahedral	TET (10)	10	AA 6061-T6

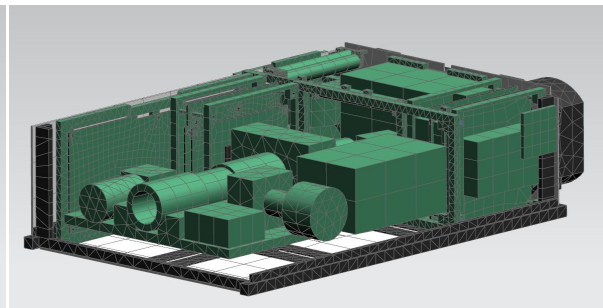Figure 7- 10 shows the mesh used.
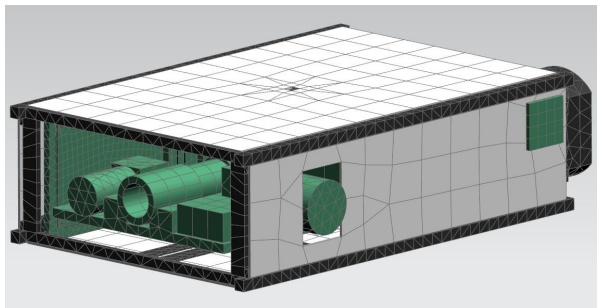
Figure 7: CubeSat Mesh

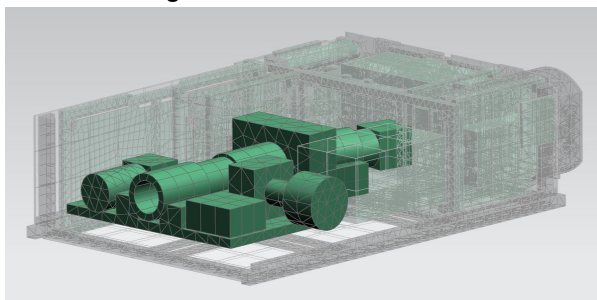*Figure 8: Payload Mesh on frame*

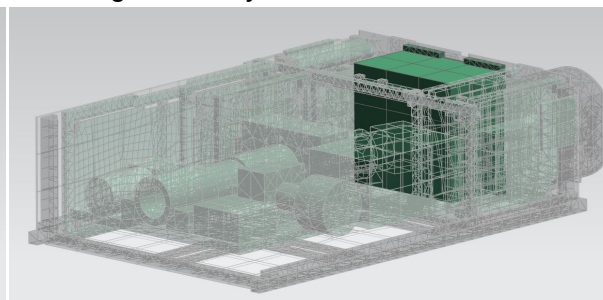*Figure 9: HSI Assembly Mesh*

Figure 10: Simplified SDR Mesh

5.3 Simulation Objects

Simulation objects contain all information regarding thermal interfaces, and internal heat generation in the CubeSat. The following simulation objects were used to define the model:

Solar heat radiation, albedo, and earth infrared radiation were simulated using the simulation object *Orbital Heating*. Orbital and space environmental parameters were defined in the object following the values tabulated in table 4 and 5. The object was applied to all surfaces by using the *Illuminate All Surfaces* function, which considers all surfaces in the model visible to the sun and earth. However, by considering all surfaces, the simulation time increases. Even so, this was done to save time on the set-up side, as simulations can be ran parallel to other work. Radiation was calculated using the Monte Carlo method with a ray density control based on an error criterion of 0.05 and confidence level at 95% [RD11].

Radiation between and from all objects were simulated using the simulation object *Radiation*. The calculation method was chosen to be the same as for orbital heating. All radiation in the simulation used the thermo-optical properties listed in table 8. Because of the number of parts in the model, the function *All Radiation* was used. This did however increase the simulation time considerably.

In order to model the conduction between every surface in the satellite, two types of simulation objects were used. These were *Surface to Surface Contact* and *Advanced Thermal Coupling*. Most of the connections in the satellite was modelled using Surface to Surface contact because of the function to only consider overlapping surfaces between two faces with dissimilar areas. Because proper conductive properties were not known, the true heat transfer was approximated to be somewhere between perfect conduction, and radiation as close parallel plates. Perfect conduction simulates the temperature to be the exact same between the two surfaces, while close parallel plate radiation assumes the view factor to be equal to 1 between the two surfaces. The resulting gray body view factor (GBVF) is calculated as $GBVF = 1/(1 + \varepsilon_1/\varepsilon_2 - \varepsilon_1)$, where ε_1, ε_2 are the emissivity factors of the primary and secondary regions. The conductance between two surfaces heavily depend on multiple factors such as the level of roughness on the surfaces, as well as pressure between them [RD12]. In some cases, the actual amount of contacting surfaces may be as low as one percent [RD13]. In these cases, most of the conduction is through close parallel plate radiation. Because of this, components outside the interest of this simulation were modelled with close parallel plate radiation. To more accurately define the conductive properties, thermal vacuum testing would be required. Thermal coupling was used in cases where the conductive surfaces did not exist due to not being designed yet, or excluded for simplicity. The HSI camera objectives to brackets and HSI platform were also simulated using close parallel plates assuming the full area of cylinder surface area and the grooves and walls of the platform. This was done due to the complexity of heat transfer between the brackets and camera cylinders as well as the time constraints of the analysis.

Heat dissipation of parts were modelled using the *Heat Load* object, which allowed the total amount of heat energy for a surface to be directly specified. The object was applied to the surfaces of all the components specified in table 4 with their respective heat dissipation values. Because some of the heat generating systems were combined in physical models, the schematic in figure 11 was followed when distributing the heat dissipation.
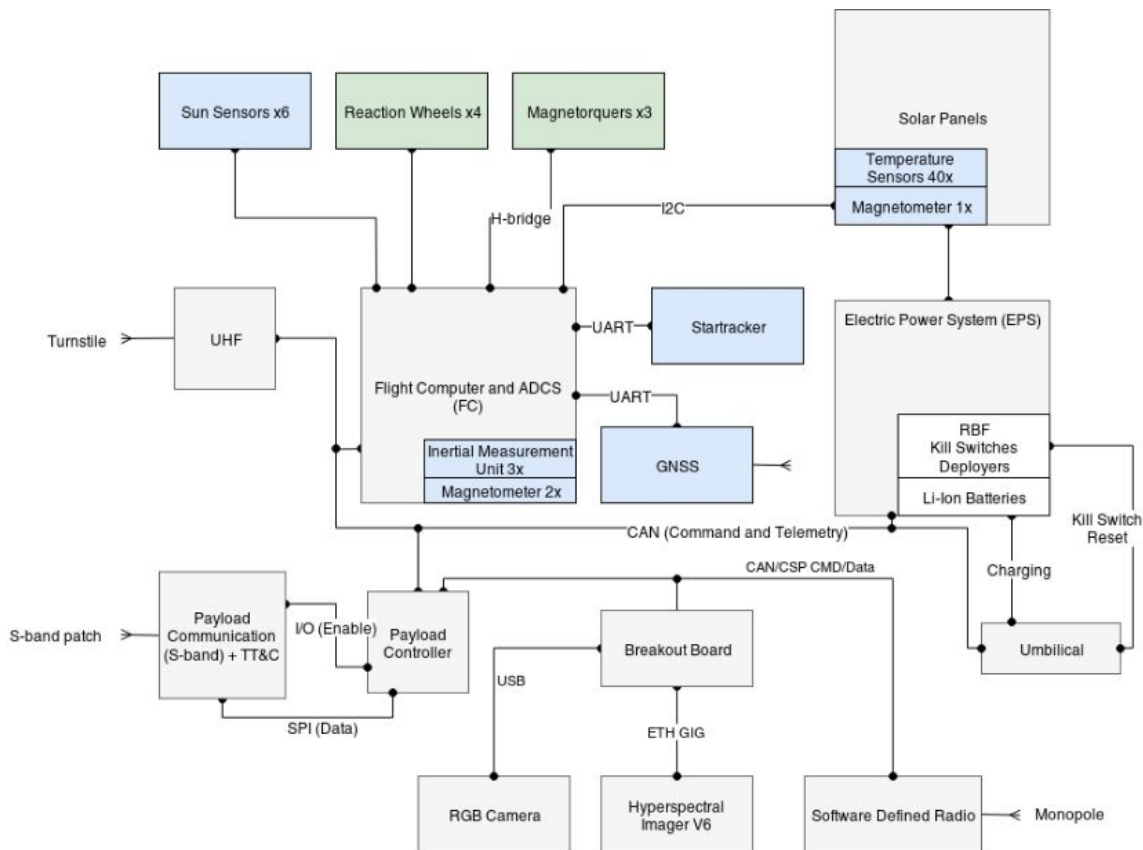

Figure 11: HYPSO Payload Schematics [RD04]

In order to model the dampeners in the simulation, the simulation object thermal coupling was used between the bottom of the HSI platform and satellite frame. Because the amount and positioning of the dampeners, as well as specific property had not been decided at the time of the simulation, various assumptions had to be made. What was known was that the *1114S damper from SMAC* as can be seen in figure 12 would be implemented. The number of dampeners assumed in the simulation was set to 9, which was the recommended amount by SMAC.
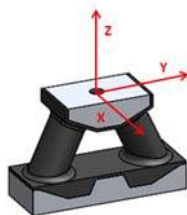

Figure 12: 1114S damper

Using the conductive gap function, the conductivity was calculated following the equation $G = \frac{kA}{L}$, where G equals the total conductance coefficient, k is the thermal conductivity of the gap, A the area of the contacting surfaces and L the distance between the two surface element. The total area was calculated as the sum of the number of dampeners, which each had two oval shaped rods. The largest diameter of the oval was used to approximate a circular cross-section. Using these assumptions, cross-section A was calculated to be 904.78mm^2. The distance L was measured to be 9 mm. For the conductivity k, 0.3W/mK was used based on higher ranges of conductances of elastomers, based on worst case values (high heat transference) for aerospace elastomers from EduPack. G was calculated to be 0.03016W/ΔK. Due to the approach, the mass of the dampeners and their interfaces were not considered in the simulation. These were also unknown at the time the analysis was conducted.

6. Results

6.1 Hot Case Results

The following figures shows the results for the hot case. Figure 13 provides an overview of the thermal fluctuations of all payloads and directly attached systems. The following figures present the Thermal Fluctuations in the parts as a function of the transient orbit, the exact nodes used for probing are listed and noted in the corresponding Probe Node Locations figure for the corresponding thermal graph.
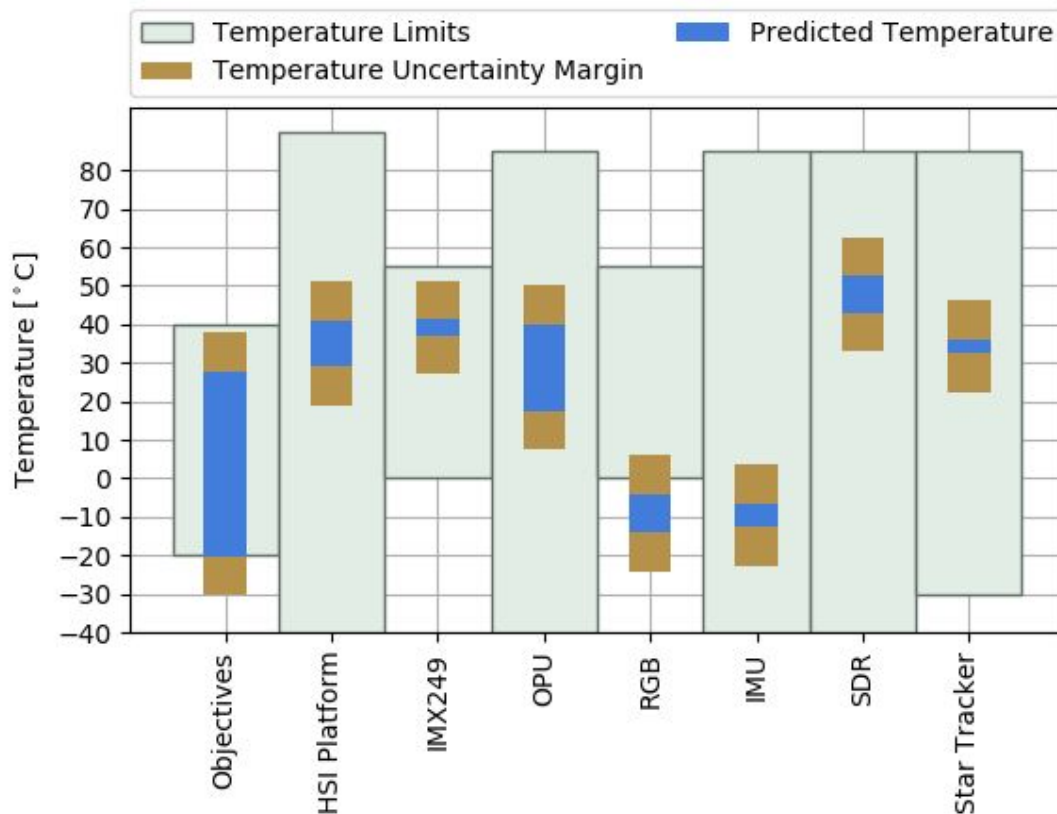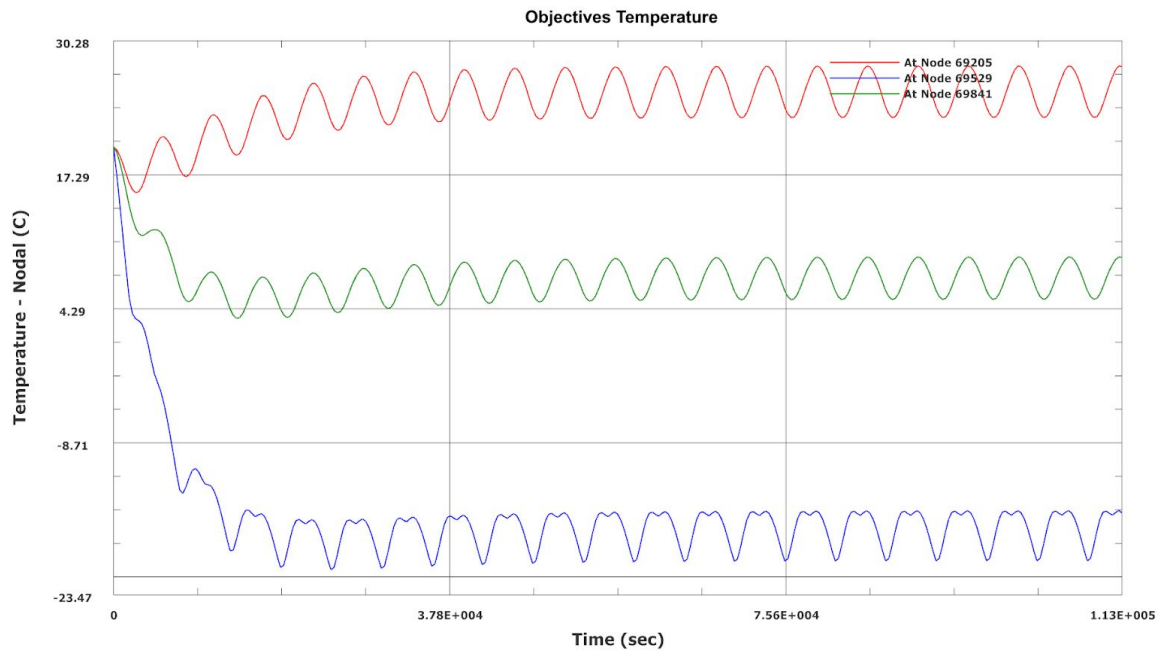

Figure 13: Hot Case Temperature Overview

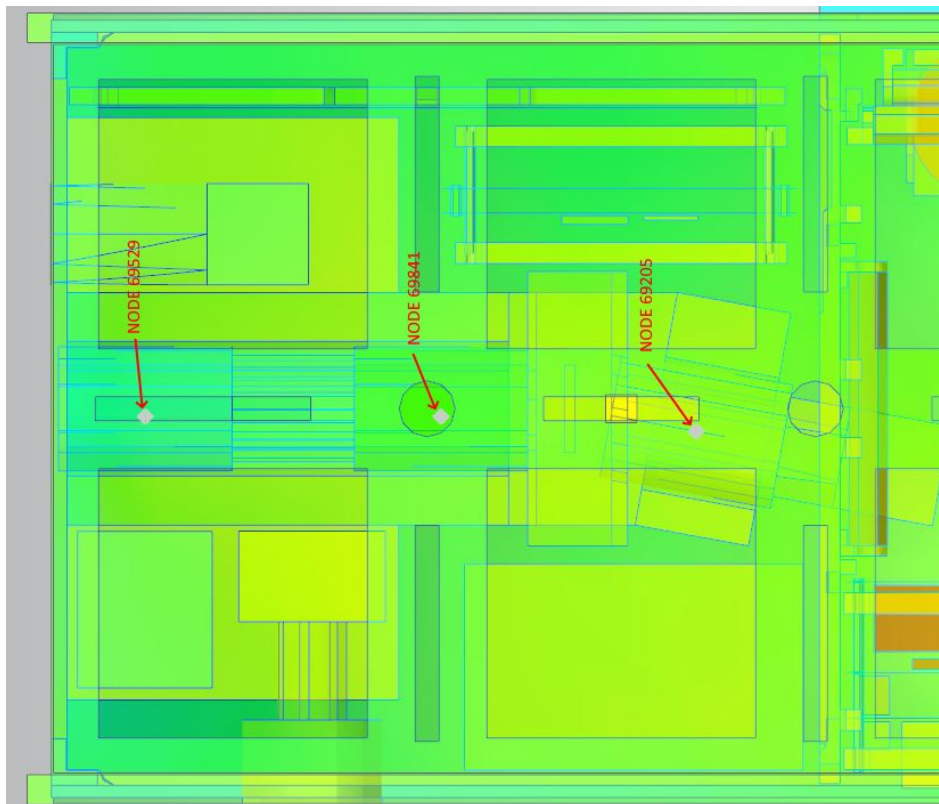*Figure 14 Objectives Orbital Thermal Fluctuations*
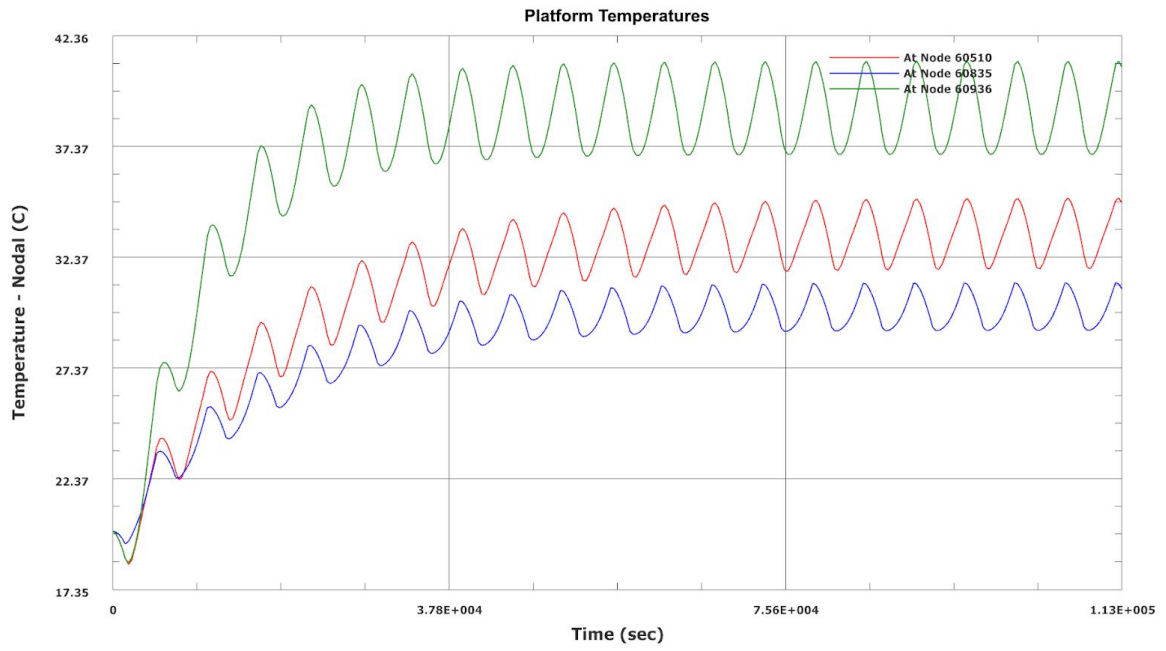

Figure 15: Objectives Probe Node Locations
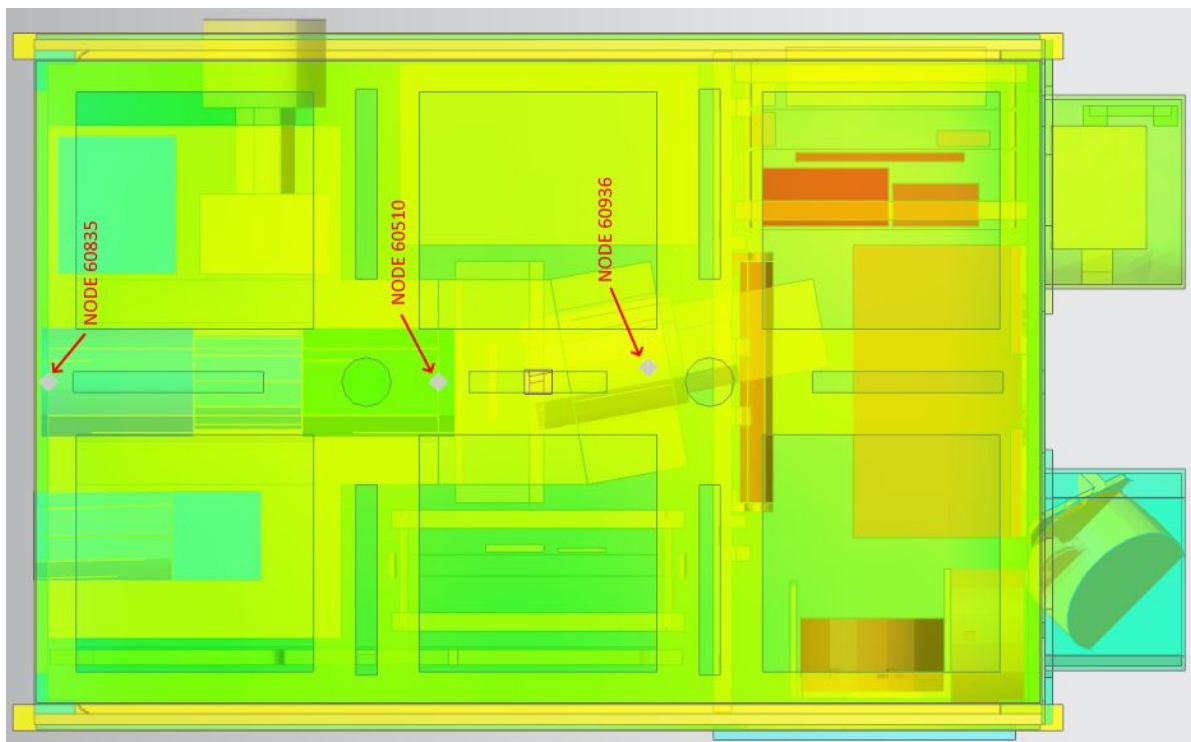
Figure 16: HSI Platform Orbital Thermal Fluctuations

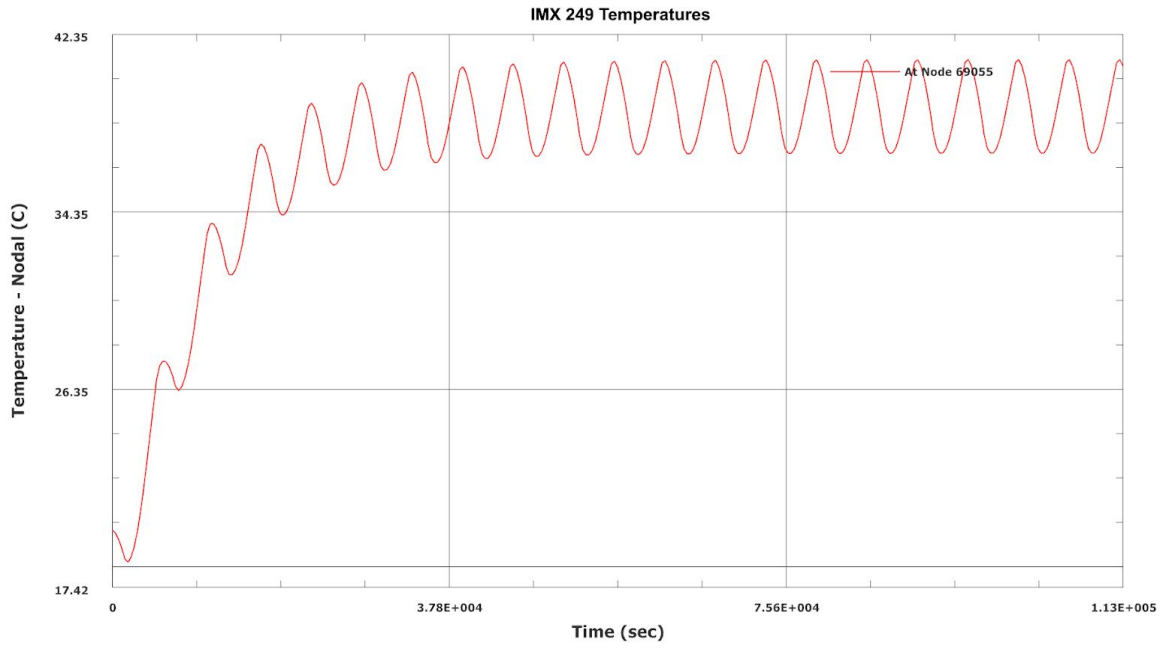*Figure 17: Platform Probe Node Locations*

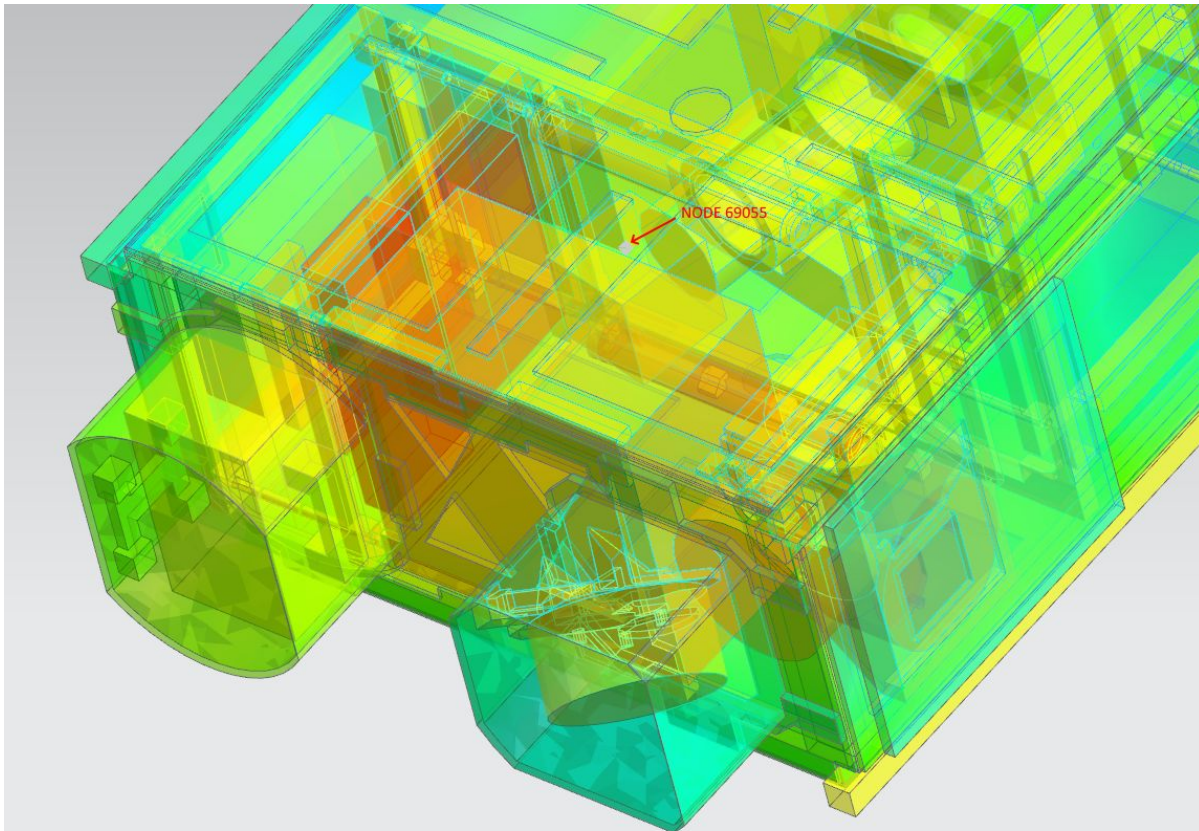*Figure 18: IMX 249 Orbital Thermal Fluctuation*

Figure 19: IMX 249 Probe Node Location

Figure 20: OPU Orbital Thermal Fluctuation

Figure 21: OPU Probe Node Location

Figure 22: RGB Orbital Thermal Fluctuation

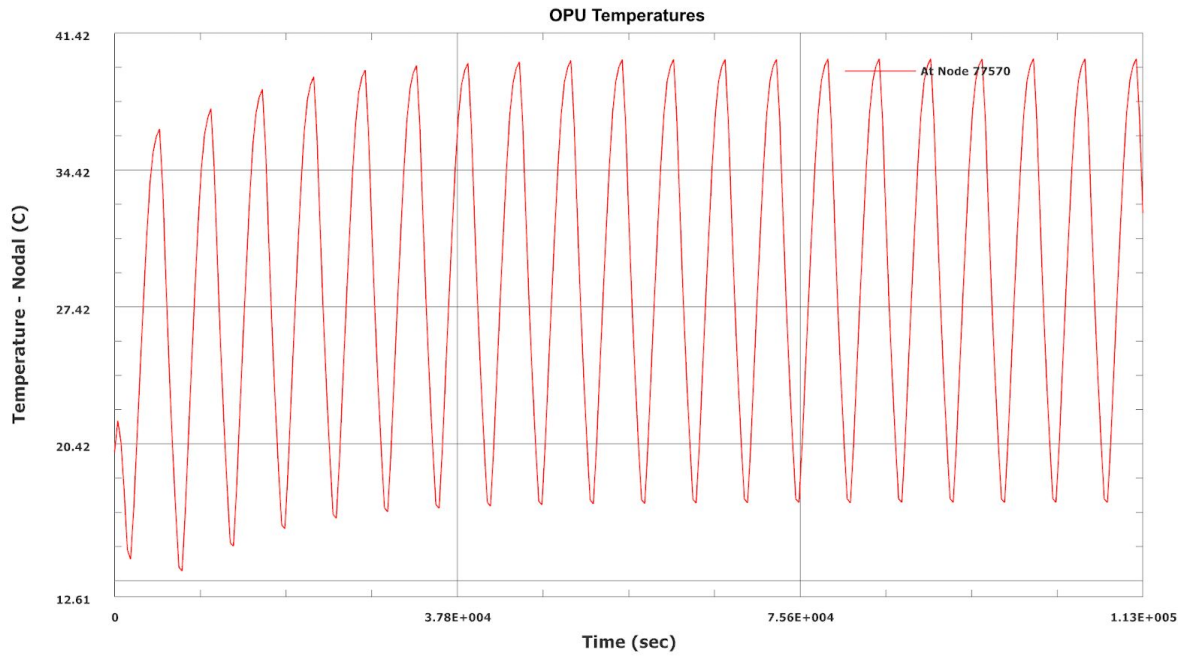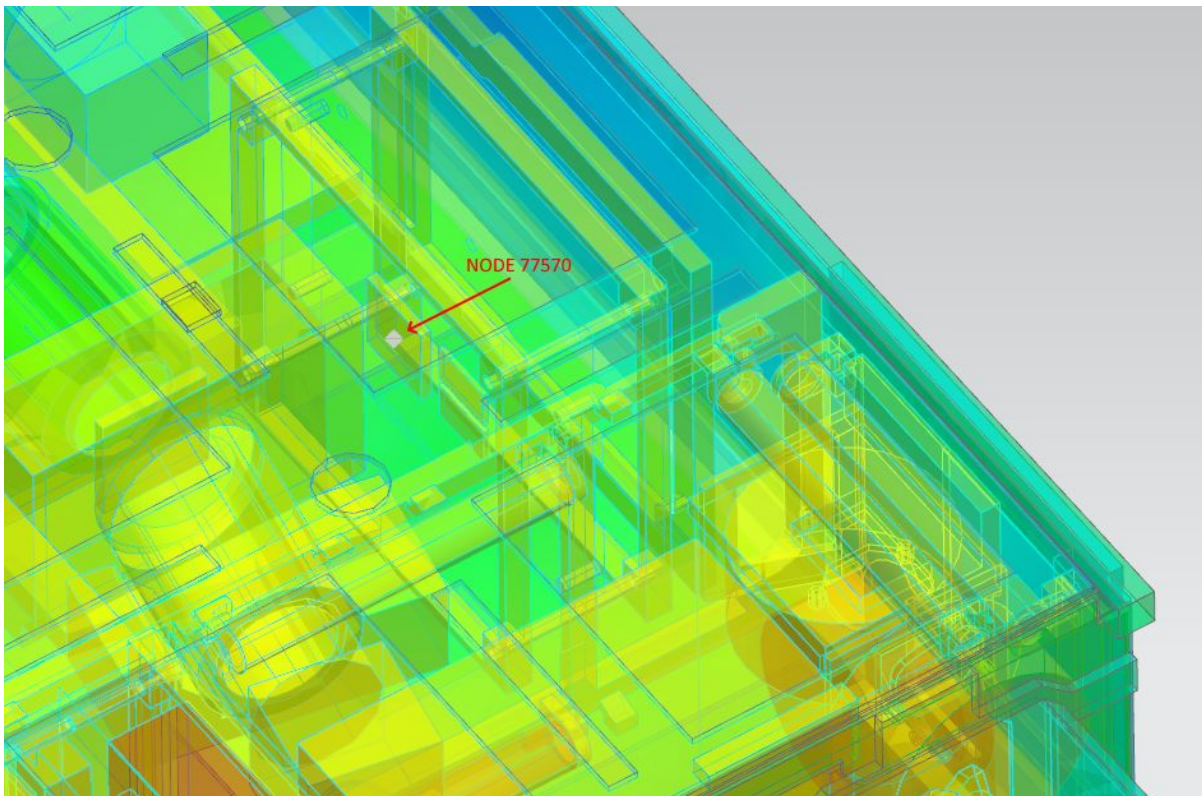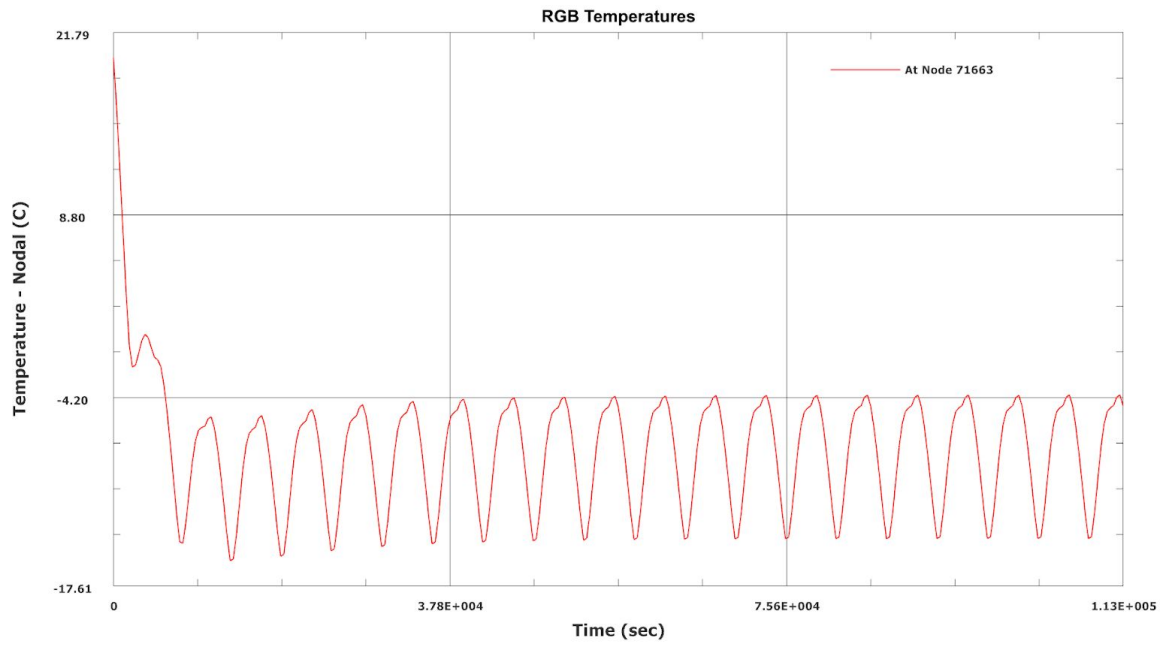*Figure 23: RGB Probe Node Location*

Figure 24: IMU Orbital Thermal Fluctuation

Figure 25: IMU Probe Node Location

Figure 26: SDR Orbital Thermal Fluctuation

Figure 27: SDR Probe Node Location
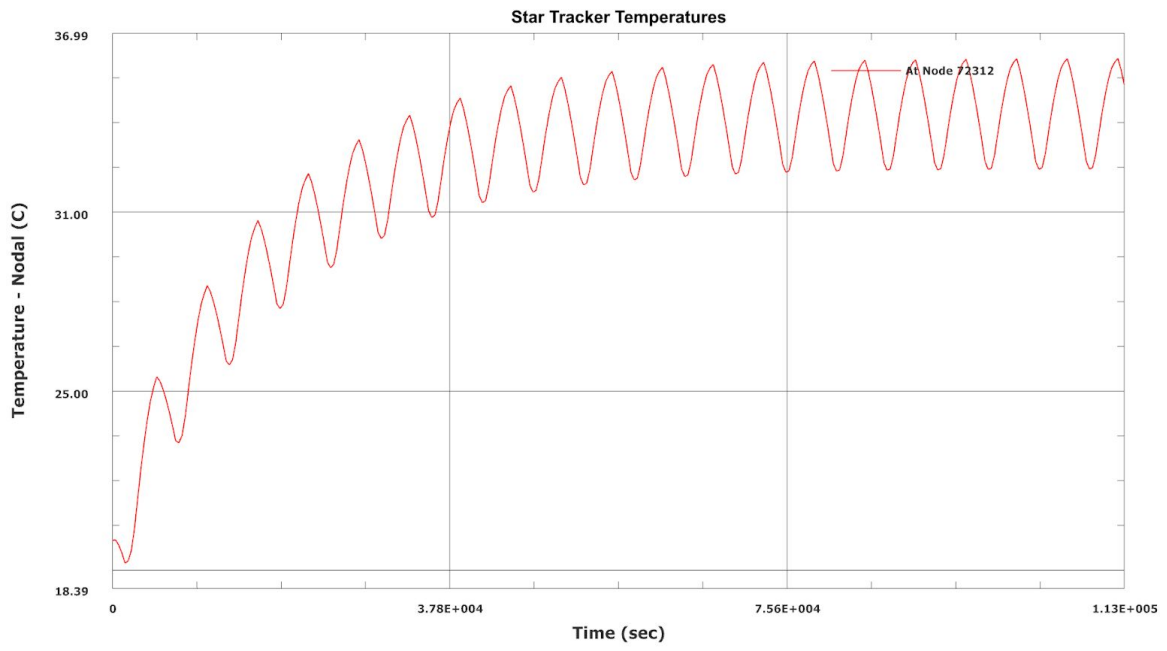
Figure 28: Star Tracker Orbital Thermal Fluctuation

Figure 29: Star Tracker Probe Node Location

6.2 Cold Case Results

The following figures shows the results for the cold case. Figure 30 provides an overview of the thermal fluctuations of all payloads and directly attached systems. The following figures present the Thermal Fluctuations in the parts as a function of the transient orbit, the exact nodes used for probing are listed and noted in the corresponding Probe Node Locations figure for the corresponding thermal graph.
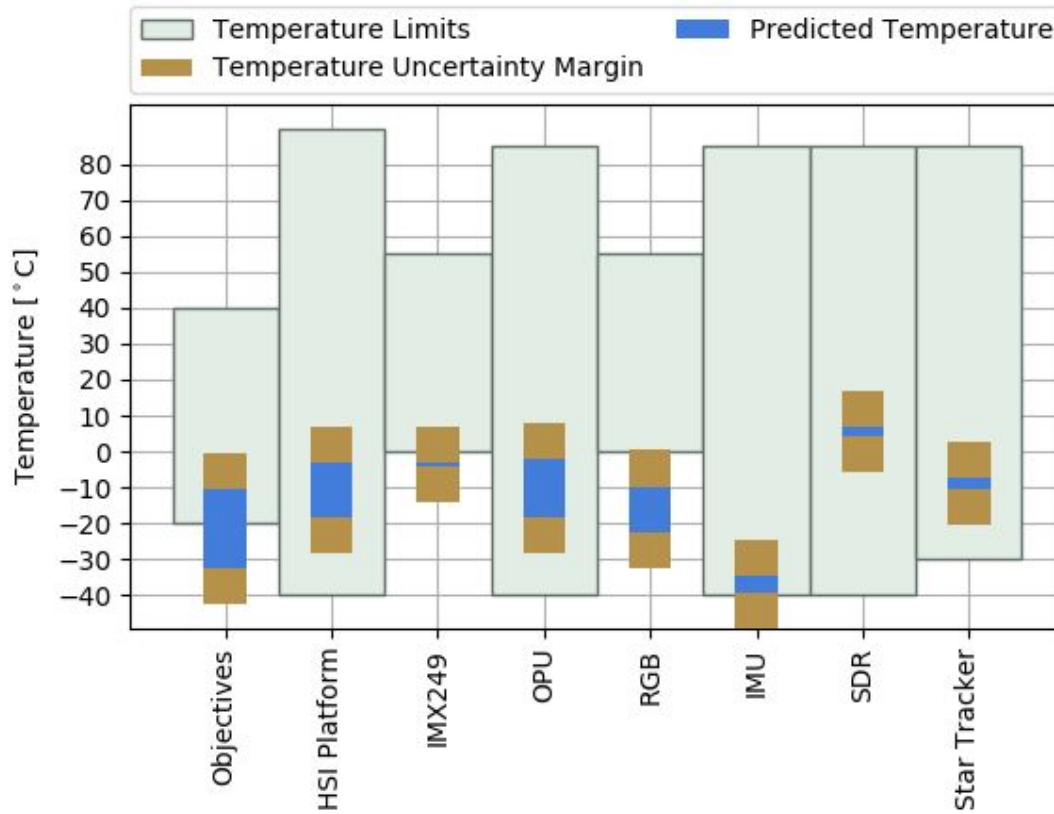
Figure 30: Cold Case Thermal Overview
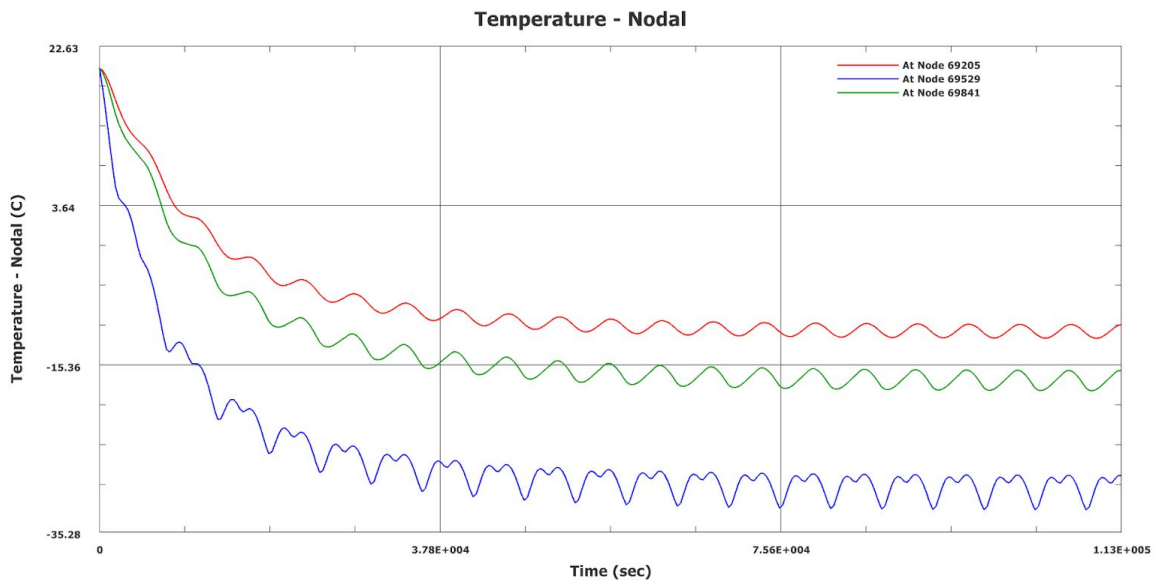
Figure 31: Objectives Orbital Thermal Fluctuations
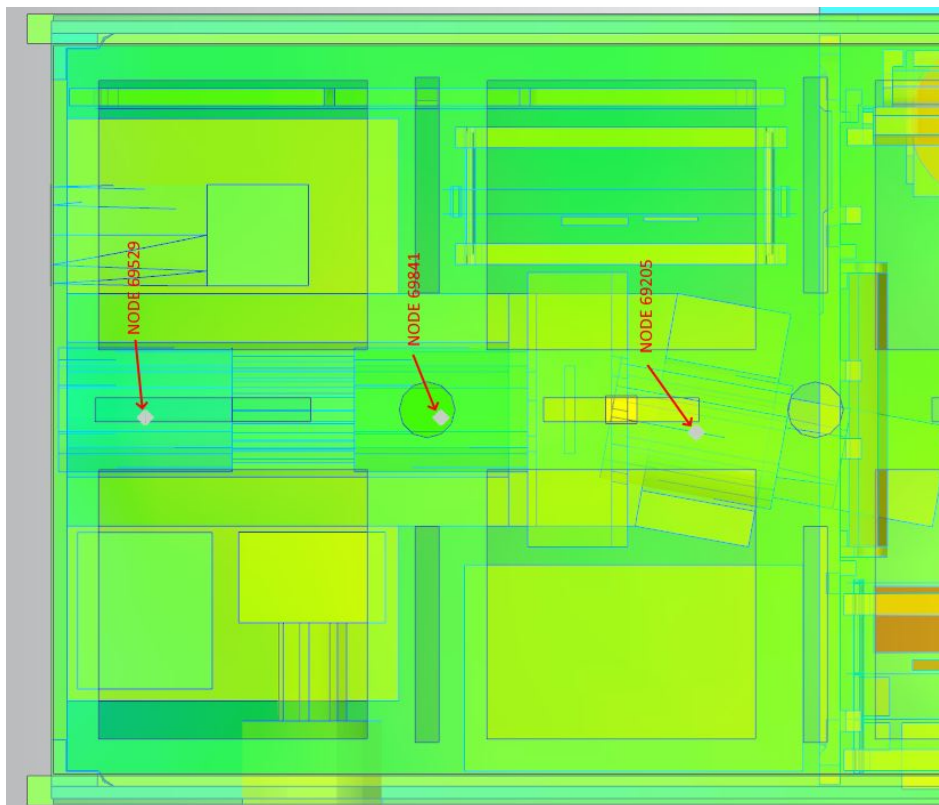
Figure 32: Objectives Probe Node Locations
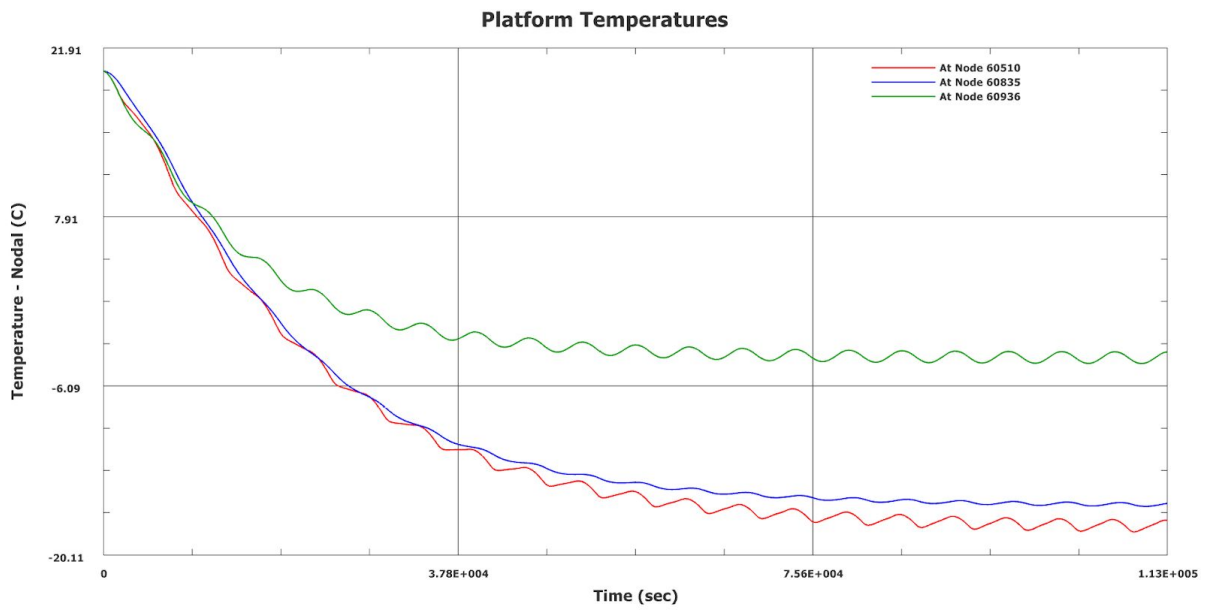
Figure 33: HSI Platform Orbital Thermal Fluctuations

Figure 34: Platform Probe Node Locations

Figure 35: IMX 249 Orbital Thermal Fluctuation
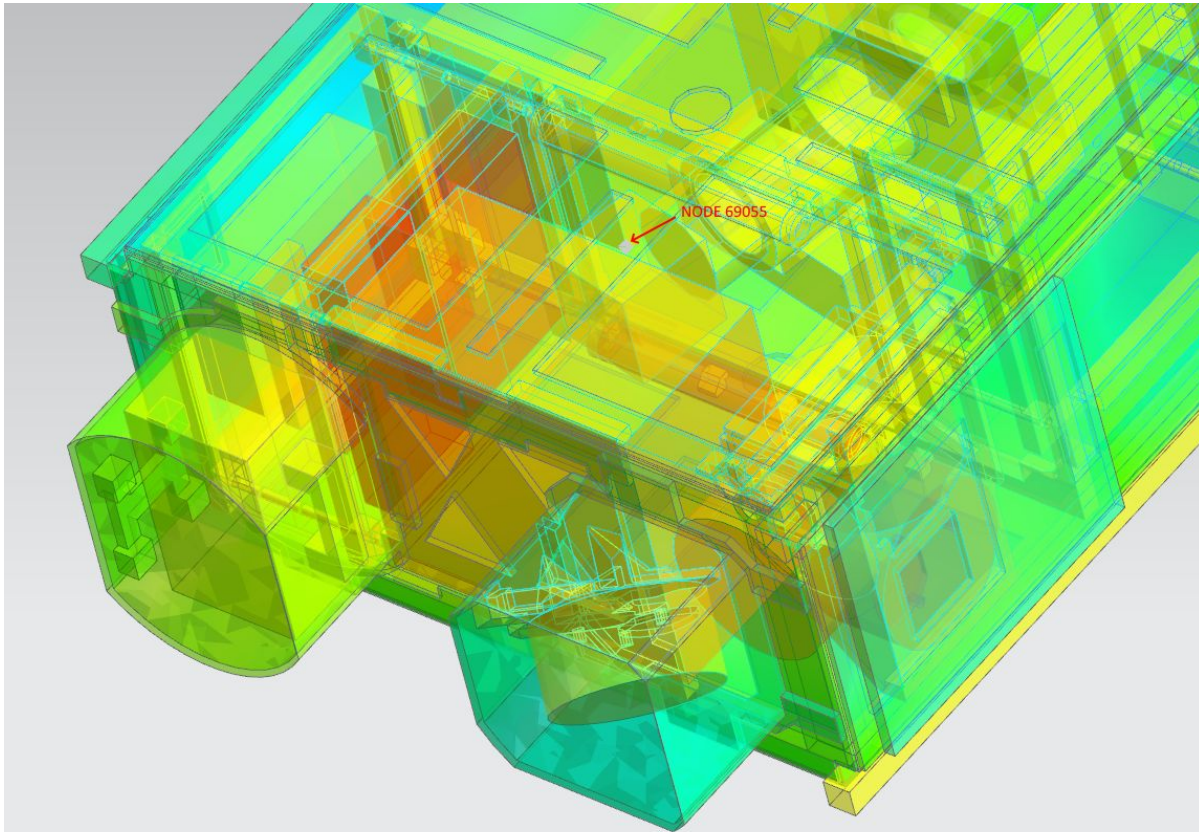
Figure 36: IMX 249 Probe Node Location
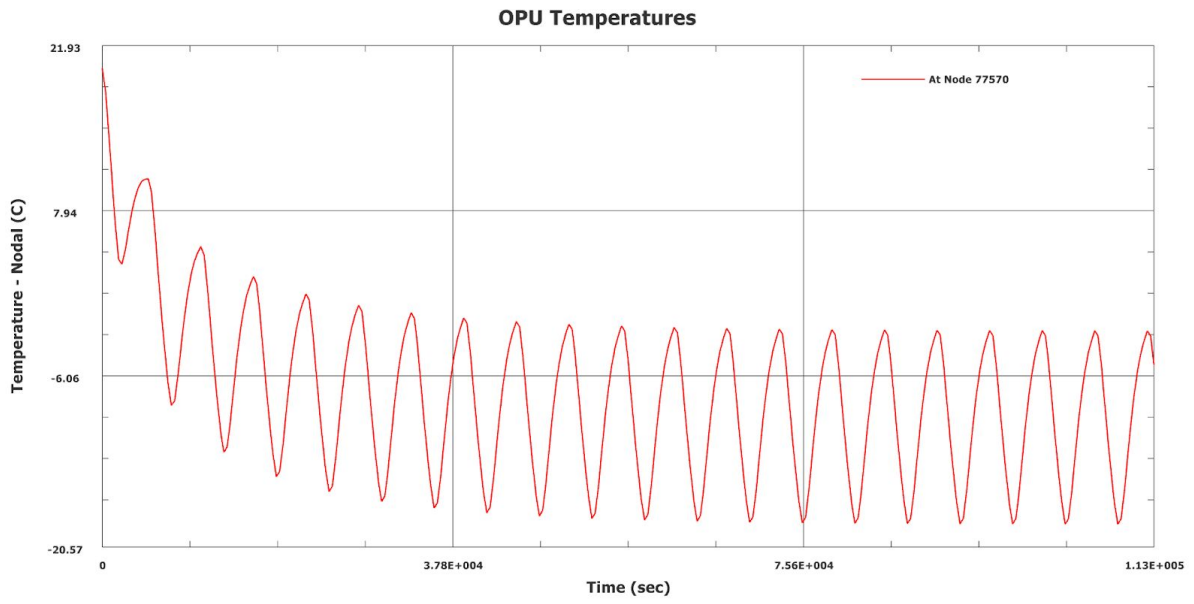
Figure 37: OPU Orbital Thermal Fluctuation
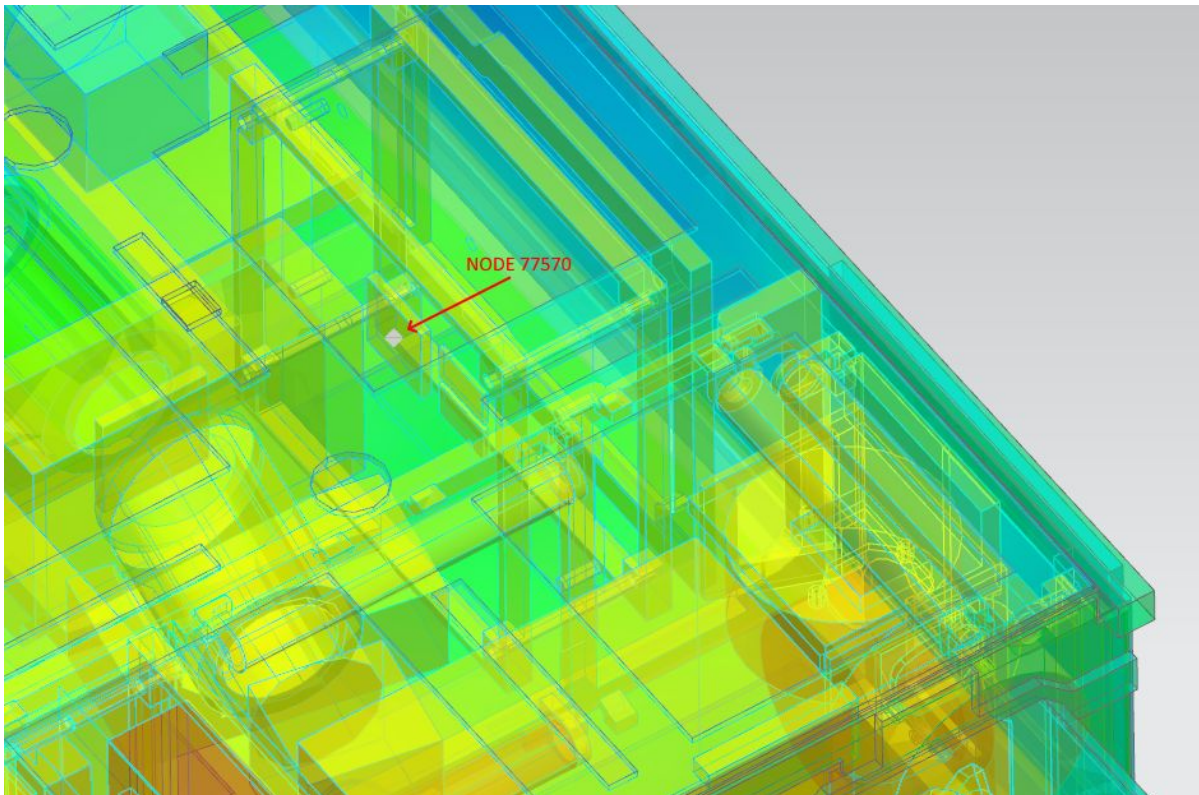
Figure 38: OPU Probe Node Location
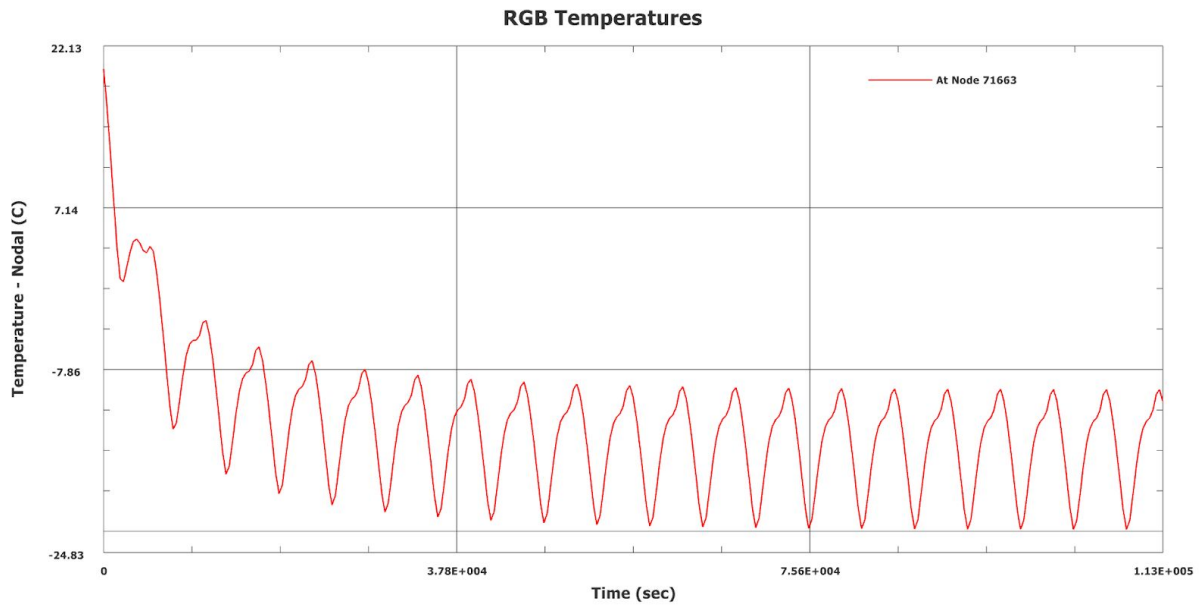
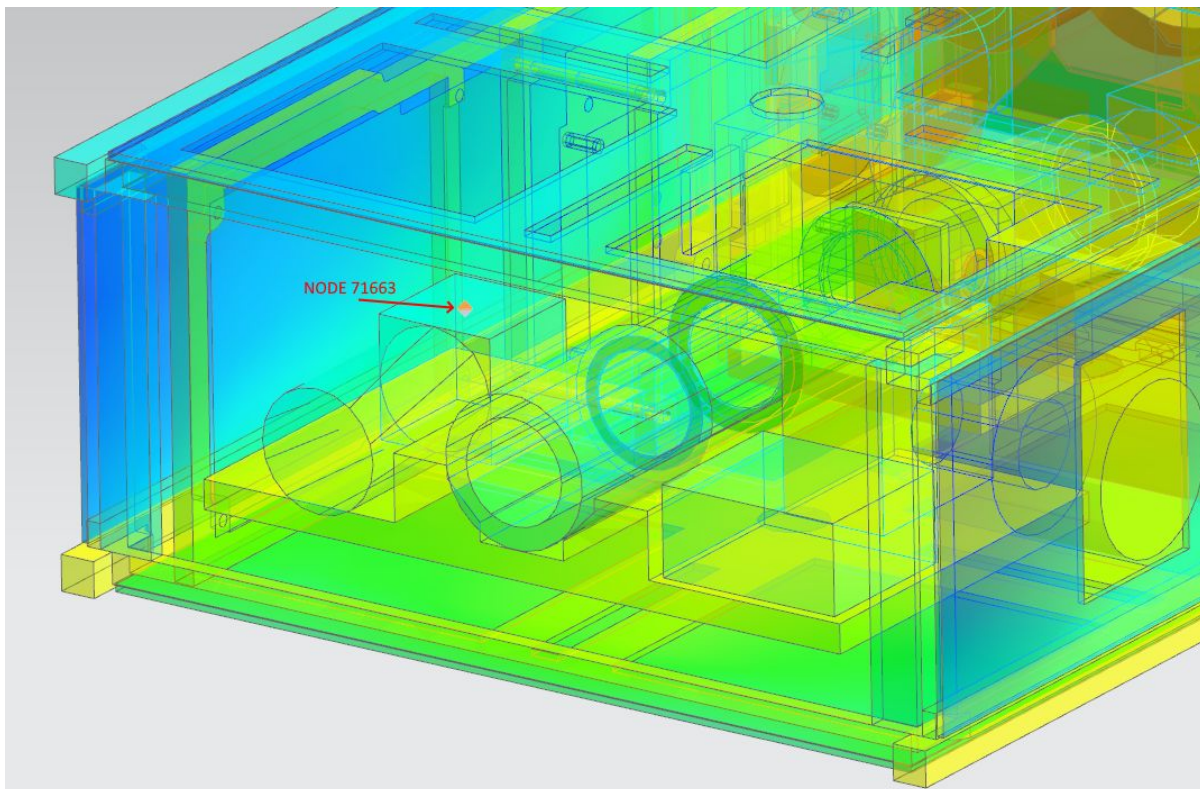*Figure 39: RGB Orbital Thermal Fluctuation*
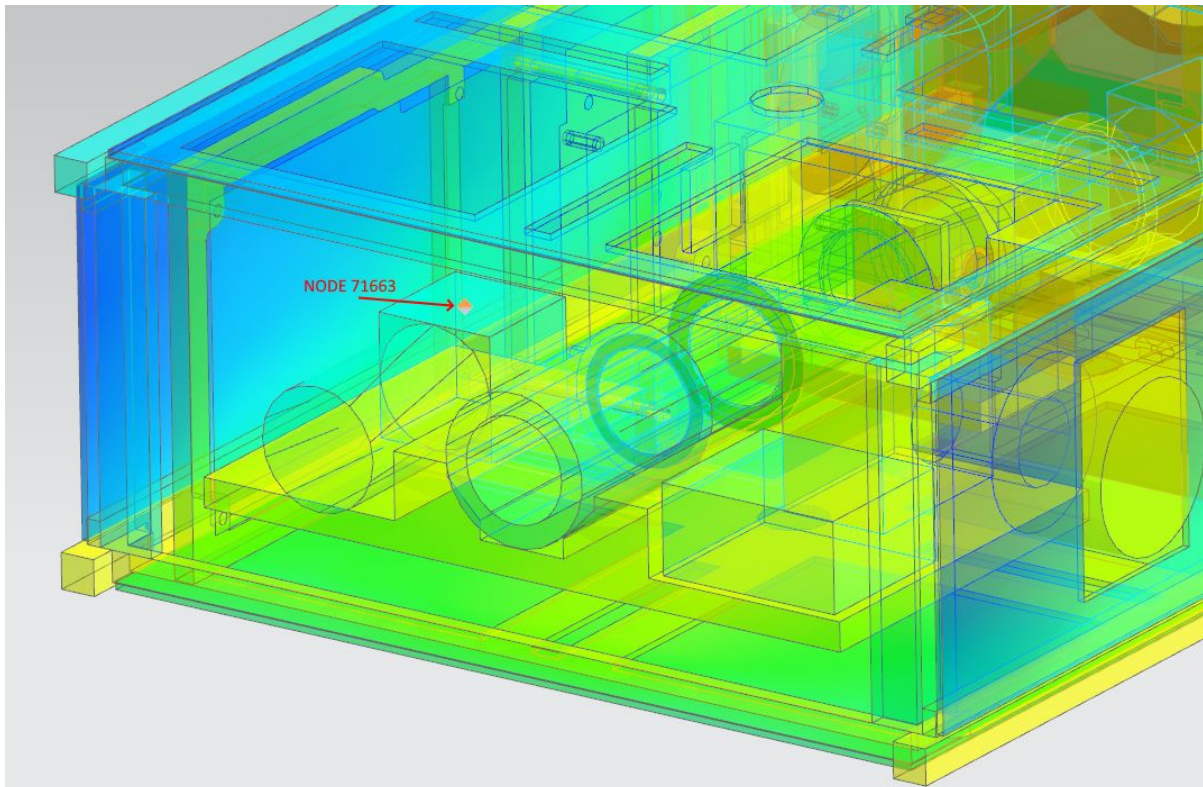
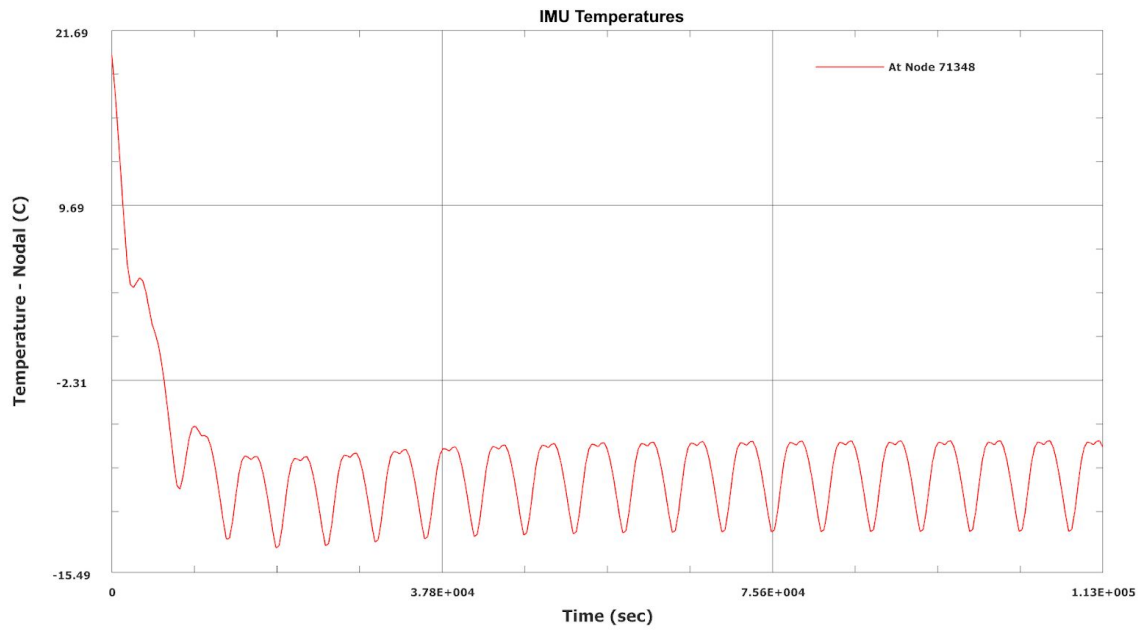*Figure 40: RGB Probe Node Location*
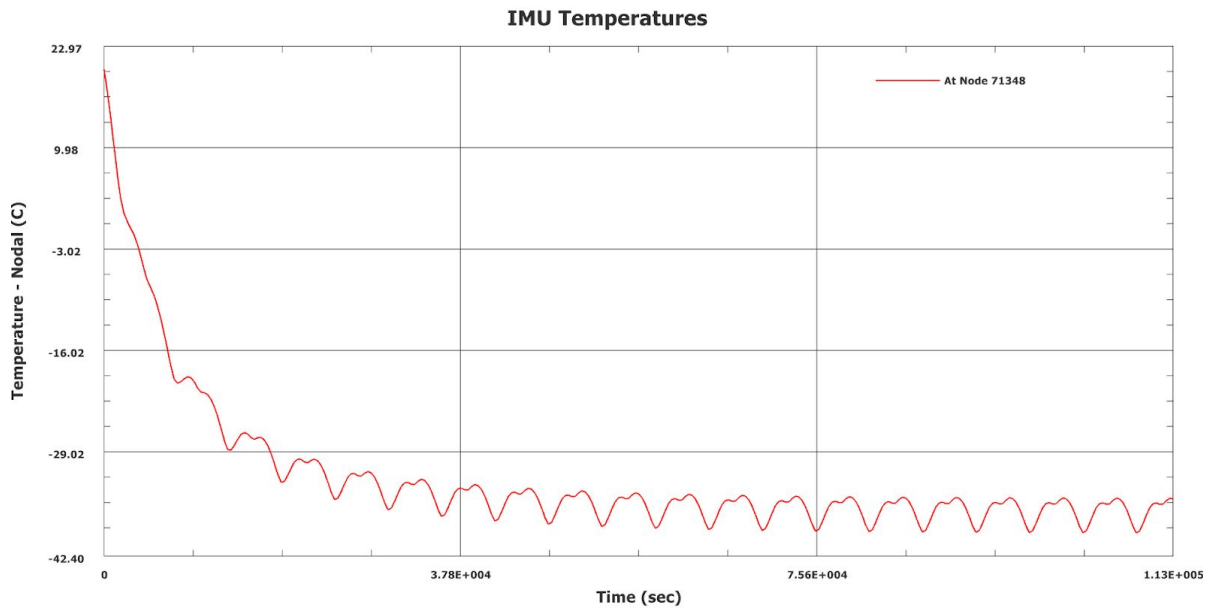
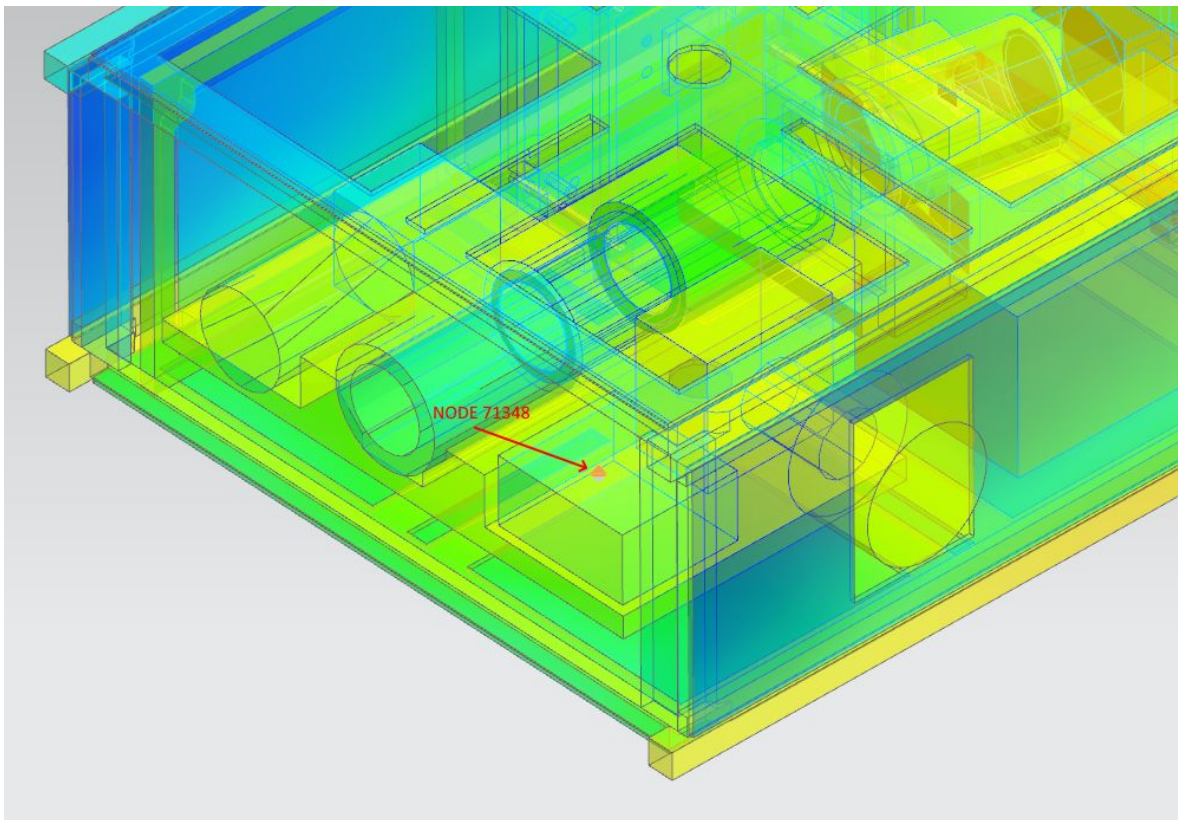*Figure 41: IMU Orbital Thermal Fluctuation*
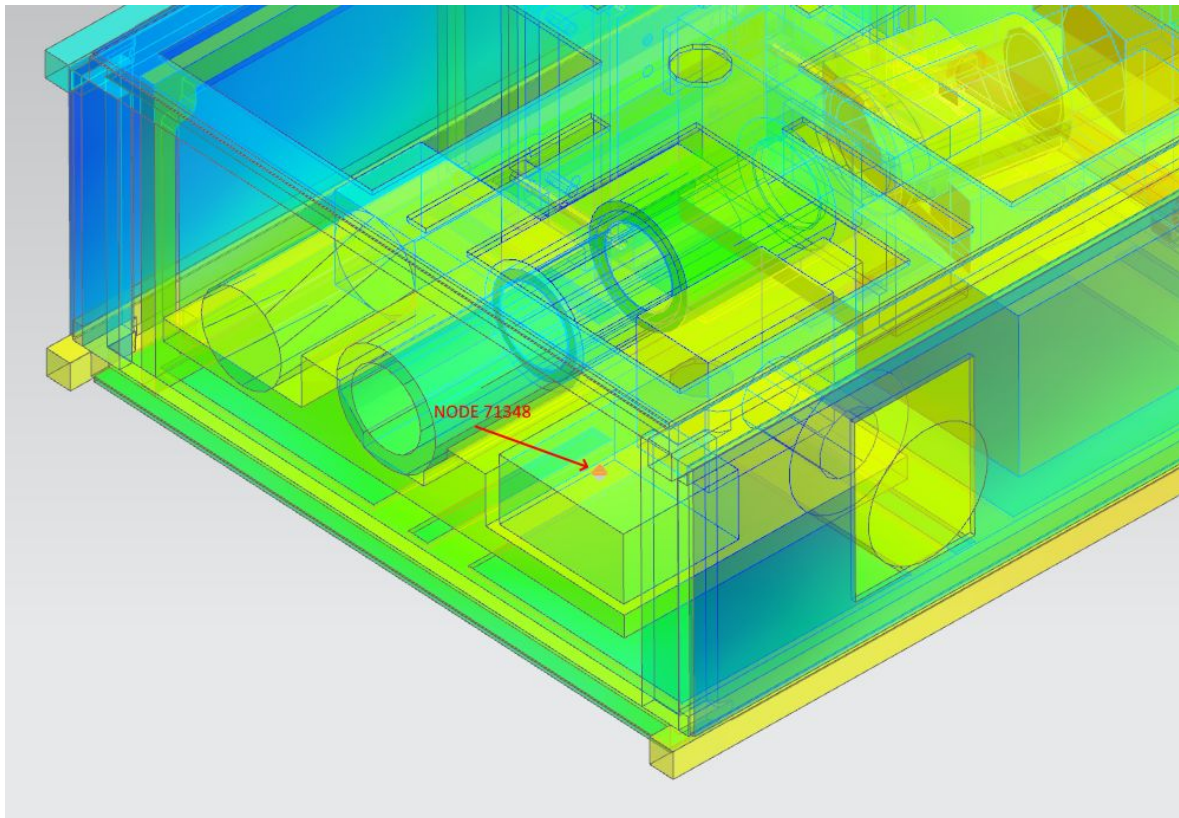
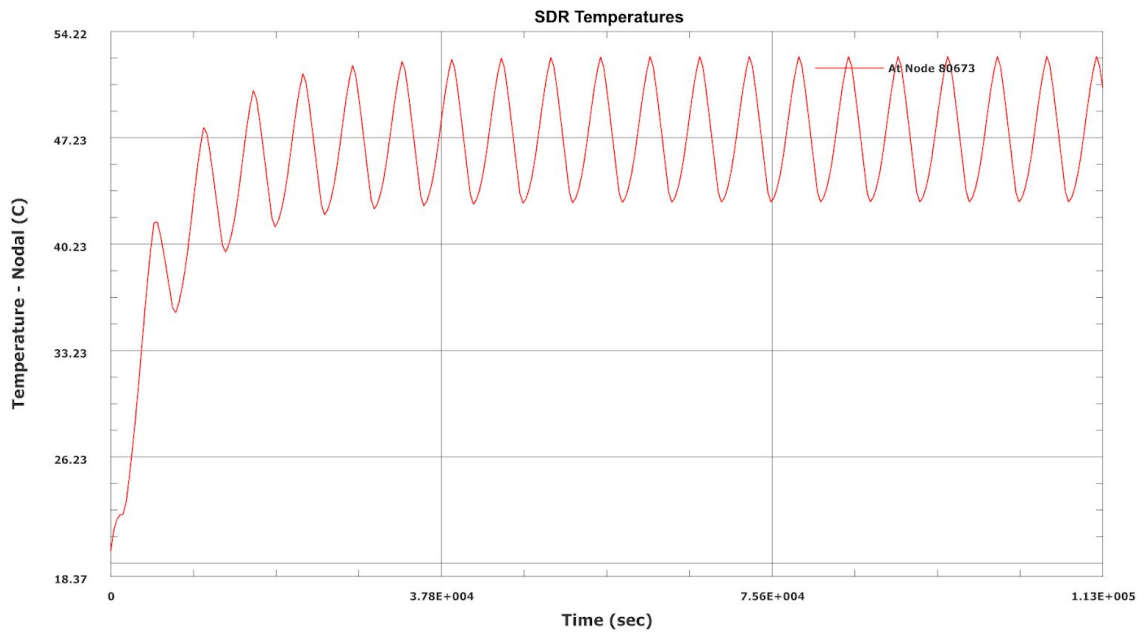*Figure 42: IMU Probe Node Location*
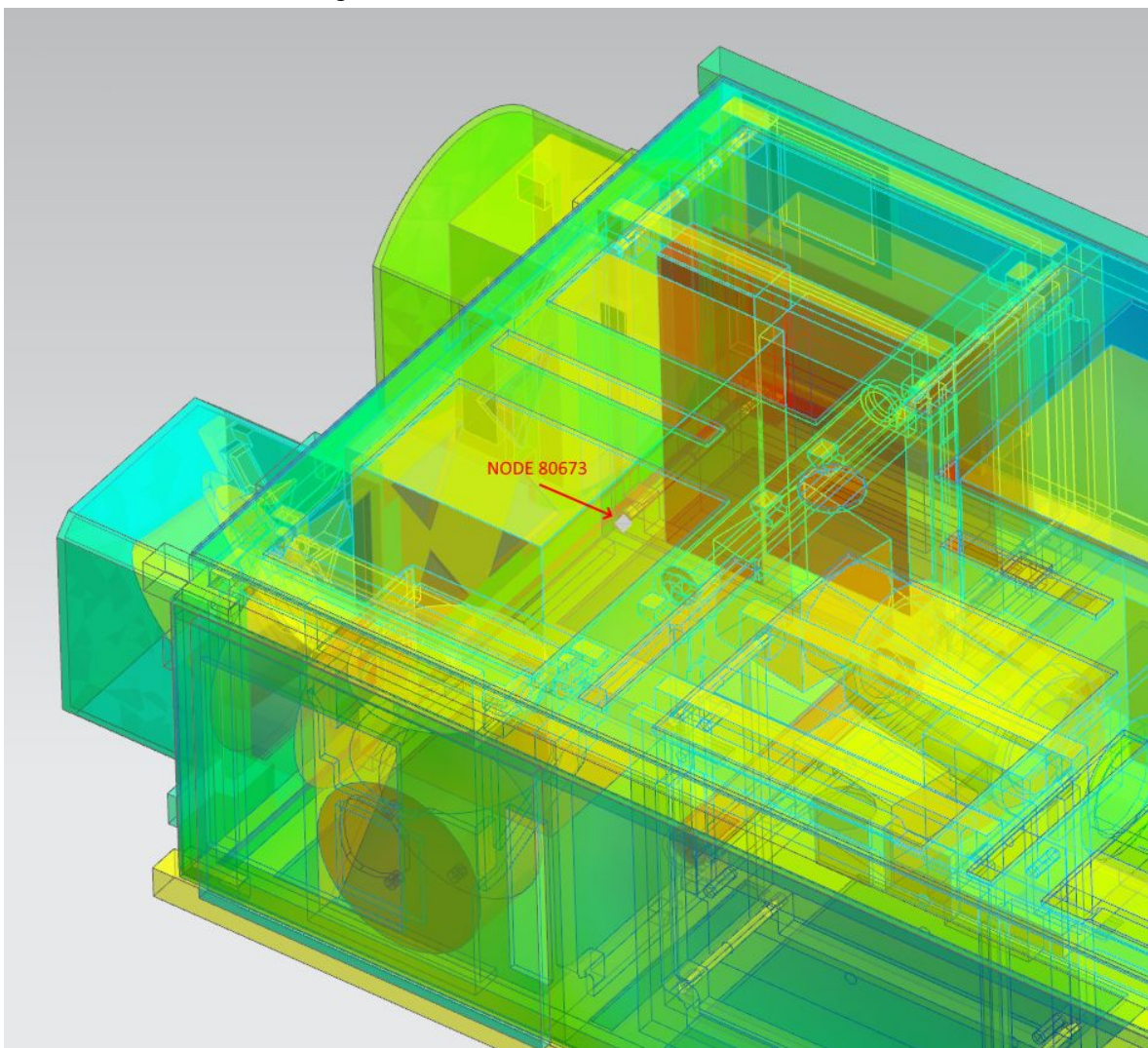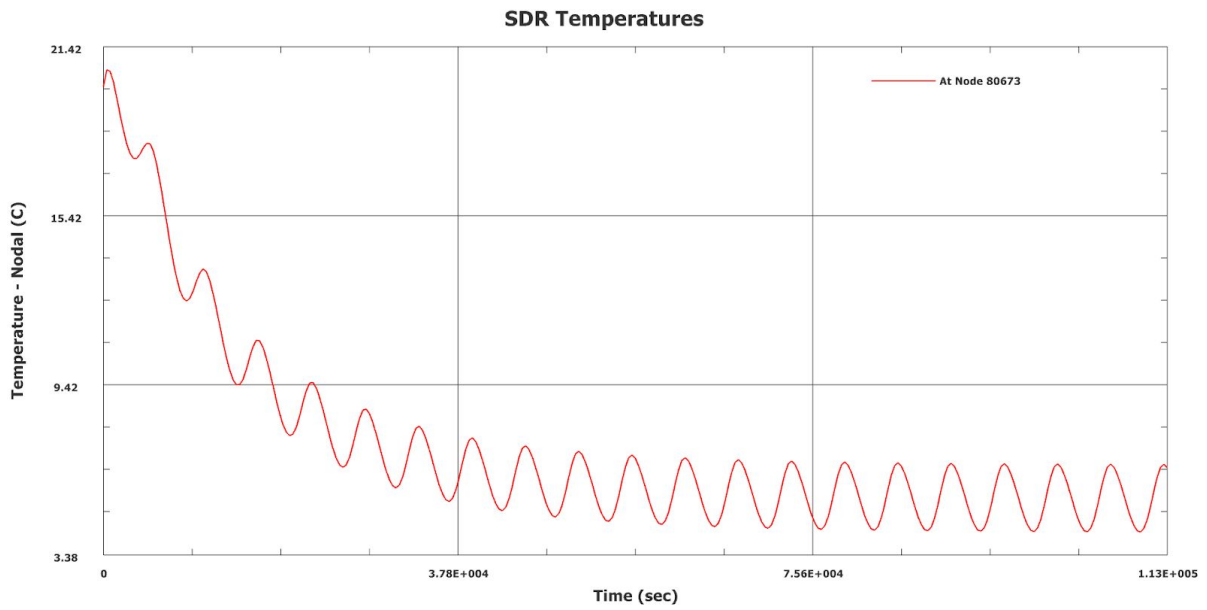
Figure 43: SDR Orbital Thermal Fluctuation
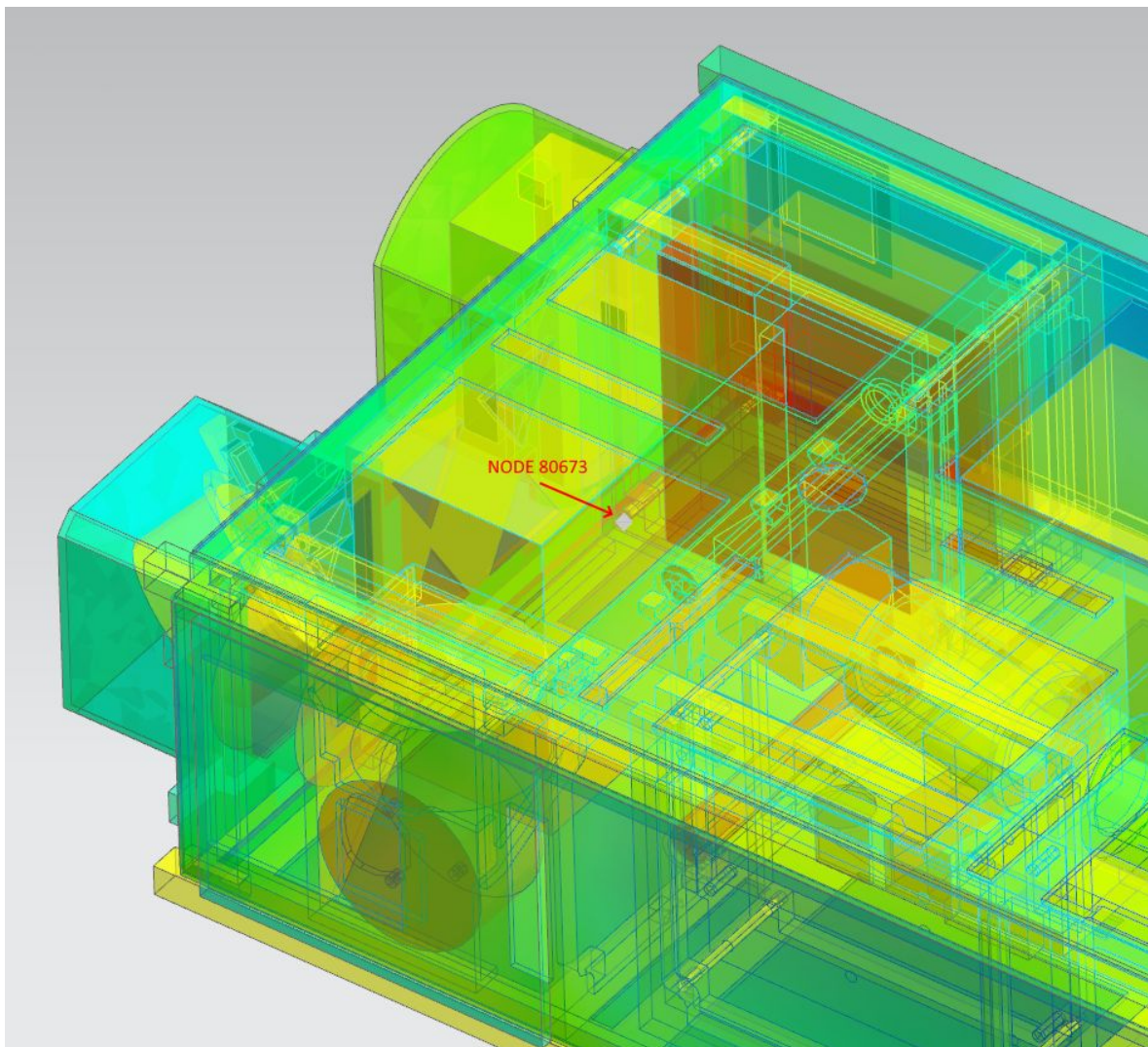
Figure 44: SDR Probe Node Location
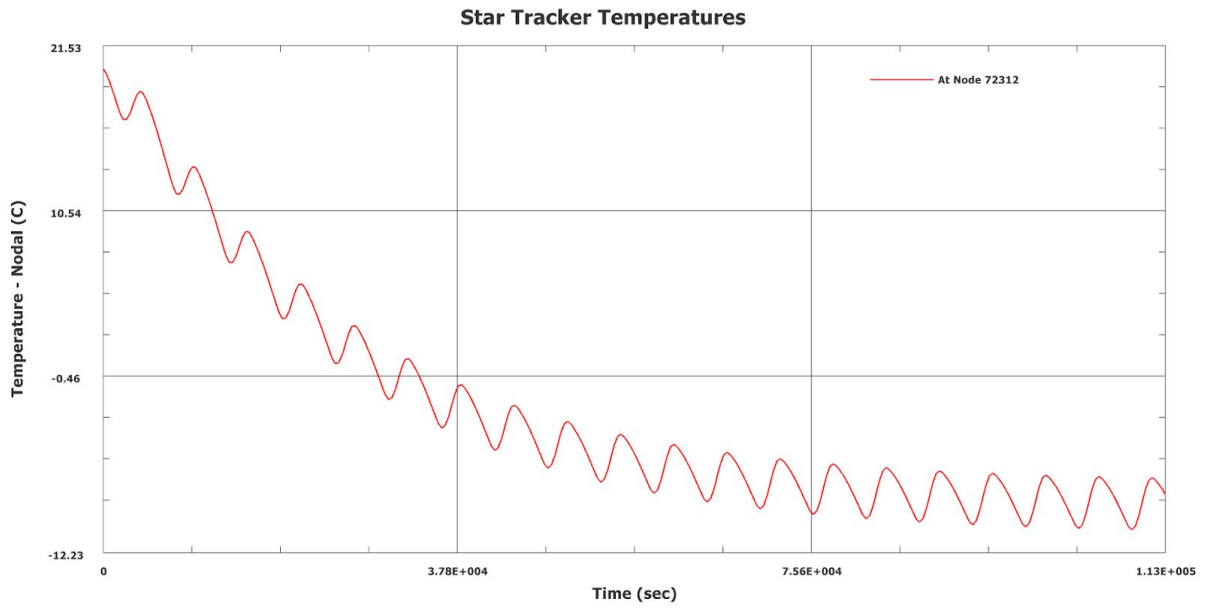
Figure 45: Star Tracker Orbital Thermal Fluctuation

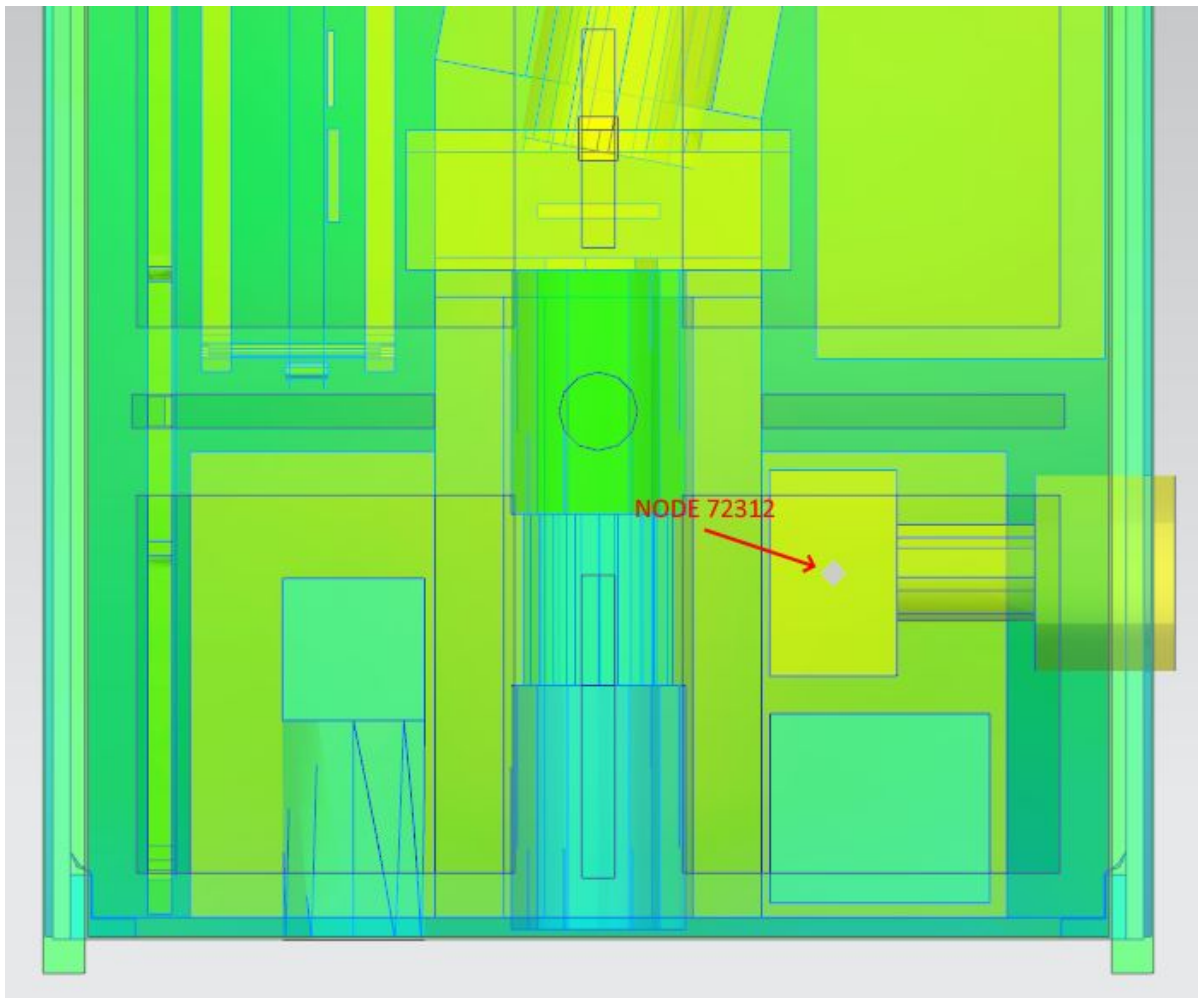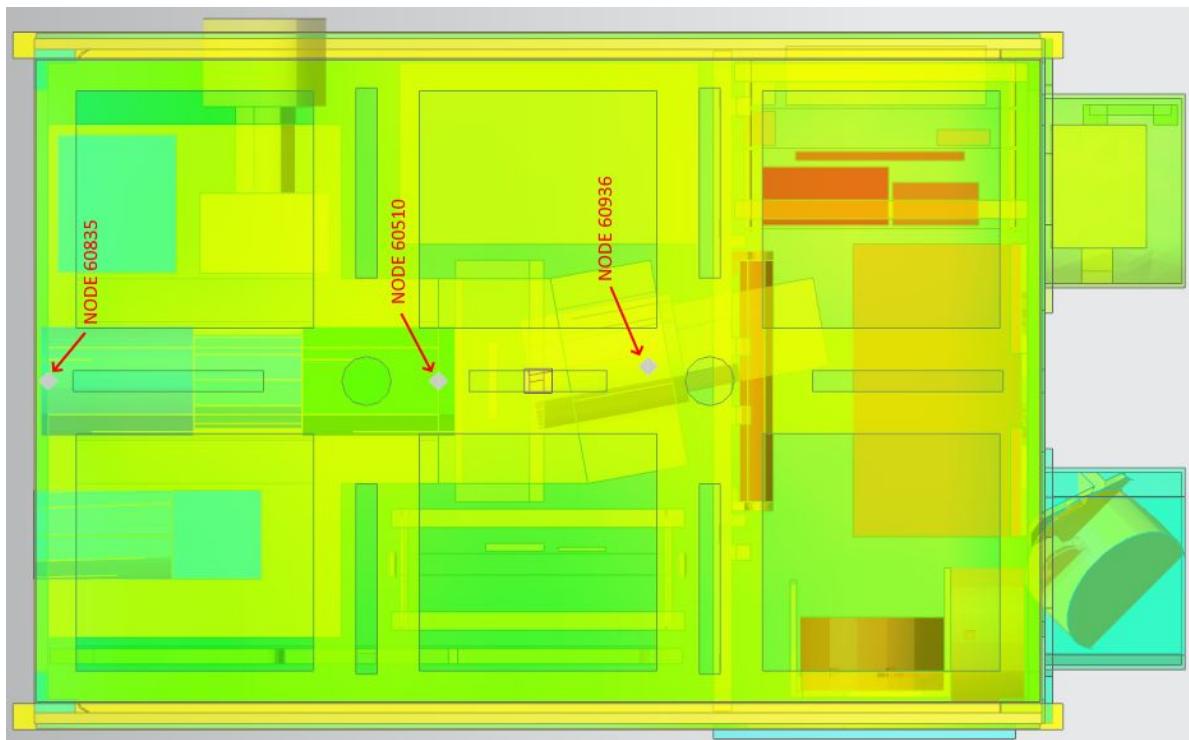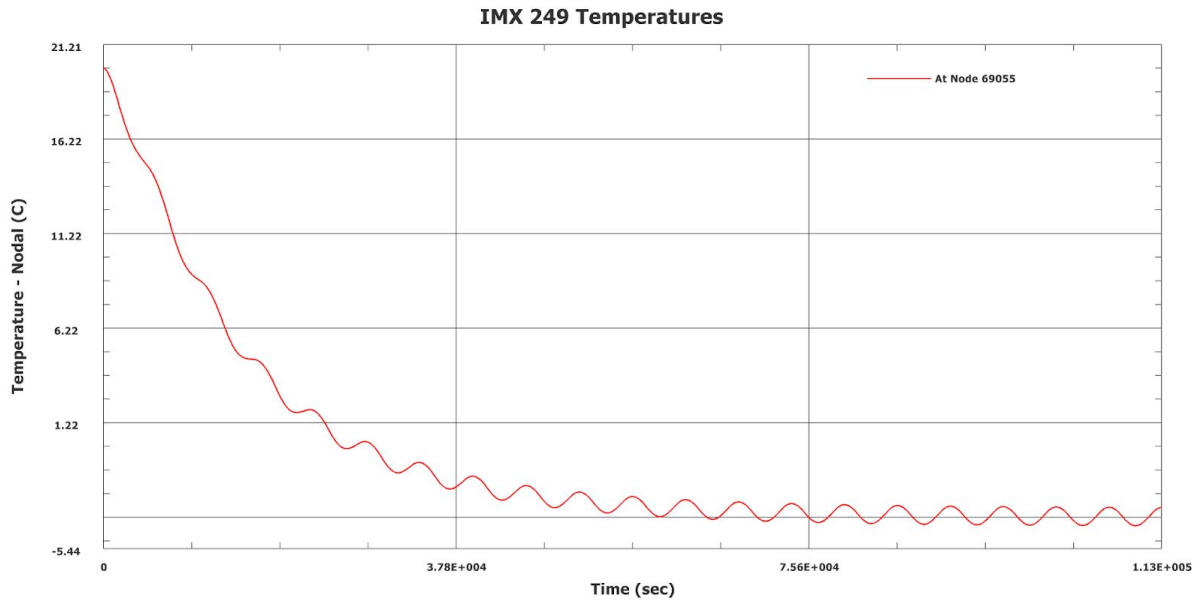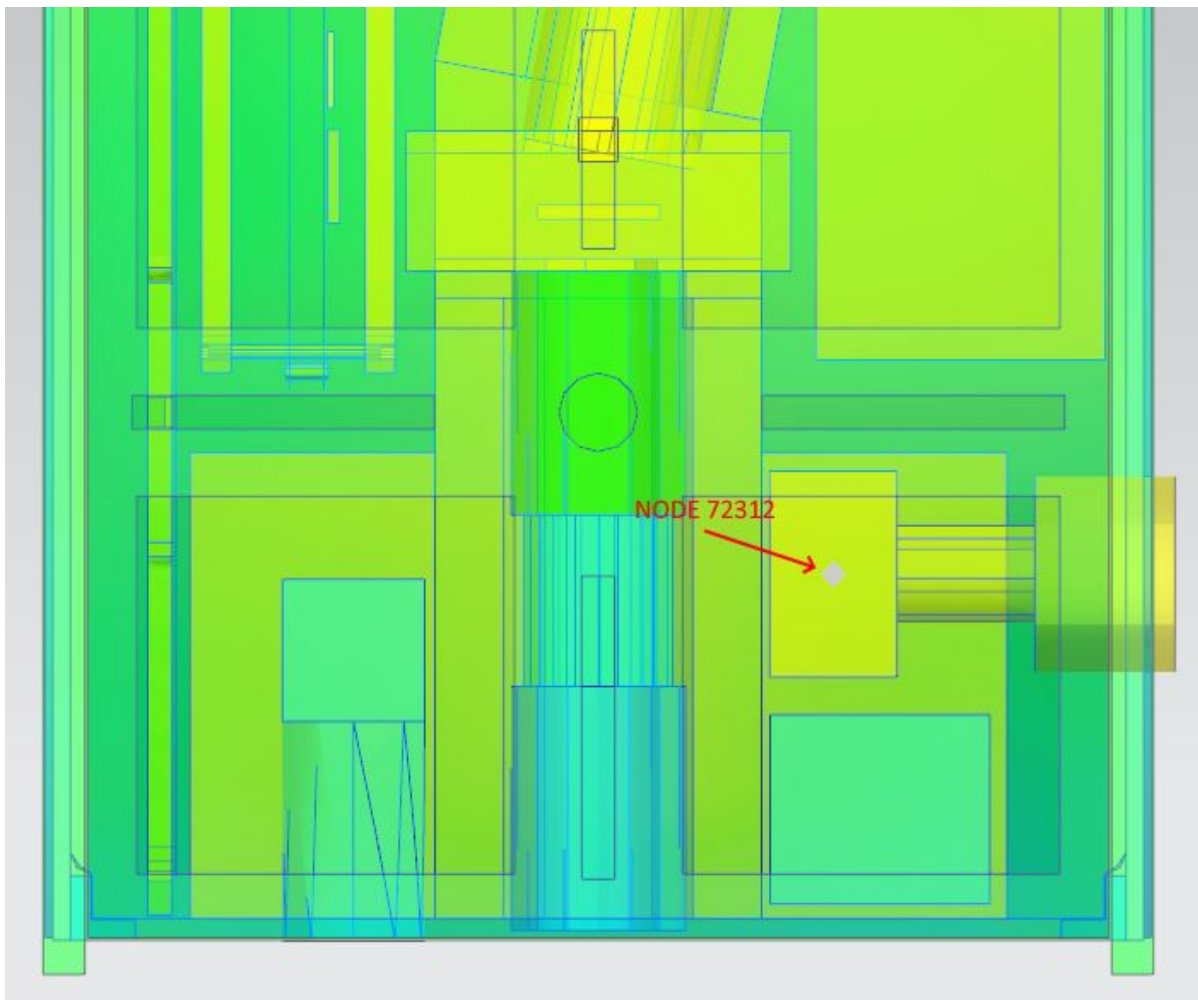*Figure 46: Star Tracker Probe Node Location*

7. Discussion

7.1 Thermal Results

The results show that the payloads are mostly within the required temperature range with the given assumptions. The limitations of the simulations as well as all assumptions were considered during the analysis of the data.

7.1.1 Hot Case

The hot case results shows that the front objectives extremal temperature is -17.16°C. With a safety margin of 10°C the temperature is out of the acceptable range of -20°C. However, the results from the *general tolerance test,* section 9, provides evidence that the HSI camera can operate and provide sharp images in -20°C, possibly in lower temperatures as well. This is further elaborated in section 7.2.

The RGB camera assembly exhibited temperatures significantly lower temperatures than the 0°C thermal limit of the detector, at -12°C. To add thermal energy to the system, the detector could be powered on for an extended amount of time in orbit. The current power usage for the RGB amounts to 7.780 mW per orbit. An increase in the average output would provide internal heating of the component. However as the power budget is limited, a more adequate solution could be passive thermal control like thermal straps.

The rest of the payloads are within the acceptable thermal limits. The cold case however shows several components reaching low temperatures compared to the required temperature limit.

7.1.2 Cold Case

The cold case showed more severe results compared to the hot case. The objectives, detector, RGB assembly and IMU exhibited temperatures below their respective temperature range when adding a 10°C safety margin. With -32°C, -4°C, -23°C and -39°C, respectively (without the safety margin). The cold case shows that some amount of thermal control is needed to keep the components within the given temperature range. However note that the cold case is the absolute worst case scenario the CubeSat could possibly face, with all components in safe mode producing little heat, no conducting between the platform and attached items, only close plate radiation, the -Y face of the satellite locked towards the sun, resulting in the +Z open face of the satellite facing deep space for 62.22% of the orbit, while the remaining 37.78% of the orbit will facing the earth.

7.1.3 General Discussion

As stated in previous sections, a large number of assumptions were required in order to perform the analysis. These mostly concerned the material properties as well as the thermal conductivity between components. The thermal conductivity had to be estimated as pure close parallel plate radiation, which is a very exaggerated case. The result of this can be observed by looking at the temperatures of the payloads mounted on the HSI platform for both the hot and cold cases. In the front +Z face of the platform and the front objective the difference in temperature was measured to be as much as 49.22°C. This is cause of this believed to be rooted in the low estimated conductivity in combination with the thermo-optical properties of the payloads, which was assumed to be anodized clear. Calculation of the absorptive and emissive ratios between the payloads and platform yielded α/ε = 0.355 and α/ε = 7.5 respectively. Based on the fact that the platform appear much hotter than the respective components attached to it in the analysis, despite the applied heat loads to the payloads the theory is further supported. Another factor contributing to this effect is the fact that by locking the -Y face of the satellite towards the sun, the +Z open face of the satellite will be facing deep space for 62.22% of the orbit, while the remaining 37.78% of the orbit will be facing the earth. Despite the discrepancy regarding the temperatures, the general heat balance of the analysis should still be correct. A more accurate model should in theory even out the temperatures of all components in the entire satellite due to increased conduction between surfaces, thus resulting in a higher overall temperature of the connected payloads due to the large mass of the proportionally warmer platform. In addition, an uncertainty margin of 10°C was added to the results. Taking this into consideration, the results from the analysis should be reliable enough to work as an indicator to what temperatures each component may experience in the space environment.

An additional estimation of the lumped solar panels taking the conversion of solar radiation into electricity was made. NanoAvionics uses GaAs solar arrays, which have an efficiency up to η = 28.7% [RD14]. With the absorptivity of GaAs solar cells being α_c = 0.91, the effective absorptivity of this surface can be estimated as α_{eff} = α_c - η [RD15]. The back white PCB plate was estimated with a relatively high absorptivity of α_u = 0.5. The total absorptivity could then be averaged out with the following equation:

$$\alpha_{avg} = f_c \alpha_{eff} + (1 - f_c)\alpha_u$$

Where f_c=71.72% is the surface ratio between solar cells and the back white PCB plate for the ±Y faces. The averaged absorptivity was calculated to be α_{avg}=0.588. Even when using upper values for absorptivity in the solar panel back plate material, the lumped properties still appear below the provided values. This could contribute to exaggerated absorption rates of heat flux, assuming that absorptivity of the solar panels used for the calculation is correct.

7.2 Optical Integrity

The optical integrity of the HSI camera when subjected to the thermal changes is also something of great concern to the mission. A basic thermal tolerance test was done in order to gain an understanding of how the camera may operate under certain temperatures. Section 9 outlines the test conditions and findings. According to the basic tests, the camera starts to defocus at temperatures 40 to 60°C. The focus is relatively stable down even when ambient temperatures reach -20°C. This is however assuming that the focus was correctly calibrated at ambient room temperatures, which most likely was not the case as indicated by the results. Furthermore, it suggests that the imager could be calibrated to function better at certain temperatures ranges. The thermal operational range of the HSI should therefore be somewhere within a 40°C range of that can be shifted to match expected environments. Further testing and analysis of results is necessary before any conclusions can be made in regards to the thermal resilience.

7.3 Thermal Design

As mentioned in section 7.1.3, the measured temperature of the platform appears elevated when compared to other components in the satellite. This was suspected to be due to the thermo-optical properties of the untreated aluminium surface. It is therefore recommended to anodize the platform in order to gain control by knowing the properties of the surface.

The simulation did not consider the actual complexity of the camera sensor PCB components, which would lead to a considerably larger heat concentration at processing areas of the component. To combat this, thermal straps will be added from the IMX249 sensor processing chip to the platform, knowing that the heat generated will have little effect on the platform temperature. The maximum increase in temperature from heat generated by HSI platform payloads was calculated to be 1.89°K per orbit, meaning that dumping heat into it should not result in any problem.

The thermal simulations also suggest that the payload components at the front of the HSI payload are cooled too much. To account for this, a plate should be added to the front +Z side of the satellite. An additional simulation was made adding the suggested front plate. The results found in appendix B indicate that adding the plate will even out the temperatures at the front. Temperatures experienced by the front lens objective was measured to increase from -17.16°C to -8°C. The temperature for all other components are also however consequently increased as a result of the plate. Adding a front plate is therefore recommended.

Another component that is recommended thermal control is the OPU. As with the camera PCB microchip, the OPU was not modelled to high accuracy. The thermal range experienced by the OPU FPGA chip was measured to be between 17.42°C to 40.11°C. Even though the results suggest that the ranges for this component are within the defined requirements, thermal straps will still be added. The reason for this is the reduced complexity of the model, as well as the fact that the component will be encompassed by a radiation shield. In addition, with the added front plate, inside temperatures of the satellite is expected to rise. The radiation shield can be used to absorb heat generated by the FPGA due to its mass and heat capacity. When considering the transient thermal behavior of the shield

throughout the orbit, the heat should be able to radiate from the shield during the period offline time at 88.36%. Adding a thermal strap between the OPU and shield is therefore highly recommended. The solution should be tested with the OPU on and coupled to the shield should be done prior to launch.

Further TVAC chamber testing should be done to test with the additional thermal control proposed. If desired, the reliability of the results from the thermal simulations can be further enhanced with information from physical test results done in an TVAC chamber, which would help increase the confidence level of thermal analyses of future HYPSO missions. The results could provide further information regarding the temperature ranges of the components, in addition to information regarding the simulation of the space environment following the NASA standard GSFC-STD-7000A [RD05].

7.4 Sources of Error

Several sources of error were present in the simulation due to the complexity of the NX SST solver and the time limit present. The identified sources of error are listed below:

- Assumptions and simplifications done discussed in section 3. And 5. respectively.
- The idealization process can produce some amount of error in the system, however this is most prevalent on the SDR mockup
- Material properties (many of the components has simply been modelled as aluminium) and given a specified mass
- Deviation in mass and heat capacity
- Changes in touching surfaces through idealization
- Thermal coupling of touching surfaces, no direct conduction was used between the HSI platform and the objectives, detector, RBG camera, IMU and star tracker. Close plate radiation were used in order to simulate a worst case scenario. This assumption will lead to lower temperatures in the discussed items.
- By averaging out the heat dissipation, temperatures should become more even. This is why a steady state simulation should be done to determine the max temperatures by a function of temperature as well
- Exact launch times have not been considered

8. Conclusion

The results from the simulations shows that the temperatures of the objectives, detector, RGB camera, IMU and star tracker payloads are under the respective temperature limits for the cold case. The hot case shows that the front objective and RGB camera reached temperatures under the limit. The results shows the need for thermal control within the payloads, if the assumptions provided are realistic. Thermal control can be done actively or passively. Normally, active solutions are preferred on optical payloads, however due to the limited power budget, the mechanics team have been asked to strongly consider passive thermal solutions, such as thermal straps or mli shielding. The most efficient solution, found were mounting an aluminum 6082 plate at the +Z side of the CubeSat with holes allowing for a clear view for the HSI and RGB, Appendix B: Thermal Results +Z plate.

8.1 Future Work

- Testing in a TVAC should be done in order to characterize the performance of passive thermal control
- Accuracy of the simulation model can be improved based on TVAC testing
- Further testing using environmental chambers should be done to onboard custom PCB components to characterize thermal resilience
- Design and manufacture a front plate with camera hole interfaces
- Further characterization of the optical behavior and analysis of results

9. HSI Payload General Thermal Tolerance Test

9.1 Tolerance Test Setup

This section is a supplement to the thermal simulation done in NX. The main purpose of this test was to uncover if the HSI payload can stand the same temperature ranges as its individual components. The tested HSI prototype was the TTH Mk.1. The HSI wat put through a general thermal tolerance test to get information about the basic performance under thermal loads. The test was aimed at uncovering any issues arising from a uniform increase or decrease in the payload temperature. This could include both variations in the optical performance as well as electrical faults in the imager. The test was performed in the SmallSat Labs thermal chamber where a white sheet of paper was used as target for the HSI. Due to low light inside the chamber, even with the internal lamp turned on, the chamber door had to be opened and an external lamp pointed at the target to gain a useful spectrogram. This test setup can be seen in figure 47.
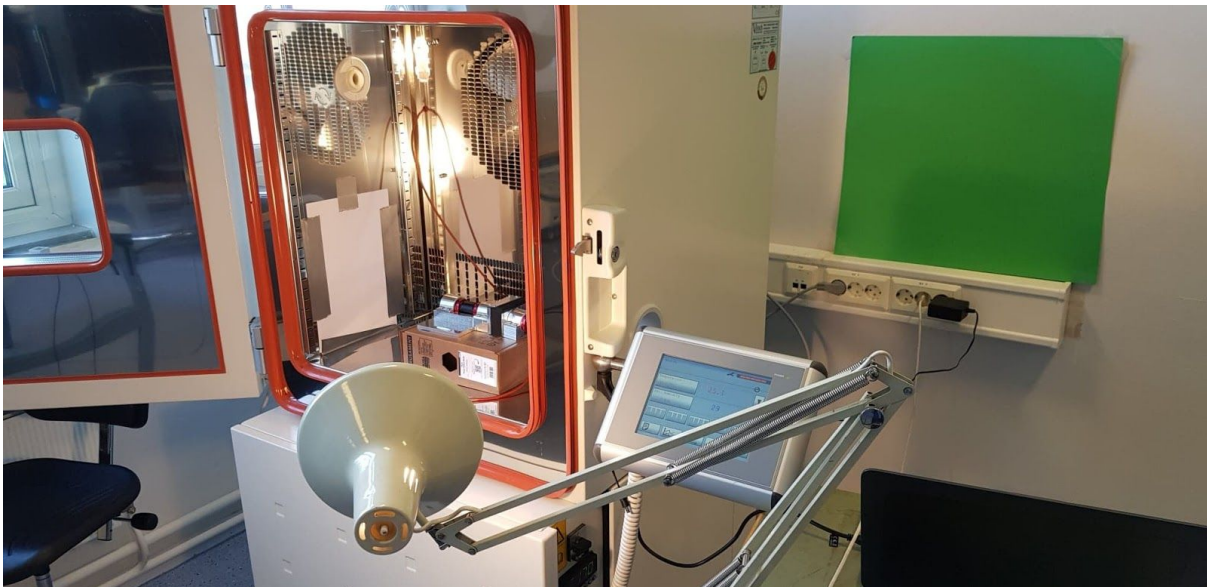
Figure 47: HSI inside the chamber and the external lamp

The chamber was manually controlled and with target temperatures set on the control unit. It was raised to the desired temperatures before being held there for 30 minutes to ensure that the whole HSI assembly had time to reach equilibrium. Figure 48 shows the temperature curve for the chamber over the whole test run.
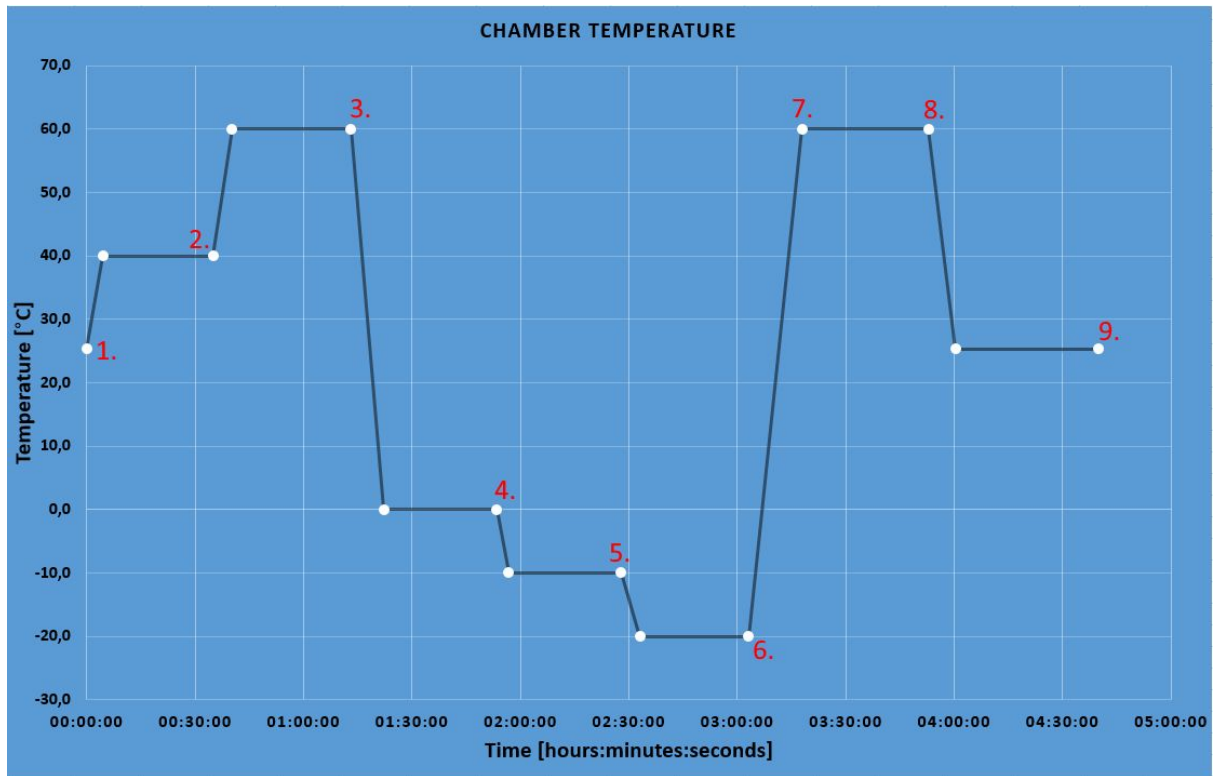
Figure 48: The chamber temperature during the test

9.2 Tolerance Tolerance Test

Figure 48 a-i shows the spectrograms produced by the HSI payload.
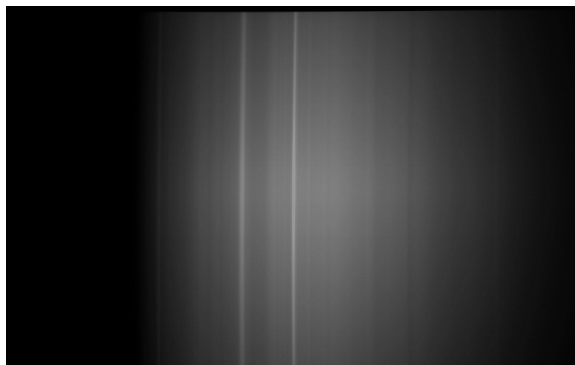
Figure 49 a: 25.3°C (1.)
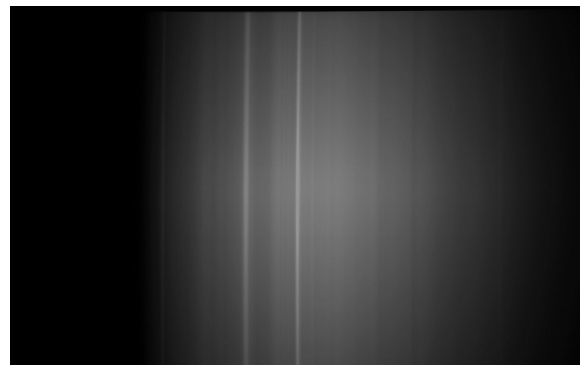
Figure 49 b: 40°C (2.)
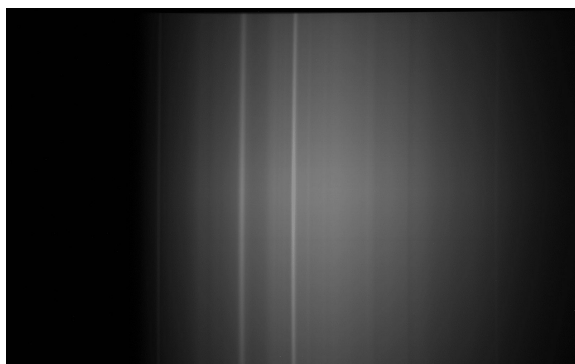
Figure 49 c: 60°C (3.)
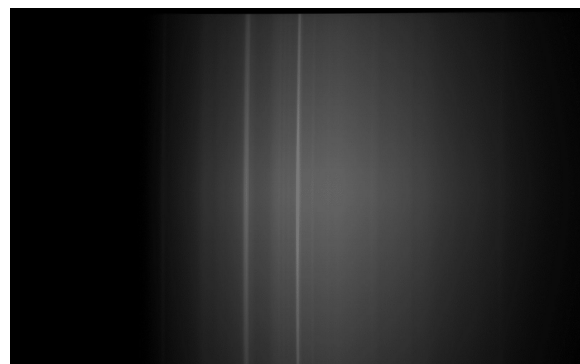
Figure 49 d: 0°C (4.)
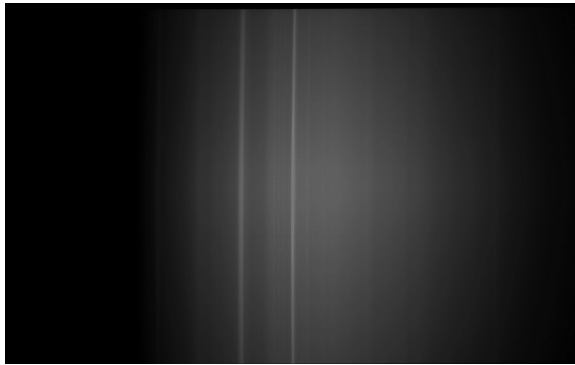
Figure 49 e: -10°C (5.)
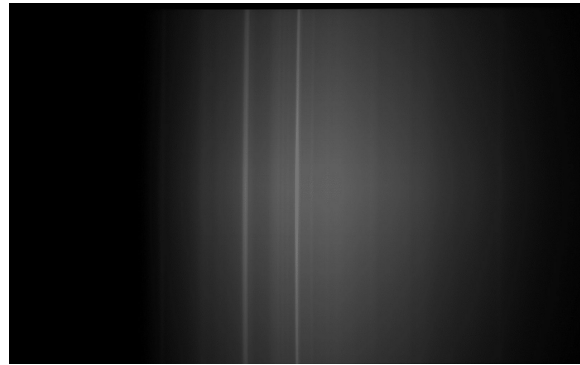
Figure 49 f: -20°C (6.)
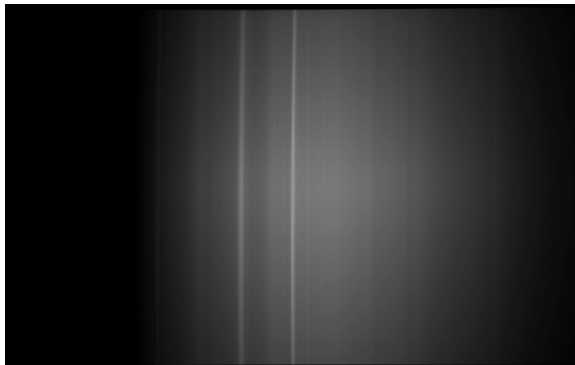
Figure 49 g: 60°C (7.)
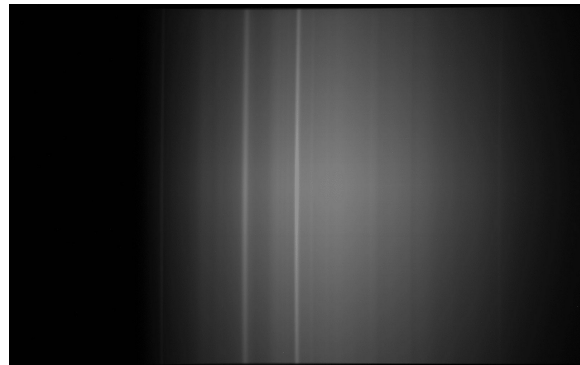
Figure 49 h: 60°C (8.)
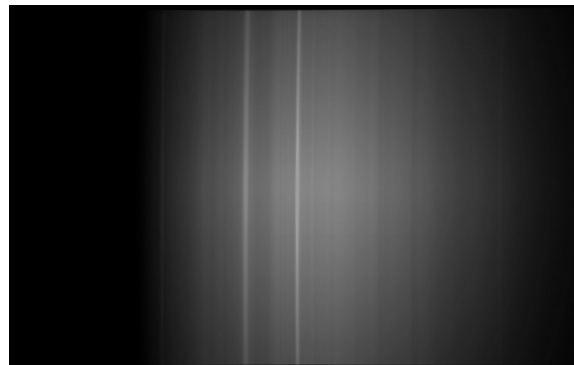
Figure 49 i: 25.3°C (9.)

9.3 Tolerance Test Discussion

The results shows that the HSI payload survives in the ambient temperature range of the detector (0 - 55°C). In addition, the camera was able to operate at -20°C without exhibiting errors or a loss in connection, which is the minimum recommended survivable storing temperature of the detector. With the detector on, the temperature range that the HSI can survive exceeds the given ranges from the datasheets, however further testing must be done to discover if these ranges change when removing the convection in vacuum. As can be seen from these spectrograms there was a defocusing effect occurring at 40°C and 60°C. At lower temperatures there was no appreciable effect on the spectrogram quality, if anything the focus might even have improved slightly but this is hard to tell from the captured spectrograms as the light environment seems to have been slightly different from the baseline image. However, this can be an indication that the baseline focus was slightly off, something that was suspected due to the difficulty with tuning the slit to its exact location based on the flange focal theoretical length. For the flight model, the HSI should be configured to have perfect focus at the expected operating temperature and this small test could serve as a template for that process.

10. List of Abbreviations

Table 10: Abbreviations

Abbrv.	Description
ADCS	Attitude Determination and Control System
AUV	Autonomous Underwater Vehicle
BoB	Breakout Board
COTS	Commercial Off-The-Shelf
EPS	Electric Power System
ESA	European Space Agency
FEA	Finite Element Analysis
FEM	Finite Element Method
FPGA	Field-Programmable Gate Array
GBVF	Gray Body View Factor
GPS	Global Positioning System
HSI	Hyperspectral Imager
ICD	Interface Control Document
IMU	Inertial Measurement Unit
IR	Infrared
LEO	Low Earth Orbit
NASA	National Aeronautics and Space Administration
OPU	Onboard Processing Unit
PCB	Printed Circuit Board
RGB	Red Green Blue
SDR	Software Defined Radio
SMAD	Space Mission Analysis and Design
SST	Space Systems Thermal
TVAC	Thermal Vacuum
UAV	Unmanned Aerial Vehicle
UHF	Ultra High Frequency
USV	Unmanned Surface Vehicle

11. Symbols

Table 11: Symbols

Symbol	Unit	Description
η	-	Efficiency ratio
ϵ	-	Emissivity
α	-	Absorptivity
α_c	-	Absorptivity (Solar cells)
α_u	-	Absorptivity (PCB)
α_{eff}	-	Effective absorptivity
α_{avg}	-	Average absorptivity
f_c	-	Surface ratio (Solar cells/PCB)
G	$\dfrac{W}{\Delta K}$	Total Conductance Coefficient
k	$\dfrac{W}{m\Delta K}$	Thermal conductivity
A	mm^2	Area of contact
L	mm	Distance between surface elements

Appendix A: Simulation Overview

The following spreadsheet contains all information regarding the raw calculations done to determine the material properties.

Part	True Mass (g)	True Volume (mm^3)	Idealized Volume (mm^3)	Appropriate Density (g/mm^3)	Change (%)	Material	Surface
Materials resulting in a density change above 5% has been altered							
HYPSO Payloads							
HSI Platform	997.825156	267864.4175	256057.2512	0.003896883027	-4.61%	AA6082	Anodized Black
50 mm VIS NIR (3)	318	76803.32322	76803.32322	0.004140445838	0.00%	Assembly (AA6061 + Glass)	Anodized Black
IMX249	50	35942.24614	35942.24614	0.001391120627	0.00%	Assembly (Chromium + FR4)	
Collimator Tube	14.1	9938.91545	9938.91545	0.001418665857	0.00%	AA 6016	Anodized Black
Grating		1875	1875	0	#DIV/0!	B270	
Star Tracker	108	88331.66872	88331.66872	0.00122266455	0.00%	AA7075	Anodized Clear
IMU	52	37179.52	37179.52	0.001398619455	0.00%	AA7075	Anodized Clear
RGB Camera	65	53980.28952	53980.28952	0.001204143227	0.00%	AA7075	Anodized Black
SDR	131			#DIV/0!	#DIV/0!	FR4	
BoB	130	191551.8203	191551.8203	0.0006786675262	0.00%	FR4	
NanoAvionics 6U CubeSat							
Structure Assembly							
Walls (2)	672.88	227579.21	216297.2148	0.003110887325	-5.22%	AA7075	Anodized Black
Brackets (4)	55.43	19799.30	31122.9806	0.001781129922	36.38%	AA7075	Anodized Black
Solar Panels Y (2)	287.10	229240.38	230280.81	0.00124673871	0.45%	FR4 + Copper	PCB White
Solar Panel +X	132.29	37527.95				FR4 + Copper	PCB White
Solar Panel -X	120.50	36700.74				FR4 + Copper	PCB White
Solar Cell							
Splitter	23.176259	8277.826594	8565.031767	0.002705916292	3.35%	AA7075	Splitter Lumped (NA)
Tuna Can +X	63.417095	20864.73862	23251.81319	0.002727404288	10.27%	AA7075	Anodized Black (NA)
Tuna Can -X	75.399238	19786.85535	23766.21865	0.003172538261	16.74%	AA7075	Anodized Black (NA)
Stack battery pack	204.7		80353.22879	0.002547501862		Misc (AA7075)	Black Body
BAT 005 Fastener	7.171707	2561.506896	2720	0.002636656985	5.83%	AA7075	Anodized Clear
BAT 006 Fastener	6.415137	2291.283912	2747.875	0.002334581085	16.62%	AA7075	Anodized Clear
Reaction Wheel (4)	549.3	256925.2285	161569.5358	0.003399774576	-59.02%	Misc (AA7075)	Anodized Clear
RHW001	22.912567	8183.644198	11055.5	0.002072503912	25.98%	AA7075	Anodized Clear
RHW002	24.902721	8894.4643				AA7075	Anodized Clear
RHW003	4.714821	1683.985048	1734.017467	0.002719015863	2.89%	AA7075	Anodized Clear
RHW004	18.477314	6599.512077	6671.545786	0.00276957014	1.08%	AA7075	Anodized Clear
Payload Controller Ring	64.496261	23036.02448	24008.57805	0.002686384044	4.05%	AA7075	Anodized Brass
Payload Controller Structural Frame	70.954808	25342.81291	26068.18261	0.002721893162	2.78%	AA7075	Anodized Brass
Payload Controller PCB							
MQT1 (2)	66					MISC	
Coil Rod (2)	62.179368	14862.40965	14862.40965	0.004183666677	0.00%	Copper and Ferrite	Copper Oxidized
Bracket (4)	3.820632	1364.609579	1364.609579	0.002799798608	0.00%	AA7075	Clear Anodized
MQT2	33					MISC	
Coil Rod	31.556636	7431.320082	7431.320082	0.004246437463	0.00%	Copper and Ferrite	Copper Oxidized
Bracket (2)	1.443364	515.5239661	515.5239661	0.002799799999	0.00%	AA7075	Clear Anodized
MQT3	33					MISC	
Coil Rod	30.377714	7431.204826	7431.204826	0.004087858525	0.00%	Copper and Ferrite	Copper Oxidized
Bracket (2)	2.622286	936.5974708	936.5974708	0.002799800428	0.00%	AA7075	Clear Anodized
Stacking Ring NTNU (2)	28.353808	10127.08346	13227.65269	0.002143525284	23.44%	AA7075	Anodized Black
Rod Stack (4 rods)	12.5			#DIV/0!	#DIV/0!	AISl310	Clear
FC 3C2	135.6			#DIV/0!	#DIV/0!	FR4	
EPS	194.3			#DIV/0!	#DIV/0!	FR4	
Stack Battery Pack	204.7	80353.2308	80353.2308	0.002547501799	0.00%	AA7075	
GPS reciever	78.65			#DIV/0!	#DIV/0!	AA7075	
S-Band TX+RX	192.2	283288.5	283288.5	0.0006784602975	0.00%	AA7075	Clear Anodized
S-band RX						AA7075	Clear Anodized
SDR Stack							
SlinkPhy Mounting Plate	42.091615	15033.79353	15379	0.002736953963	2.24%	AA7075	Clear Anodized
	125.020302	44653.29728		#DIV/0!			
SDR Dummy	405.4		449924.7922	0.0009010394783			

Appendix B: Thermal Results +Z Plate

The following results are from a thermal simulation using the same parameters as described for the hot case in the main analysis report. The simulation was conducted by adding an aluminum 6082 shielding wall, with the thickness of 1.75 mm (same as the solar panels) to the +Z front of the CubeSat. This was done in the hope that the temperature of the optical components would have a more even value, compared with each other and the platform. Figure 1 shows the newly added plate.
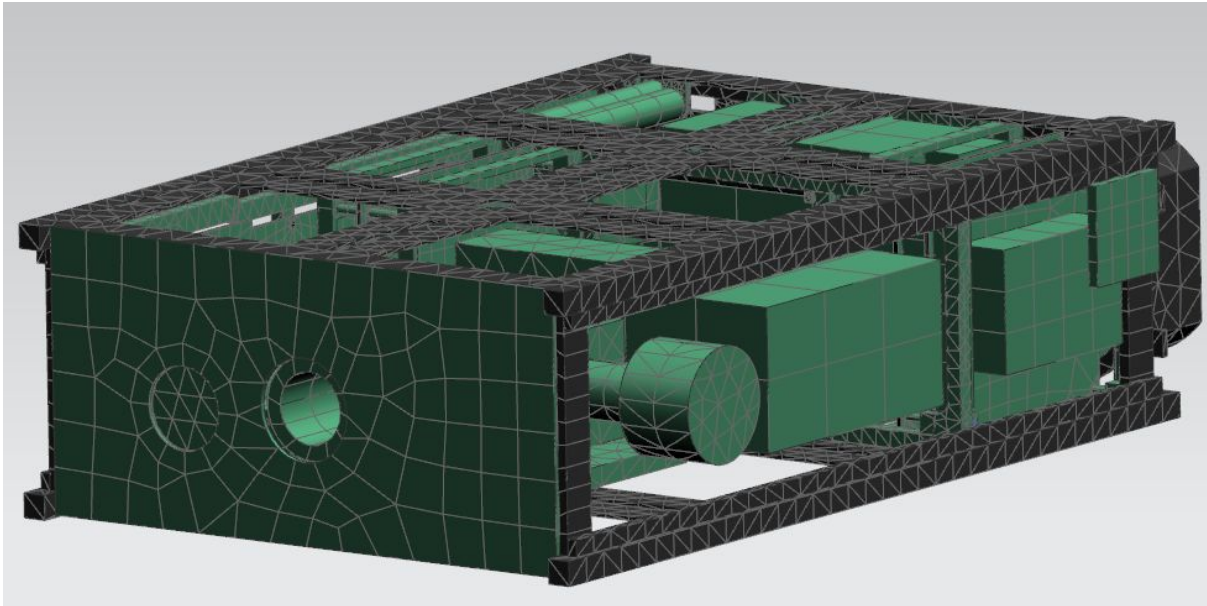
Figure 1: +Z Plate

The temperatures appears to be more homogeneous and more within the temperature limits of the optical components. The lowest experienced temperature of the front objective was changed from -17.16 to -11 degrees celsius. The plate is effective.
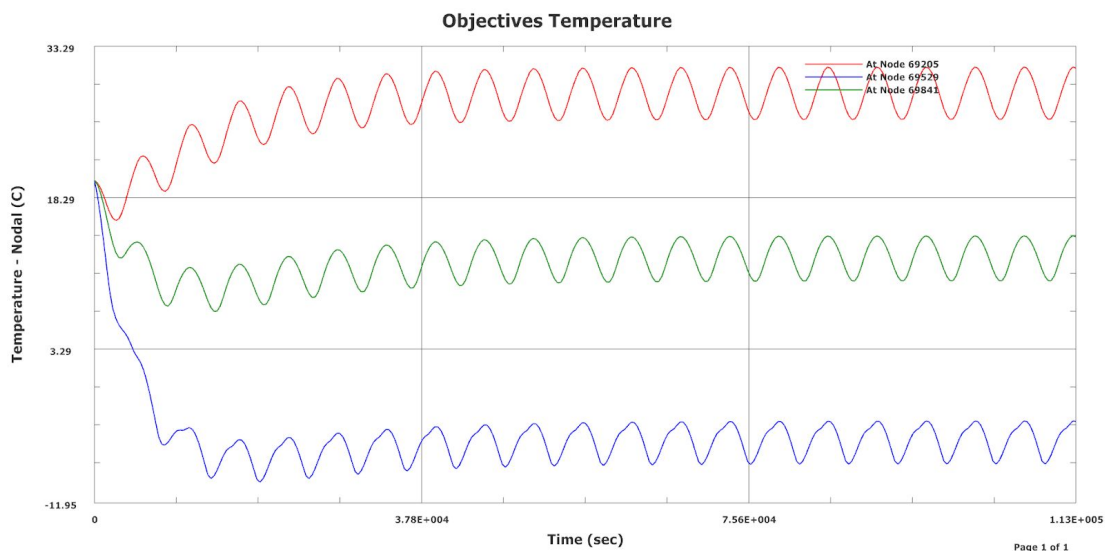
Figure 2: Temperatures of Hot Case with Front Plate
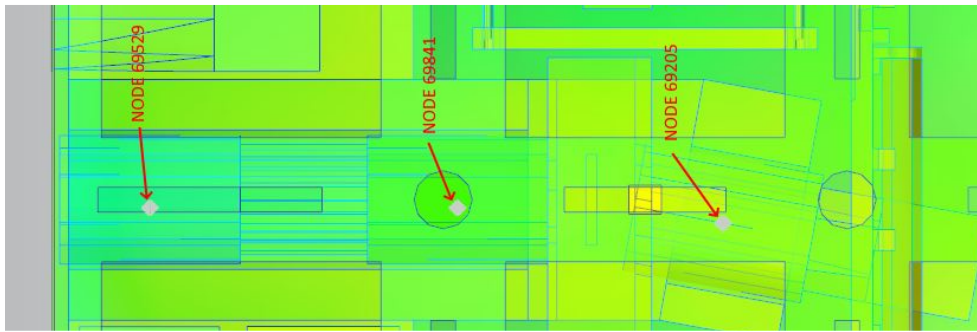
Figure 3: Node Placement on objectives
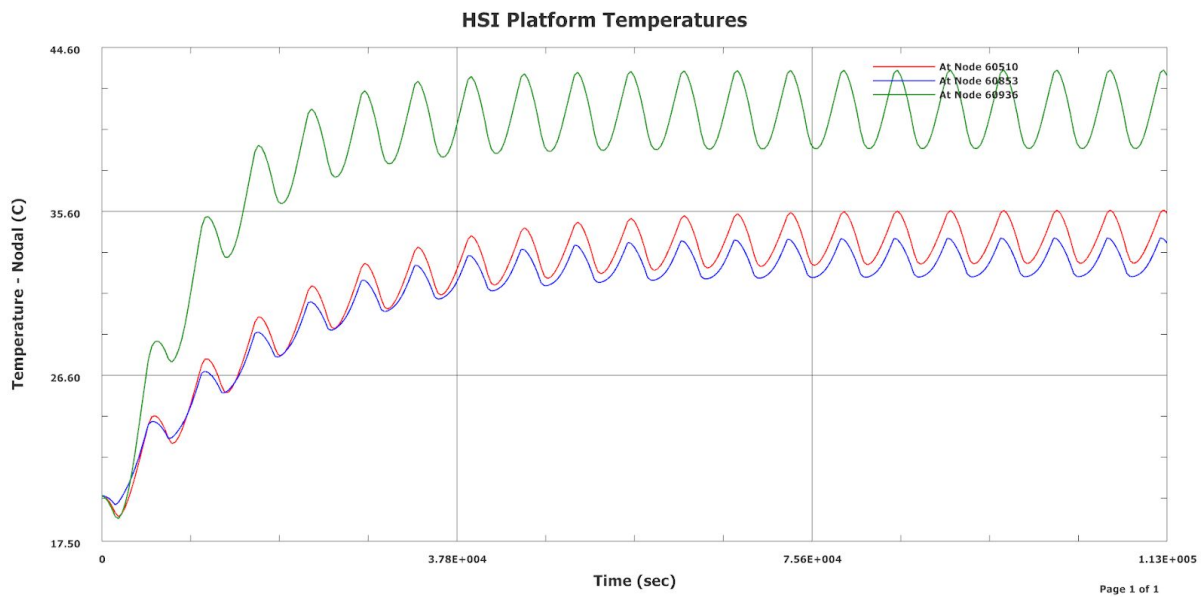
Figure 4: Temperatures of Hot Case with Front Plate

Figure 5: Node placement on platform

Appendix M

Test Plans

Vacuum Resilience Test Plan

General information

Test type:
- Development Test
- Static

Validation method:
- Visual inspection; observation by eye in a well-lit environment. Mainly look for lens cracking, condensation/material gathering on lens surfaces, general structural damage.
- Pre- and post-experimental photos following the standard procedure gives data for the performance

Test facility:
- Vacuum lab at NTNU (Berg)

Purpose

The main purpose of the test is to monitor the relevant component resistance to pressure changes experienced during the launch procedure. From normal atmospheric pressure to near vacuum. The main payload consists of COTS, with unknown mechanical properties. Most importantly is how well the lenses ventilate in relation to the change of pressure. The test will also give some data about outgassing from the various compounds in the lens as material condensation may occur. This is a separate problem and investigation from the structural rigidity of the lens assembly during pressure change. They are however tests that can be run in parallel and this saves time and resources for the project.

Risk assessment

The main risk associated with a vacuum test is the outgassing that can occur, potentially contaminating the vacuum chamber. Outgassing should be monitored. The vacuum chamber must be cleaned after use to ensure no contamination. No polymers shall be used for support in the chamber as they will contaminate the equipment. Contamination of lenses by external sources can be an issue. Make sure that the vacuum chamber is as clean as possible before and after testing occurs. Components subjected to the pressure change can get damaged or potentially break. If the same components are used for further testing, a thorough inspection of the component must be done to ensure no damage has occurred.

Items to be tested

Table 1: Test item list

Test Items	Test Description	Test date
50 mm VIS-NIR lens	COTS lenses test in vacuum chamber to obtain data regarding pressure gradient strength. Test to be done in NTNU vacuum chamber.	07.02.2019
Sony IMX249 sensor	Detector/ imager test in vacuum chamber to obtain data regarding pressure gradient strength. Test to be done in NTNU vacuum chamber.	07.02.2019

The lens and detector components will be tested in a vacuum chamber. No further components or subsystems will be tested for pressure gradient resilience.

Equipment

Table 2 lists all needed equipment to carry out the described test.

Table 2: Equipment

Equipment	#
Compact Arc Melter MAM-1 (Vacuum Chamber)	*1*
50 mm VIS-NIR lenses	*2*
Sony IMX174 sensor (Detector)	*1*
Mass scale	1
Computer with uEye Cockpit	1
Micro USB 3.0 cable	1
Checkerboard calibration pattern	1
Dark room	1
Controllable light source	1
Non latex gloves	-

Test approach

The launch of a space vehicle is a volatile process, inducing large loads on the satellite system. In addition to the mechanical loads, the rapid change in pressure can induce problems on sealed components should the components not ventilate fast enough. The rate of pressure change experienced during the HYPSO project launch unknown at this time, however the pressure behaviour can be estimated using flight information for polar satellite launch vehicle. Most vacuum chambers are not capable of simulating such rates. As a result, initial test will be done using the maximum speed of the vacuum chamber available.

Pre Procedure
- Characterization
- Visual Inspection

Set-up Procedure

1) Clean the vacuum chamber using the standard lab cleaning procedure
2) Make sure the part is correctly configured. 50mm lens should be set to 2.8 F/#
3) Clean parts using isopropyl alcohol (Find out if this is safe for part cleaning)
4) Visual inspection of the items before initiating test
5) Characterize the items using the standard characterization method
6) Place the 50mm lens in the chamber on a low outgassing interface plate using gloves
7) Start test procedure
8) Place the detector in the chamber on a low outgassing interface plate using gloves
9) Start test procedure
10) Clean the vacuum chamber using the standard lab cleaning procedure

Test Procedure

1) Begin air evacuation of vacuum chamber
2) Hold at 10^-5 Pa for 30 min
3) Repressurize over a one hour timespan
4) Remove test item from chamber using gloves
5) Visual inspection of items
6) Characterize the items

Post Procedure

Visual inspections should be done in a windowless room with as much light as possible.

Photos should be captured under the same conditions and with the same camera settings before and after the vacuum exposure. The exact settings of the camera must be adjusted and noted down according to the testing environment.

The tests shall be replicable and must therefore happen in an environment where the light can be strictly controlled. A room without windows and with a powerful lamp should be used.

Component Lifetime Radiation Test Plan

General information

Test type:
- Static

Validation method:
- Characterization test: Dark current and radiometric test
- Visual Inspection of glass opacity

Facility:
- TBA

Purpose

The main purpose of this test is to explore radiation degradation of components of the HSI. Exposure to the levels of radiation present in LEO is expected to darken the glass of the 50mm VIS-NIR lens as well as the grating itself. The performance after radiation exposure of the imager is unknown, this will therefore be an exploratory test into the performance of key components after increasingly higher doses of radiation, simulating an approximated lifetime in LEO.

Risk assessment

Testing with a high radiation dose should only be conducted in a shielded environment due to the hazard of radiation. As per the standard HYPSO test procedure, all HSE rules and procedures for the relevant lab shall be adhered to.

Radiation testing is destructive and will damage the tested components. Expected damage comprises of darkening of lenses and grating, imager malfunction, memory corruption. Tested components must be clearly marked.

Items to be tested

Table 1: Test item list

Test Items	No. of items	Approximate dimensions [mm]	Test Description	Test date
50 mm VIS-NIR lens	1	35.8x35.8x53.7	Lens to be exposed to radiation.	26.03.2019
Sony IMX249 (UI-5260CP-M-GL R2) sensor	1	29x29x48	Imager module to be exposed to radiation.	26.03.2019
Grating	1	25 x 25 x 3	Grating to be exposed to radiation.	26.03.2019
Precision Slit	1	20 x 20	Precision slit to be exposed to radiation.	26.03.2019
Sensor protective lens	1		Lens to be exposed to radiation.	26.03.2019

Test approach

Establish a baseline performance of the components, using the standard characterization: Radiometric approach. (The baseline are established by characterization tests that are developed to quantize the amount of darkening taking place.)

Two sets of imagers and lenses are required for the test, one set of test items and one set for control and to provide cross-checking between components. To acquire accurate data of the rate of darkening and other degradation it is paramount that the radiation dosing happens in increments that would at most equal a years worth of radiation per dose. Table 2 shows the radiation intervals. One grating and one precision slit will also be tested.

Characterization tests are developed to quantize the degradation of the components and these will be performed after every radiation dose, thus requiring removal and reinsertion of test objects in the radiation chamber. These tests will consist of:

- Dark current test (sensor)
- Radiometric test (sensor, lens)
- Visual inspection (sensor, lens, grating, precision slit)

Radiation amount

Calculation of radiation, effects and margin: ECSS-Q-HB-10-12A

SPENVIS Simulation software

The radiation dose simulating a lifetime of 5 years in LEO is estimated by:

Table 2: Radiation intervals (Specific values might change)

Dosage No. #	Radiation Rate [Gy/min]	Elapsed "real time" [years]	Total elapsed lifetime [years]	Radiation dose [Gy] +/-20%	Total Dose [Gy] +/-20%
1	5	0.5	0.5	10	10
2	5	0.5	1	10	20
3	5	1	2	20	40
4	5	1	3	60	100

Estimated time (with 30 min for characterization between tests): 8.5 hours

Scale of parts to be tested

Figure 1 shows the scale of the test items.

Figure 1: Item Scale

TTH Mk1 Assembly and Test Plan

General information
Test type:
- Development Test
- Static

Validation method:
- Visual inspection; observation by eye in a well-lit environment.
- Post assembly hyperspectral images, compared to the V6 models.
- *Full Assembly Characterization Test (Not Developed at this time)*

Test facility:
- NTNU SmallSat lab

Purpose
The main purpose of the test is to discover and evaluate potential flaws of the prototype. Even though several aspects in regards to machinability, assembly, tolerances and functionality have been considered during the design phase, flaws may still occur, and should always be tested for. These may comprise of misalignments, miscalculation of tolerances, impossible to reach assembly locations, and collision of parts. The functionality of the assembled HSI camera will also need to be characterized and compared to other working models. Another uncertainty of the TTH Mk1, is the unknown level of stray light protection given by the shroud. Furthermore, reflective surfaces of the platform and cassette parts may cause degradation of image quality. These aspects will also be investigated.

The tests will be done in two steps and can be treated as two separate tests:
Test 1: *Assembly and general functional test*. The general assembly will be tested and scrutinized for potential flaws and irregularities. This test can potentially highlight problems that can be addressed in the next HSI design iteration.

Test 2: *General Tolerance test.* Explore the impacts of deviations in positioning and alignment on the imaging. Since the requirements does not list measurable properties here, this testing aims to better understand the impact of changes in the geometry of the optical assembly.

Risk assessment
There is no major risk associated with this test. However, the COTS components and the custom interfacing could be damage should pieces be dropped or handled improperly. Some edges on the interfacing could be sharp, therefore the platform should be handled with care. The grating is a fragile part, and could be damaged should it be misused.

Items to be tested

Table 1 tabulates the test item, table 2 tabulates the components that make up the test item.

Table 1: Test item list

Test Items	Test Description	Test date
HSI TTH Mk 1	Functional test will be done on this system. The system is comprised of several items, shown in section table 2.	01.05.2019

Table 2: HSI Part list

HSI Part Name	Qty
HSI Platform	1
Platform Bracket	3
Cassette Front *(Grating Assembly)*	1
Cassette Back *(Grating Assembly)*	1
Clamp Bracket *(Grating Assembly)*	2
Bracket Gasket *(Grating Assembly)*	2
Shroud Front *(Shroud Assembly)*	1
Shroud Back *(Shroud Assembly)*	1
Shroud Top *(Shroud Assembly)*	1
Shroud Side *(Shroud Assembly)*	2
Shroud Gasket Front	1
Shroud Gasket Back	1
Bolts	
M2x4CSK	4
M2x6CSK	6
M2x6set	4
M2X8CH	14
M2X10CH	8
M2.5X6CSK	3

M3X6CSK	2
M3X8CSK	5
M3X10CSK	2
M4X10CH	12
COTS Components	
50mm VIS-NIR objective (OBJ-13 to OBJ-15)	3
25mm Sq. 17.5 deg Blazed Grating (300 lines/ mm)	1
SM1 lens tube 1 inch long with internal threads, and 2 threaded rings	1
Adapter ring SM1 – C-mount internal	1
Fixed high precision mounted slit	1
iDS MX249 Detector	1

Equipment

Table 3 lists all needed equipment to carry out the described test.

Table 3: Equipment

Equipment/Tools	#
Screwdriver Torx T6	*1*
Screwdriver Torx T8	*1*
Screwdriver Torx T10	*1*
Screwdriver Torx T20	1
Nitrile Gloves	2C
Isopropanol	1
Non-lint cleaning wipes	1
Optical Wipes	1
Dust-Off Canned Air	1
Angled Tweezers	1
Slit Mounting Wrench	1
Teflon Gasket	2
DP2216 3M Epoxy	-
Digital Caliper	1
Digital Scale	1
uEye Software	-
Ethernet cable	1
Socket Wrench	1

Test approach

As this is the first assembly of the prototype it is expected that the assembly order will change somewhat during the process. It is expected that unknown issues might arise and a flexible approach will be necessary. However, the steps below describe the general order of operation and will serve as a guideline during the assembly process. The main goal of this test is to learn as much as possible about the TTH Mk1 prototype and document the steps undertaken to establish a standard assembly procedure for future iterations. Steps for parts that have previously been assembled for other prototypes are taken from HYPSO-RP-006.

Pre Procedure
1. Visual inspection. Take pictures
2. Clean parts using isopropanol and wipe using non-lint cleaning wipes
3. Measure and record the weight of all parts
4. Measure geometrical dimensions and compare to specifications

Assembly Procedure

The following sections describes the planned assembly procedure. Note that the use of a clean room is recommended, however, for the purpose of this test a clean room will not be used. Neither of the V6 prototypes where assembled in a clean room. Some sections have been left open, as more information will be available during on-site during assembly. No epoxy will be applied to the assembly during this test.

Front Objective Assembly
1. Position locking ring in slit tube
2. Twist adapter on to slit tube
3. Add spacer ring to collimator objective
4. Screw together slit tube and collimator objective
5. Fix collimator objective setting

Cassette
1. Insert two M2 set screws in their respective threads from the outside of the cassette.
2. Insert the grating along with the two clamping brackets into the cassette. Note the direction of the grating to ensure correct angeling of the light
3. Hand tighten carefully
4. Apply the back plate and insert its four countersunk M2,5 screws and hand tighten them
5. Position cassette assembly on the platform and insert three M2,5 screws in the vertical direction and two M3 screws in the horizontal direction. Incrementally hand tighten these five to ensure a snug fit

Shroud
1. - On site information needed

Back Objective and Sensor
1. Screw 50mm VIS NIR lens onto IMX249 using the C-mount connections present on the parts
2. - Further on-site information needed

Positioning of Front and Back Objective Assemblies
1. Place the Front Objective Assembly into the front HSI Platform grooves
2. Slide the objectives into place within the shroud opening
3. Secure the objectives with the HSI brackets
4. Hand tighten the M4 bolts incrementally until the objectives are securely placed
5. Repeat for the back Objective and Sensor

General Functional Test
1) Inspect the spectrogram for focus, clarity and any anomalies
2) Adjust the position /orientation of various components to try to improve the quality of the spectrogram
3) Compare to spectrograms from FRED-02
4) Measure and note the positioning of all parts compared to the platform front

General Tolerance Test
Note that the steps below should be reverted to their original state before moving on to the next step. All displacements shall be measured and documented by the distance, location, and resulting spectrogram for every iteration.
1) Experiment with different spacer thicknesses and characterize what impact this has on the spectrogram
2) Displace the front optical assembly in the Z-direction and characterize what impact this has on the spectrogram
3) Displace the back optical assembly in its axial direction and characterize what impact this has on the spectrogram
4) Remove the shroud and characterize what impact this has on the spectrogram
5) Insert an M3 washer between the cassette and one of its driving surfaces. The washer should be centered on one of the bolts securing it to the platform. The goal here is to explore small rotations of the cassette relative to the incoming light beam. characterize what impact this has on the spectrogram

Post Test
The assembly process shall be well documented with photographs and in-process comments for future reference and assembly. Adjustments to any components after assembly shall be documented in text and feature before and after spectrograms. This is done to gain a better understanding of the various components role in the imaging quality. All spectrograms obtained during these tests shall be properly labeled and catalogued such that they can be used for establishing a baseline characterization of camera performance.

Appendix N

Future Test Plans

VIS-NIR Objective Shock and Vibration Test Plan

General information

Test type:
- Static

Validation method:
- Characterization test: All validations
- Visual inspection
- Measurements
- Resonance sine sweep

Facility:
- FFI Kjeller
- NTNU SmallSat lab

Purpose

The test plan comprises of the mechanical tests that will be done in order to characterize the mechanical response of the VIS-NIR 50mm objectives in regard to shock and vibration levels close to the launch environment defined by the *NanoAvionics Environmental Testing Requirements*.

To assess the amount of shock the lens component can handle before destruction, the shock will be tested at different levels up to 98G (safety factor added), or until visible damage occurs. There exists no data for the objective response to shock. This test will give the raw data needed to characterize the shock response in the objectives, and will serve as design parameters with the given safety factor.

The internal design and integrity is also unknown. If glass or parts inside the lenses start shaking or resonate at certain frequencies, this has to be known. The mechanical integrity of the set screws will also need to be investigated, as they serve as a locking mechanism for the focus and aperture. Should these vibrate loose, the image quality of the HSI may be compromised. For the vibration tests, the set screws will not be glued, as described in the HSI design document. This is to uncover whether gluing is required or not, as it introduces other potential error sources to the mission.

All the shock tests are considered destructive.

Risk assessment

There might occur damage to the tested objectives due to the shock response. This could manifest itself as misalignment of the inner optical components, cracking of the lenses or loosening of the aperture mechanism. There might also occur damage to the tested objectives due to random vibration. The damage here could manifest itself as loosening of the aperture and focus set screws, misalignment of the internal optical components, cracks in the lenses or loosening of the aperture mechanism.

Items to be tested

Table 1 tabulates the tested items.

Table 1: Test item list

Test Items	No. of items	Test Description	Test date
50 mm VIS-NIR objective (OBJ-03,10, X, X)	4	Shock in all 3 axis Sine sweep in 3 axis Random sweep in 3 axis	24.06.2019

Equipment

Table 2 tabulates all equipment necessary in order to carry out the test as described. Note that the list will be updated to include specific software and test apparatus name to ensure test repeatability.

Table 2: Test Equipment

Equipment	#
50 mm VIS-NIR lenses (OBJ-03,10, X, X)	2
Mass scale (GM-1500P)	1
Shock table (Lansmondt)	1
Accelerometers	6
Moundable adhesive putty	1
Test result recording software (Update when at FFI)	1
Shaker table (For Sine Sweep)	1
Micrometer	1
Caliper	1
Torx screwdriver set	-
Scotch-Weld Epoxy Adhesive 2216 B/A	-
Non latex gloves	-

Interfacing

Because the vibration tests have to be performed on all three axes, an interfacing unit with multi axis capability should be used. The interface unit should conform to the available fastening interface of the shaker. The hole pattern for the vibration table is also present on the shock table. The hole pattern of the shock table can be seen in figure 1.
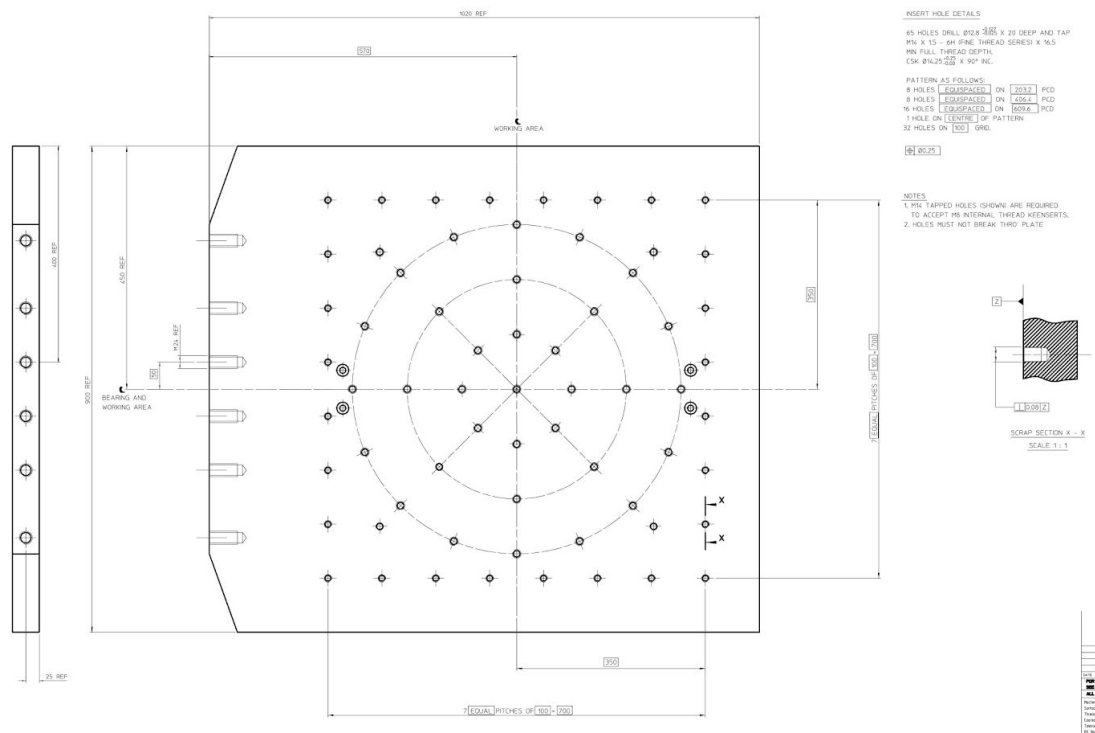

Figure 1: Hole pattern of the shock table (Appendix A)

Test Set-up

A customized platform was developed in order to test the objectives on multiple axes, given the limitations of the shock set-up at FFI. As described in section *Interfacing*, the platform shares similarities with the vibration set-up, allowing for reusability. Figure 2 shows the objective mounted on the platform. The platform was machined in aluminium 6082. It connects to the shock and vibration table by sixteen M8X16 hex head bolts and one M8X16 cap head bolt. The latter is used in the central hole to avoid problems with tool access. Technical drawings of the platform can be found in appendix B.

Figure 2: 50mm Objective mounted on the platform in the horizontal position (left), and the vertical position (right)

All parts of the test set-up was measured using a 0.05g precision scale in order to gain control of the test parameters. The weighted values are tabulated in table 3.

Table 3: Weighed parts and assemblies

Part	Mass (g)
OBJ-03	X
OBJ-10	104.95
OBJ-X	X
OBJ-X	X
Full test assembly, horizontal configuration	1204.40
Full test assembly, vertical configuration	1205.50
Interface screws*	184.35

One M8X16 cap head, sixteen M8X16 hex head.

Test Approach

Prior to the shock and vibration tests, the lens objectives will need to be properly characterized in order to detect possible changes. This will consist of a visual inspection looking for possible defects, and testing the objectives by taking spectrograms in an HSI assembly. Both of these processes should involve plenty of visual documentation. The spectrogram characterization should be done by replacing the back objective of the HSI front optical assembly with all of the tested lenses. See part (3) in figure 3. This is because the front assembly is believed to have a bigger impact on the focus of the spectrograms. The same process shall be repeated after all of the objectives have been mechanically tested.
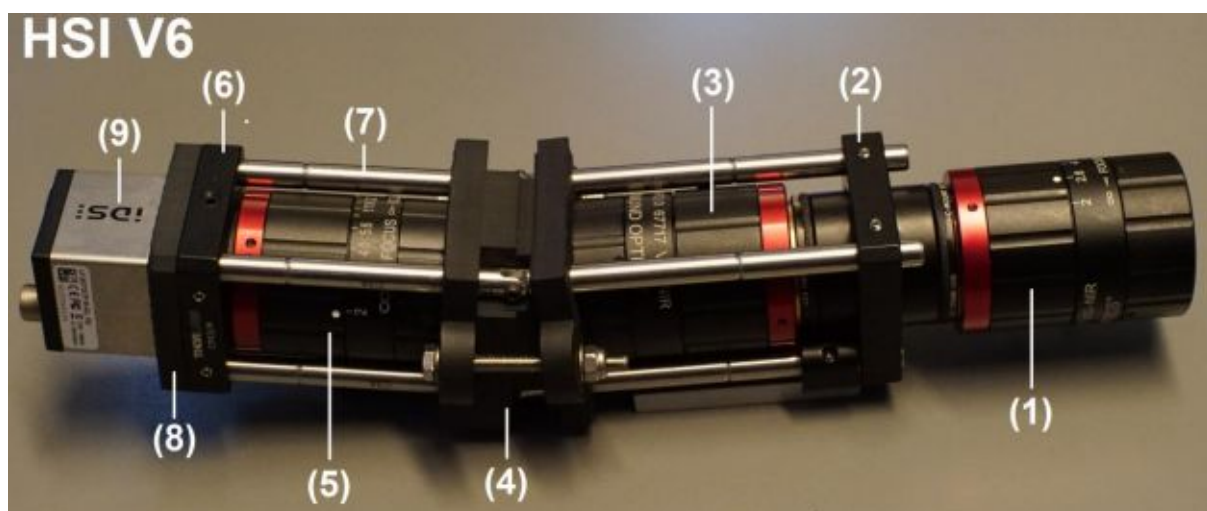

Figure 3: Hole pattern of the shock table

The objectives shall be mounted to the test platform using a tightening moment of 270Nmm on the bracket screws, as specified in the HSI design report. For the shock test, the Z-position of the objectives shall be measured relative to the brackets. This is to determine whether the objective has slid during shock due to a lack of friction or not.

Due to time restraints, the objectives will not undergo the cleaning procedure that is planned for the flight model objectives due to the presence of grease. This may be a source of error.

The payloads shall remain fully functional after a sine vibration test with the parameters noted in table 4, based on the Environmental Testing Requirements for Polar Satellite Launch Vehicle provided by NanoAvionics. The values are for a standard qualification test, the acceptance test requires a less severe profile as to not purposefully harm the flight model more than necessary. It is possible that the frequency sweep might change due to the unknown resonance frequency of the test item.

Table 4: PLSV Sine parameters

Characteristic		Qualification
Profile	Frequency, Hz	Amplitude
	5- 8	34.5 (DA)
	8- 100	4.5 G
Directions		x, y, z
Sweep Rate, oct/ min		2

The payload must also be able to survive the random vibrations that are present during the flight. The vibration band present in the PSLV can be simulated and tested in the lab. Table 5 shows the recommended values for a random vibration test, the values are for all directions X, Y and Z. Where PSD is the *power spectral density*, or the distributed power of the vibrations, and RMS is the *root mean square* a measure of the overall amplitude of the random vibrational system.

Table 5: Random Vibration Test

Characteristics		Qualification
Profile	Frequency, Hz	PSD, G^2/Hz
	20	0.002
	110	0.002
	250	0.034
	1000	0.034
	2000	0.009
Acceleration, G (RMS)		6.7
Duration, sec/ axis		120

The payload must be able to survive the shock loads present under launch. Table 6 tabulates the required shock values the payload shall survive.Where the Q-factor is the quality factor related to the system damping, a Q-factor of 10 is equivalent to 5% damping, and a normal approximation of bolted transmissions. In addition, a margin of safety of 1.4 should be incorporated in the described load factors to comply with the NASA standards.

Table 6: Half Sine Shock test

Characteristics	Qualification
Acceleration, G	70
Duration, ms	2
Q- Factor	10

With the added safety factor the actual test shock acceleration shall be 94G.

Pre-test Characterization Procedure

Make sure plenty of pictures are taken during the inspection and spectrogram steps. All measurements shall be documented.

Wear gloves

Open objective packing

Inspect objectives looking closely for:

         a) Mechanical defects on surface

         b) Defects or scratches on lenses

         c) Surface contamination on lenses

Turn the focal and aperture rings making sure they function properly

Weigh objectives

Assemble the objective into the back part of the front optical assembly (see figure 3)

Take spectrograms using the following settings: PixelClock=118, FPS=1.5, EXP=563.793, GAIN=0, the exact settings will vary depending on the light conditions.

Vibration Test Procedure

The following steps should be done twice in parallel with each on the two configurations (horizontal and vertical mounting). The unused bracket shall be removed in both configurations.

1) Mount the objective on the platform
2) Tighten the brackets with a tightening moment of 270Nmm
3) Bolt the platform to the vibration table
4) Run a sine sweep to characterize the resonance frequencies, table 4
5) Run a random sweep to check if the objectives can survive the launch conditions, table 5
6) Run a sine sweep to characterize to check for changes in the frequencies, table 4

Shock Test procedure

The following steps should be done twice in parallel with each on the two configurations (horizontal and vertical mounting). The unused bracket shall be removed in both configurations.
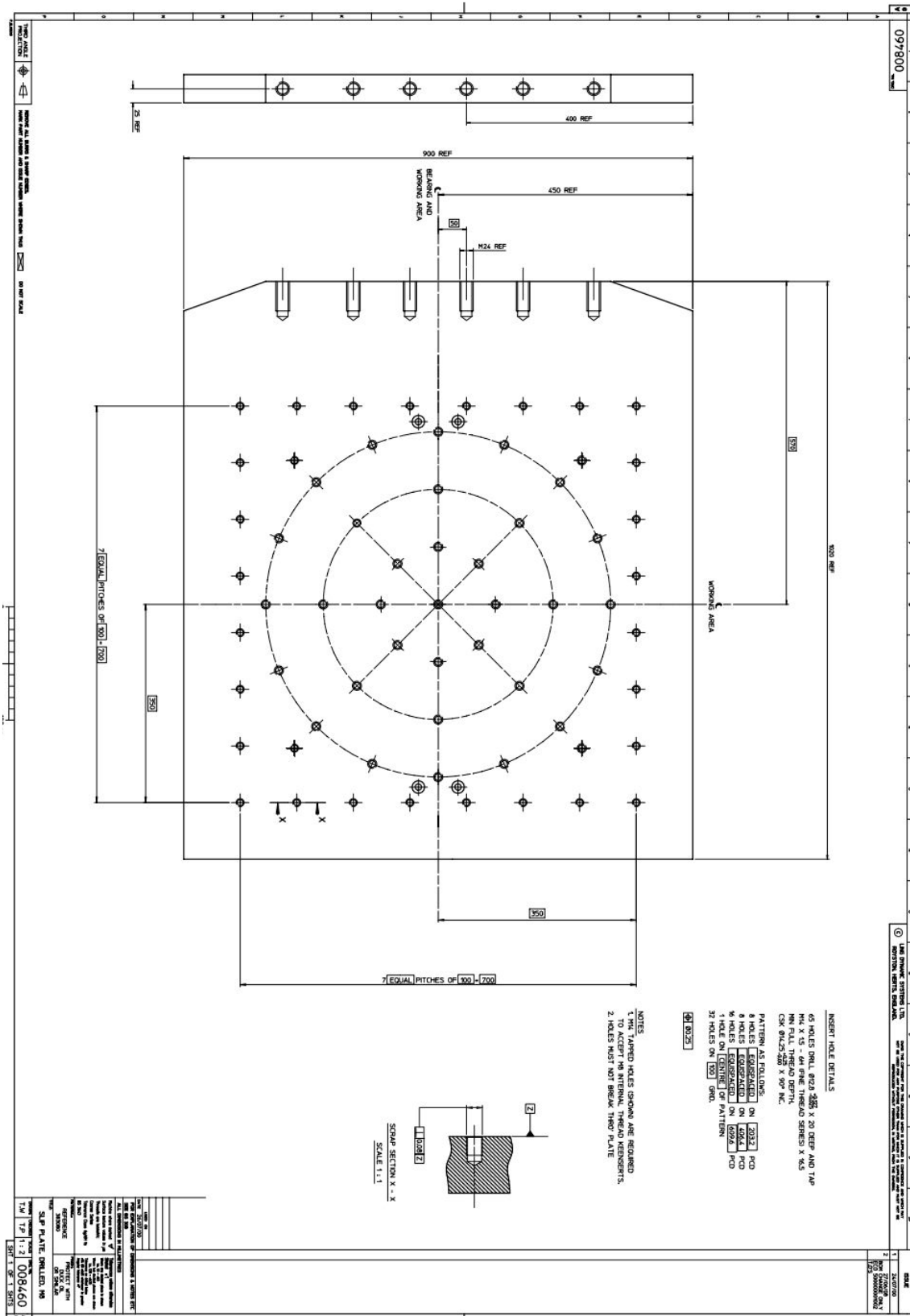
1) Mount the objective on the platform
2) Tighten the brackets with a tightening moment of 270Nmm
3) Measure the Z-position of the objective from the objective to platform bracket (this only applies to shock in the Z-direction)
4) Bolt the platform to the vibration table
5) Run a sine sweep to characterize the resonance frequencies, table 4
6) Bolt the platform to the shock table
7) Perform a shock test to the values described in table 6 with added safety factor, table 6
8) Bolt the platform to the vibrational table
9) Run a sine sweep to characterize the resonance frequencies, table 4
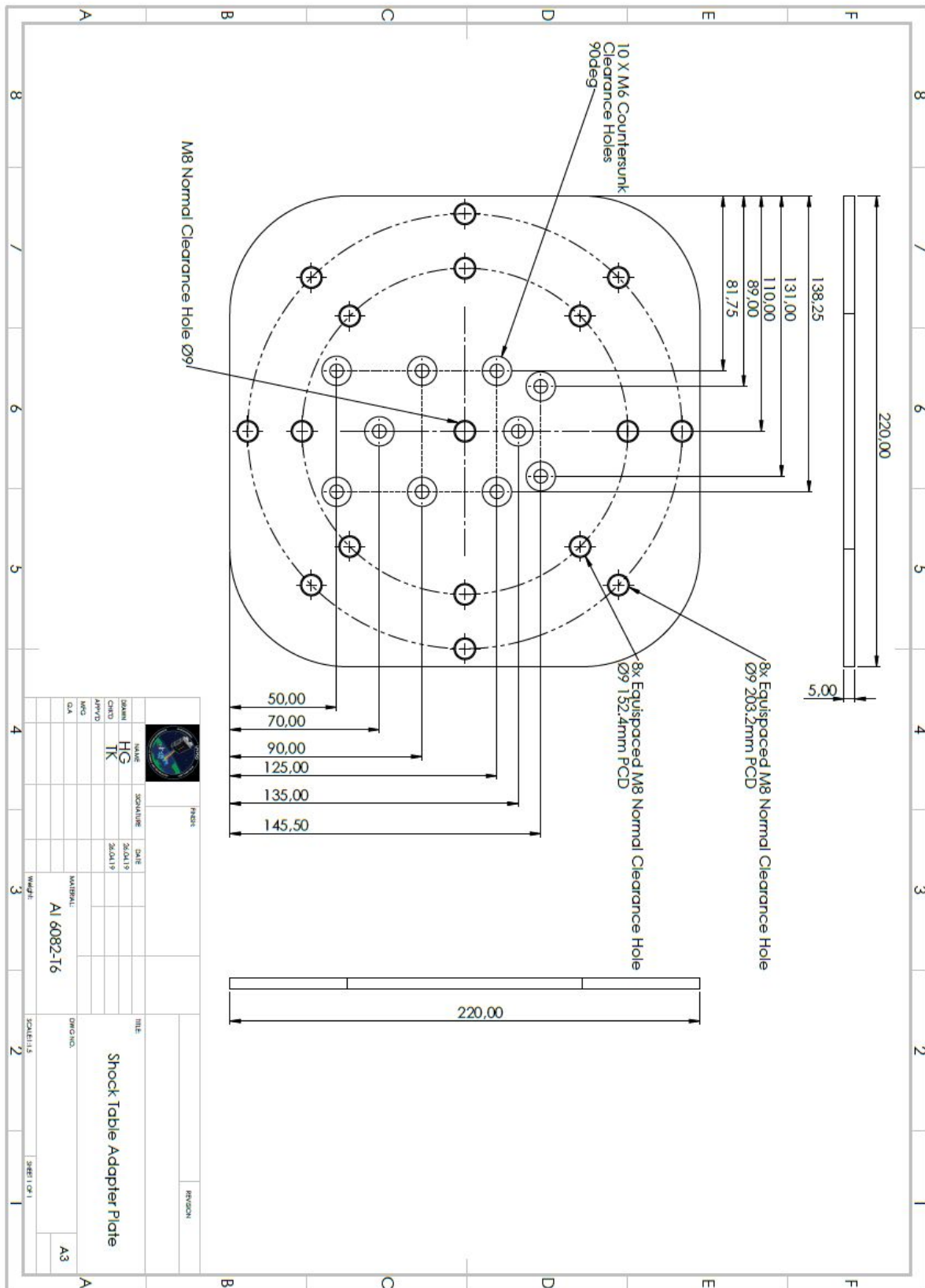
Post-test Characterization Procedure

Make sure plenty of pictures are taken during the inspection and spectrogram steps. All measurements shall be documented.

1) Wear gloves
2) Open objective packing
3) Inspect objectives looking closely for:
    a) Mechanical defects on surface
    b) Defects or scratches on lenses
    c) Surface contamination on lenses
4) Turn the focal and aperture rings making sure they function properly
5) Weigh objectives
6) Assemble the objective into the back part of the front optical assembly (see figure 3)
7) Take spectrograms using the following settings: PixelClock=118, FPS=1.5, EXP=563.793, GAIN=0, the exact settings will vary depending on the light conditions.
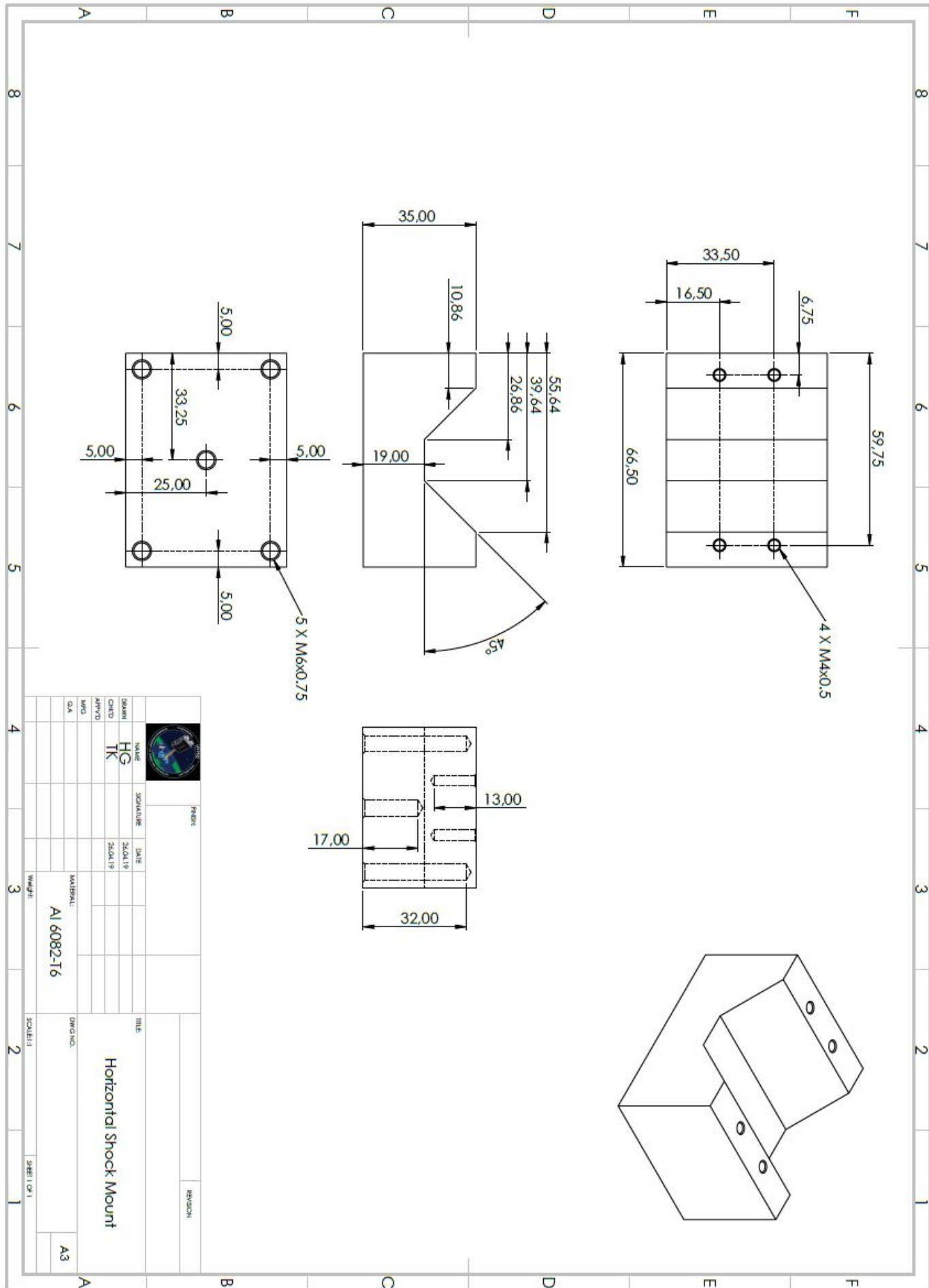
Appendix A

Appendix B

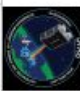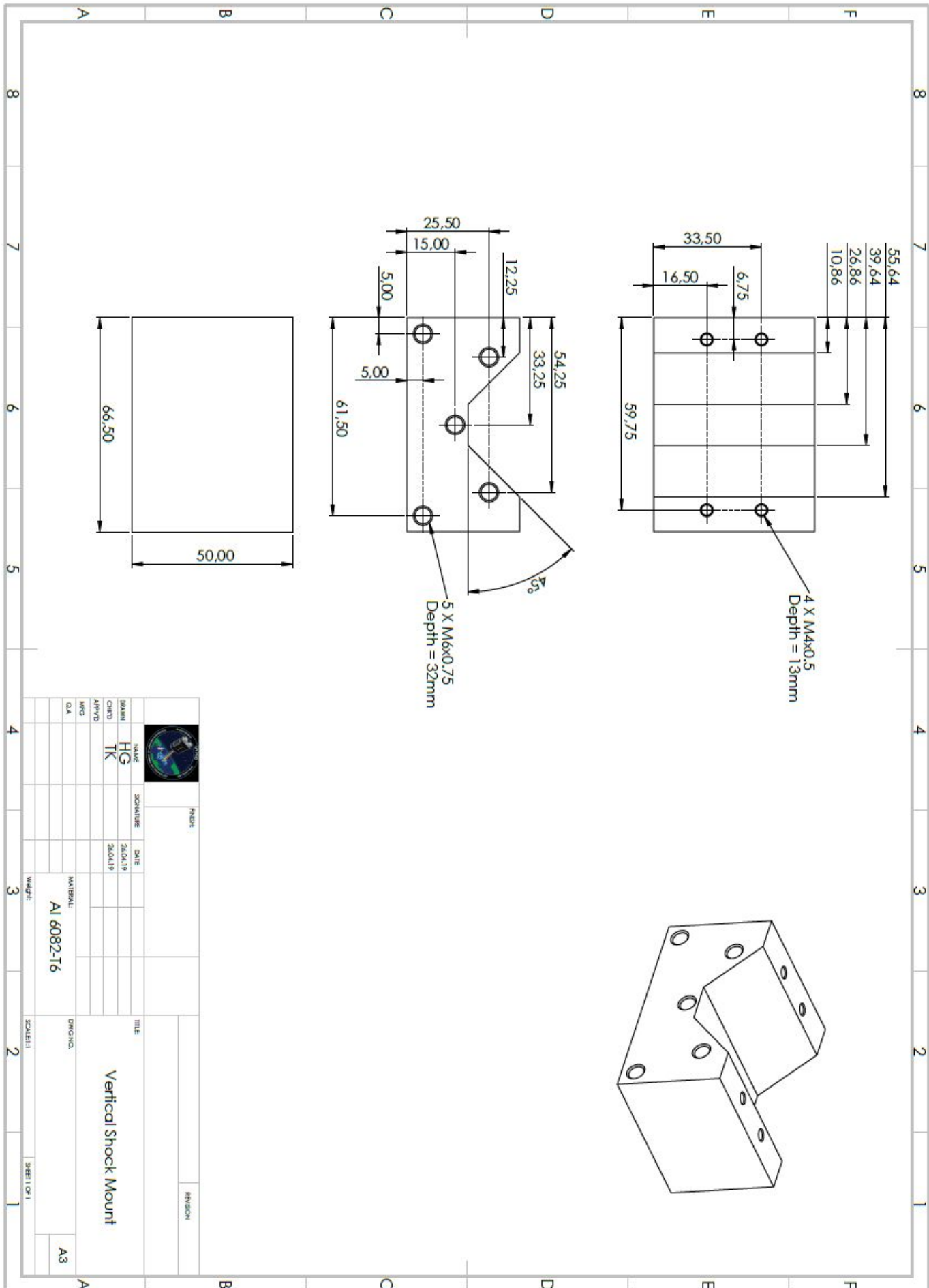Horizontal Shock Mount

MATERIAL: Al 6082-T6

NAME: HG TK

DATE: 26.04.19

35,00
10,86
19,00
55,64
39,64
26,86
45°

5,00
33,25
5,00   5,00
25,00
5,00
5 X M6x0,75

33,50
16,50   6,75
66,50   59,75
4 X M4x0,5

13,00
17,00
32,00

A3

25,50
15,00
12,25
5,00
5,00
61,50
54,25
33,25
45°
5 X M6x0.75
Depth = 32mm

33,50
16,50
6,75
55,64
39,64
26,86
10,86
59,75
4 X M4x0.5
Depth = 13mm

66,50
50,00

NAME
DRAWN HG
CHK'D TK
APP'VD
MFG
Q.A

SIGNATURE
DATE
26.04.19
26.04.19

FINISH

MATERIAL:
Al 6082-T6

WEIGHT

TITLE:
Vertical Shock Mount

DWG NO.

SCALE:1:1   SHEET 1 OF 1

REVISION

A3

Component Level Thermal Characterization Test Plan

Test Type	Static
Validation Method	Compare data as temperature increases

Purpose

The main purpose of these tests is to uncover the thermal transmission in a simple camera assembly, using the same equipment as planned for the HSI assembly. Because the tests will not be performed in vacuum, the results will deviate from the more realistic TVAC test. With the test results, thermal simulation models can also be improved upon as simulation and test results can be compared. This will allow for more knowledge about the thermal behavior of each component. However, due to the relative test simplicity and equipment availability, the test will be useful for obtaining data that can be used for further planning of more advanced tests as well as directional pointing of the thermal control. With these tests, additional unforeseen problems might also be uncovered.

Risk Assessment

The main risk is to damage the sensitive equipment needed for the test. No additional environmental equipment is required for this initial test. The test assembly consisting of a lens objective and camera detector could potentially fall down from the jig and harness.

Items to be Tested

The camera test assembly will consist of the components tabulated in table 1. selected these two for simplicity and lowest amount of error sources. The current v6 prototype consists of too many parts that will change with the new design. Additionally, the complexity of the simulations would increase significantly.

Table 1: Test Item list

Test Items	Test Description	Test date
50 mm VIS-NIR lens	The component being tested during this experiment.	7.3.2019
Sony IMX249 sensor	Tool used for gathering data before and after the vacuum exposure.	7.3.2019

The lens and detector components will be tested in a vacuum chamber. No further components or subsystems will be tested for pressure gradient resilience.

Table 2: Equipment list

Equipment	#
Sony IMX174 sensor (Detector)	1
50 mm VIS-NIR lens	1
Computer with uEye Cockpit (Software)	1
Micro USB 3.0 cable	1
FLIR i7 thermal camera	1
FLIR Tools (Software)	-
Line harness	1
Support structure	1

Test approach

The idea is to power on the camera detector and record the heat flow along a 50mm lens attached. The Detector will be powered on for 5 min with data points taken at 1 min, 2 min, 3 min, 4 min and 5 min respectively. The data points are thermal images captured by the FLIR i7 camera. During each data point, each side of the camera will need to be captured. Each side (face) of the camera will be referred to as the -Z, ±X and ±Y faces. The +Z face is the side facing the objective. Based on the detector disassembly report, the processing chip on the inside of the detector is located in the center of a PCB stack assembly. The chip is thermally coupled to the -Z face of the housing by a thermal strap that is glued on top of the chip surface. In the addition to the thermal strap, pads suspected to be thermal and shock pads are also inserted between three layers of PCB around the processor and -Z housing, as shown in figure 1.The black side face where the screw is located, now referred to as the -Y face is directly a part of the ±Z housings. This means that these surfaces should experience a quicker reaction to heat distribution.
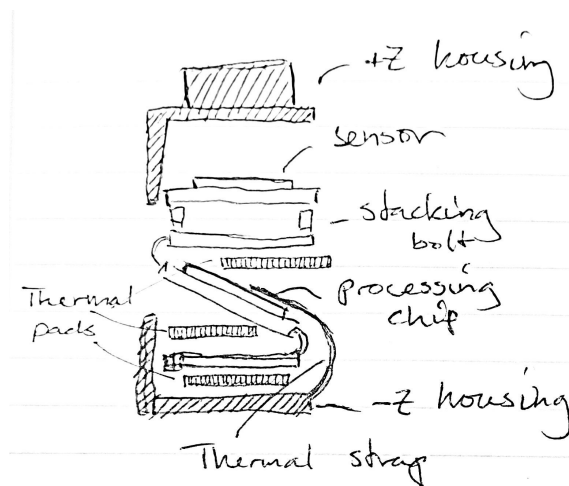
Figure 1: Detector Cross Section

A line harness and support structure makes sure that the unwanted conduction will be minimal. It is important to make sure that the surface underneath the setup is compliant to shock, should the setup drop towards the ground. Figure 2 shows the coordinate system orientations used to describe the different faces of the camera test assembly. This is based on the HSI cameras orientation inside the NanoAvionics Cubesat with respect to the CubeSat standard coordinate system.
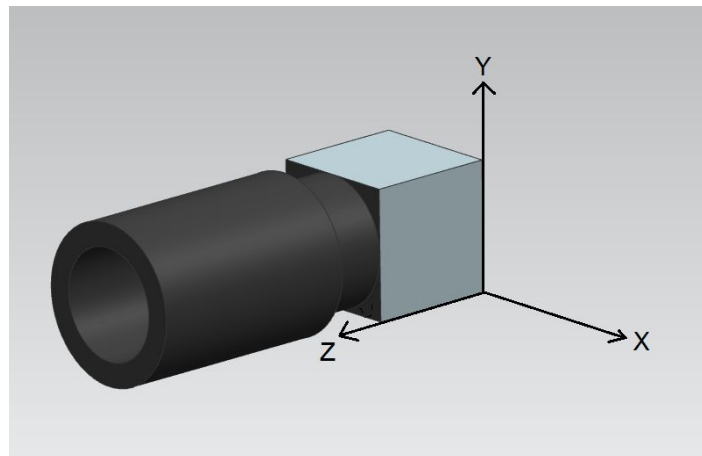

Figure 2: Coordinate System

Procedure

Take the detector and assemble the objective lens. Let the test assembly settle in room temperature. Measure the initial temperature. Connect the Micro USB 3.0 to the detector and place the camera in the line harness and connect it to the support structure. For simplicity, the Micro USB 3.0 cable will be used as a harness. Power up the camera by connecting the USB cable to a PC. This will automatically power on the IMX camera. A FLIR thermal camera will then be used to measure the ±Y and ±X faces at specified intervals. To lower the risk of damaging the objective and IMX detector, should the test assembly separate from the harness, place something soft underneath.

Settings

The thermal camera settings are tabulated in table 3. These have mostly been chosen for simplicity. FLIR Tools, the software for viewing the thermal data allows post-calibration of all settings. Thus, further calibration can be done in the future should a higher accuracy be desired. The relative increase in temperature should however remain the same.

Table 3: Camera Settings

Emissivity	0.8
Reflected Temperature	20.0°C
Distance	1.0 m
Atmospheric Temperature	20.0°C
External Optics Temperature	20.0°C
External Optics Transmittance	1.0
Relative Moisture	50.0%

Intervals

The intervals chosen for the test have been tabulated in table 4, Test Intervals. Because the test is conducted in an environment with convection, a longer total period has been chosen to capture more of the thermal behavior. The reason behind this is the cooling effect caused by air environment slowing down the heating process. The initial starting face for every interval is chosen to be the -Y face, which is the thermally coupled side.

Table 4: Test Intervals

Time (s)	Face
0	±Y and ±X
60	±Y and ±X
120	±Y and ±X
180	±Y and ±X
240	±Y and ±X
300	±Y and ±X

Tord Hansen Kaasa

Mechanical Design Analysis and Integration of a Hyperspectral Imaging Payload for a 6U CubeSat

NTNU
Norwegian University of
Science and Technology